

# HOST-GUEST CHEMISTRY OF MACROCYCLES

EDITED BY: Tangxin Xiao, Robert Elmes and Yong Yao  
PUBLISHED IN: *Frontiers in Chemistry*





# frontiers

## Frontiers eBook Copyright Statement

The copyright in the text of individual articles in this eBook is the property of their respective authors or their respective institutions or funders. The copyright in graphics and images within each article may be subject to copyright of other parties. In both cases this is subject to a license granted to Frontiers.

The compilation of articles constituting this eBook is the property of Frontiers.

Each article within this eBook, and the eBook itself, are published under the most recent version of the Creative Commons CC-BY licence.

The version current at the date of publication of this eBook is CC-BY 4.0. If the CC-BY licence is updated, the licence granted by Frontiers is automatically updated to the new version.

When exercising any right under the CC-BY licence, Frontiers must be attributed as the original publisher of the article or eBook, as applicable.

Authors have the responsibility of ensuring that any graphics or other materials which are the property of others may be included in the CC-BY licence, but this should be checked before relying on the CC-BY licence to reproduce those materials. Any copyright notices relating to those materials must be complied with.

Copyright and source acknowledgement notices may not be removed and must be displayed in any copy, derivative work or partial copy which includes the elements in question.

All copyright, and all rights therein, are protected by national and international copyright laws. The above represents a summary only. For further information please read Frontiers' Conditions for Website Use and Copyright Statement, and the applicable CC-BY licence.

ISSN 1664-8714

ISBN 978-2-88966-497-9

DOI 10.3389/978-2-88966-497-9

## About Frontiers

Frontiers is more than just an open-access publisher of scholarly articles: it is a pioneering approach to the world of academia, radically improving the way scholarly research is managed. The grand vision of Frontiers is a world where all people have an equal opportunity to seek, share and generate knowledge. Frontiers provides immediate and permanent online open access to all its publications, but this alone is not enough to realize our grand goals.

## Frontiers Journal Series

The Frontiers Journal Series is a multi-tier and interdisciplinary set of open-access, online journals, promising a paradigm shift from the current review, selection and dissemination processes in academic publishing. All Frontiers journals are driven by researchers for researchers; therefore, they constitute a service to the scholarly community. At the same time, the Frontiers Journal Series operates on a revolutionary invention, the tiered publishing system, initially addressing specific communities of scholars, and gradually climbing up to broader public understanding, thus serving the interests of the lay society, too.

## Dedication to Quality

Each Frontiers article is a landmark of the highest quality, thanks to genuinely collaborative interactions between authors and review editors, who include some of the world's best academicians. Research must be certified by peers before entering a stream of knowledge that may eventually reach the public - and shape society; therefore, Frontiers only applies the most rigorous and unbiased reviews. Frontiers revolutionizes research publishing by freely delivering the most outstanding research, evaluated with no bias from both the academic and social point of view. By applying the most advanced information technologies, Frontiers is catapulting scholarly publishing into a new generation.

## What are Frontiers Research Topics?

Frontiers Research Topics are very popular trademarks of the Frontiers Journals Series: they are collections of at least ten articles, all centered on a particular subject. With their unique mix of varied contributions from Original Research to Review Articles, Frontiers Research Topics unify the most influential researchers, the latest key findings and historical advances in a hot research area! Find out more on how to host your own Frontiers Research Topic or contribute to one as an author by contacting the Frontiers Editorial Office: [frontiersin.org/about/contact](https://frontiersin.org/about/contact)

# HOST-GUEST CHEMISTRY OF MACROCYCLES

Topic Editors:

**Tangxin Xiao**, Changzhou University, China

**Robert Elmes**, Maynooth University, Ireland

**Yong Yao**, Nantong University, China

**Citation:** Xiao, T., Elmes, R., Yao, Y., eds. (2021). Host-Guest Chemistry of Macrocycles. Lausanne: Frontiers Media SA. doi: 10.3389/978-2-88966-497-9

# Table of Contents

- 05 Editorial: Host-Guest Chemistry of Macrocycles**  
Tangxin Xiao, Robert Elmes and Yong Yao
- 08 Structural Design, Synthesis, and Preliminary Biological Evaluation of Novel Dihomooxacalix[4]arene-Based Anti-tumor Agents**  
Lin An, Chan Wang, Lili Han, Jiadong Liu, Tonghui Huang, Youguang Zheng, Chaoguo Yan and Jing Sun
- 24 Smart Molecular Recognition: From Key-to-Lock Principle to Memory-Based Selectivity**  
Askar K. Gatiatulin, Marat A. Ziganshin and Valery V. Gorbachuk
- 32 pH-Induced Transition Between Single-Chain Macrocyclic Amphiphile and [c2]Daisy Chain-Based Bola-Type Amphiphile and the Related Self-Assembly Behavior in Water**  
Pi Wang, Ruihuan Wang and Danyu Xia
- 39 A p-tert-Butyldihomooxacalix[4]arene Based Soft Gel for Sustained Drug Release in Water**  
Hao Guo, Runmiao Zhang, Ying Han, Jin Wang and Chaoguo Yan
- 45 Corrigendum: A p-tert-Butyldihomooxacalix[4]arene Based Soft Gel for Sustained Drug Release in Water**  
Hao Guo, Runmiao Zhang, Ying Han, Jin Wang and Chaoguo Yan
- 47 Corrigendum: A p-tert-Butyldihomooxacalix[4]arene Based Soft Gel for Sustained Drug Release in Water**  
Hao Guo, Runmiao Zhang, Ying Han, Jin Wang and Chaoguo Yan
- 48 Porphyrin-Based Organoplatinum(II) Metallacycles With Enhanced Photooxidation Reactivity**  
Lintao Wu, Chun Han, Zhijun Wang, Xi Wu, Feng Su, Mengyao Li, Qingyang Zhang and Xiaobi Jing
- 53 Cyclic  $\gamma$ -Peptides With Transmembrane Water Channel Properties**  
Jie Chen, Qiang Li, Pengchao Wu, Juan Liu, Dan Wang, Xiaohong Yuan, Renlin Zheng, Rongqin Sun and Liangchun Li
- 61 Facile One-Step Electrodeposition Preparation of Cationic Pillar[6]arene-Modified Graphene Films on Glassy Carbon Electrodes for Enhanced Electrochemical Performance**  
Qunpeng Duan, Lijie Wang, Fei Wang, Hongsong Zhang and Kui Lu
- 71 Calix[n]arene/Pillar[n]arene-Functionalized Graphene Nanocomposites and Their Applications**  
Qunpeng Duan, Lijie Wang, Fei Wang, Hongsong Zhang and Kui Lu
- 78 Fluorescent Supramolecular Polymers Formed by Crown Ether-Based Host-Guest Interaction**  
Jinjin Zhang, Huayu Qiu, Tian He, Yang Li and Shouchun Yin
- 97 Coordination-Driven Poly[2]Pseudorotaxanes in Highly Polar Organic Solvent**  
Hang Su, Wei Chen, Liang Li, Bin Li, Zhi-Yuan Zhang and Chunju Li



- 104** *Use of  $\alpha$ -cyclodextrin to Promote Clean and Environmentally Friendly Disinfection of Phenolic Substrates via Chlorine Dioxide Treatment*  
Sauradip Chaudhuri, Dana J. DiScenza, Thomas B. Boving, Alan Burke and Mindy Levine
- 113** *pH-Responsive Host-Guest Complexations Between a Water-Soluble Pillar[6]arene Dodecyl-Ammonium Chloride and Aromatic Sulfonic Acids*  
Qunpeng Duan, Fei Wang, Hongsong Zhang and Kui Lu
- 119** *Stimuli-Responsive Biomass Cellulose Particles Being Able to Reversibly Self-Assemble at Fluid Interface*  
Yue Zhu, Tingting Chen, Zhenggang Cui, Hong Dai and Li Cai
- 129** *Supramolecular Polymers With AIE Property Fabricated From a Cyanostilbene Motif-Derived Ditopic Benzo-21-Crown-7 and a Ditopic Dialkylammonium Salt*  
Haoran Wu and Tangxin Xiao



# Editorial: Host-Guest Chemistry of Macrocycles

Tangxin Xiao<sup>1\*</sup>, Robert Elmes<sup>2,3\*</sup> and Yong Yao<sup>4\*</sup>

<sup>1</sup> School of Petrochemical Engineering, Changzhou University, Changzhou, China, <sup>2</sup> Department of Chemistry, Maynooth University, National University of Ireland, Maynooth, Ireland, <sup>3</sup> Synthesis and Solid-State Pharmaceutical Centre, Maynooth University, National University of Ireland, Maynooth, Ireland, <sup>4</sup> School of Chemistry and Chemical Engineering, Nantong University, Nantong, China

**Keywords:** macrocycles, supramolecular chemistry, host-guest interaction, self-assembly, pillar[n]arenes

## Editorial on the Research Topic

### Host-Guest Chemistry of Macrocycles

Macrocyclic-based host-guest chemistry has played an important role in the development of supramolecular chemistry. Burgeoning progress has been continuously made in the development of supramolecular assemblies by using various host molecules, such as cyclodextrins (Li and Purdy, 1992; Szejtli, 1998; Harada et al., 2009, 2014; Antoniuk and Amiel, 2016), cucurbiturils (Lagona et al., 2005; Ni et al., 2014; Barrow et al., 2015; Murray et al., 2017), calixarenes (Shinkai et al., 1984; Böhmer, 1995; Guo and Liu, 2014), crown ethers (Pedersen, 1967; Amabilino et al., 1995; Zhang et al., 2007; Xiao et al., 2020a, 2021), pillararenes (Ogoshi et al., 2008, 2016, 2018; Xue et al., 2012; Strutt et al., 2014; Kakuta and Yamagishi, 2018; Xiao et al., 2018, 2019a,b,c), and other macrocycles (Wang et al., 2019). The architectures and properties of different hosts endow themselves with versatile abilities to bind with different guest molecules. Therefore, macrocyclic hosts show significant potential in constructing assorted functional materials, such as hydrogels (Appel et al., 2012; Xiao et al., 2019d), functional supramolecular polymers (Chen et al., 2019; Xiao et al., 2020b), artificial light harvesting systems (Xiao et al., 2019e), and so on.

Supramolecular polymers, a concept combining elements of both supramolecular chemistry and polymer science, are promising dynamic functional materials. Moreover, the incorporation of fluorophores into supramolecular polymers could endow them with interesting photophysical properties. In this context, Zhang et al. reviewed fluorescent supramolecular polymers constructed by crown ether-based host-guest interactions. They focused on fabrication strategies, properties, and potential applications of these materials. On the same Topic, Wu and Xiao contributed an article on an aggregation induced emissive (AIE) supramolecular polymer which was constructed from a cyanostilbene based ditopic benzo-21-crown-7 and a ditopic dialkylammonium salt. In another review paper, Gatiatulin et al. summarized the possible alternatives to the classical key-to-lock principle with higher selectivity for molecular recognition. These alternatives are based on cooperativity of phase transitions, which adds up the small differences in molecular structure of different bound guests. In a minireview, Duan et al. (b) summarized broad approaches for the preparation of graphene nanomaterials functionalized with calix[n]arene/pillar[n]arene, and their applications in molecular recognition, fluorescent sensors, electrochemical biosensors, and as catalytic, antibacterial, and adsorption materials.

Calixarene derivatives have played an important role in developing anti-tumor agents. The contribution of An et al. focused on novel dihomooxacalix[4]arene-based anti-tumor agents. In their work, they reported the synthesis of 19 structurally related dihomooxacalix[4]arene amide derivatives in search of optimal efficacy. Guo et al. synthesized a *p*-*tert*-butyldihomooxacalix[4]arene, which could form a soft gel in cyclohexane. Moreover, the

## OPEN ACCESS

### Edited and reviewed by:

Tony D. James,  
University of Bath, United Kingdom

### \*Correspondence:

Tangxin Xiao  
xiaotangxin@cczu.edu.cn  
Robert Elmes  
robert.elmes@mu.ie  
Yong Yao  
yaoyong1986@ntu.edu.cn

### Specialty section:

This article was submitted to  
Supramolecular Chemistry,  
a section of the journal  
Frontiers in Chemistry

**Received:** 11 November 2020

**Accepted:** 17 November 2020

**Published:** 09 December 2020

### Citation:

Xiao T, Elmes R and Yao Y (2020)  
Editorial: Host-Guest Chemistry of  
Macrocycles. *Front. Chem.* 8:628200.  
doi: 10.3389/fchem.2020.628200

xerogel with its highly interconnected and homogeneous porous network, may be used for drug storage and controlled release. Pillararenes are a relatively new macrocyclic host and have been employed to fabricate various supramolecular materials. Macrocyclic amphiphiles have attracted much attention due to their unique properties in the construction of functional nanomaterials. The work of Wang et al. investigates a pillararene-based macrocyclic amphiphile, which is responsive to pH. Interestingly, a pH-induced transition between single-chain macrocyclic amphiphile and bola-type amphiphile and the corresponding self-assembly behavior was investigated. Self-assembled peptides can also be used to fabricate new biomaterials for medical applications. Duan et al. (a) developed cationic pillar[6]arene-modified graphene films on glassy carbon electrodes directly from graphene oxide-cationic pillar[6]arene dispersions using a pulsed electrodeposition technique. Experimental results revealed that the electrochemically reduced graphene oxide-cationic pillar[6]arene films could show a much higher electrochemical response to five purine bases than unmodified reduced graphene oxide films and bare glassy carbon electrodes. In other work, Duan, Wang, Zhang et al. designed new host-guest binding motifs based on a water-soluble pillar[6]arene dodecyl-ammonium chloride with two aromatic sulfonic acids in water. Interestingly, both of these host-guest complexes can be tuned reversibly between their complexed and decomplexed states by sequential addition of a base and an acid (NaOH and HCl, respectively). Construction of polypseudorotaxanes in high-polar organic solvents is challenging owing to the weak interactions between macrocycles and axles. Su et al. prepared a novel metal-coordinated poly[2]pseudorotaxane by using pillar[5]arene, 1,4-bis(4-pyridyl pyridinium)butane, and [PdCl<sub>2</sub>(PhCN)<sub>2</sub>] in dimethyl sulfoxide.

Chaudhuri et al. developed a method to promote clean and environmentally friendly disinfection of phenolic substrates by employing  $\alpha$ -cyclodextrin to affect the product distribution in

chlorine dioxide-mediated decomposition of organic pollutants. Chen et al. synthesized and characterized two novel cyclic  $\gamma$ -peptides with hydrophobic inner surfaces, which could self-assemble into stacking nanotubes through intermolecular H-bonds and  $\pi$ - $\pi$  interactions. Notably, the nanotubes could serve as selective water channels to transport water across the lipid membrane. Metallacycles have obtained great interest in recent years. The contribution of Wu et al. constructed two porphyrin-based organoplatinum(II) metallacycles through coordination-driven self-assembly. Interestingly, these metallacycles could be utilized as catalysts for photo-oxidation with high efficiency. Zhu et al. demonstrated a simple protocol to prepare stimuli-responsive surface-active microcrystalline cellulose particles which are able to reversibly self-assemble at a fluid interface via reversible *in situ* hydrophobization to stabilize stimuli-responsive Pickering emulsions.

In summary, this Research Topic has highlighted how the fields of macrocyclic and supramolecular chemistry are still inextricably linked. The field has matured considerably in recent years and is now beginning to show more and more potential for real-world applications to address important issues across the sciences.

## AUTHOR CONTRIBUTIONS

All authors listed have made a substantial, direct and intellectual contribution to the work, and approved it for publication.

## ACKNOWLEDGMENTS

We acknowledge financial support by the National Natural Science Foundation of China (21702020, 21801139) and Science Foundation Ireland (SFI) co-funded under the European Regional Development Fund under Grant number 12/RC/2275\_P2.

## REFERENCES

- Amabilino, D. B., Ashton, P. R., Brown, C. L., Cordova, E., Godinez, L. A., Goodnow, T. T., et al. (1995). Molecular mecano. 2. Self-assembly of [n]catenanes. *J. Am. Chem. Soc.* 117, 1271–1293. doi: 10.1021/ja00109a011
- Antoniuk, I., and Amiel, C. (2016). Cyclodextrin-mediated hierarchical self-assembly and its potential in drug delivery applications. *J. Pharm. Sci.* 105, 2570–2588. doi: 10.1016/j.xphs.2016.05.010
- Appel, E. A., del Barrio, J., Loh, X. J., and Scherman, O. A. (2012). Supramolecular polymeric hydrogels. *Chem. Soc. Rev.* 41, 6195–6214. doi: 10.1039/C2CS35264H
- Barrow, S. J., Kasera, S., Rowland, M. J., del Barrio, J., and Scherman, O. A. (2015). Cucurbituril-based molecular recognition. *Chem. Rev.* 115, 12320–12406. doi: 10.1021/acs.chemrev.5b00341
- Böhmer, V. (1995). Calixarenes, macrocycles with (almost) unlimited possibilities. *Angew. Chem. Int. Ed.* 34, 713–745. doi: 10.1002/anie.199507131
- Chen, Y., Sun, S., Lu, D., Shi, Y., and Yao, Y. (2019). Water-soluble supramolecular polymers constructed by macrocycle-based host-guest interactions. *Chin. Chem. Lett.* 30, 37–43. doi: 10.1016/j.cclet.2018.10.022
- Guo, D.-S., and Liu, Y. (2014). Supramolecular chemistry of p-Sulfonatocalix[n]arenes and its biological applications. *Acc. Chem. Res.* 47, 1925–1934. doi: 10.1021/ar500009g
- Harada, A., Takashima, Y., and Nakahata, M. (2014). Supramolecular polymeric materials via cyclodextrin-guest interactions. *Acc. Chem. Res.* 47, 2128–2140. doi: 10.1021/ar500109h
- Harada, A., Takashima, Y., and Yamaguchi, H. (2009). Cyclodextrin-based supramolecular polymers. *Chem. Soc. Rev.* 38, 875–882. doi: 10.1039/B705458K
- Kakuta, T., Yamagishi, T.-a., and Ogoshi, T. (2018). Stimuli-responsive supramolecular assemblies constructed from pillar[n]arenes. *Acc. Chem. Res.* 51, 1656–1666. doi: 10.1021/acs.accounts.8b00157
- Lagona, J., Mukhopadhyay, P., Chakrabarti, S., and Isaacs, L. (2005). The Cucurbit[n]uril family. *Angew. Chem. Int. Ed.* 44, 4844–4870. doi: 10.1002/anie.200460675
- Li, S., and Purdy, W. C. (1992). Cyclodextrins and their applications in analytical chemistry. *Chem. Rev.* 92, 1457–1470. doi: 10.1021/cr00014a009
- Murray, J., Kim, K., Ogoshi, T., Yao, W., and Gibb, B. C. (2017). The aqueous supramolecular chemistry of cucurbit[n]urils, pillar[n]arenes and deep-cavity cavitands. *Chem. Soc. Rev.* 46, 2479–2496. doi: 10.1039/c7cs00095b
- Ni, X.-L., Xiao, X., Cong, H., Zhu, Q.-J., Xue, S.-F., and Tao, Z. (2014). Self-assemblies based on the “outer-surface interactions” of Cucurbit[n]urils: new opportunities for supramolecular architectures and materials. *Acc. Chem. Res.* 47, 1386–1395. doi: 10.1021/ar5000133
- Ogoshi, T., Kakuta, T., and Yamagishi, T. A. (2018). Applications of pillar[n]arene-based supramolecular assemblies. *Angew. Chem. Int. Ed.* 58, 2197–2206. doi: 10.1002/anie.201805884

- Ogoshi, T., Kanai, S., Fujinami, S., Yamagishi, T.-A., and Nakamoto, Y. (2008). Para-bridged symmetrical pillar[5]arenes: their lewis acid catalyzed synthesis and host-guest property. *J. Am. Chem. Soc.* 130, 5022–5023. doi: 10.1021/ja711260m
- Ogoshi, T., Yamagishi, T.-A., and Nakamoto, Y. (2016). Pillar-shaped macrocyclic hosts pillar[n]arenes: new key players for supramolecular chemistry. *Chem. Rev.* 116, 7937–8002. doi: 10.1021/acs.chemrev.5b00765
- Pedersen, C. J. (1967). Cyclic polyethers and their complexes with metal salts. *J. Am. Chem. Soc.* 89, 7017–7036. doi: 10.1021/ja01002a035
- Shinkai, S., Mori, S., Tsubaki, T., Sone, T., and Manabe, O. (1984). New water-soluble host molecules derived from calix[6]arene. *Tetrahedron Lett.* 25, 5315–5318. doi: 10.1016/S0040-4039(01)81592-6
- Strutt, N. L., Zhang, H., Schneebeli, S. T., and Stoddart, J. F. (2014). Functionalizing pillar[n]arenes. *Acc. Chem. Res.* 47, 2631–2642. doi: 10.1021/ar500177d
- Szejtli, J. (1998). Introduction and general overview of cyclodextrin chemistry. *Chem. Rev.* 98, 1743–1754. doi: 10.1021/cr970022c
- Wang, Y., Wang, C., Long, R., Cao, Y., Fan, D., Cen, M., et al. (2019). Synthesis and controllable self-assembly of 3D amphiphilic organoplatinum(II) metallacages in water. *Chem. Commun.* 55, 5167–5170. doi: 10.1039/c9cc02173f
- Xiao, T., Qi, L., Zhong, W., Lin, C., Wang, R., and Wang, L. (2019c). Stimuli-responsive nanocarriers constructed from pillar[n]arene-based supramolecules. *Mater. Chem. Front.* 3, 1973–1993. doi: 10.1039/c9qm00428a
- Xiao, T., Wang, J., Shen, Y., Bao, C., Li, Z.-Y., Sun, X.-Q., et al. (2021). Preparation of a fixed-tetraphenylethylene motif bridged ditopic benzo-21-crown-7 and its application for constructing AIE supramolecular polymers. *Chin. Chem. Lett.* doi: 10.1016/j.ccl.2020.10.037. [Epub ahead of print].
- Xiao, T., Xu, L., Zhong, W., Zhou, L., Sun, X.-Q., Hu, X.-Y., et al. (2018). Advanced functional materials constructed from pillar[n]arenes. *Isr. J. Chem.* 58, 1183–1193. doi: 10.1002/ijch.201800026
- Xiao, T., Xu, L., Zhou, L., Sun, X.-Q., Lin, C., and Wang, L. (2019d). Dynamic hydrogels mediated by macrocyclic host-guest interactions. *J. Mater. Chem. B* 7, 1526–1540. doi: 10.1039/C8TB02339E
- Xiao, T., Zhong, W., Xu, L., Sun, X.-Q., Hu, X.-Y., and Wang, L. (2019b). Supramolecular vesicles based on pillar[n]arenes: design, construction, and applications. *Org. Biomol. Chem.* 17, 1336–1350. doi: 10.1039/C8OB03095B
- Xiao, T., Zhong, W., Zhou, L., Xu, L., Sun, X.-Q., Elmes, R. B. P., et al. (2019e). Artificial light-harvesting systems fabricated by supramolecular host-guest interactions. *Chin. Chem. Lett.* 30, 31–36. doi: 10.1016/j.ccl.2018.05.034
- Xiao, T., Zhou, L., Sun, X.-Q., Huang, F., Lin, C., and Wang, L. (2020b). Supramolecular polymers fabricated by orthogonal self-assembly based on multiple hydrogen bonding and macrocyclic host-guest interactions. *Chin. Chem. Lett.* 31, 1–9. doi: 10.1016/j.ccl.2019.05.011
- Xiao, T., Zhou, L., Wei, X., Li, Z., and Sun, X. (2020a). Supramolecular copolymers driven by quadruple hydrogen bonding and host-guest interactions. *Chin. J. Org. Chem.* 40, 944–949. doi: 10.6023/cjoc201911014
- Xiao, T., Zhou, L., Xu, L., Zhong, W., Zhao, W., Sun, X.-Q., et al. (2019a). Dynamic materials fabricated from water soluble pillar[n]arenes bearing triethylene oxide groups. *Chin. Chem. Lett.* 30, 271–276. doi: 10.1016/j.ccl.2018.05.039
- Xue, M., Yang, Y., Chi, X., Zhang, Z., and Huang, F. (2012). Pillararenes, a new class of macrocycles for supramolecular chemistry. *Acc. Chem. Res.* 45, 1294–1308. doi: 10.1021/ar2003418
- Zhang, C., Li, S., Zhang, J., Zhu, K., Li, N., and Huang, F. (2007). Benzo-21-crown-7/secondary dialkylammonium salt [2]pseudorotaxane- and [2]rotaxane-type threaded structures. *Org. Lett.* 9, 5553–5556. doi: 10.1021/ol702510c

**Conflict of Interest:** The authors declare that the research was conducted in the absence of any commercial or financial relationships that could be construed as a potential conflict of interest.

The handling editor declared a past co-authorship with one of the authors RE.

Copyright © 2020 Xiao, Elmes and Yao. This is an open-access article distributed under the terms of the Creative Commons Attribution License (CC BY). The use, distribution or reproduction in other forums is permitted, provided the original author(s) and the copyright owner(s) are credited and that the original publication in this journal is cited, in accordance with accepted academic practice. No use, distribution or reproduction is permitted which does not comply with these terms.



# Structural Design, Synthesis, and Preliminary Biological Evaluation of Novel Dihomooxacalix[4]arene-Based Anti-tumor Agents

Lin An<sup>1,2\*</sup>, Chan Wang<sup>1,2</sup>, Lili Han<sup>3</sup>, Jiadong Liu<sup>1,2</sup>, Tonghui Huang<sup>1,2</sup>, Youguang Zheng<sup>1,2</sup>, Chaoguo Yan<sup>4\*</sup> and Jing Sun<sup>4</sup>

<sup>1</sup> College of Pharmacy, Xuzhou Medical University, Xuzhou, China, <sup>2</sup> Jiangsu Key Laboratory of New Drug Research and Clinical Pharmacy, Xuzhou Medical University, Xuzhou, China, <sup>3</sup> Children's Hospital Affiliated to Zhengzhou University, Zhengzhou, China, <sup>4</sup> College of Chemistry and Chemical Engineering, Yangzhou University, Yangzhou, China

## OPEN ACCESS

### Edited by:

Yong Yao,  
Nantong University, China

### Reviewed by:

Xiao-Yu Hu,  
Nanjing University of Aeronautics and  
Astronautics, China

Xin-Long Ni,  
Guizhou University, China

Pi Wang,  
Taiyuan University of  
Technology, China

### \*Correspondence:

Lin An  
anlinhx@sina.com.cn  
Chaoguo Yan  
cgyan@yzu.edu.cn

### Specialty section:

This article was submitted to  
Supramolecular Chemistry,  
a section of the journal  
Frontiers in Chemistry

**Received:** 26 October 2019

**Accepted:** 25 November 2019

**Published:** 13 December 2019

### Citation:

An L, Wang C, Han L, Liu J, Huang T,  
Zheng Y, Yan C and Sun J (2019)  
Structural Design, Synthesis, and  
Preliminary Biological Evaluation of  
Novel Dihomooxacalix[4]arene-Based  
Anti-tumor Agents.  
Front. Chem. 7:856.  
doi: 10.3389/fchem.2019.00856

Calixarene and its derivatives have extensively served as promising anti-tumor agents. Previously, we have synthesized a series of calix[n]arene polyhydroxyamine derivatives ( $n = 4, 6, 8$ ) and found that 5,11,17,23-*tetra-tert*-butyl-25,27-bis [N-(2-hydroxyethyl)aminocarbonylmethoxyl] calix[4]arene (**CLX-4**) displayed significant effect toward SKOV3, A549, SW1990, HeLa, Raji, and MDA-MB-231 cancer cells. In the present work, we find a replacement of calix[4]arene bone and synthesized 19 novel structurally related dihomooxacalix[4]arene amide derivatives **4A–4S** to optimize its efficacy. Their abilities to induce cytotoxicity in human lung carcinoma (A549) cells, breast cancer (MCF-7) cells, cervical cancer (HeLa) cells, hepatocellular carcinoma (HepG2) cells, as well as human umbilical vein endothelial (HUVEC) cells are evaluated *in vitro*. Encouraging results show that the majority of dihomooxacalix[4]arene amide derivatives are effective at inhibiting A549 cell proliferation with the corresponding IC<sub>50</sub> ranging from 0.6 to 20.1  $\mu$ M. In particular, compounds **4A**, **4D**, and **4L** explore markedly increased potency (IC<sub>50</sub> value is  $2.0 \pm 0.5 \mu$ M,  $0.7 \pm 0.1 \mu$ M, and  $1.7 \pm 0.4 \mu$ M) over the cytotoxicity profiles of control **CLX-4**, whose IC<sub>50</sub> value is  $2.8 \pm 0.3 \mu$ M. More interestingly, **4A** also demonstrates the perfect cytotoxic effect against MCF-7, HeLa, and HepG2 cells with IC<sub>50</sub> values of  $1.0 \pm 0.1 \mu$ M,  $0.8 \pm 0.2 \mu$ M, and  $2.7 \pm 0.4 \mu$ M. In addition, the results proved that our synthesized **4A** has much lower toxicity (41%) to normal cells at a concentration of 10  $\mu$ M than that of **4D** (90%). To reveal the mechanisms, the key indicators including the cell cycle and apoptosis are observed by the flow cytometry analysis in MCF-7 cells. The results demonstrate that both **4A** and **4D** can induce the MCF-7 cell cycle arrest in G0/G1 phase and cell apoptosis. Therefore, our finding proves that the dihomooxacalix[4]arene amide derivatives are convenient platforms for potential supramolecular anticancer agents.

**Keywords:** supramolecular chemotherapy, calixarene, structural optimization, dihomooxacalix[4]arene, X-ray diffraction, biological evaluation



## INTRODUCTION

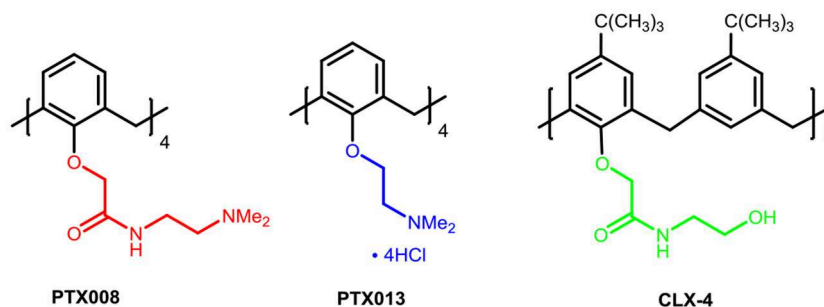
Supramolecules generally come from the aggregation of two or more molecules based on non-covalent bond forces (Lehn, 1988; Guo et al., 2018). They usually have hydrophobic cavities in which the guests can be embedded, such as crown ethers (Flink and Reinhoudt, 1999; Kralj et al., 2008; Yokoyama and Mizuguchi, 2019), cyclodextrins (Valle, 2004; Stella and He, 2008; Zhang Y. M. et al., 2019), calixarenes (Sun et al., 2009a,b; Böhmer, 2010), cucurbiturils (Lee et al., 2003; Kim et al., 2007; Bauer et al., 2019) and pillararenes (Hu et al., 2012; Sun et al., 2018, 2019; Chen et al., 2019; Zhang R. et al., 2019).

Among those supramolecules, calixarenes are cyclic oligomers composed of phenolic units linked by methylene in the ortho positions, which are considered to be the important class representing the third generation of host–guest supramolecular chemistry. A majority of studies on calixarenes have focused on the fields of molecular recognition due to their flexible nature of the basic moiety preferable for binding and transporting ions and neutral molecules (Ludwig and Dzung, 2002; Mutihac et al., 2011; Gómez-Machuca et al., 2014; Zadmand and Alavijeh, 2014; Patra et al., 2019). In addition, calixarenes have many other structural characteristics including the easy modification of their basic core and rim via covalent attachment to various chemical scaffolds, the limited toxicity and immune responses (Geraci et al., 2008). The above advantages make these cyclic oligomers ideal for the design of new drugs and building blocks for drug carriers in biomedical fields (Da Silva et al., 2004; Hussain et al., 2017). In this regard, calixarenes and their derivatives are currently being studied and used in a variety of medicinal applications beyond their traditional place in chemistry. They could be served as chemotherapy agent (Yousaf et al., 2015; Naseer et al., 2017; Zhou et al., 2017), including antibacterials (Soares et al., 2014; Muneer et al., 2017; Ali et al., 2018; Consoli et al., 2018), antivirals (Motornaya et al., 2006; Mourer et al., 2010), antimalarials (Shah et al., 2016), and anti-inflammatory (Granata et al., 2017) enzymatic inhibitors (Läppchen et al., 2015). Moreover, they especially can be used as anti-tumor drugs (Consoli et al., 2004; Hulíková et al., 2010; Neagu et al., 2010; Nasuhi Pur and Dilmaghani, 2014); which have gained considerable attention from us. Among these works, ureido-glycolix[8]arene carrying N-acetyl-D-glucosamine residue groups has been reported,

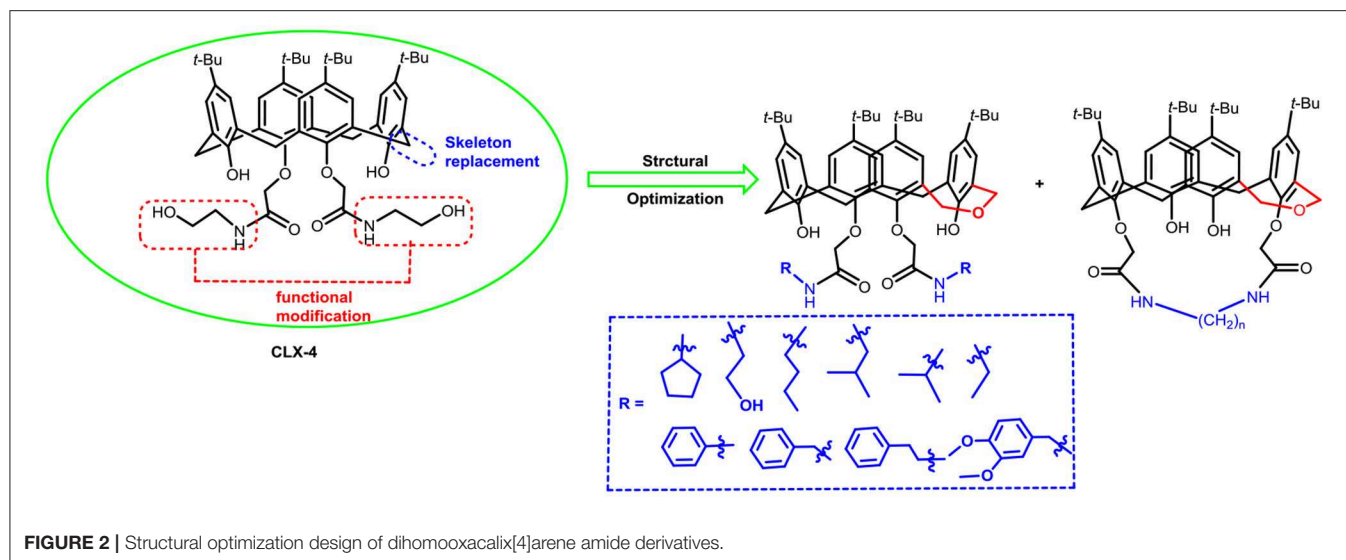
which inhibited C6 glioma cell migration and proliferation with independence of the N-acetyl-D-glucosamine residues (Sansone et al., 2008; Viola et al., 2010a,b). Dings et al. worked continuously on modifications and mechanism of calix[4]arene-based anti-tumor agents, identified galectin-1 (gal-1) as the molecular target, and explored compounds PTX008, PTX013 as potent anti-tumor agents (**Figure 1**) (Dings et al., 2012a,b, 2013; Koonce et al., 2017). Excitingly, PTX008 has been in a human Phase I clinical trial. The latest study further illustrated that PTX008 was an allosteric inhibitor that inhibits Galectin-1 due to BP-ALL survival (Paz et al., 2018).

In our previous work, we synthesized calix[4]arene polyhydroxyamine derivative **CLX-4** (**Figure 1**), which has been tested as a candidate anti-tumor drug with IC<sub>50</sub> value against A549, SKOV3, SW1990, Hela, Raji, and MDA-MB-231 cell lines ranging from 2.8 to 5.3  $\mu$ M (An et al., 2016). **CLX-4** obviously exhibited equal cytotoxic effects to those of PTX008. This inspired us to have some structural optimizations, as shown in **Figure 2**.

In our design (**Figure 2**), one possible strategy is to find alternatives to replace the material structure of **CLX-4**. Taking into account the high structural similarity, dihomooxalix[4]arene is the closest structurally calix[4]arene analog with only one CH<sub>2</sub>OCH<sub>2</sub> unit taking the place of CH<sub>2</sub> bridge, which results in improved conformational flexibility and the superior geometric shapes. Dihomooxalix[4]arene was initially reported by Gutsche et al. (1981). However, over the past several years, dihomooxalix[4]arene macrocycles and their functional derivatives were used for ion-binding application (Marcos et al., 2006, 2014; Gaeta et al., 2012; Talotta et al., 2016; Liu et al., 2017, 2018; An et al., 2018). It would seem surprising that as yet few works are so far known about the bioactivity-based approach (Harris, 1995). Therefore, dihomooxalix[4]arenes are a particularly promising alternative to replace the calix[4]arene as the new drug bone. The other way is to chemically modify the important functional OH-CH<sub>2</sub>-CH<sub>2</sub>-NH-C=O group at the lower rim of **CLX-4**, which can be expected to introduce special groups with different polarity, hydrophilicity, and compatibility, leading to screening out the optimization. Appropriate R groups can be introduced to replace the 2-hydroxyethyl group linked on the aminocarbonyl dihomooxalix[4]arene, which probably affects the anti-tumor



**FIGURE 1** | The chemical structures of calix[4]arene-based anti-tumor agents.



activity by means of rigidity, electron density, flexibility, polarity and stability. To compare the influence of activity and explore the structure–activity relationship, R position attached to the acylamino unit is varied from methyl, ethyl, propyl, isopropyl, butyl, pentyl, to cyclopentyl groups. In addition, we also intend to build the spacer chains involved in the link of amino moieties on the dihomooxalix[4]arene scaffold. As to verify our hypothesis and extend our previous work, herein we report on the synthesis, X-ray structures of a series of novel structural dihomooxalix[4]arene amide derivatives, as well as the cell-based studies related to structure–activity relationship.

## MATERIALS AND METHODS

### Synthesis and Characterization

#### Synthesis of Dihomooxalix[4]arene Amide Derivatives 4A–4S

*p*-*tert*-butyl dihomooxalix[4]arenes **1** was synthesized according to Gutsche's method (Gutsche et al., 1981). All other reagents and solvents were commercially available reagents with analytical grade and used without further purification. The products were purified by recrystallization or using preparative separations in flash column chromatography. Reactions were monitored by thin-layer chromatography (TLC) on 2.5 mm Merck silica gel F254 strips. Melting points were determined with capillaries on an YRT-3 microscope apparatus and were uncorrected. All  $^1\text{H}$  NMR and  $^{13}\text{C}$  NMR spectra were recorded at 400 MHz on a Bruker AVANCE II 400 spectrometer. IR spectra were obtained on a Nicolet FT-IR 8400 spectrometer (KBr disc). High Resolution Mass Spectrometry were carried out on (UHR-TOF) maXis 4G mass spectrometer.

#### General Procedure for the Synthesis of Dihomooxalix[4]arene Ester **2A**

Under ultrasound irradiation, a mixture of *p*-*tert*-butyl dihomooxalix[4]arene **1** (6.78 g, 10 mmol), bromoethylacetate

(6.68 ml, 60 mmol), and acetone (100 ml) was stirred at 55°C. The reaction was monitored by TLC until the start material **1** disappeared. The mixture was poured into a large amount of water and extracted with chloroform. The organic layers were collected, dried over anhydrous sodium sulfate, concentrated *in vacuo*, and further purified by silica gel column chromatography (1:4 ethyl acetate-petroleum ether) to provide the product **2A** as the white solid, which was used in the next step.

#### General Procedure for the Synthesis of Dihomooxalix[4]arene Amide **3A**

Ester **2A** (0.230 g, 0.3 mmol) was dissolved in dichloromethane (2 ml), and ethanolamine (0.037 g, 0.6 mmol) was added to the solution. Then, the resulting mixture was stirred at room temperature for 24 h. It was concentrated *in vacuo*, washing with 95% ethanol twice to give the solid precipitate, followed by filtration, purified by silica gel column chromatography (15:1 v/v, dichloromethane/methanol) to afford the desired **3A** in quantitative yield.

#### General Procedure for the Synthesis of Dihomooxalix[4]arene Amides **4A–4B**

A solution of ester **2A** (0.425 g, 0.5 mmol) and hydroxylamine (0.244 g, 4 mol) or dihydroxylamine (0.421 g, 4 mol) in refluxing ethanol/toluene (50 ml, v/v = 1:1) for 72 h. After the completion of the reaction (TLC), the solution was concentrated *in vacuo*, leaving the pale oil residue, which was washed with 95% ethanol to give the solid precipitate, followed by filtration, purified by silica gel column chromatography to yield **4A** or **4B** as a white solid.

#### General Procedure for the Synthesis of Dihomooxalix[4]arene Amides **4C–4D**

A solution of 1,4-diaminobutane or 1,6-diaminohexane (2 ml) in methanol (2 ml) kept at 0°C was added dropwise solution of ester **2A** (0.425 g, 0.5 mmol) in methanol (1 ml) for 30 min. The ice

bath was removed and the reaction mixture was warmed to room temperature and stirred for 24 h. The solution was concentrated *in vacuo*, and the residue was treated with cool water to afford the pale yellow solid precipitate, further purified by silica gel flash column chromatography to yield 4C–4D.

## General Procedure for the Synthesis of Bridged Dihomooxalix[4]arene Amides 4E–4G

A mixture of ester 2A (0.425 g, 0.5 mmol) and 2 ml of ethylenediamine (or 1,4-diaminobutane, 1,6-diaminohexane) was dissolved in ethanol (5 ml) and refluxed for 24 h. When the reaction was complete, the solution was concentrated *in vacuo*, followed by dropwise distilled water was added. The crude product was extracted and filtered to give the pale yellow solid precipitate, further purified by silica gel flash column chromatography to yield compound 4E–4G.

## General Procedure for the Synthesis of Dihomooxalix[4]arene Amides 4H–4P

A solution of ethylamine hydrochloride (2 ml) in ethanol (2 ml), kept at 0°C, was added dropwise to a solution of ester 2A (0.425 g, 0.5 mmol) in ethanol (1 ml) for 30 min. Then, the mixture was stirred at room temperature overnight. After the completion of the reaction, the solvent was removed *in vacuo*, and then the residue was treated with cool water to give the solid precipitate, further purified by silica gel flash column chromatography to yield compound 4H. Compound 4I–4P was prepared by a similar procedure.

## General Procedure for the Synthesis of 4Q–4S

A solution of 3A with cyclopentylamine (2 ml) was stirred for 4 h at room temperature. Then, the solution was concentrated *in vacuo* to give the crude product, followed by the purification with silica gel flash chromatography to give the compound 4Q, as white powder.

Compound 4R–4S was prepared by a similar procedure.

**7,13,19,25-tetra-*tert*-butyl-28,30-di-hydroxy-27,29-di-(ethoxycarbonylmethoxyl)-2,3-dihomo-3-oxalix[4]arene (2A):** White solid, m.p. 168.7–171.4°C, yield: 95.6% (**Figure S1**); <sup>1</sup>H NMR (400 MHz, CDCl<sub>3</sub>) δ (ppm): 1.11, 1.19, 1.23, 1.26 (4s, 36H), 1.30 (t, 3H, *J* = 7.2 Hz), 1.38 (t, 3H, *J* = 7.2 Hz), 3.28 (d, 1H, *J* = 12.8 Hz), 3.37 (d, 1H, *J* = 13.6 Hz), 3.46 (d, 1H, *J* = 13.2 Hz), 4.21 (d, 1H, *J* = 9.2 Hz), 4.24 (dd, 1H, *J*<sub>1</sub> = 7.2 Hz, *J*<sub>2</sub> = 1.2 Hz), 4.28 (dd, 1H, *J*<sub>1</sub> = 7.2 Hz, *J*<sub>2</sub> = 1.2 Hz), 4.31 (d, 1H, *J* = 13.2 Hz), 4.34–4.41 (m, 3H), 4.46 (d, 1H, *J* = 12.8 Hz), 4.52 (d, 1H, *J* = 15.6 Hz), 4.67 (d, 1H, *J* = 10.4 Hz), 4.71 (d, 1H, *J* = 13.6 Hz), 4.81 (d, 1H, *J* = 15.6 Hz), 4.98 (d, 1H, *J* = 10.0 Hz), 5.35 (d, 1H, *J* = 9.2 Hz), 5.53 (d, 1H, *J* = 16.0 Hz), 6.89 (d, 1H, *J* = 2.4 Hz), 6.96 (d, 1H, *J* = 2.4 Hz), 6.99 (d, 1H, *J* = 2.4 Hz), 7.03 (q, 2H, *J* = 2.4 Hz), 7.07 (d, 1H, *J* = 2.8 Hz), 7.30 (s, 1H), 7.40 (d, 1H, *J* = 2.4 Hz), 7.77 (s, 1H); <sup>13</sup>C NMR (100 MHz, CDCl<sub>3</sub>) δ (ppm): 14.3, 31.1, 31.4, 31.5, 31.6, 33.8, 34.1, 60.9, 61.4, 71.6, 72.1, 72.3, 122.6, 124.1, 125.0, 125.3, 125.4, 125.8, 126.0, 126.9, 127.6, 127.7, 128.2, 129.5, 129.8, 132.3, 132.7, 133.7, 141.1, 142.0, 146.5,

147.5, 149.4, 150.1, 152.9, 155.0, 168.8, 170.5; IR (KBr, cm<sup>−1</sup>) ν 3313, 2959, 2868, 1665, 1483, 1364, 1298, 876.

**7,13,19,25-tetra-*tert*-butyl-28,30-di-hydroxy-27-(ethoxycarbonylmethoxyl)-29-(N-(2-hydroxyethyl) amino carbonyl methoxyl)-2,3-dihomo-3-oxalix[4]arene (3A):** White solid, yield: 85.1%, m.p. 188.6–191.8°C (**Figure S2**); <sup>1</sup>H NMR (400 MHz, CDCl<sub>3</sub>) δ (ppm): 1.14, 1.22, 1.26 (3s, 36H), 1.33 (t, 3H, *J* = 7.2 Hz), 3.36 (d, 1H, *J* = 13.6 Hz), 3.42 (d, 1H, *J* = 13.2 Hz), 3.49 (d, 1H, *J* = 13.2 Hz), 3.67–3.87 (m, 4H), 4.14 (d, 1H, *J* = 13.2 Hz), 4.20 (d, 1H, *J* = 9.2 Hz), 4.24–4.35 (m, 4H), 4.39 (d, 1H, *J* = 15.6 Hz), 4.47 (d, 2H, *J* = 13.6 Hz), 4.64 (d, 1H, *J* = 16.0 Hz), 4.76 (d, 1H, *J* = 15.2 Hz), 4.94 (d, 1H, *J* = 9.6 Hz), 5.08–5.13 (m, 2H), 6.91 (d, 1H, *J* = 2.4 Hz), 6.98 (d, 1H, *J* = 2.4 Hz), 7.00 (d, 1H, *J* = 2.4 Hz), 7.10–7.12 (q, 3H, *J* = 2.4 Hz), 7.23 (d, 1H, *J* = 2.0 Hz), 7.43 (d, 1H, *J* = 2.4 Hz), 7.77 (s, 1H), 8.85 (t, 1H, *J* = 5.2 Hz); <sup>13</sup>C NMR (100 MHz, CDCl<sub>3</sub>) δ (ppm): 14.2, 30.8, 30.9, 31.0, 31.1, 31.3, 31.5, 31.6, 31.7, 32.1, 33.8, 33.9, 34.2, 42.8, 61.4, 62.8, 71.3, 71.9, 72.3, 74.1, 122.8, 124.5, 125.3, 125.4, 125.8, 126.2, 126.4, 127.1, 128.0, 128.1, 129.1, 129.6, 131.7, 132.7, 133.9, 142.4, 143.0, 147.5, 147.8, 148.9, 149.7, 152.0, 154.4, 170.1, 170.3; IR (KBr, cm<sup>−1</sup>) ν 3433, 2961, 2868, 1757, 1670, 1485, 1209, 1065, 874; MS (m/z): HRMS (ESI) Calcd for C<sub>53</sub>H<sub>71</sub>NNaO<sub>9</sub> ([M+Na]<sup>+</sup>): 888.5021, found: 888.5029.

**7,13,19,25-tetra-*tert*-butyl-28,30-di-hydroxy-27,29-di-(N-(2-hydroxyethyl)-aminocarbonylmethoxyl)-2,3-dihomo-3-oxalix[4]arene (4A):** White solid, m.p. 139.7–142.3°C, yield: 87.2% (**Figure S3**); <sup>1</sup>H NMR (400 MHz, CDCl<sub>3</sub>) δ (ppm) 1.03, 1.20, 1.26, 1.29 (4s, 36H), 3.44–3.53 (m, 5H), 3.59–3.64 (m, 2H), 3.79 (s, 4H), 4.17–4.29 (m, 4H), 4.38 (d, 1H, *J* = 10.0 Hz), 4.54 (dd, 1H, *J*<sub>1</sub> = 15.2 Hz, *J*<sub>2</sub> = 5.2 Hz), 4.60–4.68 (m, 4H), 4.84 (d, 1H, *J* = 10.0 Hz), 6.85 (d, 1H, *J* = 1.6 Hz), 6.92 (d, 1H, *J* = 2.4 Hz), 7.02 (d, 2H, *J* = 2.0 Hz), 7.16 (d, 1H, *J* = 2.0 Hz), 7.22 (d, 1H, *J* = 2.0 Hz), 7.24 (d, 1H, *J* = 2.0 Hz), 7.31 (s, 1H), 7.38 (d, 2H, *J* = 2.4 Hz), 8.78 (t, 1H, *J* = 5.2 Hz), 8.84 (t, 1H, *J* = 5.2 Hz); <sup>13</sup>C NMR (100 MHz, CDCl<sub>3</sub>) δ (ppm): 31.0, 31.2, 31.4, 31.5, 31.9, 34.0, 34.1, 34.2, 42.5, 62.0, 62.2, 70.8, 72.1, 73.9, 74.4, 76.7, 77.0, 77.2, 77.3, 122.7, 124.7, 125.9, 126.0, 126.3, 127.1, 127.4, 127.7, 127.8, 128.0, 128.8, 129.3, 131.9, 132.1, 133.6, 143.1, 143.8, 148.1, 148.4, 148.8, 149.9, 151.2, 152.6, 169.4, 169.7; IR (KBr, cm<sup>−1</sup>) ν 3389, 3366, 2959, 2870, 1666, 1545, 1485, 1447, 1362, 874; MS (m/z): HRMS (ESI) Calcd for C<sub>53</sub>H<sub>72</sub>N<sub>2</sub>NaO<sub>9</sub> ([M+Na]<sup>+</sup>): 903.5130, found: 903.5145.

**7,13,19,25-tetra-*tert*-butyl-28,30-di-hydroxy-27,29-di-(N,N-bis(2-hydroxyethyl)-aminocarbonylmethoxyl)-2,3-dihomo-3-oxalix[4]arene (4B):** White solid, m.p. 210.7–212.5°C, yield: 86.7% (**Figure S4**); <sup>1</sup>H NMR (400 MHz, DMSO-*d*<sub>6</sub>) δ (ppm): 1.11, 1.18, 1.20, 1.24 (4s, 36H), 3.42–3.49 (m, 6H), 3.54–3.62 (m, 10H), 3.67 (s, 2H), 3.87–3.91 (m, 1H), 4.19 (d, 1H, *J* = 9.2 Hz), 4.26 (d, 1H, *J* = 10.0 Hz), 4.36 (dd, 2H, *J*<sub>1</sub> = 12.8 Hz, *J*<sub>2</sub> = 6.0 Hz), 4.56 (d, 1H, *J* = 12.8 Hz), 4.66 (d, 2H, *J* = 13.2 Hz), 4.74 (d, 2H, *J* = 9.2 Hz), 4.78 (s, 1H), 4.90 (s, 1H), 4.97 (s, 1H), 5.03 (s, 1H), 5.06 (d, 1H, *J* = 4.8 Hz), 5.32 (d, 1H, *J* = 13.2 Hz), 6.89 (d, 1H, *J* = 2.4 Hz), 7.00 (d, 1H, *J* = 2.0 Hz), 7.02 (d, 1H, *J* = 2.0 Hz), 7.13 (s, 1H), 7.16 (s, 1H), 7.22 (d, 1H, *J* = 2.0 Hz), 7.36 (d, 1H, *J* = 2.0 Hz), 7.48 (d, 1H, *J* = 2.0 Hz), 7.71 (s, 1H), 8.61 (s, 1H); <sup>13</sup>C NMR (100 MHz, DMSO-*d*<sub>6</sub>) δ (ppm): 31.4, 31.6, 31.8, 31.9, 34.0, 34.3, 59.1, 122.8, 125.5, 125.7, 126.6,



126.7, 127.2, 127.9, 129.8, 132.9, 133.4, 134.5, 140.8, 141.0, 146.0, 146.7, 150.0, 152.1, 152.4, 155.3, 169.3, 169.6; IR (KBr,  $\text{cm}^{-1}$ )  $\nu$  3389, 3045, 2957, 2870, 1643, 1485, 1443, 1364, 876; MS ( $m/z$ ): HRMS (ESI) Calcd for  $\text{C}_{57}\text{H}_{80}\text{N}_2\text{NaO}_{11}$  ( $[\text{M}+\text{Na}]^+$ ): 991.5654, found: 991.5674.

**7,13,19,25-tetra-*tert*-butyl-28,30-di-hydroxy-27,29-di-(N-(4-aminobutyl)-aminocarbonylmethoxyl)-2,3-dihomo-3-oxacalix[4] arene (4C):** White solid, m.p. 129.4–131.2°C, yield: 96.2% (Figure S5);  $^1\text{H}$  NMR (400 MHz,  $\text{CDCl}_3$ )  $\delta$  (ppm): 1.16, 1.24, 1.25, 1.27 (4s, 36H), 1.32 (d, 2H,  $J = 11.2$  Hz), 1.40–1.43 (m, 2H), 1.45–1.53 (m, 3H), 1.57–1.73 (m, 4H), 2.57 (t, 2H,  $J = 7.2$  Hz), 2.68 (t, 2H,  $J = 6.8$  Hz), 3.18–3.26 (m, 2H), 3.43 (t, 2H,  $J = 12.0$  Hz), 3.52–3.66 (m, 3H), 4.10 (d, 1H,  $J = 13.6$  Hz), 4.16–4.22 (m, 2H), 4.35 (s, 1H), 4.38–4.40 (m, 2H), 4.44 (d, 1H,  $J = 9.2$  Hz), 4.50 (d, 1H,  $J = 11.2$  Hz), 4.58 (d, 1H,  $J = 10.0$  Hz), 4.80 (dd, 2H,  $J_1 = 19.2$  Hz,  $J_2 = 15.2$  Hz), 4.96 (d, 1H,  $J = 10.4$  Hz), 6.87 (d, 1H,  $J = 2.4$  Hz), 7.01 (d, 1H,  $J = 2.4$  Hz), 7.04 (d, 1H,  $J = 2.0$  Hz), 7.14 (d, 1H,  $J = 2.4$  Hz), 7.16 (d, 1H,  $J = 2.4$  Hz), 7.23 (t, 2H,  $J = 2.4$  Hz), 7.46 (d, 1H,  $J = 2.4$  Hz), 8.24 (s, 1H), 8.74 (t, 1H,  $J = 4.2$  Hz), 9.00 (t, 1H,  $J = 4.2$  Hz);  $^{13}\text{C}$  NMR (100 MHz,  $\text{CDCl}_3$ )  $\delta$  (ppm): 26.4, 26.9, 31.0, 31.1, 31.3, 31.5, 32.4, 33.9, 34.0, 34.3, 39.2, 39.5, 41.9, 42.0, 71.2, 71.9, 73.8, 74.5, 122.2, 124.4, 125.7, 126.0, 126.9, 127.0, 127.2, 127.3, 127.4, 127.6, 128.6, 129.6, 131.5, 132.4, 133.8, 143.0, 143.7, 148.0, 148.6, 148.9, 149.5, 151.4, 153.2, 168.0, 168.5; IR (KBr,  $\text{cm}^{-1}$ )  $\nu$  3369, 3194, 2959, 2866, 1674, 1483, 1296, 874; MS ( $m/z$ ): HRMS (ESI) Calcd for  $\text{C}_{57}\text{H}_{83}\text{N}_4\text{O}_7$  ( $[\text{M}+\text{H}]^+$ ): 935.6256, found: 935.6284.

**7,13,19,25-tetra-*tert*-butyl-28,30-di-hydroxy-27,29-di-(N-(6-aminohexyl)-aminocarbonylmethoxyl)-2,3-dihomo-3-oxacalix[4] arene (4D):** White solid, m.p. 123.3–125.9°C, yield: 63.3% (Figure S6);  $^1\text{H}$  NMR (400 MHz,  $\text{CDCl}_3$ )  $\delta$  (ppm): 1.18 (s, 9H), 1.27 (brs, 18H), 1.29 (s, 9H), 1.33 (d, 10H,  $J = 12.0$  Hz), 1.57–1.69 (m, 5H), 1.99 (d, 2H,  $J = 3.6$  Hz), 2.52–2.55 (m, 2H), 2.60–2.63 (m, 2H), 2.70 (t, 1H,  $J = 7.2$  Hz), 3.17–3.28 (m, 3H), 3.42–3.68 (m, 6H), 4.11 (d, 1H,  $J = 13.6$  Hz), 4.16–4.23 (m, 2H), 4.37 (s, 1H), 4.40–4.44 (m, 2H), 4.49 (d, 1H,  $J = 14.8$  Hz), 4.62 (d, 1H,  $J = 9.6$  Hz), 4.80 (t, 2H,  $J = 15.2$  Hz), 4.96 (d, 1H,  $J = 10.4$  Hz), 6.89 (d, 1H,  $J = 2.0$  Hz), 7.04 (d, 1H,  $J = 2.0$  Hz), 7.05 (d, 1H,  $J = 2.4$  Hz), 7.16 (d, 1H,  $J = 2.0$  Hz), 7.18 (d, 1H,  $J = 2.0$  Hz), 7.22–7.24 (m, 2H), 7.48 (d, 1H,  $J = 2.4$  Hz), 8.24 (s, 1H), 8.70 (t, 1H,  $J = 5.6$  Hz), 8.96 (t, 1H,  $J = 6.0$  Hz);  $^{13}\text{C}$  NMR (100 MHz,  $\text{CDCl}_3$ )  $\delta$  (ppm): 26.5, 26.9, 27.0, 29.5, 31.1, 31.3, 31.5, 33.6, 33.9, 34.3, 42.0, 42.1, 122.3, 124.4, 127.2, 127.4, 128.6, 131.5, 132.3, 133.7, 142.9, 148.6, 148.9, 151.5, 153.2, 167.9, 168.4; IR (KBr,  $\text{cm}^{-1}$ )  $\nu$  3350, 3215, 2957, 2862, 1674, 1483, 1298, 818; MS ( $m/z$ ): HRMS (ESI) Calcd for  $\text{C}_{61}\text{H}_{91}\text{N}_4\text{O}_7$  ( $[\text{M}+\text{H}]^+$ ): 991.6882, found: 991.6883.

**7,13,19,25-tetra-*tert*-butyl-28,30-di-hydroxy-27,29-N,N-(ethane-1,2-diyl)-aminocarbonylmethoxyl)-2,3-dihomo-3-oxacalix[4] arene (4E):** White solid, m.p. 204.8–206.3°C, yield: 86.6% (Figure S7);  $^1\text{H}$  NMR (400 MHz,  $\text{CDCl}_3$ )  $\delta$  (ppm): 1.16, 1.24, 1.25, 1.26 (4s, 36H), 3.10–3.23 (m, 2H), 3.40 (dd, 2H,  $J_1 = 13.2$  Hz,  $J_2 = 2.8$  Hz), 3.58 (d, 1H,  $J = 13.6$  Hz), 4.01 (d, 1H,  $J = 13.6$  Hz), 4.14–4.22 (m, 3H), 4.24 (d, 1H,  $J = 9.6$  Hz), 4.28 (d, 1H,  $J = 14.0$  Hz), 4.38–4.46 (m, 3H), 4.67 (d, 1H,  $J = 14.4$  Hz), 4.74–4.80 (m, 2H), 4.89 (d, 1H,  $J = 9.6$  Hz), 6.89 (d, 1H,  $J = 2.4$  Hz), 7.02 (dd, 2H,  $J_1 = 4.0$  Hz,  $J_2 = 2.4$  Hz), 7.08 (d, 1H,  $J = 2.4$  Hz), 7.13 (d, 2H,  $J = 3.2$  Hz), 7.25 (s, 1H), 7.28 (d, 1H,  $J = 2.4$  Hz), 7.53, 8.11 (2s, 2H), 8.30–8.33 (m, 1H), 8.60–8.63 (m, 1H);  $^{13}\text{C}$  NMR (100 MHz,  $\text{CDCl}_3$ )  $\delta$  (ppm): 29.5, 30.5, 31.2, 31.3, 31.5, 32.6, 33.9, 34.3, 39.2, 39.6, 71.3, 72.8, 73.7, 74.0, 122.6, 124.4, 125.9, 126.1, 126.2, 126.4, 126.8, 127.1, 127.8, 128.0, 128.9, 129.6, 131.4, 131.9, 143.0, 143.1, 147.5, 147.8, 148.7, 149.1, 151.9, 152.2, 167.8, 168.7; IR (KBr,  $\text{cm}^{-1}$ )  $\nu$  3373, 3180, 3049, 2961, 2868, 1692, 1530, 1483, 1364, 1296, 874; MS ( $m/z$ ): HRMS (ESI) Calcd for  $\text{C}_{51}\text{H}_{66}\text{N}_2\text{NaO}_7$  ( $[\text{M}+\text{Na}]^+$ ): 841.4762, found: 841.4771.

**7,13,19,25-tetra-*tert*-butyl-28,30-di-hydroxy-27,29-N,N-(propane-1,3-diyl)-aminocarbonylmethoxyl)-2,3-dihomo-3-oxacalix[4] arene (4F):** White solid, m.p. 189.5–191.4°C, yield: 92.0% (Figure S8);  $^1\text{H}$  NMR (400 MHz,  $\text{CDCl}_3$ )  $\delta$  (ppm): 1.16, 1.24, 1.25, 1.26 (4s, 36H), 2.29–2.38 (m, 2H), 3.26 (s, 2H), 3.42 (dd, 2H,  $J_1 = 12.4$  Hz,  $J_2 = 1.2$  Hz), 3.57 (d, 1H,  $J = 13.6$  Hz), 3.66 (d, 1H,  $J = 14.8$  Hz), 3.76 (d, 1H,  $J = 16.8$  Hz), 4.05 (d, 1H,  $J = 14.0$  Hz), 4.15 (d, 1H,  $J = 13.2$  Hz), 4.21–4.26 (m, 2H), 4.31 (d, 1H,  $J = 12.8$  Hz), 4.36–4.22 (m, 2H), 4.70–4.74 (m, 2H), 4.80–4.87 (m, 2H), 6.90 (s, 1H), 7.03 (s, 2H), 7.13 (d, 2H,  $J = 13.2$  Hz), 7.32 (s, 1H), 7.50 (s, 1H), 8.16 (s, 1H), 8.50 (s, 1H), 8.69 (s, 1H);  $^{13}\text{C}$  NMR (100 MHz,  $\text{CDCl}_3$ )  $\delta$  (ppm): 23.2, 30.0, 31.1, 31.3, 31.5, 32.3, 33.9, 34.3, 36.1, 71.0, 72.4, 73.8, 74.0, 122.7, 124.7, 125.9, 126.2, 126.3, 126.5, 126.8, 126.9, 127.5, 128.0, 129.1, 129.6, 131.2, 131.9, 133.7, 143.1, 143.3, 148.0, 148.2, 148.7, 149.1, 151.8, 152.6, 168.2, 169.3; IR (KBr,  $\text{cm}^{-1}$ )  $\nu$  3377, 3049, 2961, 2868, 1690, 1599, 1483, 1443, 1298, 874; MS ( $m/z$ ): HRMS (ESI) Calcd for  $\text{C}_{52}\text{H}_{68}\text{N}_2\text{NaO}_7$  ( $[\text{M}+\text{Na}]^+$ ): 855.4919, found: 855.4922.

**7,13,19,25-tetra-*tert*-butyl-28,30-di-hydroxy-27,29-N,N-(butane-1,4-diyl)-aminocarbonylmethoxyl)-2,3-dihomo-3-oxacalix[4] arene (4G):** White solid, m.p. 157.6–158.7°C, yield: 91.9% (Figure S9);  $^1\text{H}$  NMR (400 MHz,  $\text{DMSO}-d_6$ )  $\delta$  (ppm): 1.09, 1.19, 1.22, 1.23 (4s, 36H), 1.63 (d, 4H,  $J = 4.4$  Hz), 3.42–3.52 (m, 6H), 4.21 (d, 1H,  $J = 9.6$  Hz), 4.27–4.34 (m, 4H), 4.36–4.42 (m, 4H), 4.54 (d, 1H,  $J = 14.0$  Hz), 4.73 (d, 1H,  $J = 9.6$  Hz), 4.79 (d, 1H,  $J = 10.0$  Hz), 6.92 (d, 1H,  $J = 2.0$  Hz), 7.04 (d, 2H,  $J = 2.4$  Hz), 7.22 (d, 1H,  $J = 2.0$  Hz), 7.26 (s, 1H), 7.28 (s, 1H), 7.32 (d, 1H,  $J = 2.4$  Hz), 7.41 (d, 1H,  $J = 2.0$  Hz), 7.58 (d, 1H,  $J = 2.0$  Hz), 7.98 (s, 1H), 8.20 (t, 1H,  $J = 6.4$  Hz), 8.35 (t, 1H,  $J = 6.0$  Hz);  $^{13}\text{C}$  NMR (100 MHz,  $\text{CDCl}_3$ )  $\delta$  (ppm): 25.0, 25.4, 30.3, 31.0, 31.1, 31.3, 31.5, 31.6, 31.9, 33.9, 34.3, 38.4, 70.9, 72.5, 74.1, 74.5, 122.9, 124.6, 125.8, 126.1, 126.5, 126.6, 126.7, 127.0, 128.0, 128.7, 129.6, 131.2, 131.6, 133.8, 143.0, 143.2, 147.8, 148.4, 149.0, 149.4, 151.8, 153.0, 168.1, 169.0; IR (KBr,  $\text{cm}^{-1}$ )  $\nu$  3369, 3389, 3233, 3194, 3049, 2961, 2868, 1686, 1535, 1485, 1298, 874; MS ( $m/z$ ): HRMS (ESI) Calcd for  $\text{C}_{53}\text{H}_{70}\text{N}_2\text{NaO}_7$  ( $[\text{M}+\text{Na}]^+$ ): 869.5075, found: 869.5082.

**7,13,19,25-tetra-*tert*-butyl-28,30-di-hydroxy-27,29-N,N-(N-ethyl-aminocarbonylmethoxyl)-2,3-dihomo-3-oxacalix[4]arene (4H):** White solid, m.p. 138.9–141.2°C, yield: 87.2% (Figure S10);  $^1\text{H}$  NMR (400 MHz,  $\text{CDCl}_3$ )  $\delta$  (ppm): 1.16 (s, 9H), 1.24 (t, 6H,  $J = 14.6$  Hz), 1.25 (brs, 18H), 1.27 (s, 9H), 3.32–3.39 (m, 2H), 3.45 (t, 2H,  $J = 12.8$  Hz), 3.53 (q, 2H,  $J = 6.8$  Hz), 3.61 (q, 1H,  $J = 6.4$  Hz), 4.14 (dd, 2H,  $J_1 = 18.8$  Hz,  $J_2 = 13.6$  Hz), 4.22 (d, 1H,  $J = 10.4$  Hz), 4.33 (d, 1H,  $J = 13.2$  Hz), 4.38–4.45 (m, 2H), 4.52 (d, 1H,  $J = 15.2$  Hz), 4.64 (d, 1H,  $J = 10.0$  Hz), 4.72 (dd, 2H,  $J_1 = 18.0$  Hz,  $J_2 = 2.0$  Hz), 4.89 (d, 1H,  $J = 10.0$  Hz), 6.89 (d, 1H,  $J = 2.0$  Hz), 7.02 (d, 1H,  $J = 1.6$  Hz), 7.05 (d, 1H,

$J = 2.0$  Hz), 7.17 (dd, 2H,  $J_1 = 7.6$  Hz,  $J_2 = 2.0$  Hz), 7.22 (dd, 2H,  $J_1 = 10.4$  Hz,  $J_2 = 2.0$  Hz), 7.45 (d, 1H,  $J = 2.0$  Hz), 7.59 (s, 1H), 8.17 (s, 1H), 8.75 (t, 1H,  $J = 5.2$  Hz), 8.93 (t, 1H,  $J = 5.6$  Hz);  $^{13}\text{C}$  NMR (100 MHz,  $\text{CDCl}_3$ )  $\delta$  (ppm): 14.1, 14.8, 31.1, 31.2, 31.3, 31.5, 32.2, 33.9, 34.0, 34.2, 34.3, 34.4, 71.0, 72.0, 74.6, 122.3, 124.7, 125.7, 125.9, 126.2, 126.8, 127.2, 127.3, 127.4, 127.7, 128.8, 129.6, 131.5, 132.4, 133.7, 142.9, 143.7, 148.1, 148.6, 148.9, 149.5, 151.5, 153.1, 167.9, 168.3; IR (KBr,  $\text{cm}^{-1}$ )  $\nu$  3350, 3244, 2961, 2870, 1682, 1485, 874; MS (m/z): HRMS (ESI) Calcd for  $\text{C}_{53}\text{H}_{72}\text{N}_2\text{NaO}_7$  ( $[\text{M}+\text{Na}]^+$ ): 871.5232, found: 871.5249.

**7,13,19,25-tetra-*tert*-butyl-28,30-di-hydroxy-27,29-di-(N-isopropyl-aminocarbonylmethoxyl)-2,3-dihomo-3-oxa calix[4]arene (4I):** White solid, m.p. 133.3–135.7°C, yield: 76.3% (Figure S11);  $^1\text{H}$  NMR (400 MHz,  $\text{CDCl}_3$ )  $\delta$  (ppm): 1.16 (s, 9H), 1.20 (d, 4H,  $J = 6.4$  Hz), 1.25 (brs, 18H), 1.29 (s, 9H), 1.31 (d, 8H,  $J = 4.8$  Hz), 3.41 (t, 2H,  $J = 14.8$  Hz), 3.57 (d, 1H,  $J = 13.6$  Hz), 4.11 (d, 1H,  $J = 13.6$  Hz), 4.18–4.47 (m, 8H), 4.55 (d, 1H,  $J = 10.4$  Hz), 4.77 (dd, 2H,  $J_1 = 18.8$  Hz,  $J_2 = 15.6$  Hz), 4.99 (d, 1H,  $J = 10.4$  Hz), 6.85 (s, 1H), 7.03 (d, 2H,  $J = 14.4$  Hz), 7.15 (s, 2H), 7.23 (d, 2H,  $J = 4.0$  Hz), 7.45 (s, 1H), 7.61 (s, 1H), 7.90 (s, 1H), 8.79 (dd, 2H,  $J_1 = 19.6$  Hz,  $J_2 = 7.6$  Hz);  $^{13}\text{C}$  NMR (100 MHz,  $\text{CDCl}_3$ )  $\delta$  (ppm): 22.0, 22.3, 22.6, 31.1, 31.3, 31.5, 31.6, 33.9, 34.2, 41.4, 41.5, 71.0, 71.8, 74.2, 74.6, 121.9, 123.9, 125.6, 125.8, 126.1, 127.0, 127.4, 127.5, 127.6, 128.5, 129.7, 131.8, 132.4, 133.8, 142.8, 143.5, 147.7, 148.4, 149.0, 150.3, 151.3, 153.8, 167.4, 167.9; IR (KBr,  $\text{cm}^{-1}$ )  $\nu$  3340, 2962, 2870, 1682, 1485, 1460, 874; MS (m/z): HRMS (ESI) Calcd for  $\text{C}_{55}\text{H}_{76}\text{N}_2\text{NaO}_7$  ( $[\text{M}+\text{Na}]^+$ ): 899.5545, found: 899.5562.

**7,13,19,25-tetra-*tert*-butyl-28,30-di-hydroxy-27,29-di-(N-isobutyl-aminocarbonylmethoxyl)-2,3-dihomo-3-oxa calix[4]arene (4J):** White solid, m.p. 128.1–130.8°C, yield: 86.5% (Figure S12);  $^1\text{H}$  NMR (400 MHz,  $\text{CDCl}_3$ )  $\delta$  (ppm): 0.90–0.98 (m, 12H), 1.16 (s, 9H), 1.24 (brs, 18H), 1.26 (s, 9H), 1.85 (s, 1H), 1.99 (s, 1H), 2.94–3.04 (m, 2H), 3.38–3.46 (m, 3H), 3.56 (d, 2H,  $J = 13.6$  Hz), 4.08 (d, 1H,  $J = 15.2$  Hz), 4.21 (d, 2H,  $J = 12.4$  Hz), 4.35–4.48 (m, 4H), 4.59 (d, 1H,  $J = 10.4$  Hz), 4.75–4.84 (m, 2H), 4.96 (d, 1H,  $J = 10.4$  Hz), 6.85 (s, 1H), 7.02 (d, 2H,  $J = 6.0$  Hz), 7.14 (d, 2H,  $J = 11.2$  Hz), 7.21 (s, 2H), 7.47 (d, 2H,  $J = 14.4$  Hz), 8.09 (s, 1H), 8.62 (s, 1H), 8.94 (s, 1H);  $^{13}\text{C}$  NMR (100 MHz,  $\text{CDCl}_3$ )  $\delta$  (ppm): 20.4, 20.5, 28.5, 31.1, 31.3, 31.5, 33.9, 34.2, 34.3, 46.8, 47.0, 71.2, 72.0, 73.9, 74.5, 122.1, 124.2, 125.5, 125.9, 126.0, 126.9, 127.0, 127.2, 127.3, 127.4, 127.6, 128.6, 129.6, 131.7, 132.3, 133.8, 142.8, 143.4, 147.8, 148.5, 148.8, 149.5, 151.5, 153.2, 168.0, 168.6; IR (KBr,  $\text{cm}^{-1}$ )  $\nu$  3350, 3194, 2961, 2870, 1680, 1483, 1364; MS (m/z): HRMS (ESI) Calcd for  $\text{C}_{57}\text{H}_{80}\text{N}_2\text{NaO}_7$  ( $[\text{M}+\text{Na}]^+$ ): 927.5858, found: 927.5873.

**7,13,19,25-tetra-*tert*-butyl-28,30-di-hydroxy-27,29-di-(N-butyl-aminocarbonylmethoxyl)-2,3-dihomo-3-oxa calix[4]arene (4K):** White solid, m.p. 119.5–120.8°C, yield: 91.9% (Figure S13);  $^1\text{H}$  NMR (400 MHz,  $\text{CDCl}_3$ )  $\delta$  (ppm): 0.84 (t, 3H,  $J = 7.2$  Hz), 0.92 (t, 3H,  $J = 7.2$  Hz), 1.17 (s, 9H), 1.25 (brs, 18H), 1.28 (s, 9H), 1.32–1.43 (m, 4H), 1.56–1.71 (m, 4H), 3.19–3.31 (m, 2H), 3.44 (t, 2H,  $J = 14.0$  Hz), 3.50–3.57 (m, 2H), 3.61–3.66 (m, 1H), 4.11 (d, 1H,  $J = 13.2$  Hz), 4.17–4.24 (m, 2H), 4.35–4.42 (m, 3H), 4.49 (d, 1H,  $J = 15.2$  Hz), 4.63 (d, 1H,  $J = 10.0$  Hz), 4.76 (dd, 2H,  $J_1 = 18.8$  Hz,  $J_2 = 15.2$  Hz), 4.93 (d, 1H,  $J = 10.4$  Hz), 6.88 (d, 1H,  $J = 2.0$  Hz), 7.04 (dd, 2H,  $J_1 = 11.2$  Hz,  $J_2 = 1.6$  Hz), 7.16

(dd, 2H,  $J_1 = 8.4$  Hz,  $J_2 = 1.6$  Hz), 7.23 (dd, 2H,  $J_1 = 6.4$  Hz,  $J_2 = 1.6$  Hz), 7.46 (d, 1H,  $J = 2.0$  Hz), 7.55 (s, 1H), 8.14 (s, 1H), 8.67 (t, 1H,  $J = 5.2$  Hz), 8.91 (t, 1H,  $J = 5.2$  Hz);  $^{13}\text{C}$  NMR (100 MHz,  $\text{CDCl}_3$ )  $\delta$  (ppm): 13.7, 13.8, 20.2, 31.1, 31.3, 31.5, 34.3, 39.1, 39.3, 71.1, 72.1, 74.0, 74.5, 122.2, 124.4, 125.7, 125.9, 126.0, 126.9, 127.1, 127.2, 127.3, 127.4, 127.6, 128.7, 129.6, 131.6, 132.3, 133.8, 142.8, 143.5, 148.0, 148.5, 148.9, 149.6, 151.5, 153.2, 167.9, 168.3; IR (KBr,  $\text{cm}^{-1}$ )  $\nu$  3350, 3049, 2959, 2868, 1682, 1537, 1298, 874; MS (m/z): HRMS (ESI) Calcd for  $\text{C}_{57}\text{H}_{80}\text{N}_2\text{NaO}_7$  ( $[\text{M}+\text{Na}]^+$ ): 927.5858, found: 927.5874.

**7,13,19,25-tetra-*tert*-butyl-28,30-di-hydroxy-27,29-di-(N-pentyl-aminocarbonylmethoxyl)-2,3-dihomo-3-oxa calix[4]arene (4L):** Light yellow solid, m.p. 117.7–119.3°C, yield: 72.4% (Figure S14);  $^1\text{H}$  NMR (400 MHz,  $\text{CDCl}_3$ )  $\delta$  (ppm): 0.67 (t, 3H,  $J = 7.2$  Hz), 0.82 (t, 3H,  $J = 7.2$  Hz), 1.16, 1.24, 1.26 (4s, 36H), 1.29–1.42 (m, 7H), 1.53–1.67 (m, 5H), 3.15–3.25 (m, 2H), 3.43 (t, 2H,  $J = 14.0$  Hz), 3.50–3.65 (m, 3H), 4.09 (d, 1H,  $J = 13.6$  Hz), 4.17–4.24 (m, 2H), 4.37 (d, 2H,  $J = 14.4$  Hz), 4.41 (d, 1H,  $J = 10.4$  Hz), 4.47 (d, 1H,  $J = 14.8$  Hz), 4.61 (d, 1H,  $J = 10.0$  Hz), 4.73–4.81 (m, 2H), 4.93 (d, 1H,  $J = 10.4$  Hz), 6.87 (d, 1H,  $J = 2.0$  Hz), 7.02 (dd, 2H,  $J_1 = 11.2$  Hz,  $J_2 = 2.4$  Hz), 7.15 (dd, 2H,  $J_1 = 9.6$  Hz,  $J_2 = 2.0$  Hz), 7.22 (q, 2H,  $J = 2.4$  Hz), 7.46 (d, 1H,  $J = 2.4$  Hz), 7.54 (s, 1H), 8.19 (s, 1H), 8.68 (s, 1H), 8.95 (s, 1H);  $^{13}\text{C}$  NMR (100 MHz,  $\text{CDCl}_3$ )  $\delta$  (ppm): 13.8, 14.0, 22.4, 22.5, 29.3, 31.1, 31.3, 31.5, 33.9, 39.4, 39.6, 71.2, 72.1, 73.9, 74.5, 122.2, 124.4, 125.6, 126.0, 126.9, 127.0, 127.2, 127.3, 127.4, 127.7, 128.7, 129.6, 131.6, 132.3, 133.8, 142.9, 143.5, 147.9, 148.5, 148.9, 149.5, 151.5, 152.2, 167.8, 168.3; IR (KBr,  $\text{cm}^{-1}$ )  $\nu$  3348, 3049, 2959, 2868, 1682, 1599, 1537, 1485, 1445, 874; MS (m/z): HRMS (ESI) Calcd for  $\text{C}_{59}\text{H}_{84}\text{N}_2\text{NaO}_7$  ( $[\text{M}+\text{Na}]^+$ ): 955.6176, found: 955.6174.

**7,13,19,25-tetra-*tert*-butyl-28,30-di-hydroxy-27,29-di-(N-clopentyl-aminocarbonylmethoxyl)-2,3-dihomo-3-oxa calix[4]arene (4M):** White solid, m.p. 145.9–148.2°C, yield: 83.61% (Figure S15);  $^1\text{H}$  NMR (400 MHz,  $\text{DMSO}-d_6$ )  $\delta$  (ppm): 1.12, 1.22, 1.25, 1.26 (4s, 36H), 1.51–1.72 (m, 12H), 1.87–1.96 (m, 4H), 3.49 (q, 2H,  $J = 6.4$  Hz), 3.58 (d, 1H,  $J = 13.2$  Hz), 4.19–4.26 (m, 5H), 4.34–4.42 (m, 3H), 4.47 (d, 1H,  $J = 14.8$  Hz), 4.57 (d, 1H,  $J = 14.8$  Hz), 4.65–4.72 (m, 2H), 4.93 (d, 1H,  $J = 10.0$  Hz), 6.95, 7.05, 7.10 (3s, 3H), 7.29 (d, 2H,  $J = 8.4$  Hz), 7.35 (s, 1H), 7.46 (s, 1H), 7.60 (s, 2H), 8.14 (s, 1H), 8.32 (d, 1H,  $J = 7.6$  Hz), 8.47 (d, 1H,  $J = 7.2$  Hz);  $^{13}\text{C}$  NMR (100 MHz,  $\text{DMSO}-d_6$ )  $\delta$  (ppm): 24.1, 31.3, 31.5, 31.8, 32.4, 32.8, 33.0, 34.1, 34.4, 50.7, 50.8, 71.5, 74.1, 74.5, 122.3, 124.1, 126.0, 126.1, 126.3, 127.1, 127.3, 128.2, 129.4, 132.3, 132.9, 134.1, 142.1, 142.5, 147.2, 147.4, 149.5, 151.8, 153.9, 167.6, 168.1; IR (KBr,  $\text{cm}^{-1}$ )  $\nu$  3342, 3049, 2961, 2870, 1682, 1529, 1483; MS (m/z): HRMS (ESI) Calcd for  $\text{C}_{59}\text{H}_{80}\text{N}_2\text{NaO}_7$  ( $[\text{M}+\text{Na}]^+$ ): 951.5858, found: 951.5862.

**7,13,19,25-tetra-*tert*-butyl-28,30-di-hydroxy-27,29-di-(N-benzyl-aminocarbonylmethoxyl)-2,3-dihomo-3-oxa calix[4]arene (4N):** m.p. 183.7–186.4°C, yield: 72.0% (Figure S16);  $^1\text{H}$  NMR (400 MHz,  $\text{CDCl}_3$ )  $\delta$  (ppm): 1.12, 1.20, 1.25 (4s, 36H), 3.32 (t, 2H,  $J = 12.8$  Hz), 3.42 (d, 1H,  $J = 13.6$  Hz), 3.90 (d, 1H,  $J = 13.6$  Hz), 4.03 (dd, 2H,  $J_1 = 13.2$  Hz,  $J_2 = 4.4$  Hz), 4.15 (dd, 2H,  $J_1 = 15.6$  Hz,  $J_2 = 10.0$  Hz), 4.26–4.32 (m, 2H), 4.41–4.57 (m, 4H), 4.64 (s, 1H), 4.67 (d, 1H,  $J = 4.0$  Hz), 4.74 (dd, 1H,  $J_1 = 14.4$  Hz,  $J_2 = 6.4$  Hz), 4.83 (dd, 1H,  $J_1 = 14.4$  Hz,  $J_2 = 6.4$  Hz), 6.79 (d, 1H,  $J = 2.4$  Hz), 6.92 (d, 1H,  $J = 2.4$  Hz), 6.98 (d, 1H,  $J =$

2.8 Hz), 7.04–7.11 (m, 6H), 7.13 (s, 1H), 7.15 (d, 1H,  $J = 2.4$  Hz), 7.19–7.24 (m, 3H), 7.27 (d, 1H,  $J = 1.6$  Hz), 7.28 (s, 1H), 7.38 (dd, 3H,  $J_1 = 5.8$  Hz,  $J_2 = 2.0$  Hz), 7.74 (s, 1H), 8.93 (t, 1H,  $J = 5.6$  Hz), 9.25 (t, 1H,  $J = 5.6$  Hz);  $^{13}\text{C}$  NMR (100 MHz,  $\text{CDCl}_3$ )  $\delta$  (ppm): 31.1, 31.2, 31.5, 31.6, 33.9, 34.2, 43.6, 43.8, 72.2, 73.8, 122.3, 124.5, 125.5, 125.7, 126.1, 126.6, 126.7, 126.9, 127.0, 127.2, 127.3, 127.5, 128.4, 128.5, 128.7, 129.4, 131.4, 132.1, 133.7, 137.4, 138.0, 142.6, 143.2, 148.0, 148.3, 148.7, 149.6, 151.3, 153.0, 168.1, 168.5; IR (KBr,  $\text{cm}^{-1}$ )  $\nu$  3448, 3389, 2955, 2870, 1670, 1485, 1439; MS (m/z): HRMS (ESI) Calcd for  $\text{C}_{63}\text{H}_{77}\text{N}_2\text{O}_7$  ( $[\text{M}+\text{H}]^+$ ): 973.5725, found: 973.5716.

**7,13,19,25-tetra-tert-butyl-28,30-di-hydroxy-27,29-di-(N-phenethyl-aminocarbonylmethoxyl)-2,3-dihomo-3-oxalix [4]arene (4O):** White solid, m.p. 114.6–115.9°C, yield: 67.1% (Figure S17);  $^1\text{H}$  NMR (400 MHz,  $\text{CDCl}_3$ )  $\delta$  (ppm): 1.15, 1.24, 1.27, 1.28 (4s, 36H), 2.88–3.04 (m, 4H), 3.27 (d, 1H,  $J = 13.2$  Hz), 3.32 (d, 1H,  $J = 12.8$  Hz), 3.46–3.58 (m, 3H), 3.84–3.98 (m, 4H), 4.14 (d, 1H,  $J = 13.2$  Hz), 4.18 (d, 1H,  $J = 10.4$  Hz), 4.32 (d, 1H,  $J = 10.0$  Hz), 4.37 (d, 1H,  $J = 14.8$  Hz), 4.43 (d, 1H,  $J = 8.8$  Hz), 4.46 (d, 1H,  $J = 3.6$  Hz), 4.73 (d, 1H,  $J = 7.6$  Hz), 4.76 (d, 1H,  $J = 8.0$  Hz), 4.88 (d, 1H,  $J = 10.4$  Hz), 6.85 (d, 1H,  $J = 1.6$  Hz), 6.94–6.99 (m, 2H), 7.03–7.22 (m, 14H), 7.43 (d, 1H,  $J = 2.0$  Hz), 7.48 (s, 1H), 8.05 (s, 1H), 8.79 (t, 1H,  $J = 5.2$  Hz), 9.01 (t, 1H,  $J = 5.6$  Hz);  $^{13}\text{C}$  NMR (100 MHz,  $\text{CDCl}_3$ )  $\delta$  (ppm): 31.1, 31.3, 31.6, 32.4, 33.9, 34.2, 35.1, 35.5, 40.6, 40.6, 71.1, 72.0, 73.9, 74.4, 122.2, 124.2, 125.5, 125.9, 126.0, 126.1, 126.2, 126.8, 127.0, 127.2, 127.5, 127.7, 128.2, 128.4, 128.5, 128.7, 129.6, 131.6, 132.4, 133.8, 138.6, 138.9, 142.8, 143.5, 147.9, 148.5, 148.8, 149.3, 151.4, 153.0, 168.0, 168.5; IR (KBr,  $\text{cm}^{-1}$ )  $\nu$  3346, 2961, 2905, 2866, 1682, 1537, 1483, 1445, 1364; MS (m/z): HRMS (ESI) Calcd for  $\text{C}_{65}\text{H}_{80}\text{N}_2\text{NaO}_7$  ( $[\text{M}+\text{Na}]^+$ ): 1023.5860, found: 1023.5870.

**7,13,19,25-tetra-tert-butyl-28,30-di-hydroxy-27,29-di-(N-(3,4-dimethoxyphenethyl)-aminocarbonylmethoxyl)-2,3-dihomo-3-oxalix [4]arene (4P):** White solid, m.p. 117.4–120.1°C, yield: 76.4% (Figure S18);  $^1\text{H}$  NMR (400 MHz,  $\text{CDCl}_3$ )  $\delta$  (ppm): 1.14, 1.23, 1.24, 1.25 (4s, 36H), 2.86–2.95 (m, 4H), 3.34 (d, 2H,  $J = 12.0$  Hz), 3.46 (d, 1H,  $J = 13.6$  Hz), 3.50–3.60 (m, 2H), 3.72–3.82 (m, 12H), 3.90–4.07 (m, 5H), 4.15 (d, 1H,  $J = 10.4$  Hz), 4.28 (d, 1H,  $J = 9.2$  Hz), 4.35–4.46 (m, 3H), 4.68 (t, 2H,  $J = 14.4$  Hz), 4.81 (d, 1H,  $J = 10.0$  Hz), 6.49 (d, 1H,  $J = 8.0$  Hz), 6.58 (d, 1H,  $J = 7.2$  Hz), 6.64 (d, 1H,  $J = 7.6$  Hz), 6.73 (s, 3H), 6.84 (s, 1H), 7.00 (d, 2H,  $J = 12.8$  Hz), 7.15 (t, 4H,  $J = 17.6$  Hz), 7.41 (s, 1H), 7.51 (s, 1H), 7.94 (s, 1H), 8.76 (s, 1H), 8.90 (s, 1H);  $^{13}\text{C}$  NMR (100 MHz,  $\text{CDCl}_3$ )  $\delta$  (ppm): 30.9, 31.1, 31.2, 31.5, 33.9, 34.2, 34.3, 34.8, 35.1, 40.7, 55.8, 55.9, 70.9, 71.8, 73.9, 111.2, 111.3, 111.8, 112.0, 120.6, 120.7, 122.3, 127.1, 127.2, 127.4, 128.6, 131.3, 131.6, 133.8, 142.8, 143.3, 147.4, 148.0, 148.6, 148.9, 149.1, 151.4, 152.8, 168.0, 168.5; IR (KBr,  $\text{cm}^{-1}$ )  $\nu$  3348, 3049, 2957, 2868, 1682, 1516, 1485, 1362, 874.

**7,13,19,25-tetra-tert-butyl-28,30-di-hydroxy-27-(N-clopentyl-aminocarbonylmethoxyl)-29-(N-(2-hydroxyethyl)-aminocarbonylmethoxyl)-2,3-dihomo-3-oxalix[4]arene (4Q):** White solid, yield: 82.5%, m.p. 138.3–140.5°C (Figure S19);  $^1\text{H}$  NMR (400 MHz,  $\text{CDCl}_3$ )  $\delta$  (ppm): 1.14, 1.19, 1.24, 1.26 (4s, 36H), 1.59–1.80 (m, 8H), 3.32–3.52 (m, 4H), 3.56 (d, 1H,  $J = 13.8$  Hz), 3.67–3.79 (m, 4H), 4.05–4.22 (m, 4H),

4.31–4.45 (m, 5H), 4.52–4.60 (m, 2H), 4.69–4.91 (m, 3H), 4.99 (d, 1H,  $J = 10.8$  Hz), 6.86–7.13 (m, 6H), 7.22 (d, 2H,  $J = 8.0$  Hz), 7.37 (d, 1H,  $J = 5.6$  Hz), 7.86 (d, 1H,  $J = 14.0$  Hz), 8.70–9.01 (m, 2H);  $^{13}\text{C}$  NMR (100 MHz,  $\text{CDCl}_3$ )  $\delta$  (ppm): 23.9, 24.1, 31.0, 31.2, 31.4, 31.6, 32.0, 32.4, 32.9, 33.3, 33.9, 42.6, 51.2, 62.0, 71.5, 72.0, 122.3, 124.2, 125.5, 125.8, 126.1, 126.9, 127.1, 127.3, 127.5, 127.7, 128.4, 129.4, 131.7, 132.2, 133.6, 143.0, 143.5, 147.7, 148.0, 148.5, 148.9, 149.6, 150.0, 151.3, 153.6, 168.8, 169.0; IR (KBr,  $\text{cm}^{-1}$ )  $\nu$  3350, 2961, 2870, 1674, 1485, 1298, 1196, 1070; MS (m/z): HRMS (ESI) Calcd for  $\text{C}_{56}\text{H}_{76}\text{N}_2\text{NaO}_8$  ( $[\text{M}+\text{Na}]^+$ ): 927.5499, found: 927.5486.

**7,13,19,25-tetra-tert-butyl-28,30-di-hydroxy-27-(N-phenethyl-aminocarbonylmethoxyl)-29-(N-(2-hydroxyethyl)-aminocarbonylmethoxyl)-2,3-dihomo-3-oxalix[4]arene (4R):** White solid, m.p. 120.7–123.3°C, yield: 81.6% (Figure S20);  $^1\text{H}$  NMR (400 MHz,  $\text{CDCl}_3$ )  $\delta$  (ppm): 1.00 (s, 3H), 1.14 (s, 6H), 1.18 (s, 6H), 1.21 (s, 3H), 1.24 (s, 6H), 1.26 (s, 9H), 1.28 (s, 3H), 2.87–3.04 (m, 3H), 3.26–3.38 (m, 1H), 3.42–3.53 (m, 3H), 3.54–3.64 (m, 2H), 3.70–3.78 (m, 2H), 4.00–4.11 (m, 2H), 4.23 (dd, 2H,  $J_1 = 12.0$  Hz,  $J_2 = 7.8$  Hz), 4.30 (d, 1H,  $J = 10.4$  Hz), 4.38–4.43 (m, 2H), 4.50 (dd, 2H,  $J_1 = 14.8$  Hz,  $J_2 = 9.6$  Hz), 4.61 (dd, 1H,  $J = 16.4$ , 6.6 Hz), 4.71 (dd, 1H,  $J_1 = 15.4$  Hz,  $J_2 = 5.8$  Hz), 4.83 (dd, 1H,  $J_1 = 10.2$  Hz,  $J_2 = 5.6$  Hz), 6.79–6.89 (m, 1H), 6.94–7.03 (m, 3H), 7.03–7.11 (m, 2H), 7.11–7.15 (m, 3H), 7.16 (d, 3H,  $J = 4.4$  Hz), 7.22 (s, 1H), 7.34–7.41 (m, 2H), 7.94 (s, 1H), 8.69–8.80 (m, 1H), 8.90 (t, 1H,  $J = 5.6$  Hz);  $^{13}\text{C}$  NMR (100 MHz,  $\text{CDCl}_3$ )  $\delta$  (ppm): 30.9, 31.1, 31.2, 31.5, 31.6, 32.2, 33.9, 34.2, 35.3, 35.5, 40.6, 40.7, 42.5, 62.0, 62.4, 70.9, 71.8, 73.9, 74.3, 122.3, 124.5, 125.6, 125.9, 126.1, 126.2, 126.6, 127.2, 127.3, 127.7, 128.3, 128.4, 128.5, 128.6, 128.7, 129.4, 131.6, 132.2, 133.5, 133.9, 138.7, 138.8, 143.0, 143.6, 148.0, 148.5, 148.7, 148.8, 149.4, 151.3, 152.7, 168.7, 168.9, 169.3; IR (KBr,  $\text{cm}^{-1}$ )  $\nu$  3366, 2961, 2868, 1670, 1541, 1485, 1200, 1072, 874, 579; MS (m/z): HRMS (ESI) Calcd for  $\text{C}_{59}\text{H}_{76}\text{N}_2\text{NaO}_8$  ( $[\text{M}+\text{Na}]^+$ ): 963.5494, found: 963.5491.

**7,13,19,25-tetra-tert-butyl-28,30-di-hydroxy-27-(N-N-bis(2-hydroxyethyl)-aminocarbonylmethoxyl)-29-(N-(2-hydroxyethyl)-aminocarbonylmethoxyl)-2,3-dihomo-3-oxalix[4]arene (4S):** White solid, m.p. 144.4–146.2°C, yield: 85.9% (Figure S21);  $^1\text{H}$  NMR (400 MHz,  $\text{CDCl}_3$ )  $\delta$  (ppm): 1.07, 1.23, 1.25, 1.26 (4s, 36H), 3.31–3.58 (m, 8H), 3.68–3.89 (m, 8H), 4.00 (s, 2H), 4.22 (d, 1H,  $J = 13.2$  Hz), 4.36 (d, 1H,  $J = 13.2$  Hz), 4.58 (d, 1H,  $J = 14.8$  Hz), 4.91–5.02 (m, 4H), 6.81 (s, 1H), 6.89 (s, 1H), 7.02 (s, 2H), 7.10 (s, 1H), 7.16 (d, 2H,  $J = 6.8$  Hz), 7.43 (s, 1H), 7.83 (s, 1H), 8.99 (s, 1H);  $^{13}\text{C}$  NMR (100 MHz,  $\text{CDCl}_3$ )  $\delta$  (ppm): 30.6, 31.0, 31.1, 31.6, 31.7, 33.9, 34.1, 34.3, 42.4, 49.9, 51.3, 59.9, 60.0, 62.0, 71.2, 72.2, 72.7, 74.0, 122.8, 124.2, 125.1, 125.5, 15.8, 125.9, 126.6, 128.2, 129.0, 129.2, 129.4, 132.0, 132.2, 134.4, 142.4, 143.0, 146.8, 148.0, 148.9, 150.9, 151.7, 153.7, 170.3, 170.4; IR (KBr,  $\text{cm}^{-1}$ )  $\nu$  3398, 2961, 2870, 1485, 1364, 1202, 1068, 874; MS (m/z): HRMS (ESI) Calcd for  $\text{C}_{55}\text{H}_{76}\text{N}_2\text{NaO}_{10}$  ( $[\text{M}+\text{Na}]^+$ ): 947.5398, found: 947.5408.

## Crystallography

The single crystal of dihomooxalix[4]arene amide 4L and 4N were obtained in ethanol and their single crystal structures were determined on a Bruker Smart Apex

single crystal diffractometer. The data were processed with HKL2000. The structure was solved by direct methods of SHELX86 and subsequent Fourier-difference synthesis and refined by full-matrix least-squares on  $F^2$  with SHELXS-97 (Sheldrick, 1997). No absorption correction was done. All non-hydrogen atoms were refined with anisotropic displacement parameters.

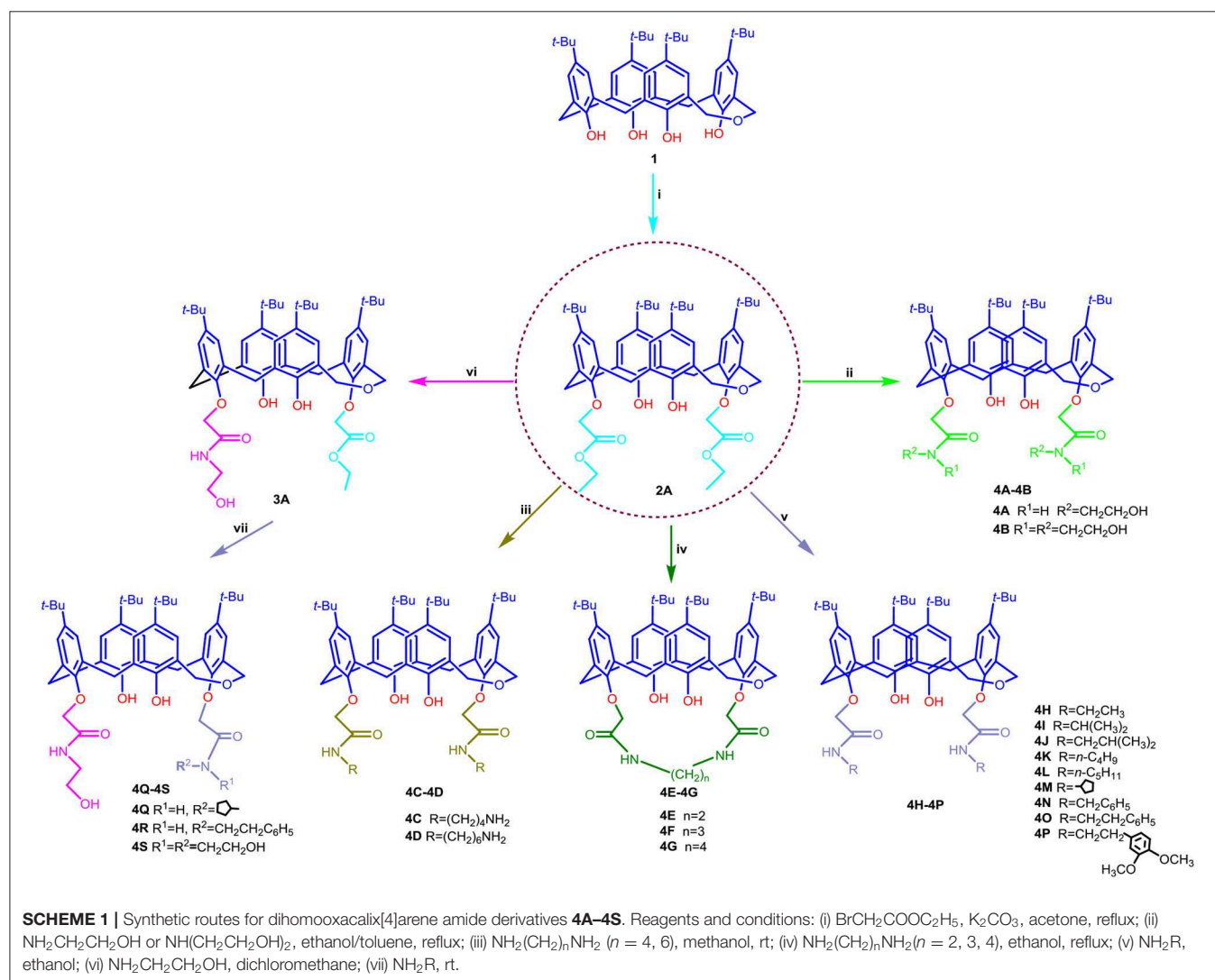
## Cell Culture

A549 cells (human lung carcinoma cells), MCF-7 cells (human breast cancer cells), HeLa cells (human cervical cancer cells), HepG2 cells (human hepatocellular carcinoma cells), and HUVEC cells (human umbilical vein endothelial cells) were kindly provided by WeiFang Caleb Pharmaceuticals, Inc. A549 cells were cultured in Ham's F12K medium containing 10% fetal bovine serum, 2 mM L-glutamine, and 1.5 g/L sodium bicarbonate; MCF-7 cells were cultured on cell culture flask using RPMI 1640 medium with 2 mM L-glutamine adjusted to contain 1.5 g/L sodium bicarbonate, 4.5 g/L glucose, 10 mM

HEPES, 1.0 mM sodium pyruvate, and 10% fetal bovine serum. Hela cells were cultured on Cell culture flask using 2 mM L-glutamine adjusted to contain 1.5 g/L sodium bicarbonate, 4.5 g/L glucose, 10 mM HEPES, and 1.0 mM sodium pyruvate in RPMI 1640 medium supplemented with 0.5 mg/ml G418 and 10% fetal bovine serum. HepG2 cells were cultured in minimum essential medium (Eagle) with 2 mM L-glutamine, Earle's BSS, 1.5 g/L sodium bicarbonate, 0.1 mM non-essential amino acids, 1.0 mM sodium pyruvate, and 10% fetal bovine serum. HUVEC cells were cultured in M199 medium containing 2 mM L-glutamine adjusted to contain 1.5 g/L sodium bicarbonate, 4.5 g/L glucose, 10 mM HEPES, 1.0 mM sodium pyruvate, ECGS, and 10% fetal bovine serum. All cells were cultured at 37°C in 5% CO<sub>2</sub>.

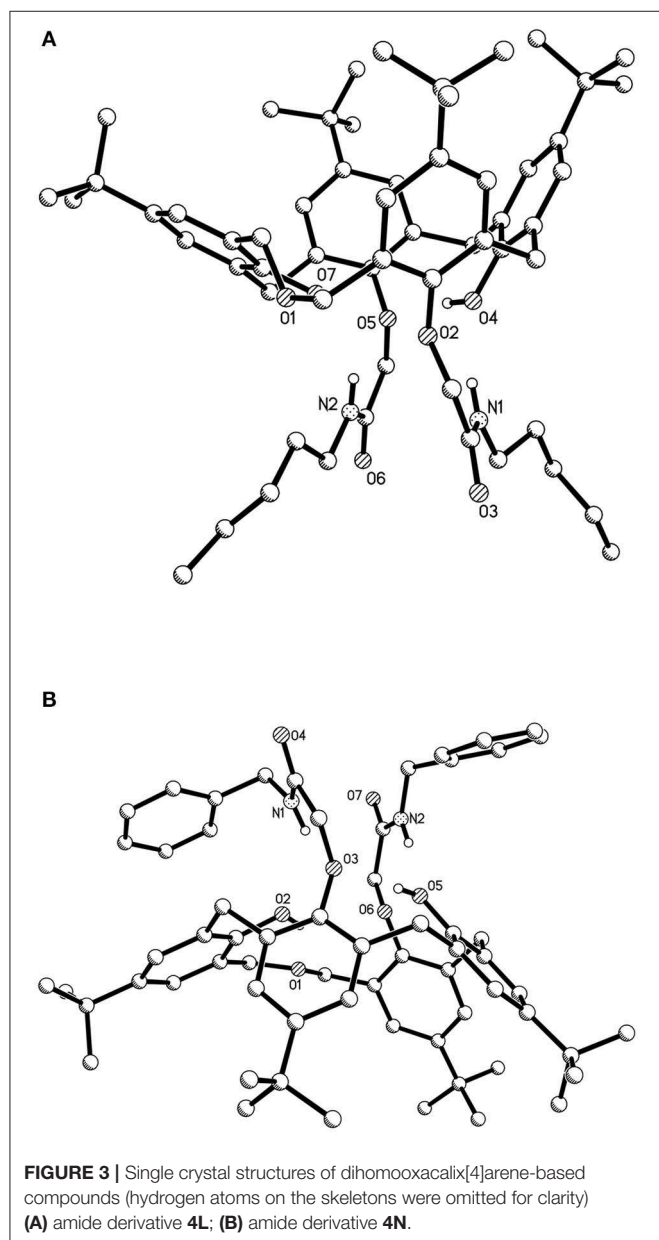
## Cytotoxicity Assay

The cell proliferation of adherent cells was determined by sulforhodamine B assay (SRB) (Quan et al., 2009; Li et al., 2017). All cells were cultured in culture medium containing 10%





fetal bovine serum and have been in the logarithmic growth phase. All cell types were seeded in a 96-well culture plate at a concentration of  $1-5 \times 10^4$  cells per well at  $37^\circ\text{C}$  in a 5%  $\text{CO}_2$  incubator for 24 h. The cells were then exposed to seven drug concentrations of dihomooxalix[4]arene derivatives for 72 h with each concentration located in three wells. Then, the cells were fixed with trichloroacetic acid (TCA). After washing, SRB working solution was added to the cells to clean them. SRB combined with protein was dissolved in Tris base. OD values were measured for each well with a SPECTRA max 190 Cell microplate reader under 540 nm wavelength. According to the OD value, the cell growth inhibition rate was calculated.



## Flow Cytometry

### Flow Cytometry for Cell Cycle Analysis

For flow cytometric analysis of DNA content, MCF-7 cells in exponential growth were treated with compound for 48 h. The cells treated with compound were collected, washed twice with PBS, and then fixed with 75% alcohol overnight. Then, the cells were washed with PBS and resuspended in 100  $\mu\text{l}$  of PBS, 200 mg/ml RNase was added for 30 min to eliminate the interference of RNA, and 20 ml/L propidium iodide (PI; Sigma) was added for 30 min. Then, the cells were washed, and the DNA content was detected by a flow cytometer (BD Accuri C6).

### Flow Cytometry for Cell Apoptosis Analysis

MCF-7 cells ( $5 \times 10^5$  cells/ml) were seeded in six-well plates and treated with compounds at different concentrations for 48 h. The cells were then harvested by trypsinization and washed twice with cold PBS. After centrifugation and removal of the supernatants, cells were resuspended in 400  $\mu\text{l}$  of  $1\times$  binding buffer, which was then added to 5  $\mu\text{l}$  of annexin V-FITC and incubated at room temperature for 15 min. After adding 10  $\mu\text{l}$  of PI, the cells were incubated at room temperature for another 15 min in the dark. The stained cells were analyzed by a flow cytometer (BD Accuri C6).

## Statistical Analysis

Data were calculated using the non-parametric variance. Comparisons among groups were statistically analyzed.  $P < 0.05$  was considered statistically significant. Statistical analyses were conducted using SPSS 16.0 (SPSS, Chicago, IL, USA).

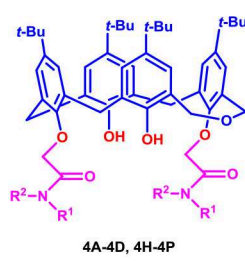
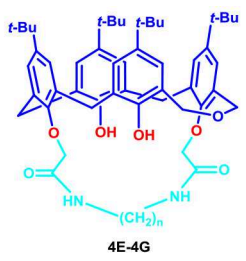
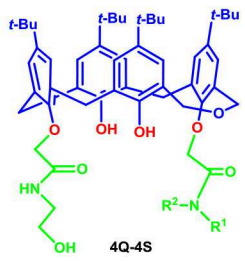
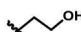
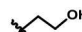
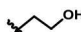
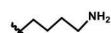


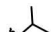
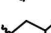
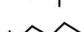
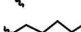

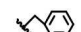

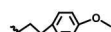
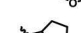
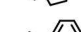


## RESULTS AND DISCUSSION

### Synthesis Investigation

The routes used for the synthesis of the target compounds 4A–4S are outlined in Scheme 1.

As outlined in Scheme 1, all the targets 4A–4S consist of 1,3-alternate dihomooxalix[4]arene conformers. As a first step in our development of dihomooxalix[4] arene amide derivatives, 1,3-di-ethoxycarbonyl substituted dihomooxalix[4]arene intermediate 2A initially synthesized as the key intermediate from known *tert*-butyl dihomooxalix[4]arene 1 by esterification with bromoethyl acetate in the presence of potassium carbonate in refluxing acetone. Subsequently, refluxing ester 2A with excess ethanolamine or diethanolamine in the mixed ethanol/toluene readily afforded the desired amide derivative 4A–4B in good yield of 87.2 and 86.7%, respectively. The derivatives 4C–4D were obtained by reacting ester 2A with an excess amount of diamines in methanol at low temperature (initially stirring in ice bath, and then up to room temperature) and the satisfying yields was 63.3 to 96.2%. Interestingly, on replacement of methanol with refluxing ethanol, but under otherwise similar conditions, the two amino groups on the diamine were found to react with ester 2A simultaneously to give amino-bridging products 4E–4G. To investigate the effect on affinity of different linker groups attached to the amino and dihomooxalix[4]arene components, compounds 4H–4P were successfully accomplished by ester

**TABLE 1 |** Single concentration inhibition of dihomooxacalix[4]arene derivatives **4A–4S** on cell viability.

<div><div></div><div></div><div></div></div>							
Compd.	R <sup>1</sup> /n	R <sup>2</sup>	% inhibition at 10 μM				
			A549	MCF-7	HeLa	HepG2	HUVEC
4A	H		100	100	100	86	41
4B			66	73	100	39	23
4C	H		42	78	96	64	55
4D	H		99	99	100	72	90
4E	2	–	60	50	46	21	26
4F	3	–	63	46	59	9	42
4G	4	–	21	34	40	16	34
4H	H		31	37	41	31	6
4I	H		45	17	44	9	16
4J	H		54	40	35	10	0
4K	H		65	41	42	6	1
4L	H		66	41	49	18	12
4M	H		66	29	52	12	14
4N	H		64	43	49	10	21
4O	H		63	45	60	9	35
4P	H		22	0	37	11	0
4Q	H		34	0	49	23	18
4R	H		2	0	4	–1	85
4S			89	96	97	94	21
CLX-4	–	–	93	99	92	94	16
Paclitaxel	–	–	IC <sub>50</sub> = 0.59 nM	IC <sub>50</sub> = 0.8 nM	IC <sub>50</sub> = 2.7 nM	IC <sub>50</sub> = 5.0 nM	IC <sub>50</sub> = 1.0 nM

**2A** with aliphatic primary amine by method similar to that for compounds **4C–4D**. However, secondary amine was not ideal for the same condition in that of steric hindrance. In addition, treatment of **2A** with ethanolamine in dichloromethane resulted in the partial aminolysis, leading to the generation of mono-N-(2-hydroxyethyl)-aminocarbonyl dihomooxacalix[4]arene compound **3A**, which was further reacted with aliphatic primary amine in methanol to yield the amide derivatives **4Q–4S**. Separation of the reaction products into the pure compounds **4A–4S** was achieved by column chromatography. All the synthesized compounds were further characterized by IR, <sup>1</sup>H NMR, <sup>13</sup>C NMR, and HR-MS spectrometry.

### Single Crystal Structure Analysis

The single crystal structures of dihomooxacalix[4]arene amide derivatives **4L** and **4N** are shown in **Figure 3**. The crystal data, data collection, and structure refinements are summarized in **Table S1**.

As shown in **Figure 3A**, the conformation of dihomooxacalix[4]arene derivative **4L** crystallizes in the monoclinic space group of P 2<sub>1</sub>/c. In molecules, the two N-pentyl-aminocarbonylmethoxyl groups (27, 29-positions) at the lower rim of the rings exist in 1,3-distal position. The four phenolic rings remained standing on same side of the mean plane defined by the four phenolic oxygen atoms O2, O4, O5, and O7. One of the aromatic rings, bearing O7, is partly parallel

to the mean plane [dihedral angle:  $27.013^\circ$  (148)]. The remaining three aromatic rings, bearing O2, O4, O5, respectively, are  $70.627^\circ$  (40),  $66.852^\circ$  (38), and  $62.138^\circ$  (42). The 27, 29-di-(N-benzyl-aminocarbonylmethoxyl) dihomooxalix[4]arene amide derivatives **4N** (Figure 3B) possessing the cone conformation shows some interesting similarities with **4L**. It crystallizes the monoclinic space group of C 2/c. The two benzyl groups are located at slightly longer distances but on the same side of the mean plane defined by O2, O3, O5, and O6 atoms. The dihedral angles of the four aromatic rings are  $20.904^\circ$  (71),  $78.442^\circ$  (69),  $52.4762^\circ$  (57), and  $54.069^\circ$  (59).

## Compounds 4A–4S Reduce the Viability of Cancer Cells

The cell-based assay can provide a useful tool to screen the preliminary specificity (Zhou et al., 2006). From this point, the synthesized compounds **4A–4S** were evaluated for antitumor activity against A549 cells, MCF-7 cells, HeLa cells, and HepG2 cells, as well as HUVEC cells using the SRB method. For initial screening, the single concentration inhibition of compounds **4A–4S** on cell viability at a concentration of  $10\ \mu\text{M}$  was assessed 72 h after treatment in comparison with those of reference compound **CLX-4** and the positive control (paclitaxel). The results are summarized in Table 1.

As shown in Table 1, dihomooxalix[4] arene derivative **4A**, which still maintains the original N-(2-hydroxyethyl) aminocarbonyl group of precursor **CLX-4**, is the most effective at inducing cytotoxicity in all the four tumor cell types tested with the single concentration inhibition on the four tumor cells ranging from 86 to 100%. The potency is equivalent to that of **CLX-4**. It allows us to conclude that the replacement of calix[4]arene bone with the dihomooxalix[4]arene scaffold is successful. Encouraged by it, the modification of 2-hydroxyethyl

group adjacent to the amido unit of the benzene ring is considered. Thus, a range of substituents, such as alkyl groups with straight or branched chains, alkyl benzyl, and alkyl amino substitution are introduced to the R2 position linked on the amido unit to afford 12 amide derivatives, including **4B–4D**, **4H–4P**. It is revealed that the majority of the above 12 amide derivatives demonstrate a good selectivity profile on A549 cell lines, but display the weak anti-tumor effects on hepG2 cell lines. In this series, derivative **4C** has the selective effect on HeLa cells. In a contrast, compound **4D** with much longer alkyl chain exerts the markable inhibition on all the tested tumor cells. In addition, derivatives with hydroxyethyl or alkyl amino group, e.g., **4A–4D** are particularly more effective than those of bearing alkyl unit with low polarity and hydrophilicity (**4H–4K**) or containing alkyl benzyl group with big steric hindrance (**4P**). Therefore, the inhibition efficiency of those derivatives is significantly involved in the hydrophilicity, steric hindrance, hydrogen bonding, and polarity of the R2 functional groups.

Moreover, the toxicity of those derivatives on HUVEC cells was also investigated. The result indicates that within a reasonable range, the single concentration inhibition of **4A** is 41%, though slightly higher than 18% of **CLX-4**. However, either **4C** or **4D** has much toxicity on HUVEC cell lines with inhibition of 55 and 90%, respectively. This may be due to the influence of the bare primary amino group on the side of alkyl chain. In this way, the further structural optimization was carried and the bridged derivatives **4E–4G** were afforded. As we expected, the toxicity of **4E–4G** on HUVEC cell lines is decreased with the single concentration inhibition degree varying from 16 to 42%. Meanwhile their inhibitory activity is less potent than those of **4C** and **4D**. Thus, N-2-hydroxyethyl attached to amido unit is probably vital to the activity of those compounds. To verify our assumption, one of the N-2-hydroxyethyl groups is replaced by cyclopentyl, phenethyl, or N,N-di-2-hydroxyethyl substituent to give **4Q–4S**.

In this series, compound **4Q** indicated no effect on MCF-7 cell line and indicated about two- to threefold decrease in potency of three other tumor cell lines, compared with those of **CLX-4**. Compound **4R** exerted no viability on the tested tumor cells, but had serious toxicity on HUVEC cell lines. As a contrast, compound **4S** remains a similar antitumor level activity to **CLX-4**, which is essentially in agreement with that of **4A**. The absence of significant activity in **4Q** and **4R** proved that N-2-hydroxyethyl substituent linked on the amido unit is suggested to have a significant impact on the inhibition activity.

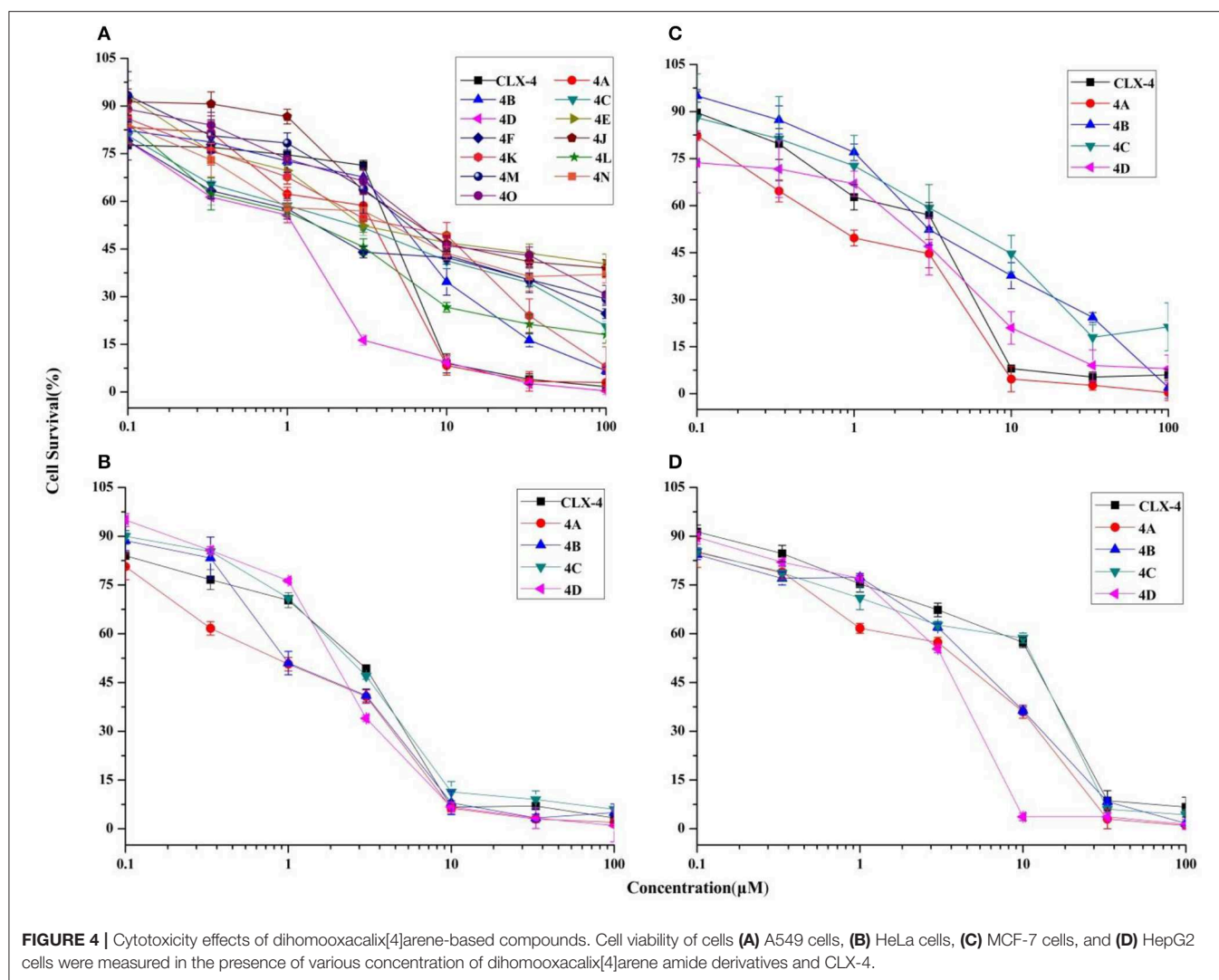
Based on the results of initial screening, the determined  $\text{IC}_{50}$  values of potent dihomooxalix[4]arene amides for tumor cell viability are measured and described in Table 2. Dose–response curves are shown in Figure 4.

Our data in Table 2 shows that almost all dihomooxalix[4]arene amides exert satisfying potency on A549 cell lines. Compounds **4A–4D** exerted potent growth inhibition against various human cancer cells with  $\text{IC}_{50}$  values ranging narrowly from 0.6 to  $8.0\ \mu\text{M}$ . In particular, **4A** demonstrates the greatest cytotoxic effect against cervical cancer (HeLa) cell line with the  $\text{IC}_{50}$  of  $0.8 \pm 0.2\ \mu\text{M}$ , which is at the

**TABLE 2** |  $\text{IC}_{50}$  values of dihomooxalix[4]arene-based compounds on tumor cells viability.

Compd.	$\text{IC}_{50}$ ( $\mu\text{M}$ )			
	A549	MCF-7	HeLa	HepG2
<b>4A</b>	$2.0 \pm 0.5$	$1.0 \pm 0.1$	$0.8 \pm 0.2$	$2.7 \pm 0.4$
<b>4B</b>	$3.9 \pm 0.5$	$4.4 \pm 0.7$	$1.1 \pm 0.5$	$3.8 \pm 0.3$
<b>4C</b>	$3.3 \pm 0.7$	$5.4 \pm 2.6$	$2.3 \pm 0.1$	$5.0 \pm 0.8$
<b>4D</b>	$0.7 \pm 0.1$	$1.8 \pm 0.7$	$1.9 \pm 0.1$	$2.6 \pm 0.2$
<b>4E</b>	$12.4 \pm 2.2$	–	–	–
<b>4F</b>	$2.9 \pm 0.7$	–	–	–
<b>4J</b>	$16.9 \pm 3.2$	–	–	–
<b>4K</b>	$4.5 \pm 1.4$	–	–	–
<b>4L</b>	$1.7 \pm 0.4$	–	–	–
<b>4M</b>	$10.1 \pm 1.8$	–	–	–
<b>4N</b>	$6.8 \pm 0.5$	–	–	–
<b>4O</b>	$12.6 \pm 2.0$	–	–	–
<b>CLX-4</b>	$2.8 \pm 0.3$	$2.1 \pm 0.4$	$1.9 \pm 0.2$	$6.6 \pm 0.8$

"N.T." means no tested.



level of submicromolar concentration. Overall, **4A** and **4D** show enhanced potency over the cytotoxicity profiles (2- to 4-fold) of **CLX-4**, suggesting that our structural optimization is successful.

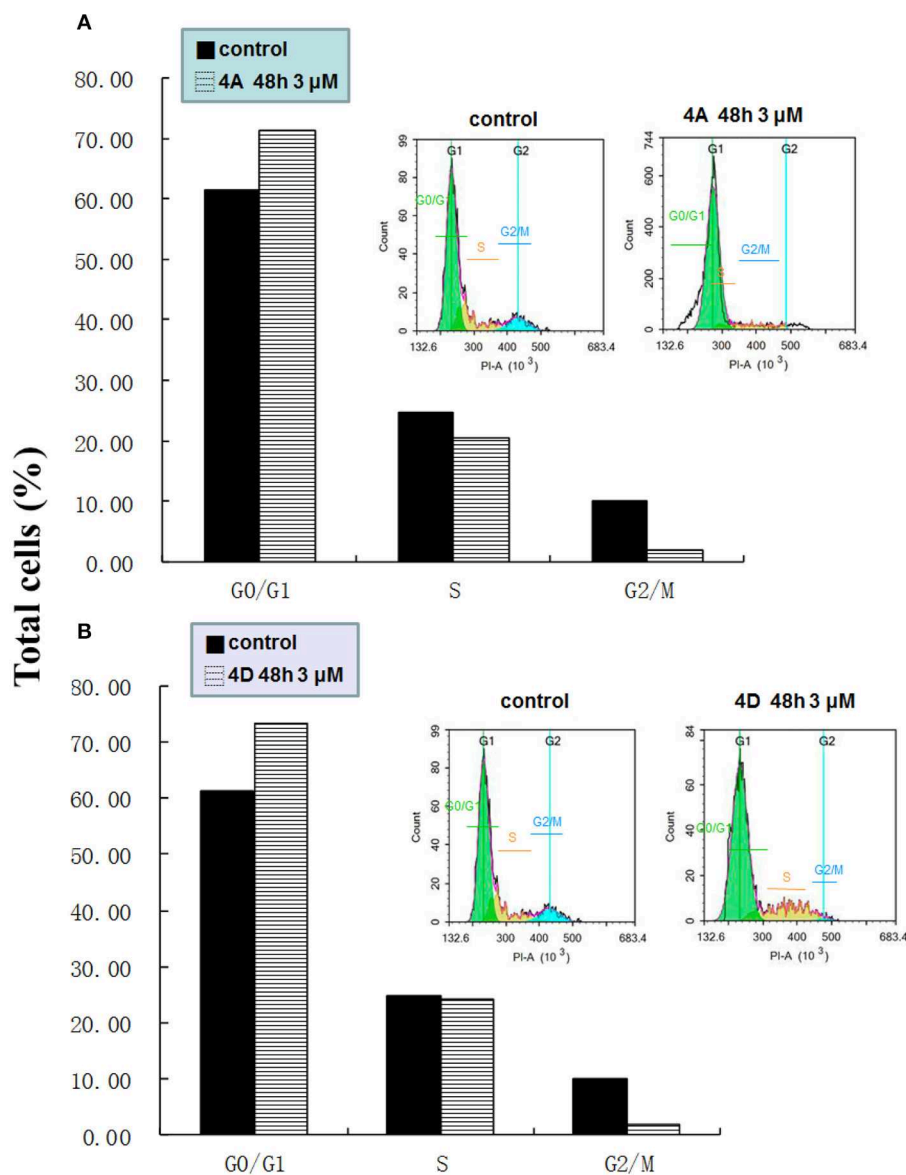
## Flow Cytometry for MCF-7 Cell Cycle and Apoptosis Analysis

Cancer progression has been suggested to include the loss of cell cycle checkpoint controls that regulate passage through the cell cycle (Pelizzarorocha et al., 2013; Ji et al., 2017). According to the literatures, Dings and co-workers (Dings et al., 2013) have revealed that calixarene amine derivative **PTX013** had good cytotoxicity to cancer cells and blockades the cell cycle of SQ20B at G0/G1 phase. In addition, Pelizzarorocha et al. (2013) found that *tert*-butyl calix[6]arenes can cause cell cycle arrest in G0/G1 phase by down-regulating key proteins, such as PIM1, CDK2, and CDK4. To have an insight into the underlying mechanism of cytotoxic effects *in vitro*, the key indicators including the cell cycle and apoptosis were observed by the flow cytometry analysis. We first tested if treatment with **4A** or **4D** affects the cell cycle of MCF-7 cells. The results are shown in Figure 5.

As exemplified with MCF-7 cells in Figure 5A, the percentage of non-treated cells was  $61.36 \pm 3.65\%$  in G0/G1 phase,  $24.69 \pm 6.30\%$  in S, and  $10.06 \pm 0.91$  in G2/M phase, whereas after the treatment with **4A** at a low concentration ( $3 \mu\text{M}$ ) for 48 h, MCF-7 cells led to an accumulation number of cells in G0/G1 phase of the cell cycle and the percentage was increased to  $71.39 \pm 11.21\%$ , whereas it correspondingly reduced to  $20.68 \pm 13.12\%$  and  $1.87 \pm 2.45\%$ , respectively, in S and G2/M phase. A similar profile in the cells treated with  $3 \mu\text{M}$  **4D** was supported by the  $73.56 \pm 3.95\%$  of cells in the G0/G1 phase, as observed in Figure 5B.

Next, we measured the apoptotic rate of MCF-7 cells at different concentrations of treatment to detect whether **4A** and **4D** can induce apoptosis. As shown in Figure 6, during treatment of MCF-7 cells for 48 h with 1 and  $3 \mu\text{M}$  of **4A**,  $19.63 \pm 0.11\%$  and  $15.40 \pm 0.13\%$  apoptotic rates are given by the contrast of  $14.50 \pm 0.68\%$  in the non-treated group, which suggests that 1 or  $3 \mu\text{M}$  of **4A** is not enough to induce apoptosis in MCF-7 cells. Subsequently, treatment of MCF-7 cells with  $10 \mu\text{M}$  of **4A** resulted in the progressive apoptotic





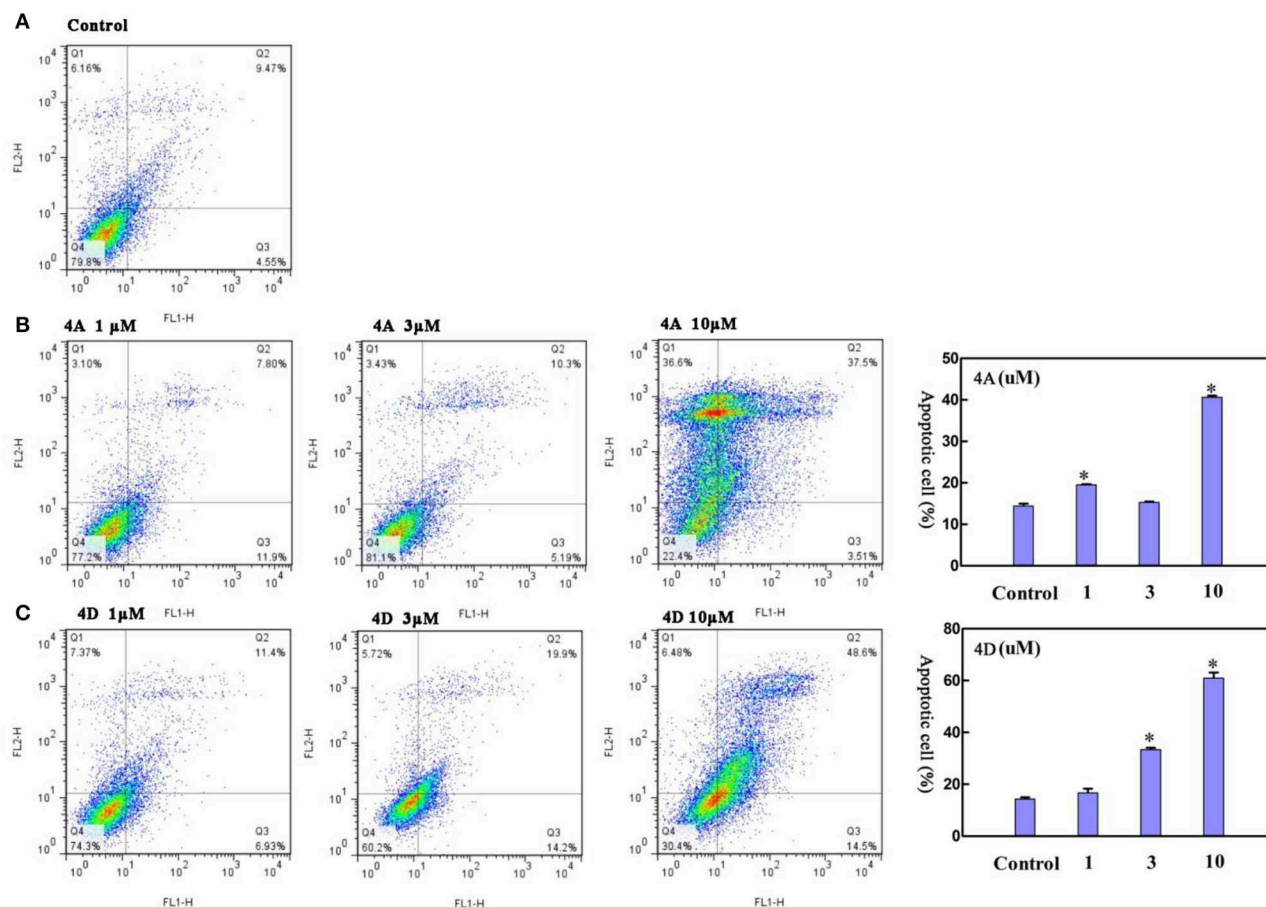
**FIGURE 5 |** Effect of **4A** and **4D** on the cell cycle of MCF-7 cells. Flow cytometric analyses of MCF-7 cells show that **4A** (A), **4D** (B) treatment induces G0/G1 arrest in MCF-7.

rate of  $40.74 \pm 0.38\%$ . This proliferation is also observed after the treatment of 4D at concentrations of 3 and  $10 \mu\text{M}$ , supported by apoptotic rates of  $33.55 \pm 0.78\%$  and  $61.15 \pm 2.76\%$  (Figure 6C). Therefore, we conclude that both 4A and 4D can induce cell apoptosis in MCF-7 cells as well as cell cycle arrest in G0/G1 phase.

## CONCLUSION

In summary, this study describes the optimization of the anti-tumor agent CLX-4 by employing the drug design strategies, X-ray crystallography, and cell-based screening. With

the comparison to CLX-4, dihomooxalix[4]arene derivative 4A demonstrates the much more efficient cytotoxic effect against the MCF-7 and HeLa cell lines with  $\text{IC}_{50}$  of  $1.0 \pm 0.1 \mu\text{M}$  and  $0.8 \pm 0.2 \mu\text{M}$ , respectively. Derivative 4D has an  $\text{IC}_{50}$  of  $0.7 \pm 0.1 \mu\text{M}$  against A549 cell lines, but failed due to the high toxicity on HUVEC cell lines. The underlying mechanism of cytotoxic effects indicates that they can induce the MCF-7 cell cycle arrest in G0/G1 phase and cell apoptosis. In this context, it is also important to note that we provide a new look into drug discovery by using the old supramolecular scaffold to design potent anti-tumor agents.



**FIGURE 6 |** Effect of **4A** and **4D** on apoptosis in MCF-7 cells. Flow cytometric analyses of MCF-7 cells after Annexin IV staining show that compared to controls (**A**), **4A** exposure (**B**) and **4D** exposure (**C**) result in apoptosis in MCF-7 cells in a concentration. Data are reported as mean  $\pm$  SD. \* $P < 0.001$ , compared to the control group.

## DATA AVAILABILITY STATEMENT

The detailed spectroscopic data including crystallographic data (CIF) of compounds are available. Single crystal data for compounds **4L** and **4N** have been deposited in the Cambridge Crystallographic Data Center and assigned to deposition numbers CCDC 1915578 and 1569156. All datasets generated for this study are included in the article/**Supplementary Material**.

## AUTHOR CONTRIBUTIONS

LA and CY designed the work. LH, CW, and JL made contributions to the experiments and collective data. The paper was written by LA. YZ, TH, and JS provide the technical

support. All authors extensively discussed the results, reviewed the manuscript, extensively discussed the results, reviewed the manuscript, and approved the final version of the manuscript to be submitted.

## FUNDING

This work was financially supported by the National Natural Science Foundation of China (Nos. 81202490 and 21871227).

## SUPPLEMENTARY MATERIAL

The Supplementary Material for this article can be found online at: <https://www.frontiersin.org/articles/10.3389/fchem.2019.00856/full#supplementary-material>

## REFERENCES

- Ali, Y., Muhamad Bunnori, N., Susanti, D., Muhammad Alhassan, A., and Abd Hamid, S. (2018). Synthesis, *in-vitro* and *in silico* studies of azo-based calix[4]arenes as antibacterial agent and neuraminidase inhibitor: a new look into an old scaffold. *Front. Chem.* 6, 210–219. doi: 10.3389/fchem.2018.00210
- An, L., Han, L. L., Zheng, Y. G., Peng, X. N., Xue, Y. S., Gu, X. K., et al. (2016). Synthesis, x-ray crystal structure and anti-tumor activity of calix[n]arene polyhydroxyamine derivatives. *Eur. J. Med. Chem.* 123, 21–30. doi: 10.1016/j.ejmech.2016.07.016
- An, L., Wang, J. W., Wang, C., Zhou, S. S., Sun, J., and Yan, C. G. (2018). 2, 3-Ethylene-bridged dihomooxacalix [4] arenes: synthesis, X-ray crystal structures and highly selective binding properties with anions. *New J. Chem.* 42, 10689–10696. doi: 10.1039/C8NJ01284A
- Bauer, D., Andrae, B., Gaß, P., Trenz, D., Becker, S., and Kubik, S. (2019). Functionalizable acyclic cucurbiturils. *Org. Chem. Front.* 6, 1555–1560. doi: 10.1039/C9QO00156E
- Böhmer, V. (2010). Calixarenes, macrocycles with (almost) unlimited possibilities. *Angew. Chem, Int. Ed. Engl.* 34, 713–745. doi: 10.1002/anie.199507131
- Chen, J., Wang, Y., Wang, C., Long, R., Chen, T., and Yao, Y. (2019). Functionalization of inorganic nanomaterials with pillar [n] arenes. *Chem. Comm.* 55, 6817–6826. doi: 10.1039/C9CC03165K
- Consoli, G. M., Cunsolo, F., Geraci, C., and Sgarlata, V. (2004). Synthesis and lectin binding ability of glycosamino acid-calixarenes exposing GlcNAc clusters. *Org. Lett.* 6, 4163–4166. doi: 10.1021/ol0485767
- Consoli, G. M. L., Granata, G., Picciotto, R., Blanco, A. R., Geraci, C., Marino, A., et al. (2018). Design, synthesis and antibacterial evaluation of a polycationic calix[4]arene derivative alone and in combination with antibiotics. *Med. Chem. Commun.* 9, 160–164. doi: 10.1039/C7MD00527J
- Da Silva, E., Lazar, A. N., and Coleman, A. W. (2004). Biopharmaceutical applications of calixarenes. *J. Drug. Deliv. Sci. TEC.* 14, 3–20. doi: 10.1016/S1773-2247(04)50001-1
- Dings, R. P., Levine, J. I., Brown, S. G., Astorguesxerri, L., Macdonald, J. R., Hoyer, T. R., et al. (2013). Polycationic calixarene ptx013, a potent cytotoxic agent against tumors and drug resistant cancer. *Invest. New Drugs* 31, 1142–1150. doi: 10.1007/s10637-013-9932-0
- Dings, R. P., Miller, M. C., Nesmelova, I., Astorguesxerri, L., Kumar, N., Serova, M., et al. (2012b). Antitumor agent calixarene 0118 targets human galectin-1 as an allosteric inhibitor of carbohydrate binding. *J. Med. Chem.* 55, 5121–5129. doi: 10.1021/jm300014q
- Dings, R. P. M., Levine, J. I., Astorgues-Xerri, L., Kumar, N., Serova, M., Macdonald, J., et al. (2012a). 568 design of ptx008 that allosterically targets galectin-1 to inhibit tumor growth in mice. *Eur. J. Cancer* 48, 174–174. 10.1016/S0959-8049(12)72365-1 doi: 10.1016/S0959-8049(12)72365-1
- Flink, S., and Reinhoudt, D. N. (1999). Recognition of cations by self-assembled monolayers of crown ethers. *J. Phys. Chem. B* 103, 6515–6520. doi: 10.1021/jp990014v
- Gaeta, C., Talotta, C., Farina, F., Teixeira, F. A., Marcos, P. M., Ascenso, J. R., et al. (2012). Alkylammonium cation complexation into the narrow cavity of Dihomooxacalix [4] arene macrocycle. *J. Org. Chem.* 77, 10285–10293. doi: 10.1021/jo3019945
- Geraci, C., Consoli, G. M., Galante, E., Bousquet, E., Pappalardo, M., and Spadaro, A. (2008). Calix[4]arene decorated with four Tn antigen glycomimetic units and P<sub>3</sub>CS immunoadjuvant: synthesis, characterization, and anticancer immunological evaluation. *Bioconjugate Chem.* 19, 751–758. doi: 10.1021/bc700411w
- Gómez-Machuca, H., Quiroga-Campano, C., Jullian, C., Fuente, J. D., Pessoa-Mahana, H., Escobar, C. A., et al. (2014). Study by fluorescence of calix[4]arenes bearing heterocycles with anions: highly selective detection of iodide. *J. Incl. Phenom. Macrocycl. Chem.* 80, 369–375. doi: 10.1007/s10847-014-0418-2
- Granata, G., Paterniti, I., Geraci, C., Cunsolo, F., Esposito, E., Cordaro, M., et al. (2017). Potential eye drop based on a calix [4] arene nanoassembly for curcumin delivery: Enhanced drug solubility, stability, and anti-inflammatory effect. *Mol. Pharmacol.* 14, 1610–1622. doi: 10.1021/acs.molpharmaceut.6b01066
- Guo, S., Song, Y., He, Y., Hu, X. Y., and Wang, L. (2018). Highly efficient artificial light-harvesting systems constructed in aqueous solution based on supramolecular self-assembly. *Angew. Chem. Int. Ed.* 57, 3163–3167. doi: 10.1002/anie.201800175
- Gutsche, C. D., Dhawan, B., No, K. H., and Muthukrishnan, R. (1981). Calixarenes. 4. The synthesis, characterization, and properties of the calixarenes from p-tert-butylphenol. *J. Am. Chem. Soc.* 103, 3782–3792. doi: 10.1021/ja00403a028
- Harris, S. J. (1995). *Calixarene-Based Compounds Having Antibacterial, Antifungal, Anticancer-HIV Activity. WO Patent No 95/19974*. Geneva: World Intellectual Property Organization International Bureau.
- Hu, X. Y., Zhang, P., Xuan, W., Wei, X., Xiao, T., Jiang, J., et al. (2012). Pillar[5]arene-based supramolecular polypseudorotaxanes constructed from quadruple hydrogen bonding. *Polymer Chem.* 3, 3060–3063. doi: 10.1039/c2py20285a
- Hulíková, K., Grobárová, V., Krivohlavá, R., and Fišerová, A. (2010). Antitumor activity of N-acetyl-D-glucosamine-substituted glycoconjugates and combined therapy with keyhole limpet hemocyanin in B16F10 mouse melanoma model. *Folia Microbiol.* 55, 528–532. doi: 10.1007/s12223-010-0087-5
- Hussain, M. A., Ashraf, M. U., Muhammad, G., Tahir, M. N., and Bukhari, S. N. A. (2017). Calixarene: a versatile material for drug design and applications. *Current Pharm. Design.* 23, 2377–2388. doi: 10.2174/1381612822666160928143328
- Ji, S., Tang, S., Li, K., Li, Z., Liang, W., Qiao, X., et al. (2017). Licoricidin inhibits the growth of sw480 human colorectal adenocarcinoma cells, *in vitro*, and, *in vivo*, by inducing cycle arrest, apoptosis and autophagy. *Toxicol. Appl. Pharm.* 326, 25–33. doi: 10.1016/j.taap.2017.04.015
- Kim, K., Selvapalam, N., Ko, Y. H., Park, K. M., Kim, D., and Kim, J. (2007). Functionalized cucurbiturils and their applications. *Cheminform* 36, 267–279. doi: 10.1039/B603088M
- Koonce, N. A., Griffin, R. J., Dings, R. P. M. (2017). Galectin-1 inhibitor otx008 induces tumor vessel normalization and tumor growth inhibition in human head and neck squamous cell carcinoma models. *Int. J. Mol. Sci.* 18, 2671–2679. doi: 10.3390/ijms18122671
- Kralj, M., Tusekbožić, L., and Frkanec, L. (2008). Biomedical potentials of crown ethers: prospective antitumor agents. *Chemmedchem* 3, 1478–1492. doi: 10.1002/cmdc.200800118
- Läppchen, T., Dings, R. P. M., Rossin, R., Simon, J. F., Visser, T. J., Bakker, M., et al. (2015). Novel analogs of antitumor agent calixarene 0118: Synthesis, cytotoxicity, click labeling with 2-[18F] fluoroethylazide, and *in vivo* evaluation. *Eur. J. Med. Chem.* 89, 279–295. doi: 10.1016/j.ejmech.2014.10.048
- Lee, J. W., Samal, S., Selvapalam, N., Kim, H. J., and Kim, K. (2003). Cucurbituril homologues and derivatives: new opportunities in supramolecular chemistry. *Cheminform* 34, 621–630. doi: 10.1021/ar020254k
- Lehn, J. (1988). Supramolecular chemistry—scope and perspectives molecules, supermolecules, and molecular devices (nobel lecture). *Angew. Chem. Int. Ed.* 27, 89–112. doi: 10.1002/anie.198800891
- Li, D. H., Hu, P., Xu, S. T., Fang, C. Y., Tang, S., Wang, X. Y., et al. (2017). Lasiokaurin derivatives: synthesis, antimicrobial and antitumor biological evaluation, and apoptosis-inducing effects. *Arch. Pharm. Res.* 40, 796–806. doi: 10.1007/s12272-016-0867-9
- Liu, Y., Sun, J., and Yan, C. G. (2017). Synthesis and crystal structures of p-tert-butylidihomooxacalix [4] arene mono-Schiff bases. *J. Incl. Phenom. Macrocycl. Chem.* 87, 157–166. doi: 10.1007/s10847-016-0687-z
- Liu, Y., Zhao, L. L., Sun, J., and Yan, C. G. (2018). Convenient synthesis and coordination properties of p-tert-butylidihomooxacalix[4]arene mono-schiff bases. *Polycycl. Aromat. Comp.* 5, 1–16. doi: 10.1080/10406638.2018.1469520
- Ludwig, R., and Dzung, N. T. K. (2002). Calixarene-based molecules for cation recognition. *Sensors* 22, 397–416. doi: 10.3390/s21000397

- Marcos, P. M., Félix, S., Ascenso, J. R., Segurado, M. A., Mellah, B., Abidi, R., et al. (2006). Complexation and transport of alkali and alkaline earth metal cations by p-tert-butylidihomooxacalix [4] arene tetraketone derivatives: erratum. *Supramol. Chem.* 18, 285–297. doi: 10.1080/10610270600773006
- Marcos, P. M., Teixeira, F. A., Segurado, M. A., Ascenso, J. R., Bernardino, R. J., Michel, S., et al. (2014). Bidentate urea derivatives of p-tert-butylidihomooxacalix [4] arene: neutral receptors for anion complexation. *J. Org. Chem.* 79, 742–751. doi: 10.1021/jo4026012
- Motornaya, A. E., Alimbarova, L. M., Shokova, E. A., and Kovalev, V. V. (2006). Synthesis and antihypertensive activity of N-(3-amino-1-adamantyl) calix [4] arenes. *Pharm. Chem. J.* 40, 68–72. doi: 10.1007/s11094-006-0060-4
- Mourer, M., Psychogios, N., Laumond, G., Aubertin, A. M., and Regnouf-de-Vains, J. B. (2010). Synthesis and anti-HIV evaluation of water-soluble calixarene-based bithiazolyl podands. *Bioorg. Med. Chem.* 18, 36–45. doi: 10.1016/j.bmc.2009.11.016
- Muneer, S., Memon, S., Pahnwar, Q. K., Bhatti, A. A., and Khokhar, T. S. (2017). Synthesis and investigation of antimicrobial properties of pyrrolidine appended calix [4] arene. *J. Anal. Sci. Technol.* 8, 3–8. doi: 10.1186/s40543-017-0111-3
- Mutihac, L., Lee, J. H., Kim, J. S., and Vican, J. (2011). Recognition of amino acids by functionalized calixarenes. *Chem. Soc. Rev.* 40, 2777–2796. doi: 10.1039/c0cs00005a
- Naseer, M. M., Ahmed, M., and Hameed, S. (2017). Functionalized calix[4]arenes as potential therapeutic agents, *Chem. Biol. Drug Des.* 89, 243–256. doi: 10.1111/cbdd.12818
- Nasuhi Pur, F., and Dilmaghani, K. A. (2014). Calixplatin: novel potential anticancer agent based on the platinum complex with functionalized calixarene. *J. Coord. Chem.* 67, 440–448. doi: 10.1080/00958972.2014.890718
- Neagu, M., Ion, R. M., Manda, G., Constantin, C., Radu, E., and Cristu, Z. (2010). Antitumoral effect of calixarenes in experimental photodynamic therapy with K562 tumor cell line. *Rom. J. Biochem.* 47, 17–35.
- Patra, S., Boricha, V. P., and Paul, P. (2019). Dual-mode calixarene-based chemosensor: highly selective fluorogenic detection of  $Hg^{2+}$  and chromogenic detection of  $Cu^{2+}$  with a single ionophore. *Eur. J. Inorg. Chem.* 2019, 199–205. doi: 10.1002/ejic.201800925
- Paz, H., Joo, E. J., Chou, C. H., Fei, F., Mayo, K. H., and Abdel-Azim, H. (2018). Treatment of B-cell precursor acute lymphoblastic leukemia with the Galectin-1 inhibitor PTX008. *J. Exp. Clin. Cancer Res.* 37, 67–91. doi: 10.1186/s13046-018-0721-7
- Pelizarorocha, K. J., de Jesus, M. B., Rueladesousa, R. R., Nakamura, C. V., Reis, F. S., de Fátima, A., et al. (2013). Calix[6]arene bypasses human pancreatic cancer aggressiveness: downregulation of receptor tyrosine kinases and induction of cell death by reticulum stress and autophagy. *Biochim Biophys Acta.* 1833, 2856–2865. doi: 10.1016/j.bbamer.2013.07.010
- Quan, H., Liu, H., Li, C., and Lou, L. (2009). 1,4-diamino-2,3-dicyano-1,4-bis(methylthio)butadiene (u0126) enhances the cytotoxicity of combretastatin a4 independently of mitogen-activated protein kinase kinase. *J. Pharmacol. Exp. Ther.* 330, 326–333. doi: 10.1124/jpet.109.153320
- Sansone, F., Baldini, L., Casnati, A., and Ungaro, R. (2008). Conformationally mobile glucosylthioureidocalix [6]-and calix[8]arenes: Synthesis, aggregation and lectin binding. *Supramol. Chem.* 20, 161–168. doi: 10.1080/10610270701777344
- Shah, R. B., Valand, N. N., Sutariya, P. G., and Menon, S. K. (2016). Design, synthesis and characterization of quinoline–pyrimidine linked calix [4] arene scaffolds as anti-malarial agents. *J. Inclusion Phenom. Macro. Chem.* 84, 173–178. doi: 10.1007/s10847-015-0581-0
- Sheldrick, G. M. (1997). *SHELXS-97 and SHELXL-97*. Gottingen: University of Gottingen.
- Soares, M. N. Jr., Gáscón, T. M., Fonseca, F. L., Ferreira, K. S., and Bagatin, I. A. (2014). Evaluation of the biological effects of 5-Cl-8-oxyquinolinepropoxycalix [4] arene and 8-oxyquinolinepropoxycalix [4] arene *in vitro* and *in vivo*. *J. Mater. Sci. Eng. C-Mater.* 40, 260–266. doi: 10.1016/j.msec.2014.04.002
- Stella, V. J., and He, Q. (2008). Cyclodextrins. *Toxicol. Pathol.* 36, 30–42. doi: 10.1177/0192623307310945
- Sun, G., Pu, L., Pangannaya, S., Xiao, T., Hu, X. Y., Jiang, J., et al. (2019).  $\beta$ -D-galactose-functionalized pillar [5] arene with interesting planar-chirality for constructing chiral nanoparticles. *Front. Chem.* 7:743. doi: 10.3389/fchem.2019.00743
- Sun, J., Liu, D. M., Wang, J. X., and Yan, C. G. (2009a). Regioselective synthesis of calix [4] arene 1, 3-di-and monosubstituted sulfur-containing Schiff bases. *J. Incl. Phenom. Macro. Chem.* 64, 317–324. doi: 10.1007/s10847-009-9570-5
- Sun, J., Liu, D. M., and Yan, C. G. (2009b). Transition metal complexes of bidentate p-tert-butylcalix [4] arene S-alkyldithio carbazate Schiff bases. *J. Coord. Chem.* 62, 2337–2346. doi: 10.1080/00958970902818208
- Sun, S., Geng, M., Huang, L., Chen, Y., and Yao, Y. (2018). A new amphiphilic pillar[5]arene: synthesis, controllable self-assembly in water and application in white-light-emitting system. *Chem. Commun.* 54, 13006–13009. doi: 10.1039/C8CC07658H
- Talotta, C., Gaeta, C., De Rosa, M., Ascenso, J. R., Marcos, P. M., and Neri, P. (2016). Alkylammonium guest induced-fit Recognition by a flexible dihomooxacalix [4] arene derivative. *Eur. J. Org. Chem.* 2016, 158–167. doi: 10.1002/ejoc.201501319
- Valle, E. M. D. (2004). Cyclodextrins and their uses: a review. *Process Biochem.* 39, 1033–1046. doi: 10.1016/S0032-9592(03)00258-9
- Viola, S., Consoli, G. M., Merlo, S., Drago, F., Sortino, M. A., and Geraci, C. (2010a). Inhibition of rat glioma cell migration and proliferation by a calix[8]arene scaffold exposing multiple glcnac and ureido functionalities. *NeuroChem.* 107, 1047–1055. doi: 10.1111/j.1471-4159.2008.05656.x
- Viola, S., Merlo, S., Consoli, G. M., Drago, F., Geraci, C., and Sortino, M. A. (2010b). Modulation of C6 glioma cell proliferation by ureido-calix[8]arenes. *Pharmacology* 3, 182–188. doi: 10.1159/000317518
- Yokoyama, T., and Mizuguchi, M. (2019). Crown ethers as transthyretin amyloidogenesis inhibitors. *J. Med. Chem.* 62, 2076–2082. doi: 10.1021/acs.jmedchem.8b01700
- Yousaf, A., Hamid, S. A., Bunnori, N. M., and Ishola, A. A. (2015). Applications of calixarenes in cancer chemotherapy: facts and perspectives. *Drug Design, Dev. Therapy.* 9, 2831–2838. doi: 10.2147/DDDT.S83213
- Zadmard, R., and Alavijeh, N. S. (2014). Protein surface recognition by calixarenes. *RSC Advances* 4, 41529–41542. doi: 10.1039/C4RA05181E
- Zhang, R., Wang, C., Long, R., Chen, T., Yan, C., and Yao, Y. (2019). Pillar[5]arene based [1]rotaxane systems with redox-responsive host-guest property: design, synthesis and the key role of chain length. *Front. Chem.* 7:508. doi: 10.3389/fchem.2019.00508
- Zhang, Y. M., Xu, Q. Y., and Liu, Y. (2019). Molecular recognition and biological application of modified  $\beta$ -cyclodextrins. *Sci. Chin.* 62, 1–12. doi: 10.1007/s11426-018-9405-3
- Zhou, H., Wang, D. A., Baldini, L., Ennis, E., Jain, R., Carie, A., et al. (2006). Structure-activity studies on a library of potent calix[4]arene-based PDGF antagonists that inhibit PDGF-stimulated PDGFR tyrosine phosphorylation. *Org. Biomol. Chem.* 4, 2376–2386. doi: 10.1039/B515483A
- Zhou, J., Yu, G., and Huang, F. (2017). Supramolecular chemotherapy based on host–guest molecular recognition: a novel strategy in the battle against cancer with a bright future. *Chem. Soc. Rev.* 46, 7021–7053. doi: 10.1039/C6CS00898D

**Conflict of Interest:** The authors declare that the research was conducted in the absence of any commercial or financial relationships that could be construed as a potential conflict of interest.

Copyright © 2019 An, Wang, Han, Liu, Huang, Zheng, Yan and Sun. This is an open-access article distributed under the terms of the Creative Commons Attribution License (CC BY). The use, distribution or reproduction in other forums is permitted, provided the original author(s) and the copyright owner(s) are credited and that the original publication in this journal is cited, in accordance with accepted academic practice. No use, distribution or reproduction is permitted which does not comply with these terms.





# Smart Molecular Recognition: From Key-to-Lock Principle to Memory-Based Selectivity

Askar K. Gatiatulin, Marat A. Ziganshin and Valery V. Gorbachuk\*

Department of Physical Chemistry, A. M. Butlerov Institute of Chemistry, Kazan Federal University, Kazan, Russia

The formation and decomposition of inclusion compounds with a solid-solid phase transition may be very selective to the guest molecular structure. This selectivity may function in essentially different ways than defined by the classical concept of molecular recognition, which implies the preferential binding of complementary molecules. Solid inclusion compounds may take part as an initial or/and final state in several processes of different types summarized in this review, which selectivity is boosted by cooperativity of participating molecular crystals. Some of these processes resemble switching electronic devices and can be called smart giving practically absolute molecular recognition.

## OPEN ACCESS

### Edited by:

Yong Yao,  
Nantong University, China

### Reviewed by:

Pi Wang,  
Taiyuan University of  
Technology, China  
Lin An,  
Xuzhou Medical University, China

### \*Correspondence:

Valery V. Gorbachuk  
valery.gorbachuk@kpfu.ru

### Specialty section:

This article was submitted to  
Supramolecular Chemistry,  
a section of the journal  
Frontiers in Chemistry

**Received:** 27 November 2019

**Accepted:** 23 December 2019

**Published:** 21 January 2020

### Citation:

Gatiatulin AK, Ziganshin MA and  
Gorbachuk VV (2020) Smart  
Molecular Recognition: From  
Key-to-Lock Principle to  
Memory-Based Selectivity.  
Front. Chem. 7:933.  
doi: 10.3389/fchem.2019.00933

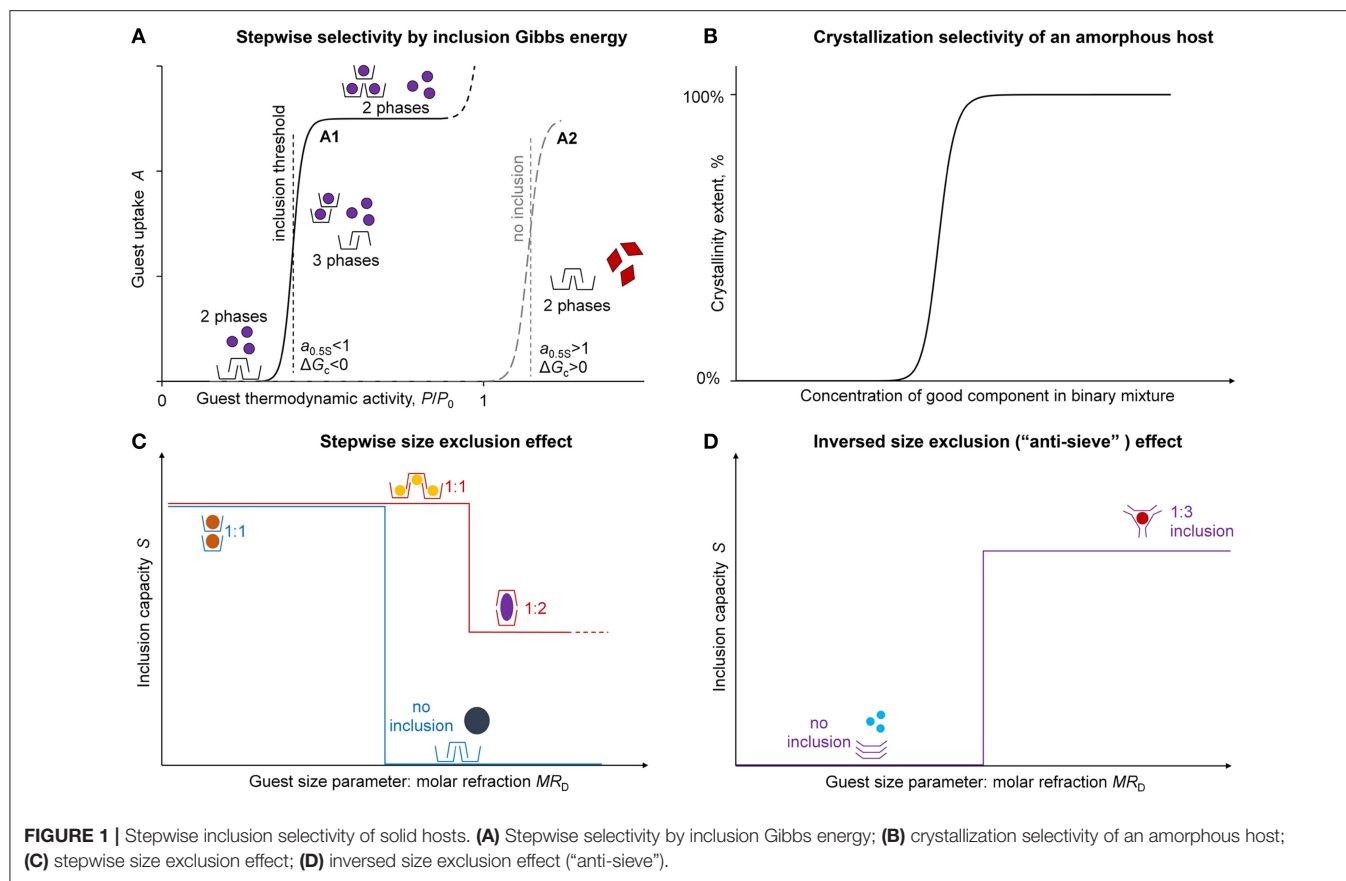
**Keywords:** molecular recognition, selectivity, inclusion compound, clathrate, phase transition

## INTRODUCTION

Molecular recognition of neutral molecules is one of the key problems in chemical technologies and in analytical and biotechnological applications (Reinhoudt, 2013; Persch et al., 2015; Shu et al., 2018). To reach a sufficient selectivity, host compounds with very complex structure are synthesized (Ariga et al., 2012; Zhang et al., 2019) to fit the well-known key-to-lock concept of molecular recognition formulated by Fischer (1894). This concept later developed in supramolecular chemistry is based on complementarity of two interacting molecules, where the host interacts with guest cooperatively through several more or less strong coordinate, donor-acceptor, and hydrogen bonds having a specific spatial arrangement (Joyce et al., 2010; Sonnenberg et al., 2012). The most studies of molecular recognition are conducted in liquid solutions (Ariga et al., 2012; Persch et al., 2015; Shu et al., 2018; Zhang et al., 2019) and perform a sufficient selectivity only if guest forms at least two such bonds with host (Yao et al., 2018).

This review describes the possible alternatives to the classical key-to-lock principle with a higher selectivity of molecular recognition. These alternatives are based on cooperativity of phase transitions, which adds up the small differences in molecular structure of different included guests. Some of the described recognition principles can be called smart because they resemble the function of electronic devices.

Quantitatively, the cooperativity of phase transition at guest inclusion by solid host can be seen in a stepwise sigmoidal shape of guest sorption isotherm (Gorbachuk et al., 1997a; Dewa et al., 1998). According to the Gibbs phase rule, a sorption isotherm in system with two independent components (guest and host) should have a threshold concentration, vapor pressure or thermodynamic activity of guest corresponding to formation of three phases of guest, host, and clathrate (inclusion compound) at constant temperature, **Figure 1A** (Gorbachuk et al., 2002). Below this threshold activity, the guest is not included, and below and above this threshold the composition of the solid phase does not change.



In solid state, this phase transition is observed if the initial host is non-porous (Gorbachuk et al., 2002). If the host has a permanent porosity combined with flexible structure, like that of some metal organic frameworks (MOFs) (Hiraide et al., 2016; Engel et al., 2017) or silicalites (DeJaco et al., 2019), the initial part of sorption isotherm may have the shape of Langmuir isotherm followed by a sigmoidal step. This step is called the gate-opening or breathing (Afonso et al., 2012; Lee et al., 2019). A similar cooperative phenomena were observed for biological objects, e.g., for oxygen binding by aqueous solution of hemoglobin (Yuan et al., 2015).

The sigmoidal isotherms of guest inclusion by solid host and related cooperativity of guest release from the inclusion compound may boost the selectivity of these processes. Depending on the initial and final states of host, several specific types of selectivity may be observed, which are described in this review.

## CRYSTALLIZATION SELECTIVITY OF AMORPHOUS HOST

Selectivity of guest inclusion may be visualized if the initial state of host is amorphous. The amorphous state is a high-energy state, so its transition to the crystalline state may be spontaneous (Faizullin et al., 2019). The activation of this process with guest vapors may be selective. Such selectivity was observed visually for a compact glass of calixarene (Gataullina et al., 2015, 2017) and

using an atomic force microscopy for thin amorphous films of dipeptides (Ziganshin et al., 2015). Amorphous dipeptides may have three options in contact with guest vapors depending on the guest molecular structure: (1) crystallization, (2) gel formation, (3) intact host morphology (Ziganshin et al., 2017).

The amorphous calixarenes in the form of a compact transparent glass can be used to detect visually the composition of a binary guest mixture, where only one (good) component has an ability to induce the host crystallization. The mixture should have the concentration of this guest above a certain threshold value for this crystallization to be apparent, **Figure 1B**. For example, glassy *tert*-butylthiacalix[4]arene derivative crystallizes in contact with vapors of the aqueous solution of ethanol if its concentration is above 24 vol.% (Gataullina et al., 2015). The glass of the same calixarene in another conformation allows detecting 1% vol. of benzene in hexane (Gataullina et al., 2017). A similar crystallization behavior was observed for glassy polymers (Gao et al., 2012), which have a less pronounced concentration threshold for the good component in binary solvent due to the incomplete crystallization.

## SELECTIVITY BY CAPACITY AND GIBBS ENERGY OF GUEST INCLUSION

The guest inclusion by the host with the phase transition complicates much the structure-property relationships for this process. The related selectivity can be described using

approximation parameters of sigmoidal isotherms of guest inclusion, **Figure 1A**. These isotherms may be fitted with Hill equation adjusted to “guest uptake  $A$  vs. relative vapor pressure  $P/P_0$ ” coordinates (Gorbachuk et al., 1997a):

$$A = SC(P/P_0)^N/[1 + C(P/P_0)^N] \quad (1)$$

where  $S$  is guest contents in a saturated inclusion compound (clathrate) in mol of guest per 1 mol of host,  $C$  is a sorption constant,  $N$  is a cooperativity parameter, which in ideal case of phase transition should have an infinitely high value,  $N \rightarrow \infty$ . The integration of sigmoidal sorption isotherms fitted by this equation gives the inclusion Gibbs energy  $\Delta G_c$  of guest transfer from its pure liquid or solid state to the saturated inclusion compound (Gorbachuk et al., 1999a):

$$\Delta G_c = RT \int_0^1 \ln(P/P_0) dY \quad (2)$$

$$\Delta G_c = RT \ln a_{0.5S} = -RT (\ln C)/N \quad (3)$$

Here  $Y = A/S$  is the extent of host saturation with guest,  $a_{0.5S}$  is the guest activity  $P/P_0$  at  $Y = 0.50$ .

The thermodynamics defined by Equations (1–3) means the stepwise selectivity of guest inclusion. If two guests have very small difference in molecular structure, but the first guest has sorption constant  $C$  slightly below unity and for the second one this parameter should be slightly above this level, only the first guest will be included, **Figure 1A**. As a result, a high selectivity of guest inclusion may be observed discriminating the close homologs. For example, *tert*-butylthiacalix[4]arene includes methanol from the vapor phase, but not ethanol (Galyaltidinov et al., 2012).

The same inclusion thermodynamics may produce a stepwise change in the guest inclusion capacity  $S$  at the variation of the guest molecular structure, **Figure 1C**. A good example is *tert*-butylcalix[4]arene including a lot of guests inside its molecular cavity (Ripmeester et al., 2006) with a regular stepwise size exclusion effect between the inclusion capacity  $S$  and guest molar refraction  $MR_D$ , which is a good molecular size parameter (Gorbachuk et al., 1999b). The exclusions are the guests, which can break the host intramolecular cyclic H-bond, like 1-butylamine (Udachin et al., 2002).

In those cases, where also interstitial guest inclusion is possible, the structure-property relationship for the host inclusion capacity  $S$  may be more complex. *tert*-Butylcalix[5]arene with such structure of inclusion compounds has a very irregular relationship between  $S$  and  $MR_D$  values (Ziganshin et al., 2007). The same was observed for diol host (Gorbachuk et al., 2000), adamantylcalix[4]arene (Yakimova et al., 2008), and *tert*-butylcalix[6]arene (Safina et al., 2013).

Rather regular size exclusion effect may be expected for hosts with strong intermolecular H-bonding in their crystals. This was observed for dry hydrophilic receptors  $\alpha$ -cyclodextrin (Gatiatulin et al., 2018) and  $\beta$ -cyclodextrin (Gatiatulin et al., 2016). In both cases, hydrophilic guests are included better than hydrophobic ones. In this relation, the inclusion selectivity of dry cyclodextrins is similar to those of dry glassy hydrophilic

receptors like human serum albumin (Gorbachuk et al., 1997b, 1999c),  $\beta$ -lactoglobulin (Mironov et al., 2003), and cross-linked polyacrylamide derivative (Gorbachuk et al., 2004).

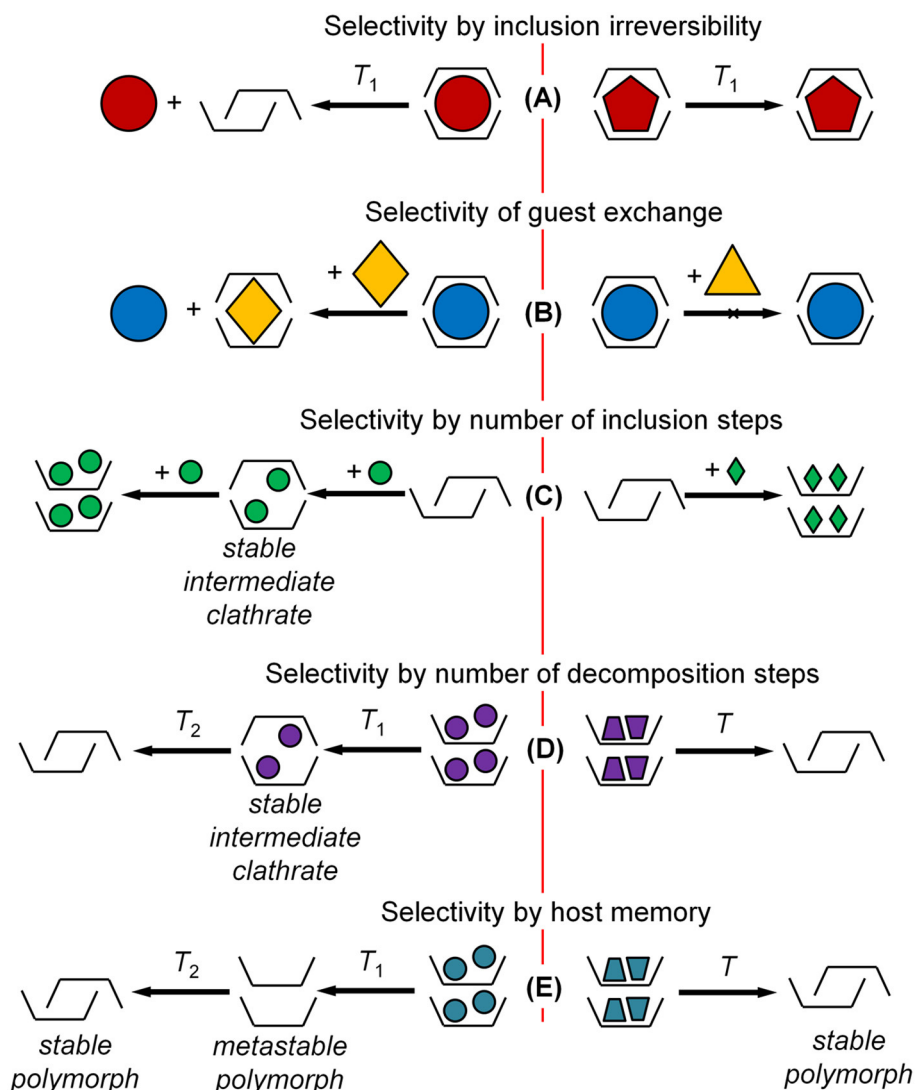
The second type of host selectivity to the guest size is an inverted size exclusion or “anti-sieve” effect, where the host prefers larger molecules, while the smaller are not included, **Figure 1D**. Such selectivity was observed for thiacalix[4]arene, which may include guests into the interstitial space formed by too many calixarene macrocycles where a sufficient driving force apparently needed to push them aside (Galyaltidinov et al., 2014).

The solid-phase transition at guest inclusion by solid host implies also the host selectivity by inclusion threshold of guest thermodynamic activity, and accordingly, by inclusion Gibbs energy  $\Delta G_c$ , **Figure 1A**. The range of the observed  $\Delta G_c$  values depends much on the size of host cavity that does not require work to be created (Gorbachuk et al., 2002; Gatiatulin et al., 2018). For example, for the *tert*-butylcalix[4]arene, which includes the most guests studied inside its molecular cavity (Ripmeester et al., 2006; Ramon et al., 2011), there is a significant variation in  $\Delta G_c$  from  $-1.2$  to  $-8.9$  kJ/mol for different guests (Gorbachuk et al., 2002). *tert*-Butylthiacalix[4]arene with the same type of guest inclusion but with a smaller effective cavity has the  $\Delta G_c$  values from  $-0.4$  to  $-2.0$  kJ/mol (Gorbachuk et al., 2002). *tert*-Butylcalix[5]arene (Ziganshin et al., 2007), adamantylcalix[4]arene (Yakimova et al., 2008), and  $\beta$ -cyclodextrin (Gorbachuk et al., 2013), which may include guests into interstitial space of their crystal packing, have an intermediate position by this parameter: with  $\Delta G_c$  less negative than  $-4.6$ ,  $-3.6$  and  $-3.8$  kJ/mol, respectively. If the interstitial inclusion is possible, the higher values of inclusion capacity  $S$  corresponds mostly to the less negative  $\Delta G_c$  values (Ziganshin et al., 2007; Yakimova et al., 2008).

This type of selectivity explains the described above stepwise size exclusion effect in the guest inclusion by solid hosts. When the guest molecule is too big for the host molecular cavity, the structure-property relationship may have two options. Either there is a stepwise change to no inclusion, e.g., for *tert*-butylthiacalix[4]arene (Gorbachuk et al., 2002), or a stepwise change to a different packing pattern with a lower guest content observed for *tert*-butylcalix[4]arene (Gorbachuk et al., 1999b). One should not compare the selectivity by inclusion Gibbs energy  $\Delta G_c$  and the selectivity by host-guest association constants  $K_a$  in liquid solutions from NMR titration experiments, which may give a huge overestimation of  $K_a$  values (Gorbachuk et al., 2017).

## SELECTIVITY OF INCLUSION IRREVERSIBILITY

Cooperativity of the guest inclusion process creates the additional selectivity options that can be used to enhance the efficient molecular recognition. Molecular structure of host and guest may have a strong impact also on the process of guest release, **Figure 2A**, e.g., in host regeneration of the sensor experiment. Being kinetically controlled through a strong sorption/desorption hysteresis (Dewa et al., 1998), guest release from the host-guest clathrate may have a



**FIGURE 2 |** Specific types of molecular recognition using solid-solid phase transitions. **(A)** Selectivity by inclusion irreversibility; **(B)** selectivity of guest exchange; **(C)** selectivity by number of inclusion steps; **(D)** selectivity by number of decomposition steps; **(E)** selectivity by host memory.

different structure-property relationship than guest inclusion, which is under a thermodynamic control described above. This irreversibility may be detrimental in sensor experiments (Yakimova et al., 2008; Gorbachuk et al., 2017), and the undesired history effect may be removed by high-temperature treatment of the host layer giving a normal sigmoidal shape of sorption isotherm by sensor unit (Matsuura et al., 2000).

The dependence of inclusion irreversibility on the guest molecular structure may be used to increase the selectivity of sensor experiment. A good example is the vapor sensor with a thin layer of adamantylcalix[4]arene on the quartz microbalance (Yakimova et al., 2008). The first run of this sensor experiment at 25°C and the second run after the host intermediate regeneration at 45°C by air purge give the sensor responses  $R_1$  and  $R_2$ , respectively. The ratio of these responses  $R_2/R_1$  is mostly

different for different guests being a parameter of guest inclusion reversibility with  $R_2/R_1 \leq 1$ . Using this parameter helps to increase the selectivity of single sensor analysis and to ensure recognition of more individual guests.

## SELECTIVITY OF GUEST EXCHANGE IN INCLUSION COMPOUND

Along with the inclusion selectivity in binary host-guest systems, the selectivity of guest exchange in the solid phase of inclusion compound may be used for molecular recognition, **Figure 2B**. An efficiency of this exchange may depend on guest molecular structure in a different way than that of guest inclusion in binary system (Galyaltdinov et al., 2012; Amombo Noa et al., 2016). This gives an additional dimension to molecular



recognition of guest compounds using the same host. For example, for thiacalix[4]arene (Galyaltdinov et al., 2014) and *tert*-butylthiacalix[4]arene (Galyaltdinov et al., 2012; Morohashi et al., 2019), the guest exchange increases the range of included compounds thus decreasing the inclusion selectivity. Still, this selectivity remains essentially stepwise. In some cases, the guest capable of inclusion in binary system cannot replace another guest in inclusion compound.

The guest inclusion by the host with a partial exchange of the already included water is a standard experimental procedure for solid hydrophilic hosts, such as native cyclodextrins (Ho et al., 2011, 2016; Gatiatulin et al., 2019) that do not include large hydrophobic guests in binary host-guest systems in the absence of water (Gorbachuk et al., 2013; Gatiatulin et al., 2018). To activate this inclusion without water, the guest exchange in anhydrous inclusion compounds of cyclodextrins may be used (Gorbachuk et al., 2013; Gatiatulin et al., 2014), which selectivity and efficiency depends much on molecular structure of the leaving guest. For example, 1-propanol and propionitrile cannot replace water in the saturated  $\beta$ -cyclodextrin hydrate but can exchange benzene, ethanol and acetonitrile in anhydrous clathrates with this host (Gorbachuk et al., 2013; Gatiatulin et al., 2016).

## SELECTIVITY BY A NUMBER OF STEPS OF GUEST INCLUSION AND RELEASE

The geometric constraints for guest inclusion changing with the variation of guest content in inclusion compound (clathrate) may give another type of selectivity. This is the selective formation of stable intermediate clathrates, **Figures 2C,D**, which can be seen in two-step sorption isotherms (Ziganshin et al., 2007; Safina et al., 2010) and thermogravimetric (TG) curves (Yakimov et al., 2008). Sorption isotherms and TG curves of this type are relatively rare. So for *tert*-butylcalix[4]arene (Ziganshin et al., 2007), *tert*-butylcalix[5]arene (Ziganshin et al., 2007), and adamantylcalix[4]arene (Yakimova et al., 2008), two-step sorption isotherms or TG curves are observed for 2 out of 15, 3 out of 8, 2 out of 7 studied guests, respectively.

An example of absolute molecular recognition of benzene by a number of guest inclusion steps was observed for tetra(ethoxycarbonyl)methoxy thiacalix[4]arene (Safina et al., 2010). This calixarene performs a two-step inclusion only for benzene in experiments with quartz-crystal microbalance sensors, while all other studied guests are included in one step. This type of selectivity was observed also for benzene in mixtures with its close homologs. It fundamentally differs from the classical key-to-lock model.

## SMART MOLECULAR RECOGNITION: SELECTIVITY BY HOST MEMORY FOR PREVIOUSLY INCLUDED AND RELEASED GUEST

The irreversibility of guest inclusion and release with solid-solid phase transition can be a source of one more type of selectivity. This is selectivity of guest-induced polymorphism, which is a

well-studied phenomenon used for screening of polymorphs (Braga et al., 2010; Petkune et al., 2012; Newman, 2013; Lee, 2014). A corresponding screening technique involves preparing the inclusion compound and removing the included guest (Lee et al., 2013; Gataullina et al., 2017). This is a smart process, where the host may remember molecular structure of a released guest by formation of a specific metastable polymorph (Gataullina et al., 2015).

An ideal case for molecular recognition is the host ability to form two polymorphs: stable and metastable ones, **Figure 2E**, where the metastable polymorph is formed after inclusion and release of only one guest and not of any other. Such an absolute selectivity for chloroform and methanol was found for *N*-(2-hydroxyethyl)carbamoylmethoxy *tert*-butylthiacalix[4]arene (Safina et al., 2011) and for *tert*-butylthiacalix[4]arene (Galyaltdinov et al., 2012), respectively. For *tert*-butylthiacalix[4]arene, metastable polymorph is formed from its clathrate prepared only by solid-phase exchange of included 1,2-dichloroethane with methanol. In both cases, the formation of metastable polymorph can be detected by exothermic solid-solid phase transition of guest-free host in simultaneous experiment of TG and differential scanning calorimetry (DSC).

For comparison, *tert*-butylcalix[6]arene is less selective breaking the studied guest compounds into two groups: (1) remembered guests inducing formation of metastable polymorphs, and (2) non-remembered guests without such ability (Yakimov et al., 2008). This selectivity of *tert*-butylcalix[6]arene may be used in the analysis of binary mixtures if at least one of their components is from the first group. The efficiency of this analysis was demonstrated using DSC for the binary mixtures with one (Safina et al., 2013) and two (Gabdulkhaev et al., 2016) remembered components.

Guest-induced metastable polymorphs of calixarenes capable of an exothermic solid-phase transition have also a potential in 100% separation of binary mixtures of close homologs (Morohashi et al., 2017; Morohashi and Hattori, 2018) or compounds with close boiling points (Gabdulkhaev et al., 2016).

The phenomenon of polymorphism is more variable than the examples given in this review. In many cases, metastability of a polymorph is in its lower melting point than that of the stable form. Such polymorphs may have more than one melting point with an intermediate exothermic cold crystallization to the more stable forms (Gataullina et al., 2017, 2019). The formation of such polymorphs by guest inclusion and release may be also a kind of molecular recognition when it is selective enough, but in this case the problem is to find sufficient experimental proofs that the host treatment with different guests gives different polymorphs.

## CONCLUSIONS

Cooperativity of guest inclusion by solid host with phase transition provides specific types of selectivity for neutral guest compounds that cannot be observed in liquid solutions. In some cases, this selectivity gives practically absolute molecular

recognition and may be called smart because it uses the host polymorphism with a very selective and easily detectable memory of the guest included and released. Besides, of the same molecular recognition level is the very selective formation of stable intermediate inclusion compounds, which may be detected by mass-sensitive sensor and in thermogravimetric curves. This process resembles a smart switch of the initial host crystals recognizing only one guest or few guest compounds.

The specific types of structure-property relationships and molecular recognition caused by phase transition at guest inclusion and release may be expected for any solid host capable of clathrate formation. Still, discovery of the host-guest systems

with a genuine selectivity for neutral molecules requires an extensive screening, which success cannot be predicted.

## AUTHOR CONTRIBUTIONS

VG supervised the project and mainly wrote the paper. AG and MZ co-wrote the paper. All authors discussed the reviewed results and commented on the manuscript.

## FUNDING

This work was financially supported by RFBR, grant No. 17-03-01311.

## REFERENCES

- Afonso, R., Mendes, A., and Gales, L. (2012). Peptide-based solids: porosity and zeolitic behavior. *J. Mater. Chem.* 22, 1709–1723. doi: 10.1039/C1JM13568F
- Amombo Noa, F. M., Bourne, S. A., Su, H., and Nassimbeni, L. R. (2016). Guest exchange in halogenated host-guest compounds: structures and kinetics. *Cryst. Growth Des.* 16, 1636–1642. doi: 10.1021/acs.cgd.5b01728
- Ariga, K., Ito, H., Hill, J. P., and Tsukube, H. (2012). Molecular recognition: from solution science to nano/materials technology. *Chem. Soc. Rev.* 41, 5800–5835. doi: 10.1039/c2cs35162e
- Braga, D., Grepioni, F., and Maini, L. (2010). The growing world of crystal forms. *Chem. Commun.* 46, 6232–6242. doi: 10.1039/c0cc01195a
- DeJaco, R. F., de Mello, M. D., Nguyen, H. G. T., Jeon, M. Y., Zee, R. D., Tsapatsis, M., et al. (2019). Vapor and liquid phase adsorption of alcohol and water in silicalite-1 synthesized in fluoride media. *AIChE J.* e16868. doi: 10.1002/aic.16868. [Epub ahead of print].
- Dewa, T., Endo, K., and Aoyama, Y. (1998). Dynamic aspects of lattice inclusion complexation involving a phase change. Equilibrium, kinetics, and energetics of guest-binding to a hydrogen-bonded flexible organic network. *J. Am. Chem. Soc.* 120, 8933–8940. doi: 10.1021/ja9812453
- Engel, E. R., Jouaiti, A., Bezuidenhout, C. X., Hosseini, M. W., and Barbour, L. J. (2017). Activation-dependent breathing in a flexible metal-organic framework and the effects of repeated sorption/desorption cycling. *Angew. Chemie Int. Ed.* 56, 8874–8878. doi: 10.1002/anie.201704044
- Faizullin, M. Z., Vinogradov, A. V., Tomin, A. S., and Koverda, V. P. (2019). Kinetics of decay of highly non-equilibrium metastable states of gas-saturated amorphous ice in the presence of artificially introduced crystal centers. *Int. J. Heat Mass Transf.* 143, 118592. doi: 10.1016/j.ijheatmasstransfer.2019.118592
- Fischer, E. (1894). Einfluss der configuration auf die wirkung der enzyme. II. Berichte der dtsch. Chem. Gesellschaft 27, 3479–3483. doi: 10.1002/cber.189402703169
- Gabdulkhaev, M. N., Gatiatulin, A. K., Ziganshin, M. A., and Gorbachuk, V. V. (2016). Nonlinear effect of two remembered guests in their mixtures on the host memory for guest inclusion and release. *J. Therm. Anal. Calorim.* 126, 627–632. doi: 10.1007/s10973-016-5558-8
- Galyaltdinov, S. F., Ziganshin, M. A., Drapailo, A. B., and Gorbachuk, V. V. (2012). Unusually high selectivity of guest exchange in *tert*-butylthiacalix[4] arene clathrate producing more thermostable inclusion and memory of guest. *J. Phys. Chem. B* 116, 11379–11385. doi: 10.1021/jp3065739
- Galyaltdinov, S. F., Ziganshin, M. A., Gubaidullin, A. T., Vyshnevsky, S. G., Kalchenko, O. I., and Gorbachuk, V. V. (2014). Anti-sieve effect in guest inclusion by thiacalix[4]arene giving a surge in thermal stability of its clathrates prepared by solid-phase guest exchange. *CrystEngComm* 16, 3781–3787. doi: 10.1039/C3CE42304B
- Gao, J., Duan, L., Yang, G., Zhang, Q., Yang, M., and Fu, Q. (2012). Manipulating poly(lactic acid) surface morphology by solvent-induced crystallization. *Appl. Surf. Sci.* 261, 528–535. doi: 10.1016/j.apsusc.2012.08.050
- Gataullina, K. V., Buzyurov, A. V., Ziganshin, M. A., Padnya, P. L., Stoikov, I. I., Schick, C., et al. (2019). Using fast scanning calorimetry to detect guest-induced polymorphism by irreversible phase transitions in the nanogram scale. *CrystEngComm* 21, 1034–1041. doi: 10.1039/C8CE01865K
- Gataullina, K. V., Ziganshin, M. A., Stoikov, I. I., Gubaidullin, A. T., and Gorbachuk, V. V. (2015). Twice as smart behavior of *tert*-butylthiacalix[4]arene derivative in glassy and crystalline form. *Phys. Chem. Chem. Phys.* 17, 15887–15895. doi: 10.1039/C5CP02042E
- Gataullina, K. V., Ziganshin, M. A., Stoikov, I. I., Klimovitskii, A. E., Gubaidullin, A. T., Suwinska, K., et al. (2017). Smart polymorphism of thiacalix[4]arene with long-chain amide containing substituents. *Cryst. Growth Des.* 17, 3512–3527. doi: 10.1021/acs.cgd.7b00463
- Gatiatulin, A. K., Osel'skaya, V. Y., Ziganshin, M. A., and Gorbachuk, V. V. (2018). Size exclusion effect in binary inclusion compounds of  $\alpha$ -cyclodextrin. *Phys. Chem. Chem. Phys.* 20, 26105–26116. doi: 10.1039/C8CP03104E
- Gatiatulin, A. K., Osel'skaya, V. Y., Ziganshin, M. A., and Gorbachuk, V. V. (2019). Smart control of guest inclusion by  $\alpha$ -cyclodextrin using its hydration history. *RSC Adv.* 9, 37778–37787. doi: 10.1039/C9RA08710A
- Gatiatulin, A. K., Ziganshin, M. A., and Gorbachuk, V. V. (2014). Selective preparation of beta-cyclodextrin clathrates by solid-phase exchange of included tetrahydrofuran for volatile guests in absence of water. *J. Therm. Anal. Calorim.* 118, 987–992. doi: 10.1007/s10973-014-3800-9
- Gatiatulin, A. K., Ziganshin, M. A., Yumaeva, G. F., Gubaidullin, A. T., Suwinska, K., and Gorbachuk, V. V. (2016). Using water-mimic organic compounds to activate guest inclusion by initially dry beta-cyclodextrin. *RSC Adv.* 6, 61984–61995. doi: 10.1039/C6RA11378H
- Gorbachuk, V. V., Antipin, I. S., Tsifarkin, A. G., Solomonov, B. N., and Konovalov, A. I. (1997a). The cooperative effect of the third component on the isotherms of guest vapour inclusion in solid *tert*-butylcalix[4]arene. *Mendeleeev Commun.* 7, 215–217. doi: 10.1070/MC1997v007n06ABEH000807
- Gorbachuk, V. V., Gatiatulin, A. K., and Ziganshin, M. A. (2017). “Gas/solid complexation and inclusion” in *Comprehensive Supramolecular Chemistry II, Vol II*, ed J. L. Atwood, G. W. Gokel, and L. J. Barbour (Oxford: Elsevier), 139–150. doi: 10.1016/B978-0-12-409547-2.12499-0
- Gorbachuk, V. V., Gatiatulin, A. K., Ziganshin, M. A., Gubaidullin, A. T., and Yakimova, L. S. (2013). Unusually high efficiency of  $\beta$ -cyclodextrin clathrate preparation by water-free solid-phase guest exchange. *J. Phys. Chem. B* 117, 14544–14556. doi: 10.1021/jp408059b
- Gorbachuk, V. V., Mironov, N. A., Solomonov, B. N., and Habicher, W. D. (2004). Biomimetic cooperative interactions of dried cross-linked poly(N-6-aminohexylacrylamide) with binary mixtures of solvent vapors. *Biomacromolecules* 5, 1615–1623. doi: 10.1021/bm049743t
- Gorbachuk, V. V., Tsifarkin, A. G., Antipin, I. S., Solomonov, B. N., and Konovalov, A. I. (1999a). Estimation of the free energy of the supramolecular effect on host-guest complex formation between solid *tert*-butylcalix[4]arene and vapors of organic compounds. *J. Incl. Phenom. Macrocycl. Chem.* 35, 389–396. doi: 10.1023/A:1008136124183
- Gorbachuk, V. V., Tsifarkin, A. G., Antipin, I. S., Solomonov, B. N., and Konovalov, A. I. (1999b). Influence of the guest molecular size on the thermodynamic parameters of host-guest complexes between solid

- tert-butylcalix[4]arene and vapours of organic compounds. *Mendelev Commun.* 9, 11–13. doi: 10.1070/MC1999v009n01ABEH000989
- Gorbachuk, V. V., Tsifarkin, A. G., Antipin, I. S., Solomonov, B. N., Kononov, A. I., Lhotak, P., et al. (2002). Nonlinear structure - affinity relationships for vapor guest inclusion by solid calixarenes. *J. Phys. Chem. B* 106, 5845–5851. doi: 10.1021/jp014352j
- Gorbachuk, V. V., Tsifarkin, A. G., Antipin, I. S., Solomonov, B. N., Kononov, A. I., Seidel, J., et al. (2000). Thermodynamic comparison of molecular recognition of vaporous guests by solid calixarene and diol hosts. *J. Chem. Soc. Perkin Trans. 2*, 2287–2294. doi: 10.1039/b003477k
- Gorbachuk, V. V., Ziganshin, M. A., and Solomonov, B. N. (1999c). Supramolecular interactions of solid human serum albumin with binary mixtures of solvent vapors. *Biophys. Chem.* 81, 107–123. doi: 10.1016/S0301-4622(99)00087-3
- Gorbachuk, V. V., Ziganshin, M. A., Solomonov, B. N., and Borisover, M. D. (1997b). Vapor sorption of organic compounds on human serum albumin. *J. Phys. Org. Chem.* 10, 901–907. doi: 10.1002/(SICI)1099-1395(199712)10:12<901::AID-POC956>3.0.CO;2-J
- Hiraide, S., Tanaka, H., and Miyahara, M. T. (2016). Understanding gate adsorption behaviour of CO<sub>2</sub> on elastic layer-structured metal-organic framework-11. *Dalton Trans.* 45, 4193–4202. doi: 10.1039/C5DT03476K
- Ho, B. T., Joyce, D. C., and Bhandari, B. R. (2011). Encapsulation of ethylene gas into  $\alpha$ -cyclodextrin and characterisation of the inclusion complexes. *Food Chem.* 127, 572–580. doi: 10.1016/j.foodchem.2011.01.043
- Ho, T. M., Howes, T., and Bhandari, B. R. (2016). Encapsulation of CO<sub>2</sub> into amorphous alpha-cyclodextrin powder at different moisture contents – part 1: encapsulation capacity and stability of inclusion complexes. *Food Chem.* 203, 348–355. doi: 10.1016/j.foodchem.2016.02.076
- Joyce, L. A., Shabbir, S. H., and Anslyn, E. V. (2010). The uses of supramolecular chemistry in synthetic methodology development: examples of anion and neutral molecular recognition. *Chem. Soc. Rev.* 39, 3621–3632. doi: 10.1039/b926224p
- Lee, E. H. (2014). A practical guide to pharmaceutical polymorph screening & selection. *Asian J. Pharm. Sci.* 9, 163–175. doi: 10.1016/j.ajps.2014.05.002
- Lee, J., Boerrigter, S. X. M., Jung, Y. W., Byun, Y., Yuk, S. H., Byrn, S. R., et al. (2013). Organic vapor sorption method of isostructural solvates and polymorph of tenofovir disoproxil fumarate. *Eur. J. Pharm. Sci.* 50, 253–262. doi: 10.1016/j.ejps.2013.07.004
- Lee, J. H., Jeoung, S., Chung, Y. G., and Moon, H. R. (2019). Elucidation of flexible metal-organic frameworks: research progresses and recent developments. *Coord. Chem. Rev.* 389, 161–188. doi: 10.1016/j.ccr.2019.03.008
- Matsuura, K., Ariga, K., Endo, K., Aoyama, Y., and Okahata, Y. (2000). Dynamic analyses on induced-fit gaseous guest binding to organic crystals with a quartz-crystal microbalance. *Chem. Eur. J.* 6, 1750–1756. doi: 10.1002/(sici)1521-3765(20000515)6:10<1750::aid-chem1750>3.0.co;2-a
- Mironov, N. A., Breus, V. V., Gorbachuk, V. V., Solomonov, B. N., and Haertlé, T. (2003). Effects of hydration, lipids, and temperature on the binding of the volatile aroma terpenes by  $\beta$ -lactoglobulin powders. *J. Agric. Food Chem.* 51, 2665–2673. doi: 10.1021/jf020896m
- Morohashi, N., and Hattori, T. (2018). Selective guest inclusion by crystals of calixarenes: potential for application as separation materials. *J. Incl. Phenom. Macrocycl. Chem.* 90, 261–277. doi: 10.1007/s10847-018-0783-3
- Morohashi, N., Miyoshi, I., Sasaki, T., Nakaji, Y., Nakayama, H., and Hattori, T. (2019). Inclusion of alkanes with a crystal consisting of exocavity complexes of p-tert-butylthiacalix[4]arene with diethylamine: extension of guest scope by changing the structure of inclusion crystals. *Cryst. Growth Des.* 19, 7022–7029. doi: 10.1021/acs.cgd.9b00837
- Morohashi, N., Tonosaki, A., Kitagawa, T., Sasaki, T., Ebata, K., and Hattori, T. (2017). Competitive inclusion of disubstituted benzene regioisomers with crystals of p-tert-butylcalix[4]arene. *Cryst. Growth Des.* 17, 5038–5043. doi: 10.1021/acs.cgd.7b01007
- Newman, A. (2013). Specialized solid form screening techniques. *Org. Process Res. Dev.* 17, 457–471. doi: 10.1021/op300241f
- Persch, E., Dumele, O., and Diederich, F. (2015). Molecular recognition in chemical and biological systems. *Angew. Chemie Int. Ed.* 54, 3290–3327. doi: 10.1002/anie.201408487
- Petkune, S., Bobrovs, R., and Actinš, A. (2012). Organic solvents vapor pressure and relative humidity effects on the phase transition rate of  $\alpha$  and  $\beta$  forms of tegafur. *Pharm. Dev. Technol.* 17, 625–631. doi: 10.3109/10837450.2011.565346
- Ramon, G., Jacobs, A., Nassimbeni, L. R., and Yav-Kabwit, R. (2011). Inclusion compounds of p-tert-butylcalixarenes: structures, kinetics, and selectivity. *Cryst. Growth Des.* 11, 3172–3182. doi: 10.1021/cg2004084
- Reinhoudt, D. N. (2013). “Supramolecular chemistry and heterocycles,” in *Reference Module in Chemistry, Molecular Sciences, and Chemical Engineering* (Elsevier), 1–2. doi: 10.1016/B978-0-12-409547-2.05396-8
- Ripmeester, J. A., Enright, G. D., Ratcliffe, C. I., Udachin, K. A., and Moudrakovski, I. L. (2006). What we have learned from the study of solid p-tert-butylcalix[4]arene compounds. *Chem. Commun.* 48, 4986–4996. doi: 10.1039/b605275d
- Safina, G. D., Gavrilova, O. M., Ziganshin, M. A., Stoikov, I. I., Antipin, I. S., and Gorbachuk, V. V. (2011). Molecular recognition of chloroform by divergent polymorphic transitions in tert-butylthiacalix[4]arene tetrasubstituted with N-(2-hydroxyethyl)carbamoylmethoxy groups in a lower rim. *Mendelev Commun.* 21, 291–292. doi: 10.1016/j.mencom.2011.09.022
- Safina, G. D., Validova, L. R., Ziganshin, M. A., Stoikov, I. I., Antipin, I. S., and Gorbachuk, V. V. (2010). Using clathrate pseudopolymorphism for a single sensor detection of target component in the headspace of liquid mixture. *Sens. Actu. B Chem.* 148, 264–268. doi: 10.1016/j.snb.2010.04.032
- Safina, G. D., Ziganshin, M. A., Gubaidullin, A. T., and Gorbachuk, V. V. (2013). Analysis of guest binary mixtures by tert-butylcalix[6]arene using host memory of previously bound guests. *Org. Biomol. Chem.* 11, 1318–1325. doi: 10.1039/c2ob27164h
- Shu, X., Xu, K., Hou, D., and Li, C. (2018). Molecular recognition of water-soluble pillar[n]arenes towards biomolecules and drugs. *Isr. J. Chem.* 58, 1230–1240. doi: 10.1002/ijch.201800115
- Sonnenberg, C., Hartmann, A., and Mazik, M. (2012). Molecular recognition of carbohydrates: evaluation of the binding properties of pyrazole-based receptors and their comparison with imidazole- and indole-based systems. *Nat. Prod. Commun.* 7, 321–326. doi: 10.1177/1934578X1200700311
- Udachin, K. A., Enright, G. D., Brown, P. O., and Ripmeester, J. A. (2002). Pseudopolymorphism in the p-tert-butylcalix[4]arene-n-butylamine system: directing the structural motifs. *Chem. Commun.* 2162–2163. doi: 10.1039/B204313K
- Yakimov, A. V., Ziganshin, M. A., Gubaidullin, A. T., and Gorbachuk, V. V. (2008). Metastable tert-butylcalix[6]arene with unusually large tunable free volume for non-threshold enclathration of volatiles. *Org. Biomol. Chem.* 6, 982–985. doi: 10.1039/b800187a
- Yakimova, L. S., Ziganshin, M. A., Sidorov, V. A., Kovalev, V. V., Shokova, E. A., Tafeenko, V. A., et al. (2008). Molecular recognition of organic vapors by adamantylcalix[4]arene in QCM sensor using partial binding reversibility. *J. Phys. Chem. B* 112, 15569–15575. doi: 10.1021/jp804277u
- Yao, H., Ke, H., Zhang, X., Pan, S.-J., Li, M.-S., Yang, L.-P., et al. (2018). Molecular recognition of hydrophilic molecules in water by combining the hydrophobic effect with hydrogen bonding. *J. Am. Chem. Soc.* 140, 13466–13477. doi: 10.1021/jacs.8b09157
- Yuan, Y., Tam, M. F., Simplaceanu, V., and Ho, C. (2015). New look at hemoglobin allostery. *Chem. Rev.* 115, 1702–1724. doi: 10.1021/cr500495x
- Zhang, Y., Xu, Q., and Liu, Y. (2019). Molecular recognition and biological application of modified  $\beta$ -cyclodextrins. *Sci. China Chem.* 62, 549–560. doi: 10.1007/s11426-018-9405-3
- Ziganshin, M. A., Gubina, N. S., Gerasimov, A. V., Gorbachuk, V. V., Ziganshina, S. A., Chuklanov, A. P., et al. (2015). Interaction of L-alanyl-L-valine and L-valyl-L-alanine with organic vapors: thermal stability

- of clathrates, sorption capacity and the change in the morphology of dipeptide films. *Phys. Chem. Chem. Phys.* 17, 20168–20177. doi: 10.1039/C5CP03309H
- Ziganshin, M. A., Safiullina, A. S., Ziganshina, S. A., Gerasimov, A. V., and Gorbachuk, V. V. (2017). Non-zeolitic properties of the dipeptide L-leucyl-L-leucine as a result of the specific nanostructure formation. *Phys. Chem. Chem. Phys.* 19, 13788–13797. doi: 10.1039/C7CP01393K
- Ziganshin, M. A., Yakimov, A. V., Safina, G. D., Solovieva, S. E., Antipin, I. S., and Gorbachuk, V. V. (2007). Nonregular structure–property relationships for inclusion parameters of *tert*-butylcalix[5]arene. *Org. Biomol. Chem.* 5, 1472–1478. doi: 10.1039/B701082F

**Conflict of Interest:** The authors declare that the research was conducted in the absence of any commercial or financial relationships that could be construed as a potential conflict of interest.

Copyright © 2020 Gatiatulin, Ziganshin and Gorbachuk. This is an open-access article distributed under the terms of the Creative Commons Attribution License (CC BY). The use, distribution or reproduction in other forums is permitted, provided the original author(s) and the copyright owner(s) are credited and that the original publication in this journal is cited, in accordance with accepted academic practice. No use, distribution or reproduction is permitted which does not comply with these terms.



# pH-Induced Transition Between Single-Chain Macrocyclic Amphiphile and [c2]Daisy Chain-Based Bola-Type Amphiphile and the Related Self-Assembly Behavior in Water

Pi Wang<sup>1\*</sup>, Ruihuan Wang<sup>1</sup> and Danyu Xia<sup>2\*</sup>

<sup>1</sup> Ministry of Education Key Laboratory of Interface Science and Engineering in Advanced Materials, Taiyuan University of Technology, Taiyuan, China, <sup>2</sup> Scientific Instrument Center, Shanxi University, Taiyuan, China

## OPEN ACCESS

### Edited by:

Yong Yao,  
Nantong University, China

### Reviewed by:

Bingbing Shi,  
Northwest Normal University, China  
Bin Hua,  
Zhejiang University, China  
Kecheng Jie,  
University of Cambridge,  
United Kingdom

### \*Correspondence:

Pi Wang  
wangpi@tyut.edu.cn  
Danyu Xia  
danyuxia@sxu.edu.cn

### Specialty section:

This article was submitted to  
Supramolecular Chemistry,  
a section of the journal  
Frontiers in Chemistry

**Received:** 28 November 2019

**Accepted:** 12 December 2019

**Published:** 24 January 2020

### Citation:

Wang P, Wang R and Xia D (2020)  
pH-Induced Transition Between  
Single-Chain Macrocyclic Amphiphile  
and [c2]Daisy Chain-Based Bola-Type  
Amphiphile and the Related  
Self-Assembly Behavior in Water.  
*Front. Chem.* 7:894.  
doi: 10.3389/fchem.2019.00894

Macrocyclic amphiphiles, a type of amphiphiles synthesized based on macrocyclic compounds, have attracted much attention over the past decades due to their unique superiority in the construction of various functional nanomaterials. The regulation of the state of macrocyclic amphiphiles by introducing stimuli-responsive motif to macrocyclic amphiphiles is an efficient way to extend their applications in diverse fields. Herein, pillararene-based macrocyclic amphiphile **H1** was prepared. **H1** can act as single-chain amphiphile to self-assemble into micelles in water when the pH was  $\geq 5.0$ . **H1** can be protonated to turn into **H2** when pH changed to  $< 5.0$ . Interestingly, **H2** formed [c2]daisy chain-based bola-type supramolecular amphiphile. This bola-type supramolecular amphiphile self-assembled into nanosheets in water. Therefore, pH-induced transition between single-chain macrocyclic amphiphile and bola-type amphiphile and the corresponding self-assembly system based on pillararene in water were constructed.

**Keywords:** macrocyclic amphiphile, stimuli responsiveness, daisy chain, self-assembly, pillararene

## INTRODUCTION

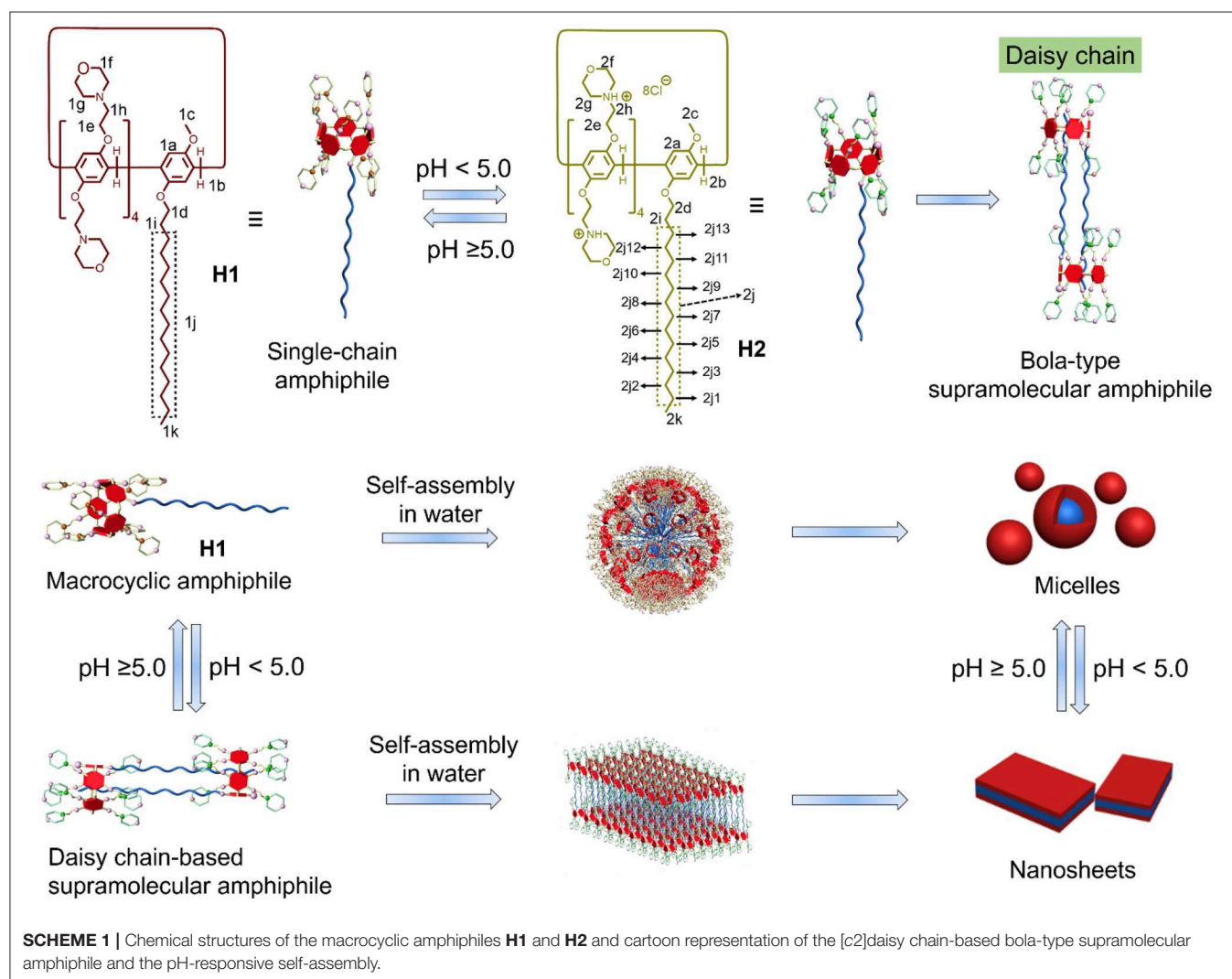
Amphiphiles, carrying both hydrophilic and hydrophobic parts connected by covalent bonds, are a class of interesting molecules to fabricate self-assembly systems (Discher and Eisenberg, 2002; Sorrenti et al., 2013; Chang et al., 2019b). Owing to their amphiphilic nature, amphiphiles can self-assemble into various nanostructures in water that can be applied in various areas, including drug/gene delivery, photodynamic therapy, and bioimaging (Zhang and Wang, 2011; Hu et al., 2013; Kelley et al., 2013; Ma and Zhao, 2015; Yu et al., 2015; Ji et al., 2016; Xia et al., 2016; Webber and Langer, 2017; Guo et al., 2018; Zuo et al., 2018; Wang S.-P. et al., 2019; Wang Y. et al., 2019). Amphiphiles synthesized based on macrocyclic compounds, namely, macrocyclic amphiphiles (Jie et al., 2015; Zhu et al., 2018), have gained growing attention in recent years. Compared with traditional amphiphiles, macrocyclic amphiphiles possess unique superiority in the construction of various functional nanomaterials, e.g., the incorporation of functional groups and intriguing properties can be achieved by host-guest interactions without extra additives and tedious synthesis



(Wei et al., 2014; Wang et al., 2015; Shulov et al., 2016; Geng et al., 2017; Redondo-Gomez et al., 2019). In addition, the regulation of the state of macrocyclic amphiphiles by introducing stimuli-responsive motif to macrocyclic amphiphiles is an efficient way to extend their applications. Therefore, external stimuli-responsive macrocyclic amphiphiles play important roles in many fields, such as injectable materials, sensing, and cell imaging (Chang et al., 2014; Himmelein et al., 2014; Wang et al., 2015; Yang et al., 2016; Himmelein and Ravoo, 2017; Gao et al., 2018; Hu et al., 2018; Sun et al., 2018; Lee et al., 2019; Li et al., 2019).

Pillararenes, the generation of macrocycles next to crown ethers, cyclodextrins, calixarenes, and cucurbiturils, have been widely studied in the past decade (Li et al., 2017; Ping et al., 2017; Sathiyajith et al., 2017; Hua et al., 2018, 2019; Chen et al., 2019; Xu et al., 2019). Owing to their facile synthesis, easy functionalization and excellent host–guest recognition property, pillararenes have been widely applied to construct amphiphilic self-assembly systems (Shi et al., 2016; Xia et al., 2017; Zhang et al., 2018; Xiao et al., 2019). The rigid and symmetric structure

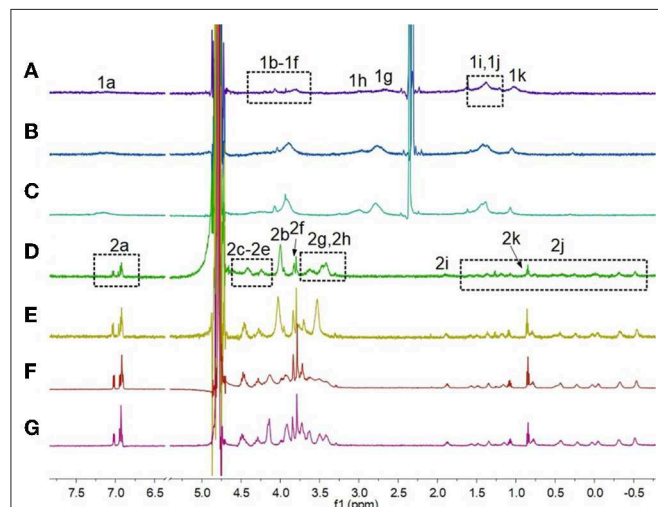
of pillararenes make them good candidates for the construction of macrocyclic amphiphiles. Several types of pillararenes-based macrocyclic amphiphiles have been reported up to now: (1) the non-symmetric pillararenes with half hydrophilic groups and half hydrophobic groups from non-symmetric monomers (Yao et al., 2012; Yu et al., 2013); (2) the difunctionalized pillararene-based macrocyclic amphiphiles from copillar[5]arenes (Gao et al., 2013); (3) monofunctionalized pillararene-based macrocyclic amphiphiles by linking hydrophobic tails to symmetric pillararenes (Jie et al., 2014); and (4) the symmetric *per*-functionalized pillararenes-based amphiphiles (Nierengarten et al., 2013; Chang et al., 2014, 2019a; Yang et al., 2016; Sun et al., 2018). The obtained macrocyclic amphiphiles from these methods displayed interesting stimuli-responsiveness and applications, indicating the importance of pillararenes-based macrocyclic amphiphiles. Herein, we developed a new efficient way to synthesize pillararenes-based macrocyclic amphiphiles. First, we synthesized a long alkyl-containing copillar[5]arene from previous literature. Then, pH-sensitive morpholine



groups were covalently linked to the copillar[5]arene to prepare a single-chain macrocyclic amphiphile **H1**. Interestingly, **H1** transformed into protonated state **H2**, which formed [c2]daisy chains in water when the pH-value decreased under 5.0. As a result, single-chain amphiphile **H1** turned into bola-type supramolecular amphiphile. Moreover, the pH-responsive self-assembly behavior was investigated. Single-chain amphiphile **H1** self-assembled into micelles in water. When the value of pH decreased to under 5.0, micelles transformed into nanosheets due to the formation of bola-type supramolecular amphiphiles based on the [c2]daisy chain structure (Scheme 1).

## MATERIALS AND METHODS

All reagents were commercially available and used as supplied without further purification. Compounds **a** were prepared according to published procedures (Shi et al., 2014). NMR spectra were recorded with a Bruker Avance DMX 600 spectrophotometer or a Bruker Avance DMX 400 spectrophotometer. Low-resolution electrospray ionization mass spectra were recorded with a Bruker Esquire 3000 Plus spectrometer. High-resolution mass spectrometry experiments were performed with a Waters UPLC H-Class QDA instrument. The melting points were collected on a SGW X-4 automatic melting point apparatus. The determination of the critical aggregation concentration (CAC) values was carried out on a FE38 instrument. Transmission electron microscopy investigations were carried out on a JEM-1200EX instrument. Atomic force microscopy experiments were performed by a Bruker Multi-Mode 8.0 instrument.



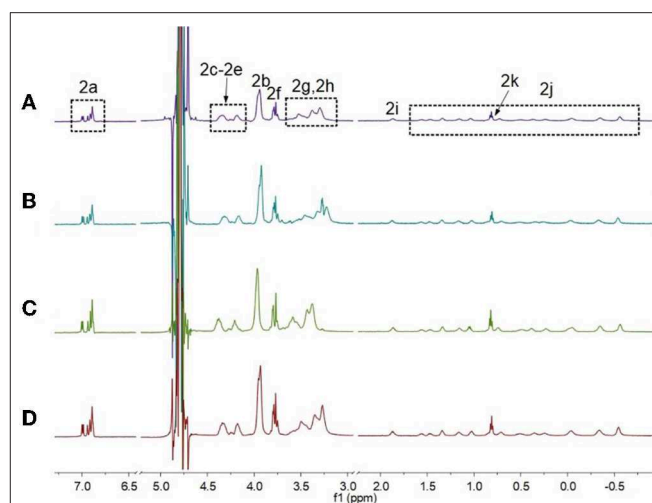
**FIGURE 1** | Partial  $^1\text{H}$  NMR spectra (600 MHz, 3:1  $\text{D}_2\text{O}/\text{CD}_3\text{CN}$ , room temperature) of **H1** (2.50 mM) under different pH conditions: (A) pH 7.0, (B) pH 6.0, (C) pH 5.0; partial  $^1\text{H}$  NMR spectra (600 MHz,  $\text{D}_2\text{O}$ , room temperature) of **H1** (2.50 mM) under different pH conditions: (D) pH 4.0, (E) pH 3.0, (F) pH 2.0, (G) pH 1.0.

## Synthesis of H1

**H1** was synthesized from compound **a** and morpholine (Scheme S1). Compound **a** (1.08 g, 0.622 mmol) and morpholine (0.566 g, 6.50 mmol) were added to acetonitrile (10.0 ml). The solution was refluxed overnight. Then, the crude product was purified by a silica gel column using dichloromethane as eluent (0.421 g, 38%) (Mp: 75.0–77.0°C). The  $^1\text{H}$  NMR spectrum of **H1** is shown in Figure S1.  $^1\text{H}$  NMR (400 MHz,  $\text{CDCl}_3$ , 298 K)  $\delta$  (ppm): 6.85 (s, 10H), 4.14–4.09 (m, 8H), 3.98–3.92 (m, 9H), 3.75–3.73 (m, 47H), 2.88–2.75 (m, 16H), 2.62–2.61 (m, 32H), 1.95–1.86 (m, 2H), 1.84–1.72 (m, 2H), 1.56–1.47 (m, 2H), 1.41–1.32 (m, 2H), 1.16–1.07 (m, 20H), 0.85 (t,  $J = 8.0$  Hz, 3H). The  $^{13}\text{C}$  NMR spectrum of **H1** is shown in Figure S2.  $^{13}\text{C}$  NMR (100 MHz,  $\text{CDCl}_3$ , 298 K)  $\delta$  (ppm): 149.47, 148.84, 148.77, 127.82, 127.65, 127.50, 127.45, 127.06, 114.32, 114.18, 112.90, 67.69, 65.99, 65.99, 65.81, 57.23, 54.93, 53.27, 52.34, 30.91, 28.78, 28.72, 28.64, 28.59, 28.44, 28.39, 28.35, 28.28, 25.13, 21.68, 13.13. High-resolution electrospray ionization mass spectrometry is shown in Figure S3:  $m/z$  calcd for  $[\text{M} + 2\text{H} + \text{e}]^+$   $\text{C}_{102}\text{H}_{158}\text{N}_8\text{O}_{18}$ , 1,783.16941, found 1,783.16784, error  $-0.9$  ppm;  $m/z$  calcd for  $[\text{M} + 3\text{H} + \text{e}]^{2+}$   $\text{C}_{102}\text{H}_{159}\text{N}_8\text{O}_{18}$ , 892.08862, found 892.08527, error  $-3.8$  ppm.

## Critical Aggregation Concentration Determination

The CAC determination is based on the dependence of the solution conductivity on the solution concentration. Generally, the slope value of the change in conductivity vs. the concentration above CAC is higher than the slope below the CAC. As a result, the CAC-value is the junction of the conductivity-concentration plot. To measure the CAC of **H1** and **H2**, the conductivities of their solutions at different concentrations (from 0 to 0.16 mM and from 0 to 0.25 mM, respectively) were determined. Therefore, through plotting the changes of the



**FIGURE 2** | Partial  $^1\text{H}$  NMR spectra of **H2** (600 MHz,  $\text{D}_2\text{O}$ , room temperature) at different concentrations when the pH-value of the solutions was 3.0: (A) 0.500 mM, (B) 1.00 mM, (C) 2.50 mM, and (D) 5.00 mM.

conductivity vs. the concentration, the CAC of **H1** and **H2** can be obtained.

## Transmission Electron Microscopy Experiments

The self-assembled structures of **H1** and **H2** were investigated by TEM. A solution of  $1.00 \times 10^{-4}$  M **H1** was made first in water. The samples of **H1** were prepared by drop coating this solution onto a carbon-coated copper grid. The solution of **H2** were obtained by adding hydrochloride acid to the solution of **H1**. Then, the TEM samples of **H2** was prepared by drop coating the solution on a carbon-coated copper grid. TEM experiments were performed on a JEM-1200EX instrument.

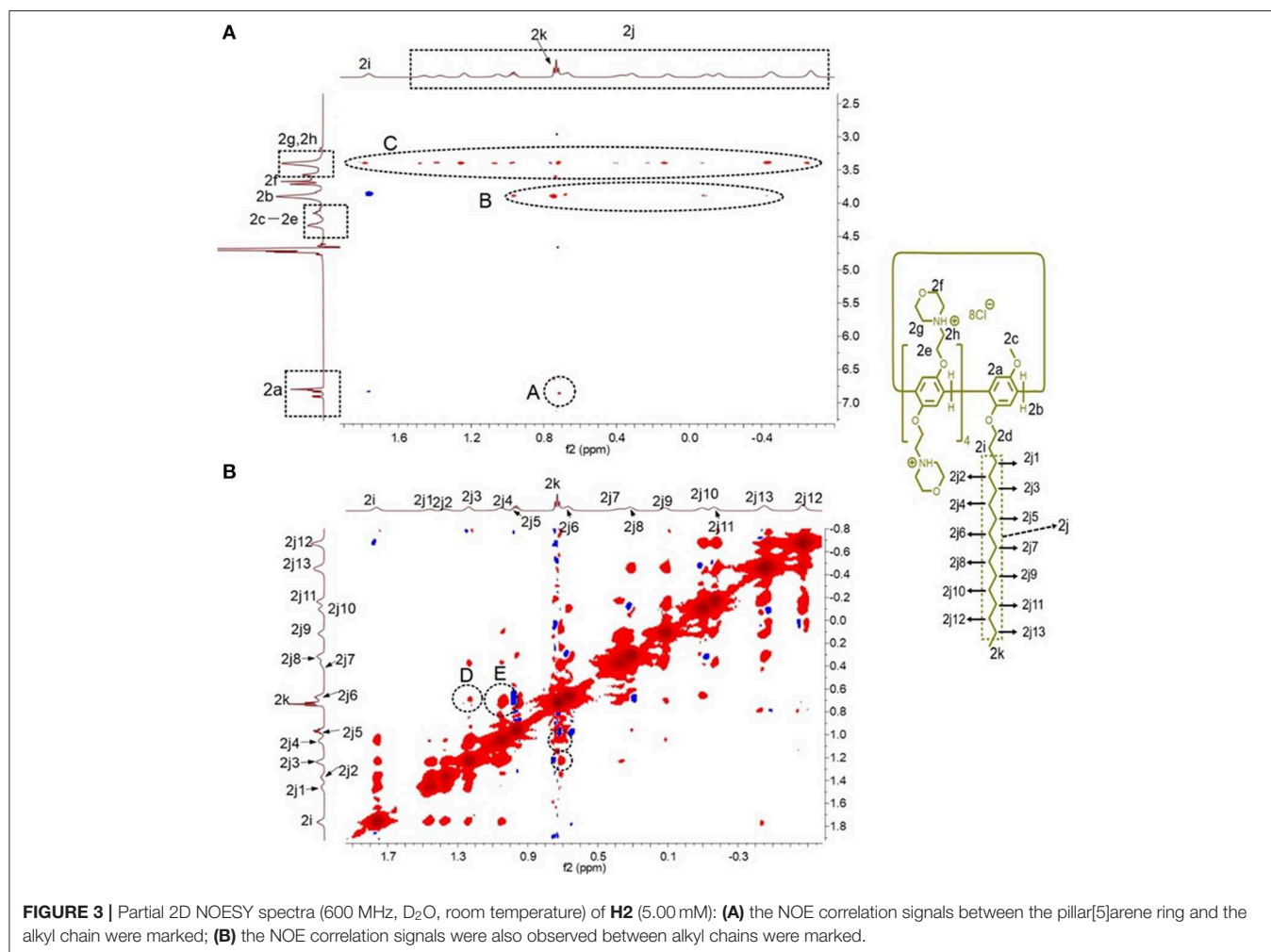
## Atomic Force Microscopy Experiments

The self-assembled structure **H2** was investigated by atomic force microscopy (AFM). A solution of  $1.00 \times 10^{-4}$  M **H1** was prepared in water. The solution of **H2** were obtained by adding hydrochloride acid to the solution of **H1**. Then, the TEM samples of **H2** was prepared by drop coating the solution on a Si substrate. AFM experiments were carried out on a Bruker Multi-Mode 8.0 instrument.

## RESULTS AND DISCUSSIONS

### $^1\text{H}$ NMR Spectroscopy Experiments

First,  $^1\text{H}$  NMR spectroscopy experiments were performed to study the pH-induced transition between **H1** and **H2**. Owing to the poor solubility of **H1** in water, the  $^1\text{H}$  NMR experiments of **H1** was done in the mixture of  $\text{D}_2\text{O}$  and  $\text{CD}_3\text{CN}$  (Figures 1A–C). With the decrease in the pH-value of the aqueous solution of **H1**, the morpholine groups on **H1** were protonated, and **H1** changed into **H2**. Therefore, the peaks corresponding to the protons on **H2** were quite different from that of **H1**. As shown in Figures 1D–G, the signals for protons  $\text{H}_{2g}$  and  $\text{H}_{2h}$  appeared in upfield comparing to the protons  $\text{H}_{1g}$  and  $\text{H}_{1h}$  on **H1**. In addition, the signals for the protons  $\text{H}_{2i}$ – $\text{H}_{2k}$  on the alkyl chain of **H2** appeared in upfield and splitted compared to the related protons on **H1**. This phenomenon was because the alkyl chain threaded into the cavity of **H2**, forming cyclic oligomers. To investigate whether the specific structures of **H2** occur only at low concentrations, concentration-dependent  $^1\text{H}$  NMR experiments were carried out. As shown in Figure 2, with the increase in the concentration from 0.500 to 5.00 mM, the peaks related to **H2** did not show changes.





In addition, at first, we assumed that **H2** can also act as monomers for supramolecular polymers like other systems (Shi et al., 2014). However, **H2** showed poorer solubility in water than other monomers. That is why the concentration-dependent  $^1\text{H}$  NMR experiments were only done in the range of 0.500–5.00 mM. Therefore, the conclusion can be drawn that **H2** formed [2]daisy chains in water, which did not change with its concentration (Zhang et al., 2011).

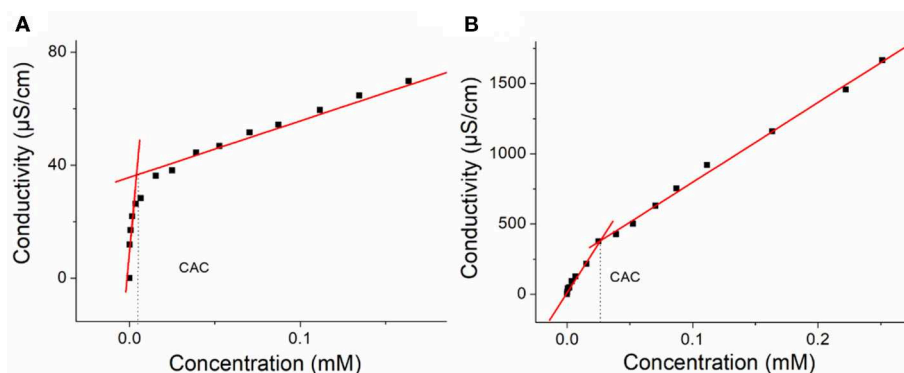
## 2D Nuclear Overhauser Effect Spectroscopy Study

2D nuclear overhauser effect spectroscopy (NOESY) was performed to monitor the formation of the [c2]daisy chain based on **H2**. As shown in Figure 3, NOE correlation signals were observed between the protons  $\text{H}_{2a}$  on the phenyl rings and  $\text{H}_{2k}$  on the alkyl chain (A), between  $\text{H}_{2b}$  on the methylene

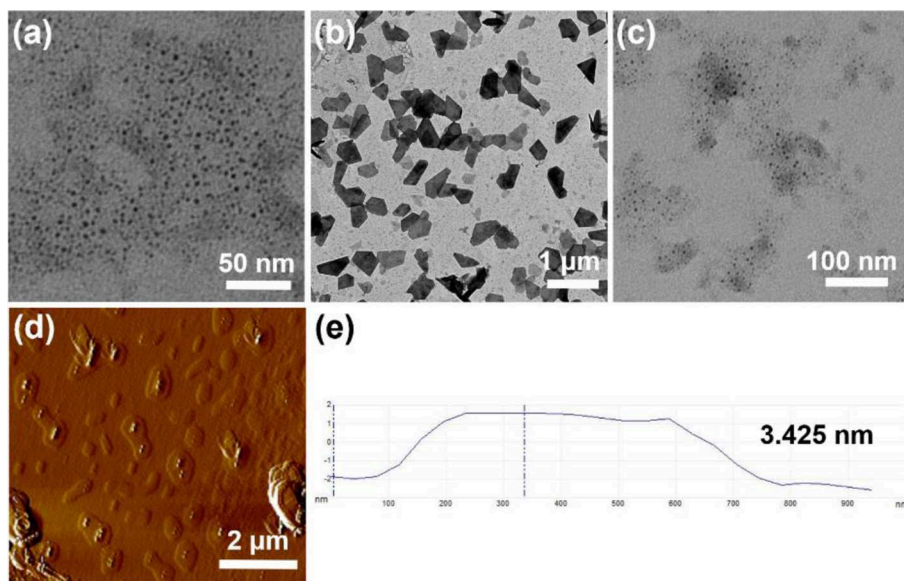
bridge and  $\text{H}_{2k}-\text{H}_{2j}$  on the alkyl chain (B), and between protons  $\text{H}_{2g}$ ,  $\text{H}_{2h}$  on the morpholine groups and  $\text{H}_{2i}-\text{H}_{2k}$  on the alkyl chain (C), suggesting that the alkyl chain thread into the cavity of **H2**. In addition, NOE correlation signals were also observed between alkyl chains, including the signals between protons  $\text{H}_{2j3}$  and  $\text{H}_{2k}$  (D) and between protons  $\text{H}_{2j4}$  and  $\text{H}_{2k}$  (E), confirming the formation of the [c2]daisy chain based on **H2**.

## Critical Aggregation Concentration Determinations

The CACs of **H1** and **H2** were measured. As shown in Figure 4, the CACs of **H1** and **H2** were measured to be  $3.69 \times 10^{-6}$  M and  $2.67 \times 10^{-5}$  M, respectively, using the concentration-dependent conductivity measurements.



**FIGURE 4 | (A)** The concentration-dependent conductivity of **H1**. The critical aggregation concentration (CAC) was determined to be  $3.69 \times 10^{-6}$  M and **(B)** the concentration-dependent conductivity of the **H2**. The CAC was determined to be  $2.67 \times 10^{-5}$  M.



**FIGURE 5 | (a)** TEM image of **H1** ( $1.00 \times 10^{-4}$  M) aggregates in water; **(b)** TEM image of a after addition of hydrochloric acid; **(c)** TEM image of **(b)** after addition of sodium hydroxide; **(d)** AFM image of **(b)**; **(e)** measured thickness of **(d)**.

## Transmission Electron Microscopy and Atomic Force Microscopy Investigations

The self-assembly morphologies in water were investigated by TEM and AFM. As shown in **Figure 5a**, **H1** formed micelles with an average diameter of  $\sim 6$  nm, which was near to the length of two **H1** molecules. After adding hydrochloride acid to the solution of **H1** to adjust the pH-value to 4.0, **H1** turned into **H2**, the micelles changed into nanosheets (**Figure 5b**). After further addition of sodium hydroxide to the solution of **H2**, the nanosheets turned back to micelles (**Figure 5c**). AFM experiments were also carried out to investigate the self-assembled morphology by **H2**. As shown in **Figures 5d,e**, the nanosheet morphology was confirmed and the wall thickness was  $\sim 3.425$  nm from AFM results, which was about the extended length of the [c2]daisy chain, suggesting that the nanosheets had a bilayer wall.

## CONCLUSION

In summary, a pillararene-based macrocyclic amphiphile **H1** was prepared. **H1** can act as a single-chain amphiphile and self-assembled into micelles in water. After changing the pH of the solution of **H1** to below 5.0, the single-chain amphiphiles turned into [c2]daisy chain-based bola-type supramolecular amphiphiles. As a result, the micelles turned into nanosheets when self-assembling in water. This pH-induced transition between macrocyclic single-chain amphiphile and [c2]daisy chain-based bola-type supramolecular amphiphiles based on pillararenes was first reported, providing a new strategy to tailor the structure

and self-assembly property of macrocyclic amphiphiles. The corresponding pH-responsive self-assembly system provides a promising candidate for advanced material such as controlled release, drug delivery systems, and surface modification.

## DATA AVAILABILITY STATEMENT

Compound characterization, full synthetic details for this study are included in the article/**Supplementary Material**.

## AUTHOR CONTRIBUTIONS

PW, RW, and DX made contributions to the experiments. All authors extensively discussed the results. The paper was written by PW. All authors reviewed the manuscript. All authors extensively discussed the results, reviewed the manuscript, and approved the final version of the manuscript to be submitted.

## FUNDING

This work was supported by National Science Foundation for Young Scientists of China (21704073, 21901149).

## SUPPLEMENTARY MATERIAL

The Supplementary Material for this article can be found online at: <https://www.frontiersin.org/articles/10.3389/fchem.2019.00894/full#supplementary-material>

## REFERENCES

- Chang, Y., Chen, J.-Y., Yang, J., Lin, T., Zeng, L., Xu, J.-F., et al. (2019a). Targeting the cell membrane by charge-reversal amphiphilic pillar[5]arene for the selective killing of cancer cells. *ACS Appl. Mater. Interfaces* 11, 38497–38502. doi: 10.1021/acsami.9b13492
- Chang, Y., Jiao, Y., Symons, H. E., Xu, J. F., Faul, C. F. J., and Zhang, X. (2019b). Molecular engineering of polymeric supra-amphiphiles. *Chem. Soc. Rev.* 48, 989–1003. doi: 10.1039/C8CS00806J
- Chang, Y., Yang, K., Wei, P., Huang, S., Pei, Y., Zhao, W., et al. (2014). Cationic vesicles based on amphiphilic pillar[5]arene capped with ferrocenium: a redox-responsive system for drug/siRNA co-delivery. *Angew. Chem. Int. Ed.* 53, 13126–13130. doi: 10.1002/anie.201407272
- Chen, J., Wang, Y., Wang, C., Long, R., Chen, T., and Yao, Y. (2019). Functionalization of inorganic nanomaterials with pillar[n]arenes. *Chem. Commun.* 55, 6817–6826. doi: 10.1039/C9CC03165K
- Discher, D. E., and Eisenberg, A. (2002). Polymer vesicles. *Science* 297, 967–973. doi: 10.1126/science.1074972
- Gao, J., Li, J., Geng, W.-C., Chen, F.-Y., Duan, X., Zheng, Z., et al. (2018). Biomarker displacement activation: a general host-guest strategy for targeted phototheranostics *in vivo*. *J. Am. Chem. Soc.* 140, 4945–4953. doi: 10.1021/jacs.8b02331
- Gao, L., Zheng, B., Yao, Y., and Huang, F. (2013). Responsive reverse giant vesicles and gel from self-organization of a bolaamphiphilic pillar[5]arene. *Soft Matter* 9, 7314–7319. doi: 10.1039/c3sm51047f
- Geng, W.-C., Liu, Y.-C., Wang, Y.-Y., Xu, Z., Zheng, Z., Yang, C.-B., et al. (2017). A self-assembled white-light-emitting system in aqueous medium based on a macrocyclic amphiphile. *Chem. Commun.* 53, 392–395. doi: 10.1039/C6CC09079F
- Guo, S., Song, Y., He, Y., Hu, X.-Y., and Wang, L. (2018). Highly efficient artificial light-harvesting systems constructed in aqueous solution based on supramolecular self-assembly. *Angew. Chem. Int. Ed.* 57:1363. doi: 10.1002/anie.201800175
- Himmelein, S., Lewe, V., Stuart, M. C. A., and Ravoo, B. J. (2014). A carbohydrate-based hydrogel containing vesicles as responsive non-covalent cross-linkers. *Chem. Sci.* 5, 1054–1058. doi: 10.1039/c3sc52964a
- Himmelein, S., and Ravoo, B. J. (2017). A self-assembled sensor for carbohydrates on the surface of cyclodextrin vesicles. *Chem. Eur. J.* 23, 6034–6041. doi: 10.1002/chem.201603115
- Hu, X., Hu, J., Tian, J., Ge, Z., Zhang, G., Luo, K., et al. (2013). Polyprodrug amphiphiles: hierarchical assemblies for shape-regulated cellular internalization, trafficking, and drug delivery. *J. Am. Chem. Soc.* 135, 17617–17629. doi: 10.1021/ja409686x
- Hu, X. Y., Gao, L., Mosel, S., Ehlers, M., Zellermann, E., Jiang, H., et al. (2018). From supramolecular vesicles to micelles: controllable construction of tumor-targeting nanocarriers based on host-guest interaction between a pillar[5]arene-based prodrug and a RGD-sulfonate guest. *Small* 14:e1803952. doi: 10.1002/smll.201803952
- Hua, B., Shao, L., Zhang, Z., Liu, J., and Huang, F. (2019). Cooperative silver ion-pair recognition by peralkylated pillar[5]arenes. *J. Am. Chem. Soc.* 141, 15008–15012. doi: 10.1021/jacs.9b08257
- Hua, B., Zhou, W., Yang, Z., Zhang, Z., Shao, L., Zhu, H., et al. (2018). Supramolecular solid-state microlaser constructed from pillar[5]arene-based host-guest complex microcrystals. *J. Am. Chem. Soc.* 140, 15651–15654. doi: 10.1021/jacs.8b11156

- Ji, X., Wang, H., Li, Y., Xia, D., Li, H., Tang, G., et al. (2016). Controlling amphiphilic copolymer self-assembly morphologies based on macrocycle/anion recognition and nucleotide-induced payload release. *Chem. Sci.* 7, 6006–6014. doi: 10.1039/C6SC01851C
- Jie, K., Yao, Y., Chi, X., and Huang, F. (2014). A CO(2)-responsive pillar[5]arene: synthesis and self-assembly in water. *Chem. Commun.* 50, 5503–5505. doi: 10.1039/c4cc01704h
- Jie, K., Zhou, Y., Yao, Y., and Huang, F. (2015). Macrocyclic amphiphiles. *Chem. Soc. Rev.* 44, 3568–3587. doi: 10.1039/C4CS00390J
- Kelley, E. G., Albert, J. N., Sullivan, M. O., and Epps, T. H. III. (2013). Stimuli-responsive copolymer solution and surface assemblies for biomedical applications. *Chem. Soc. Rev.* 42, 7057–7071. doi: 10.1039/c3cs35512h
- Lee, H. J., Le, P. T., Kwon, H. J., and Park, K. D. (2019). Supramolecular assembly of tetronic–adamantane and poly( $\beta$ -cyclodextrin) as injectable shear-thinning hydrogels. *J. Mater. Chem. B* 7, 3374–3382. doi: 10.1039/C9TB00072K
- Li, B., Meng, Z., Li, Q., Huang, X., Kang, Z., Dong, H., et al. (2017). A pH responsive complexation-based drug delivery system for oxaliplatin. *Chem. Sci.* 8, 4458–4464. doi: 10.1039/C7SC01438D
- Li, P. Y., Chen, Y., Chen, C. H., and Liu, Y. (2019). Amphiphilic multi-charged cyclodextrins and vitamin K co-assembly as a synergistic coagulant. *Chem. Commun.* 55, 11790–11793. doi: 10.1039/C9CC06545H
- Ma, X., and Zhao, Y. (2015). Biomedical applications of supramolecular systems based on host–guest interactions. *Chem. Rev.* 115, 7794–7839. doi: 10.1021/cr500392w
- Nierengarten, I., Nothisen, M., Sigwalt, D., Biellmann, T., Holler, M., Remy, J.-S., et al. (2013). Polycationic pillar[5]arene derivatives: interaction with DNA and biological applications. *Chem. A Eur. J.* 19, 17552–17558. doi: 10.1002/chem.201303029
- Ping, G., Wang, Y., Shen, L., Wang, Y., Hu, X., Chen, J., et al. (2017). Highly efficient complexation of sanguinarine alkaloid by carboxylatopillar[6]arene: pKa shift, increased solubility and enhanced antibacterial activity. *Chem. Commun.* 53, 7381–7384. doi: 10.1039/C7CC02799K
- Redondo-Gomez, C., Abdouni, Y., Becer, C. R., and Mata, A. (2019). Self-assembling hydrogels based on a complementary host–guest peptide amphiphile pair. *Biomacromolecules* 20, 2276–2285. doi: 10.1021/acs.biomac.9b00224
- Sathiyajith, C., Shaikh, R. R., Han, Q., Zhang, Y., Meguellati, K., and Yang, Y.-W. (2017). Biological and related applications of pillar[n]arenes. *Chem. Commun.* 53, 677–696. doi: 10.1039/C6CC08967D
- Shi, B., Jie, K., Zhou, Y., Zhou, J., Xia, D., and Huang, F. (2016). Nanoparticles with near-infrared emission enhanced by pillararene-based molecular recognition in water. *J. Am. Chem. Soc.* 138, 80–83. doi: 10.1021/jacs.5b11676
- Shi, B., Xia, D., and Yao, Y. (2014). A water-soluble supramolecular polymer constructed by pillar[5]arene-based molecular recognition. *Chem. Commun.* 50, 13932–13935. doi: 10.1039/C4CC06971D
- Shulov, I., Rodik, R. V., Arntz, Y., Reisch, A., Kalchenko, V. I., and Klymchenko, A. S. (2016). Protein-sized bright fluorogenic nanoparticles based on cross-linked calixarene micelles with cyanine corona. *Angew. Chem. Int. Ed.* 55, 15884–15888. doi: 10.1002/anie.201609138
- Sorrenti, A., Illa, O., and Ortuno, R. M. (2013). Amphiphiles in aqueous solution: well beyond a soap bubble. *Chem. Soc. Rev.* 42, 8200–8219. doi: 10.1039/c3cs60151j
- Sun, S., Geng, M., Huang, L., Chen, Y., Cen, M., Lu, D., et al. (2018). A new amphiphilic pillar[5]arene: synthesis and controllable self-assembly in water and application in white-light-emitting systems. *Chem. Commun.* 54, 13006–13009. doi: 10.1039/C8CC07658H
- Wang, K. P., Chen, Y., and Liu, Y. (2015). A polycation-induced secondary assembly of amphiphilic calixarene and its multi-stimuli responsive gelation behavior. *Chem. Commun.* 51, 1647–1649. doi: 10.1039/C4CC08721F
- Wang, S.-P., Lin, W., Wang, X., Cen, T.-Y., Xie, H., Huang, J., et al. (2019). Controllable hierarchical self-assembly of porphyrin-derived supra-amphiphiles. *Nat. Commun.* 10:1399. doi: 10.1038/s41467-019-09363-y
- Wang, Y., Cai, Y., Cao, L., Cen, M., Chen, Y., Zhang, R., et al. (2019). An amphiphilic metallaclip with enhanced fluorescence emission in water: synthesis and controllable self-assembly into multi-dimensional micro-structures. *Chem. Commun.* 55, 10132–10134. doi: 10.1039/C9CC04809J
- Webber, M. J., and Langer, R. (2017). Drug delivery by supramolecular design. *Chem. Soc. Rev.* 46, 6600–6620. doi: 10.1039/C7CS00391A
- Wei, P., Cook, T. R., Yan, X., Huang, F., and Stang, P. J. (2014). A discrete amphiphilic organoplatinum(II) metallacycle with tunable lower critical solution temperature behavior. *J. Am. Chem. Soc.* 136, 15497–15500. doi: 10.1021/ja5093503
- Xia, D., Li, Y., Jie, K., Shi, B., and Yao, Y. (2016). A water-soluble cyclotrimeratrylene-based supra-amphiphile: synthesis, pH-responsive self-assembly in water, and its application in controlled drug release. *Org. Lett.* 18, 2910–2913. doi: 10.1021/acs.orglett.6b01264
- Xia, D., Wang, P., and Shi, B. (2017). Cu(II) ion-responsive self-assembly based on a water-soluble pillar[5]arene and a rhodamine B-containing amphiphile in aqueous media. *Org. Lett.* 19, 202–205. doi: 10.1021/acs.orglett.6b03486
- Xiao, T., Qi, L., Zhong, W., Lin, C., Wang, R., and Wang, L. (2019). Stimuli-responsive nanocarriers constructed from pillar[n]arene-based supra-amphiphiles. *Mater. Chem. Front.* 3, 1973–1993. doi: 10.1039/C9QM00428A
- Xu, L., Wang, Z., Wang, R., Wang, L., He, X., Jiang, H., et al. (2019). A conjugated polymeric supramolecular network with aggregation-induced emission enhancement: an efficient light-harvesting system with an ultrahigh antenna effect. *Angew. Chem. Int. Ed.* 58:1. doi: 10.1002/anie.201907678
- Yang, K., Chang, Y., Wen, J., Lu, Y., Pei, Y., Cao, S., et al. (2016). Supramolecular vesicles based on complex of trp-modified pillar[5]arene and galactose derivative for synergistic and targeted drug delivery. *Chem. Mater.* 28, 1990–1993. doi: 10.1021/acs.chemmater.6b00696
- Yao, Y., Xue, M., Chen, J., Zhang, M., and Huang, F. (2012). An amphiphilic pillar[5]arene: synthesis, controllable self-assembly in water, and application in calcein release and TNT adsorption. *J. Am. Chem. Soc.* 134, 15712–15715. doi: 10.1021/ja3076617
- Yu, G., Jie, K., and Huang, F. (2015). Supramolecular amphiphiles based on host–guest molecular recognition motifs. *Chem. Rev.* 115, 7240–7303. doi: 10.1021/cr5005315
- Yu, G., Ma, Y., Han, C., Yao, Y., Tang, G., Mao, Z., et al. (2013). A sugar-functionalized amphiphilic pillar[5]arene: synthesis, self-assembly in water, and application in bacterial cell agglutination. *J. Am. Chem. Soc.* 135, 10310–10313. doi: 10.1021/ja405237q
- Zhang, H., Liu, Z., and Zhao, Y. (2018). Pillararene-based self-assembled amphiphiles. *Chem. Soc. Rev.* 47, 5491–5528. doi: 10.1039/C8CS00037A
- Zhang, X., and Wang, C. (2011). Supramolecular amphiphiles. *Chem. Soc. Rev.* 40, 94–101. doi: 10.1039/B919678C
- Zhang, Z., Yu, G., Han, C., Liu, J., Ding, X., Yu, Y., et al. (2011). Formation of a cyclic dimer containing two mirror image monomers in the solid state controlled by van der Waals forces. *Org. Lett.* 13, 4818–4821. doi: 10.1021/ol2018938
- Zhu, H., Shangguan, L., Shi, B., Yu, G., and Huang, F. (2018). Recent progress in macrocyclic amphiphiles and macrocyclic host-based supra-amphiphiles. *Mater. Chem. Front.* 2, 2152–2174. doi: 10.1039/C8QM00314A
- Zuo, M., Qian, W., Xu, Z., Shao, W., Hu, X.-Y., Zhang, D., et al. (2018). Multiresponsive supramolecular theranostic nanoplatfrom based on pillar[5]arene and diphenylboronic acid derivatives for integrated glucose sensing and insulin delivery. *Small* 14:1801942. doi: 10.1002/smll.201801942

**Conflict of Interest:** The authors declare that the research was conducted in the absence of any commercial or financial relationships that could be construed as a potential conflict of interest.

Copyright © 2020 Wang, Wang and Xia. This is an open-access article distributed under the terms of the Creative Commons Attribution License (CC BY). The use, distribution or reproduction in other forums is permitted, provided the original author(s) and the copyright owner(s) are credited and that the original publication in this journal is cited, in accordance with accepted academic practice. No use, distribution or reproduction is permitted which does not comply with these terms.



# *p*-tert-Butyldihomooxalix[4]arene Based Soft Gel for Sustained Drug Release in Water

Hao Guo<sup>1,2</sup>, Runmiao Zhang<sup>1,2</sup>, Ying Han<sup>1\*</sup>, Jin Wang<sup>2\*</sup> and Chaoguo Yan<sup>1</sup>

<sup>1</sup> School of Chemistry and Chemical Engineer, Yangzhou University, Yangzhou, China, <sup>2</sup> School of Chemistry and Chemical Engineer, Nantong University, Nantong, China

## OPEN ACCESS

### Edited by:

Tangxin Xiao,  
Changzhou University, China

### Reviewed by:

Dong-Sheng Guo,  
Nankai University, China  
De-Xian Wang,  
Institute of Chemistry Chinese  
Academy of Sciences, China

### \*Correspondence:

Ying Han  
hanying@yzu.edu.cn  
Jin Wang  
wangjin107@ntu.edu.cn

### Specialty section:

This article was submitted to  
Supramolecular Chemistry,  
a section of the journal  
Frontiers in Chemistry

**Received:** 19 November 2019

**Accepted:** 09 January 2020

**Published:** 28 February 2020

### Citation:

Guo H, Zhang R, Han Y, Wang J and  
Yan C (2020)  
*p*-tert-Butyldihomooxalix[4]arene  
Based Soft Gel for Sustained Drug  
Release in Water. *Front. Chem.* 8:33.  
doi: 10.3389/fchem.2020.00033

*P*-tert-butylidihomooxalix[4]arene is a well-known calix[4]arene analog in which one CH<sub>2</sub> bridge is replaced by one -CH<sub>2</sub>OCH<sub>2</sub>- group. Thus, dihomooxalix[4]arene has a slightly larger cavity than that of calix[4]arene and usually possesses a more flexible cone conformation, and the bridged oxygen atom might provide additional binding sites. Here, we synthesized a new functional *p*-tert-butylidihomooxalix[4]arene **1** through Ugi reaction with good yield (70%), starting from condensed *p*-tert-butylidihomooxalix[4]arene *O*-alkoxy-substituted benzaldehydes, benzoic acid, benzylamine, and cyclohexyl isocyanide. Proton nuclear magnetic resonance spectroscopy (<sup>1</sup>H NMR), <sup>13</sup>C NMR, IR, and diffusion-ordered <sup>1</sup>H NMR spectroscopy (DOSY) methods were used to characterize the structure of **1**. Then soft gel was prepared by adding **1** into cyclohexane directly. It shows remarkable thermoreversibility and can be demonstrated for several cycles. As is revealed by scanning electron microscopy (SEM) images, xerogel showed highly interconnected and homogeneous porous network structures, and hence, the gel is suitable for storage and controlled release.

**Keywords:** calixarenes, gel, controlled release, macrocyclic compounds, Ugi reaction

## INTRODUCTION

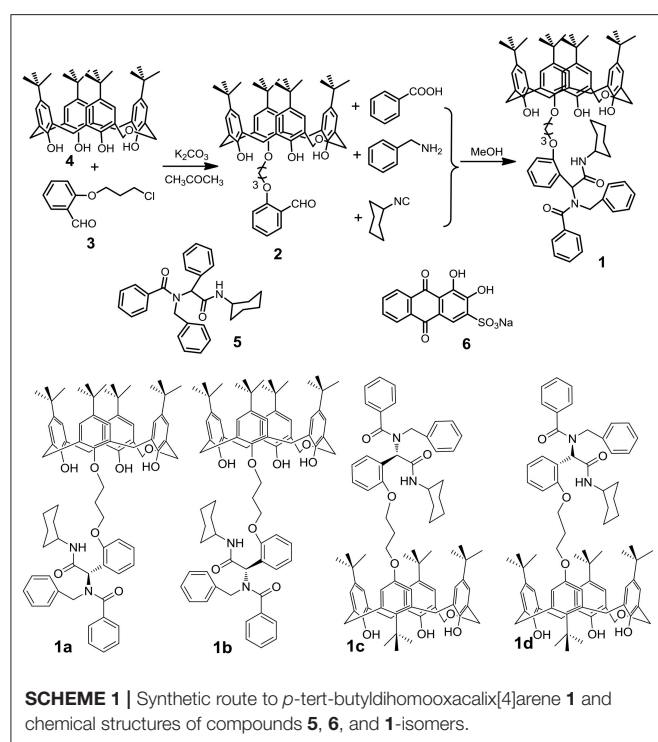
The designed and prepared macrocyclic hosts [mainly including crown ethers (Liu et al., 2017; Morrison et al., 2017), cyclodextrins (Zhang et al., 2018; Larsen and Beeren, 2019), calixarenes (Wang et al., 2015; Tian et al., 2019), cucurbiturils (Kim et al., 2007; Wu et al., 2018; Xiao B. et al., 2019), and pillar[*n*]arenes (Xue et al., 2012; Sun et al., 2018; Chen et al., 2019; Ogoshi et al., 2019; Xiao T. et al., 2019)] and the investigations of their host-guest properties are the foundation of the development of supramolecular chemistry (Zheng et al., 2012; Yao et al., 2018; Zhang et al., 2019). As the third generation of macrocyclic compounds in supramolecular chemistry, calixarenes possess several advantages, such as excellent flexibility, improved conformational mobility, and easy modification (Kim et al., 2012; Nimse and Kim, 2013).

*P*-tert-butylidihomooxalix[4]arene is a well-known *p*-tert-butylcalix[4]arene analog in which one CH<sub>2</sub> bridge is replaced by one -CH<sub>2</sub>OCH<sub>2</sub>- group (Marcos et al., 2002). Thus, dihomooxalix[4]arene has a slightly larger cavity than that of calix[4]arene and usually possesses a more flexible cone conformation. What's more, the bridged oxygen atom might provide additional



binding sites (Teixeira et al., 2017; An et al., 2018; Zhao et al., 2019). On the other hand, gels are interesting soft materials owing to their functional properties, leading to potential applications (Yao et al., 2017). Using gels as drug carriers has attracted tremendous attention for their numerous advantages in medical treatments, including prolonged drug release time, reduced side effects of drugs, and maintained effective plasma concentration (Nishimura et al., 2019; Teng et al., 2019; Thamizhanban et al., 2019). For example, Prof. Yao and co-workers prepared a soft gel based on pillar[5]arene by using a carbazone reaction and found that dyes such as TPP or TPPE can be incorporated into this gel and then released in a sustained way in water due to solvent exchange (Yao et al., 2017). However, investigations about supramolecular gels based on *p*-tert-butyldihomooxalix[4]arene and their applications are rarely reported.

Herein, we designed and synthesized a novel functionalized *p*-tert-butyldihomooxalix[4]arene **1** with two H-bonding sites through Ugi reaction (Scheme 1), which was prepared with good yield (70%). Then the soft gel was constructed by adding **1** into cyclohexane, heating the mixture, and leaving it cooled in the refrigerator for 2 min. **1**-based gel showed remarkable thermoreversibility, and this can be demonstrated for several cycles. The morphology of xerogel was revealed by scanning electron microscopy (SEM) images, which showed highly interconnected and homogeneous porous network structures. What's more, this gel can persist in its shape in water. Organic dyes such as alizarin red S **6** can be incorporated into this gel and are observed to be released in a sustained way in water. This may be very useful for preparing future smart materials by the implementation of related macrocyclic derivatives.



## MATERIALS AND METHODS

### Synthesis of

#### *p*-tert-Butyldihomooxalix[4]-Arene **1**

*P*-tert-butyldihomooxalix[4]arene **4** (4.0 g, 5.9 mmol), Cl-alkoxy-substituted salicylaldehyde (1.8 g, 9.0 mmol), K<sub>2</sub>CO<sub>3</sub> (1.2 g, 9.0 mmol), and KI (1.5 g) was added in 150 ml acetone. The mixture was stirred at 75°C for 24 h (Scheme S1). After removal of the inorganic salt, the solvent was evaporated, and the residue was purified by chromatography on silica gel (petroleum ether/ethyl acetate, v/v 5:1) to give **2** as a white solid (Liu et al., 2018). Then **2** (0.1 mmol, 0.885 g), benzyl amine (0.1 mmol, 0.107 g), benzoic acid (0.1 mmol, 0.122 g), and isocyanocyclohexane (0.1 mmol, 0.109 g) were added into 7 ml methanol for reacting for 36 h. Then the solvent was evaporated, and the residue was purified by chromatography on silica gel (petroleum ether/ethyl acetate, v/v 3:1) to give **1** as a light yellow solid.

**1**: Yellow solid, 70%, m.p. 163.6–164.8°C; proton nuclear magnetic resonance spectroscopy (<sup>1</sup>H NMR) (400 MHz, CDCl<sub>3</sub>) (Figure S1) δ: A-isomer: 9.18 (brs, 1H, OH), 8.52 (s, 1H, OH), 7.74 (s, 1H, OH), 7.45–7.28 (m, 7H, pH), 7.26–7.82 (m, 15H, pH), 6.12 (s, 1H, CH), 5.23 (s, 1H, CH), 5.01–4.91 (m, 1H, CH<sub>2</sub>), 4.77–4.65 (m, 2H, CH<sub>2</sub>), 4.55–4.03 (m, 10H, CH<sub>2</sub>), 3.83–3.73 (m, 1H, CH<sub>2</sub>), 3.32–3.26 (m, 1H, CH<sub>2</sub>), 2.48–2.41 (m, 3H, CH<sub>2</sub>), 1.88–1.52 (m, 7H, CH<sub>2</sub>), 1.37–0.88 (m, 36H, CH<sub>3</sub>); B-isomer: 8.85 (s, 1H, OH), 6.28 (s, 1H, CH), 5.59 (s, 1H, CH); C-isomer: 8.33 (s, 1H, OH), 6.12 (s, 1H, CH), 5.48 (s, 1H, CH); D-isomer: 8.15 (s, 1H, OH), 5.69 (s, 1H, CH), 5.29 (s, 1H, CH); ratio of A/B/C/D-isomer = 0.2:0.1:0.1:0.1; <sup>1</sup>H NMR (400 MHz, cyclohexane-d) δ: A-isomer: 9.50 (s, 1H, OH), 8.70 (s, 1H, OH), 7.90 (s, 1H, OH), 7.54–7.01 (m, 13H, pH), 6.87–6.72 (m, 9H, pH), 5.87–5.42 (m, 2H, CH), 4.88–3.91 (m, 14H, CH<sub>2</sub>), 3.67–3.08 (m, 6H, CH<sub>2</sub>), 2.48–2.37 (m, 2H, CH<sub>2</sub>), 1.86–1.45 (m, 6H, CH<sub>2</sub>), 1.23–1.18 (m, 27H, CH<sub>3</sub>), 1.17–1.15 (m, 9H, CH<sub>3</sub>); B-isomer: 8.33 (s, 1H, OH); ratio of A/B-isomer = 0.9:1 (Figure S9, Scheme S3); <sup>13</sup>C NMR (100 MHz, CDCl<sub>3</sub>) (Figure S2) δ: 173.2, 157.4, 157.2, 152.7, 151.2, 149.1, 148.0, 147.8, 143.8, 142.7, 141.8, 141.7, 136.9, 132.8, 132.6, 131.9, 131.5, 130.3, 129.6, 128.4, 128.2, 128.2, 128.0, 127.8, 127.5, 127.5, 126.9, 126.9, 126.8, 126.8, 126.6, 126.0, 125.9, 125.8, 125.7, 125.3, 123.9, 122.8, 122.7, 120.7, 111.7, 77.4, 77.2, 77.0, 73.0, 72.6, 72.1, 71.7, 64.8, 64.4, 48.6, 34.3, 34.0, 33.9, 32.9, 32.8, 32.6, 31.7, 31.6, 31.5, 31.5, 31.5, 31.3, 30.3, 30.3, 30.1, 29.9, 29.8, 25.5, 25.1, 25.0; IR (KBr) ν: 3,386, 3,056, 2,959, 2,864, 1,735, 1,681, 1,637, 1,489, 1,453, 1,399, 1,361, 1,297, 1,246, 1,203, 1,077, 1,051, 876, 788, 735, 698, 596 cm<sup>-1</sup>; MS (*m/z*): HRMS (ESI) calcd. for C<sub>76</sub>H<sub>92</sub>N<sub>2</sub>O<sub>8</sub>Na ([M+Na]<sup>+</sup>): 1183.6751, found: 1183.6797 (Figure S3).

### Materials

All reagents and solvents were commercially available in analytical grade and used as received. Further purification and drying by standard methods were employed, and distillation was done prior to use when necessary. All evaporations of organic solvents were carried out with a rotary evaporator in conjunction with a water aspirator. *p*-tert-Butyldihomooxalix[4]arenes were prepared according to published methods (Marcos et al., 2002). Melting point measurements were taken on a hot-plate



microscope apparatus and are uncorrected.  $^1\text{H}$  and  $^{13}\text{C}$  NMR spectra were recorded with an Avance III 400 MHz or 600 MHz liquid-state NMR spectrometer. IR spectra were obtained on a Bruker Tensor 27 spectrophotometer (KBr disk). HRMS was determined on a Bruker maXis mass spectrometer. Fluorescence spectra were recorded on a Shimadzu HITACHI F-4500 spectrophotometer. Rheological studies were performed on an AR-G2 rheometer (TA Instruments, USA) using a plate-plate geometry. The SEM image was obtained from a ZEISS Gemini SEM 300 instrument.

## RESULTS AND DISCUSSION

### Gelation Tests

The gelation test results obtained for calix[4]arene **1** in different solvents are shown in **Figure 1**. We chose methanol, ethanol, pentanol, *tert*-butanol, acetonitrile, ethyl acetate, tetrahydrofuran, toluene, cyclopentane, cyclohexane, and hexane as the solvents and found that **1** can disperse well in all these solvents with the concentration at about 100 mmol at 40°C. However, when the temperature cooled to 25°C, **1** could form a gel in cyclohexane (**Figure 1**, under, sample j) but could not form a gel in methanol, ethanol, pentanol, *tert*-butanol, acetonitrile, ethyl acetate, tetrahydrofuran, toluene, and hexane, as the samples flowed under gravity (**Figure 1**, under, samples a, b, c, d, e, f, g, h, k). Sample i seemed to be gelled but also flowed under slight vibrations. For comparison, compound **5** in **Scheme S2** (**Figures S4** and **S5**) without the calix[4]arene framework could not form a gel in the same condition, indicating that the calix[4]arene framework is an integral part of the gel formation process. Further investigation found that the critical concentration of compound **1** to form a gel in cyclohexane is 10.9 wt%. It should be pointed out that the compound **1** we used to construct gel contains both conformers.

### $^1\text{H}$ NMR Studies

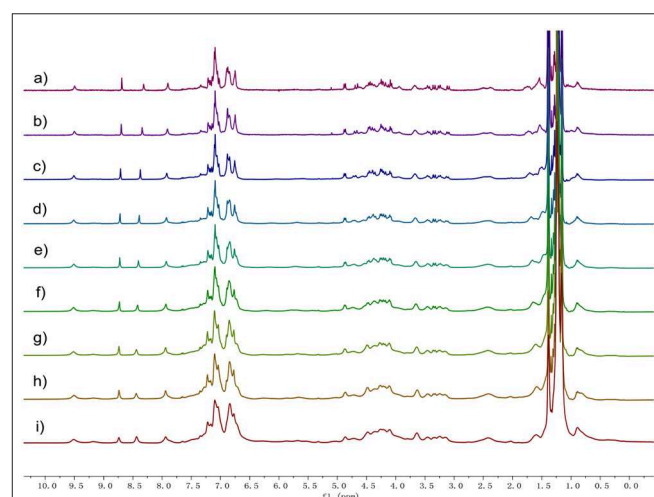
In order to investigate the intermolecular interactions during gel formation,  $^1\text{H}$  NMR and 2D diffusion-ordered  $^1\text{H}$  NMR spectroscopy (DOSY) were performed. As shown in **Figure 2**,  $^1\text{H}$  NMR spectra of **1** in *d*-cyclohexanes were recorded over the concentration range of 5.00 up to 80 mM. As the concentration

increased, all the signals of protons on compound **1** became broad, which demonstrated the formation of high-molecular-weight aggregates (Yan et al., 2012).

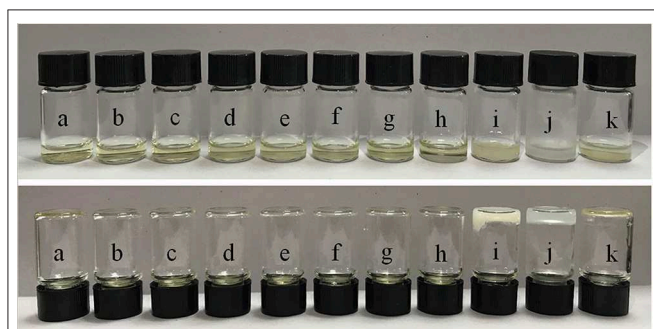
DOSY showed that the weight-average diffusion coefficient ( $D$ ) of **1** in cyclohexane-*d* decreased gradually from  $2.03 \times 10^{-10}$  to  $3.15 \times 10^{-11} \text{ m}^2 \text{ s}^{-1}$  upon the concentration of **1** increasing from 5.0 up to 80 mM (**Figure S7**, ESI<sup>†</sup>). FT-IR investigation confirmed the formation of H-bond after **1** self-assembly into gel (**Figure S8**). These observations proved that there is an increase in the average aggregation size owing to the concentration going on, indicating the formation of polymeric structures in cyclohexane.

### Rheological Properties

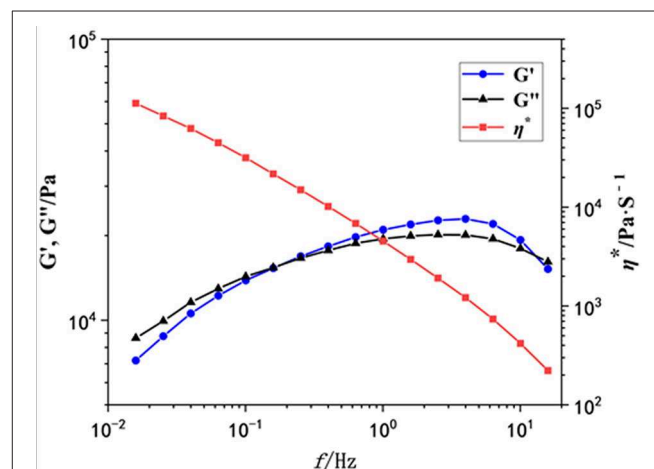
Then we used oscillatory rheological characterization to investigate the mechanical properties of this gel in detail. The



**FIGURE 2** | Proton nuclear magnetic resonance spectroscopy ( $^1\text{H}$ ) NMR spectra (400 MHz, cyclohexane-*d*, 20°C) of **1** at different concentrations: (a) 5, (b) 10, (c) 20, (d) 30, (e) 40, (f) 50, (g) 60, (h) 70, and (i) 80 mM.



**FIGURE 1** | Gelation test of compound **1** in different solvents: (a) methanol; (b) ethanol; (c) pentanol; (d) *tert*-butanol; (e) acetonitrile; (f) ethyl acetate; (g) tetrahydrofuran; (h) toluene; (i) cyclopentane; (j) cyclohexane; and (k) hexane.

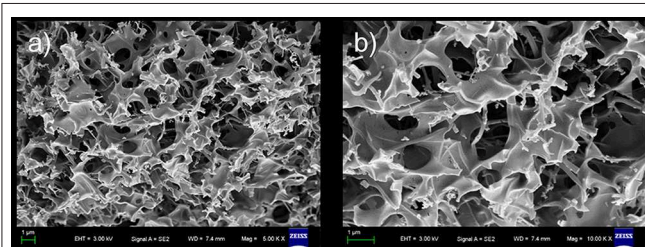


**FIGURE 3** | The rheological property of the gel as a function of the scanning frequency (Hz).  $G'$ : blue points;  $G''$ , black points;  $\eta^*$ , red points.

storage ( $G'$ ) and loss ( $G''$ ) moduli of the obtained gel as a function of the scanning frequency ( $f$ ) were investigated. As shown in **Figure 3**, when the  $f$  increased to 0.2, the intersection point of  $G'$  and  $G''$  ( $G' = G''$ ) appeared, indicating the formation of a gel. However,  $G'$  is larger than  $G''$  at frequencies from 0.2 to 20 Hz, and both  $G'$  and  $G''$  are independent of the frequency, indicating the existence of network structures in the gel. The value of  $G'$  is about 10,000 Pa, so this gel exhibits moderate mechanical properties. Additionally, the viscometry ( $\eta^*$ , red line) decreased sharply with the scanning frequency increasing.

## SEM

The morphology of this xerogel, which was obtained using a freeze-drying methodology to remove cyclohexane, was then examined by SEM. As shown in **Figure 4**, SEM revealed that the xerogel was an interconnected honeycomb-like porous structure in which large open plate-like structures and fibrils with diameters of 200 nm and lengths of several micrometers aggregated into very distinct micro-structured networks. It is worth pointing out that porous materials have attracted a great deal of interest in both science and technology due to their potential applications in many areas. Interestingly, at room temperature, our gel was stable for about 2 months in aqueous solution (pH from 3 to 11, **Figure S6**). Furthermore, the fresh gel can persist in its shape after pressing by heavy weight.



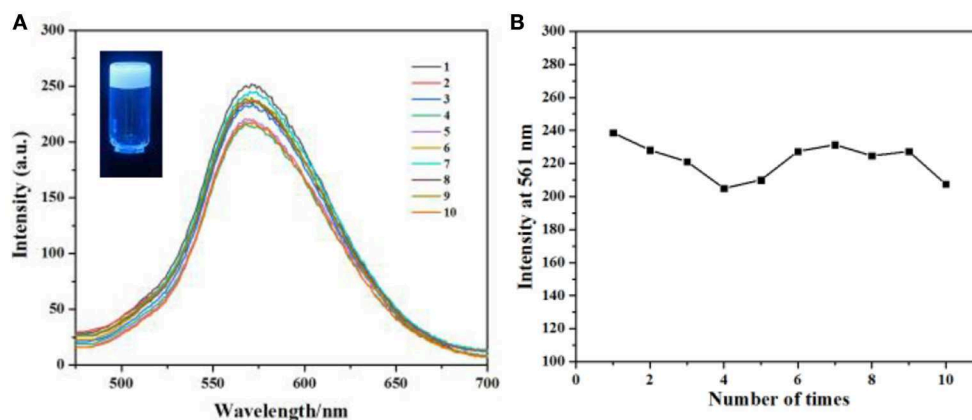
**FIGURE 4 |** Scanning electron microscopy (SEM) images of three-dimensional network of **1**-based xerogel. **(b)** is partial enlarge of **(a)**.

## Sustained Release

As we all known, gel is a new type of soft material, has obtained great interest from both chemistry and materials scientists, and has shown useful applications in various areas. When gel is applied in drug release, the major disadvantage is that most drugs will release in a rapid and complete way. In this condition, the concentration of the drug could not maintain a good value, so the efficiency of the uptake of the drug is very low. However, our supramolecular gel can incorporate some small molecules and then release them in a sustained way in water. So our gel can be used in sustained drug release for cancer therapy with good efficiency. Herein, alizarin red S **6** was used as a model compound to investigate the potential of our gel as a platform for sustained drug release. **6** can be incorporated in our soft gel to form a fluorescence gel (**Figure 5**, inset). Then when we immersed this gel in water and changed the water every 12 h, the fluorescence intensity of the solution also remained a certain value after repeating 10 times (**Figure 5**), indicating that **6** was released from calixarene-based gel in a sustained way.

## CONCLUSIONS

In this paper, we synthesized a new calix[4]arene **1** through Ugi reaction, which was prepared with good yield (70%), starting from condensed *p*-tert-butylidihomooxcalix[4]arene O-alkoxy-substituted benzaldehydes, benzoic acid, benzylamine, and cyclohexyl isocyanide. Then soft gel was prepared by adding the **1** into cyclohexane directly through a heating/cooling process. The gel shows remarkable thermoreversibility, and this can be demonstrated for several cycles.  $^1\text{H}$  NMR, FT-IR, DOSY, rheological characterization, FL, and SEM were employed to study the formation process and resultant gel. Furthermore, compound **6** as a model drug can be incorporated into our supramolecular gel and was observed to be released in a sustained way in water. This may have potential applications in sustained drug release for cancer therapy. Our next study will focus on cell and animal experiments of this gel in sustained drug release for cancer therapy.



**FIGURE 5 | (A)** Fluorescence emission spectra (the excitation wavelength is 365 nm) of **6** loaded gel vs. number of times water was changed. **(B)** The maximum intensity of **(A)** with the extraction times.

## DATA AVAILABILITY STATEMENT

The raw data supporting the conclusions of this article will be made available by the authors, without undue reservation, to any qualified researcher.

## AUTHOR CONTRIBUTIONS

Individual authors contributed to the present paper as follows: HG and RZ prepared all the compounds. YH and CY analyzed the data. JW and CY wrote the paper.

## REFERENCES

- An, L., Wang, J.-W., Wang, C., Zhou, S.-S., Sun, J., and Yan, C.-G. (2018). 2, 3-Ethylene-bridged dihomooxalix[4]arenes: synthesis, X-ray crystal structures and highly selective binding properties with anions. *New J. Chem.* 42:10689. doi: 10.1039/C8NJ01284A
- Chen, J., Wang, Y., Wang, C., Long, R., Chen, T., and Yao, Y. (2019). Functionalization of inorganic nanomaterials with pillar[n]arenes. *Chem. Commun.* 55, 6817–6826. doi: 10.1039/c9cc03165k
- Kim, H. J., Lee, M. H., Mutihac, L., Vicens, J., and Kim, J. S. (2012). Host-guest sensing by calixarenes on the surfaces. *Chem. Soc. Rev.* 41, 1173–1190. doi: 10.1039/c1cs15169j
- Kim, K., Selvapalam, N., Ko, Y. H., Park, K. M., Kim, D., and Kim, J. (2007). Functionalized cucurbiturils and their applications. *Chem. Soc. Rev.* 36, 267–279. doi: 10.1039/b603088m
- Larsen, D., and Beeren, S. R. (2019). Enzyme-mediated dynamic combinatorial chemistry allows out-of-equilibrium template-directed synthesis of macrocyclic oligosaccharides. *Chem. Sci.* 10, 9981–9987. doi: 10.1039/C9SC03983J
- Liu, Z., Nalluri, S. K. M., and Stoddart, J. F. (2017). Surveying macrocyclic chemistry: from flexible crown ethers to rigid cyclophanes. *Chem. Soc. Rev.* 46, 2459–2478. doi: 10.1039/c7cs00185a
- Liu, Y., Zhao, L.-L., Sun, J., and Yan, C.-G. (2018). Convenient synthesis and coordination properties of p-tert-butylidihomooxalix[4]arene mono-schiff bases. *Polycyclic Aromat. Compd.* 40, 644–659. doi: 10.1080/10406638.2018.1469520
- Marcos, P., Ascenso, J., and Pereira, J. L. C. (2002). Synthesis and NMR conformational studies of p-tert-butylidihomooxalix[4]arene derivatives bearing pyridyl pendant groups at the lower rim. *Eur. J. Org. Chem.* 2002, 3034–3041. doi: 10.1002/1099-0690(200209)2002:17<3034::AID-EJOC3034>3.0.CO;2-I
- Morrison, P. W. J., Porfiryeva, N. N., Chahal, S., Salakhov, I. A., Lacourt, C., Semina, I. I., et al. (2017). Crown ethers: novel permeability enhancers for ocular drug delivery? *Mol. Pharmaceutics* 14, 3528–3538. doi: 10.1021/acs.molpharmaceut.7b00556
- Nimse, S. B., and Kim, T. (2013). Biological application of functionalized calixarenes. *Chem. Soc. Rev.* 42, 366–386. doi: 10.1039/C2CS35233H
- Nishimura, T., Sumi, N., Mukai, S.-A., Sasaki, Y., and Akiyoshi, K. (2019). Supramolecular injectable hydrogels by crystallization-driven self-assembly of carbohydrate-conjugated poly(2-isopropylloxazoline)s for biomedical applications. *J. Mater. Chem. B* 7, 6362–6369. doi: 10.1039/c9tb00918c
- Ogoshi, T., Kakuta, T., and Yamagishi, T. A. (2019). Application of pillar[n]arene-based supramolecular assemblies. *Angew. Chem. Int. Ed.* 58, 2197–2206. doi: 10.1002/anie.201805884
- Sun, S., Geng, M., Huang, L., Chen, Y., Cen, M., Lu, D., et al. (2018). A new amphiphilic pillar[5]arene: synthesis and controllable self-assembly in water and application in white-light-emitting systems. *Chem. Commun.* 54, 13006–13009. doi: 10.1039/c8cc07658h
- Teixeira, F. A., Marcos, P. M., Ascenso, J. R., Brancatelli, G., Hickey, N., and Geremia, S. (2017). Selective binding of spherical and linear anions by tetraphenyl(thio)urea-based dihomooxalix[4]arene receptors. *J. Org. Chem.* 21, 11383–11390. doi: 10.1021/acs.joc.7b01801
- Teng, L., Chen, Y., Jia, Y.-G., and Ren, L. (2019). Supramolecular and dynamic covalent hydrogel scaffolds: from gelation chemistry to enhanced cell retention and cartilage regeneration. *J. Mater. Chem. B* 7, 6705–6736. doi: 10.1039/c9tb01698h
- Thamizhanban, A., Lalitha, K., Sarvepalli, G. P., Maheswari, C. U., Sridharan, V., Rayappan, J. B. B., et al. (2019). Smart supramolecular gels of enolizable amphiphilic glycosylfuran. *J. Mater. Chem. B* 7, 6238–6246. doi: 10.1039/c9tb01480b
- Tian, H.-W., Liu, Y.-C., and Guo, D.-S. (2019). Assembling features of calixarene-based amphiphilic and supra-amphiphiles. *Mater. Chem. Front.* 4, 46–98. doi: 10.1039/C9QM00489K
- Wang, Y.-X., Zhang, Y.-M., and Liu, Y. (2015). Photolysis of an amphiphilic assembly by calixarene-induced aggregation. *J. Am. Chem. Soc.* 137, 4543–4549. doi: 10.1021/jacs.5b01566
- Wu, W., Song, S., Cui, X., Sun, T., Zhang, J.-X., and Ni, X.-L. (2018). pH-Switched fluorescent pseudorotaxane assembly of cucurbit[7]uril with bispyridinium ethylene derivatives. *Chin. Chem. Lett.* 29, 95–98. doi: 10.1016/j.ccl.2017.08.049
- Xiao, B., Wang, Q., Zhang, S., Li, X.-Y., Long, S.-Q., Xiao, Y., et al. (2019). Cucurbit[7]uril-anchored polymer vesicles enhance photosensitization in the nucleus. *J. Mater. Chem. B* 7, 5966–5971. doi: 10.1039/c9tb01526d
- Xiao, T., Qi, L., Zhong, W., Lin, C., Wang, R., and Wang, L. (2019). Stimuli-responsive nanocarriers constructed from pillar[n]arene-based supra-amphiphiles. *Mater. Chem. Front.* 3, 1973–1993. doi: 10.1039/C9QM00428A
- Xue, M., Yang, Y., Chi, X., Zhang, Z., and Huang, F. (2012). Pillararenes, a new class of macrocycles for supramolecular chemistry. *Acc. Chem. Res.* 45, 1294–1308. doi: 10.1021/ar2003418
- Yan, X., Xu, D., Chi, X., Chen, J., Dong, S., Ding, X., et al. (2012). A multiresponsive, shape-persistent, and elastic supramolecular polymer network gel constructed by orthogonal self-assembly. *Adv. Mater.* 24, 362–369. doi: 10.1002/adma.201103220
- Yao, Y., Sun, Y., Yu, H., Chen, W., Dai, H., and Shi, Y. (2017). A pillar[5]arene based gel from a low molecular weight gelator for sustained dye release in water. *Dalton Trans.* 46, 16802–16806. doi: 10.1039/c7dt04001f
- Yao, Y., Zhao, R., Shi, Y., Cai, Y., Chen, J., Sun, S., et al. (2018). 2D amphiphilic organoplatinum(ii) metallacycles: their syntheses, self-assembly in water and potential application in photodynamic therapy. *Chem. Commun.* 54, 8068–8071. doi: 10.1039/c8cc04423f
- Zhang, R., Wang, C., Long, R., Chen, T., Yan, C., and Yao, Y. (2019). Pillar[5]arene based [1]rotaxane systems with redox-responsive host-guest property: design, synthesis and the key Role of chain length. *Front. Chem.* 7:508. doi: 10.3389/fchem.2019.00508

## FUNDING

This work was supported by the National Natural Science Foundation of China (21801139, 21871227) and Natural Science Foundation of Jiangsu Province (BK20180942).

## SUPPLEMENTARY MATERIAL

The Supplementary Material for this article can be found online at: <https://www.frontiersin.org/articles/10.3389/fchem.2020.00033/full#supplementary-material>

- Zhang, Y.-M., Zhang, N.-Y., Xiao, K., Yu, Q.-L., and Liu, Y. (2018). Photo-controlled reversible microtubule assembly mediated by paclitaxel-modified cyclodextrin. *Angew. Chem. Int. Ed.* 57, 8649–8653. doi: 10.1002/anie.201804620
- Zhao, L.-L., Yang, X.-S., Chong, H., Wang, Y., and Yan, C.-G. (2019). Multi-point interaction-based recognition of fluoride ions by tert-butylidihomooxcalix[4]arenes bearing phenolic hydroxyls and thiourea. *New J. Chem.* 43, 5503–5511. doi: 10.1039/C8NJ06333H
- Zheng, B., Wang, F., Dong, S., and Huang, F. (2012). Supramolecular polymers constructed by crown ether-based molecular recognition. *Chem. Soc. Rev.* 41, 1621–1636. doi: 10.1039/c1cs15220c

**Conflict of Interest:** The authors declare that the research was conducted in the absence of any commercial or financial relationships that could be construed as a potential conflict of interest.

Copyright © 2020 Guo, Zhang, Han, Wang and Yan. This is an open-access article distributed under the terms of the Creative Commons Attribution License (CC BY). The use, distribution or reproduction in other forums is permitted, provided the original author(s) and the copyright owner(s) are credited and that the original publication in this journal is cited, in accordance with accepted academic practice. No use, distribution or reproduction is permitted which does not comply with these terms.



# Corrigendum: A *p*-tert-Butyldihomooxacalix[4]arene Based Soft Gel for Sustained Drug Release in Water

Hao Guo<sup>1,2</sup>, Runmiao Zhang<sup>1,2</sup>, Ying Han<sup>1\*</sup>, Jin Wang<sup>2\*</sup> and Chaoguo Yan<sup>1</sup>

<sup>1</sup> School of Chemistry and Chemical Engineer, Yangzhou University, Yangzhou, China, <sup>2</sup> School of Chemistry and Chemical Engineer, Nantong University, Nantong, China

**Keywords:** calixarenes, gel, controlled release, macrocyclic compounds, Ugi reaction

## A Corrigendum on

### A *p*-tert-Butyldihomooxacalix[4]arene Based Soft Gel for Sustained Drug Release in Water

by Guo, H., Zhang, R., Han, Y., Wang, J., and Yan, C. (2020). *Front. Chem.* 8:33. doi: 10.3389/fchem.2020.00033

## OPEN ACCESS

### Edited by:

Tangxin Xiao,  
Changzhou University, China

### Reviewed by:

Shengyi Dong,  
Hunan University, China

### \*Correspondence:

Ying Han  
hanying@yzu.edu.cn  
Jin Wang  
wangjin107@ntu.edu.cn

### Specialty section:

This article was submitted to  
Supramolecular Chemistry,  
a section of the journal  
Frontiers in Chemistry

**Received:** 15 June 2020

**Accepted:** 13 July 2020

**Published:** 21 August 2020

### Citation:

Guo H, Zhang R, Han Y, Wang J and  
Yan C (2020) Corrigendum: A  
*p*-tert-Butyldihomooxacalix[4]arene  
Based Soft Gel for Sustained Drug  
Release in Water. *Front. Chem.* 8:721.  
doi: 10.3389/fchem.2020.00721

In the original article, there was an error. In the title, “*p*-tert-Tutyldihomooxacalix[4]arene” was misspelled. A correction has been made to the title which should read “A *p*-tert-Butyldihomooxacalix[4]arene Based Soft Gel for Sustained Drug Release in Water”.

There was an error in the abstract: “one CH<sub>2</sub> bridge is replaced by one -O- group” was misspelled. A correction has been made to the first sentence abstract which should read as follows: “*P*-tert-butyldihomooxacalix[4]arene is a well-known calix[4]arene analog in which one CH<sub>2</sub> bridge is replaced by one -CH<sub>2</sub>OCH<sub>2</sub>- group.”

Also, “one CH<sub>2</sub> bridge is replaced by one -O- group” was misspelled in Introduction, in the first sentence of the second paragraph. The corrected sentence should read as follows: “*P*-tert-butyldihomooxacalix[4]arene is a well-known *p*-tert-butylcalix[4]arene analog in which one CH<sub>2</sub> bridge is replaced by one -CH<sub>2</sub>OCH<sub>2</sub>- group (Marcos et al., 2002).”

In the original article, the following reference was not cited in the article: Liu, Y., Zhao, L.-L., Sun, J., and Yan, C.-G. (2018). Convenient synthesis and coordination properties of *p*-tert-butyldihomooxacalix[4]arene mono-schiff bases. *Polycyclic Aromat. Compd.* 40, 644–659. doi: 10.1080/10406638.2018.1469520. The citation has now been inserted in Materials and Methods, in section Synthesis of *p*-tert-Butyldihomooxacalix[4]-Arene 1, in the first paragraph which should read:

*P*-tert-butyldihomooxacalix[4]arene 4 (4.0 g, 5.9 mmol), Cl-alkoxy-substituted salicylaldehyde (1.8 g, 9.0 mmol), K<sub>2</sub>CO<sub>3</sub> (1.2 g, 9.0 mmol), and KI (1.5 g) was added in 150 ml acetone. The mixture was stirred at 75°C for 24 h (Scheme S1). After removal of the inorganic salt, the solvent was evaporated, and the residue was purified by chromatography on silica gel (petroleum ether/ethyl acetate, v/v 5:1) to give 2 as a white solid (Liu et al., 2018). Then 2 (0.1 mmol, 0.885 g), benzyl amine (0.1 mmol, 0.107 g), benzoic acid (0.1 mmol, 0.122 g), and isocyanocyclohexane (0.1 mmol, 0.109 g) were added into 7 ml methanol for reacting for 36 h. Then the solvent was evaporated, and the residue was purified by chromatography on silica gel (petroleum ether/ethyl acetate, v/v 3:1) to give 1 as a light yellow solid.

Additionally, in the original article, Scheme 1 indicates compound 1 in the cone and partial cone conformations, but these two conformers are not explained. A correction has been made to Results and Discussion, section Gelation tests, end of the second paragraph by adding the



following sentence: “It should be pointed out that the compound **1** we used to construct gel contains both conformers.”

The authors apologize for these errors and state that these do not change the scientific conclusions of the article in any way. The original article has been updated.

## REFERENCES

- Liu, Y., Zhao, L.-L., Sun, J., and Yan, C.-G. (2018). Convenient synthesis and coordination properties of *p*-tert-Butyldihomooxalix[4]arene mono-schiff bases. *Polycyclic Aromat. Compd.* 40, 644–659. doi: 10.1080/10406638.2018.1469520
- Marcos, P., Ascenso, J., and Pereira, J. L. C. (2002). Synthesis and NMR conformational studies of *p*-tert-butyldihomooxalix[4]arene derivatives bearing pyridyl pendant groups at the lower rim. *Eur. J. Org. Chem.* 2002, 3034–3041. doi: 10.1002/1099-0690(200209)2002:17<3034::AID-EJOC3034>3.0.CO;2-I

Copyright © 2020 Guo, Zhang, Han, Wang and Yan. This is an open-access article distributed under the terms of the Creative Commons Attribution License (CC BY). The use, distribution or reproduction in other forums is permitted, provided the original author(s) and the copyright owner(s) are credited and that the original publication in this journal is cited, in accordance with accepted academic practice. No use, distribution or reproduction is permitted which does not comply with these terms.



# Corrigendum: A *p*-tert-Butyldihomooxacalix[4]arene Based Soft Gel for Sustained Drug Release in Water

## OPEN ACCESS

### Edited by:

Tangxin Xiao,  
Changzhou University, China

### Reviewed by:

Xiao-Yu Hu,  
Nanjing University of Aeronautics and  
Astronautics, China

### \*Correspondence:

Ying Han  
hanying@yzu.edu.cn  
Jin Wang  
wangjin107@ntu.edu.cn

### Specialty section:

This article was submitted to  
Supramolecular Chemistry,  
a section of the journal  
Frontiers in Chemistry

**Received:** 02 November 2020

**Accepted:** 19 November 2020

**Published:** 16 December 2020

### Citation:

Guo H, Zhang R, Han Y, Wang J and  
Yan C (2020) Corrigendum: A  
*p*-tert-Butyldihomooxacalix[4]arene  
Based Soft Gel for Sustained Drug  
Release in Water.  
Front. Chem. 8:624978.  
doi: 10.3389/fchem.2020.624978

Hao Guo<sup>1,2</sup>, Runmiao Zhang<sup>1,2</sup>, Ying Han<sup>1\*</sup>, Jin Wang<sup>2\*</sup> and Chaoguo Yan<sup>1</sup>

<sup>1</sup> School of Chemistry and Chemical Engineer, Yangzhou University, Yangzhou, China, <sup>2</sup> School of Chemistry and Chemical Engineer, Nantong University, Nantong, China

**Keywords:** calixarenes, gel, controlled release, macrocyclic compounds, Ugi reaction

## A Corrigendum on

**A *p*-tert-Butyldihomooxacalix[4]arene Based Soft Gel for Sustained Drug Release in Water**  
by Guo, H., Zhang, R., Han, Y., Wang, J., and Yan, C. (2020). *Front. Chem.* 8:33.  
doi: 10.3389/fchem.2020.00033

In the original Supporting Information, we missed **Scheme S2**, **Scheme S3**, and **Figures S6, S7, S8, S9**, please update it with the new ESI document we provided below.

The authors apologize for this error and state that this does not change the scientific conclusions of the article in any way. The original article has been updated.

## SUPPLEMENTARY MATERIAL

The Supplementary Material for this article can be found online at: <https://www.frontiersin.org/articles/10.3389/fchem.2020.624978/full#supplementary-material>

Copyright © 2020 Guo, Zhang, Han, Wang and Yan. This is an open-access article distributed under the terms of the Creative Commons Attribution License (CC BY). The use, distribution or reproduction in other forums is permitted, provided the original author(s) and the copyright owner(s) are credited and that the original publication in this journal is cited, in accordance with accepted academic practice. No use, distribution or reproduction is permitted which does not comply with these terms.



# Porphyrin-Based Organoplatinum(II) Metallacycles With Enhanced Photooxidization Reactivity

Lintao Wu<sup>1</sup>, Chun Han<sup>1</sup>, Zhijun Wang<sup>1</sup>, Xi Wu<sup>1</sup>, Feng Su<sup>1</sup>, Mengyao Li<sup>1</sup>, Qingyang Zhang<sup>2\*</sup> and Xiaobi Jing<sup>3\*</sup>

<sup>1</sup> Department of Chemistry, Changzhi University, Changzhi, China, <sup>2</sup> State Key Laboratory of Bioactive Substances and Function of Natural Medicine, Institute of Materia Medica, Chinese Academy of Medical Sciences and Peking Union Medical College, Beijing, China, <sup>3</sup> School of Chemistry and Chemical Engineering, Yangzhou University, Yangzhou, China

## OPEN ACCESS

### Edited by:

Yong Yao,  
Nantong University, China

### Reviewed by:

Mingliang Liu,  
Chinese Academy of Medical  
Sciences and Peking Union Medical  
College, China  
Yang Wang,  
Nantong University, China

### \*Correspondence:

Qingyang Zhang  
zhangqingyang@imm.ac.cn  
Xiaobi Jing  
xbjing@yzu.edu.cn

### Specialty section:

This article was submitted to  
Supramolecular Chemistry,  
a section of the journal  
Frontiers in Chemistry

**Received:** 17 February 2020

**Accepted:** 18 March 2020

**Published:** 28 April 2020

### Citation:

Wu L, Han C, Wang Z, Wu X, Su F,  
Li M, Zhang Q and Jing X (2020)  
Porphyrin-Based Organoplatinum(II)  
Metallacycles With Enhanced  
Photooxidization Reactivity.  
Front. Chem. 8:262.  
doi: 10.3389/fchem.2020.00262

In recent years, metal coordination macrocycles have obtained great interests due to the fact that they combined the rich host-guest properties of macro-cyclic hosts and the unique optical properties of the organic ligands. In this work, we constructed two porphyrin-based organoplatinum(II) metallacycles (**MC1** and **MC2**) through coordination-driven self-assembly. <sup>1</sup>H NMR, <sup>31</sup>P NMR, and HRMS technologies were used to characterize the structures of **MC1** and **MC2**. Interestingly, **MC1** and **MC2** can be used as catalysts for photooxidization under light irradiation with higher efficiency compared with the porphyrin ligand only. We hope that the coordination-driven self-assembly strategy can provide an efficient method to construct photo-active materials.

**Keywords:** self-assembly, macrocycle, porphyrin, photooxidization, coordination

## INTRODUCTION

Macrocyclic host compounds, mainly including crown ethers (Zhu et al., 2012; Liu et al., 2017), cyclodextrins (Lai et al., 2017; Li et al., 2019), calixarenes (Kim et al., 2012; Nimse and Kim, 2013), cucurbiturils (Kim et al., 2007; Barrow et al., 2015), and pillararenes (Xue et al., 2012; Ogoshi et al., 2016; Yao et al., 2017; Chen J. et al., 2019), are the foundation of the development of supramolecular chemistry (Dong et al., 2014; Sun et al., 2018; Gao L. et al., 2019; Xiao et al., 2019). During the past two decades, the syntheses, host-guest properties, and applications of macrocycles have been widely investigated (Chen Y. et al., 2019; Wu and Yang, 2019). Among various macrocycles, discrete organoplatinum(II) metallacycles, which was fabricated by a new valuable strategy called “coordination-driven self-assembly,” attracted great interests from both chemists and materials scientists (Gao S. et al., 2019; Zhang et al., 2019). A remarkable advantage of the “coordination-driven self-assembly” is that two-dimensional metallacycles or three-dimensional metallacycles can be easily obtained by the formation of metal-ligand bonds between metal acceptors and organic donors when combining simple building blocks (Wang et al., 2019a; Yan et al., 2019). Up to now, discrete organoplatinum(II) metallacycles have been investigated a lot and widely applied in many areas, such as fluorescent detection, homogeneous catalysis, functional materials, bioengineering, photodynamic therapy, and so on (Cai et al., 2020; Qin et al., 2019).

Porphyrin derivatives, which contain a large  $\pi$ -conjugated aromatic structure, are a class of famous photo-activities (Liang et al., 2011; Ou et al., 2019; Wang et al., 2019b). Porphyrins usually have very intense absorption bands in the UV-visible region. However, due to the strong  $\pi$ - $\pi$  stacking between the aromatic systems, porphyrins are easily aggregated in solvents, especially in aqueous solution (Zou et al., 2017). Commonly, porphyrins aggregate more seriously as

the concentration increased. This aggregation phenomenon greatly decreases the efficiency of porphyrins to generate  $^1\text{O}_2$  and therefore restrained their potentially wide applications (Zhou et al., 2019). To address the aggregation of porphyrins in water, chemistry and materials scientists usually introduce a large substituent onto the platform of the porphyrin core (Slater et al., 2015). However, these chemical synthesis and purification processes have some other disadvantages, such as being time-consuming, tedious, and with higher costs of preparation.

Herein we designed and synthesized two new metallacycles (**MC1** and **MC2**) with *p*-bipyridine-modified porphyrin (**Scheme S1**, **Scheme 1**) as organic donor and organoplatinum(II) (**2** or **3**) as the metal acceptor (**Scheme 1**). The weak metal–ligand bonds will prevent the  $\pi$ - $\pi$  stacking of the conjugated aromatic porphyrin units, thus improving the efficiency of generating  $^1\text{O}_2$  under irradiation. Interestingly, compared with ligand **1** (**Figure S1**), the resultant metallacycle **MC1** or **MC2** can be used as catalyst for photo-oxidizing phenols much more efficiently.

## MATERIALS AND METHODS

### Synthesis of Metallacycles **MC1** and **MC2**

Ligand **1** and organoplatinum(II) **2** (**Figure 1A**) and **3** (**Figure 1C**) were prepared according to a previous report (Grishagin et al., 2014). In a 1:1 molar ratio, bipyridylporphyrin **1** (1.85 mg, 3.00  $\mu\text{mol}$ ) and  $60^\circ\text{Pt}$  (II) acceptor **2** (4.01 mg, 3.00  $\mu\text{mol}$ ) were placed in a 2-ml vial, followed by addition of acetone (1 ml). After stirring overnight at  $50^\circ\text{C}$ , the mixture was filtered to remove insoluble materials (**Scheme S2**). Then, the solvent was removed by  $\text{N}_2$  flow to about 0.2 ml, and **MC1** was obtained by the addition of diethyl ether (5.22 mg, 89%). **MC2** was prepared by the same method (**Scheme S3**).

#### **MC1**

Purple solid, 89%.  $^1\text{H}$  NMR (400 MHz,  $\text{CD}_3\text{COCD}_3$ )  $\delta$  (ppm): 10.17 (d, 4H), 9.21 (s, 2H), 8.92–8.90 (m, 10H), 8.27–8.25 (m, 8H), 7.89–7.85 (m, 12H), 2.47–2.43 (m, 24H), 1.70–1.62 (m, 36H).  $^{31}\text{P}$   $\{^1\text{H}\}$  NMR (acetone, room temperature, 121.4

MHz)  $\delta$  = 9.53 ( $^{195}\text{Pt}$  satellites,  $^1J_{\text{Pt-P}} = 2,662$  Hz). HR-ESI-MS: calculated for  $\text{C}_{203}\text{H}_{288}\text{F}_9\text{N}_{18}\text{O}_9\text{P}_{12}\text{Pt}_6\text{S}_3$  ( $[\text{M} - 3 \text{ OTf}]^{3+}$ ): 1,646.78, found: 1,646.77.

#### **MC2**

Purple solid, 87%.  $^1\text{H}$  NMR (400 MHz,  $\text{CD}_3\text{COCD}_3$ )  $\delta$  (ppm): 9.73 (s, 1H), 9.61 (s, 1H), 9.06 (s, 2H), 8.90 (s, 4H), 8.67–8.65 (m, 2H), 8.29–8.19 (m, 4H), 7.86–7.74 (m, 12H), 1.83–1.81 (m, 24H), 1.49–1.41 (m, 36H).  $^{31}\text{P}$   $\{^1\text{H}\}$  NMR (acetone, room temperature, 121.4 MHz)  $\delta$  =  $-5.04$  ppm ( $^{195}\text{Pt}$  satellites,  $^1J_{\text{Pt-P}} = 3,156$  Hz). HR-ESI-MS: calculated for  $\text{C}_{244}\text{H}_{280}\text{F}_{12}\text{N}_{24}\text{O}_{20}\text{P}_8\text{Pt}_4\text{S}_4$  ( $[\text{M} + 8 \text{ CH}_3\text{COCH}_3 - 4 \text{ OTf}]^{4+}$ ): 1,316.97, found: 1,316.92.

## Materials

All reagents and solvents were commercially available in analytical grade and used as received. Further purification and drying by standard methods were employed and these were distilled prior to use when necessary. Deuterated solvents were purchased from Cambridge Isotope Laboratory (Andover, MA, USA). All evaporations of organic solvents were carried out with a rotary evaporator in conjunction with a water aspirator. Melting point measurements were taken on a hot-plate microscope apparatus and are uncorrected.  $^1\text{H}$  and  $^{13}\text{C}$  NMR spectra were recorded with an Avance III 400 MHz or 600 MHz liquid-state NMR spectrometer.  $^{31}\text{P}\{^1\text{H}\}$  NMR chemical shifts are referenced to an external unlocked sample of 85%  $\text{H}_3\text{PO}_4$  ( $\delta$  0.0). Mass spectra were recorded on a Micromass Quattro II triple-quadrupole mass spectrometer using electrospray ionization with a MassLynx operating system. UV-vis spectra were recorded on a Hitachi F-7000 fluorescence spectrophotometer.

## RESULTS AND DISCUSSION

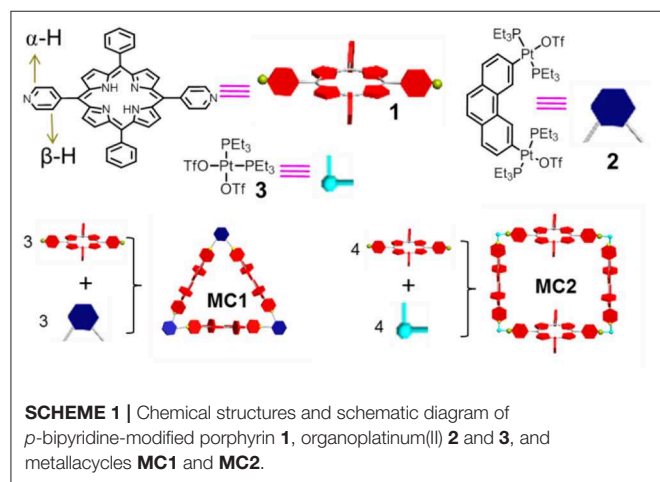
### NMR Studies

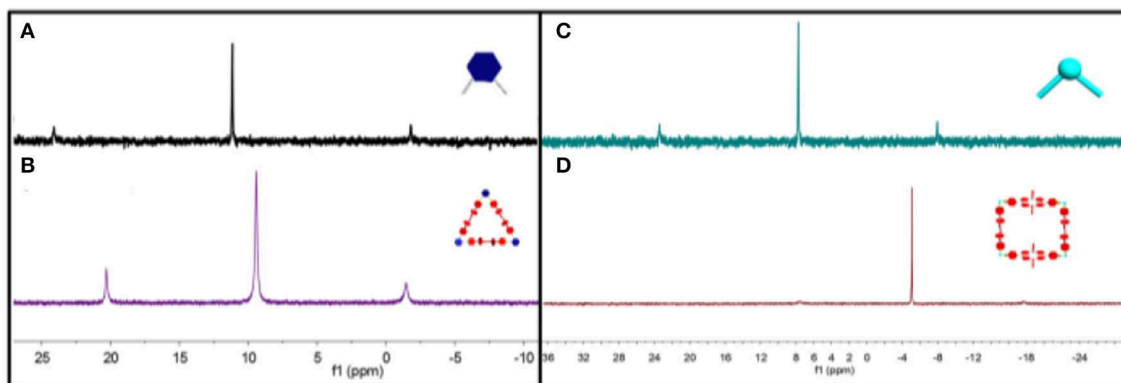
The formation of discrete organoplatinum(II) metallacycles **MC1** and **MC2** were characterized by multinuclear NMR ( $^{31}\text{P}$  and  $^1\text{H}$ ) analysis. The  $^{31}\text{P}$   $\{^1\text{H}\}$  NMR spectra of **MC1** and **MC2** showed a sharp singlet with concomitant  $^{195}\text{Pt}$  satellites at 9.53 ppm for **MC1** and at  $-5.04$  ppm for **MC2** (**Figures 1B,D**) corresponding to a single phosphorous environment, indicating the formation of discrete and symmetric metallacycles (Wei et al., 2014).

At the same time, downshifts were observed for  $\beta$ -pyridyl hydrogen in  $^1\text{H}$  NMR spectra. As shown in **Figure 2**,  $\beta$ -pyridyl hydrogen changed from 9.04 to 9.51 and 9.72 ppm in **MC1** and from 9.04 to 10.21 ppm in **MC2**.  $\beta$ -pyridyl hydrogen also showed a downfield chemical shift. These chemical shift changes in  $^1\text{H}$  NMR spectra are similar with the previous analogous organoplatinum(II) system, indicating the formation of discrete metallacycles (Yao et al., 2018).

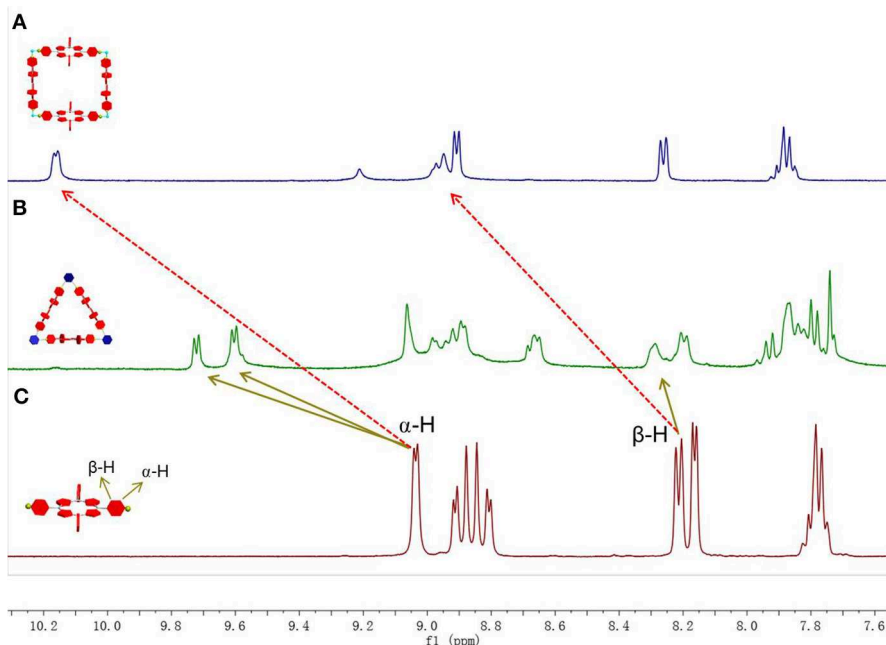
### Electrospray Ionization Time of Flight Mass Spectrometry Studies

Electrospray ionization time of flight mass spectrometry (ESI-TOF-MS) provided further evidence for the stoichiometry formation of discrete metallacycles **MC1** and **MC2**. In the mass spectrum of **MC1**, the peak at  $m/z = 1,646.77$  is consistent with





**FIGURE 1** |  $^{31}\text{P}\{^1\text{H}\}$  NMR spectra (room temperature, 121.4 MHz) of (A) 60° acceptor **2**, (B) metallacycle **MC1**, (C) 90° acceptor **3**, and (D) metallacycle **MC2** in acetone.



**FIGURE 2** |  $^1\text{H}$  NMR spectra ( $\text{CD}_3\text{COCD}_3$ , room temperature) of (A) bipyridylporphyrin **1**, (B) metallacycle **MC1**, and (C) metallacycle **MC2**.

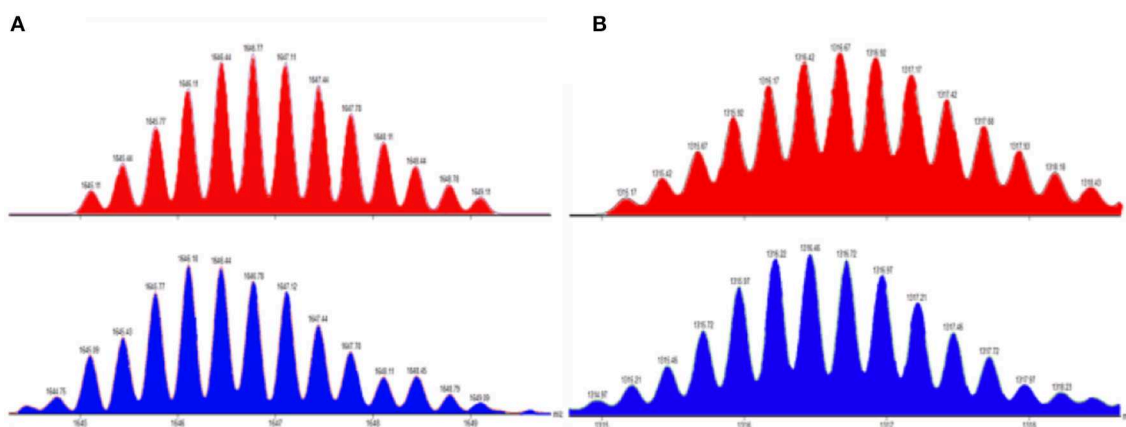
an intact  $[\text{M} - 3\text{OTf}]^{3+}$  charge state, which supported a  $[3 + 3]$  metallacycle (**Figure 3A**). Similarly, for metallacycle **MC2**, the peak at  $m/z = 1,316.92$  is consistent with an intact  $[\text{M} + 8\text{CH}_3\text{COCH}_3 - 4\text{OTf}]^{4+}$  charge state, which is expected only for a  $[4 + 4]$  metallacycle (**Figure 3B**). All the evidence from  $^1\text{H}$  NMR,  $^{31}\text{P}$  NMR, and ESI-TOF-MS confirmed the formation of a discrete structure as the sole assembly product.

## Photooxidation Studies

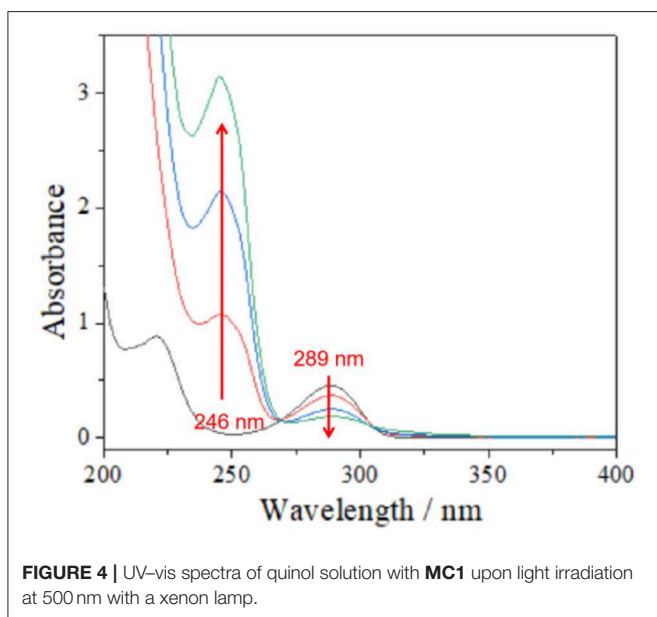
As we all know, porphyrins have the ability to generate  $^1\text{O}_2$  due to the fact that they could be excited into  $^3\text{O}_2$  state under irradiation and the energy transfer process is accompanied with molecular  $\text{O}_2$ . However, due to the strong  $\pi$ - $\pi$  interactions,

most porphyrins applied as photosensitizers are easily aggregated in aqueous solution (**Figures S4, S5**). This aggregation will greatly restrain the ability of the porphyrins to generate reactive oxygen species. For our obtained metallacycles **MC1** and **MC2**, the coordination bonds will decrease the self-quenching of the excited states and improve the photooxidation efficiency. Therefore, metallacycles **MC1** and **MC2** can be used as an expected catalyst for the photoreaction mediated by  $^1\text{O}_2$ . Herein quinol was selected as a model substrate for detecting the reactivity, and UV-vis spectroscopy was used to monitor the process. As shown in **Figure 4**, after 20 ml of aqueous solution of quinol ( $10^{-2} \text{ mmol L}^{-1}$ ) was irradiated by a LED lamp (500 nm) under air with **MC1** (5 mg) as catalyst, the absorption band





**FIGURE 3** | Experimental (blue) and calculated (red) ESI-TOF-MS spectra of **(A)**  $[M - 3OTf]^{3+}$  and **(B)**  $[M + 8 CH_3COCH_3 - 4OTf]^{4+}$ .



**FIGURE 4** | UV-vis spectra of quinol solution with **MC1** upon light irradiation at 500 nm with a xenon lamp.

of the phenyl moiety in quinol in 289 nm gradually decreased, and 65% of quinol was consumed after irradiation for 60 min (**Figure 4**). As expected, **MC2** has a similar catalytic efficiency with **MC1** (**Figure S2**). However, in the control experiments using the ligand **1** as catalyst instead of **MC1**, only 8% of quinol was reacted after irradiation at 500 for 60 min under the same conditions (**Figure S2**). Importantly, the investigation for the recyclability of **MC1** showed that they could be recovered by simple filtration and reused without significant loss of catalytic activity (yield loss within 5% for six cycles, **Figure S3**).

## CONCLUSIONS

In this paper, we synthesized two metallocycles, **MC1** and **MC2**, with *p*-bipyridines modified porphyrin as the ligands through coordination-driven self-assembly. Then, the obtained

metallocycles were characterized by  $^{31}P$  NMR,  $^1H$  NMR, and ESI-TOF-MS methods. Furthermore, the metallocycles **MC1** and **MC2** can be used as an expected catalyst for the photoreaction mediated by  $^1O_2$  due to the coordination bonds that will decrease the self-quenching of the excited states of porphyrin units and improve the photooxidization efficiency. Our next study will focus on the application of our metallocycles in photodynamic therapy.

## DATA AVAILABILITY STATEMENT

All datasets generated for this study are included in the article/**Supplementary Material**.

## AUTHOR CONTRIBUTIONS

LW, CH, and ZW prepared the ligands. LW, XW, and FS constructed the metallocycles. ML and QZ did the photooxidization. LW and XJ analyzed the data. LW, QZ, and XJ wrote the paper.

## FUNDING

This work was supported by the National Natural Science Foundation of China (Award Nos. 21907010 and 21402012), the Natural Science Foundation of Shanxi Province (Award No. 201801D221082), the Scientific and Technological Innovation Programs of Higher Education Institutions in Shanxi (Award No. 2019L0913), and the Shanxi 1331 Project Key Innovative Research Team and the Undergraduate Innovation and Entrepreneurship Project of Shanxi Province (Award No. 2019603).

## SUPPLEMENTARY MATERIAL

The Supplementary Material for this article can be found online at: <https://www.frontiersin.org/articles/10.3389/fchem.2020.00262/full#supplementary-material>

## REFERENCES

- Barrow, S. J., Kasera, S., Rowland, M. J., Barrio, J., and Scherman, O. A. (2015). Cucurbituril-based molecular recognition. *Chem. Rev.* 115:12320. doi: 10.1021/acs.chemrev.5b00341
- Cai, Y., Wang, Y., Wang, C., Long, R., Cao, L., Chen, Y., et al. (2020). Hierarchical self-assembly of 3D amphiphilic discrete organoplatinum(II) metallacage in water. *Chin. Chem. Lett.* 31, 689–692. doi: 10.1016/j.ccl.2019.08.036
- Chen, J., Wang, Y., Wang, C., Long, R., Chen, T., and Yao, Y. (2019). Functionalization of inorganic nanomaterials with pillar[n]arenes. *Chem. Commun.* 55, 6817–6826. doi: 10.1039/C9CC03165K
- Chen, Y., Sun, S., Lu, D., Shi, Y., and Yao, Y. (2019). Water-soluble supramolecular polymers constructed by macrocycle-based host-guest interactions. *Chin. Chem. Lett.* 30, 37–43. doi: 10.1016/j.ccl.2018.10.022
- Dong, S., Zheng, B., Wang, F., and Huang, F. (2014). Supramolecular polymers constructed from macrocycle-based host-guest molecular recognition motifs. *Acc. Chem. Res.* 47, 1982–1994. doi: 10.1021/ar5000456
- Gao, L., Li, M., Ehrmann, S., Tu, Z., and Haag, R. (2019). Positively charged nanoaggregates based on zwitterionic pillar[5]arene that combat planktonic bacteria and disrupt biofilms. *Angew. Chem. Int. Ed.* 58, 3645–3649. doi: 10.1002/anie.201810314
- Gao, S., Yan, X., Xie, G., Zhu, M., Ju, X., Stang, P. J., et al. (2019). Membrane intercalation-enhanced photodynamic inactivation of bacteria by a metallacycle and TAT-decorated virus coat protein. *Proc. Natl. Acad. Sci. U.S.A.* 116, 23437–23443. doi: 10.1073/pnas.1911869116
- Grishagin, I. V., Pollock, J. B., Kushal, S., Cook, T. R., Stang, P. J., and Olenyuk, B. Z. (2014). *In vivo* anticancer activity of rhomboidal Pt(II) metallacycles. *Proc. Natl. Acad. Sci. U.S.A.* 111, 18448–18453. doi: 10.1073/pnas.1418712111
- Kim, H. J., Lee, M. H., Mutihac, L., Vicens, J., and Kim, J. S. (2012). Host-guest sensing by calixarenes on the surfaces. *Chem. Soc. Rev.* 41, 1173–1190. doi: 10.1039/C1CS15169J
- Kim, K., Selvapalam, N., Ko, Y. H., Park, K. M., Kim, D., and Kim, J. (2007). Functionalized cucurbiturils and their applications. *Chem. Soc. Rev.* 36, 267–279. doi: 10.1039/B603088M
- Lai, W.-F., Rogach, A. L., and Wong, W.-T. (2017). Chemistry and engineering of cyclodextrins for molecular imaging. *Chem. Soc. Rev.* 46, 6379–6419. doi: 10.1039/C7CS00040E
- Li, P.-Y., Chen, Y., Chen, C.-H., and Liu, Y. (2019). Amphiphilic multi-charged cyclodextrins and vitamin K co-assembly as a synergistic coagulant. *Chem. Commun.* 55:11790. doi: 10.1039/C9CC06545H
- Liang, X., Li, X., Yue, X., and Dai, Z. (2011). Conjugation of porphyrin to nanohybrid cerasomes for photodynamic diagnosis and therapy of cancer. *Angew. Chem. Int. Ed.* 50, 11622–11627. doi: 10.1002/anie.201103557
- Liu, Z., Nalluri, S. K. M., and Stoddart, J. F. (2017). Surveying macrocyclic chemistry: from flexible crown ethers to rigid cyclophanes. *Chem. Soc. Rev.* 46, 2459–2478. doi: 10.1039/C7CS00185A
- Nimse, S. B., and Kim, T. (2013). Biological applications of functionalized calixarenes. *Chem. Soc. Rev.* 42, 366–386. doi: 10.1039/C2CS35233H
- Ogoshi, T., Yamagishi, T.-a., and Nakamoto, Y. (2016). Pillar-shaped macrocyclic hosts pillar[n]arenes: new key players for supramolecular chemistry. *Chem. Rev.* 116, 7937–8002. doi: 10.1021/acs.chemrev.5b00765
- Ou, C., Zhang, Y., Pan, D., Ding, K., Zhang, S., Xu, W., et al. (2019). Zinc Porphyrin-polydopamine core-shell nanostructures for enhanced photodynamic/photothermal cancer therapy. *Mater. Chem. Front.* 3, 1786–1792. doi: 10.1039/C9QM00197B
- Qin, Y., Chen, L.-J., Dong, F., Jiang, S.-T., Yin, G.-Q., Li, X., et al. (2019). Light-controlled generation of singlet oxygen within a discrete dual-stage metallacycle for cancer therapy. *J. Am. Chem. Soc.* 141, 8943–8950. doi: 10.1021/jacs.9b02726
- Slater, A. G., Hu, Y., Yang, L., Argent, S. P., Lewis, W., Blunt, M. O., et al. (2015). Thymine functionalised porphyrins, synthesis and heteromolecular surface-based self-assembly. *Chem. Sci.* 5, 1562–1569. doi: 10.1039/C4SC03531C
- Sun, S., Geng, M., Huang, L., Chen, Y., Cen, M., Lu, D., et al. (2018). A new amphiphilic pillar[5]arene: synthesis and controllable self-assembly in water and application in white-light-emitting systems. *Chem. Commun.* 54, 13006–13009. doi: 10.1039/C8CC07658H
- Wang, Y., Cai, Y., Cao, L., Cen, M., Chen, Y., Zhang, R., et al. (2019a). An amphiphilic metallacage with enhanced fluorescence emission in water: synthesis and controllable self-assembly into multi-dimensional microstructures. *Chem. Commun.* 55, 10132–10134. doi: 10.1039/C9CC04809J
- Wang, Y., Wang, C., Long, R., Cao, Y., Fan, D., Cen, M., et al. (2019b). Synthesis and controllable self-assembly of 3D amphiphilic organoplatinum(II) metallacycles in water. *Chem. Commun.* 55, 5167–5170. doi: 10.1039/C9CC02173F
- Wei, P., Cook, T. R., Yan, X., Huang, F., and Stang, P. J. (2014). A discrete amphiphilic organoplatinum(II) metallacycle with tunable lower critical solution temperature behavior. *J. Am. Chem. Soc.* 136, 15497–15500. doi: 10.1021/ja5093503
- Wu, Y.-R., and Yang, Y.-W. (2019). New opportunities in synthetic macrocyclic arenes. *Chem. Commun.* 55, 1533–1543. doi: 10.1039/C8CC09374A
- Xiao, T., Zhou, L., Xu, L., Zhong, W., Zhao, W., Sun, X.-Q., et al. (2019). Dynamic materials fabricated from water soluble pillar[n]arenes bearing triethylene oxide groups. *Chin. Chem. Lett.* 30, 271–276. doi: 10.1016/j.ccl.2018.05.039
- Xue, M., Yang, Y., Chi, C., Zhang, Z., and Huang, F. (2012). Pillararenes, a new class of macrocycles for supramolecular chemistry. *Acc. Chem. Res.* 45, 1294–1308. doi: 10.1021/ar2003418
- Yan, X., Wei, P., Liu, Y., Wang, M., Chen, C., Zhao, J., et al. (2019). Endo- and exo-functionalized tetraphenylethylene M12L24 nanospheres: fluorescence emission inside a confined space. *J. Am. Chem. Soc.* 141, 9673–9679. doi: 10.1021/jacs.9b03885
- Yao, Y., Sun, Y., Yu, H., Chen, W., Dai, H., and Shi, Y. (2017). A pillar[5]arene based gel from a low-molecular-weight gelator for sustained dye release in water. *Dalton Trans.* 46, 16802–16806. doi: 10.1039/C7DT04001F
- Yao, Y., Zhao, R., Shi, Y., Cai, Y., Chen, J., Sun, S., et al. (2018). 2D amphiphilic organoplatinum(II) metallacycles: their syntheses, self-assembly in water and potential application in photodynamic therapy. *Chem. Commun.* 54, 8068–8071. doi: 10.1039/C8CC04423F
- Zhang, Z., Zhao, Z., Hou, Y., Wang, H., Li, X., He, G., et al. (2019). Aqueous platinum(II) cage-based light-harvesting system for photocatalytic cross-coupling hydrogen evolution reaction. *Angew. Chem. Int. Ed.* 58, 8862–8866. doi: 10.1002/anie.201904407
- Zhou, W.-L., Zhao, X., Chen, Y., and Liu, Y. (2019). Construction and heterogeneous photooxidation reactivity of a cyclodextrin/porphyrin polyrotaxane network. *Org. Chem. Front.* 6, 10–14. doi: 10.1039/C8QO00790J
- Zhu, K., Vukotic, V. N., Noujeim, N., and Loeb, S. J. (2012). Bis(benzimidazolium) axles and crown ether wheels: a versatile templating pair for the formation of [2]rotaxane molecular shuttles. *Chem. Sci.* 3, 3265–3271. doi: 10.1039/c2sc20986a
- Zou, Q., Abbas, M., Zhao, L., Li, S., Shen, G., and Yan, X. (2017). Biological photothermal nanodots based on self-assembly of peptide-porphyrin conjugates for antitumor therapy. *J. Am. Chem. Soc.* 139, 1921–1927. doi: 10.1021/jacs.6b11382

**Conflict of Interest:** The authors declare that the research was conducted in the absence of any commercial or financial relationships that could be construed as a potential conflict of interest.

The reviewer ML declared a shared affiliation, with no collaboration, with one of the authors QZ to the handling editor at time of review.

Copyright © 2020 Wu, Han, Wang, Wu, Su, Li, Zhang and Jing. This is an open-access article distributed under the terms of the Creative Commons Attribution License (CC BY). The use, distribution or reproduction in other forums is permitted, provided the original author(s) and the copyright owner(s) are credited and that the original publication in this journal is cited, in accordance with accepted academic practice. No use, distribution or reproduction is permitted which does not comply with these terms.



# Cyclic $\gamma$ -Peptides With Transmembrane Water Channel Properties

Jie Chen<sup>1</sup>, Qiang Li<sup>1</sup>, Pengchao Wu<sup>1</sup>, Juan Liu<sup>1</sup>, Dan Wang<sup>1</sup>, Xiaohong Yuan<sup>1</sup>, Renlin Zheng<sup>1</sup>, Rongqin Sun<sup>2</sup> and Liangchun Li<sup>1\*</sup>

<sup>1</sup> School of Life Science and Engineering, Southwest University of Science and Technology, Mianyang, China, <sup>2</sup> School of Materials Science and Engineering, Southwest University of Science and Technology, Mianyang, China

## OPEN ACCESS

### Edited by:

Tangxin Xiao,  
Changzhou University, China

### Reviewed by:

Xiuling Liu,  
Michigan Technological University,  
United States  
Jinlin He,  
Soochow University, China

### \*Correspondence:

Liangchun Li  
lilc76@gmail.com

### Specialty section:

This article was submitted to  
Supramolecular Chemistry,  
a section of the journal  
Frontiers in Chemistry

**Received:** 10 January 2020

**Accepted:** 08 April 2020

**Published:** 30 April 2020

### Citation:

Chen J, Li Q, Wu P, Liu J, Wang D,  
Yuan X, Zheng R, Sun R and Li L  
(2020) Cyclic  $\gamma$ -Peptides With  
Transmembrane Water Channel  
Properties. *Front. Chem.* 8:368.  
doi: 10.3389/fchem.2020.00368

Self-assembling peptides can be used to design new materials for medical and biological applications. Here we synthesized and characterized two novel cyclic  $\gamma$ -peptides ( $\gamma$ -CPs) with hydrophobic inner surfaces. The NMR and FT-IR studies confirmed that the CPs could self-assemble into parallel stacking structures via intermolecular H-bonds and  $\pi$ - $\pi$  interactions. The morphologies of the self-assembly CPs showed bundles of nanotubes via transmission electron microscopy (TEM); these nanotubes form water channels to transport water across the lipid membrane. The properties of blocking the transport of protons like natural water channels showed that the hydrophobic inner surfaces are important in artificial transmembrane water channel designs. These studies also showed that water transport was a function of pore size and length of the assemblies.

**Keywords:** cyclic peptide, self-assembling, nanotube, hydrophobic inner cavity, water channels

## INTRODUCTION

Artificial compounds can form channels for ions and water that mimic natural channels (Sakai and Matile, 2013; Si et al., 2015; Barboiu, 2016; Huo and Zeng, 2016). These synthetic channels often contain structural motifs from biological assemblies including peptides (Hille, 2001; Hsieh and Liaw, 2019), DNA (Langecker et al., 2012), and steroids (Chen et al., 2005). Recent studies have shown that the integration of these assemblies with non-covalent forces, such as hydrogen bonding, electrostatic forces, hydrophobic and  $\pi$ - $\pi$  interactions, and metal-organic architectures, can produce various synthetic channels and pores. Nevertheless, tools to tightly control the selectivity of the water or ions across the lipid membrane remain scarce (Si et al., 2015; Barboiu, 2016; Huo and Zeng, 2016; Gong, 2018).

Versus biological channels, most synthetic pores are hydrophilic with poor ion selectivity; only a few have demonstrated water selectivity. Pores with a diameter of  $\sim 3$  Å are a critical requirement for ion-exclusion properties [e.g., I-quarter (Le Duc et al., 2011) and aquafoldamer (Fu et al., 2013; Zhao et al., 2014)] such pores can mimic the functions of natural Aquaporins (AQPs). Percec et al. recently showed that aquapores can transport water and exclude ions except protons through bilayer membranes (Percec et al., 2004). They used dendritic dipeptides that self-assemble via enhanced peripheral  $\pi$ -stacking of aromatic dendrons to form stable helical pores (14.5 Å average diameter). The ion-exclusion phenomena in these aquapores are based on hydrophobic effects, which seem to be more important than steric constraints. However, little work has been done since then to harness these hydrophobic effects in artificial transmembrane water channels.

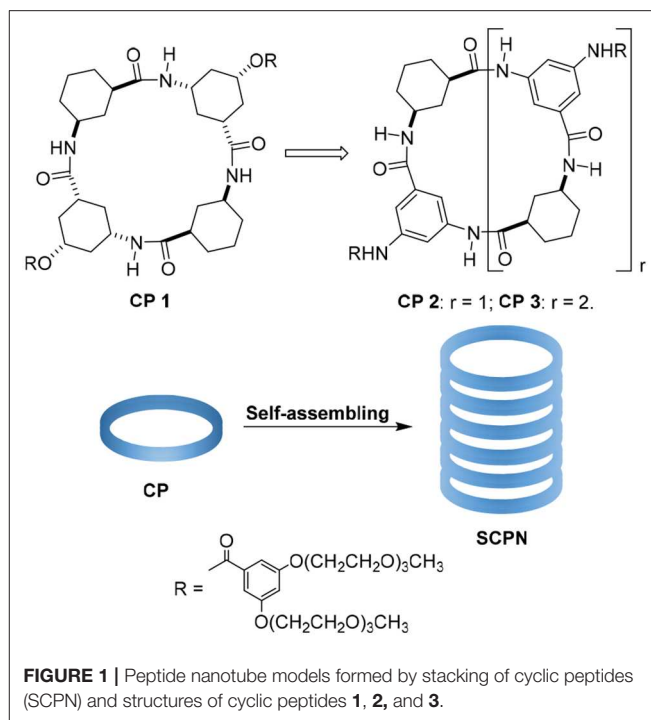
Self-assembling peptides are critical to the design of new materials for medical and biological applications (Abbas et al., 2017; Li et al., 2017; Zou et al., 2017; Otter and Besenius, 2019). Self-assembling cyclic peptide nanotubes (SCPNs) are tubular supramolecular aggregates obtained by stacking flat cyclic peptides (Bong et al., 2001; Rodriguez-Vazquez et al., 2017; Silk et al., 2019; Song et al., 2019). One of their key features is precise control of their internal diameter; the properties of their outer surface can also be tuned via the constituent amino acids (Chapman et al., 2012; Lamas et al., 2018; Mendez-Ardoy et al., 2018; Shaikh et al., 2018). Most SCPNs have a hydrophilic inner cavity to transport hydrophilic molecules (Brea et al., 2010). However, the ion transport properties of a partially hydrophobic nanotube channel like  $\alpha$ ,  $\gamma$ -CP have also been described by Granja (Montenegro et al., 2013).

The tubular assemblies of **1** can self-assemble into nanotubes through hydrogen-bond-mediated parallel stacking, and this work further studies and optimizes their structure/function relationship (Li et al., 2012). Unfortunately, the structure of **1** is not amenable to extensive changes in the inner pore diameter because the  $\gamma$ -Ach is rigid and the corresponding molecules is not flat enough and favors the tetramer; this makes it difficult to obtain larger pores. In addition, the ester side chains are not stable enough for applications in physiological environment. Gong's designs are another tube system and can form hexamers when selecting the 1,3-disubstituted benzene residues as basic building blocks (Wu et al., 2015). Inspired by these studies, we designed two cyclic peptides by replacing the 3-amino-5-hydroxycyclohexane-1-carboxylic acid with 3,5-diaminobenzoic acid (Figure 1). After preparing the materials, we studied their transport properties. **2** is a tetrameric  $\gamma$ -peptide with an approximate Van der Waals internal diameter of 4 Å. **3** is a hexameric CP with an internal diameter of 8 Å that was used with **2** to test the effect of pore diameter on transport properties.

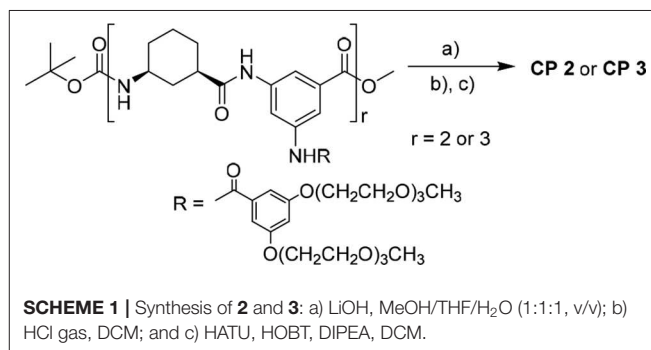
## RESULTS AND DISCUSSION

The prior solubility studies from our lab (Li et al., 2012; Lin et al., 2013) showed that the 3,5-diaminobenzoic acid was linked with 3,5-bis(triethylene glycol monomethyl ether)benzoate and contained two tri-EG (TEG) monomethyl ethers that improve peptide solubility. The integration of dendritic EG chains and hydrophobic cyclic peptides in the amphiphilic nanotubes can control the width and the length of the nanofibers that aggregate via  $\beta$ -sheet-like hydrogen-bonding between the cyclic hexapeptides of the hybrids. Thus, after removal of the N-terminal and C-terminal groups of **4a** and **4b**, the synthetic linear tetramer and hexamer were finally cyclized to form **2** and **3** that were then purified by column chromatography for 67 and 41% yields, respectively (Scheme 1).

The  $^1\text{H}$  NMR spectra of **2** and **3** displayed sharp and well-resolved signals in DMSO- $d_6$  (Figure 2). In  $\text{CDCl}_3$ , the broad and poorly-resolved peaks suggest self-assembly of cyclic peptides in the non-polar solution. The  $^1\text{H}$  NMR spectra in  $\text{CDCl}_3$  have three amide signals ( $\delta = 8.8, 9.0$  and  $10.6$  ppm) indicating that the 4 or 6 residue peptide adopts a symmetrical

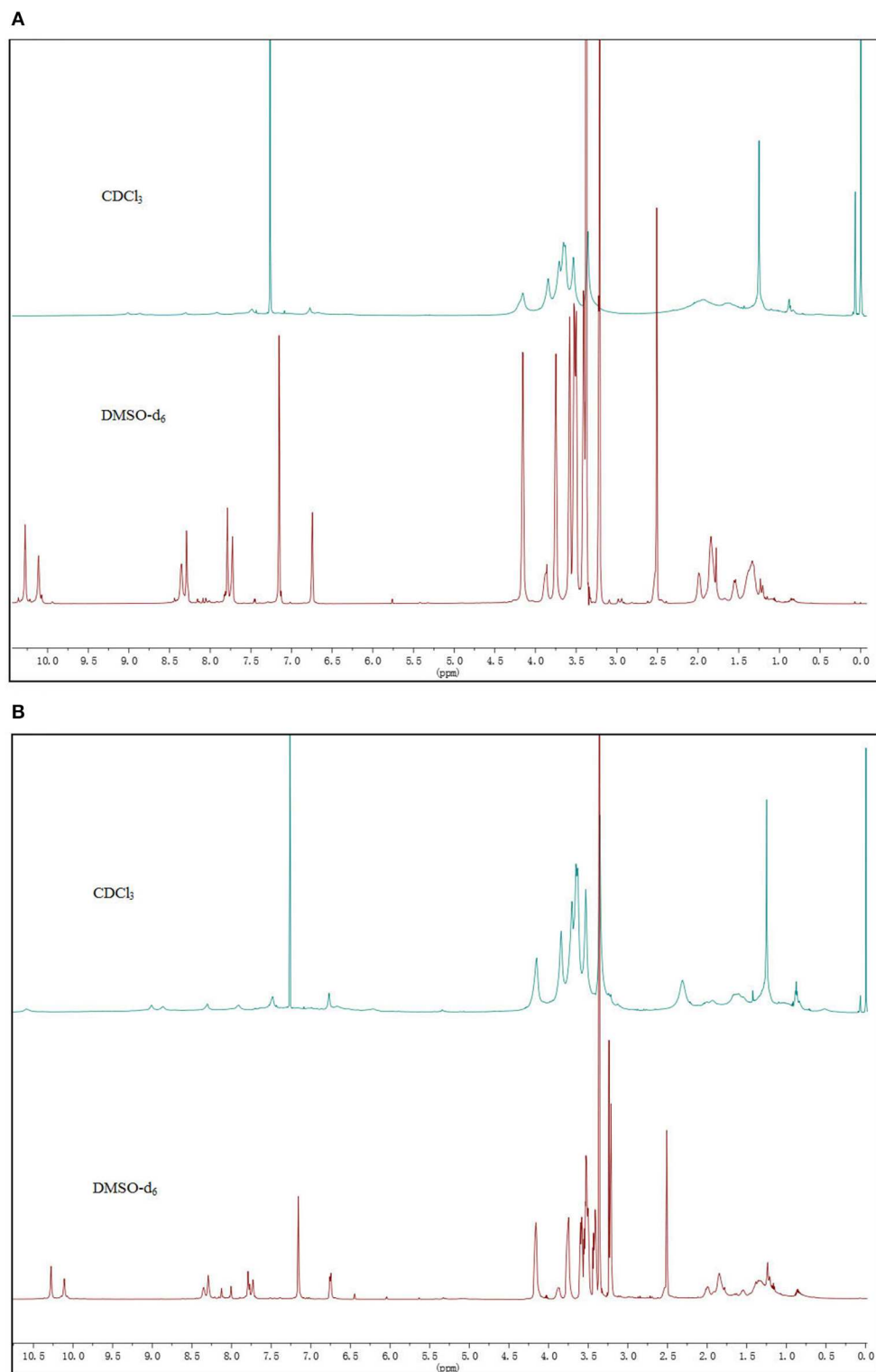


**FIGURE 1** | Peptide nanotube models formed by stacking of cyclic peptides (SCPN) and structures of cyclic peptides **1**, **2**, and **3**.



**SCHEME 1** | Synthesis of **2** and **3**: a) LiOH, MeOH/THF/H<sub>2</sub>O (1:1:1, v/v); b) HCl gas, DCM; and c) HATU, HOBT, DIPEA, DCM.

conformation. The downfield chemical shifts suggest that the proton is hydrogen bonded with the carbonyl group. Variable concentration (12 to 1 mM) experiments were performed on **2** and **3** but only a small upfield shift was observed for the NH proton (see Figures S4-2, S4-4 in Supporting Information); the variable temperature experiments in  $\text{CDCl}_3$  (2 mM) showed that the signals of the NH proton were shifted upfield by almost 0.1 ppm from 10 to 50°C for both **2** and **3** (see label 1 and 3 of N-H in Figure 3), which implies that the amide formed a stable intermolecular hydrogen-bonding (Brea et al., 2007). Furthermore, Ar-H resonance in the ring (label 9 in Figure 3) was upfield shifted from  $\delta$  6.43 to 6.04 as the temperature increase, while Ar-H resonance in the side-chain (label 4 in Figure 3) was downfield shifted from  $\delta$  8.29 to 8.35. Thus, the variable temperature experiments also showed that some Ar-H signals were shifted downfield or upfield as the temperature varied, implying that the aryl groups formed intermolecular  $\pi$ - $\pi$  stacking aggregates.

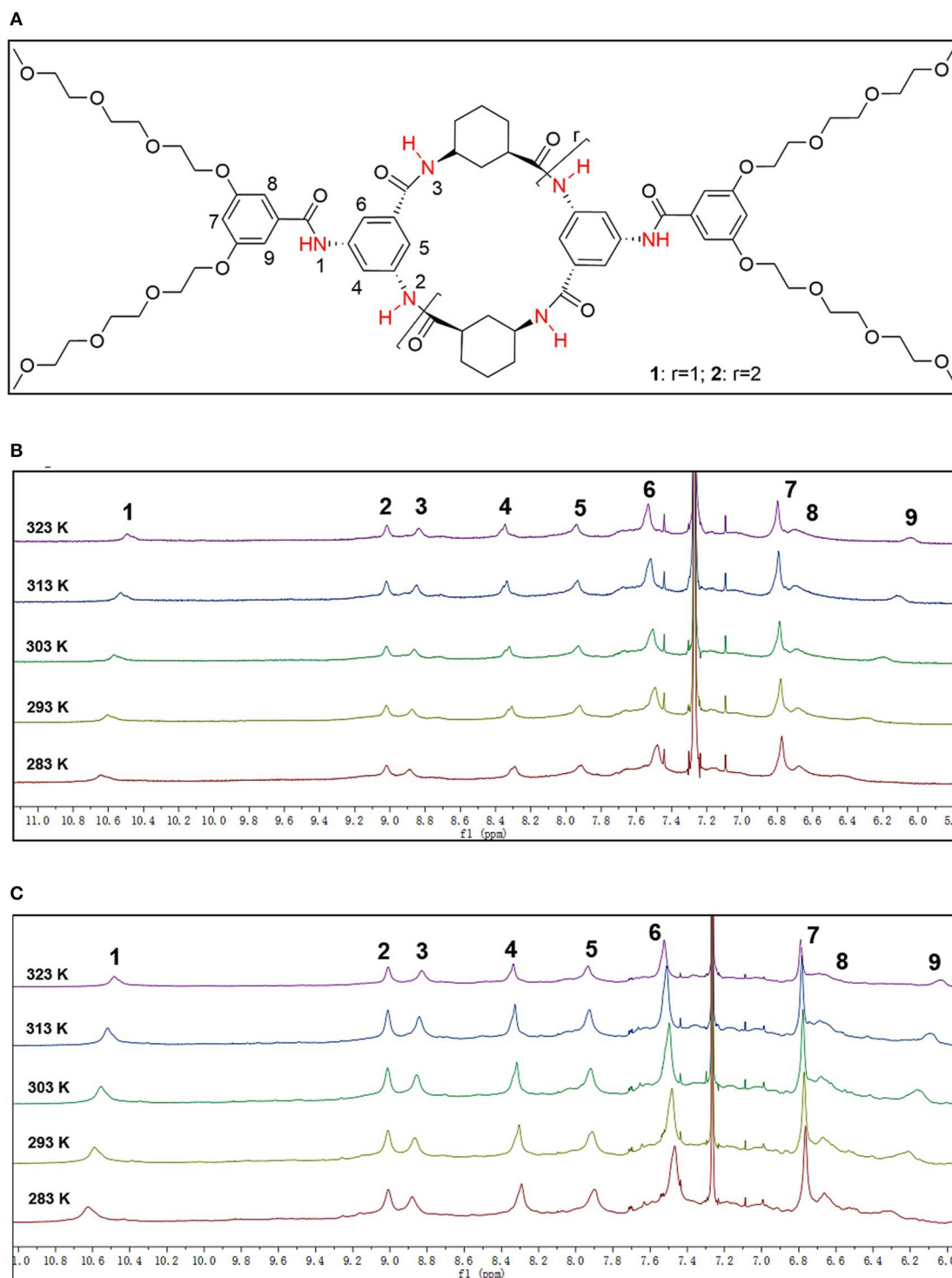


**FIGURE 2** | The  $^1\text{H}$  NMR spectra of CPs in DMSO and  $\text{CDCl}_3$ : **(A)** **2** and **(B)** **3**.

The UV/Vis absorption spectra of CPs were measured in DCM at room temperature with different concentrations. Species **2** and **3** exhibited strong UV/Vis absorption at about 250 nm,

which is due to the  $\pi$ - $\pi^*$  transition of the aryl moieties (Perkampus, 1992). The intensity increased as the concentration varied from 0.02 to 1 mM. However, it is difficult to identify the



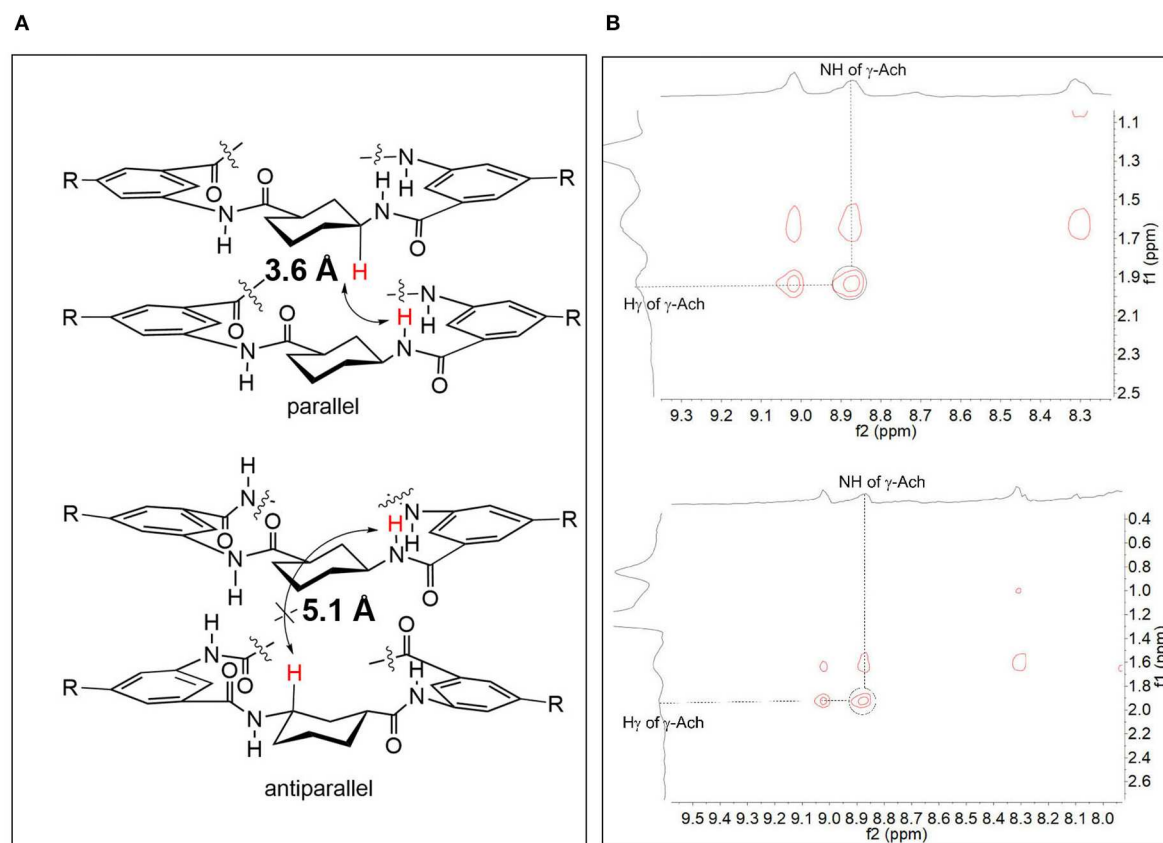


**FIGURE 3 | (A)** The structure of the CPs, and the select 6.0–11.0 ppm region of variable temperature  $^1\text{H}$  NMR spectrum of **(B) 2** and **(C) 3** in  $\text{CDCl}_3$  (2 mM) showing the downfield shift of Ph-H and NH signals [NH signals (about 8.80–10.80 ppm) and Ar-H signals (about 6.00–8.4 ppm)].

absorption bands and research the  $\pi$ - $\pi$  stacking aggregates via signal shifting.

We next performed further DFT calculations on **2** and **3** to study the conformations of the CPs (Frisch et al., 2009).

The results confirmed that the parallel stackings of **2** and **3** are much more energetically favorable than the antiparallel ones. The antiparallel stacking of **2** is not stable in solution (similar to **1**, Table S13). The calculations showed that the



**FIGURE 4 | (A)** The arrow shows the NH protons of  $\gamma$ -Ach and the  $H_\gamma$  of  $\gamma$ -Ach in the parallel stacking dimer and in the antiparallel stacking dimer (both calculated dimers of **2** and **3** are almost the same and the repeat structures are cut for clarity); **(B)** Selected region of the NOESY spectra of **2** (top) and **3** (bottom) in  $CDCl_3$ .

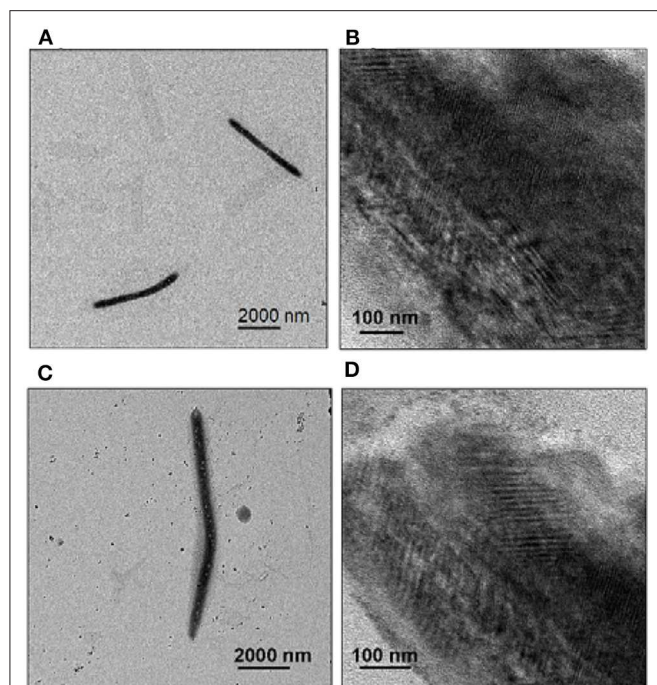
distances between the benzene rings in the parallel stacking conformation were  $<5$  Å (about 4.7–4.8 Å, see **Figure S13-2** in **Supporting Information**), which support the presence of  $\pi$ - $\pi$  stacking interactions. We also determined that the distances of the NH protons of  $\gamma$ -Ach and the  $H_\gamma$  of  $\gamma$ -Ach in the parallel stacking dimers (about 3.6 Å) are closer than those in the antiparallel stacking dimers (about 5.1 Å) (**Figure 4A**). We then performed NOESY experiments to verify whether NOE cross-peaks exist. **Figure 4B** shows NOE cross peaks between NH protons of  $\gamma$ -Ach (about 8.85 ppm) and the  $H_\gamma$  of the  $\gamma$ -Ach (about 1.92 ppm) in both **2** and **3**. Such peaks are consistent with the proposed parallel stacking structure.

A solution of **2** and **3** in  $CHCl_3$  (2 mM) was equilibrated against n-hexane via vapor-phase diffusion. A colorless gel was formed after incubating at room temperature for 3–4 days. Fourier transform infrared (FT-IR) studies of the dried gel deposited on KBr pellets showed substantial evidence for the self-assembly of the peptides; the spectroscopy of **2** and **3** (**Figure S6** in **Supporting Information**) are nearly identical. The spectra showed sharp peaks at  $1,647\text{ cm}^{-1}$  in the amide I region and  $1,596\text{ cm}^{-1}$  in the amide II region. These are characteristic of extensive hydrogen-bonding  $\beta$ -sheet-like networks. Moreover, the broad signal at  $3,307\text{ cm}^{-1}$  also corresponds to the tightly hydrogen

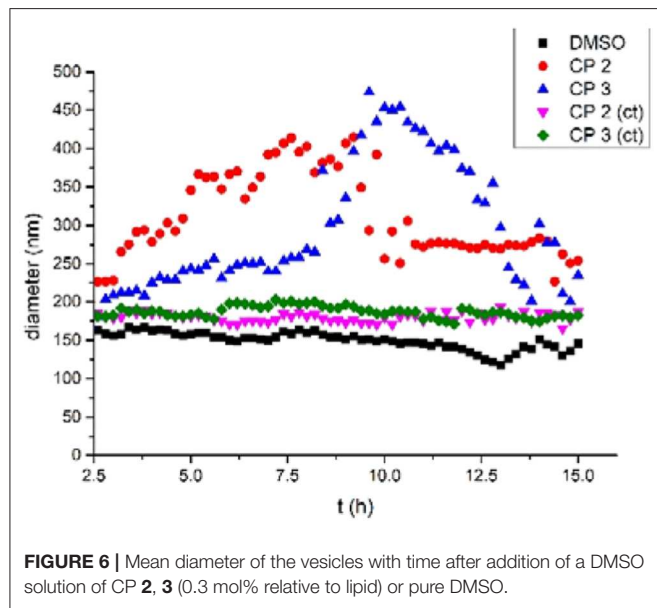
bonded ring-stacked networks (Bong et al., 2001; Rodriguez-Vazquez et al., 2017). These results suggest that the gels are constructed from tightly packed nanotubes formed during self-assembly of CPs; the basis for these nanotubes is  $\beta$ -sheet-like hydrogen-bonding. In the meantime, the absence of signal near  $1,690\text{ cm}^{-1}$  corresponding to antiparallel  $\beta$ -sheet in **2** or **3** further suggests parallel  $\beta$ -sheet structures in these compounds (Clark et al., 1998; Li et al., 2012).

The organogel was then dried and dispersed in n-hexane by sonication for transmission electron microscopy (TEM). TEM images of **2** confirmed that the nanofibers were 250 nm wide and 4–5  $\mu\text{m}$  long (**Figure 5A**). This implies the formation of nanotube bundles because a single CP nanotube is about 5 nm wide. Some of the thin nanofibers were about 6 nm wide and 100–200 nm long (**Figure 5B**), which implied side-by-side packing of single nanotubes. Similarly, TEM images of assembly organogel samples formed by **3** showed that nanofibers had a width of 300–350 nm and length of 9–10  $\mu\text{m}$  (**Figure 5C**); the thin nanofibers were about 10–14 nm width and 400–500 nm long (**Figure 5D**). The fibers formed by **3** were longer than those formed by **2**.

After confirming tube formation, we next evaluated their functions. The water transport properties of the tubular structures across lipid bilayers were investigated using dynamic



**FIGURE 5 |** TEM images of gels formed by **2** (A,B) and **3** (C,D). Each compound (2 mM in  $\text{CHCl}_3$ ) was equilibrated against n-hexane via vapor-phase diffusion for several days to obtain the gels for sampling. TEM images were obtained after the gels were dispersed in n-hexane.



**FIGURE 6 |** Mean diameter of the vesicles with time after addition of a DMSO solution of CP **2**, **3** (0.3 mol% relative to lipid) or pure DMSO.

light scattering (DLS) (Hallett et al., 1993). Large unilamellar vesicles in buffer containing NaCl (100 mM) were first prepared from egg yolk L- $\alpha$ -phosphatidylcholine (EYPC) and then suspended in pure water to produce different osmotic pressures inside and outside the vesicles. Aliquots of DMSO solutions of **2** and **3** (0.3% molar ratio relative to lipid) were injected into the vesicle suspensions. The light scattering and vesicle diameters

were then monitored for 15 h. **Figure 6** shows that adding the solution of **2** and **3** in DMSO caused the mean vesicle diameter to increase from ca. 180 nm to ca. 450 nm within 9 h. In contrast, adding pure DMSO did not lead to a detectable influence.

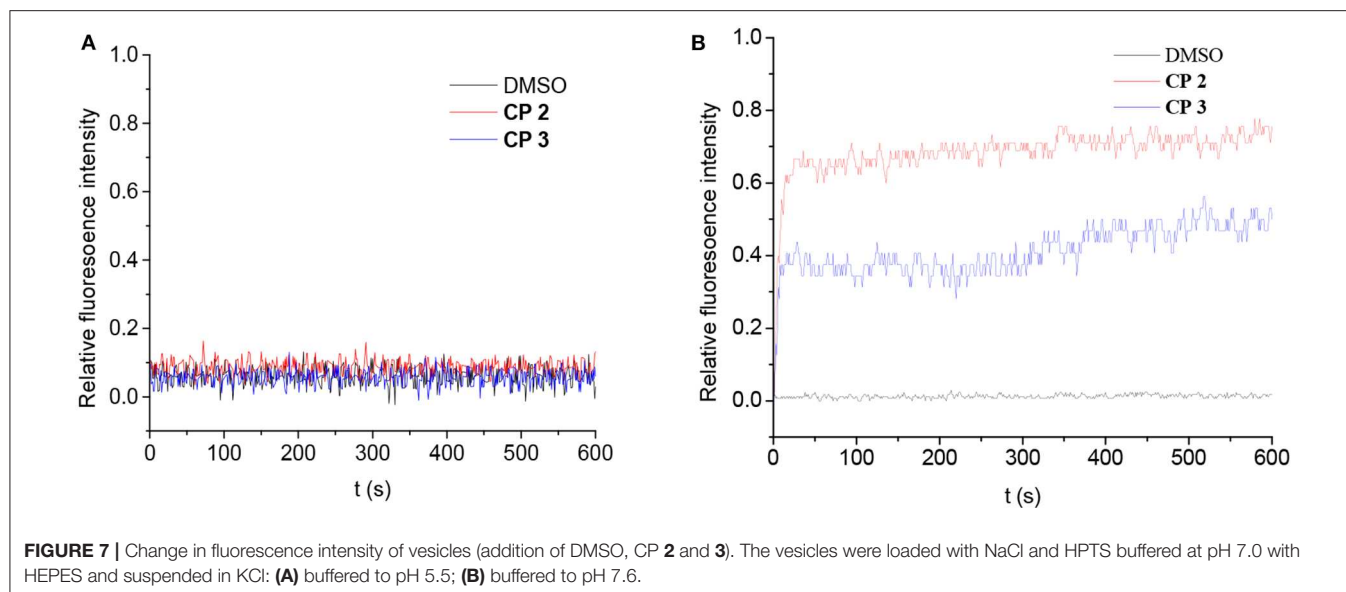
When the vesicles were suspended in buffer containing NaCl (100 mM), the osmotic pressure was the same inside and outside the vesicles. Adding **2** and **3** to the suspension did not change the size of the vesicles within 15 h (CP **2** (ct) and CP **3** (ct) in **Figure 6**). This implies that **2** and **3** did not promote vesicle fusion. Thus, based on prior work about water channels (Hu et al., 2012), we suspect that the vesicle increase is due to water transport from outside the vesicles to the inside via osmotic pressure differences. The transport of water was detected after almost 2.5 h, which is quite late vs. other artificial water channels. This suggests that the formation of cyclic peptide tubes is slow in membranes. However, the size of the vesicles increased 2-fold within 7 h for **2** and 9 h for **3**, which implied that the tubes formed by **2** were more efficient than **3** in membranes. After 9–11 h, the vesicle diameters decreased gradually because of the precipitation of large vesicles.

The transport-originating properties of **2** and **3** were then evaluated for the  $\text{H}^+/\text{OH}^-$  transport (**Figure 7**) using a pH gradient across the vesicle membranes (Jeon et al., 2004). Large unilamellar vesicles were prepared from egg yolk L-R-phosphatidylcholine (EYPC) with and without **2** or **3** (1 mol %) as described in the literature. The  $\text{H}^+/\text{OH}^-$  flux through the membranes was assessed by changes in fluorescence intensity of the pH-sensitive dye 8-hydroxypyrene-1,3,6-trisulfonate (HPTS) entrapped inside the vesicles. A suspension of vesicles entrapping the HPTS and HEPES buffer (pH 7.0 inside the vesicles) was prepared and **2** or **3** in DMF (5.0 mM, 20.0  $\mu\text{L}$ ) were added with gentle stirring. We then added these vesicles to HEPES buffers with a pH of 5.5 or 7.6 to produce higher  $\text{H}^+$  or  $\text{OH}^-$  concentrations outside the vesicles.

Compounds **2** and **3** had no change in fluorescence intensity of HPTS at pH 5.5, suggesting that they did not transport protons across the membrane. However, there was  $\text{OH}^-$  flux through the membrane. Adding **2** or **3** to the vesicle suspension in higher  $\text{OH}^-$  buffer changed the fluorescence intensity. One of the key features of natural water channels is blocking of the proton flux; these results suggest that the cyclic peptides act as natural water channels (Jensen et al., 2005). Furthermore, **2** exhibited higher transport ability, which implies that the bigger diameter of the cyclic peptide does not improve the  $\text{OH}^-$  transport rate but does improve the water diffusion ability (Possibly due to the shorter length of nanotubes formed by **2**). It is interesting that the results of blocking proton flux were different from Granja's CP, which suggested the formation of the proton-transport channel (Brea et al., 2010; Rodriguez-Vazquez et al., 2016).

## CONCLUSION

In summary, we designed and synthesized two cyclic  $\gamma$ -peptides with hydrophobic inner surfaces. The NMR, IR, and TEM showed that CPs **2** and **3** could aggregate to form nanotubes via intermolecular stacking. The CPs form selective water channels



that block  $H^+$  flux to transport water across the lipid membrane. Prior work has shown that proton transport was not blocked by the cyclic peptide nanotubes (including hydrophilic inner surfaces and Granja's partial hydrophobic inner surfaces of CPs) (Brea et al., 2010; Chapman et al., 2012). Thus, these results show that the fully hydrophobic inner surfaces affect the behavior of cyclic peptide nanotubes in transport properties. These cyclic peptide systems may have utility for biomimicking water channels.

## DATA AVAILABILITY STATEMENT

All datasets generated for this study are included in the article/**Supplementary Material**.

## AUTHOR CONTRIBUTIONS

LL designed the study and wrote the protocol. JC undertook the main experimental works, performed the SEM/TEM analysis, managed the literature search and wrote the

first draft of the manuscript with assistance from RS. QL performed the ion channel experiments and synthetic works with the assistance from XY. PW did part of synthetic works about the cyclic peptides with assistance from DW. JL did part of synthetic works with assistance from RZ.

## FUNDING

This work was supported by the National Transgenic Major Project of China (2019ZX08010-004) and the National Natural Science Foundation of China (21002099).

## SUPPLEMENTARY MATERIAL

The Supplementary Material for this article can be found online at: <https://www.frontiersin.org/articles/10.3389/fchem.2020.00368/full#supplementary-material>

## REFERENCES

- Abbas, M., Zou, Q., Li, S., and Yan, X. (2017). Self-assembled peptide- and protein-based nanomaterials for antitumor photodynamic and photothermal therapy. *Adv. Mater.* 29:1605021. doi: 10.1002/adma.201605021
- Barboiu, M. (2016). Artificial water channels—incipient innovative developments. *Chem. Commun.* 52, 5657–5665. doi: 10.1039/c6cc01724j
- Bong, D. T., Clark, T. D., Granja, J. R., and Ghadiri, M. R. (2001). Self-assembling organic nanotubes. *Angew. Chem. Int. Ed.* 40, 988–1011. doi: 10.1002/1521-3773(20010316)40:6<988::AID-ANIE9880>3.0.CO;2-N3.0.CO;2
- Brea, R. J., Castedo, L., and Granja, J. R. (2007). Large-diameter self-assembled dimers of alpha,gamma-cyclic peptides, with the nanotubular solid-state structure of cyclo-[(l-Leu-D-(Me)N-gamma-Acp)(4)-].4CHCl(2)COOH. *Chem. Commun.* 3267–3269. doi: 10.1039/b703659k
- Brea, R. J., Reiriz, C., and Granja, J. R. (2010). Towards functional bionanomaterials based on self-assembling cyclic peptide nanotubes. *Chem. Soc. Rev.* 39, 1448–1456. doi: 10.1039/b805753m
- Chapman, R., Danial, M., Koh, M. L., Jolliffe, K. A., and Perrier, S. (2012). Design and properties of functional nanotubes from the self-assembly of cyclic peptide templates. *Chem. Soc. Rev.* 41, 6023–6041. doi: 10.1039/c2cs35172b
- Chen, W.-H., Shao, X.-B., and Regen, S. L. (2005). Poly (choloyl)-based amphiphiles as pore-forming agents: transport-active monomers by design. *J. Am. Chem. Soc.* 127, 12727–12735. doi: 10.1021/ja053527q
- Clark, T. D., Buriak, J. M., Kobayashi, K., Isler, M. P., McRee, D. E., and Ghadiri, M. R. et al. (1998). Cylindrical  $\beta$ -sheet peptide assemblies. *J. Am. Chem. Soc.* 120, 8949–8962. doi: 10.1021/ja981485i



- Frisch, M. J. E. A., Trucks, G. W., Schlegel, H. B., Scuseria, G. E., Robb, M. A., Cheeseman, J. R., et al. (2009). *Gaussian 09, revision a. 02*. Wallingford, CT: Gaussian, Inc.
- Fu, H., Liu, Y., and Zeng, H. (2013). Shape-persistent H-bonded macrocyclic aromatic pentamers. *Chem. Commun.* 49, 4127–4144. doi: 10.1039/c2cc36698c
- Gong, B. (2018). Artificial water channels: inspiration, progress, and challenges. *Faraday Discuss.* 209, 415–427. doi: 10.1039/C8FD00132D
- Hallett, F. R., Marsh, J., Nickel, B. G., and Wood, J. M. (1993). Mechanical properties of vesicles. II. A model for osmotic swelling and lysis. *Biophys. J.* 64, 435–442. doi: 10.1016/S0006-3495(93)81384-5
- Hille, B. (2001). *Ion Channels of Excitable Membranes*, Vol. 507. Sunderland, MA: Sinauer.
- Hsieh, W. H., and Liaw, J. (2019). Applications of cyclic peptide nanotubes cPNTs. *J. Food Drug Anal.* 27, 32–47. doi: 10.1016/j.jfda.2018.09.004
- Hu, X. B., Chen, Z., Tang, G., Hou, J. L., and Li, Z. T. (2012). Single-molecular artificial transmembrane water channels. *J. Am. Chem. Soc.* 134, 8384–8387. doi: 10.1021/ja302292c
- Huo, Y., and Zeng, H. (2016). “Sticky”-ends-guided creation of functional hollow nanopores for guest encapsulation and water transport. *Acc. Chem. Res.* 49, 922–930. doi: 10.1021/acs.accounts.6b00051
- Jensen, M. O., Rothlisberger, U., and Rovira, C. (2005). Hydroxide and proton migration in aquaporins. *Biophys. J.* 89, 1744–1759. doi: 10.1529/biophysj.104.058206
- Jeon, Y. J., Jon, S., Selvapalam, N., Oh, D. H., Seo, I., Park, C.-S., et al. (2004). Artificial ion channel formed by cucurbit[n]uril derivatives with a carbonyl group fringed portal reminiscent of the selectivity filter of K<sup>+</sup> channels. *J. Am. Chem. Soc.* 126, 15944–15945. doi: 10.1021/ja044748j
- Lamas, A., Guerra, A., Amorin, M., and Granja, J. R. (2018). New self-assembling peptide nanotubes of large diameter using delta-amino acids. *Chem. Sci.* 9, 8228–8233. doi: 10.1039/c8sc02276c
- Langecker, M., Arnaut, V., Martin, T. G., List, J., Renner, S., Mayer, M., et al. (2012). Synthetic lipid membrane channels formed by designed DNA nanostructures. *Science* 338, 932–936. doi: 10.1126/science.1225624
- Le Duc, Y., Michau, M., Gilles, A., Gence, V., Legrand, Y. M., van der Lee, A., et al. (2011). Imidazole-quartet water and proton dipolar channels. *Angew. Chem. Int. Ed. Engl.* 50, 11366–11372. doi: 10.1002/anie.201103312
- Li, J., Du, X., Hashim, S., Shy, A., and Xu, B. (2017). Aromatic-aromatic interactions enable  $\alpha$ -helix to  $\beta$ -sheet transition of peptides to form supramolecular hydrogels. *J. Am. Chem. Soc.* 139, 71–74. doi: 10.1021/jacs.6b11512
- Li, L., Zhan, H., Duan, P., Liao, J., Quan, J., Hu, Y., et al. (2012). Self-assembling nanotubes consisting of rigid cyclic  $\gamma$ -peptides. *Adv. Funct. Mater.* 22, 3051–3056. doi: 10.1002/adfm.201200488
- Lin, Z., Li, L., Yang, Y., Zhan, H., Hu, Y., Zhou, Z., et al. (2013). The self-assembly of cystine-bridged  $\gamma$ -peptide-based cyclic peptide-dendron hybrids. *Org. Biomol. Chem.* 11, 8443–8451. doi: 10.1039/c3ob40532j
- Mendez-Ardoy, A. M., Granja, J. R., and Montenegro, J. (2018). pH-Triggered self-assembly and hydrogelation of cyclic peptide nanotubes confined in water micro-droplets. *Nanoscale Horiz.* 3, 391–396. doi: 10.1039/c8nh00009c
- Montenegro, J., Ghadiri, M. R., and Granja, J. R. (2013). Ion channel models based on self-assembling cyclic peptide nanotubes. *Acc. Chem. Res.* 46, 2955–2965. doi: 10.1021/ar400061d
- Otter, R., and Besenius, P. (2019). Supramolecular assembly of functional peptide-polymer conjugates. *Org. Biomol. Chem.* 17, 6719–6734. doi: 10.1039/c9ob01191a
- Perkampus, H.-H. (1992). *UV-VIS Spectroscopy and Its Applications*. Berlin; Heidelberg: Springer. doi: 10.1007/978-3-642-77477-5
- Percec, V., Dulcey, A. E., Balagurusamy, V. S. K., Miura, Y., Smirndkal, J., and Peterca, M. et al. (2004). Self-assembly of amphiphilic dendritic dipeptides into helical pores. *Nature*, 430, 764–68. doi: 10.1038/nature02770
- Rodriguez-Vazquez, N., Amorin, M., Alfonso, I., and Granja, J. R. (2016). Anion recognition and induced self-assembly of an  $\alpha,\gamma$ -Cyclic peptide to form spherical clusters. *Angew. Chem. Int. Ed.* 55, 4505–4508. doi: 10.1002/anie.201511857
- Rodriguez-Vazquez, N., Amorin, M., and Granja, J. R. (2017). Recent advances in controlling the internal and external properties of self-assembling cyclic peptide nanotubes and dimers. *Org. Biomol. Chem.* 15, 4490–4505. doi: 10.1039/c7ob00351j
- Sakai, N., and Matile, S. (2013). Synthetic ion channels. *Langmuir* 29, 9031–9040. doi: 10.1021/la400716c
- Shaikh, H., Rho, J. Y., Macdougall, L. J., Gurnani, P., Lunni, A. M., Yang, J., et al. (2018). Hydrogel and organogel formation by hierarchical self-assembly of cyclic peptides nanotubes. *Chem. Eur. J.* 24, 19066–19074. doi: 10.1002/chem.201804576
- Si, W., Xin, P., Li, Z. T., and Hou, J. L. (2015). Tubular unimolecular transmembrane channels: construction strategy and transport activities. *Acc. Chem. Res.* 48, 1612–1619. doi: 10.1021/acs.accounts.5b00143
- Silk, M. R., Mohanty, B., Sampson, J. B., Scanlon, M. J., Thompson, P. E., and Chalmers, D. K. (2019). Controlled construction of cyclic  $\alpha$  /  $\beta$  peptide nanorods. *Angew. Chem. Int. Ed.* 58, 596–601. doi: 10.1002/anie.201811910
- Song, Q., Yang, J., Rho, J. Y., and Perrier, S. (2019). Supramolecular switching of the self-assembly of cyclic peptide-polymer conjugates via host-guest chemistry. *Chem. Commun.* 55, 5291–5294. doi: 10.1039/c9cc01914f
- Wu, X., Liu, R., Sathyamoorthy, B., Yamato, K., Liang, G., Shen, L., et al. (2015). Discrete stacking of aromatic oligoamide macrocycles. *J. Am. Chem. Soc.* 137, 5879–5882. doi: 10.1021/jacs.5b02552
- Zhao, H., Sheng, S., Hong, Y., and Zeng, H. (2014). Proton gradient-induced water transport mediated by water wires inside narrow aquapores of aquafoldamer molecules. *J. Am. Chem. Soc.* 136, 14270–14276. doi: 10.1021/ja5077537
- Zou, Q., Abbas, M., Zhao, L., Li, S., Shen, G., and Yan, X. (2017). Biological photothermal nanodots based on self-assembly of peptide-porphyrin conjugates for antitumor therapy. *J. Am. Chem. Soc.* 139, 1921–1927. doi: 10.1021/jacs.6b11382

**Conflict of Interest:** The authors declare that the research was conducted in the absence of any commercial or financial relationships that could be construed as a potential conflict of interest.

Copyright © 2020 Chen, Li, Wu, Liu, Wang, Yuan, Zheng, Sun and Li. This is an open-access article distributed under the terms of the Creative Commons Attribution License (CC BY). The use, distribution or reproduction in other forums is permitted, provided the original author(s) and the copyright owner(s) are credited and that the original publication in this journal is cited, in accordance with accepted academic practice. No use, distribution or reproduction is permitted which does not comply with these terms.





# Facile One-Step Electrodeposition Preparation of Cationic Pillar[6]arene-Modified Graphene Films on Glassy Carbon Electrodes for Enhanced Electrochemical Performance

## OPEN ACCESS

### Edited by:

Tangxin Xiao,  
Changzhou University, China

### Reviewed by:

Xiao-Yu Hu,  
Nanjing University of Aeronautics and  
Astronautics, China  
Peter Cragg,  
University of Brighton,  
United Kingdom  
Yingjie Ma,  
National Center for Nanoscience and  
Technology (CAS), China

### \*Correspondence:

Qunpeng Duan  
qpduan@haue.edu.cn  
Fei Wang  
wf2003@haue.edu.cn  
Kui Lu  
lucky Luke@haue.edu.cn

### Specialty section:

This article was submitted to  
Supramolecular Chemistry,  
a section of the journal  
Frontiers in Chemistry

**Received:** 27 February 2020

**Accepted:** 23 April 2020

**Published:** 04 June 2020

### Citation:

Duan Q, Wang L, Wang F, Zhang H  
and Lu K (2020) Facile One-Step  
Electrodeposition Preparation of  
Cationic Pillar[6]arene-Modified  
Graphene Films on Glassy Carbon  
Electrodes for Enhanced  
Electrochemical Performance.  
*Front. Chem.* 8:430.  
doi: 10.3389/fchem.2020.00430

Qunpeng Duan<sup>1\*</sup>, Lijie Wang<sup>1</sup>, Fei Wang<sup>1\*</sup>, Hongsong Zhang<sup>1</sup> and Kui Lu<sup>1,2\*</sup>

<sup>1</sup> School of Materials and Chemical Engineering, Henan University of Engineering, Zhengzhou, China, <sup>2</sup> School of Chemical Engineering and Food Science, Zhengzhou Institute of Technology, Zhengzhou, China

In the present work, we have developed a facile one-step route for preparing electrochemically reduced graphene oxide-cationic pillar[6]arene (ErGO-CP6) nanocomposite films on glassy carbon electrodes (GCEs) directly from graphene oxide-cationic pillar[6]arene (GO-CP6) colloidal solution by using a pulsed electrodeposition technique. The electrocatalytic activity of ErGO-CP6 was examined by studying the oxidations of five purine bases [adenine (A), guanine (G), xanthine (X), hypoxanthine (HX), and uric acid (UA)]. It enhanced the oxidation currents of A, G, X, HX, and UA when compared to unmodified ErGO films and bare GCE, which is considered to be the synergetic effects of the graphene (excellent electrical properties and large surface area) and CP6 molecules (high inclusion complexation and enrichment capability).

**Keywords:** electrodeposition, pillar[6]arene, host-guest inclusion, graphene films, electrochemical performance

## INTRODUCTION

Graphene, a 2D  $sp^2$ -hybridized carbon sheet, has attracted considerable attention in academia and industry due to its fascinating electronic, chemical, mechanical, thermal, and optical properties as well as for its tremendous potential in applications in various fields, such as nanoelectronics (Son et al., 2006), supercapacitors (Maiti et al., 2014), batteries (Takamura et al., 2007), sensors (Shao et al., 2010b), and nanocomposites (Vickery et al., 2009). The reduced graphene oxide (rGO) is the product of treating graphene oxide (GO) under reducing conditions. Although rGO has a relatively lower conductivity than that of the graphene made with a mechanical cleaving method, it is nevertheless a versatile material. In particular, it can be used as a perfect candidate for carbon-based electrode materials to produce electrochemical sensors or biosensors owing to its large active surface area, good electrical conductivity, and electrocatalytic activity (Zhou et al., 2009). However, the practical applications of rGO are challenged by its irreversible agglomeration in an aqueous solution, which significantly reduces its effectiveness. Interestingly, introducing water-soluble macrocyclic hosts as functional molecules can effectively disperse graphene and further introduce new or enhanced functions through combining their individual characteristics. Therefore, macrocyclic-host-functionalized rGO nanocomposites that simultaneously possess the

unique properties of rGO (a large surface area and good conductivity) and the macrocyclic host (high supramolecular recognition and good enrichment capability) have been intensively exploited as electrocatalysts for improving the analyte detection sensitivity (Guo et al., 2010, 2011; Xu et al., 2011; Zhou et al., 2013a,b,c; Li et al., 2017; Singh et al., 2018; Sun et al., 2019; Tan et al., 2019a). The commonly reported approach for the preparation of the macrocyclic-host-functionalized rGO nanocomposite modified electrode is the drop-casting of chemically reduced graphene oxide-macrocyclic host suspension onto the electrode surface. Obviously, such a preparation methodology involves highly toxic chemicals, such as hydrazine hydrate, and, moreover, chemical reduction of the graphene oxide-macrocyclic host suspension cannot completely reduce oxygen-containing functional groups, which may result in a decrease in the electrochemical performance.

More recently, electrochemical reduction of GO to rGO has attracted considerable attention because it is regarded as a simple, fast, and green method; in addition, graphene film can be obtained by this method on conductive substrates (Guo et al., 2009; Shao et al., 2010a). More importantly, the high negative potential employed in the electrochemically reduced graphene oxide (ErGO) can efficiently reduce the oxygen-rich functional groups present on the GO surface (Wang et al., 2012). Up to now, various electrochemical methods, including cyclic voltammetry (CV) (Chen et al., 2011) and the potentiostatic method (Kong et al., 2013), have been employed. However, the pulsed electrodeposition method (Davies et al., 2011), having some advantages of simplicity, cost efficiency, time saving, and in the production of high-purity deposits, has rarely been applied in the ErGO field till now.

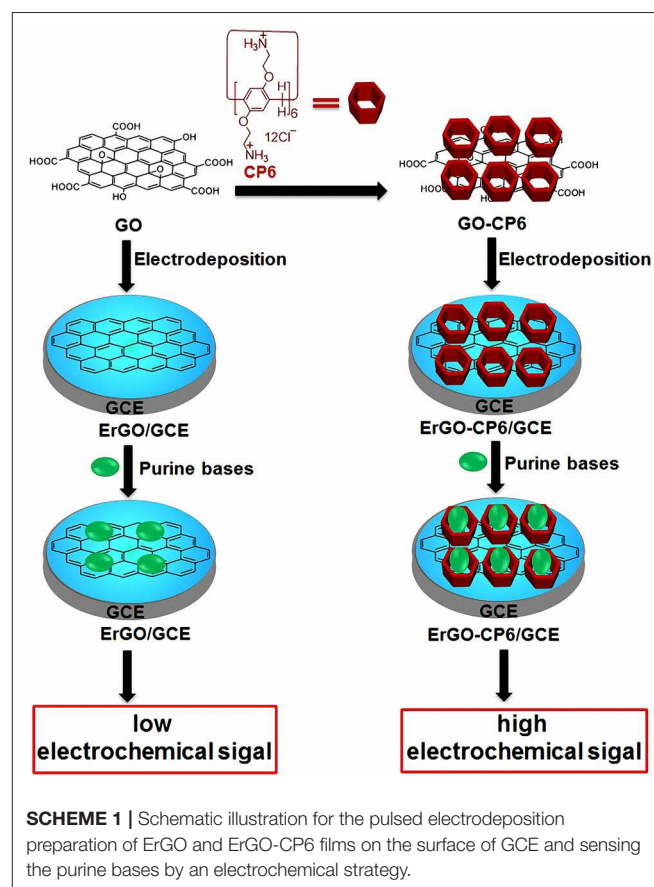
Pillararenes (Ogoshi et al., 2008, 2016; Cao et al., 2009, 2014; Cragg and Sharma, 2012; Xue et al., 2012; Yao et al., 2012; Si et al., 2014; Cragg, 2018; Wang et al., 2019), as a relatively new class of macrocyclic hosts, have received continuous attention owing to their symmetrical rigid pillar-shaped structures, adjustable cavity size, easy functionalization, and unique host-guest recognition capabilities. Practically, a series of pillararenes with good water solubility and recognition capability have been applied to fabricate graphene hybrids to improve their water stability and dispersity as well as to enhance their supramolecular recognition capability in many applications, including sensors, luminescence, electrocatalysis, and electronics; they have therefore attracted wide research interest (Zhou et al., 2013a,b,c; Zhang et al., 2014; Ye et al., 2015; Zhou et al., 2015; Liu et al., 2016; Mao et al., 2016; Yu et al., 2017, 2018; Zhao et al., 2017; Hou et al., 2019; Sun et al., 2019; Tan et al., 2019b,c; Tan S. et al., 2019). Recently, a water-soluble cationic pillar[6]arene (CP6) with 12- $\text{NH}_3^+$  groups on both rims was designed and synthesized by our group (Duan et al., 2019). CP6 contains not only one hydrophobic cavity but also 12 hydrophilic ammonium groups on both rims, which can produce electrostatic interaction with the negatively charged groups present in GO to form GO-CP6 nanocomposites with potential applications in materials science.

In this work, we report that CP6 functionalized graphene films were prepared onto glassy carbon electrodes (GCEs) directly from GO-CP6 dispersions by facile one-step pulsed

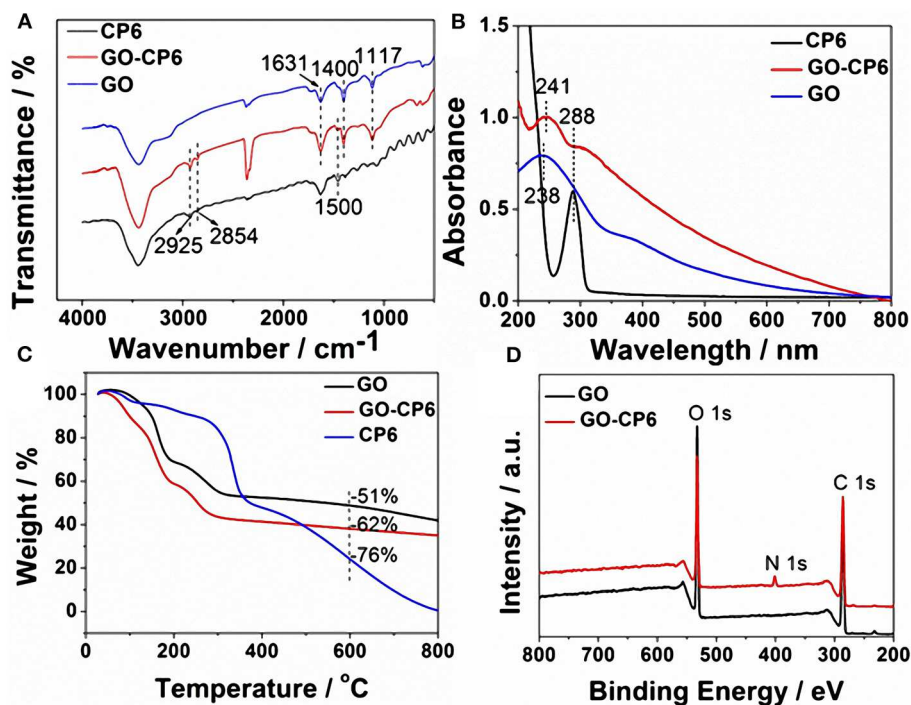
electrodeposition technique (Scheme 1). The electrodeposited nanocomposite films were characterized by scanning electron microscopy (SEM) and Raman spectra. The electrocatalytic activity of the present ErGO-CP6-modified GCE (ErGO-CP6/GCE) was examined by taking five purine bases [adenine (A), guanine (G), xanthine (X), hypoxanthine (HX), and uric acid (UA)] as the probes. The electrochemical behaviors of five purine bases at the ErGO-CP6/GCE displayed higher electrochemical performance than at those of ErGO/GCE and bare GCE, indicating that the CP6-modified graphene films not only show the excellent electrical properties of graphene but also exhibit high inclusion complexation and enrichment capability of CP6 through the formation of host-guest inclusion complexes between CP6 and the five purine bases.

## MATERIALS AND METHODS

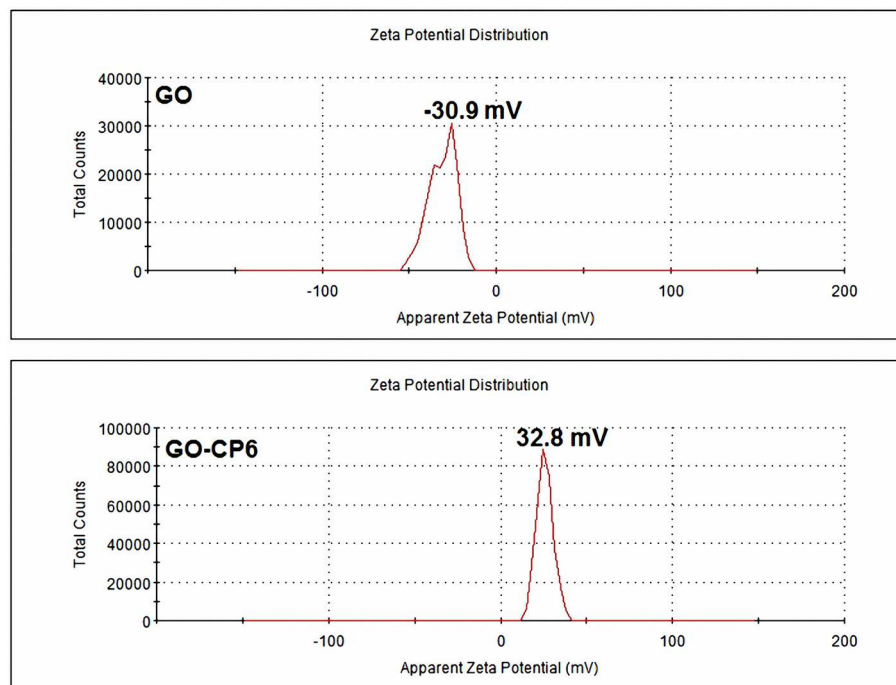
Graphite was obtained from XFNANO Materials Tech Co., Ltd (Nanjing, China). A, G, X, HX, and UA were purchased from Adamas-beta Ltd. All other reagents were analytically pure and were used as supplied without further purification. Doubly distilled water (DDW) was used for preparing all solutions. Fourier transform infrared (FTIR) spectroscopy measurements were conducted on a Thermo Fisher Nicolet 6700. UV-vis spectroscopy data were collected by a Shimadzu



**SCHEME 1** | Schematic illustration for the pulsed electrodeposition preparation of ErGO and ErGO-CP6 films on the surface of GCE and sensing the purine bases by an electrochemical strategy.



**FIGURE 1 |** Characterization of materials. FTIR spectra (A), UV-vis absorption spectra (B), and TGA curves of CP6, GO-CP6, and GO (C). XPS survey spectra of GO and GO-CP6 (D).



**FIGURE 2 |** Zeta potentials of GO and GO-CP6.

UV-3600 spectrophotometer (UV-3600, Shimadzu, Japan). Thermogravimetric analysis (TGA) was performed using NETZSCH STA449F3 thermogravimetric analyzer at a heating rate of  $10^{\circ}\text{C}\cdot\text{min}^{-1}$  under nitrogen atmosphere from 30 to  $800^{\circ}\text{C}$ . Raman spectra were recorded using an inVia Reflex Raman spectrometer (Renishaw Co., England). A Quanta-250 scanning electron microscope (SEM) (FEI, Czech) was used for imaging. X-ray photoelectron spectroscopy (XPS) data were collected with Thermo Fisher Scientific ESCALAB-250XI spectrometer. Al K alpha radiation was used as an X-ray source ( $1486.6\text{ eV}$ ). Zeta potential measurements were conducted on a Malvern Zetasizer Nano series. All fluorescence titration experiments were conducted on a Cary Eclipse fluorescence spectrophotometer (Agilent, Australia) at room temperature. All electrochemical experiments were carried out using a CHI 650A electrochemical analyzer (CHI Instrument, China) and RST5000 electrochemical workstation (Zhengzhou Shiruisi Technology, China). A conventional three-electrode system was employed, where a saturated calomel electrode (SCE) served as the reference electrode, a platinum (Pt) wire electrode as the auxiliary electrode, and the modified GCE ( $d = 3.0\text{ mm}$ ) as the working electrode. All pH values were measured with a PHS-3C

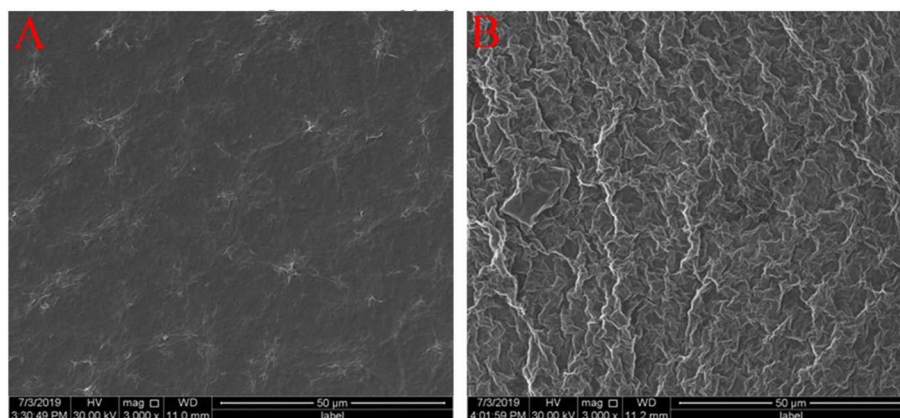
digital pH meter (Shanghai Leici Instrument Factory, Shanghai, China), which was calibrated daily at  $25^{\circ}\text{C}$ .

### Preparation of GO-CP6 Composite

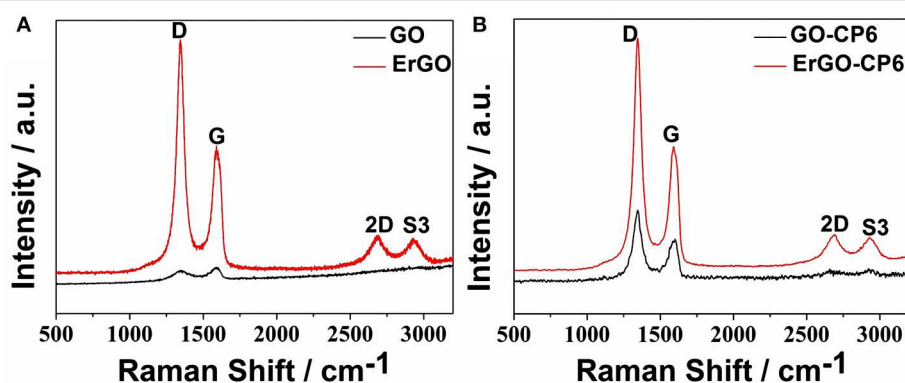
GO was prepared from natural graphite powder by a modified Hummer's method (Hummers and Offeman, 1958), and CP6 was prepared according to our previously published procedure (Duan et al., 2019). A GO-CP6 composite was prepared: CP6 (6 mg) and GO (6 mg) were dissolved in 10 mL of DDW by sonication for 10 min, and then the mixture reacted for 12 h at room temperature under continuous stirring. The black dispersion was separated by centrifuging at 18,000 rpm for 20 min, thoroughly rinsed with DDW three times, and dried under vacuum to obtain GO-CP6 composite. The GO-CP6 powder, which can be easily dispersed in a 0.2 M pH 6.8 PBS by ultrasonication again was obtained by freeze drying for further characterization.

### Pulsed Electrodeposition Preparation of ErGO and ErGO-CP6 Films Onto GCE

Prior to use, the GCE surface was successively polished with 0.3 and  $0.05\text{ }\mu\text{m}$   $\text{Al}_2\text{O}_3$  powder and washed thoroughly with



**FIGURE 3 |** SEM images of ErGO films (A) and ErGO-CP6 films (B) modified GCE.



**FIGURE 4 |** (A) Raman spectra of GO and ErGO; (B) Raman spectra of GO-CP6 and ErGO-CP6.



DDW between each polishing step, and then the polished GCE was sonicated in ethanol and DDW for 2 min prior to each experiment before then being dried under  $N_2$  blowing. After drying, the cleaned GCE was immersed in the aforementioned PBS (pH 6.8) containing  $0.8 \text{ mg}\cdot\text{mL}^{-1}$  GO-CP6, and the GO-CP6 was electrodeposited onto the GCE by a pulse potentiostatic method under constant stirring at room temperature. The optimum pulse electrodeposition parameters were set: anodic potential,  $-0.1 \text{ V}$ ; cathodic potential,  $-1.3 \text{ V}$ ; anodic pulse duration time,  $0.7 \text{ s}$ ; cathodic pulse duration time,  $0.3 \text{ s}$ ; and the total experimental time,  $100 \text{ s}$ . After electrodeposition, the ErGO-CP6/GCE was thoroughly washed with DDW and then kept under ambient conditions prior to use. For comparison purposes, we also prepared ErGO/GCE through the similar pulse potentiostatic method except that the anodic potential of  $0.1 \text{ V}$  was used to deposit GO on GCE.

## RESULTS AND DISCUSSION

### Characterization of GO-CP6 Composite

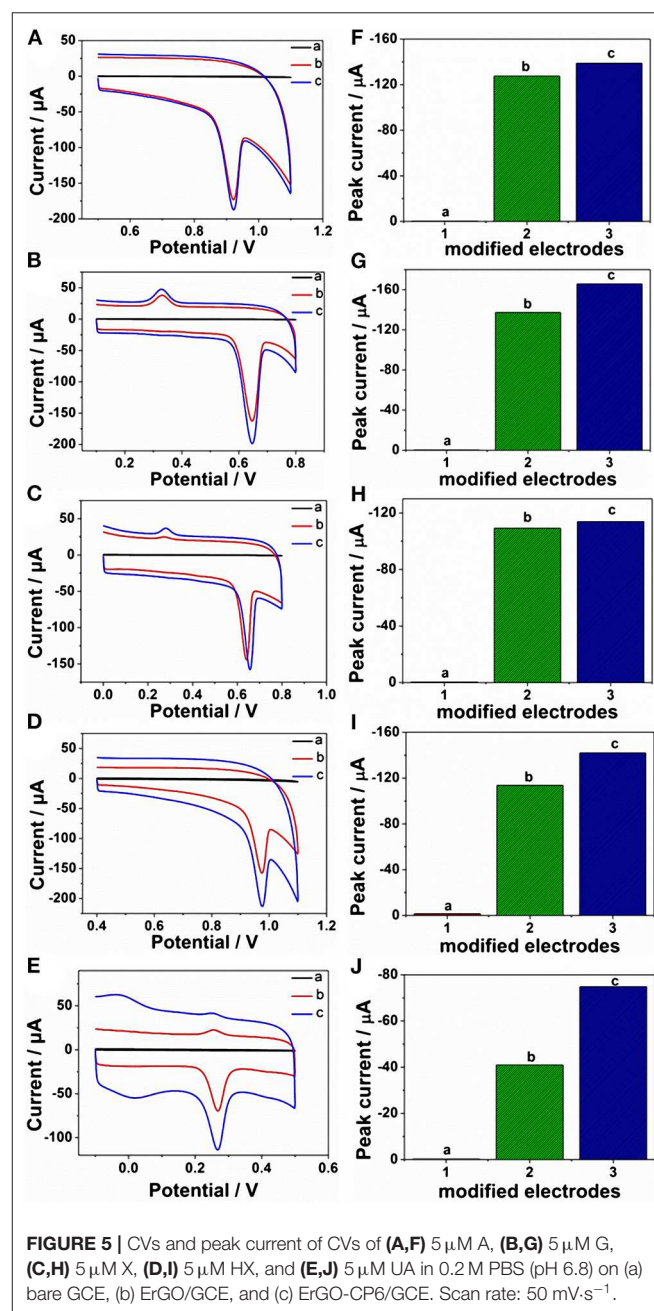
FTIR spectra supported the successful functionalization of GO with CP6. As can be seen from **Figure 1A**, the FTIR spectrum of GO displays the stretching vibrations of  $-\text{OH}$  ( $3,436 \text{ cm}^{-1}$ ),  $\text{C}=\text{C}$  ( $1,631 \text{ cm}^{-1}$ ),  $\text{C}-\text{OH}$  ( $1,400 \text{ cm}^{-1}$ ), and  $\text{C}-\text{O}$  ( $1,117 \text{ cm}^{-1}$ ). In the spectrum of GO-CP6, the new bands observed at  $2,925$  and  $2,854 \text{ cm}^{-1}$  correspond to asymmetric and symmetric  $\text{CH}_2$  stretching vibrations, respectively, and the bands centered at  $1,500 \text{ cm}^{-1}$  are observed which are assigned to the typical CP6 absorption features of the phenyl stretching vibrations, indicating that the CP6 molecules have been successfully attached to the surface of GO (Allen et al., 2010). The successful preparation of GO-CP6 composites is further confirmed by UV-vis absorption spectra. As shown in **Figure 1B**, the characteristic absorption peak of CP6 is located at  $288 \text{ nm}$ . The absorption peak of GO is about  $238 \text{ nm}$ . When CP6 was loaded onto GO, GO-CP6 composites present two main absorption peaks, which are assigned to the absorption peaks of CP6 ( $\sim 288 \text{ nm}$ ) and GO ( $241 \text{ nm}$ ). Therefore, the successful chemical modification of CP6 on GO is further confirmed by UV-vis absorption spectra.

TGA measurement was further used to determine the mass fraction of CP6 in GO-CP6 composites. As shown in **Figure 1C**, pure CP6 slowly decomposed at  $\sim 300^\circ\text{C}$ . The GO has a mass loss ( $51\%$ ) at  $\sim 600^\circ\text{C}$  because of the pyrolysis of the labile oxygen-containing functional groups. The loss in mass of the GO-CP6 was about  $62 \text{ wt}\%$  at  $\sim 600^\circ\text{C}$ . The mass loss caused by CP6 decomposition was evaluated to be  $11 \text{ wt}\%$  by deducting the mass loss of the GO, suggesting that the mass fraction of CP6 molecules loaded on the surface of GO is  $11 \text{ wt}\%$ . This result is exciting because GO loading plentiful CP6 molecules will provide a good opportunity to expand the inclusion complexation and enrichment ability of CP6.

To further illustrate the formation of GO-CP6, XPS analysis was also performed to determine the compositions of GO and GO-CP6. As shown in **Figure 1D**, a significant  $\text{N}1\text{s}$  peak was observed for the GO-CP6 sample, which comes

from the  $-\text{NH}_3^+$  groups of CP6, but there was no  $\text{N}$  signal on the GO, further revealing the successful loading of CP6 onto GO.

The average zeta potentials of GO and GO-CP6 are  $-30.9$  and  $32.8 \text{ mV}$ , respectively, as shown in **Figure 2**. Compared to the zeta potential of GO, the zeta potential of GO-CP6 increases by  $\sim 63.7 \text{ mV}$ , and this is caused by the introduced positive charges of  $-\text{NH}_3^+$  in the CP6 molecule. The introduced positive charges in GO-CP6 facilitate the stability of nanocomposite owing to the increased repulsion of positive charges. Furthermore, the zeta potential of GO-CP6 is higher than  $30 \text{ mV}$ , suggesting that the stability and dispersion of GO-CP6 are very high (Fu et al., 2013).





Therefore, these results of FTIR, UV-vis, TGA, XPS, and zeta potential suggest that CP6 has been successfully grafted on the surface of GO.

## Pulsed Electrodeposition of ErGO and ErGO-CP6 Films on GCE

GO colloids are negatively charged in weak acid solution (Chen et al., 2011), while the surface charge of GO-CP6 is positively charged in weak acid solutions (Figure 2). When positive and negative potentials were applied on the GCE, respectively, GO and GO-CP6 could be spontaneously deposited onto the surface of GCE due to the strong electrostatic attraction. In accordance with the literature (Chen et al., 2011), the as-deposited GO can be electrochemically reduced at  $E = -1.1$  V vs. SCE. Herein, pulse potentiostatic method was used to achieve the electrodeposition of ErGO and ErGO-CP6 films in which 0.1 and  $-0.1$  V vs. SCE were used to deposit GO and GO-CP6 on GCE, respectively, followed by employing  $-1.3$  V vs. SCE to electrochemically reduce the as-deposited GO and GO-CP6 to ErGO and ErGO-CP6.

## Characterization of the ErGO/GCE and ErGO-CP6/GCE

The surface morphologies of ErGO and ErGO-CP6 films electrodeposited on GCE were examined by SEM. Figure 3 shows the SEM images of the ErGO and ErGO-CP6 films electrodeposited on the surface of GCE. As can be seen from Figure 3A, the ErGO films exhibit a curly morphology consisting a thin wrinkling paper-like structure and distribute homogeneously on the surface of GCE. In contrast, the ErGO-CP6 films (Figure 3B) possess more crumpled sheets closely associated with each other. Furthermore, aggregation barely occurs on the thin films, suggesting that the electrodeposition of ErGO-CP6 films on GCE by pulse potentiostatic method can obtain well-dispersed ErGO-CP6 films and prevent the aggregation.

Raman spectra of GO, ErGO, GO-CP6, and ErGO-CP6 are shown in Figure 4. The Raman spectrum of GO-CP6 (Figure 4B) displays D and G bands at  $1,344$  and  $1,587$   $\text{cm}^{-1}$ , respectively,

which is similar to those of GO prepared through the chemical oxidation of graphite (Figure 4A). The D band at  $\sim 1,350$   $\text{cm}^{-1}$  corresponds to the presence of defects due to  $\text{sp}^3$  hybridized carbon, while the G band at  $\sim 1,575$   $\text{cm}^{-1}$  indicates the  $\text{sp}^2$  hybridized carbon (Zhu et al., 2010). The intensity ratio of the D band to the G band ( $I_D/I_G$ ) of carbon products is generally used to evaluate the extent of disorder or defects that result from vacancies, distortion, and edges (Tuinstra and Koenig, 1970; Stankovich et al., 2007). The larger value of  $I_D/I_G$  is an indication of smaller  $\text{sp}^2$  domains (Tuinstra and Koenig, 1970). After electrochemical reduction of GO and CP6-GO, the

**TABLE 1** | Comparison with other modified electrodes in the literatures for the detection of UA.

Modified electrode	Linear range ( $\mu\text{M}$ )	Detection limit ( $\mu\text{M}$ )	Analytical methods	References
Au/RGO <sup>a</sup> /GCE	8.8–530	1.8	DPV	Wang et al., 2014
MoS <sub>2</sub> /PEDOT <sup>b</sup> /GCE	2–25	0.95	DPV	Li et al., 2016
RGO-ZnO <sup>c</sup> /GCE	1–70	0.33	DPV	Zhang et al., 2016
Au-Cu <sub>2</sub> O/RGO/GCE	100–900	6.5	DPV	Aparna et al., 2018
PANI-GO <sup>d</sup> /GCE	2–18	0.2	DPV	Manivel et al., 2013
CNC <sup>e</sup> /GCE	2–110	0.83	DPV	Liu et al., 2019
AuNPs <sup>f</sup> /GCE	2.8–57.5	2.8	DPV	Shi et al., 2017
ZnO-Au HCs <sup>g</sup> /GCE	10–400	2.375	DPV	Hou et al., 2016
ErGO-CP6/GCE	0.1–88.2	0.02	DPV	This work

<sup>a</sup>RGO: reduced graphene oxide.

<sup>b</sup>PEDOT: poly(3,4-ethylenedioxythiophene).

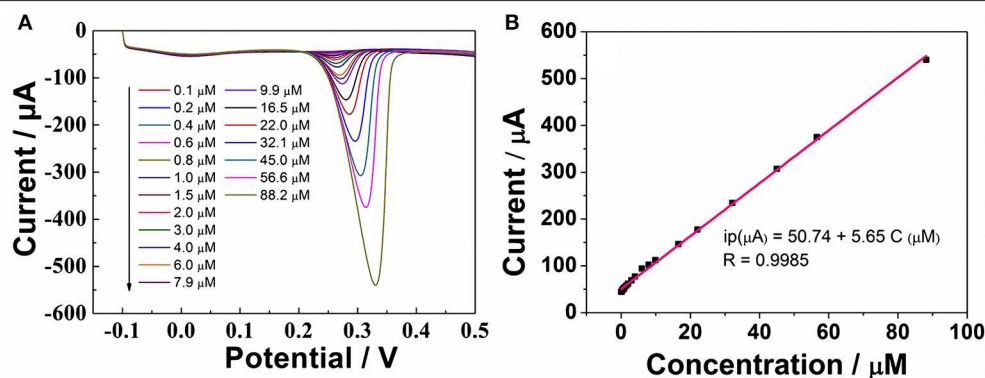
<sup>c</sup>RGO-ZnO: reduced graphene oxide-zinc oxide composite.

<sup>d</sup>PANI-GO: polyaniline/graphene oxide.

<sup>e</sup>CNC: N, Co-doped porous carbon.

<sup>f</sup>AuNPs: Au nanoparticles.

<sup>g</sup>ZnO-Au HCs: ZnO nanorods-Au nanoparticles hybrids composite.



**FIGURE 6** | (A) DPV response for the different concentrations of UA on ErGO-CP6/GCE in 0.2 M PBS (pH 6.8). (B) The calibration curve of UA.

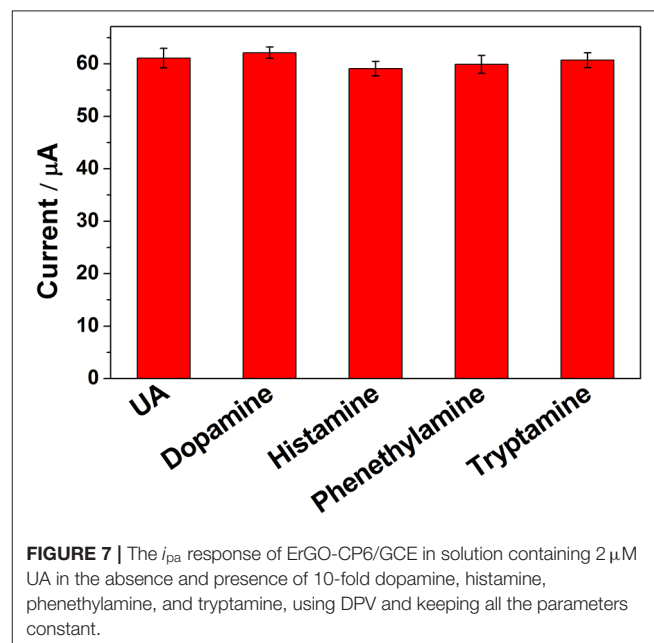
Raman spectra both displayed an increase in the intensities of D band compared to those of G band (**Figures 4A,B**). After the electrodeposition, the  $I_D/I_G$  ratios increased from 0.85 (for GO) to 1.81 (for ErGO) and 1.60 (for GO-CP6) to 1.84 (for ErGO-CP6), respectively, suggesting that smaller  $sp^2$  carbon domains are formed upon the electrochemical reduction of the GO and GO-CP6 (Stankovich et al., 2007). The two weak and broad 2D bands at  $\sim 2,690\text{ cm}^{-1}$  also indicated disorder due to an out-of-plane vibrational mode, and the cooperation between D and G bands also gave rise to an S3 band near  $2,932\text{ cm}^{-1}$ . The appearance of 2D and S3 bands at ErGO and ErGO-CP6 indicates that electrochemical reduction of GO and GO-CP6 can generate better graphitization compared to chemical reduction (Tung et al., 2009). The above results revealed that the electrochemical reduction of GO and GO-CP6 had indeed taken place, and their electrochemical reduction retained the  $sp^2$  hybridization of graphene's lattice.

### Electrochemical Characterization of the ErGO/GCE and ErGO-CP6/GCE

Given the above discussion, it can be demonstrated that CP6-modified graphene nanocomposite films had been prepared on GCE by pulsed electrodeposition, which could not only improve the stability and dispersion of graphene but also enhance sensitivity for detecting some important biological molecules through supramolecular host-guest complex formation between CP6 and the guest molecules that fit spatially within CP6 cavities. To confirm this conception (**Scheme 1**), the electrochemical behaviors of five purine bases [adenine (A), guanine (G), xanthine (X), hypoxanthine (HX), and uric acid (UA)] were investigated. CVs and peak currents of the above five purine bases on (a) GCE, (b) ErGO/GCE, and (c) ErGO-CP6/GCE are shown in **Figures 5A–J**, respectively. As shown in **Figures 5A–E** (curve a), very weak redox peaks currents on bare GCE were observed for five purine bases. Meanwhile, there were increases in the oxidation peak currents of five purine bases at ErGO/GCE compared to the currents at the bare GCE (**Figures 5A–E**, curve b), which may be ascribed to excellent conductivity and large surface area of ErGO arising from its specific structure. Much to our excitement, at the ErGO-CP6/GCE (**Figures 5A–E**, curve c), all the oxidation peak currents were noticeably increased and were  $\sim 1.2$ – $1.9$  times as much as those on ErGO/GCE. This illustrated that CP6 molecules immobilized on the surface of ErGO with excellent supramolecular enrichment ability can form host-guest complexes with all the examined purine bases (the association constants; see **Supplementary Figures 1–4** and **Supplementary Table 1**). The host-guest interactions between the CP6 and the purine bases can further improve the accumulation effect of ErGO-CP6/GCE and therefore increase the concentration of purine bases on the surface of the modified electrode, which would result in the noticeable enhancement in the oxidation peak current as compared with ErGO/GCE. These phenomena demonstrated that ErGO-CP6/GCE not only displayed the excellent properties of ErGO but also exhibited the outstanding supramolecular inclusion complexation and enrichment capability of CP6. Thus, the

enhanced electrochemical reactivity of the above five purine bases at the ErGO-CP6/GCE relative to the reactivity of those at the other two electrodes made the ErGO-CP6/GCE a better choice for the electrochemical detection of the above five purine bases at physiological pH.

According to the above discussion, ErGO-CP6 is an excellent electrode material for improving the electrochemical response for different purine bases. To evaluate the sensing performance of ErGO-CP6 toward certain purine bases, UA (UA is a vital product of purine metabolism and a crucial biomolecule in biological fluids, such as serum and urine; its detection is of great importance for pathological and physiological diagnosis) was chosen as a representative analyte. **Figure 6A** displays the differential pulse voltammetric (DPV) response of ErGO-CP6/GCE for different concentration additions of UA. Under the optimized conditions, the DPV response of UA is linearly proportional to the concentration within  $0.1$ – $88.2\text{ }\mu\text{M}$ , and the corresponding linear regression equation can be expressed as  $I_{pa}\text{ (}\mu\text{A)} = 50.74 + 5.65 C_{UA}\text{ (}\mu\text{M)}$  with the correlation coefficient ( $R^2$ ) of  $0.9985$ . The detection limit was estimated as  $0.02\text{ }\mu\text{M}$  based on  $S/N = 3$  (**Figure 6B**). Additionally, we compared our developed sensor with previous reports. As shown in **Table 1**, the developed ErGO-CP6/GCE electrode is better than or comparable with previously reported UA sensors regarding its analytical parameters, including the detection limit and linear range. The comparative results clearly reveal that the ErGO-CP6/GCE exhibited an excellent electrochemical performance toward the target molecules. Furthermore, the present method of preparation of ErGO-CP6/GCE is easy, simple, and saves time when compared to other carbon-based nanomaterials modified electrode. Therefore, based on a pulsed electrodeposition technique, ErGO-CP6/GCE can be prepared and used as a promising



**FIGURE 7** | The  $I_{pa}$  response of ErGO-CP6/GCE in solution containing  $2\text{ }\mu\text{M}$  UA in the absence and presence of 10-fold dopamine, histamine, phenethylamine, and tryptamine, using DPV and keeping all the parameters constant.

electrode material for sensitive detection of a wide variety of electroactive compounds.

To evaluate the influence of potential interfering biomolecules, some cyclic biogenic amines, such as dopamine, histamine, phenethylamine, and tryptamine, were studied as a potential interfering compound. Interfering experiments were carried out with 2  $\mu$ M UA in the absence and presence of 10-fold of dopamine, histamine, phenethylamine, and tryptamine. The observed results (Figure 7) clearly indicated that the peak current of UA was not affected even in the presence of excess concentration of the interfering bioorganic amines, which clearly confirmed that the ErGO-CP6/GCE displayed reasonable selectivity.

## CONCLUSIONS

In conclusion, the present work demonstrated a simple, rapid, and green pulsed electrodeposition method for the preparation of ErGO-CP6 films on the surface of GCE. More significantly, due to the unique properties of graphene and CP6, the ErGO-CP6 films at the modified electrode could exhibit outstanding enrichment capabilities and higher electrochemical responses toward A, G, X, HX, and UA than those of ErGO/GCE and bare electrodes. Under optimal conditions, the detection limit of UA was 0.02  $\mu$ M. The results indicate that the directly electrodeposited reduced graphene oxide-cationic pillar[6]arene composite films may be an attractive and a promising platform for analytical sensing.

## REFERENCES

- Allen, M. J., Tung, V. C., and Kaner, R. B. (2010). Honeycomb carbon: a review of graphene. *Chem. Rev.* 110, 132–145. doi: 10.1021/cr90070d
- Aparna, T. K., Sivasubramanian, R., and Dar, M. A. (2018). One-pot synthesis of Au-Cu<sub>2</sub>O/rGO nanocomposite based electrochemical sensor for selective and simultaneous detection of dopamine and uric acid. *J. Alloys Compd.* 741, 1130–1141. doi: 10.1016/j.jallcom.2018.01.205
- Cao, D., Kou, Y., Liang, J., Chen, Z., Wang, L., and Meier, H. (2009). A facile and efficient preparation of pillararenes and a pillarquinone. *Angew. Chem. Int. Ed.* 48, 9721–9723. doi: 10.1002/anie.200904765
- Cao, Y., Hu, X.-Y., Li, Y., Zou, X., Xiong, X., Lin, C., et al. (2014). Multistimuli-responsive supramolecular vesicles based on water-soluble pillar[6]arene and SAINT complexation for controllable drug release. *J. Am. Chem. Soc.* 136, 10762–10769. doi: 10.1021/ja505344t
- Chen, L., Tang, Y., Wang, K., Liu, C., and Luo, S. (2011). Direct electrodeposition of reduced graphene oxide on glassy carbon electrode and its electrochemical application. *Electrochem. Commun.* 13, 133–137. doi: 10.1016/j.elecom.2010.11.033
- Cragg, P. J. (2018). Pillar[n]arenes at the chemistry-biology interface. *Isr. J. Chem.* 58, 1158–1172. doi: 10.1002/ijch.201800013
- Cragg, P. J., and Sharma, K. (2012). Pillar[5]arenes: fascinating cyclophanes with a bright future. *Chem. Soc. Rev.* 41, 597–607. doi: 10.1039/C1CS15164A
- Davies, A., Audette, P., Farrow, B., Hassan, F., Chen, Z., Choi, J.-Y., et al. (2011). Graphene-based flexible supercapacitors: pulse-electropolymerization of polypyrrole on free-standing graphene films. *J. Phys. Chem. C* 115, 17612–17620. doi: 10.1021/jp205568v
- Duan, Q., Zhang, H., Mai, W., Wang, F., and Lu, K. (2019). Acid/base- and base/acid-switchable complexation between anionic-/cationic-pillar[6]arenes

## DATA AVAILABILITY STATEMENT

All datasets generated for this study are included in the article/Supplementary Material.

## AUTHOR CONTRIBUTIONS

QD and KL designed the work. LW and QD made contributions to the experiments and collective data. The paper was written by QD. All authors extensively discussed the results, reviewed the manuscript, and approved the final version of the manuscript to be submitted.

## FUNDING

This work was supported by the National Natural Science Foundation of China (no. 21402040, 21572046), Henan province science and technology research program (192102210197), and Program for Innovative Research Team (in Science and Technology) at the University of Henan Province (no. 20IRTSTHN008). Financial support from the Program of 543 team at Henan University of Engineering is gratefully acknowledged.

## SUPPLEMENTARY MATERIAL

The Supplementary Material for this article can be found online at: <https://www.frontiersin.org/articles/10.3389/fchem.2020.00430/full#supplementary-material>

- and a viologen dityosylate salt. *Org. Biomol. Chem.* 17, 4430–4434. doi: 10.1039/C9OB00398C
- Fu, G., Tao, L., Zhang, M., Chen, Y., Tang, Y., Lin, J., et al. (2013). One-pot, water-based and high-yield synthesis of tetrahedral palladium nanocrystal decorated graphene. *Nanoscale* 5, 8007–8014. doi: 10.1039/C3NR02179C
- Guo, H., Wang, X., Qian, Q., Wang, F., and Xia, X. (2009). A green approach to the synthesis of graphene nanosheets. *ACS Nano* 3, 2653–2659. doi: 10.1021/nn900227d
- Guo, Y., Guo, S., Li, J., Wang, E., and Dong, S. (2011). Cyclodextrin-graphene hybrid nanosheets as enhanced sensing platform for ultrasensitive determination of carbendazim. *Talanta* 84, 60–64. doi: 10.1021/j.talanta.2010.12.007
- Guo, Y., Guo, S., Ren, J., Zhai, Y., Dong, S., and Wang, E. (2010). Cyclodextrin functionalized graphene nanosheets with high supramolecular recognition capability: synthesis and host-guest inclusion for enhanced electrochemical performance. *ACS Nano* 4, 4001–4010. doi: 10.1021/nn100939n
- Hou, C., Liu, H., Zhang, D., Yang, C., and Zhang, M. (2016). Synthesis of ZnO nanorods-Au nanoparticles hybrids via *in-situ* plasma sputtering-assisted method for simultaneous electrochemical sensing of ascorbic acid and uric acid. *J. Alloys Compd.* 666, 178–184. doi: 10.1016/j.jallcom.2016.01.092
- Hou, X., Liu, X., Li, Z., Zhang, J., Du, G., Ran, X., et al. (2019). Electrochemical determination of methyl parathion based on pillar[5]arene@AuNPs/reduced graphene oxide hybrid nanomaterials. *New J. Chem.* 43, 13048–13057. doi: 10.1039/C9NJ02901J
- Hummers, W. S. Jr., and Offeman, R. E. (1958). Preparation of graphitic oxide. *J. Am. Chem. Soc.* 80, 1339–1339. doi: 10.1021/ja01539a017
- Kong, Y., Ren, X., Huo, Z., Wang, G., Tao, Y., and Yao, C. (2013). Electrochemical detection of pyrosine with electrochemically reduced graphene oxide modified glassy carbon electrode. *Eur. Food Res. Technol.* 236, 955–961. doi: 10.1007/s00217-013-1964-3

- Li, C., Wu, Z., Yang, H., Deng, L., and Chen, X. (2017). Reduced graphene oxide-cyclodextrin-chitosan electrochemical sensor: effective and simultaneous determination of o- and p-nitrophenols. *Sens. Actuators B* 251, 446–454. doi: 10.1016/j.snb.2017.05.059
- Li, Y., Lin, H., Peng, H., Qi, R., and Luo, C. (2016). A glassy carbon electrode modified with MoS<sub>2</sub> nanosheets and poly(3,4-ethylenedioxythiophene) for simultaneous electrochemical detection of ascorbic acid, dopamine and uric acid. *Microchim. Acta* 183, 2517–2523. doi: 10.1007/s00604-016-1897-1
- Liu, L., Liu, L., Wang, Y., and Ye, B.-C. (2019). A novel electrochemical sensor based on bimetallic metal-organic framework-derived porous carbon for detection of uric acid. *Talanta* 199, 478–484. doi: 10.1016/j.talanta.2019.03.008
- Liu, X., Wang, W., Li, X., Li, C., Qin, L., Sun, J., et al. (2016). Preparation of per-hydroxylated pillar[5]arene decorated graphene and its electrochemical behavior. *Electrochim. Acta* 210, 720–728. doi: 10.1016/j.electacta.2016.05.211
- Maiti, U. N., Lim, J., Lee, K. E., Lee, W. J., and Kim, S. O. (2014). Three-dimensional shape engineered, interfacial gelation of reduced graphene oxide for high rate, large capacity supercapacitors. *Adv. Mater.* 26, 615–619. doi: 10.1002/adma.201303503
- Manivel, P., Dhakshnamoorthy, M., Balamurugan, A., Ponpandian, N., Mangalaraj, D., and Viswanathan, C. (2013). Conducting polyaniline-graphene oxide fibrous nanocomposites: preparation, characterization and simultaneous electrochemical detection of ascorbic acid, dopamine and uric acid. *RSC Adv.* 3, 14428–14437. doi: 10.1039/C3RA42322K
- Mao, X., Liu, T., Bi, J., Luo, L., Tian, D., and Li, H. (2016). The synthesis of pillar[5]arene functionalized graphene as a fluorescent probe for paraquat in living cells and mice. *Chem. Commun.* 52, 4385–4388. doi: 10.1039/C6CC00949b
- Ogoshi, T., Kanai, S., Fujinami, S., Yamagishi, T.-A., and Nakamoto, Y. (2008). para-Bridged symmetrical pillar[5]arenes: their Lewis acid catalyzed synthesis and host-guest property. *J. Am. Chem. Soc.* 130, 5022–5023. doi: 10.1021/ja711260m
- Ogoshi, T., Yamagishi, T.-A., and Nakamoto, Y. (2016). Pillar-shaped macrocyclic hosts pillar[n]arenes: new key players for supramolecular chemistry. *Chem. Rev.* 116, 7937–8002. doi: 10.1021/acs.chemrev.5b00765
- Shao, Y., Wang, J., Engelhard, M., Wang, C., and Lin, Y. (2010a). Facile and controllable electrochemical reduction of graphene oxide and its applications. *J. Mater. Chem.* 20, 743–748. doi: 10.1039/B917975E
- Shao, Y., Wang, J., Wu, H., Liu, J., Aksay, I. A., and Lin, Y. (2010b). Graphene based electrochemical sensors and biosensors: a review. *Electroanalysis* 22, 1027–1036. doi: 10.1002/elan.200900571
- Shi, Y., Wang, J., Li, S., Yan, B., Xu, H., Zhang, K., et al. (2017). The enhanced photo-electrochemical detection of uric acid on Au nanoparticles modified glassy carbon electrode. *Nanoscale Res. Lett.* 12, 455. doi: 10.1186/s11671-017-2225-3
- Si, W., Li, Z.-T., and Hou, J.-L. (2014). Voltage-driven reversible insertion into and leaving from a lipid bilayer: tuning transmembrane transport of artificial channels. *Angew. Chem. Int. Ed.* 53, 4578–4581. doi: 10.1002/anie.201311249
- Singh, M., Jaiswal, N., Tiwari, I., Foster, C. W., and Banks, C. E. (2018). A reduced graphene oxide-cyclodextrin-platinum nanocomposite modified screen printed electrode for the detection of cysteine. *J. Electroanal. Chem.* 829, 230–240. doi: 10.1016/j.jelechem.2018.09.018
- Son, Y., Cohen, M. L., and Louie, S. G. (2006). Half-metallic graphene nanoribbons. *Nature* 444, 347–349. doi: 10.1038/nature05180
- Stankovich, S., Dikin, D. A., Piner, R. D., Kleinhammes, K. A., Jia, Y., Wu, Y., et al. (2007). Synthesis of graphene-based nanosheets via chemical reduction of exfoliated graphite oxide. *Carbon* 45, 1558–1565. doi: 10.1016/j.carbon.2007.02.034
- Sun, J., Guo, F., Shi, Q., Wu, H., Sun, Y., Chen, M., et al. (2019). Electrochemical detection of paraquat based on silver nanoparticles/water-soluble pillar[5]arene functionalized graphene oxide modified glassy carbon electrode. *J. Electroanal. Chem.* 847, 113221. doi: 10.1016/j.jelechem.2019.113221
- Takamura, T., Endo, K., Fu, L., Wu, Y., Lee, K. J., and Matsumoto, T. (2007). Identification of nano-sized holes by TEM in the graphene layer of graphite and the high rate discharge capability of Li-ion battery anodes. *Electrochim. Acta* 53, 1055–1061. doi: 10.1016/j.electacta.2007.03.052
- Tan, S., Han, R., Wu, S., Liang, H., Zhao, Y., Zhao, H., et al. (2019). A novel fluorescent sensing platform for insulin detection based on competitive recognition of cationic pillar[6]arene. *Talanta* 197, 130–137. doi: 10.1016/j.talanta.2019.01.004
- Tan, X., Liu, Y., Zhang, T., Luo, S., Liu, X., Tian, H., et al. (2019a). Ultrasensitive electrochemical detection of methyl parathion pesticide based on cationic water-soluble pillar[5]arene and reduced graphene nanocomposite. *RSC Adv.* 9, 345–353. doi: 10.1039/C8RA08555B
- Tan, X., Wu, Y., Yu, S., Zhang, T., Tian, H., He, S., et al. (2019b). The synthesis of water-soluble phosphate pillar[5]arenes functionalized graphene as a fluorescent probe for sensitive detection of paraquat. *Talanta* 195, 472–479. doi: 10.1016/j.talanta.2018.11.099
- Tan, X., Zhang, T., Zeng, W., He, S., Liu, X., Tian, H., et al. (2019c). A fluorescence sensing determination of 2,4,6-trinitrophenol based on cationic water-soluble pillar[6]arene graphene nanocomposite. *Sensors* 19:91. doi: 10.3390/s19010091
- Tuinstra, F., and Koenig, J. L. (1970). Raman spectrum of graphite. *J. Chem. Phys.* 53, 1126–1130. doi: 10.1063/1.1674108
- Tung, V. C., Allen, M. J., Yang, Y., and Kaner, R. B. (2009). High-throughput solution processing of large-scale graphene. *Nat. Nanotechnol.* 4, 25–29. doi: 10.1038/nnano.2008.329
- Vickery, J. L., Patil, A. J., and Mann, S. (2009). Fabrication of graphene-polymer nanocomposites with higher-order three-dimensional architectures. *Adv. Mater.* 21, 2180–2184. doi: 10.1002/adma.200803606
- Wang, C., Du, J., Wang, H., Zou, C., Jiang, F., Yang, P., et al. (2014). A facile electrochemical sensor based on reduced graphene oxide and Au nanoplates modified glassy carbon electrode for simultaneous detection of ascorbic acid, dopamine and uric acid. *Sens. Actuators B Chem.* 204, 302–309. doi: 10.1016/j.snb.2014.07.077
- Wang, X., Liu, Z.-J., Hill, E. H., Zheng, Y., Guo, G., Wang, Y., et al. (2019). Organic-inorganic hybrid pillarene-based nanomaterial for label-free sensing and catalysis. *Matter* 1, 848–861. doi: 10.1016/j.matt.2019.03.005
- Wang, Z., Wu, S., Zhang, J., Chen, P., Yang, G., Zhou, X., et al. (2012). Comparative studies on single-layer reduced graphene oxide films obtained by electrochemical reduction and hydrazine vapor reduction. *Nanoscale Res. Lett.* 7, 1–7. doi: 10.1186/1556-276X-7-161
- Xu, C., Wang, J., Wan, L., Lin, J., and Wang, X. (2011). Microwave-assisted covalent modification of graphene nanosheets with hydroxypropyl-β-cyclodextrin and its electrochemical detection of phenolic organic pollutants. *J. Mater. Chem.* 2, 10463–10471. doi: 10.1039/C1JM10478K
- Xue, M., Yang, Y., Chi, X., Zhang, Z., and Huang, F. (2012). Pillararenes, a new class of macrocycles for supramolecular chemistry. *Acc. Chem. Res.* 45, 1294–1308. doi: 10.1021/ar2003418
- Yao, Y., Xue, M., Chen, J., Zhang, M., and Huang, F. (2012). An amphiphilic pillar[5]arene: synthesis, controllable self-assembly in water, and application in calcein release and TNT adsorption. *J. Am. Chem. Soc.* 134, 15712–15715.
- Ye, J., Ma, L., Chen, W., Ma, Y., Huang, F., Gao, C., et al. (2015). Supramolecule-mediated synthesis of MoS<sub>2</sub>/reduced graphene oxide composites with enhanced electrochemical performance for reversible lithium storage. *J. Mater. Chem. A* 3, 6884–6893. doi: 10.1039/c5ta00006h
- Yu, G., Yang, J., Fu, X., Wang, Z., Shao, L., Mao, Z., et al. (2018). Supramolecular hybrid material constructed from graphene oxide and pillar[6]arene-based host-guest complex as an ultrasound and photoacoustic signals nanoamplifier. *Mater. Horiz.* 5, 429–435. doi: 10.1039/C8MH00128F
- Yu, Z., Ye, J., Chen, W., and Xu, S. (2017). Fabrication of MoS<sub>2</sub>/reduced graphene oxide hybrid as an earth-abundant hydrogen evolution electrocatalyst. *Mater. Lett.* 188, 48–51. doi: 10.1016/j.matlet.2016.10.088
- Zhang, H., Ma, X., Nguyen, K. T., Zeng, Y., Tai, S., and Zhao, Y. (2014). Water-soluble pillararene-functionalized graphene oxide for *in vitro* raman and fluorescence dual-mode imaging. *ChemPlusChem* 79, 462–469. doi: 10.1002/cplu.201300408
- Zhang, X., Zhang, Y.-C., and Ma, L.-X. (2016). One-pot facile fabrication of graphene-zinc oxide composite and its enhanced sensitivity for simultaneous electrochemical detection of ascorbic acid, dopamine and uric acid. *Sens. Actuators B Chem.* 227, 488–496. doi: 10.1016/j.snb.2015.12.073
- Zhao, G., Yang, L., Wu, S., Zhao, H., Tang, E., and Li, C.-P. (2017). The synthesis of amphiphilic pillar[5]arene functionalized reduced graphene oxide and its application as novel fluorescence sensing platform for the determination of acetaminophen. *Biosens. Bioelectron.* 91, 863–869. doi: 10.1016/j.bios.2017.01.053



- Zhou, J., Chen, M., and Diao, G. (2013a). Calix[4,6,8]arenesulfonates functionalized reduced graphene oxide with high supramolecular recognition capability: fabrication and application for enhanced host–guest electrochemical recognition. *ACS Appl. Mater. Interfaces* 5, 828–836. doi: 10.1021/am302289v
- Zhou, J., Chen, M., and Diao, G. (2013b). Assembling Gold and Platinum nanoparticles on resorcinarene modified graphene and their electrochemical applications. *J. Mater. Chem. A* 1, 2278–2285. doi: 10.1039/C2TA01146H
- Zhou, J., Chen, M., Xie, J., and Diao, G. (2013c). Synergistically enhanced electrochemical response of host–guest recognition based on ternary nanocomposites: reduced graphene oxide-amphiphilic pillar[5]arene-Gold nanoparticles. *ACS Appl. Mater. Interfaces* 5, 11218–11224. doi: 10.1021/am403463p
- Zhou, M., Zhai, Y., and Dong, S. (2009). Electrochemical sensing and biosensing platform based on chemically reduced graphene oxide. *Anal. Chem.* 81, 5603–5613. doi: 10.1021/ac900136z
- Zhou, T., Yu, H., Liu, M., and Yang, Y.-W. (2015). Carboxylatopillararene-modified reduced graphene oxides with high water dispersibility for fluorescent dye sensing. *Chin. J. Chem.* 33, 125–130. doi: 10.1002/cjoc.201400238
- Zhu, C., Guo, S., Fang, Y., and Dong, S. (2010). Reducing sugar: new functional molecules for the green synthesis of graphene nanosheets. *ACS Nano* 4, 2429–2437. doi: 10.1021/nn1002387

**Conflict of Interest:** The authors declare that the research was conducted in the absence of any commercial or financial relationships that could be construed as a potential conflict of interest.

Copyright © 2020 Duan, Wang, Wang, Zhang and Lu. This is an open-access article distributed under the terms of the Creative Commons Attribution License (CC BY). The use, distribution or reproduction in other forums is permitted, provided the original author(s) and the copyright owner(s) are credited and that the original publication in this journal is cited, in accordance with accepted academic practice. No use, distribution or reproduction is permitted which does not comply with these terms.





# Calix[n]arene/Pillar[n]arene-Functionalized Graphene Nanocomposites and Their Applications

Qunpeng Duan<sup>1\*</sup>, Lijie Wang<sup>1</sup>, Fei Wang<sup>1</sup>, Hongsong Zhang<sup>1</sup> and Kui Lu<sup>1,2\*</sup>

<sup>1</sup> School of Materials and Chemical Engineering, Henan University of Engineering, Zhengzhou, China, <sup>2</sup> School of Chemical Engineering and Food Science, Zhengzhou Institute of Technology, Zhengzhou, China

## OPEN ACCESS

### Edited by:

Tangxin Xiao,  
Changzhou University, China

### Reviewed by:

Xuan Wu,  
Wenzhou Institute of Biomaterials and  
Engineering (CAS), China  
Qi Wang,  
Nanjing University of Posts and  
Telecommunications, China

### \*Correspondence:

Qunpeng Duan  
qpduan@haue.edu.cn  
Kui Lu  
lucky Luke@haue.edu.cn

### Specialty section:

This article was submitted to  
Supramolecular Chemistry,  
a section of the journal  
Frontiers in Chemistry

**Received:** 26 April 2020

**Accepted:** 15 May 2020

**Published:** 12 June 2020

### Citation:

Duan Q, Wang L, Wang F, Zhang H  
and Lu K (2020)  
Calix[n]arene/Pillar[n]arene-  
Functionalized Graphene  
Nanocomposites and Their  
Applications. *Front. Chem.* 8:504.  
doi: 10.3389/fchem.2020.00504

Calix[n]arenes and pillar[n]arenes, which contain repeating units of phenol and methane, are class of synthetic cyclic supramolecules. Their rigid structure, tunable cavity size, flexible functionalization, and rich host-guest properties make them ideal surface modifiers to construct functional hybrid materials. Introduction of the calix[n]arene/pillar[n]arene species to the graphene may bring new interesting or enhanced physicochemical/biological properties by combining their individual characteristics. Reported methods for the surface modification of graphene with calix[n]arene/pillar[n]arene utilize either covalent or non-covalent approaches. This mini-review presents the recent advancements in the functionalization of graphene nanomaterials with calix[n]arene/pillar[n]arene and their applications. At the end, the future outlook and challenges for the continued research of calix[n]arene/pillar[n]arene-functionalized graphene nanohybrids in the development of applied nanoscience are thoroughly discussed.

**Keywords:** calix[n]arene, pillar[n]arene, graphene, nanocomposites, functionalization

## INTRODUCTION

In recent years, as a two-dimensional  $sp^2$ -hybridized carbon nanomaterial, graphene has attracted intense scientific interest since its discovery in 2004. It is described as the World's "thinnest" material, and it presents fascinating mechanical, electronic, thermal, optical, and chemical properties that have made it a promising material for potential use in various scientific fields such as nanoelectronics (Son et al., 2006), supercapacitors (Maiti et al., 2014), batteries (Takamura et al., 2007), sensors (Shao et al., 2010), and nanocomposites (Watcharotone et al., 2007). The development of these applications requires preservation of the single-layer of graphene in common solvents. However, it is difficult to construct single-layer graphene at ambient temperature. Graphene sheets tend to form irreversible agglomerates due to the attractive van der Waals forces between the graphene sheets or even re-aggregate through those same attractive forces if the sheets are not well-separated from each other (Li et al., 2008; Shan et al., 2009). Aggregation can be greatly reduced by attachment of other functionality to the graphene sheets. Such functionality should bring new properties, produce some desirable effects, and open up a new avenue to further utilize the resulting nanostructure as novel composite materials. One of the most promising strategies for the creation of functionalized graphene is using water-soluble supramolecules capable of

forming host-guest complexes with the target substrate (Guo et al., 2010; Kasprzak and Poplawska, 2018). The introduction of water-soluble supramolecules as functional molecules can effectively disperse graphene, and further introduce new or enhanced functions through combining their individual characteristics.

Calix[n]arenes and pillar[n]arenes are class of synthetic cyclic oligomers which contain repeating phenolic units and methane. Calix[n]arenes are generally known as the third class of supramolecules (Gutsche, 1998). Most of the supramolecular self-assembly and substrate-recognition patterns were first realized with calix[n]arenes and thereafter so were other supramolecules. Ease functionalization of both the upper and lower rims of calix[n]arenes have made them attractive versatile building blocks for supramolecular hybrid materials. Emerging as a relatively new class of calix[n]arene analogs, pillar[n]arenes and their derivatives have attracted particular interest in supramolecular chemistry and materials science during past decades (Ogoshi et al., 2008; Ogoshi, 2015; Wang et al., 2018a,b). Different from conventional calix[n]arenes, their symmetrical rigid pillar-shaped structures, tunable cavity size, easy functionalization, and unique host-guest recognition abilities inspire researchers to construct pillar[n]arene-based functional nanocomposite materials. In the present mini-review, we summarize the recent achievements in the design and application of graphene functionalized with calix[n]arene/pillar[n]arene (Figure 1). The structures of calix[n]arenes and pillar[n]arenes utilized to construct graphene hybrids are shown in Figure 2. Besides, the potential and challenges of the study of calix[n]arene/pillar[n]arene-functionalized graphene nanomaterials are summarized.

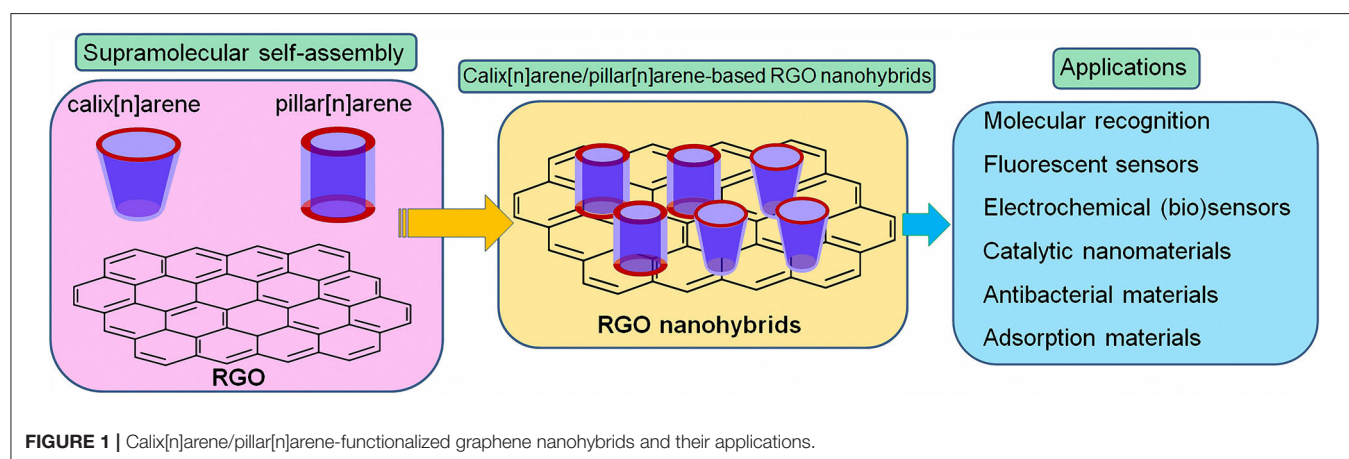
## FUNCTIONALIZATION OF GRAPHENE WITH CALIX[N]ARENES

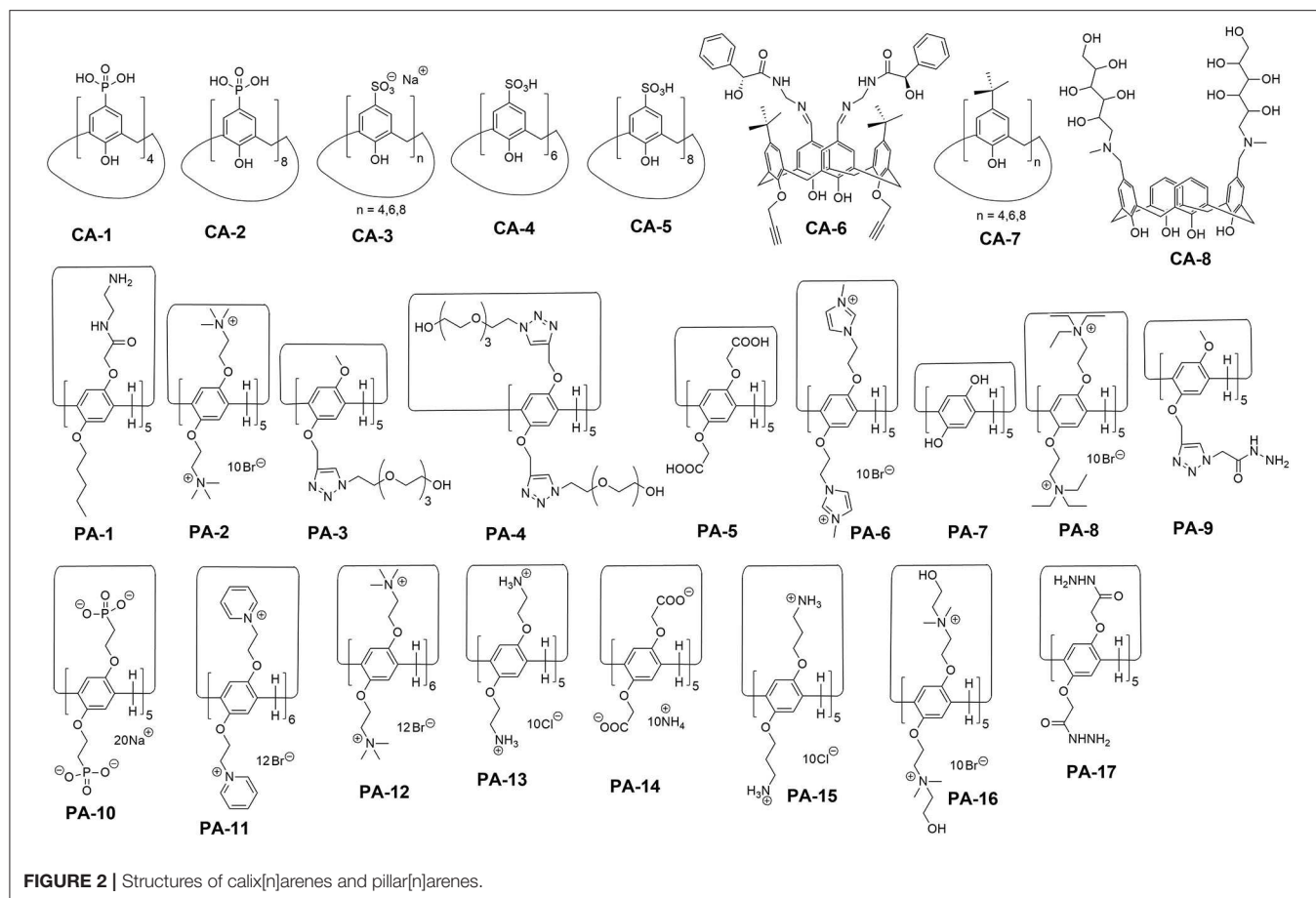
As the third-generation host molecules after crown ethers and cyclodextrins, calix[n]arenes have attracted continuous interest since they can form stable host-guest complexes with various

guest molecules (Diamond and McKerver, 1996; Gutsche, 1998). It is noteworthy that calix[n]arenes can be used as modifiers to form calix[n]arenes-functionalized graphene composites by  $\pi$ - $\pi$  stacking interactions and hydrogen-bonding interactions (Eroglu et al., 2013; Zhou et al., 2013a). The advantage of water-soluble calix[n]arenes, particularly, *p*-phosphonate and *p*-sulfonated derivatives, is that it brings graphene high water-solubility and guest molecules trapped into calix[n]arenes are easily accessible to graphene.

*p*-Phosphonic acid calix[n]arene, an amphiphilic supramolecule with the phosphonate groups and hydroxide groups on the upper and lower rim, respectively, has been employed as a versatile stabilizing surfactant to effectively stabilize graphenes in water. In 2011, Zou et al. (2011) successfully prepared the first example of *p*-phosphonic acid calix[4]arene (CA-1) modified graphene. CA-1 gives high stability to graphene in water. This CA-1 modified graphene (CA-1@graphene) can be utilized as a highly effective template on nucleate ultra-small palladium nanoparticles (Pd NPs), which in turn stabilizes graphene. High-density 2D nano-arrays of platinum nanoparticles (Pt NPs) were achieved by using Pd-CA-1@graphene as galvanic reaction templates. Subsequently, Chen et al. (2013a,b); Chen et al. (2014) reported non-covalent functionalization of reduced graphene oxide (RGO) in an aqueous medium with *p*-phosphonic acid calix[8]arene (CA-2). Employing a simple and versatile drop-casting technique on interdigital electrodes, electrocatalytic ternary Pd/Pt/Ru-CA-2@graphene nanocomposite has been incorporated into a device for effective hydrogen sensing, which provides an attractive perspective in replacing traditional graphene oxide (GO) or RGO as an effective supporting material for noble metal nanostructures in energy storage, sensors, catalysis, and devices. In 2013, Eroglu et al. (2013) also constructed CA-2 stabilized graphene for reversible nitrate uptake from aquatic effluents.

In supramolecular chemistry, fragments of sulfonic acids are usually employed in order to increase water solubility, which gives surficial active properties based on acid-base or ionic interactions. A significant contribution in the preparation and application of sulfonatocalix[n]arene-stabilized graphene has





been made by many research groups. In 2013, Zhou et al. (2013a) reported that three kinds of *p*-sulfonatocalix[4,6,8]arenes sodium (CA-3) were successfully loaded onto RGO surface by utilizing a simple wet-chemical method. Significantly, CA-3@RGO-modified glassy carbon electrode (GCE) exhibited an enhanced electrochemical response to dye molecules and biomolecules due to the high supramolecular recognition and enrichment effect between CA-3 and the biological and organic dye molecules. Subsequently, Yang et al. (2016b) developed an electrochemical sensing platform based on CA-4 functionalized reduced graphene oxide (CA-4@RGO). Based on competitive host-guest recognition between CA-4 and methylene blue/ cholesterol, CA-4@RGO-modified GCE was used as an electrochemical sensor for the efficient and selective detection of cholesterol without any enzyme or antibody. Later in 2018, Song et al. (2018) constructed a CA-4@RGO-modified gold electrode for the sensitive and selective detection of caspase-3. CA-4@RGO can be attached onto the gold electrode surface through host-guest recognition. Owing to the host-guest recognition of CA-4, electrical signal molecules methylene blue has more binding sites on the CA-4@RGO surface, which resulted in a higher electrochemical response to caspase-3.

In the meantime, Yang et al. (2015, 2016a) also constructed two simple and convenient fluorescence sensing platforms based on CA-4 and CA-5 functionalized reduced graphene oxide

(CA-4@RGO and CA-5@RGO). Based on competitive host-guest recognition, CA-4@RGO and CA-5@RGO were used as a fluorescent probe for the sensitive and selective detection of tadalafil and aconitine, respectively. Later in 2016, Ye et al. (2016) also reported a facile competitive fluorescent sensing platform by using CA-4-MnO<sub>2</sub>@RGO composite as a receptor. The ternary nanocomposites CA-4-MnO<sub>2</sub>@RGO simultaneously possess the excellent quenching performance of MnO<sub>2</sub>@RGO and the high supramolecular recognition capability of CA-4, which was used as a fluorescent probe for the sensitive and selective detection of labetalol in human serum samples. Later in 2016, CA-4 was also used as an effective particle stabilizer to create silver-graphene nanocomposites with enhanced antibacterial activity (Kellici et al., 2016).

In 2015, Mao et al. (2015) designed and synthesized a chiral *R*-mandelic acid calix[4]arene (CA-6). CA-6 was successfully covalently grafted to GO through a click reaction to obtain CA-6 modified graphene (CA-6@G). By taking advantages of both the functional calixarene and graphene, CA-6@G was used as a chiral probe for the highly sensitive and selective sensing of amino propanol enantiomers in a serum sample at the nM levels. Later in 2016, Zhang et al. (2016) reported that three kinds of calix[4,6,8]arenes (CA-7) were covalently anchored onto the surface of GO by esterification and polymerization of CA-7 onto GO surfaces. Ongoing research confirms that the introduction

of **CA-7** onto the GO surface facilitates the adsorption capacity toward neodymium ions. In 2018, Nurerk et al. (2018) prepared calix[4]arene-functionalized GO via covalent attachment of 4-tert-butylcalix[4]arene [**CA-7** ( $n = 4$ )] and GO. Subsequently, the prepared calix[4]arene@GO was absorbed and entrapped in porous polydopamine-coated cellulose acetate fiber (PDA-CFs) to fabricate calix[4]arene@GO/PDA-CFs. The developed calix[4]arene@GO/PDA-CFs was successfully applied as an adsorbent for analyzing aflatoxins from corn samples. Later in 2019, Nodeh et al. (2019) synthesized magnetic graphene on basis of *N*-methyl-*D*-glucamine functionalized calix[4]arene (**CA-8**) nanocomposite (**CA-8@MGO**) by covalent attachment of *N*-methyl-*D*-glucamine calix[4]arene (**CA-8**) and Fe<sub>3</sub>O<sub>4</sub>-graphene oxide (MGO). The synthesized **CA-8@MGO** was successfully utilized as an effective adsorbent for the removal of chlorpyrifos and hexaconazole pesticides from water samples.

## FUNCTIONALIZATION OF GRAPHENE WITH PILLAR[N]ARENES

Pillar[n]arenes are a relatively new class of macrocyclic hosts, which was first reported in 2008 (Ogoshi et al., 2008). These macrocyclic hosts have attracted much attention due to their synthetic accessibility and pillar-shaped three-dimensional structures. Practically, a series of pillar[n]arenes with good water solubility and recognition capability have been exploited to construct graphene hybrid materials to improve their water stability and dispersity, as well as to enhance their supramolecular recognition capability in many applications, including sensors, luminescence, electrocatalysis, and electronics, and therefore attracted wide research interest.

Zhou et al. (2013b) reported the first example of non-covalent functionalization of RGO with an amphiphilic pillar[5]arene (**PA-1**). The resulting functionalized graphene nanocomposite (**PA-1@RGO**) exhibits good water dispersibility. It also possesses excellent selective supramolecular recognition and enrichment capability toward guest molecules. In order to obtain ternary nanocomposites **PA-1@RGO-AuNPs**, gold nanoparticles (AuNPs) were self-assembled onto the surface of **PA-1@RGO**. Furthermore, these ternary nanocomposites **PA-1@RGO-AuNPs** exhibit enhanced electrochemical performance due to the synergistic effects of AP5 supramolecular recognition capability, high catalysis of AuNPs and excellent electron transport performances of RGO. Later in 2019, based on cationic pillar [5]arene (**PA-2**) modified RGO and PtPd bimetallic nanoparticles (PtPd NPs), Liang et al. (2019) also reported ternary nanocomposites **PA-2@RGO-PtPd**. To obtain these ternary nanocomposites, **PA-2**-decorated RGO was firstly prepared and then loaded with PtPd NPs. Glassy carbon electrode modified with **PA-2@RGO-PtPd** was employed for BPA detection with enhanced electrochemical performance, which is also caused by synergistic influences of **PA-2** host-guest recognition performance, high catalysis of PtPd NPs and conductivity of RGO.

In 2014, supramolecular functionalized graphene hybrid materials with conjugated tadpole-like (**PA-3**) and bola-amphiphilic pillar[5]arenes (**PA-4**) have been successfully

prepared by Zhang et al. (2014). The strong interfacial adhesion between these pillar[5]arenes and graphene oxide was attributed to the strong hydrogen-bonding interactions. Ongoing research shows that these functionalized graphene hybrid materials have excellent biocompatibility and low cytotoxicity, which was used for *in vitro* dual-mode Raman and fluorescence imaging.

In 2015, Zhou et al. (2015) designed a sensing platform by the functionalization of RGO with a water-soluble carboxylated pillar[5]arene (**PA-5**) via covalent bonds. The resulting functionalized graphene exhibits good water dispersibility and enhanced fluorescence-quenching resistance as compared with native RGO. This fabricated sensing platform opens up prospects to sense and detect organic dye molecules and pesticides in aqueous solution.

Later in 2015, Chen's group investigated the role of cationic water-soluble pillar[5]arene (**PA-2**) containing 10 trimethylammonium groups on the microstructure of MoS<sub>2</sub>/RGO composites. They found that the modification of pillar[5]arene onto the surface of graphene oxide sheets (GOS) enhances the lithium storage performance of MoS<sub>2</sub>/RGO composites (Ye et al., 2015). A later study from the same research group showed that the functionalization of *N*-methylimidazole water-soluble pillar[5]arene (**PA-6**) on the GOS surface also enhances the lithium storage performance of MoS<sub>2</sub>/RGO composites (Yu et al., 2017).

In 2016, Liu et al. (2016) reported the preparation of graphene-based hybrid material modified with per-hydroxylated pillar[5]arene (**PA-7**) via covalent bonds and its electrochemical behavior. The resulting functionalized graphene modified electrode exhibits high sensitivity and selectivity to dopamine. This sensing platform opens an attractive perspective in practical sensing and detection of dopamine in biological samples. Tan et al. (2019a) later also developed an ultrasensitive electrochemical sensor for detecting methyl parathion based on cationic water-soluble pillar[5]arene (**PA-8**) modified RGO. This sensor has been utilized to determine methyl parathion in wastewater and soil samples with satisfactory results.

In 2016, Mao et al. (2016) developed a new strategy of introducing hydrazine-pillar[5]arene (**PA-9**) onto biocompatible graphene via covalent bonds. The resulting functionalized graphene can be used as an effective fluorescence sensing platform for the detection of paraquat both in living cells and mice with low cellular toxicity. This method provides an attractive perspective in developing a new methodology for quantifying intracellular imaging in live cells.

In 2017, Zhao et al. (2017) designed a fluorescence sensing platform for the detection of acetaminophen (AP) by utilizing amphiphilic pillar[5]arene functionalized reduced graphene oxide (**PA-1@RGO**) as a sensor. Because of the host-guest interaction, both acetaminophen and acridine orange can thread into the hydrophobic inner cavity of **PA-1** to form 1:1 inclusion complex with **PA-1**. The obtained **PA-1@RGO** can detect acetaminophen by the host-guest competition due to the stronger interaction between AP and **PA-1**. Subsequently, Tan et al. (2019b,c) reported two selective and sensitive fluorescence sensing platforms based on phosphate pillar[5]arene (**PA-10**) functionalized reduced graphene oxide (**PA-10@RGO**) and pyridinium pillar[6]arene (**PA-11**) modified



reduced graphene oxide (**PA-11@RGO**). Based on competitive host-guest recognition, **PA-10@RGO** and **PA-11@RGO** were used as a fluorescent probe for sensitively detecting paraquat and 2,4,6-Trinitrophenol, respectively. At the same time, Tan et al. (2019d) also reported a fluorescent sensing platform for the detection of insulin based on fluorescence resonance energy transfer through competitive supramolecular recognition between cationic pillar[6]arene (**PA-12**) functionalized reduced graphene oxide (**PA-12@RGO**) and probe/insulin molecules. Rhodamine B, whose fluorescence is quenched by RGO-based fluorescence resonance energy transfer, was used as a probe molecule. When insulin was added into **PA-12@RGO**, Rhodamine B was displaced by insulin and an inclusion complex between **PA-12@RGO** and insulin was formed, which resulted in a “turn-on” fluorescent signal. The constructed fluorescent sensing platform has been successfully used to detect insulin in artificial serum.

Later in 2018, Yang's group developed a rapid and convenient electrochemical method for selectively recognizing tryptophan isomers (L-/D-Trp) based on the co-assembly of water-soluble cationic pillar[5]arene (**PA-13**) and anionic pillar[5]arene (**PA-14**) on the carboxylic graphene (C-Gra) modified electrode (Zhao et al., 2018). Differential pulse voltammetry results show that the peak currents of tryptophan isomers decrease with the increasing of the assembled pillar[5]arene layer number, whereas the difference in the value of the peak current between L-Trp and D-Trp increase with the increased layers, demonstrating an effective route for the immobilization of pillar[5]arene for discriminating the tryptophan isomers. The same research group later reported the same co-assembly of water-soluble cationic pillar[5]arene (**PA-15**) and anionic pillar[5]arene (**PA-14**) on the C-Gra-modified electrode for the selective recognition of nitrophenol isomers (Tan et al., 2018).

In 2019, Sun et al. (2019) reported that silver nanoparticles (AgNPs) functionalized by carboxylated pillar[5]arene (**PA-5**) could be immobilized on GO surface by hydrogen bond and  $\pi$ - $\pi$  stacking interaction between **PA-5** molecules and GO. GCE modified with **PA-5@AgNPs-GO** hybrid material demonstrates pronounced sensitivity toward paraquat, with limit detection for paraquat of  $1.0 \times 10^{-8}$  M. Such excellent performance can be explained by the synergic electrocatalytic effect of AgNPs and GO, and the host-guest recognition of **PA-5** for paraquat. Hou et al. (2019) later successfully prepared a simple and sensitive electrochemical sensor, in which hydroxylatopillar[5]arene (**PA-16**) stabilized AuNPs were anchored on electrochemically reduced graphene oxide (ERGO) by  $\pi$ - $\pi$  stacking interaction between **PA-16** molecules and ERGO. The obtained hybrid composites **PA-16@AuNPs-ERGO** modified electrode show excellent detection sensitivity toward methyl parathion due to the combined advantages of high catalysis of AuNPs, **PA-16** host-guest recognition performance and conductivity of ERGO.

In 2020, Guo et al. (2020) developed a simple strategy for one-pot preparation of hydrazide-pillar[5]arene (**PA-17**) modified RGO (**PA-17@RGO**) hybrid material by the redox reaction between GO and **PA-17** in aqueous solution, in which **PA-17** served as the reducing agent and stabilizer. In the whole process, there was no need to add additional reducing agents. The few-layer **PA-17@RGO** composites constructed exhibited good

water dispersibility and stability. The **PA-17@RGO** composite as electrode material displayed a high initial specific capacitance and great rate capability due to the synergistic effect of RGO and **PA-17**. This study provides an attractive perspective in expanding the development of supramolecular composites in energy storage.

## CONCLUSION AND OUTLOOK

In this mini-review, we overviewed recent progress in functionalization and applications of graphene nanomaterials with calix[n]arene/pillar[n]arene. New interesting approaches for constructing calix[n]arene/pillar[n]arene-functionalized graphene nanocomposites are reported. Bridging the supramolecular host-guest properties of calix[n]arene/pillar[n]arene hosts and the unique properties of graphene still inspires the scientific community to generate various important findings. However, some challenges remain in this emerging research field. First, the separation of excess calix[n]arene/pillar[n]arene modifiers from the functionalized graphene is a major concern. Therefore, special consideration should be given to the appropriate design of the modification protocol. Second, low-cost, efficient, and environmentally friendly approaches have to be developed for the preparation of calix[n]arene/pillar[n]arene-functionalized graphene sheets in large quantities with controllable sizes, layer thickness, compositions, and defects. Third, the properties and functions of the calix[n]arene/pillar[n]arene-functionalized graphene nanocomposites depend strongly on their microstructures. Therefore, in order to synthesize calix[n]arene/pillar[n]arene-functionalized graphene nanocomposites with desirable nanostructured architectures, the assembly behaviors of graphene with calix[n]arene/pillar[n]arene require to be studied more clearly. Finally, the applications of calix[n]arene/pillar[n]arene-functionalized graphene nanocomposites are at their initial stages. They need to be investigated systematically from both experimental and theoretical aspects. Altogether, we believe the combination of graphene materials with calix[n]arene/pillar[n]arene will produce a series of advanced materials with highly specific functionalities and potential applications having as the limit only the imagination.

## AUTHOR CONTRIBUTIONS

QD supervised the project and mainly wrote the paper. All authors extensively reviewed the manuscript and approved the final version of the manuscript to be submitted.

## FUNDING

This work was supported by the National Natural Science Foundation of China (No. 21402040), Henan province science and technology research program (192102210197) and Program for Innovative Research Team (in Science and Technology) in University of Henan Province (No. 20IRTSTHN008). Financial support from the Program of 543 team of Henan University of Engineering is gratefully acknowledged.



## REFERENCES

- Chen, X., Vimalanathan, K., Zang, W., Slattery, A. D., Boulos, R. A., Gibson, C. T., et al. (2014). Self-assembled calixarene aligned patterning of noble metal nanoparticles on graphene. *Nanoscale* 6, 4517–4520. doi: 10.1039/C3NR06857A
- Chen, X., Yasin, F. M., Eggers, P. K., Boulos, R. A., Duan, X., Lamb, R. N., et al. (2013a). Non-covalently modified graphene supported ultrafine nanoparticles of palladium for hydrogen gas sensing. *RSC Adv.* 3, 3213–3217. doi: 10.1039/c3ra22986f
- Chen, X., Zang, W., Vimalanathan, K., Iyer, K. S., and Raston, C. L. (2013b). A versatile approach for decorating 2D nanomaterials with Pd or Pt nanoparticles. *Chem. Commun.* 49, 1160–1162. doi: 10.1039/c2cc37606g
- Diamond, D., and McKervey, M. A. (1996). Calixarene-based sensing agents. *Chem. Soc. Rev.* 25, 15–24. doi: 10.1039/CS9962500015
- Eroglu, E., Zang, W. Z., Eggers, P. K., Chen, X. J., Boulos, R. A., Haniff Wahid, M., et al. (2013). Nitrate uptake by p-phosphonic acid calix[8]arene stabilized graphene. *Chem. Commun.* 49, 8172–8174. doi: 10.1039/C3CC44093A
- Guo, F., Xiao, P., Yan, B., Hahn, M., Kong, Y., Zhang, W., et al. (2020). One-pot synthesis of hydrazide-pillar[5]arene functionalized reduced graphene oxide for supercapacitor electrode. *Chem. Eng. J.* 391:123511. doi: 10.1016/j.cej.2019.123511
- Guo, Y., Guo, S., Ren, J., Zhai, Y., Dong, S., and Wang, E. (2010). Cyclodextrin functionalized graphene nanosheets with high supramolecular recognition capability: synthesis and host-guest inclusion for enhanced electrochemical performance. *ACS Nano* 4, 4001–4010. doi: 10.1021/nn100939n
- Gutsche, C. D. (1998). “Calixarenes revisited,” in *Monographs in Supramolecular Chemistry*, ed J. F. Stoddart (Cambridge: Royal Society of Chemistry), 1–250.
- Hou, X., Liu, X., Li, Z., Zhang, J., Du, D., Ran, X., et al. (2019). Electrochemical determination of methyl parathion based on pillar[5]arene@AuNPs@reduced graphene oxide hybrid nanomaterials. *New J. Chem.* 43, 13048–13057. doi: 10.1039/C9NJ02901J
- Kasprzak, A., and Poplowska, M. (2018). Recent developments in the synthesis and applications of graphene-family materials functionalized with cyclodextrins. *Chem. Commun.* 54, 8547–8562. doi: 10.1039/C8CC04120B
- Kellici, S., Acord, J., Vaughn, A., Power, N. P., Morgan, D. J., Heil, T., et al. (2016). Calixarene assisted rapid synthesis of silver-graphene nanocomposites with enhanced antibacterial activity. *ACS Appl. Mater. Interfaces* 29, 19038–19046. doi: 10.1021/acsami.6b06052
- Li, D., Müller, M. B., Gjilje, S., Kaner, R. B., and Wallace, G. G. (2008). Processable aqueous dispersions of graphene nanosheets. *Nat. Nanotechnol.* 3, 101–105. doi: 10.1038/nnano.2007.451
- Liang, H., Zhao, Y., Ye, H., and Li, C.-P. (2019). Ultrasensitive and ultrawide range electrochemical determination of bisphenol A based on PtPd bimetallic nanoparticles and cationic pillar[5]arene decorated graphene. *J. Electroanal. Chem.* 855:113487. doi: 10.1016/j.jelechem.2019.113487
- Liu, X., Wang, W., Li, X., Li, C., Qin, L., Sun, J., et al. (2016). Preparation of per-hydroxylated pillar[5]arene decorated graphene and its electrochemical behavior. *Electrochim. Acta* 210, 720–728. doi: 10.1016/j.electacta.2016.05.211
- Maiti, U. N., Lim, J., Lee, K. E., Lee, W. J., and Kim, S. O. (2014). Three-dimensional shape engineered, interfacial gelation of reduced graphene oxide for high rate, large capacity supercapacitors. *Adv. Mater.* 26, 615–619. doi: 10.1002/adma.201303503
- Mao, X., Liu, T., Bi, J., Luo, L., Tian, D., and Li, H. (2016). The synthesis of pillar[5]arene functionalized graphene as a fluorescent probe for paraquat in living cells and mice. *Chem. Commun.* 52, 4385–4388. doi: 10.1039/c6cc00949b
- Mao, X., Zhao, H., Luo, L., Tian, D., and Li, H. (2015). Highly sensitive chiral recognition of amino propanol in serum with R-mandelic acid-linked calix[4]arene modified graphene. *J. Mater. Chem. C* 3, 1325–1329. doi: 10.1039/C4TC02365J
- Nodeh, H. R., Kamboh, M. A., Ibrahim, W. A. W., Jume, B. H., Sereshti, H., and Sanagi, M. M. (2019). Equilibrium, kinetic and thermodynamic study of pesticides removal from water using novel glucamine-calix[4]arene functionalized magnetic graphene oxide. *Environ. Sci. Processes Impacts* 21, 714–726. doi: 10.1039/C8EM00530C
- Nurer, P., Bunkoed, W., Kanatharana, P., and Bunkoed, O. (2018). Miniaturized solid-phase extraction adsorbent of calix[4]arene-functionalized graphene oxide/polydopamine-coated cellulose acetate for the analysis of aflatoxins in corn. *J. Sep. Sci.* 41, 3892–3901. doi: 10.1002/jssc.201800440
- Ogoshi, T. (2015). “Pillararenes,” in *Monographs in Supramolecular Chemistry*, ed J. F. Stoddart (Cambridge: Royal Society of Chemistry), 1–315. doi: 10.1039/9781782622321
- Ogoshi, T., Kanai, S., Fujinami, S., Yamagishi, T. A., and Nakamoto, Y. (2008). para-Bridged symmetrical pillar[5]arenes: their lewis acid catalyzed synthesis and host-guest property. *J. Am. Chem. Soc.* 130, 5022–5023. doi: 10.1021/ja711260m
- Shan, C., Yang, H., Han, D., Zhang, Q., Ivaska, and, A., and Niu, L. (2009). Water-soluble graphene covalently functionalized by biocompatible poly-L-lysine. *Langmuir* 25, 12030–12033. doi: 10.1021/la903265p
- Shao, Y., Wang, J., Wu, H., Liu, J., Aksay, I. A., and Lin, Y. (2010). Graphene based electrochemical sensors and biosensors: a review. *Electroanalysis* 22, 1027–1036. doi: 10.1002/elan.200900571
- Son, Y., Cohen, M. L., and Louie, S. G. (2006). Half-metallic graphene nanoribbons. *Nature* 444, 347–349. doi: 10.1038/nature05180
- Song, S., Shang, X., Zhao, J., Hu, X., Koh, K., Wang, K., et al. (2018). Sensitive and selective determination of caspase-3 based on calixarene functionalized reduction of graphene oxide assisted signal amplification. *Sens. Actuators B Chem.* 267, 357–365. doi: 10.1016/j.snb.2018.03.185
- Sun, J., Guo, F., Shi, Q., Wu, H., Sun, Y., Chen, M., et al. (2019). Electrochemical detection of paraquat based on silver nanoparticles/water-soluble pillar[5]arene functionalized graphene oxide modified glassy carbon electrode. *J. Electroanal. Chem.* 847:113221. doi: 10.1016/j.jelechem.2019.113221
- Takamura, T., Endo, K., Fu, L., Wu, Y., Lee, K. J., and Matsumoto, T. (2007). Identification of nano-sized holes by TEM in the graphene layer of graphite and the high rate discharge capability of Li-ion battery anodes. *Electrochim. Acta* 53, 1055–1061. doi: 10.1016/j.electacta.2007.03.052
- Tan, S., Han, R., Wu, S., Liang, H., Zhao, Y., Zhao, H., et al. (2019d). A novel fluorescent sensing platform for insulin detection based on competitive recognition of cationic pillar[6]arene. *Talanta* 197, 130–137. doi: 10.1016/j.talanta.2019.01.004
- Tan, X., Liu, Y., Zhang, T., Luo, S., Liu, X., Tian, H., et al. (2019a). Ultrasensitive electrochemical detection of methyl parathion pesticide based on cationic water-soluble pillar[5]arene and reduced graphene nanocomposite. *RSC Adv.* 9, 345–353. doi: 10.1039/c8ra08555b
- Tan, X., Wu, Y., Yu, S., Zhang, T., Tian, H., He, S., et al. (2019b). The synthesis of water-soluble phosphate pillar[5]arenes functionalized graphene as a fluorescent probe for sensitive detection of paraquat. *Talanta* 195, 472–479. doi: 10.1016/j.talanta.2018.11.099
- Tan, X., Zhang, T., Zeng, W., He, S., Liu, X., Tian, H., et al. (2019c). A fluorescence sensing determination of 2,4,6-trinitrophenol based on cationic water-soluble pillar[6]arene graphene nanocomposite. *Sensors* 19:91. doi: 10.3390/s19010091
- Tan, X., Zhao, G., Zhou, X., Li, T., Lei, H., Du, G., et al. (2018). Electrochemical recognition of nitrophenol isomers by assembly of pillar[5]arenes multilayers. *Anal. Chim. Acta* 1036, 49–57. doi: 10.1016/j.aca.2018.06.085
- Wang, Q., Tian, L., Xu, J., Xia, B., Li, J., Lu, F., et al. (2018a). Multifunctional supramolecular vesicles for combined photothermal/photodynamic/hypoxia-activated chemotherapy. *Chem. Commun.* 54, 10328–10331. doi: 10.1039/C8CC05560B
- Wang, Q., Zhang, P., Xu, J., Xia, B., Tian, L., Chen, J., et al. (2018b). NIR-absorbing dye functionalized supramolecular vesicles for chemo-photothermal synergistic therapy. *ACS Appl. Bio Mater.* 1, 70–78. doi: 10.1021/acsabm.8b00014
- Watcharotone, S., Dikin, D. A., Stankovich, S., Piner, R., Jung, I., Dommett, G. H. B., et al. (2007). Graphene-silica composite thin films as transparent conductors. *Nano Lett.* 7, 1888–1892. doi: 10.1021/nl070477+
- Yang, L., Xie, X., Cai, L., Ran, X., Li, Y., Yin, T., et al. (2016a). p-sulfonated calix[8]arene functionalized graphene as a “turn on” fluorescent sensing platform for aconitine determination. *Biosens. Bioelectron.* 82, 146–154. doi: 10.1016/j.bios.2016.04.005
- Yang, L., Zhao, H., Li, Y., Ran, X., Deng, G., Xie, X., et al. (2015). Fluorescent detection of tadalafil based on competitive host-guest interaction using p-sulfonated calix[6]arene functionalized graphene. *ACS Appl. Mater. Interfaces* 48, 26557–26565. doi: 10.1021/acsami.5b07833
- Yang, L., Zhao, H., Li, Y., Ran, X., Deng, G., Zhang, Y., et al. (2016b). Indicator displacement assay for cholesterol electrochemical sensing using

- a calix[6]arene functionalized graphene-modified electrode. *Analyst* 141, 270–278. doi: 10.1039/c5an01843a
- Ye, H., Yang, L., Zhao, G., Zhang, Y., Ran, X., Wu, S., et al. (2016). A FRET-based fluorescent approach for labelol sensing using calix[6]arene functionalized MnO<sub>2</sub>@graphene as a receptor. *RSC Adv.* 6, 79350–79360. doi: 10.1039/C6RA14835B
- Yu, J., Ma, L., Chen, W., Ma, Y., Huang, F., Gao, C., et al. (2015). Supramolecule-mediated synthesis of MoS<sub>2</sub>/reduced graphene oxide composites with enhanced electrochemical performance for reversible lithium storage. *J. Mater. Chem. A* 3, 6884–6893. doi: 10.1039/c5ta00006h
- Yu, Z., Ye, J., Chen, W., Xu, S., and Huang, F. (2017). Fabrication of few-layer molybdenum disulfide/reduced graphene oxide hybrids with enhanced lithium storage performance through a supramolecule-mediated hydrothermal route. *Carbon* 114, 125–133. doi: 10.1016/j.carbon.2016.12.002
- Zhang, H., Ma, X., Nguyen, K. T., Zeng, Y., Tai, S., and Zhao, Y. (2014). Water-soluble pillararene-functionalized graphene oxide for *in vitro* raman and fluorescence dual-mode imaging. *ChemPlusChem* 79, 462–469. doi: 10.1002/cplu.201300408
- Zhang, P., Wang, Y., Zhang, D., Bai, H., and Tarasov, V. V. (2016). Calixarene-functionalized graphene oxide composites for adsorption of neodymium ions from the aqueous phase. *RSC Adv.* 6, 30384–30394. doi: 10.1039/C5RA27509A
- Zhao, G., Yang, L., Wu, S., Zhao, H., Tang, E., and Li, C.-P. (2017). The synthesis of amphiphilic pillar[5]arene functionalized reduced graphene oxide and its application as novel fluorescence sensing platform for the determination of acetaminophen. *Biosens. Bioelectron.* 91, 863–869. doi: 10.1016/j.bios.2017.01.053
- Zhao, G., Zhou, X., Ran, X., Tan, X., Li, T., Cao, M., et al. (2018). Layer-by-layer assembly of anionic-/cationic-pillar[5]arenes multilayer films as chiral interface for electrochemical recognition of tryptophan isomers. *Electrochim. Acta* 277, 1–8. doi: 10.1016/j.electacta.2018.04.196
- Zhou, J., Chen, M., and Diao, G. W. (2013a). Calix[4,6,8]arenesulfonates functionalized reduced graphene oxide with high supramolecular recognition capability: fabrication and application for enhanced host-guest electrochemical recognition. *ACS Appl. Mater. Interfaces* 5, 828–836. doi: 10.1021/am302289v
- Zhou, J., Chen, M., Xie, J., and Diao, G. (2013b). Synergistically enhanced electrochemical response of host-guest recognition based on ternary nanocomposites: reduced graphene oxide-amphiphilic pillar[5]arene-Gold nanoparticles. *ACS Appl. Mater. Interfaces* 5, 11218–11224. doi: 10.1021/am403463p
- Zhou, T., Yu, H., Liu, M., and Yang, Y.-W. (2015). Carboxylatopillararene-modified reduced graphene oxides with high water dispersibility for fluorescent dye sensing. *Chin. J. Chem.* 33, 125–130. doi: 10.1002/cjoc.201400238
- Zou, J., Martin, A. D., Zdyrko, B., Luzinov, I., Raston, C. L., and Iyer, K. S. (2011). Pd-induced ordering of 2D Pt nanoarrays on phosphonated calix[4]arenes stabilised graphenes. *Chem. Commun.* 47, 5193–5195. doi: 10.1039/c1cc10408j

**Conflict of Interest:** The authors declare that the research was conducted in the absence of any commercial or financial relationships that could be construed as a potential conflict of interest.

Copyright © 2020 Duan, Wang, Wang, Zhang and Lu. This is an open-access article distributed under the terms of the Creative Commons Attribution License (CC BY). The use, distribution or reproduction in other forums is permitted, provided the original author(s) and the copyright owner(s) are credited and that the original publication in this journal is cited, in accordance with accepted academic practice. No use, distribution or reproduction is permitted which does not comply with these terms.



# Fluorescent Supramolecular Polymers Formed by Crown Ether-Based Host-Guest Interaction

Jinjin Zhang<sup>1</sup>, Huayu Qiu<sup>1,2</sup>, Tian He<sup>1\*</sup>, Yang Li<sup>1\*</sup> and Shouchun Yin<sup>1\*</sup>

<sup>1</sup> College of Material, Chemistry and Chemical Engineering, Hangzhou Normal University, Hangzhou, China, <sup>2</sup> Key Laboratory of Organosilicon Chemistry and Materials Technology of Ministry of Education, Hangzhou Normal University, Hangzhou, China

## OPEN ACCESS

### Edited by:

Yong Yao,  
Nantong University, China

### Reviewed by:

Bingbing Shi,  
Northwest Normal University, China  
Da-Hui Qu,  
East China University of Science and  
Technology, China  
Chen Lin,  
Nanjing Normal University, China  
Shengyi Dong,  
Hunan University, China

### \*Correspondence:

Tian He  
het@hznu.edu.cn  
Yang Li  
oceanlee136@163.com  
Shouchun Yin  
yinsc@hznu.edu.cn

### Specialty section:

This article was submitted to  
Supramolecular Chemistry,  
a section of the journal  
Frontiers in Chemistry

**Received:** 17 April 2020

**Accepted:** 02 June 2020

**Published:** 24 July 2020

### Citation:

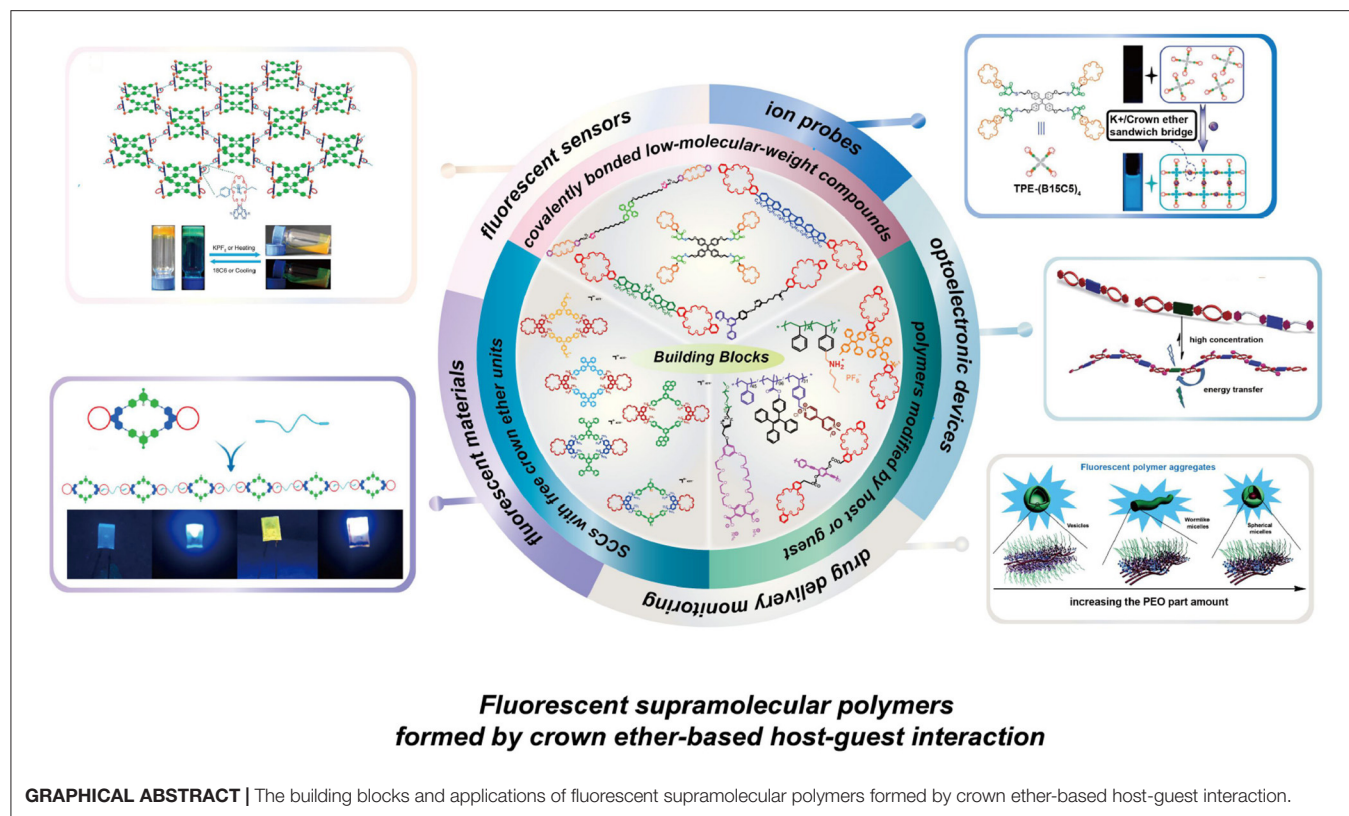
Zhang J, Qiu H, He T, Li Y and Yin S  
(2020) Fluorescent Supramolecular  
Polymers Formed by Crown  
Ether-Based Host-Guest Interaction.  
Front. Chem. 8:560.  
doi: 10.3389/fchem.2020.00560

Inspired by the vast array of assemblies present in nature, supramolecular chemistry has attracted significant attention on account of its diverse supra-structures, which include micelles, vesicles, and fibers, in addition to its extensive applications in luminescent materials, sensors, bioimaging, and drug delivery over the past decades. Supramolecular polymers, which represent a combination of supramolecular chemistry and polymer science, are constructed by non-covalent interactions, such as host-guest interactions, hydrogen bonding, hydrophobic or hydrophilic interactions, metal-ligand interactions,  $\pi$ - $\pi$  stacking, and electrostatic interactions. To date, numerous host-guest recognition systems have been reported, including crown ethers, cyclodextrins, calixarenes, cucurbituril, pillararenes, and other macrocyclic hosts. Among them, crown ethers, as the first generation of macrocyclic hosts, provide a promising and facile alternative route to supramolecular polymers. In addition, the incorporation of fluorophores into supramolecular polymers could endow them with multiple properties and functions, thereby presenting potential advantages in the context of smart materials. Thus, this review focuses on the fabrication strategies, interesting properties, and potential applications of fluorescent supramolecular polymers based on crown ethers. Typical examples are presented and discussed in terms of three different types of building blocks, namely covalently bonded low-molecular-weight compounds, polymers modified by hosts or guests, and supramolecular coordination complexes.

**Keywords:** supramolecular polymer, fluorescence, crown ether, host-guest interaction, supramolecular coordination complex

## INTRODUCTION

Molecular self-assembly is the key to obtaining complicated biomolecules in natural systems, such as proteins, nucleic acids, phospholipid membranes, ribosomes, and microtubules (Chen et al., 2016; Laurent et al., 2017; Sun et al., 2019). Drawing inspiration from the vast number of assemblies present in nature, functional materials for applications in luminescent materials, sensors, bioimaging, and drug delivery (Chen L. -J. et al., 2015; Yan et al., 2015; Zhang M. et al., 2016; Yu et al., 2017; Zhang et al., 2017a) have been obtained through molecular self-assembly to form diverse supra-structures, such as micelles, vesicles, ribbons, and fibers (Ji et al., 2013a; Yan et al., 2013; Shi et al., 2016). In contrast to molecules based on traditional covalent bonds, supramolecular self-assembled structures exhibit specific characteristics, such as self-healing, coordinability, and responsiveness to stimuli, due to the dynamic and reversible nature of the non-covalent bonds or dynamic



covalent bonds (Yan et al., 2012a; Yu et al., 2013, 2014; Zhang et al., 2018, 2019a; Deng et al., 2020). Among them, supramolecular polymers, in which repeating units are held together to form polymeric arrays through intermolecular bonds (e.g., host-guest interactions, hydrogen bonding, hydrophobic/hydrophilic interactions, metal-ligand interactions, and  $\pi$ - $\pi$  stacking) are considered to be promising smart materials.

To date, host-guest recognition systems have been widely employed to construct supramolecular polymers, where the hosts are often crown ethers, cyclodextrins, calixarenes, cucurbituril, pillararenes, and other macrocyclic hosts (Ma and Zhao, 2015; Qu et al., 2015; Yu et al., 2015; Liu et al., 2018; Shi et al., 2019). Among them, crown ethers, which were the first artificial macrocycles, are a type of macrocyclic polyether containing multiple oxygen methylene units, with examples including 18-crown-6, 21-crown-7, 24-crown-8, and other analogous derivatives, which can be host to positive ions and neutral molecules (Yamaguchi et al., 1998; Gibson et al., 2002; Huang and Gibson, 2004; Wei et al., 2015). In 1967, Pedersen reported, for the first time, stable complexes formed by crown ethers and certain cations that interacted via ion-dipole interactions between the cations and the high electron-density oxygen atoms of the crown ethers (Pedersen, 1967). Other studies have focused on the recognition between crown ethers and metal cations, such as  $K^+$ ,  $Li^+$ , and  $Na^+$  (Pedersen, 1967; Ma et al., 2015); however, in the wake of in-depth studies, complexes constructed from crown ethers and organic cations or organic neutral molecules

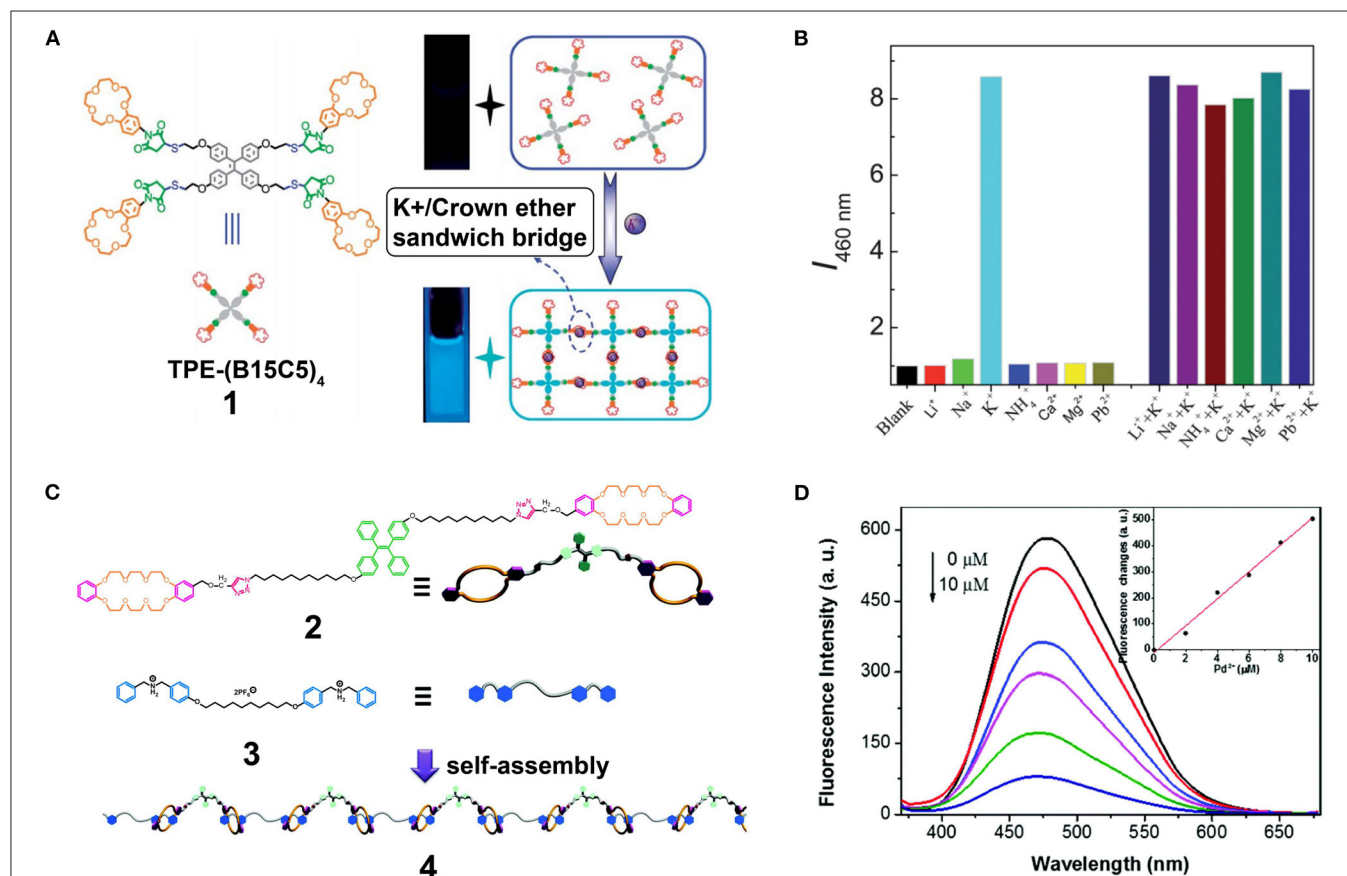
were discovered, with examples including secondary ammonium salts, diazonium salts, and paraquat (Yamaguchi and Gibson, 1999; Gibson et al., 2003; Huang et al., 2007; Zhang et al., 2007). Crown ethers are known to accommodate a variety of guests, and they tend to exhibit strong binding affinities for specific guests due to their multidentate structure and relatively strong non-covalent interactions. Therefore, host-guest recognition systems based on crown ethers offer distinct advantages in terms of fabricating supramolecular polymers (Yan et al., 2012b; Zheng et al., 2012; Ding et al., 2013; Li X. et al., 2018; Li et al., 2019b; Xiao et al., 2020). Importantly, the formation of supramolecular polymers can overcome issues related to the preparation of traditional polymers, since the latter methods tend to require an auxiliary initiator, high temperatures, and long reaction times. Furthermore, the introduction of host-guest interactions can also endow the constructed supramolecular polymers with dynamic and reversible properties (Dong et al., 2012; Yan et al., 2014; Zhan et al., 2014a,b; Huang et al., 2018; Wang et al., 2020). For example, Dong and co-workers made a supramolecular polymer network with dynamic reversibility, good malleability, and processability that depended on the formation of host-guest interactions between crown ethers and ammonium motifs of H2G2-type monomer (Wang et al., 2020). Moreover, recently, a crown ether-based interaction has been used to enhance the mechanical strength of a supramolecular polymer, which is promising for more exciting applications (Shi et al., 2020). Although a range of supramolecular polymers have been constructed based on host-guest interactions,



the development of crown ether-based supramolecular polymers with additional multiple functionalities remains of interest.

Fluorescence refers to a cold luminescence phenomenon caused by photoluminescence, which is light emitted by a substance after it absorbs light or other electromagnetic radiation. In recent years, fluorescent materials have been widely used in life and material science. Fluorophores, which can emit fluorescence, are often incorporated into supramolecular polymers, since the resulting polymers inherit the fluorescence properties of the fluorogens in addition to exhibiting the dynamic and reversible properties originating from the non-covalent interactions. This renders them capable of exhibiting a fluorescence response to various external stimuli (Dong et al., 2016; Li et al., 2016, 2020; Wang et al., 2017). Fluorescent supramolecular polymers have therefore been widely applied in fluorescent materials, fluorescent probing, data storage, bio-imaging, drug delivery, and cancer therapy (Lou and Yang, 2018; Li et al., 2019a). Indeed, various kinds of organic

fluorogens exist, such as coumarins, fluoresceins, cyanine naphthalimide rhodamine, conjugated polymer groups, and aggregation-induced emission (AIE) luminogens (Dsouza et al., 2011; Fermi et al., 2014; Ma et al., 2016; Peng et al., 2017; Li Y. et al., 2018). In addition, when conventional organic chromophores were combined with supramolecular polymers, the resulting polymers were found to exhibit weak fluorescence, since the formation of supramolecular polymers must be carried out at high concentrations, thereby causing aggregation-caused quenching (ACQ) of the traditional fluorescent chromophore. This issue can be efficiently resolved through the use of AIE luminogens, which were initially developed by Luo et al. (2001) and were found to exhibit faint luminescence in a dilute solution but strong luminescence in the solid or aggregate state due to the restriction of intramolecular vibrations and rotations. Furthermore, Lou and Yang focused on the combination of AIEgens with supramolecular macrocyclics, with a recent review of the supra-structures obtained, which included supramolecular nanocomplexes/polymers,

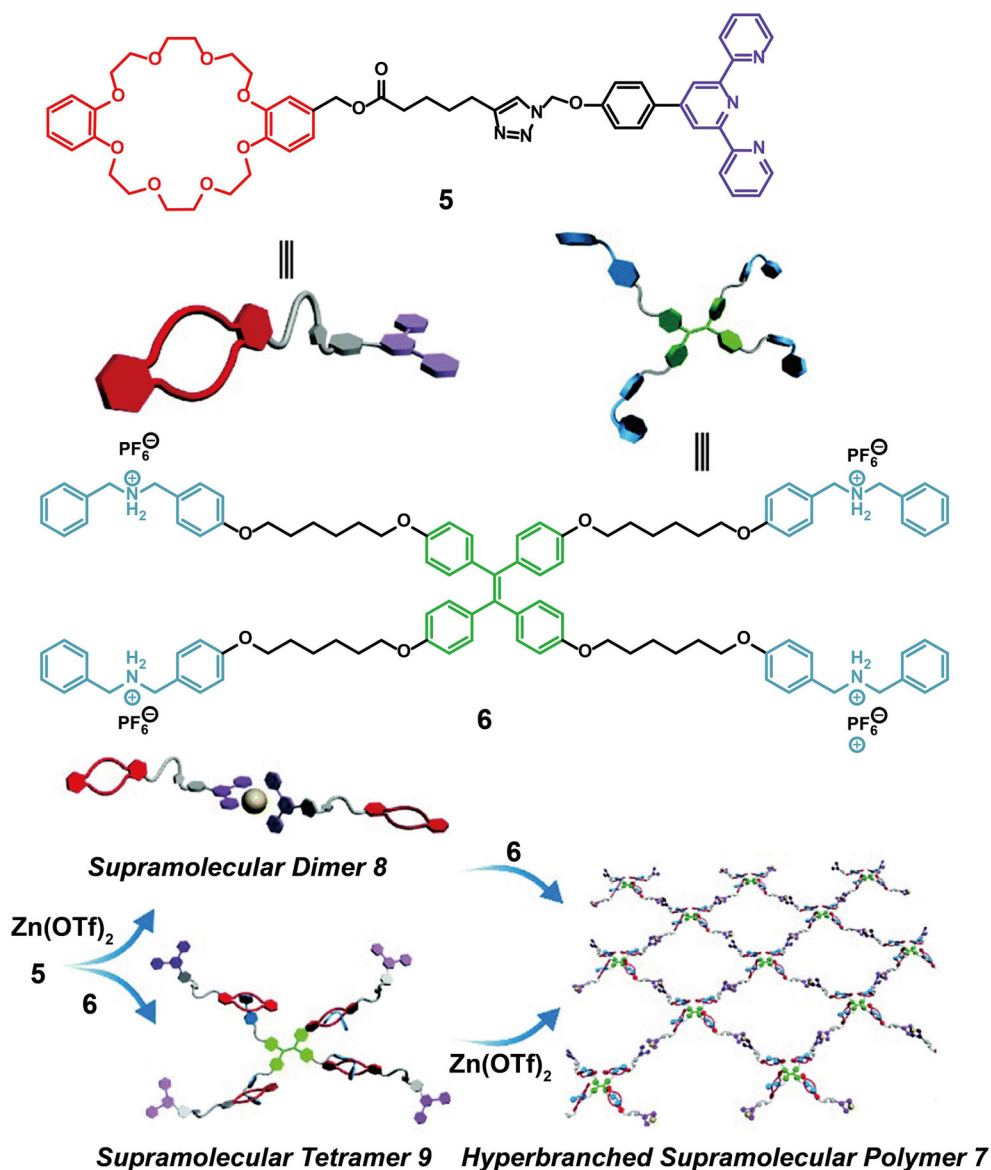


**FIGURE 1 | (A)** Schematic illustration of the AIE of TPE-(B15C5)<sub>4</sub> induced by recognition between the crown ether moieties and K<sup>+</sup> ions. **(B)** Relative fluorescence intensity at  $\lambda_{em} = 460$  nm of TPE-(B15C5)<sub>4</sub> in THF solution recorded under the addition of K<sup>+</sup> ions in the absence or presence of other interfering ions (i.e., Li<sup>+</sup>, Na<sup>+</sup>, NH<sub>4</sub><sup>+</sup>, Ca<sup>2+</sup>, Mg<sup>2+</sup>, and Pb<sup>2+</sup>) ( $\lambda_{ex} = 360$  nm; slit width: Ex. 5 nm, Em. 5 nm; 25°C). Adapted with permission from Wang et al. (2012); copyright 2012, Royal Society of Chemistry. **(C)** Cartoon representations of the formation of the linear fluorescent supramolecular polymer **4** from host **2** and guest **3**. **(D)** Fluorescence emission spectra of **4** with different concentrations of Pd<sup>2+</sup> (0–10 μM) in the solid state ( $\lambda_{ex} = 350$  nm). Inset: Linear relationship between the fluorescence intensity of **4** and the concentration of Pd<sup>2+</sup> at  $\lambda_{em} = 577$  nm. Adapted with permission from Chen D. et al. (2015); copyright 2015, Royal Society of Chemistry.

supramolecular nanoparticles, and host-guest complexes on nanosurfaces (Lou and Yang, 2018). Thus, in the next parts of this review, we will focus on fluorescent supramolecular polymers based on crown ethers, which are not confined to AIE-active luminogens, and discuss their fabrication strategies, interesting properties, and potential applications. In addition, we present diverse methods for combining free crown ether units with various building blocks, including covalently bonded low-molecular-weight compounds, polymers modified by hosts or guests, and supramolecular coordination complexes (SCCs), and representative examples are scrutinized over a comprehensive scope.

## CROWN ETHER-BASED FLUORESCENT SUPRAMOLECULAR POLYMERS CONSTRUCTED BY COVALENTLY BONDED LOW-MOLECULAR-WEIGHT COMPOUNDS

The most efficient and straightforward method of constructing fluorescent supramolecular polymers is to design and prepare fluorescent hosts or guests through the rational chemical modification of chromophores. Subsequently, certain crown ethers and guests are brought together through host-guest

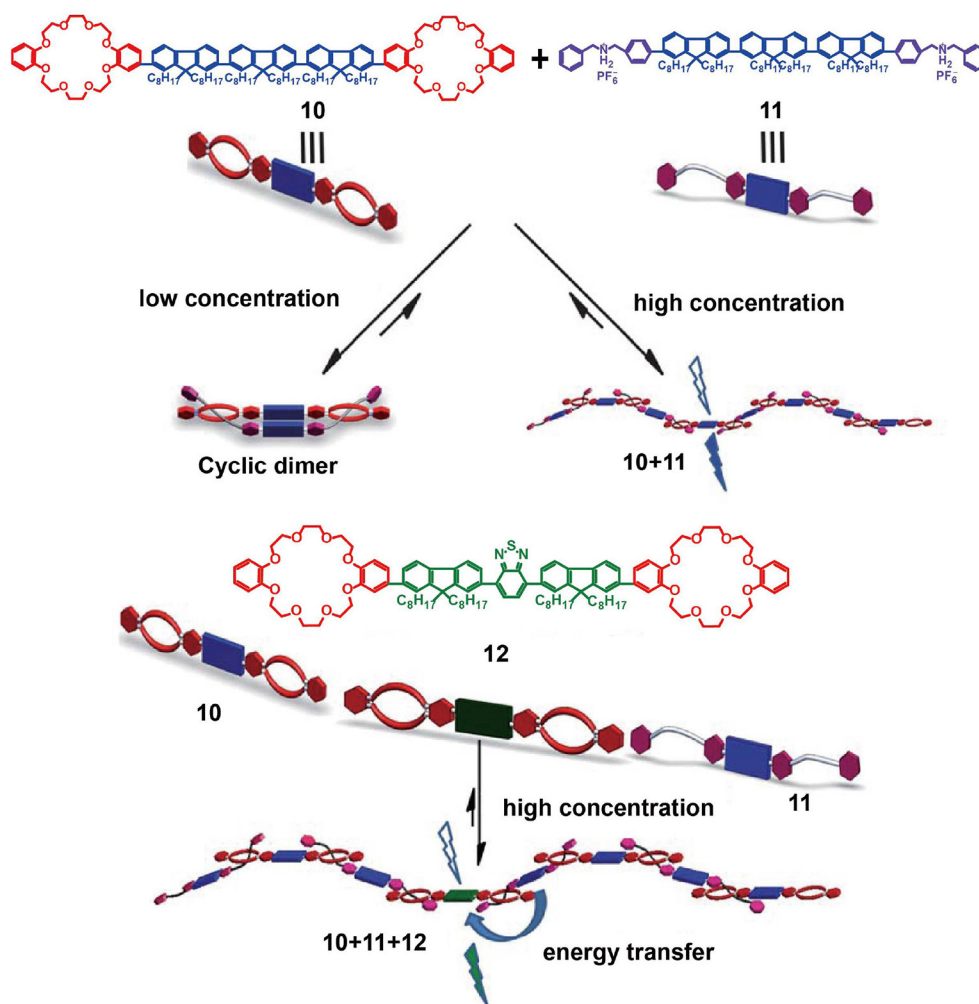


**FIGURE 2 |** Schematic illustration of monomers **5** and **6** and cartoon representations of the formation of supramolecular dimer **8**, supramolecular tetramer **9**, and hyperbranched supramolecular polymer **7**. Adapted with permission from Zhang J. et al. (2016); copyright 2016, Royal Society of Chemistry.

interactions along with  $\pi$ - $\pi$  stacking (Ma et al., 2015) and/or donor-acceptor interactions (Roy et al., 2016).

More specifically, Wang et al. reported the application of AIE-active supramolecular polymers based on the recognition system of crown ethers (Wang et al., 2012). They designed a novel and effective fluorometric  $K^+$  probe via host-guest molecular recognition and aggregation-induced emission. The host molecule TPE-(B15C5)<sub>4</sub> (**1**) was synthesized by the functionalization of a four peripheral benzo-15-crown-5 (B15C5) with tetraphenylethylene (TPE) as the core (**Figure 1A**). The AIE feature of the TPE cores and the formation of cross-linked supramolecular polymers resulted in the aggregation of **1** and an enhancement in fluorescence emission; this system was suitable for application in  $K^+$  detection. Moreover, **1** exhibited an excellent selectivity toward  $K^+$  compared to other interfering ions (e.g.,  $Li^+$ ,  $Na^+$ ,  $NH_4^+$ ,  $Ca^{2+}$ ,  $Mg^{2+}$ , and  $Pd^{2+}$ ) (**Figure 1B**), with a detection limit of  $\sim 1.0 \mu M$ . This work opened a new avenue for the development of sensitive

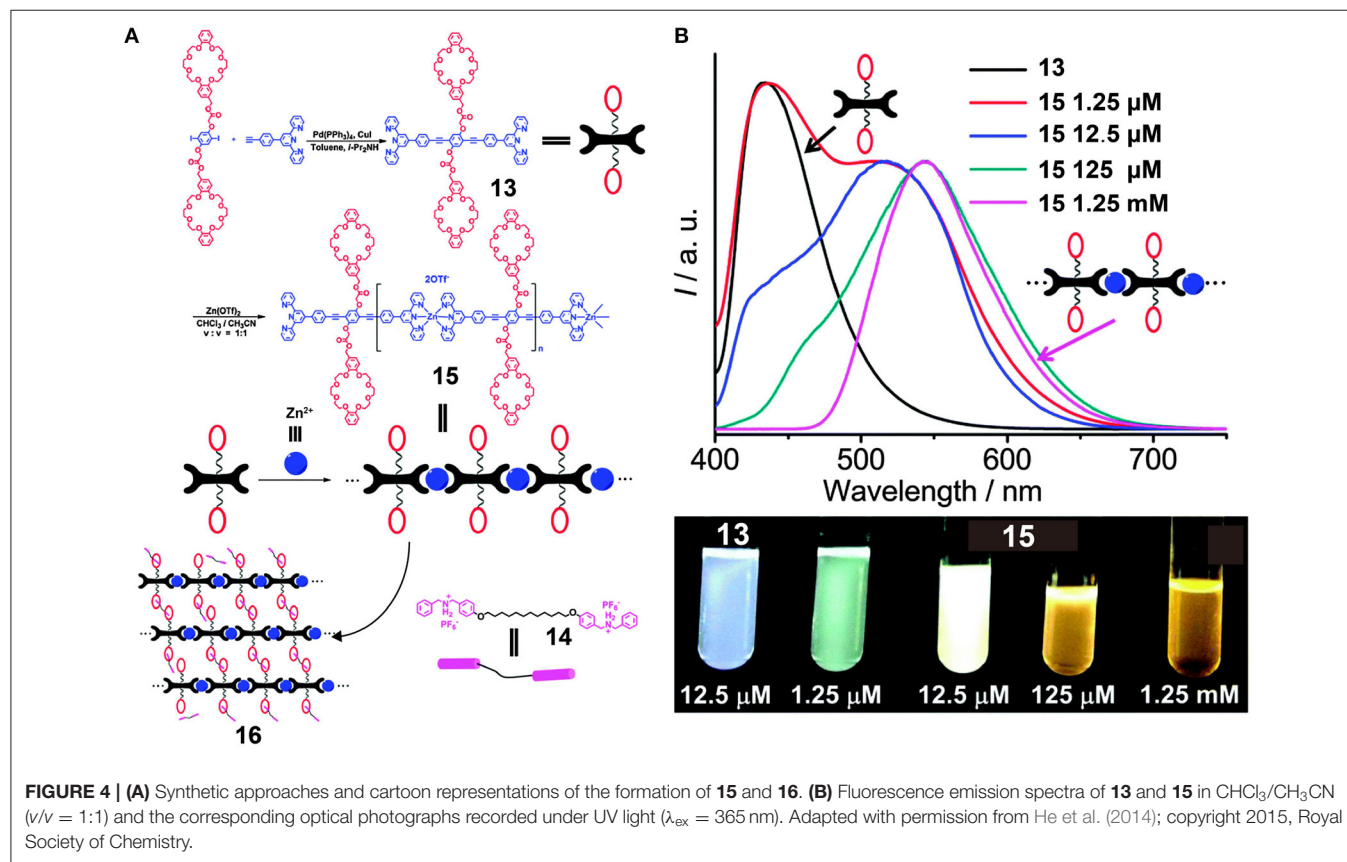
and selective fluorometric off-on probes. Similarly, Chen D. et al. (2015) designed monomer **2**, wherein the host TPE core was linked with two dibenzo-24-crown-8 (DB24C8) and two 1,2,3-triazole units, and a dibenzylammonium (DBA) salt monomer **3** was employed as the guest. Consequently, an AIE-active supramolecular polymer **4** (**Figure 1C**) was obtained through host-guest interactions by mixing monomers **2** and **3** in a 1:1 molar ratio. The characteristic AIE properties of supramolecular polymer **4** originated from restriction of the TPE group intramolecular rotational motion. These properties were confirmed by observation that the fluorescence intensity of **4** was 6-fold stronger than that of monomer **1** at the same concentration. In addition, the enhanced fluorescence intensity of **4** was accompanied by a 13-nm red-shift upon increasing its concentration from 75 to 200 mM. Furthermore, the fluorescence intensity of **4** in the solid state was further increased along with a 79-nm blue-shift due to morphological changes in the aggregates. Interestingly, the fluorescence intensity of **4** decreased linearly



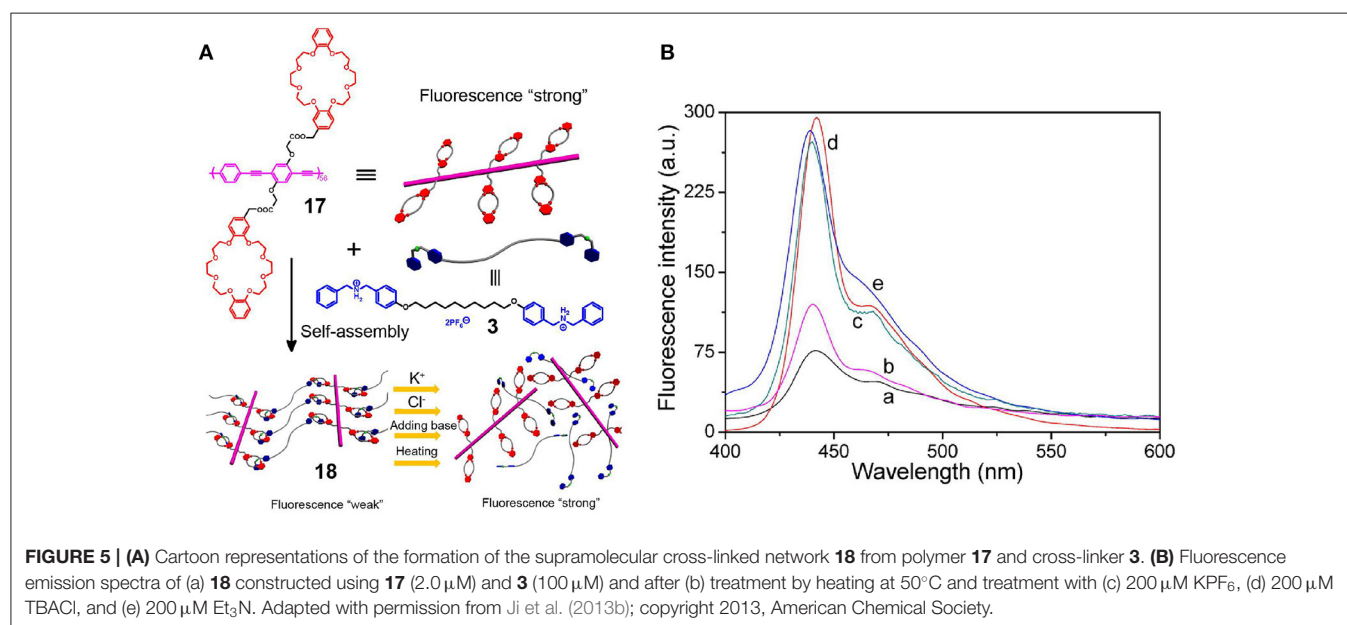
**FIGURE 3** | Cartoon representations of the formation of SLEPs from host **10**, guest **11**, and doping host **12**. Adapted with permission from Zhang et al. (2012); copyright 2012, Royal Society of Chemistry.

upon the addition of  $\text{Pd}^{2+}$  (**Figure 1D**) owing to coordination interactions and energy transfer between the 1,2,3-triazole units and  $\text{Pd}^{2+}$ . Thus, **4** can be employed as a  $\text{Pd}^{2+}$  fluorescent probe in the solid state, thereby enriching the application of supramolecular polymeric materials.

In addition to their application as ion sensors, crown ether-based fluorescent supramolecular polymers formed using TPE-functionalized monomers can also be employed as smart and adaptive luminescent materials. For example, Zhang J. et al. (2016) designed two monomers, one (**5**) with a DB24C8 group



**FIGURE 4 | (A)** Synthetic approaches and cartoon representations of the formation of **15** and **16**. **(B)** Fluorescence emission spectra of **13** and **15** in  $\text{CHCl}_3/\text{CH}_3\text{CN}$  ( $v/v = 1:1$ ) and the corresponding optical photographs recorded under UV light ( $\lambda_{\text{ex}} = 365 \text{ nm}$ ). Adapted with permission from He et al. (2014); copyright 2015, Royal Society of Chemistry.



**FIGURE 5 | (A)** Cartoon representations of the formation of the supramolecular cross-linked network **18** from polymer **17** and cross-linker **3**. **(B)** Fluorescence emission spectra of **18** constructed using **17** (2.0  $\mu\text{M}$ ) and **3** (100  $\mu\text{M}$ ) and after (b) treatment by heating at  $50^\circ\text{C}$  and treatment with (c) 200  $\mu\text{M}$   $\text{KPF}_6$ , (d) 200  $\mu\text{M}$   $\text{TBACl}$ , and (e) 200  $\mu\text{M}$   $\text{Et}_3\text{N}$ . Adapted with permission from Ji et al. (2013b); copyright 2013, American Chemical Society.

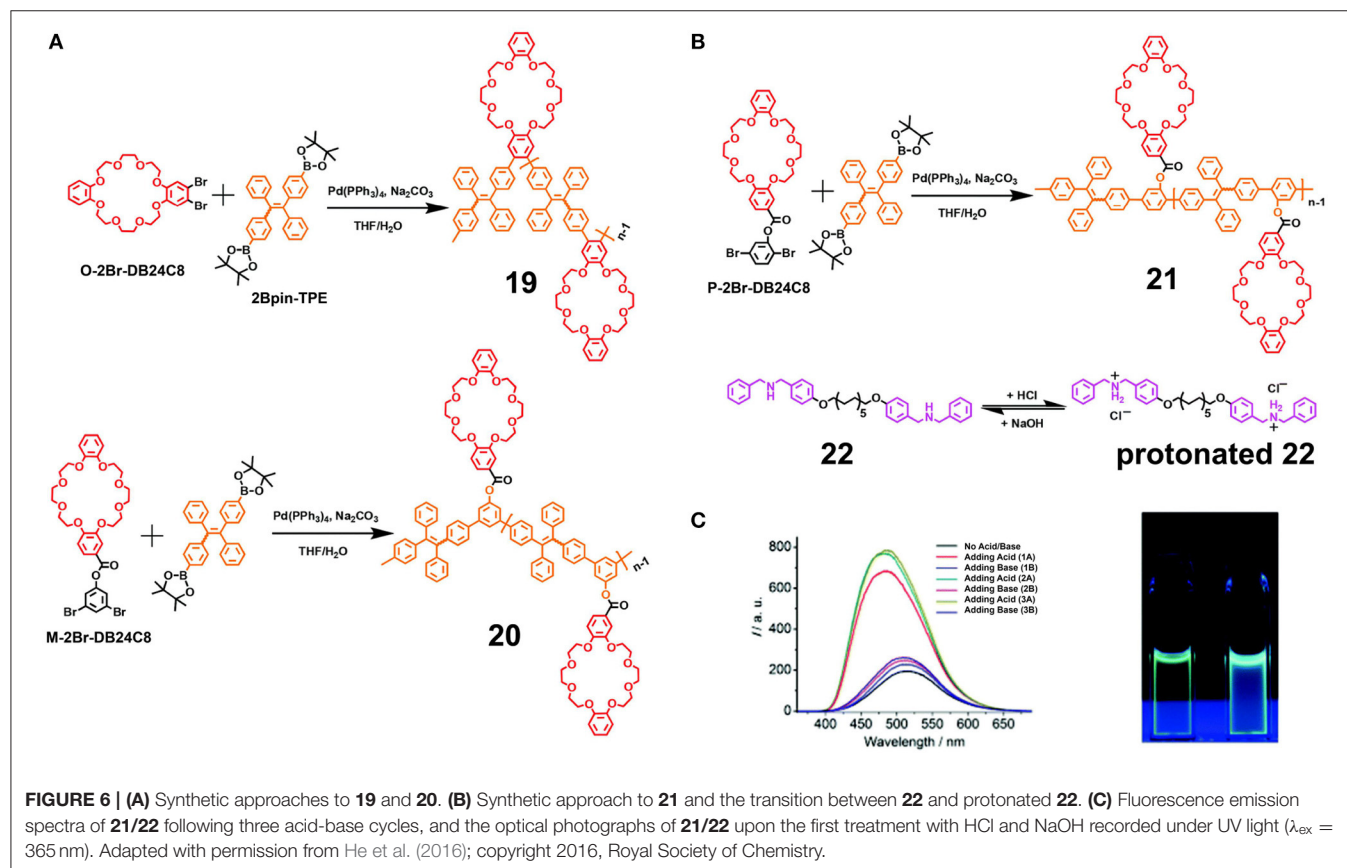


at one end and a terpyridine moiety at the other end, and another (**6**) with a TPE core and four outer DBA salts. A hyperbranched fluorescent supramolecular polymer, **7**, was constructed through the connection of  $\text{Zn}(\text{OTf})_2$  with monomers **5** and **6** via terpyridine-based metal-ligand interactions and crown ether-based host-guest interactions (**Figure 2**). The hyperbranched fluorescent supramolecular polymer **7** displayed a strong emission, while supramolecular dimer **8** and supramolecular tetramer **9**, which were formed by only one kind of non-covalent interaction, exhibited a reduced luminescence due to inefficient restriction of the intramolecular rotation/torsion of the TPE groups in **8** and **9**. In addition, **7** exhibited responsiveness to multiple stimuli, including temperature, pH,  $\text{K}^+$ , and  $\text{Cl}^-$ , due to the dynamic and reversible nature of the two orthogonal non-covalent interactions. Coincidentally, a further pH-responsive supramolecular polymer was fabricated by Bai et al. (2015) based on a similar principle, whereby the polymer consisted of TPE entities bearing DB24C8 or DBA on opposite phenyl rings. These results therefore provide a representative demonstration of self-assembly-induced emission (SAIE), which is conducive to the development of novel supramolecular materials exhibiting a stimulus-responsive fluorescence transition.

In addition to the introduction of AIEgens such as TPE as luminescent groups, the use of fluorescent conjugated oligomers would also present potential advantages in the development of optoelectronic devices or fluorescence materials. For example, Zhang et al. (2012) reported supramolecular light-emitting

polymers (SLEPs) prepared from blue-emitting conjugated oligomer **10** and green-emitting conjugated oligomer **12** as the hosts and blue-emitting conjugated oligomer **11** as the guest (**Figure 3**). The resulting polymer, based on host-guest interactions, exhibited good film formation abilities, a stable film morphology, and facile solution processability. Furthermore, the polymer emission was tuneable by controlling the content of dopant host **12**. More specifically, by doping 10 or 30% of **12** into the supramolecular system to promote efficient energy transfer among the oligomers, the resulting SLEPs showed a large red-shift photoluminescent emission, significantly enhanced photoluminescent efficiencies, and achieved superior device performance. Due to these advantages, SLEPs have the potential to promote the development of solution-processed optoelectronic devices.

To endow supramolecular polymers with more versatile topological structures and increase their suitability for practical applications, He et al. (2014) constructed a cross-linked metallosupramolecular polymer, **16**, by employing metal-ligand interactions between conjugated bis-terpyridine ligand **13** and  $\text{Zn}^{2+}$  as the chromophore in addition to host-guest interactions between the two DB24C8 moieties in **13** and the two DBA groups in **14** (**Figure 4A**). The resulting linear conjugated supramolecular polymer **15** based on the terpyridine/ $\text{Zn}$  recognition motifs exhibited concentration-controllable emission varying in color from cyan to white to yellow (**Figure 4B**) due to the presence of components



**FIGURE 6 | (A)** Synthetic approaches to **19** and **20**. **(B)** Synthetic approach to **21** and the transition between **22** and protonated **22**. **(C)** Fluorescence emission spectra of **21/22** following three acid-base cycles, and the optical photographs of **21/22** upon the first treatment with HCl and NaOH recorded under UV light ( $\lambda_{\text{ex}} = 365 \text{ nm}$ ). Adapted with permission from He et al. (2016); copyright 2016, Royal Society of Chemistry.

bearing different numbers of repeat units, including monomers, oligomers, and polymers. Interestingly, when the concentration of **15** is  $12.5\ \mu\text{M}$ , nearly white emission occurred in the absence of other complementary fluorescence groups. Moreover, upon increasing the quantities of added guest molecules **14** into **15**, the fluorescence intensity decreased gradually due to the formation of cross-linked metallosupramolecular polymer **16** via host-guest interactions between the DB24C8 moieties and the DBA moieties. In addition, the fluorescence intensity of **16** varied with changes in pH, which renders **16** suitable for application in acid-base stimulus-responsive materials. With such dual responsiveness, this supramolecular polymer represents an important advance in the design of fluorescent materials and molecular devices.

## CROWN ETHER-BASED FLUORESCENT SUPRAMOLECULAR POLYMERS CONSTRUCTED USING POLYMERS

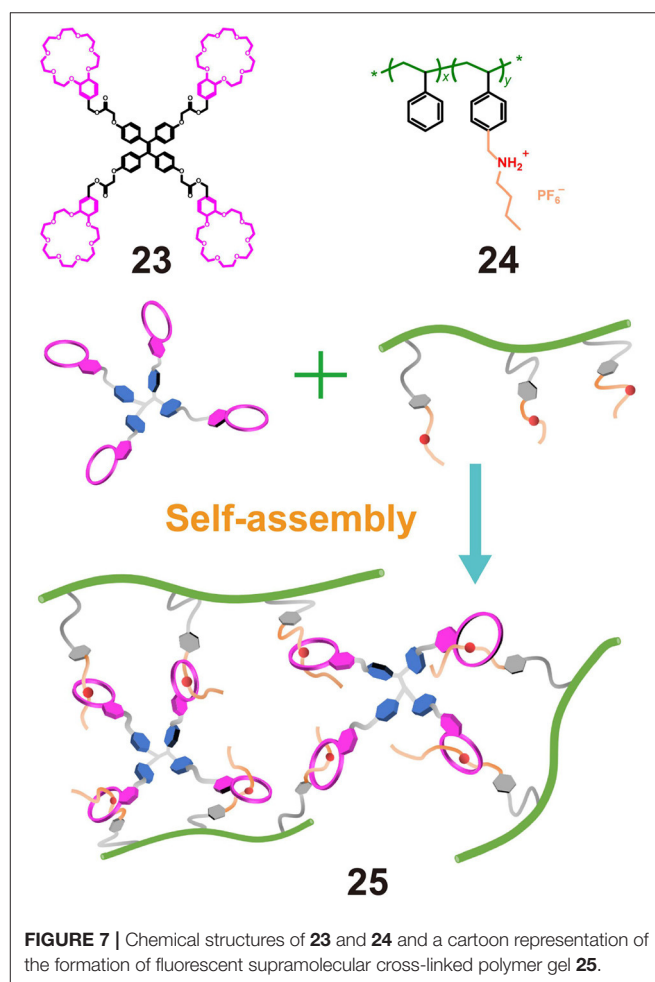
The construction of crown ether-based fluorescent supramolecular polymers using covalently bonded low-molecular-weight compounds has a number of advantages, including simple synthetic routes, clear molecular structures, and ease of building supramolecular polymers with complicated topological structures. However, the stabilities and mechanical properties of the resulting supramolecular polymers tend to be poor, and so to overcome this issue, the incorporation of covalently bonded polymers into the supramolecular polymeric systems is an option. Indeed, with the development of supramolecular chemistry and polymer science, growing numbers of tailor-made covalent polymers have been employed as building blocks to construct supramolecular polymers through non-covalent interactions, and these polymers inherit the properties of both covalent and non-covalent bonding, including the associated mechanical properties, photophysical properties, reversibility, and stimuli-responsiveness. In such cases, polymers can play the roles of the host, the guest, or both.

### Polymers as Hosts and Micromolecules as Guests

In the case where polymers are employed as hosts and micromolecules as guests, crown ethers are modified into the traditional polymer hosts, while low-molecular-weight secondary ammonium salts, diazonium, salts, and paraquat are used as the guests. More specifically, Ji et al. (2013b) developed a supramolecular cross-linked network **18** via host-guest interactions through the use of fluorescent conjugated polymer chains grafted with the DB24C8 groups of **17** as the host and a bisammonium salt as the guest (**3**) (Figure 5A). Compared with the fluorescence intensity of polymer **17**, that of the supramolecular cross-linked network **18** was significantly lower due to the ACQ properties of the conjugated poly(phenylene ethynylene) polymeric backbones. The structure of polymer network **18** could be destroyed by multiple stimuli, such as variations in the temperature or pH change or the addition of  $\text{K}^+$  or  $\text{Cl}^-$  ions, and this was accompanied by an increase

in the fluorescence intensity due to the presence of dynamic non-covalent bonds (Figure 5B). Interestingly, the cross-linked polymer network thin film emitted a stronger fluorescence upon exposure to an alkaline gas, such as ammonia vapor, since the deprotonation of cross-linker **3** resulted in dissociation of the aggregated state of the poly(phenylene ethynylene) polymer main chains. Hence, this system could be employed to probe various stimuli, and in particular, the presence of an alkaline gas, and so can be considered an attractive candidate for advanced sensor materials.

To overcome the weak fluorescence exhibited by traditional conjugated polymers upon aggregation, He et al. (2016) constructed a series of crown ether-based fluorescent polymers **19–21** with AIE properties by coupling 2Bpin-TPE as an AIEgen with O-2Br-DB24C8, M-2Br-DB24C8, and P-2Br-DB24C8, in addition to a bisammonium salt **22** (Figures 6A,B). It should be noted here that the structural difference between polymers **19–21** was the linkage position of the TPE group. Thus, polymers **19–21** exhibited different degrees of aggregation-induced emission enhancement (AIEE) upon increasing the fraction of the poor solvent present in the mixture. For example, **19** exhibited a relatively bright emission in the dilute solution state, while its fluorescence enhancement was limited upon aggregation. This



**FIGURE 7** | Chemical structures of **23** and **24** and a cartoon representation of the formation of fluorescent supramolecular cross-linked polymer gel **25**.

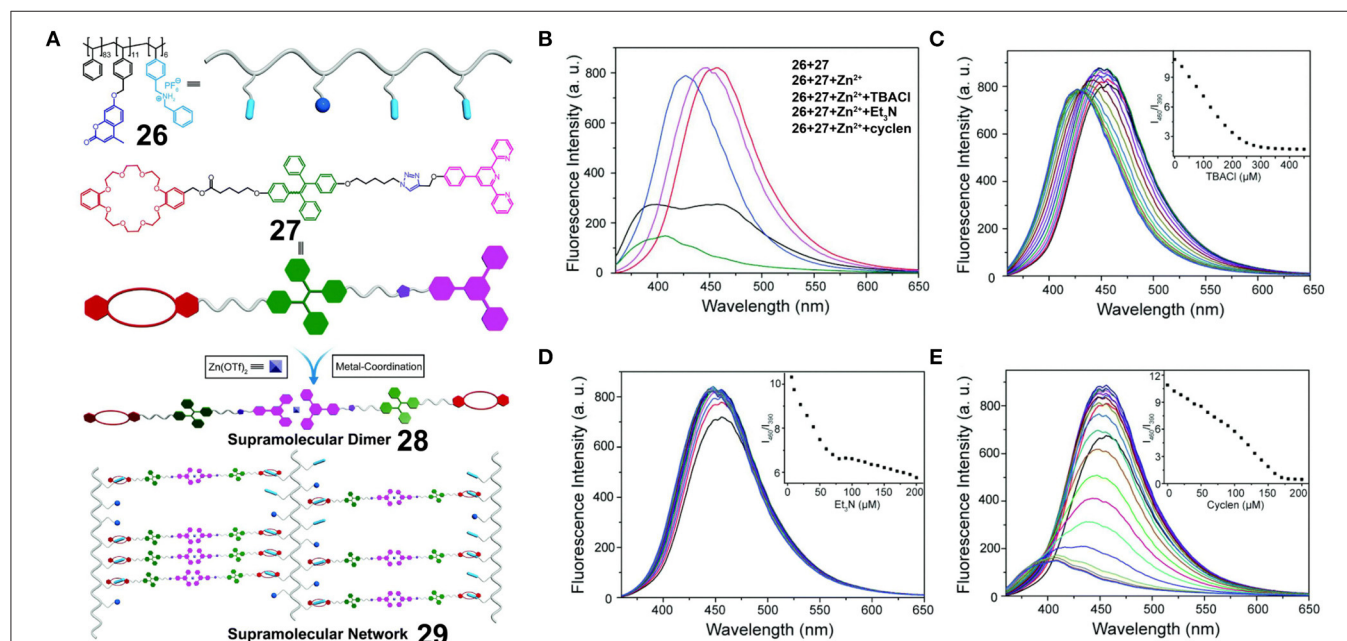
was accounted for by considering that the suppression of the intramolecular motion of the TPE moieties in **19** connected at the *ortho*-position was more efficient than the associated suppression in **20** at the *meta*-position and in **21** at the *para*-position. Interestingly, following treatment with three acid-base cycles, the system formed using **21** and **22** exhibited a highly reversible fluorescence intensity and emission wavelength (Figure 6C), while the systems formed from **19** and **22** or **20** and **22** exhibited stepwise increases in their fluorescence intensities. This was attributed to recognition between DB24C8 and DBAS and the efficient salting-out effect of NaCl generated from the acid-base process, which in turn facilitated morphological evolution from micelles to larger vesicles. However, due to the more rigid conformation of the polymer chain of **21**, the construction of vesicles from the **21/22** system was more challenging, and so stabilization of the fluorescence intensity was less efficient. Based on such findings, these polymers can be considered promising materials for use in the field of optoelectronic devices and fluorescent sensors.

## Polymers as Guests and Micromolecules as Hosts

In the case where polymers are employed as guests and micromolecules as hosts, secondary ammonium salts are commonly hung on traditional polymers to make the guest, while low-molecular-weight crown ethers are employed as the hosts. For example, Ji X. F. et al. (2015) synthesized polystyrene polymer **24** bearing dialkylammonium salt moieties

as pendent groups and benzo-21-crown-7 (B21C7) macrocycles **23** functionalized on the four arms of TPE molecules. Upon mixing **24** and **23**, a fluorescent supramolecular polymer gel was obtained via host-guest interactions between the B21C7 units and the dialkylammonium salts (Figure 7). The gel emitted a strong fluorescence, while a solution of **23** containing the same molar concentration of TPE units showed almost no fluorescence, thereby indicating that gelation induced the fluorescence emission. In addition, the presence of non-covalent interactions rendered the gel responsive to changes in temperature and pH. Thus, upon heating or with the addition of triethylamine, the recognition between B21C7 and the dialkylammonium salts was destroyed, resulting in disassembly of the gel and the formation of a sol, which was accompanied by fluorescence quenching. However, the recognition between B21C7 and the dialkylammonium salts was easily recovered by cooling or by the addition of trifluoroacetic acid. This work therefore provided a strategy for the construction of functional supramolecular polymers.

Employing the above-mentioned method, Xu et al. (2018a) prepared a polystyrene polymer **26** bearing coumarin moieties and dialkylammonium salts and combined this with a TPE derivative **27** bearing a DB24C8 unit and a terpyridine moiety at each side. A supramolecular network was constructed by the simple mixing of **26**, **27**, and  $\text{Zn}(\text{OTf})_2$  through DB24C8/dialkylammonium salt and terpyridine/Zn recognition moieties (Figure 8A). Upon increasing the concentration of the



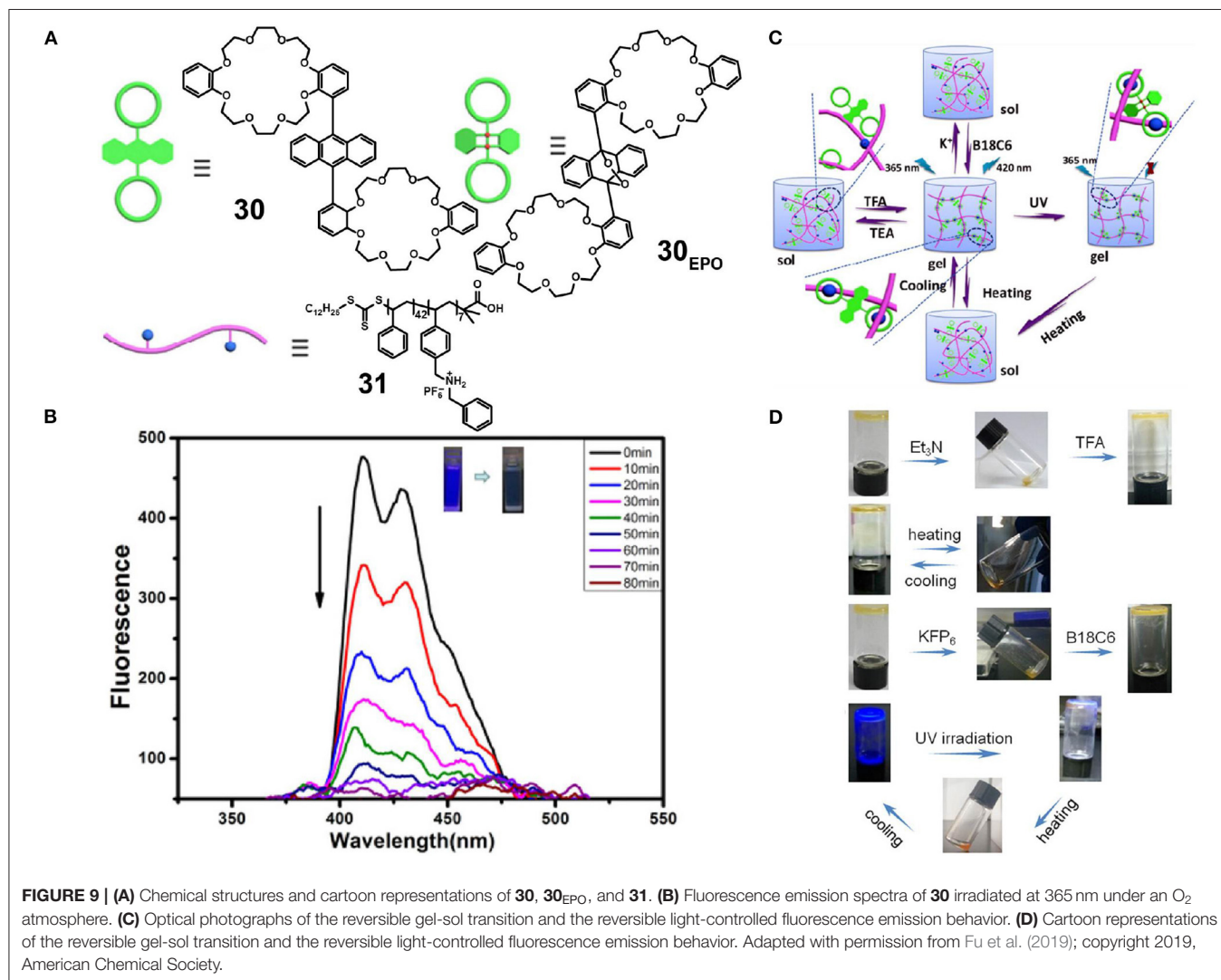
**FIGURE 8 | (A)** Chemical structures of **26** and **27**, and cartoon representations of the formation of supramolecular dimer **28** and fluorescent supramolecular cross-linked polymer **29**. **(B)** Fluorescence emission spectra of the mixture of **26** (18.6  $\mu\text{M}$ ) and **27** (100  $\mu\text{M}$ ) and upon the addition of  $\text{Zn}(\text{OTf})_2$  (50  $\mu\text{M}$ ), TBACl (450  $\mu\text{M}$ ),  $\text{Et}_3\text{N}$  (200  $\mu\text{M}$ ), or cyclen (200  $\mu\text{M}$ ). Fluorescence emission spectra of the network upon the stepwise addition of **(C)** TBACl, **(D)**  $\text{Et}_3\text{N}$ , and **(E)** cyclen. The insets show the plots of  $I_{460}/I_{390}$  vs. the amount of **(C)** TBACl, **(D)**  $\text{Et}_3\text{N}$ , and **(E)** cyclen added. Adapted with permission from Xu et al. (2018a); copyright 2018, Royal Society of Chemistry.



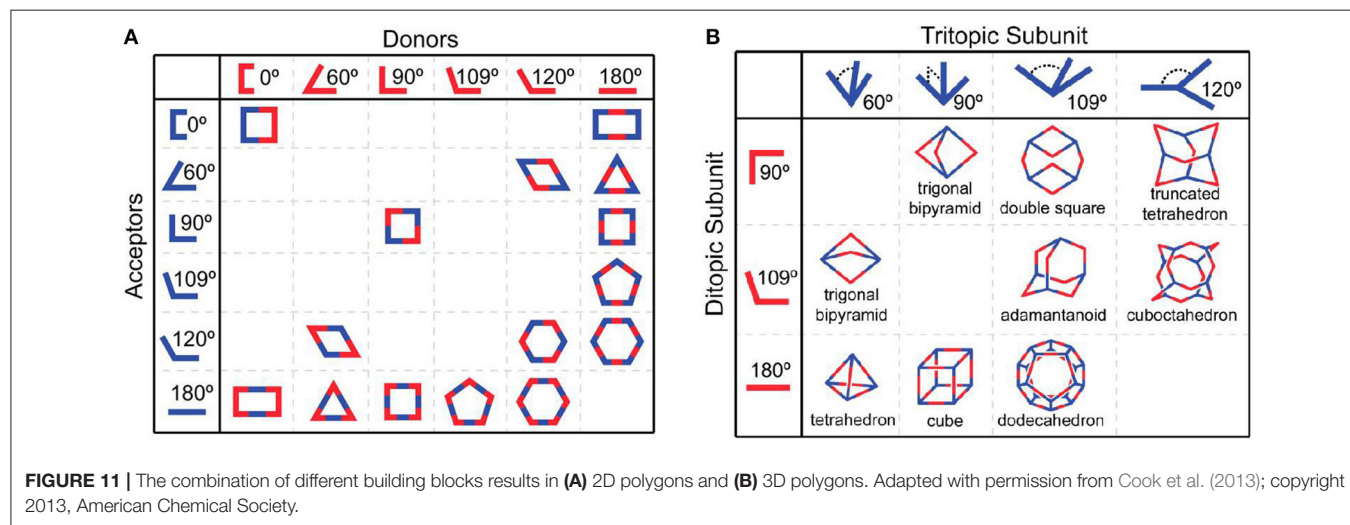
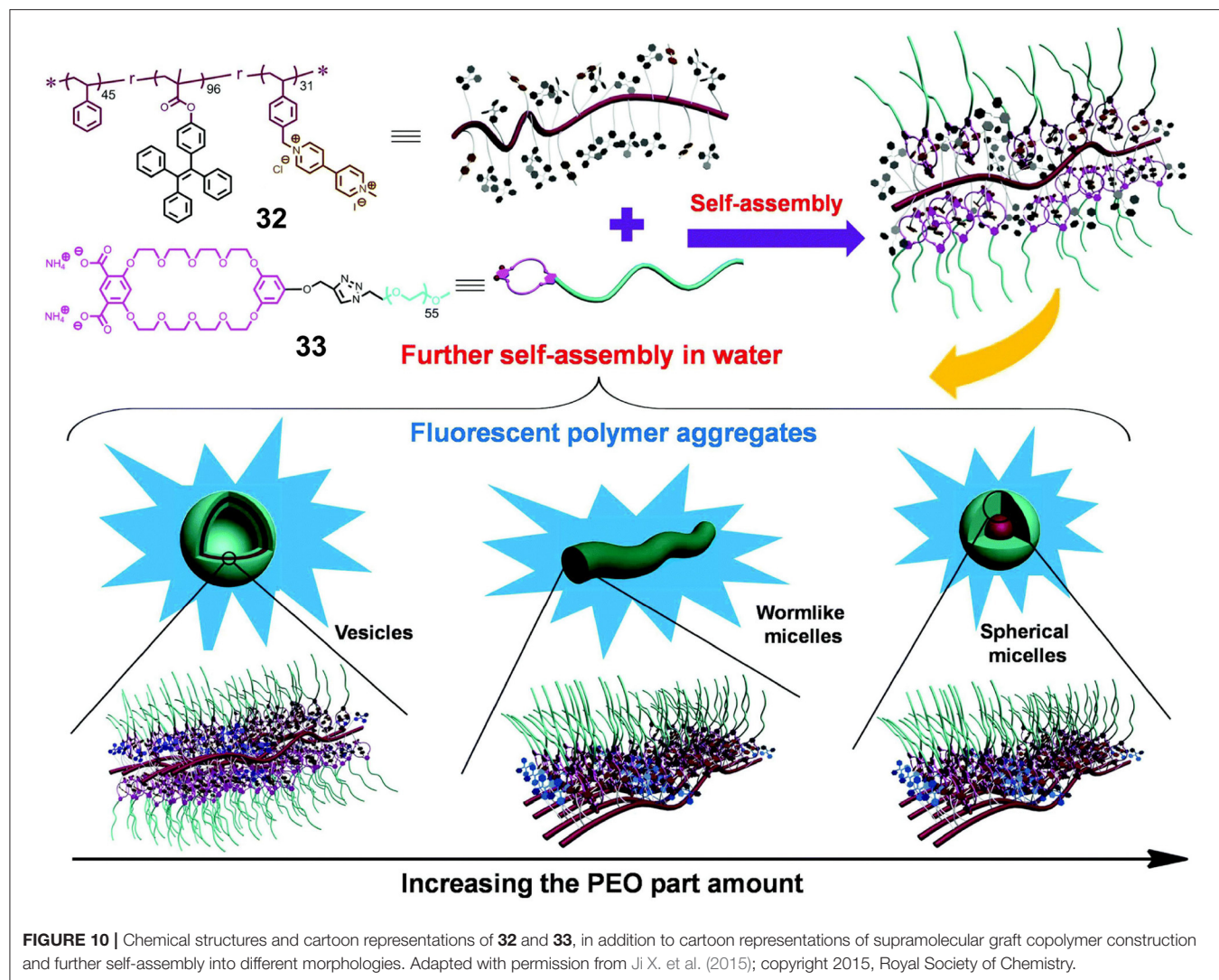
system, the emission intensity of the supramolecular polymer network **29** at 460 nm (originating from the TPE units) was found to increase, while that at 390 nm (originating from the coumarin units) was found to decrease due to the AIE property of the TPE units and the ACQ property of the coumarin units. In this case, no obvious Förster resonance energy transfer (FRET) took place between **26** and **27** due to a lack of spectral overlap. Furthermore, the ratio between the emission intensities at 460 and 390 nm ( $I_{460}/I_{390}$ ) varied linearly within a certain range upon the dissociation of **29** when  $\text{NEt}_3$ ,  $\text{Cl}^-$ , or cyclen was added. Thus, the supramolecular polymer network **29** could be employed as a ratiometric sensor for pH, cyclen, and  $\text{Cl}^-$  with precise results (Figures 8B–E). Upon further increasing the concentration of the supramolecular polymer network **29**, a cross-linked supramolecular gel exhibiting multiple stimulus responsiveness and self-healing behavior was formed. Based on the above results, this fluorescent supramolecular polymer provided a representative illustration of a fluorescent material to serve as a ratiometric sensor,

whereby monitoring was possible through self-calibration from two emission peaks.

Fu et al. (2019) also prepared polystyrene **31** containing DBAS units as pendant groups. In addition, they synthesized an anthracene-bridged divalent crown ether **30** (Figure 9A) in which anthracene adopted the *cis*-conformation to prevent  $\pi$ - $\pi$  stacking between the anthracene units. Upon the simple mixing of **30** and **31** at an appropriately high concentration, a fluorescent supramolecular polymer gel formed based on DB24C8/DBAS recognition, and this polymer displayed a reversible gel-sol transition upon the addition of competitive guest or through pH or thermal stimuli, due to the nature of the dynamic and reversible non-covalent bond (Figures 9C,D). Furthermore, this luminescent supramolecular polymer gel possessed an attractive photo-controlled property due to the fact that host **30**, which contains two bulky groups in the 9 and 10 positions of the anthracene skeleton, could react with singlet oxygen through a  $[4 + 2]$  cycloaddition reaction upon irradiation with UV light, therefore leading to a decrease in fluorescence (Figure 9B).







This supramolecular system exhibits potential for application in fluorescent materials and, in particular, photo-controlled sensors.

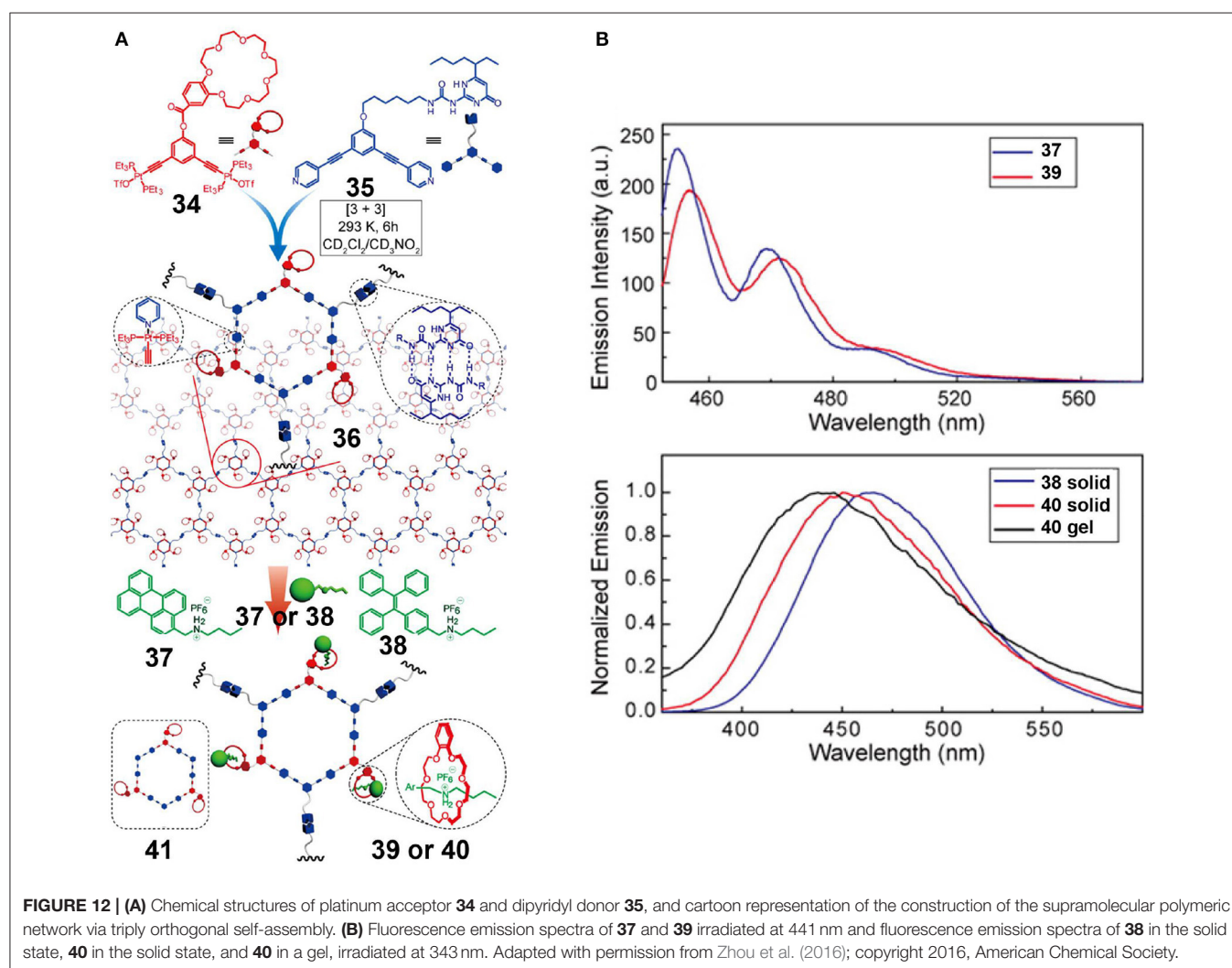
## Polymers as Both Hosts and Guests

In the case where polymers are employed both as the hosts and the guests, crown ethers and secondary ammonium salts are both employed to modify traditional polymers. In this context, Ji X. et al. (2015) investigated the influence of the aggregation morphology on the functions of fluorescent polymeric aggregation through constructing supramolecular systems based on hydrophobic polymer **32** and hydrophilic polymer **33** in water. More specifically, polymer **32** consisted of polystyrene with pendent TPE moieties and paraquat units, while polymer **33** consisted of a water-soluble poly(ethylene oxide) (PEO) terminated with a bis-(*m*-phenylene)-32-crown-10 (BMP32C10) unit containing two COO<sup>−</sup> groups. Unlike traditional intricate methods for the construction of fluorescent polymeric aggregates through the synthesis of a series of polymers, host-guest interactions between the BMP32C10 and paraquat units in **32** and **33** resulted in the formation of supramolecular amphiphilic graft copolymers. By adjusting the proportion of hydrophilic

polymer **33**, different aggregation morphologies, such as vesicles, wormlike micelles, and spherical micelles, can be formed (Figure 10). Thus, due to their amphipathy and special morphology, these supramolecular graft copolymers could encapsulate non-fluorescent drugs and subsequently release these drugs with the appropriate pH stimulus due to the stimulus responsiveness of BMP32C10/paraquat recognition. This could be detected by changes in the intensity of fluorescence. Furthermore, due to the low cytotoxicities of **32** and **33** and the resulting polymer aggregates, this supramolecular system shows promise for application in the field of drug delivery.

## CROWN ETHER-BASED FLUORESCENT SUPRAMOLECULAR POLYMERS CONSTRUCTED BY SCCs

In addition to the aforementioned strategies, discrete supramolecular coordination complexes (SCCs) with well-defined sizes, shapes, and geometries have been proven to be rational building blocks for the construction of fluorescent



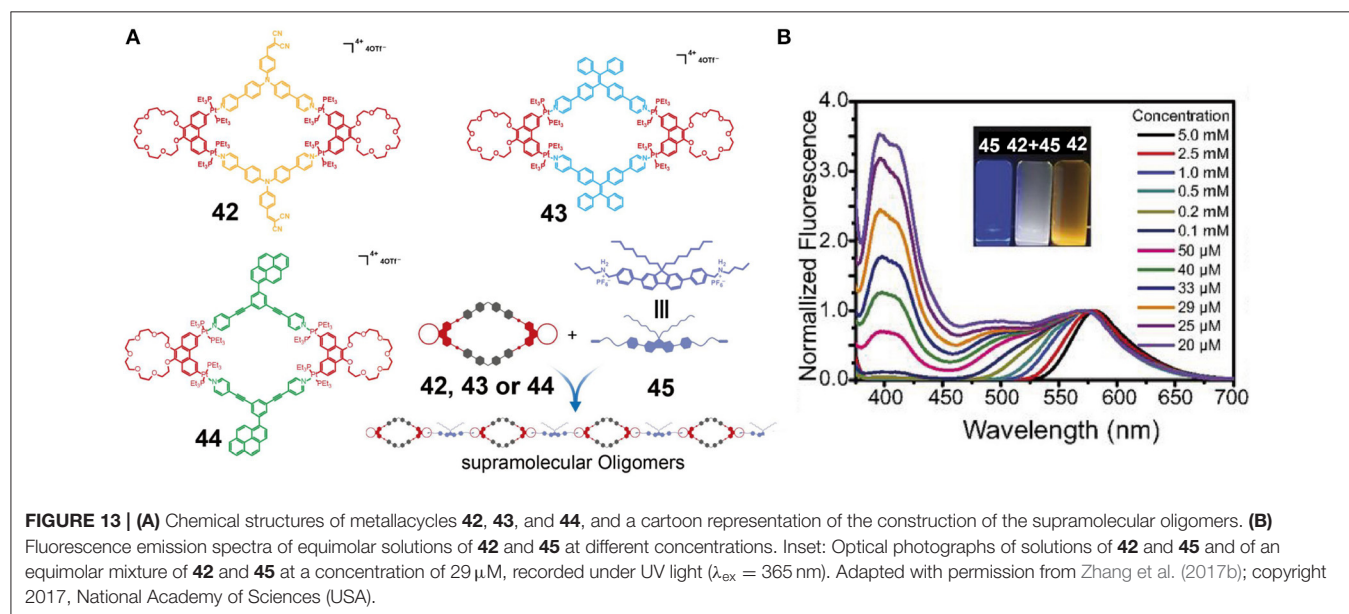
supramolecular polymers. In a similar manner to natural self-assembly processes, SCCs with superior properties have been efficiently developed by coordination-driven self-assembly, wherein the spontaneous connection between metal acceptors and organic donors via metal-ligand bonds resulted in the formation of non-covalent interactions and complicated structures (Smulders et al., 2013; Wei et al., 2015; Li et al., 2019a; Sun et al., 2019). In addition, over the past few decades, Stang (Sepehrpour et al., 2019), Fujita (Sawada et al., 2014), Raymond (Zhao et al., 2013), Mirkin (Mendez-Arroyo et al., 2014), Newkome (Chakraborty et al., 2017), Nitschke (Mosquera et al., 2016), and Yang (Chen L. -J. et al., 2015) have made enormous contributions to the development of a series of discrete SCCs with various shapes covering two-dimensional metallacycles and three-dimensional metallacages (**Figure 11**) (Cook et al., 2013). It is necessary to emphasize the difference between the metallic linkage applied in the cases of **Figures 1, 2, 8** and that of SCCs. The former could comprise infinite linear polymers or cross-linked networks in which the metal centers and organic ligands bridged through metal-ligand coordination bonds, such as terpyridine-based metal-ligand interactions. The latter could form discrete systems where organometallic receptors and organic donors with specific angularity undergo self-assembly to generate finite supramolecular complexes. Due to the range of supramolecular structures, the stimulus-responsive nature of metal-ligand coordination interactions, and the introduction of metal atoms, SCCs have profound implications for the future development of light-emitting materials (Yan et al., 2015), sensors (Zhang et al., 2017b), molecular flasks (Inokuma et al., 2011), cell imaging (Zhang M. et al., 2016), and bioengineering (Zhou et al., 2019).

In addition, since the formation of metal-ligand coordination interactions does not interfere with other non-covalent interactions, complicated supramolecular polymer systems

could be constructed using metal-ligand coordination-based interactions to construct metallacycles or metallacages as repetitive units with other non-covalent interactions, such as crown ether-based recognition systems (Wei et al., 2015). Utilizing two or more non-covalent bond forces to construct supramolecular polymers could not only give them richer stimulus responsiveness and other functions but could also provide a new flexible method for developing the topological structures of supramolecular polymers.

## Metallacycles as Building Blocks

Zhou et al. (2016) reported a crown ether-based supramolecular polymer network using three orthogonal interactions, including coordination-driven self-assembly, hydrogen bonding, and host-guest interactions (**Figure 12A**). More specifically, a platinum acceptor **34** bearing a B21C7 moiety and a corresponding dipyridyl donor **35** with a pendant 2-ureido-4-pyrimidinone (UPy) unit was used to assemble a metalla-hexagon that was then converted into supramolecular polymer network **36** by the complementary hydrogen-bonding interactions of the UPy units. In addition, the resultant supramolecular polymer network **36** could be functionally modified using the free B21C7 moieties. Driven by host-guest interactions based on the recognition between the B21C7 moieties and dialkylammonium salts, two fluorescent supramolecular polymer networks (**39** and **40**) were developed by the introduction of perylene-decorated (**37**) and TPE-decorated (**38**) dialkylammonium salts, respectively. As evidenced by the fluorescence emission spectra of **37–40** (**Figure 12B**), the functional supramolecular polymer networks inherited the emission properties of independent precursors in the premise that the preassembly was not disrupted, suggesting that the construction strategy developed here was a feasible, efficient, and imitable methodology for fabricating fluorescent supramolecular polymers through tailored fluorophores.

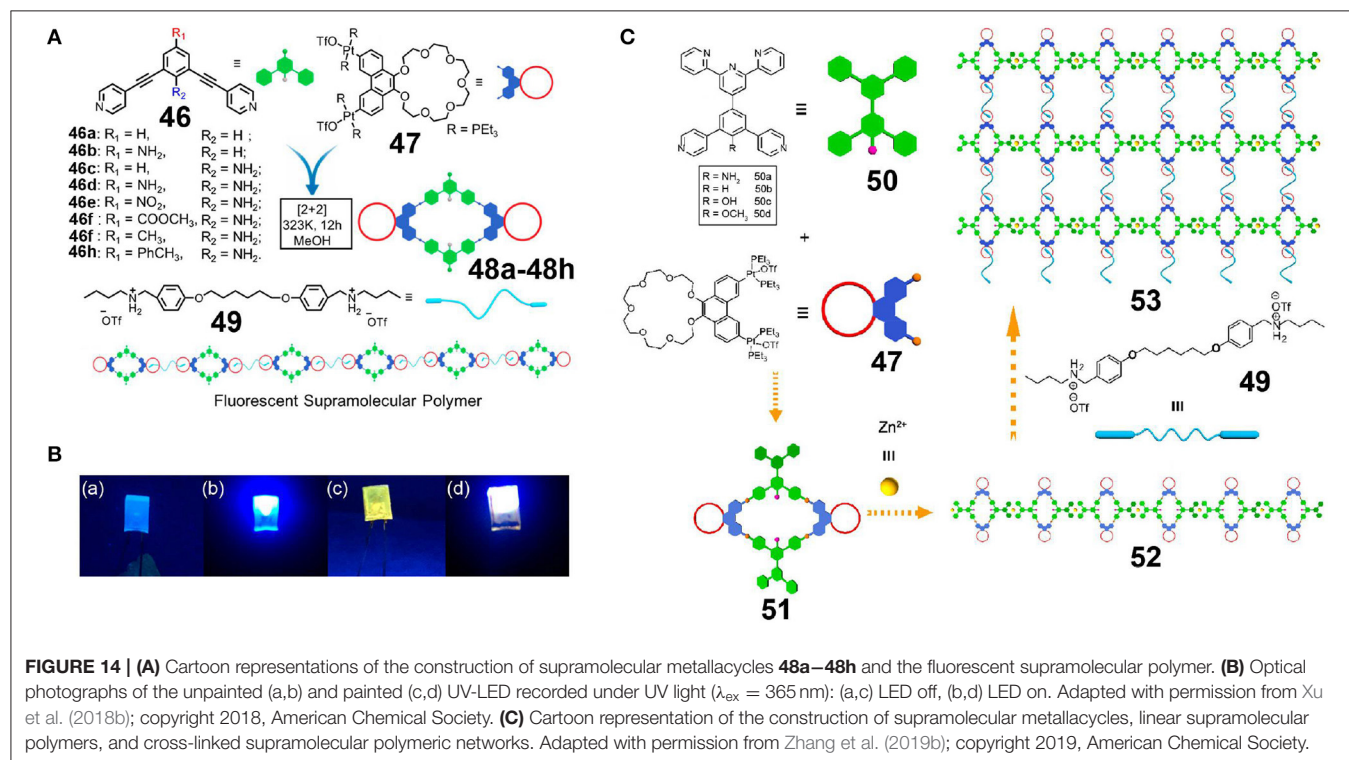




Zhang et al. (2017b) constructed metallacycles **42–44** by the coordination-driven self-assembly of well-established 120° dipyriddy donors with phenanthrene-21-crown-7 (P21C7)-based 60° diplatinum(II) acceptors. Metallacycles **42–44** exhibited orange, cyan, and green emission colors, respectively, originating from the triphenylamine, tetraphenylethene, and pyrene fluorogens. Further polymerization could be efficiently achieved via crown ether-diaklyammonium salt-based host-guest interactions between the P21C7 units of metallacycles **42–44** and a fluorene-functionalized bis-ammonium salt **45** (Figure 13A). The supramolecular assemblies constructed using **42** and **45** mainly gave blue fluorescence in the dilute solution state (molar concentration of **42** or **45** < 25  $\mu$ M), while they displayed orange emission at high concentrations (molar concentrations of **42** or **45** > 0.5 mM) since the ACQ properties of fluorene and the AIE properties of the triphenylamine moiety exhibited strong emissions only in dilute and concentrated solutions, respectively. As a result, this supramolecular system showed a strongly concentration-dependent emission from blue to orange. In addition, at a concentration of 29  $\mu$ M, this supramolecular system simultaneously displayed white emission because its fluorescence emission covered the entire region from 400 to 700 nm (Figure 13B). Thus, the emission properties of given assemblies can be precise and can also be controlled on a large scale simply by adjusting the system concentration. However, the supramolecular assemblies formed from **43** to **45** and from **44** to **45** did not exhibit a pronounced tuneable emission over a large range due to their similar fluorescence color. Overall, the emissions of such supramolecular systems could be adjusted over a large range by changing the concentration of the system when complementary host-guest interactions (crown-ethers

and diammonium salts), complementary emissions (blue and orange), and complementary fluorescence properties (AIE and ACQ) are combined into the same system, thereby providing a simple and effective method for the construction of fluorescent supramolecular assemblies. Such systems therefore play an important role in promoting the application of fluorescent supramolecular assemblies in the field of biotechnology and optoelectronics.

Light-emitting supramolecular assemblies play an important role in the fields of chemical sensors, biological imaging, and organic photoelectric materials. However, control of the fluorescence properties of supramolecular assemblies in a simple way and over a large range is one of the greatest challenges associated with the construction of fluorescent supramolecular assemblies. As an example, Xu et al. (2018b) first synthesized a series of P21C7-functionalized rhomboidal metallacycles **48a–48h** by variation of the substituents present on dipyriddy donor **46** and on P21C7-based 60° diplatinum(II) acceptor **47** (Figure 14A). As a result, the structures of metallacycles **48** differed in the number and position of amino groups on the pyridine ligands or in the electronic effect and the conjugated structure of the aniline moiety at the *para*-position. Metallacycles bearing an endohedral amino group, with strong electron-donating substituents *para* to the aniline group, or presenting a longer conjugated structure, were found to exhibit higher quantum yields both in the solution and thin film states. Fluorescent supramolecular polymers emitting over a wide range from blue to red were then constructed through host-guest interactions between metallacycles **48** and bis-ammonium salts **49**. These supramolecular polymers exhibited higher quantum yields than their corresponding discrete metallacycles both in





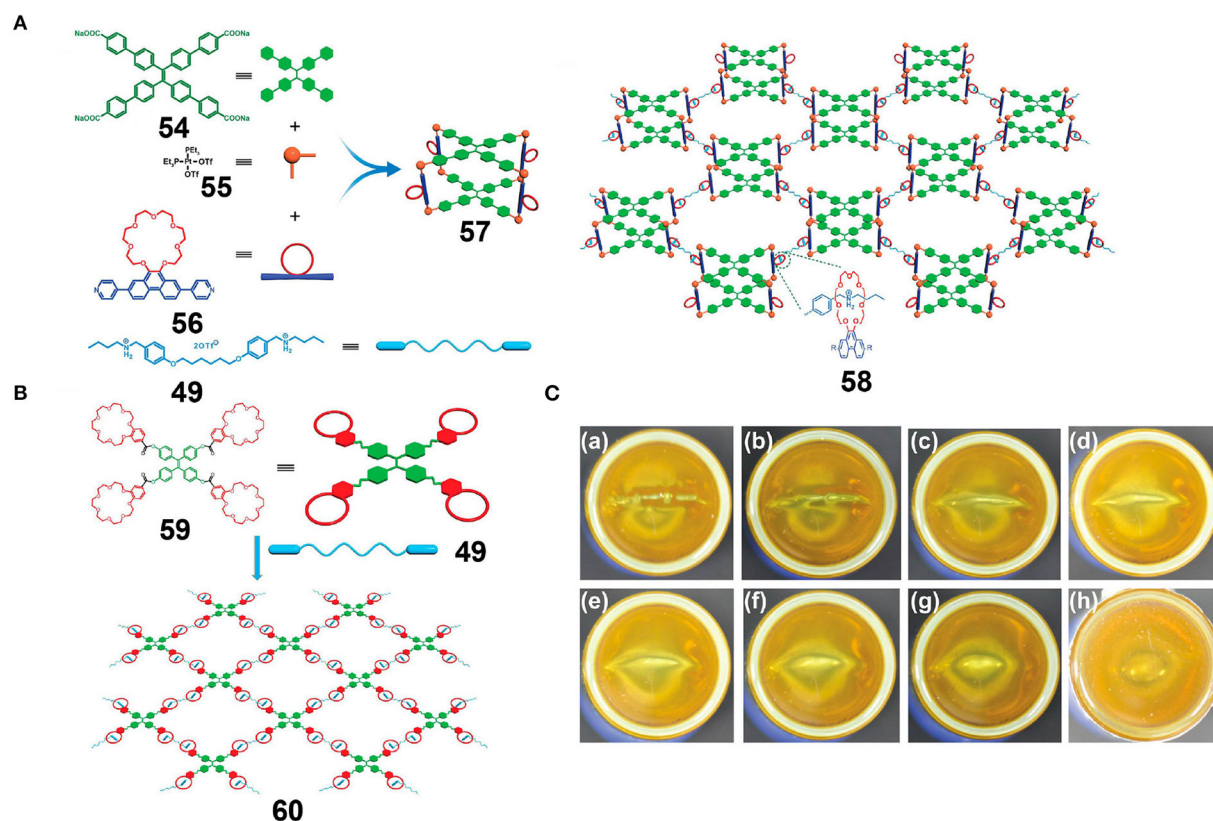
the solution and thin film states, likely due to the formation of supramolecular polymers inhibiting tight packing of the assemblies, in turn facilitating an alternative stacking pattern that enhanced the emission efficiency. In addition, a white emission light-emitting diode (LED) was obtained by the incorporation of a yellow-emitting supramolecular polymer **48h** with good solubility and a high quantum yield along with a blue-emitting LED source (**Figure 14B**). The presented system therefore represents a new strategy for the preparation of tuneable fluorescent supramolecular polymers through modification of the functional groups of organic ligands and lays a foundation for the development of self-assembled polymer materials for photoelectric materials, biological imaging, biosensors, and other applications.

The bottom-up method of hierarchical self-assembly based on miscellaneous non-covalent interactions to prepare complex supramolecular structures is a powerful means of building novel functional supramolecular materials. However, the preparation of organometallic materials with precise structural control via hierarchical self-assembly remains a challenge, in particular in the case of systems containing heterometals. For example, Zhang et al. (2019b) reported the construction of four rhomboidal metallacycles **50a–50d** bearing

a P21C7 group and a conjugately-linked tripyridine moiety by platinum(II)-ligand coordination-driven self-assembly (**Figure 14C**). A linear bimetallic supramolecular polymer was then formed through metal-coordination between Zn and the tripyridine moiety. Finally, a bimetallic cross-linked supramolecular polymer was constructed through host-guest interactions between crown-ethers and diammonium salts. These three kinds of orthogonal non-covalent interactions do not interfere with one another, and so at high concentrations, the cross-linked supramolecular polymer can form a gel with multiple-stimulus-responsive properties in addition to good self-healing properties. Furthermore, the emission properties of such supramolecular polymers can be effectively controlled by changing the electron-donor ability of the pyridine ligands present in the metallacycles, thereby providing a new route to novel functional supramolecular polymers through various metal-ligand coordination interactions.

## Metallacycles as Building Blocks

Lu et al. (2018) reported a tetragonal prismatic metallacycle, **57**, bearing pendant B21C7 moieties through the incorporation of  $\text{cis-Pt}(\text{PEt}_3)_2(\text{OTf})_2$ , TPE-functionalized sodium benzoate



**FIGURE 15 | (A)** Cartoon representations of the construction of supramolecular metallacycle **57** and metallacycle-cored fluorescent supramolecular polymer **58**. **(B)** Cartoon representation of the construction of cross-linked supramolecular polymer **60**. **(C)** Optical photographs of the self-healing process of gel **58**, and images showing the gel after cutting and allowing to stand for (a) 0, (b) 0.5, (c) 1.0, (d) 1.5, (e) 2, (f) 2.5, (g) 3, and (h) 4 min. Adapted with permission from Lu et al. (2018); copyright 2018, American Chemical Society.

ligands, and linear dipyrrolyl ligands via metal-coordination-driven self-assembly. Upon the addition of bis-ammonium linkers, a supramolecular polymer network (SPN) was formed via host-guest interactions (**Figure 15A**), and upon increasing the concentration of the SPN to a relatively high level, a supramolecular polymer gel was obtained that inherited the AIE properties originating from the TPE moieties. Moreover, due to the reversibility and environmental responsiveness of platinum(II)-ligand coordination interactions and the host-guest interactions based on the B21C7 units and bis-ammonium salts, transitions between the metallacage-cored fluorescent supramolecular polymer gel and the disassembled sol with weak fluorescence were achieved by the addition of competing coordination compounds and thermal stimuli. Dynamic and reversible non-covalent interactions endowed the resultant gel with self-healing properties that allowed crack repair over a short time (**Figure 15C**). To gain some insight into the effect of metallacages as cores in the gel, a model gel **60** (**Figure 15B**) was prepared via host-guest interactions between crown ether-functionalized TPE derivatives and bis-ammonium linkers. In comparison with gel **60**, gel **58** displayed a significantly stiffer structure due to the presence of rigid metallacages and higher branch functionalities. Thus, the above system provided a simple yet highly efficient strategy for obtaining multi-functional fluorescent supramolecular gels and laid a foundation for the development of dynamic but robust supramolecular materials. The authors also reported an improvement in the mechanical properties and self-healing properties of these fluorescent supramolecular gel systems when rigid metallacages were introduced through host-guest interactions, thereby showing promise for the application of metal-organic metallacages in intelligent soft materials, luminescent materials, drug carriers, and other fields.

## CONCLUSIONS

We herein summarized the current published research works in the field of fluorescent supramolecular polymers formed by crown ether-based host-guest interactions. Depending on the building blocks employed, the fabrication strategies could be divided into three categories, including linking covalently bonded low-molecular weight compounds with the association units of hosts and guests, modifying hosts and guests with polymers, and the use of supramolecular coordination complexes (SCCs) bearing free crown ether units. The examples covered in this review comprehensively describe the superior performances of fluorescent materials based on the marriage of fluorophores and crown ether-based supramolecular macrocyclic compounds, which have demonstrated value in applications such as solid-state or gel-state fluorescent materials, fluorescent sensors, drug delivery monitoring, and optoelectronic devices. Aggregation-induced emission luminogens and conjugated oligomers such as tetraphenylethylene, triphenylamine, and oligomers of fluorene are usually selected to serve as the luminescent groups due to their facile modification and good luminescence. In addition, novel multifunctional supramolecular polymeric

materials can be obtained through the combination of crown-ether-based host-guest interactions and other interactions, such as metal-ligand coordination interactions, and multiple hydrogen-bonding interactions. Furthermore, responsiveness to multiple stimuli is a particularly pronounced characteristic of crown ether-based supramolecular polymers, which arises from the dynamic and reversible non-covalent bonding present in such structures. Moreover, crown ether-based fluorescent supramolecular polymers bearing more topological structures possess the desired properties of both rigidity and reversibility, thereby rendering it possible for them to be easily functionalized and developed.

Although there have been important advances in fluorescent supramolecular polymers formed through crown ether-based host-guest interactions, efforts still should be devoted to exploiting uncharted terrains and addressing remaining challenges to ensure more extensive practical applications. Firstly, additional attention should be paid to utilizing existing fluorophores but also to creating novel fluorophores with unique characteristics. Secondly, there is a lack of depth and system in the research into fluorescent supramolecular polymers with various morphologies. However, the construction of amphipathic fluorescent nanoparticles from supramolecular polymers via crown ether-based recognition is one of the developments that could expand the potential applications in biology, such as cell imaging. Moreover, a feasible method for enriching the properties of fluorescent supramolecular polymeric materials is the introduction of more non-covalent interactions, such as  $\pi$ - $\pi$  stacking interactions, electrostatic interactions, and van der Waals forces. Finally, SCCs and, in particular, metallacages have been proven to be a novel kind of building block that is conducive to the emergence of new fluorescent supramolecular polymers. It can be anticipated that the combination of various fluorescent properties and the unique responsiveness and reversibility of crown ether-based supramolecular macrocyclic chemistry may broaden the application range of developing smart materials in areas such as photocatalysis, information transition, and data storage. We therefore expect continual endeavors to be carried out to ensure the development of novel fluorescent supramolecular polymers that exhibit desirable and enhanced properties as well as to ensure their subsequent practical application.

## AUTHOR CONTRIBUTIONS

HQ, TH, YL, and SY designed the proposal and revised the manuscript. JZ wrote the first draft of the manuscript and prepared the figures. All authors read and approved the final manuscript prior to submission.

## ACKNOWLEDGMENTS

We thank the National Natural Science Foundation of China (21971049 and 51903070) and the Zhejiang Provincial Natural Science Foundation of China (LQ18B040001 and LY16B040006) for financial support.

## REFERENCES

- Bai, W., Wang, Z., Tong, J., Mei, J., Qin, A., Sun, J. Z., et al. (2015). A self-assembly induced emission system constructed by the host-guest interaction of AIE-active building blocks. *Chem. Commun.* 51, 1089–1091. doi: 10.1039/C4CC06510G
- Chakraborty, S., Hong, W., Endres, K. J., Xie, T.-Z., Wojtas, L., Moorefield, C. N., et al. (2017). Terpyridine-based, flexible tripods: from a highly symmetric nanosphere to temperature-dependent, irreversible, 3D isomeric macromolecular nanocages. *J. Am. Chem. Soc.* 139, 3012–3020. doi: 10.1021/jacs.6b11784
- Chen, D., Zhan, J., Zhang, M., Zhang, J., Tao, J., Tang, D., et al. (2015). A fluorescent supramolecular polymer with aggregation induced emission (AIE) properties formed by crown ether-based host-guest interactions. *Polym. Chem.* 6, 25–29. doi: 10.1039/C4PY01206B
- Chen, L.-J., Ren, Y.-Y., Wu, N.-W., Sun, B., Ma, J.-Q., Zhang, L., et al. (2015). Hierarchical self-assembly of discrete organoplatinum(II) metallacycles with polysaccharide via electrostatic interactions and their application for heparin detection. *J. Am. Chem. Soc.* 137, 11725–11735. doi: 10.1021/jacs.5b06565
- Chen, P.-Z., Weng, Y.-X., Niu, L.-Y., Chen, Y.-Z., Wu, L.-Z., Tung, C.-H., et al. (2016). Light-harvesting systems based on organic nanocrystals to mimic chlorosomes. *Angew. Chem.* 128, 2809–2813. doi: 10.1002/ange.201510503
- Cook, T. R., Zheng, Y.-R., and Stang, P. J. (2013). Metal-organic frameworks and self-assembled supramolecular coordination complexes: comparing and contrasting the design, synthesis, and functionality of metal-organic materials. *Chem. Rev.* 113, 734–777. doi: 10.1021/cr3002824
- Deng, Y., Zhang, Q., Feringa, B. L., Tian, H., and Qu, D.-H. (2020). Toughening a self-healable supramolecular polymer by ionic cluster-enhanced iron-carboxylate complexes. *Angew. Chem. Int. Ed.* 59, 5278–5283. doi: 10.1002/anie.201913893
- Ding, Y., Wang, P., Tian, Y.-K., Tian, Y.-J., and Wang, F. (2013). Formation of stimuli-responsive supramolecular polymeric assemblies via orthogonal metal-ligand and host-guest interactions. *Chem. Commun.* 49, 5951–5953. doi: 10.1039/c3cc42511h
- Dong, R., Ravinathan, S. P., Xue, L., Li, N., Zhang, Y., Zhou, L., et al. (2016). Dual-responsive aggregation-induced emission-active supramolecular nanoparticles for gene delivery and bioimaging. *Chem. Commun.* 52, 7950–7953. doi: 10.1039/C6CC02794F
- Dong, S., Zheng, B., Xu, D., Yan, X., Zhang, M., and Huang, F. (2012). A crown ether appended super gelator with multiple stimulus responsiveness. *Adv. Mater.* 24, 3191–3195. doi: 10.1002/adma.201200837
- Dsouza, R. N., Pischel, U., and Nau, W. M. (2011). Fluorescent dyes and their supramolecular host/guest complexes with macrocycles in aqueous solution. *Chem. Rev.* 111, 7941–7980. doi: 10.1021/cr200213s
- Ferri, A., Bergamini, G., Roy, M., Gingras, M., and Ceroni, P. (2014). Turn-on phosphorescence by metal coordination to a multivalent terpyridine ligand: a new paradigm for luminescent sensors. *J. Am. Chem. Soc.* 136, 6395–6400. doi: 10.1021/ja501458s
- Fu, H.-G., Chen, Y., and Liu, Y. (2019). Multistimuli-responsive and photocontrolled supramolecular luminescent gels constructed by anthracene-bridged bis(dibenzo-24-crown-8) with secondary ammonium salt polymer. *ACS Appl. Mater. Interfaces* 11, 16117–16122. doi: 10.1021/acsami.9b04323
- Gibson, H. W., Yamaguchi, N., Hamilton, L., and Jones, J. W. (2002). Cooperative self-assembly of dendrimers via pseudorotaxane formation from a homotritopic guest molecule and complementary monotopic host dendrons. *J. Am. Chem. Soc.* 124, 4653–4665. doi: 10.1021/ja012155s
- Gibson, H. W., Yamaguchi, N., and Jones, J. W. (2003). Supramolecular pseudorotaxane polymers from complementary pairs of homoditopic molecules. *J. Am. Chem. Soc.* 125, 3522–3533. doi: 10.1021/ja020900a
- He, L., Li, L., Liu, X., Wang, J., Huang, H., and Bu, W. (2016). Acid-base-controlled and dibenzylammonium-assisted aggregation induced emission enhancement of poly(tetraphenylethene) with an impressive blue shift. *Polym. Chem.* 7, 3722–3730. doi: 10.1039/C6PY00275G
- He, L., Liang, J., Cong, Y., Chen, X., and Bu, W. (2014). Concentration and acid-base controllable fluorescence of a metallosupramolecular polymer. *Chem. Commun.* 50, 10841–10844. doi: 10.1039/C4CC04243C
- Huang, D., Zhang, Q., Deng, Y., Luo, Z., Li, B., Shen, X., et al. (2018). Polymeric crown ethers: LCST behavior in water and stimuli-responsiveness. *Polym. Chem.* 9, 2574–2579. doi: 10.1039/C8PY00412A
- Huang, F., and Gibson, H. W. (2004). Formation of a supramolecular hyperbranched polymer from self-organization of an AB2 monomer containing a crown ether and two paraquat Moieties. *J. Am. Chem. Soc.* 126, 14738–14739. doi: 10.1021/ja044830e
- Huang, F., Nagvekar, D. S., Zhou, X., and Gibson, H. W. (2007). Formation of a linear supramolecular polymer by self-assembly of two homoditopic monomers based on the bis(m-phenylene)-32-crown-10/paraquat recognition motif. *Macromolecules* 40, 3561–3567. doi: 10.1021/ma062080i
- Inokuma, Y., Kawano, M., and Fujita, M. (2011). Crystalline molecular flasks. *Nat. Chem.* 3, 349–358. doi: 10.1038/nchem.1031
- Ji, X., Dong, S., Wei, P., Xia, D., and Huang, F. (2013a). A novel diblock copolymer with a supramolecular polymer block and a traditional polymer block: preparation, controllable self-assembly in water, and application in controlled release. *Adv. Mater.* 25, 5725–5729. doi: 10.1002/adma.201301654
- Ji, X., Li, Y., Wang, H., Zhao, R., Tang, G., and Huang, F. (2015). Facile construction of fluorescent polymeric aggregates with various morphologies by self-assembly of supramolecular amphiphilic graft copolymers. *Polym. Chem.* 6, 5021–5025. doi: 10.1039/C5PY00801H
- Ji, X., Yao, Y., Li, J., Yan, X., and Huang, F. (2013b). A supramolecular cross-linked conjugated polymer network for multiple fluorescent sensing. *J. Am. Chem. Soc.* 135, 74–77. doi: 10.1021/ja3108559
- Ji, X. F., Wang, P., Wang, H., and Huang, F.-H. (2015). A fluorescent supramolecular crosslinked polymer gel formed by crown ether based host-guest interactions and aggregation induced emission. *Chin. J. Polym. Sci.* 33, 890–898. doi: 10.1007/s10118-015-1639-6
- Laurent, J., Blin, G., Chatelain, F., Vanneaux, V., Fuchs, A., Larghero, J., et al. (2017). Convergence of microengineering and cellular self-organization towards functional tissue manufacturing. *Nat. Biomed. Eng.* 1, 939–956. doi: 10.1038/s41551-017-0166-x
- Li, B., He, T., Fan, Y., Yuan, X., Qiu, H., and Yin, S. (2019a). Recent developments in the construction of metallacycle/metallacage-cored supramolecular polymers via hierarchical self-assembly. *Chem. Commun.* 55, 8036–8059. doi: 10.1039/C9CC02472G
- Li, B., He, T., Shen, X., Tang, D., and Yin, S. (2019b). Fluorescent supramolecular polymers with aggregation induced emission properties. *Polym. Chem.* 10, 796–818. doi: 10.1039/C8PY01396A
- Li, B., Lin, C., Lu, C., Zhang, J., He, T., Qiu, H., et al. (2020). A rapid and reversible thermochromic supramolecular polymer hydrogel and its application in protected quick response codes. *Mater. Chem. Front.* 4, 869–874. doi: 10.1039/C9QM00699K
- Li, J., Shi, K., Drechsler, M., Tang, B. Z., Huang, J., and Yan, Y. (2016). A supramolecular fluorescent vesicle based on a coordinating aggregation induced emission amphiphile: insight into the role of electrical charge in cancer cell division. *Chem. Commun.* 52, 12466–12469. doi: 10.1039/C6CC06432A
- Li, X., Wang, L., Deng, Y., Luo, Z., Zhang, Q., Dong, S., et al. (2018). Preparation of cross-linked supramolecular polymers based on benzo-21-crown-7/secondary ammonium salt host-guest interactions. *Chem. Commun.* 54, 12459–12462. doi: 10.1039/C8CC07657J
- Li, Y., Dong, Y., Miao, X., Ren, Y., Zhang, B., Wang, P., et al. (2018). Shape-controllable and fluorescent supramolecular organic frameworks through aqueous host-guest complexation. *Angew. Chem. Int. Ed.* 57, 729–733. doi: 10.1002/anie.201710553
- Liu, Y., Zhang, Y., Zhu, H., Wang, H., Tian, W., and Shi, B. (2018). A supramolecular hyperbranched polymer with multi-responsiveness constructed by pillar[5]arene-based host-guest recognition and its application in the breath figure method. *Mater. Chem. Front.* 2, 1568–1573. doi: 10.1039/C8QM00220G
- Lou, X.-Y., and Yang, Y.-W. (2018). Manipulating aggregation-induced emission with supramolecular macrocycles. *Adv. Optical Mater.* 6:1800668. doi: 10.1002/adom.201800668
- Lu, C., Zhang, M., Tang, D., Yan, X., Zhang, Z., Zhou, Z., et al. (2018). Fluorescent metallacage-core supramolecular polymer gel formed by orthogonal metal coordination and host-guest interactions. *J. Am. Chem. Soc.* 140, 7674–7680. doi: 10.1021/jacs.8b03781



- Luo, J., Xie, Z., Lam, J. W. Y., Cheng, L., Chen, H., Qiu, C., et al. (2001). Aggregation-induced emission of 1-methyl-1,2,3,4,5-pentaphenylsilole. *Chem. Commun.*, 1740–1741. doi: 10.1039/b105159h
- Ma, X., Xie, J., Tang, N., and Wu, J. (2016). AIE-caused luminescence of a thermally-responsive supramolecular organogel. *New J. Chem.* 40, 6584–6587. doi: 10.1039/C6NJ01211F
- Ma, X., and Zhao, Y. (2015). Biomedical applications of supramolecular systems based on host–guest interactions. *Chem. Rev.* 115, 7794–7839. doi: 10.1021/cr500392w
- Ma, Y., Marszalek, T., Yuan, Z., Stangenberg, R., Pisula, W., Chen, L., et al. (2015). A crown ether decorated dibenzocoronene tetracarboxydiimide chromophore: synthesis, sensing, and self-organization. *Chem. Asian J.* 10, 139–143. doi: 10.1002/asia.201403037
- Mendez-Arroyo, J., Barroso-Flores, J., Lifschitz, A. M., Sarjeant, A. A., Stern, C. L., and Mirkin, C. A. (2014). A multi-state, allosterically-regulated molecular receptor with switchable selectivity. *J. Am. Chem. Soc.* 136, 10340–10348. doi: 10.1021/ja503506a
- Mosquera, J., Ronson, T. K., and Nitschke, J. R. (2016). Subcomponent flexibility enables conversion between D4-symmetric  $Cd^{II}_8L_8$  and T-symmetric  $Cd^{II}_4L_4$  assemblies. *J. Am. Chem. Soc.* 138, 1812–1815. doi: 10.1021/jacs.5b12955
- Pedersen, C. J. (1967). Cyclic polyethers and their complexes with metal salts. *J. Am. Chem. Soc.* 89, 7017–7036. doi: 10.1021/ja01002a035
- Peng, H.-Q., Zheng, X., Han, T., Kwok, R. T. K., Lam, J. W. Y., Huang, X., et al. (2017). Dramatic differences in aggregation-induced emission and supramolecular polymerizability of tetraphenylethene-based stereoisomers. *J. Am. Chem. Soc.* 139, 10150–10156. doi: 10.1021/jacs.7b05792
- Qu, D.-H., Wang, Q.-C., Zhang, Q.-W., Ma, X., and Tian, H. (2015). Photoresponsive host–guest functional systems. *Chem. Rev.* 115, 7543–7588. doi: 10.1021/cr5006342
- Roy, B., Noguchi, T., Yoshihara, D., Yamamoto, T., Sakamoto, J., and Shinkai, S. (2016). Amplified fluorescence emission of bolaamphiphilic perylene-azacrown ether derivatives directed towards molecular recognition events. *PCCP* 18, 13239–13245. doi: 10.1039/C6CP01545J
- Sawada, T., Hisada, H., and Fujita, M. (2014). Mutual induced fit in a synthetic host–guest system. *J. Am. Chem. Soc.* 136, 4449–4451. doi: 10.1021/ja500376x
- Sepehrpour, H., Fu, W., Sun, Y., and Stang, P. J. (2019). Biomedically relevant self-assembled metallacycles and metallacages. *J. Am. Chem. Soc.* 141, 14005–14020. doi: 10.1021/jacs.9b06222
- Shi, B., Jie, K., Zhou, Y., Zhou, J., Xia, D., and Huang, F. (2016). Nanoparticles with near-infrared emission enhanced by pillararene-based molecular recognition in water. *J. Am. Chem. Soc.* 138, 80–83. doi: 10.1021/jacs.5b11676
- Shi, B., Zhou, Z., Vanderlinden, R. T., Tang, J.-H., Yu, G., Acharyya, K., et al. (2019). Spontaneous supramolecular polymerization driven by discrete platinum metallacycle-based host–guest complexation. *J. Am. Chem. Soc.* 141, 11837–11841. doi: 10.1021/jacs.9b06181
- Shi, C.-Y., Zhang, Q., Yu, C.-Y., Rao, S.-J., Yang, S., Tian, H., et al. (2020). An ultrastrong and highly stretchable polyurethane elastomer enabled by a zipper-like ring-sliding effect. *Adv. Mater.* 32:2000345. doi: 10.1002/adma.202000345
- Smulders, M. M. J., Riddell, I. A., Browne, C., and Nitschke, J. R. (2013). Building on architectural principles for three-dimensional metallasupramolecular construction. *Chem. Soc. Rev.* 42, 1728–1754. doi: 10.1039/C2CS35254K
- Sun, Y., Chen, C., and Stang, P. J. (2019). Soft materials with diverse suprastructures via the self-assembly of metal–organic complexes. *Acc. Chem. Res.* 52, 802–817. doi: 10.1021/acs.accounts.8b00663
- Wang, H., Ji, X., Li, Z., Zhu, C. N., Yang, X., Li, T., et al. (2017). Preparation of a white-light-emitting fluorescent supramolecular polymer gel with a single chromophore and use of the gel to fabricate a protected quick response code. *Mater. Chem. Front.* 1, 167–171. doi: 10.1039/C6QM00164E
- Wang, L., Cheng, L., Li, G., Liu, K., Zhang, Z., Li, P., et al. (2020). A self-cross-linking supramolecular polymer network enabled by crown-ether-based molecular recognition. *J. Am. Chem. Soc.* 142, 2051–2058. doi: 10.1021/jacs.9b12164
- Wang, X., Hu, J., Liu, T., Zhang, G., and Liu, S. (2012). Highly sensitive and selective fluorometric off–on K<sup>+</sup> probe constructed via host–guest molecular recognition and aggregation-induced emission. *J. Mater. Chem.* 22, 8622–8628. doi: 10.1039/c2jm16510d
- Wei, P., Yan, X., and Huang, F. (2015). Supramolecular polymers constructed by orthogonal self-assembly based on host–guest and metal–ligand interactions. *Chem. Soc. Rev.* 44, 815–832. doi: 10.1039/C4CS00327F
- Xiao, T., Zhou, L., Sun, X.-Q., Huang, F., Lin, C., and Wang, L. (2020). Supramolecular polymers fabricated by orthogonal self-assembly based on multiple hydrogen bonding and macrocyclic host–guest interactions. *Chin. Chem. Lett.* 31, 1–9. doi: 10.1016/j.ccl.2019.05.011
- Xu, L., Chen, D., Zhang, Q., He, T., Lu, C., Shen, X., et al. (2018a). A fluorescent cross-linked supramolecular network formed by orthogonal metal-coordination and host–guest interactions for multiple ratiometric sensing. *Polym. Chem.* 9, 399–403. doi: 10.1039/C7PY01788J
- Xu, L., Shen, X., Zhou, Z., He, T., Zhang, J., Qiu, H., et al. (2018b). Metallacycle-cored supramolecular polymers: fluorescence tuning by variation of substituents. *J. Am. Chem. Soc.* 140, 16920–16924. doi: 10.1021/jacs.8b10842
- Yamaguchi, N., and Gibson, H. W. (1999). Formation of supramolecular polymers from homoditopic molecules containing secondary ammonium ions and crown ether moieties. *Angew. Chem. Int. Ed.* 38, 143–147.
- Yamaguchi, N., Nagvekar, D. S., and Gibson, H. W. (1998). Self-organization of a heteroditopic molecule to linear polymolecular arrays in solution. *Angew. Chem. Int. Ed.* 37, 2361–2364.
- Yan, X., Cook, T. R., Pollock, J. B., Wei, P., Zhang, Y., Yu, Y., et al. (2014). Responsive supramolecular polymer metallo gel constructed by orthogonal coordination-driven self-assembly and host/guest interactions. *J. Am. Chem. Soc.* 136, 4460–4463. doi: 10.1021/ja412249k
- Yan, X., Cook, T. R., Wang, P., Huang, F., and Stang, P. J. (2015). Highly emissive platinum(II) metallacycles. *Nat. Chem.* 7, 342–348. doi: 10.1038/nchem.2201
- Yan, X., Li, S., Cook, T. R., Ji, X., Yao, Y., Pollock, J. B., et al. (2013). Hierarchical self-assembly: well-defined supramolecular nanostructures and metallohydrogels via amphiphilic discrete organoplatinum(II) metallacycles. *J. Am. Chem. Soc.* 135, 14036–14039. doi: 10.1021/ja406877b
- Yan, X., Wang, F., Zheng, B., and Huang, F. (2012a). Stimuli-responsive supramolecular polymeric materials. *Chem. Soc. Rev.* 41, 6042–6065. doi: 10.1039/c2cs35091b
- Yan, X., Xu, D., Chi, X., Chen, J., Dong, S., Ding, X., et al. (2012b). A multiresponsive, shape-persistent, and elastic supramolecular polymer network gel constructed by orthogonal self-assembly. *Adv. Mater.* 24, 362–369. doi: 10.1002/adma.201103220
- Yu, G., Jie, K., and Huang, F. (2015). Supramolecular amphiphiles based on host–guest molecular recognition motifs. *Chem. Rev.* 115, 7240–7303. doi: 10.1021/cr5005315
- Yu, G., Yan, X., Han, C., and Huang, F. (2013). Characterization of supramolecular gels. *Chem. Soc. Rev.* 42, 6697–6722. doi: 10.1039/c3cs60080g
- Yu, G., Zhang, M., Saha, M. L., Mao, Z., Chen, J., Yao, Y., et al. (2017). Antitumor activity of a unique polymer that incorporates a fluorescent self-assembled metallacycle. *J. Am. Chem. Soc.* 139, 15940–15949. doi: 10.1021/jacs.7b09224
- Yu, X., Chen, L., Zhang, M., and Yi, T. (2014). Low-molecular-mass gels responding to ultrasound and mechanical stress: towards self-healing materials. *Chem. Soc. Rev.* 43, 5346–5371. doi: 10.1039/C4CS00066H
- Zhan, J., Li, Q., Hu, Q., Wu, Q., Li, C., Qiu, H., et al. (2014a). A stimuli-responsive orthogonal supramolecular polymer network formed by metal–ligand and host–guest interactions. *Chem. Commun.* 50, 722–724. doi: 10.1039/C3CC47468B
- Zhan, J., Zhang, M., Zhou, M., Liu, B., Chen, D., Liu, Y., et al. (2014b). A multiple-responsive self-healing supramolecular polymer gel network based on multiple orthogonal interactions. *Macromol. Rapid Commun.* 35, 1424–1429. doi: 10.1002/marc.201400216
- Zhang, C., Li, S., Zhang, J., Zhu, K., Li, N., and Huang, F. (2007). Benzo-21-crown-7/secondary dialkylammonium salt [2]pseudorotaxane- and [2]rotaxane-type threaded structures. *Org. Lett.* 9, 5553–5556. doi: 10.1021/ol702510c
- Zhang, J., Zhang, K., Huang, X., Cai, W., Zhou, C., Liu, S., et al. (2012). Supramolecular light-emitting polymers for solution-processed optoelectronic devices. *J. Mater. Chem.* 22, 12759–12766. doi: 10.1039/c2jm31773g
- Zhang, J., Zhu, J., Lu, C., Gu, Z., He, T., Yang, A., et al. (2016). A hyperbranched fluorescent supramolecular polymer with aggregation induced emission (AIE) properties. *Polym. Chem.* 7, 4317–4321. doi: 10.1039/C6PY00872K
- Zhang, M., Li, S., Yan, X., Zhou, Z., Saha, M. L., Wang, Y.-C., et al. (2016). Fluorescent metallacycle-cored polymers via covalent linkage and their use



- as contrast agents for cell imaging. *Proc. Natl. Acad. Sci. U.S.A.* 113:11100. doi: 10.1073/pnas.1612898113
- Zhang, M., Saha, M. L., Wang, M., Zhou, Z., Song, B., Lu, C., et al. (2017a). Multicomponent platinum(II) cages with tunable emission and amino acid sensing. *J. Am. Chem. Soc.* 139, 5067–5074. doi: 10.1021/jacs.6b12536
- Zhang, M., Yin, S., Zhang, J., Zhou, Z., Saha, M. L., Lu, C., et al. (2017b). Metallacycle-cored supramolecular assemblies with tunable fluorescence including white-light emission. *Proc. Natl. Acad. Sci. U.S.A.* 114:3044. doi: 10.1073/pnas.1702510114
- Zhang, Q., Deng, Y.-X., Luo, H.-X., Shi, C.-Y., Geise, G. M., Feringa, B. L., et al. (2019a). Assembling a natural small molecule into a supramolecular network with high structural order and dynamic functions. *J. Am. Chem. Soc.* 141, 12804–12814. doi: 10.1021/jacs.9b05740
- Zhang, Q., Shi, C.-Y., Qu, D.-H., Long, Y.-T., Feringa, B. L., and Tian, H. (2018). Exploring a naturally tailored small molecule for stretchable, self-healing, and adhesive supramolecular polymers. *Sci. Adv.* 4:eaat8192. doi: 10.1126/sciadv.aat8192
- Zhang, Q., Tang, D., Zhang, J., Ni, R., Xu, L., He, T., et al. (2019b). Self-Healing heterometallic supramolecular polymers constructed by hierarchical assembly of triply orthogonal interactions with tunable photophysical properties. *J. Am. Chem. Soc.* 141, 17909–17917. doi: 10.1021/jacs.9b09671
- Zhao, C., Sun, Q.-F., Hart-Cooper, W. M., DiPasquale, A. G., Toste, F. D., Bergman, R. G., et al. (2013). Chiral amide directed assembly of a diastereo- and enantiopure supramolecular host and its application to enantioselective catalysis of neutral substrates. *J. Am. Chem. Soc.* 135, 18802–18805. doi: 10.1021/ja411631v
- Zheng, B., Wang, F., Dong, S., and Huang, F. (2012). Supramolecular polymers constructed by crown ether-based molecular recognition. *Chem. Soc. Rev.* 41, 1621–1636. doi: 10.1039/C1CS15220C
- Zhou, Z., Liu, J., Huang, J., Rees, T. W., Wang, Y., Wang, H., et al. (2019). A self-assembled Ru–Pt metallacage as a lysosome-targeting photosensitizer for 2-photon photodynamic therapy. *Proc. Natl. Acad. Sci. U.S.A.* 116:20296. doi: 10.1073/pnas.1912549116
- Zhou, Z., Yan, X., Cook, T. R., Saha, M. L., and Stang, P. J. (2016). Engineering functionalization in a supramolecular polymer: hierarchical self-organization of triply orthogonal non-covalent interactions on a supramolecular coordination complex platform. *J. Am. Chem. Soc.* 138, 806–809. doi: 10.1021/jacs.5b12986

**Conflict of Interest:** The authors declare that the research was conducted in the absence of any commercial or financial relationships that could be construed as a potential conflict of interest.

Copyright © 2020 Zhang, Qiu, He, Li and Yin. This is an open-access article distributed under the terms of the Creative Commons Attribution License (CC BY). The use, distribution or reproduction in other forums is permitted, provided the original author(s) and the copyright owner(s) are credited and that the original publication in this journal is cited, in accordance with accepted academic practice. No use, distribution or reproduction is permitted which does not comply with these terms.



# Coordination-Driven Poly[2]Pseudorotaxanes in Highly Polar Organic Solvent

Hang Su<sup>1,2†</sup>, Wei Chen<sup>2†</sup>, Liang Li<sup>1\*</sup>, Bin Li<sup>2</sup>, Zhi-Yuan Zhang<sup>3\*</sup> and Chunju Li<sup>2,3</sup>

<sup>1</sup> School of Chemical and Environmental Engineering, Shanghai Institute of Technology, Shanghai, China, <sup>2</sup> Department of Chemistry, Center for Supramolecular Chemistry and Catalysis, Shanghai University, Shanghai, China, <sup>3</sup> Tianjin Key Laboratory of Structure and Performance for Functional Molecules, College of Chemistry, Tianjin Normal University, Tianjin, China

## OPEN ACCESS

### Edited by:

Yong Yao,  
Nantong University, China

### Reviewed by:

Bin Hua,  
Zhejiang University, China  
Peifa Wei,  
Anhui University, China  
Lin Xu,  
East China Normal University, China  
Xiao-Yu Hu,  
Nanjing University of Aeronautics and  
Astronautics, China

### \*Correspondence:

Liang Li  
lilianglcx@sit.edu.cn  
Zhi-Yuan Zhang  
zzy@tjnu.edu.cn

<sup>†</sup>These authors have contributed  
equally to this work

### Specialty section:

This article was submitted to  
Supramolecular Chemistry,  
a section of the journal  
Frontiers in Chemistry

**Received:** 16 May 2020

**Accepted:** 04 June 2020

**Published:** 30 July 2020

### Citation:

Su H, Chen W, Li L, Li B, Zhang Z-Y  
and Li C (2020) Coordination-Driven  
Poly[2]Pseudorotaxanes in Highly  
Polar Organic Solvent.  
Front. Chem. 8:579.  
doi: 10.3389/fchem.2020.00579

Self-assembly of polypseudorotaxanes in high-polar organic solvents is difficult due to remarkably weak interactions between macrocycles and axles. Reported here is a novel metal-coordinated poly[2]pseudorotaxane constructed by pillar[5]arene, 1,4-bis(4-pyridyl pyridinium)butane, and [PdCl<sub>2</sub>(PhCN)<sub>2</sub>] in highly polar organic solvent of dimethyl sulfoxide (DMSO). Utilizing a combination of <sup>1</sup>H NMR, NOESY, DOSY, DLS, SEM, and viscosity measurements, the formation of polypseudorotaxane was shown to be dependent on the concentration of [2]pseudorotaxanes/[PdCl<sub>2</sub>(PhCN)<sub>2</sub>] and temperature. Furthermore, a temperature-responsive supramolecular gel with reversibly gel-sol transformation was obtained via spontaneous assembly of the polypseudorotaxanes at high concentrations.

**Keywords:** pillararenes, host-guest interactions, coordination polymers, polypseudorotaxanes, supramolecular chemistry

## INTRODUCTION

Over the past 20 years, supramolecular architectures of (pseudo)rotaxanes and catenanes have played a significant role in supramolecular topology and the fabrication of mechanically interlocked molecules (Loeb, 2007; Serre et al., 2007; Hunter, 2011; Lehn, 2017). Poly(pseudo)rotaxanes constructed by threading repeated macrocyclic rings onto linear-chain polymeric backbones have attracted tremendous attention for their specific and unique molecular recognition structures and diverse potential applications in various fields (Forgan et al., 2011; Du et al., 2012; Rambo et al., 2012; Rotzler and Mayor, 2013; Guo and Liu, 2014; Ma and Tian, 2014; Hou et al., 2016; Lefebvre et al., 2016; Kato et al., 2018; Hashidzume et al., 2019; Xiao et al., 2020).

Macrocycles are the basic building blocks in the construction of pseudorotaxanes because of the strong binding ability between macrocyclic hosts and guests. Therefore, there is no doubt that introducing new macrocycles and novel non-covalent interactions into polypseudorotaxanes will expand the applications of polypseudorotaxanes. Furthermore, variations in supramolecular structures allow them to show unique responsivity to stimuli. Pillar[n]arenes, the fifth generation of host macrocycles, have been applied to the formation of various functional supramolecular materials, owing to their rigid pillar architecture, easy functionalization, and outstanding binding properties in host-guest chemistry (Cao et al., 2009; Xue et al., 2012; Li, 2014; Ogoshi et al., 2016; Li et al., 2017; Hua et al., 2018, 2019; Chen et al., 2019; Xia et al., 2019; Shao et al., 2020; Wang et al., 2020). To date, a variety of supramolecular poly(pseudo)rotaxanes based on pillar[n]arenes have been investigated (Hu et al., 2012; Eichstaedt et al., 2016; Cui et al., 2017; Zeng et al., 2018; Li B. et al., 2019; Yang et al., 2019).

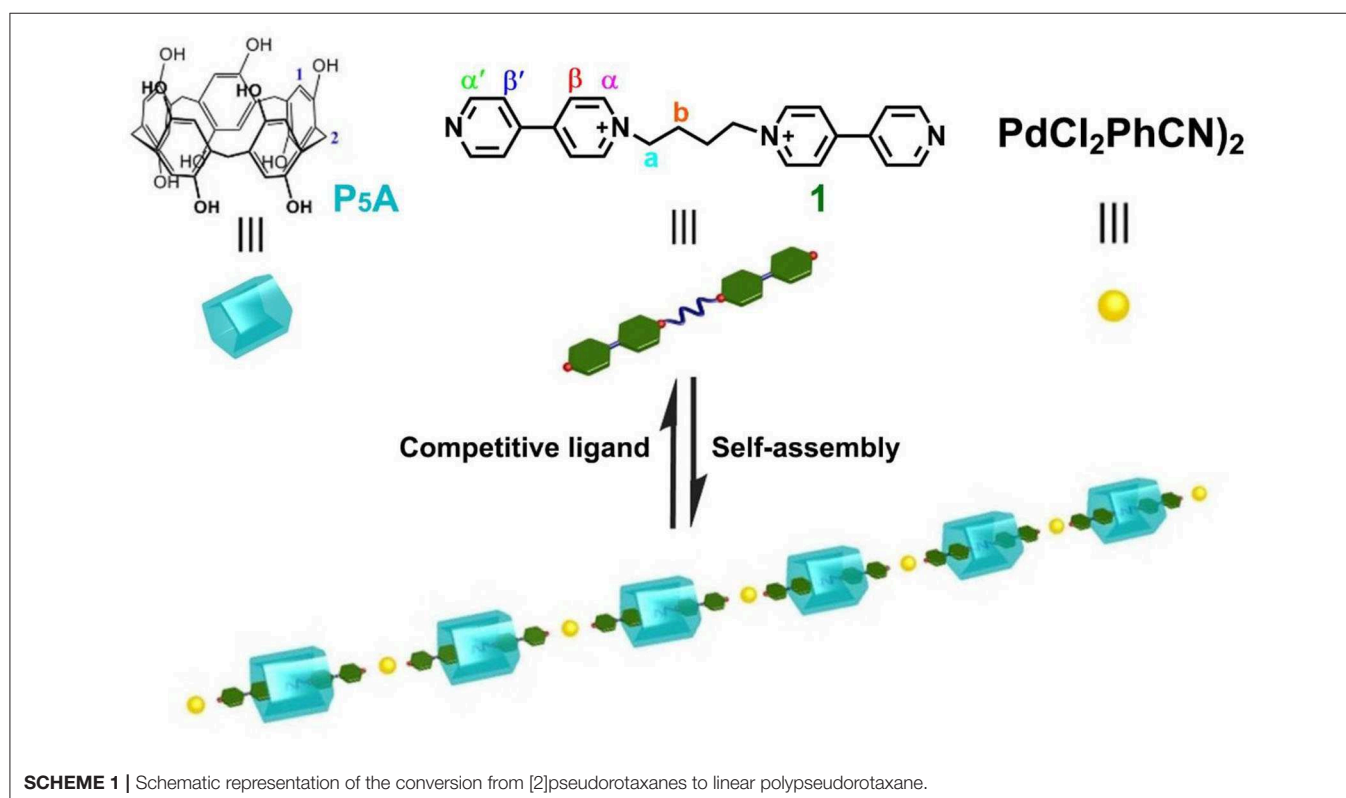
Metal coordination interactions, as a class of non-covalent interactions possessing remarkable stability and unique properties, can be used to effectively and conveniently generate polypseudorotaxane (Lee et al., 2001; Liu et al., 2003; Harada et al., 2009; Wei et al., 2014; Yan et al., 2014; Krogsgaard et al., 2016; Tian et al., 2016; Winter and Schubert, 2016; Wu et al., 2016; Huang et al., 2017; Wang et al., 2018 Xia et al., 2018; Wang L. et al., 2019; Zhu et al., 2019). However, most of the (poly)rotaxanes and (poly)pseudorotaxanes are constructed in water, low polar organic solvents, or the crystalline state. Highly polar organic solvent such as dimethyl sulfoxide (DMSO) seems to be not working because, generally, the non-covalent interactions between the wheels and axles, which greatly depend on the sorts and polarity of solvents, are quite weak in DMSO. Aqueous solution and low polar organic solvents can maintain these non-covalent interactions well. But highly polar solvents such as DMSO inhibit non-covalent bonds involving hydrogen bonding and complementary  $\pi\cdots\pi$ -stacking, through powerful solvation of the interacting components.

In the past 10 years, our group focused on the host-guest chemistry of pillararenes and biphenarenes (Li, 2014; Ma et al., 2016; Li H. et al., 2019; Wang Y. et al., 2019; Xu et al., 2020). The association constant,  $(7.4 \pm 0.3) \times 10^2 \text{ M}^{-1}$ , of **P<sub>5</sub>A** and bis(pyridinium)dicationic guest **1** in DMSO is surprisingly high, leading to the formation of a [2]pseudorotaxane-type complex (Li et al., 2010). Herein, to provide new insight into supramolecular polypseudorotaxanes in highly polar solvents, we extended

our research target to novel **P<sub>5</sub>A**-based polypseudorotaxane bridging by palladium(II)-containing coordination interactions [ $\text{PdCl}_2(\text{PhCN})_2$ ]. Therefore, a linear polypseudorotaxane was constructed by [2]pseudorotaxanes making up of **P<sub>5</sub>A** and bis(pyridinium)dicationic (**1**) via metal-coordination interactions in DMSO (**Scheme 1**). It was expected that the utilization of **P<sub>5</sub>A**-based [2]pseudorotaxanes and metal-ligand coordination would be quite suitable for fabricating polymeric assemblies in highly polar solvents due to their robust interactions. Interestingly, the obtained polypseudorotaxane could continuously self-assemble at higher concentrations to form a dynamic supramolecular gel, which responded to environmental stimuli.

## MATERIALS AND METHODS

All reagents and solvents were commercially available and used without further purification, unless otherwise noted. Compound (**P<sub>5</sub>A**) (Ogoshi et al., 2008; Cao et al., 2009) and bis(pyridinium)dicationic **1** (Joseph et al., 2003; Li et al., 2010) were synthesized according to literature procedures.  $^1\text{H}$  NMR and DOSY spectra were recorded on a Bruker AV500 instrument. Viscosity measurements were carried out with Ubbelohde micro dilution viscometers (Shanghai Liangjing Glass Instrument Factory, 0.40 mm inner diameter) at 298 K in DMSO. Dynamic light scattering (DLS) was analyzed on a Malvern Zetasizer 3000HSA at 298 K. Scanning electron microscopy (SEM) images were recorded on SHIMADZU SSX-550.

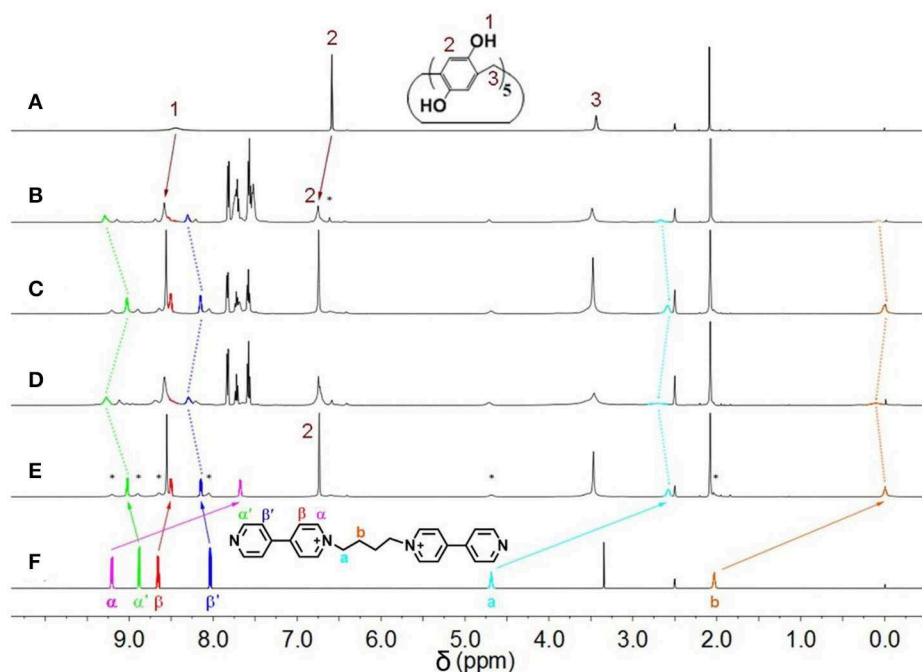


## RESULTS AND DISCUSSION

Initially, host–guest complexation of **P<sub>5</sub>A** and **1** was carried out in DMSO-*d*<sub>6</sub> and investigated through <sup>1</sup>H NMR spectroscopy. As shown in **Figures 1A,E,F**, the <sup>1</sup>H NMR spectra of **1** were recorded in the absence and presence of the **P<sub>5</sub>A** host, where evident upfield chemical shifts and a broadening effect inside the pyridine motif and methylene protons (H<sub>a</sub>, H<sub>b</sub>, H<sub>α</sub>, and H<sub>β</sub>) on guest **1** could be observed in the presence of **P<sub>5</sub>A** owing to the shielding effects in the cavity, while no apparent change was observed in the proton signals of H<sub>α'</sub> and H<sub>β'</sub> on guest **1**. When comparing to the corresponding signals of the uncomplexed **P<sub>5</sub>A** and **1**, new peaks were observed, demonstrating a slow exchange on the NMR timescale for this binding process. The results are in agreement with the spatial structure that the host **P<sub>5</sub>A** as a wheel was fully threaded by the axle of guest **1** and left pyridine moiety outside its cavity, indicating the formation of a [2]pseudorotaxane between **P<sub>5</sub>A** and **1** in DMSO (**Scheme 1**). Besides, distinct NOE correlation signals between the protons H<sub>a</sub>, H<sub>b</sub>, and H<sub>α</sub> on **1** and H<sub>1–3</sub> on **P<sub>5</sub>A** in a 2D NOESY spectrum further confirmed the formation of the [2]pseudorotaxanes (**Supplementary Figure 1**). As shown in the energy-minimized structure of the [2]pseudorotaxanes calculated by DFT (Materials Studio), multiple hydrogen bonding and C–H...π interactions between **P<sub>5</sub>A** and **1** provided enough non-covalent interactions and guaranteed the existence of [2]pseudorotaxanes in DMSO. And the pyridine moiety on **1** was located outside the cavity of

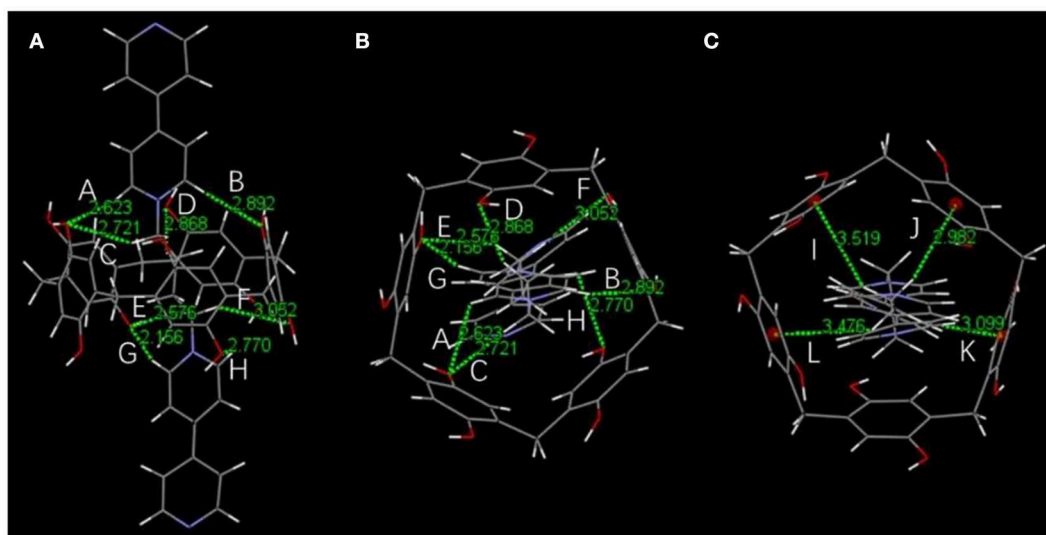
**P<sub>5</sub>A**, which reserved indispensable sites for the coordination of metal (**Figure 2**).

Subsequently, after dissolving 1.0 equiv of [PdCl<sub>2</sub>(PhCN)<sub>2</sub>] into 60 mM premixed solution of **P<sub>5</sub>A** and **1**, all of the main peaks broadened remarkably, and the signals of H<sub>α'</sub> and H<sub>β'</sub> on guest **1** clearly shifted downfield (**Figure 1D**). These observations provided clear evidence of the complexation between pyridine nitrogen atoms and palladium(II) ligands. Furthermore, binding stoichiometry between [PdCl<sub>2</sub>(PhCN)<sub>2</sub>] and **1** was investigated. To a mixture of **1** and **P<sub>5</sub>A** ([**1**]: [**P<sub>5</sub>A**] = 1:5) in DMSO-*d*<sub>6</sub>, [PdCl<sub>2</sub>(PhCN)<sub>2</sub>] was added in different ratios and <sup>1</sup>H NMR spectra were recorded. As shown in **Supplementary Figure 2**, upon increasing [PdCl<sub>2</sub>(PhCN)<sub>2</sub>], both the proton signals of H<sub>α'</sub> and H<sub>β'</sub> on the pyridine rings of **1** shifted downfield significantly, suggesting the coordination of metal to the pyridine rings. No obvious change was observed for the signals of H<sub>α'</sub> and H<sub>β'</sub> when the molar ratio of [**1**]: [PdCl<sub>2</sub>(PhCN)<sub>2</sub>] was increased to 1:1, indicating that the binding ratio between [PdCl<sub>2</sub>(PhCN)<sub>2</sub>] and **1** was 1:1 or n:n, which fitted well with the coordination characteristics between pyridine and [PdCl<sub>2</sub>(PhCN)<sub>2</sub>] (Kaminker et al., 2011). The 255 nm of the hydrodynamic radius measured by dynamic light scattering (DLS) manifested the formation of large aggregates, which excluded the 1:1 mode and confirmed that the binding ratio was n:n. The small amount of specie in several nanometers was deduced as unreacted [2]pseudorotaxanes (**Figure 3**). These results verified the formation of metal supramolecular polypseudorotaxane between [PdCl<sub>2</sub>(PhCN)<sub>2</sub>] and [2]pseudorotaxane.

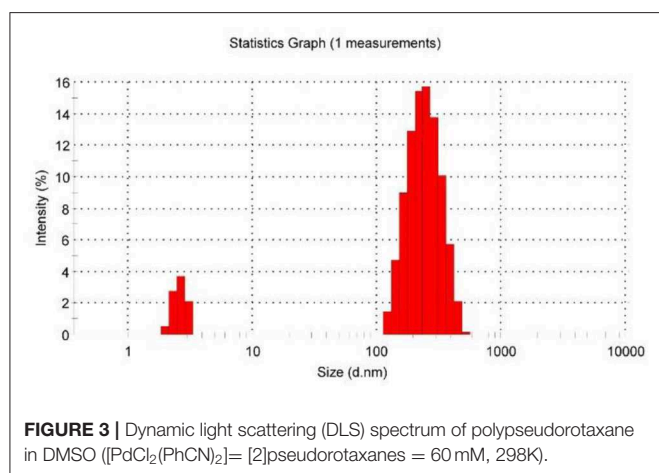


**FIGURE 1** | <sup>1</sup>H NMR spectra (DMSO-*d*<sub>6</sub>, 298 K, 500 MHz) of polypseudorotaxane and building units. (A) **P<sub>5</sub>A**; (B) **P<sub>5</sub>A** + **1** + [PdCl<sub>2</sub>(PhCN)<sub>2</sub>] + PPh<sub>3</sub> + [PdCl<sub>2</sub>(PhCN)<sub>2</sub>]; (C) **P<sub>5</sub>A** + **1** + [PdCl<sub>2</sub>(PhCN)<sub>2</sub>] + PPh<sub>3</sub>; (D) **P<sub>5</sub>A** + **1** + [PdCl<sub>2</sub>(PhCN)<sub>2</sub>]; (E) **P<sub>5</sub>A** + **1**; (F) **1**. ([**P<sub>5</sub>A**] = [**1**] = [PdCl<sub>2</sub>(PhCN)<sub>2</sub>] = 60.0 mM; \*represent uncomplexed **P<sub>5</sub>A** and free **1**).





**FIGURE 2 |** The energy-minimized structure of [2]pseudorotaxanes calculated by DFT (Materials Studio). The green dashed lines represent hydrogen bond interactions (A–H) and C–H... $\pi$  interactions (I–L). **(A)** Front view and **(B)** top view of hydrogen bond parameters: H...O distance (Å), C(O)–H...O angle ( $^{\circ}$ ) A: 2.623, 122.75; B: 2.892, 169.46; C: 2.721, 147.14; D: 2.868, 144.38; E: 2.576, 144.90; F: 3.052, 148.60; G: 2.156, 161.67; H: 2.770, 101.37. **(C)** Top view of C–H... $\pi$  interaction parameters: C–H... $\pi$  distance (Å), C–H... $\pi$  angle ( $^{\circ}$ ) I: 3.519, 138.60; J: 2.982, 156.63; K: 3.099, 142.02; L: 3.476, 133.24.



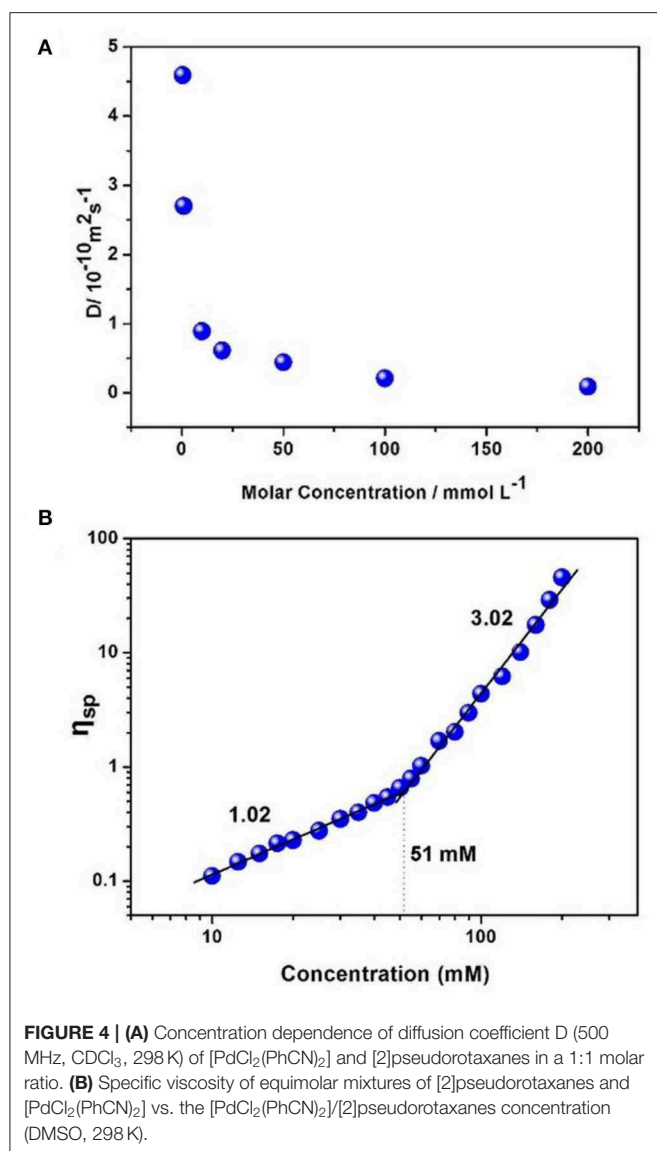
**FIGURE 3 |** Dynamic light scattering (DLS) spectrum of polypseudorotaxane in DMSO ([PdCl<sub>2</sub>(PhCN)<sub>2</sub>] = [2]pseudorotaxanes = 60 mM, 298 K).

Furthermore, the competitive ligand PPh<sub>3</sub> was employed to bind palladium(II) ions to investigate the phase transition between polypseudorotaxane and [2]pseudorotaxane. Upon adding **1** equiv of PPh<sub>3</sub> to the polypseudorotaxane, a precipitate formed at the bottom of the mixed system solution. As shown in **Figure 1C**, the <sup>1</sup>H NMR spectrum was almost the same with the spectrum of [2]pseudorotaxane (**Figure 1E**), which indicated the formation of the more stable complex between PPh<sub>3</sub> and palladium(II) ions, resulting in the disassembly of the polypseudorotaxane (Wang et al., 2010). After filtrating off the precipitate, one equiv of [PdCl<sub>2</sub>(PhCN)<sub>2</sub>] was added to the solution, and the peaks of protons on guest **1** returned to their original positions (**Figure 1B**). This result suggested that metallosupramolecular polypseudorotaxane was reconstructed. Therefore, the reversible transition between polypseudorotaxane and [2]pseudorotaxane can be realized.

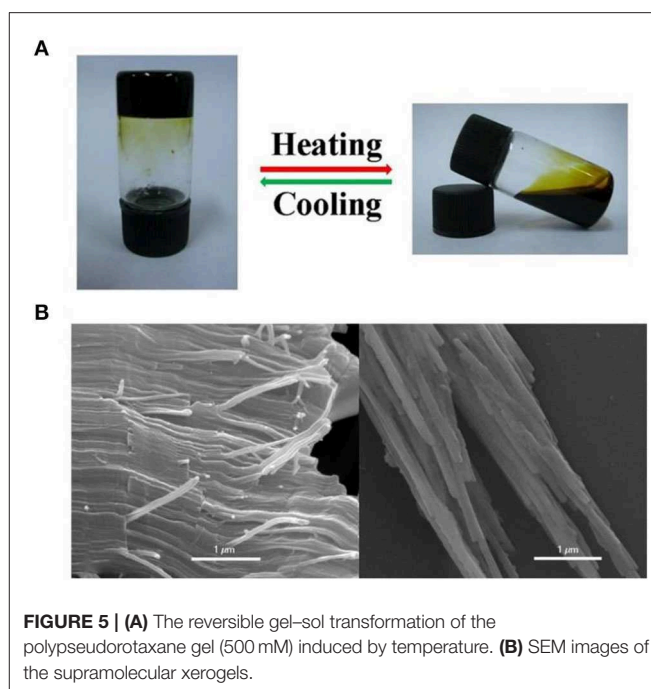
Two-dimensional diffusion-ordered NMR experiments (DOSY) were adopted to explore the polypseudorotaxane. When the concentration of [2]pseudorotaxane/[PdCl<sub>2</sub>(PhCN)<sub>2</sub>] increased from 0.5 to 200 mM, the weight average diffusion coefficient (*D*) decreased significantly from  $4.59 \times 10^{-10}$  to  $0.88 \times 10^{-11} \text{ m}^2 \text{ s}^{-1}$ , suggesting an increase in the average size of the polymeric structure owing to the generation of polypseudorotaxane from the small oligomers (**Figure 4A**).

Viscosity is a characteristic property index for metallosupramolecular polypseudorotaxane. Therefore, viscosity measurements of an equimolar mixture of [2]pseudorotaxanes and [PdCl<sub>2</sub>(PhCN)<sub>2</sub>] were carried out in DMSO at 298 K. A double-logarithmic plot of specific viscosity vs. the initial concentrations of [2]pseudorotaxanes is shown in **Figure 4B**. The slopes of the curves in the low-concentration region tended to 1 (1.02 for [PdCl<sub>2</sub>(PhCN)<sub>2</sub>]/[2]pseudorotaxanes), implying that no linear polypseudorotaxane formed (Söntjens et al., 2001; Xiao et al., 2012). When the concentrations of the mixture of [2]pseudorotaxanes and [PdCl<sub>2</sub>(PhCN)<sub>2</sub>] increased above the critical polymerization concentration (CPC, approximately 51 mM), a sharp increase in the viscosity was obtained (slope = 3.02), which indicated the formation of linear polypseudorotaxane resulting from strong interactions between [2]pseudorotaxanes and [PdCl<sub>2</sub>(PhCN)<sub>2</sub>] (Söntjens et al., 2001; Xiao et al., 2012). This result is also in agreement with the above NMR experiments.

Interestingly, when the concentration exceeded 500 mM, a cross-linked supramolecular gel was observed. That was, upon increasing the concentration of [2]pseudorotaxane and [PdCl<sub>2</sub>(PhCN)<sub>2</sub>], metallosupramolecular polypseudorotaxane transformed into a supramolecular gel. Notably, the metal-coordinated polypseudorotaxane gel was sensitive to temperature



and could transform into sol reversibly by heating to 60°C and cooling to room temperature (25°C) (Figure 5A). A possible reason for the reversible gel–sol transition is reversible entanglement among linear polypseudorotaxane and the coordination interaction between [2]pseudorotaxane and [PdCl<sub>2</sub>(PhCN)<sub>2</sub>]. Heating decreased that interaction and decomposed the polypseudorotaxane, and therefore, gel changed to sol. However, upon cooling, the intermolecular entanglement restored, resulting in the recovery of the supramolecular gel. The morphology of polypseudorotaxane xerogels prepared by freeze-drying was investigated by scanning electron microscopy (SEM). Regular long and fine fiber structures were observed, and the diameter was determined to be 0.2–0.3 μm (Figure 5B). These observations provided further proof that the metallosupramolecular gel was constructed by polypseudorotaxane fibers resulting from [2]pseudorotaxanes and bridging palladium(II).



## CONCLUSIONS

In summary, a novel metallosupramolecular polypseudorotaxane was successfully fabricated from pillar[5]arene-based [2]pseudorotaxanes and [PdCl<sub>2</sub>(PhCN)<sub>2</sub>] in a highly polar solvent of DMSO, which was comprehensively confirmed by various techniques, such as <sup>1</sup>H NMR, NOESY, DOSY, DLS, Viscometry, and SEM. The formation of polypseudorotaxane was shown to be dependent on the concentration of [2]pseudorotaxanes/[PdCl<sub>2</sub>(PhCN)<sub>2</sub>] and temperature. Moreover, the reversal transition between polypseudorotaxane and [2]pseudorotaxanes can be realized by the successive addition of metal linker [PdCl<sub>2</sub>(PhCN)<sub>2</sub>] and competitive ligand PPh<sub>3</sub>. Significantly, the metal polypseudorotaxane could transform into supramolecular gel when the concentration was above 500 mM, which showed reversibly temperature-induced gel–sol transformation. This study provides a new insight into the construction of macrocycles-based polypseudorotaxane in highly polar organic solvent and benefits to the fabrication of smart materials.

## DATA AVAILABILITY STATEMENT

The raw data supporting the conclusions of this article will be made available by the authors, without undue reservation.

## AUTHOR CONTRIBUTIONS

CL, BL, and LL conceived of this project and designed the experiments. HS and WC contributed to most of the experimental work. All authors analyzed the data. CL, WC, and Z-YZ co-wrote the paper. All authors discussed and commented on the paper.

## FUNDING

This work was supported by the National Natural Science Foundation of China (21772118 and 21971192).

## REFERENCES

- Cao, D., Kou, Y., Liang, J., Chen, Z., Wang, L., and Meier, H. (2009). A facile and efficient preparation of pillararenes and a pillarquinone. *Angew. Chem. Int. Ed.* 48, 9721–9723. doi: 10.1002/anie.200904765
- Chen, J., Ni, H., Meng, Z., Wang, J., Huang, X., Dong, Y., et al. (2019). Supramolecular trap for catching polyamines in cells as an anti-tumor strategy. *Nat. Commun.* 10:3546. doi: 10.1038/s41467-019-11553-7
- Cui, W., Tang, H., Xu, L., Wang, L., Meier, H., and Cao, D. (2017). Pillar[5]arene-diketopyrrolopyrrole fluorescent copolymer: a promising recognition and adsorption material for adiponitrile by selective formation of a conjugated polypseudorotaxane. *Macromol. Rapid Commun.* 38:1700161. doi: 10.1002/marc.201700161
- Du, G., Moulin, E., Jouault, N., Buhler, E., and Giuseppone, N. (2012). Muscle-like supramolecular polymers: integrated motion from thousands of molecular machines. *Angew. Chem. Int. Ed.* 51, 12504–12508. doi: 10.1002/anie.201206571
- Eichstaedt, K., Wicher, B., Gdaniec, M., and Polonski, T. (2016). Halogen bonded polypseudorotaxanes based on a pillar[5]arene host. *Cryst. Eng. Comm.* 18, 5807–5810. doi: 10.1039/C6CE01416J
- Forgan, R. S., Sauvage, J.-P., and Stoddart, J. F. (2011). Chemical topology: complex molecular knots, links, and entanglements. *Chem. Rev.* 111, 5434–5464. doi: 10.1021/cr200034u
- Guo, D.-S., and Liu, Y. (2014). Supramolecular chemistry of p-sulfonatocalix[n]arenes and its biological applications. *Acc. Chem. Res.* 47, 1925–1934. doi: 10.1021/ar500009g
- Harada, A., Hashidzume, A., Yamaguchi, H., and Takashima, Y. (2009). Polymeric rotaxanes. *Chem. Rev.* 109, 5974–6023. doi: 10.1021/cr9000622
- Hashidzume, A., Yamaguchi, H., and Harada, A. (2019). Cyclodextrin-based rotaxanes: from rotaxanes to polyrotaxanes and further to functional materials. *Eur. J. Org. Chem.* 2019, 3344–3357. doi: 10.1002/ejoc.201900090
- Hou, X., Ke, C., and Fraser Stoddart, J. (2016). Cooperative capture synthesis: yet another playground for copper-free click chemistry. *Chem. Soc. Rev.* 45, 3766–3780. doi: 10.1039/C6CS00055J
- Hu, X.-Y., Wu, X., Duan, Q., Xiao, T., Lin, C., and Wang, L. (2012). Novel Pillar[5]arene-based dynamic polyrotaxanes interlocked by the quadruple hydrogen bonding ureidopyrimidinone motif. *Org. Lett.* 14, 4826–4829. doi: 10.1021/ol302149t
- Hua, B., Shao, L., Zhang, Z., Liu, J., and Huang, F. (2019). Cooperative silver ion-pair recognition by peralkylated pillar[5]arenes. *J. Am. Chem. Soc.* 141, 15008–15012. doi: 10.1021/jacs.9b08257
- Hua, B., Zhou, W., Yang, Z., Zhang, Z., Shao, L., Zhu, H., et al. (2018). Supramolecular solid-state microlaser constructed from pillar[5]arene-based host–guest complex microcrystals. *J. Am. Chem. Soc.* 140, 15651–15654. doi: 10.1021/jacs.8b11156
- Huang, C.-B., Xu, L., Zhu, J.-L., Wang, Y.-X., Sun, B., Li, X., et al. (2017). Real-time monitoring the dynamics of coordination-driven self-assembly by fluorescence-resonance energy transfer. *J. Am. Chem. Soc.* 139, 9459–9462. doi: 10.1021/jacs.7b04659
- Hunter, C. (2011). Bigger and better synthesis. *Nature* 469, 39–41. doi: 10.1038/469039a
- Joseph, J., Eldho, N. V., and Ramaiah, D. (2003). Design of photoactivated DNA oxidizing agents: synthesis and study of photophysical properties and DNA interactions of novel viologen-linked acridines. *Chem. Eur. J.* 9, 5926–5935. doi: 10.1002/chem.200304936
- Kaminker, R., Popovitz-Biro, R., and van der Boom, M. E. (2011). Coordination-polymer nanotubes and spheres: a ligand-structure effect. *Angew. Chem. Int. Ed.* 50, 3224–3226. doi: 10.1002/anie.201008193
- Kato, K., Hori, A., and Ito, K. (2018). An efficient synthesis of low-covered polyrotaxanes grafted with poly( $\epsilon$ -caprolactone) and the mechanical properties of its cross-linked elastomers. *Polymer* 147, 67–73. doi: 10.1016/j.polymer.2018.05.072
- Krogsgaard, M., Nue, V., and Birkedal, H. (2016). Mussel-inspired materials: self-healing through coordination chemistry. *Chem. Eur. J.* 22, 844–857. doi: 10.1002/chem.201503380
- Lee, E., Kim, J., Heo, J., Whang, D., and Kim, K. (2001). A two-dimensional polyrotaxane with large cavities and channels: a novel approach to metal–organic open-frameworks by using supramolecular building blocks. *Angew. Chem. Int. Ed.* 40, 399–402. doi: 10.1002/1521-3773(20010119)40:2<399::aid-anie399>3.0.co;2-w
- Lefebvre, H., Bheda, M., and Gibson, H. W. (2016). Main chain polyamide rotaxanes from aliphatic crown ethers. *Polymer* 90, 317–330. doi: 10.1016/j.polymer.2016.02.048
- Lehn, J.-M. (2017). Supramolecular chemistry: where from? Where to? *Chem. Soc. Rev.* 46, 2378–2379. doi: 10.1039/C7CS00115K
- Li, B., Meng, Z., Li, Q., Huang, X., Kang, Z., Dong, H., et al. (2017). A pH responsive complexation-based drug delivery system for oxaliplatin. *Chem. Sci.* 8, 4458–4464. doi: 10.1039/C7SC01438D
- Li, B., Wang, B., Huang, X., Dai, L., Cui, L., Li, J., et al. (2019). Terphen[n]arenes and quaterphen[n]arenes (n=3–6): one-pot synthesis, self-assembly into supramolecular gels, and iodine capture. *Angew. Chem. Int. Ed.* 58, 3885–3889. doi: 10.1002/anie.201813972
- Li, C. (2014). Pillararene-based supramolecular polymers: from molecular recognition to polymeric aggregates. *Chem. Commun.* 50, 12420–12433. doi: 10.1039/C4CC03170A
- Li, C., Xu, Q., Li, J., Feina, Y., and Jia, X. (2010). Complex interactions of pillar[5]arene with paraquats and bis(pyridinium) derivatives. *Org. Biomol. Chem.* 8, 1568–1576. doi: 10.1039/b920146g
- Li, H., Yang, Y., Xu, F., Liang, T., Wen, H., and Tian, W. (2019). Pillararene-based supramolecular polymers. *Chem. Commun.* 55, 271–285. doi: 10.1039/C8CC08085B
- Liu, Y., Zhao, Y.-L., Zhang, H.-Y., and Song, H.-B. (2003). Polymeric rotaxane constructed from the inclusion complex of  $\beta$ -cyclodextrin and 4,4'-dipyridine by coordination with nickel(II) ions. *Angew. Chem. Int. Ed.* 42, 3260–3263. doi: 10.1002/anie.200351128
- Loeb, S. J. (2007). Rotaxanes as ligands: from molecules to materials. *Chem. Soc. Rev.* 36, 226–235. doi: 10.1039/B605172N
- Ma, J., Meng, Q., Hu, X., Li, B., Ma, S., Hu, B., et al. (2016). Synthesis of a water-soluble carboxylatobiphenyl[4]arene and its selective complexation toward acetylcholine. *Org. Lett.* 18, 5740–5743. doi: 10.1021/acs.orglett.6b03005
- Ma, X., and Tian, H. (2014). Stimuli-responsive supramolecular polymers in aqueous solution. *Acc. Chem. Res.* 47, 1971–1981. doi: 10.1021/ar500033n
- Ogoshi, T., Kanai, S., Fujinami, S., Yamagishi, T.-A., and Nakamoto, Y. (2008). Para-bridged symmetrical pillar[5]arenes: their lewis acid catalyzed synthesis and host–guest property. *J. Am. Chem. Soc.* 130, 5022–5023. doi: 10.1021/ja711260m
- Ogoshi, T., Yamagishi, T.-A., and Nakamoto, Y. (2016). Pillar-shaped macrocyclic hosts pillar[n]arenes: new key players for supramolecular chemistry. *Chem. Rev.* 116, 7937–8002. doi: 10.1021/acs.chemrev.5b00765
- Rambo, B. M., Gong, H.-Y., Oh, M., and Sessler, J. L. (2012). The “texas-sized” molecular box: a versatile building block for the construction of anion-directed mechanically interlocked structures. *Acc. Chem. Res.* 45, 1390–1401. doi: 10.1021/ar300076b
- Rotzler, J., and Mayor, M. (2013). Molecular daisy chains. *Chem. Soc. Rev.* 42, 44–62. doi: 10.1039/C2CS35217F
- Serrelli, V., Lee, C.-F., Kay, E. R., and Leigh, D. A. (2007). A molecular information ratchet. *Nature* 445, 523–527. doi: 10.1038/nature05452

## SUPPLEMENTARY MATERIAL

The Supplementary Material for this article can be found online at: <https://www.frontiersin.org/articles/10.3389/fchem.2020.00579/full#supplementary-material>

- Shao, L., Hua, B., Hu, X., Stalla, D., Kelley, S. P., and Atwood, J. L. (2020). Construction of polymeric metal-organic nanocapsule networks via supramolecular coordination-driven self-assembly. *J. Am. Chem. Soc.* 142, 7270–7275. doi: 10.1021/jacs.0c00640
- Söntjens, S. H. M., Sijbesma, R. P., van Genderen, M. H. P., and Meijer, E. W. (2001). Selective formation of cyclic dimers in solutions of reversible supramolecular polymers. *Macromolecules* 34, 3815–3818. doi: 10.1021/ma002010q
- Tian, J., Xu, Z.-Y., Zhang, D.-W., Wang, H., Xie, S.-H., Xu, D.-W., et al. (2016). Supramolecular metal-organic frameworks that display high homogeneous and heterogeneous photocatalytic activity for H<sub>2</sub> production. *Nat. Commun.* 7:11580. doi: 10.1038/ncomms11580
- Wang, F., Zhang, J., Ding, X., Dong, S., Liu, M., Zheng, B., et al. (2010). Metal coordination mediated reversible conversion between linear and cross-linked supramolecular polymers. *Angew. Chem. Int. Ed.* 49, 1090–1094. doi: 10.1002/anie.200906389
- Wang, L., Xia, D., Chao, J., Zhang, J., Wei, X., and Wang, P. (2019). A dimethoxypillar[5]arene/azastilbene host-guest recognition motif and its applications in the fabrication of polypseudorotaxanes. *Org. Biomol. Chem.* 17, 6038–6042. doi: 10.1039/C9OB00862D
- Wang, P., Wang, R., and Xia, D. (2020). pH-induced transition between single-chain macrocyclic amphiphile and [c<sub>2</sub>]daisy chain-based bola-type amphiphile and the related self-assembly behavior in water. *Front. Chem.* 7:894. doi: 10.3389/fchem.2019.00894
- Wang, X.-Q., Wang, W., Li, W.-J., Chen, L.-J., Yao, R., Yin, G.-Q., et al. (2018). Dual stimuli-responsive rotaxane-branched dendrimers with reversible dimension modulation. *Nat. Commun.* 9, 3190. doi: 10.1038/s41467-018-05670-y
- Wang, Y., Xu, K., Li, B., Cui, L., Li, J., Jia, X., et al. (2019). Efficient separation of cis- and trans-1,2-dichloroethene isomers by adaptive biphen[3]arene crystals. *Angew. Chem. Int. Ed.* 58, 10281–10284. doi: 10.1002/anie.201905563
- Wei, P., Li, J., Yan, X., and Zhou, Q. (2014). Metallosupramolecular poly[2]pseudorotaxane constructed by metal coordination and crown-ether-based molecular recognition. *Org. Lett.* 16, 126–129. doi: 10.1021/ol403111e
- Winter, A., and Schubert, U. S. (2016). Synthesis and characterization of metallo-supramolecular polymers. *Chem. Soc. Rev.* 45, 5311–5357. doi: 10.1039/C6CS00182C
- Wu, X., Yu, Y., Gao, L., Hu, X.-Y., and Wang, L. (2016). Stimuli-responsive supramolecular gel constructed by pillar[5]arene-based pseudo[2]rotaxanes via orthogonal metal-ligand coordination and hydrogen bonding interaction. *Org. Chem. Front.* 3, 966–970. doi: 10.1039/C6QO00197A
- Xia, D., Lv, X., Chen, K., and Wang, P. (2019). A [2]pseudorotaxane based on a pillar[6]arene and its application in the construction of a metallosupramolecular polymer. *Dalton. Trans.* 48, 9954–9958. doi: 10.1039/C9DT01713E
- Xia, D., Wang, L., Lv, X., Chao, J., Wei, X., and Wang, P. (2018). Dual-responsive [2]pseudorotaxane on the basis of a pH-sensitive pillar[5]arene and its application in the fabrication of metallosupramolecular polypseudorotaxane. *Macromolecules* 51, 2716–2722. doi: 10.1021/acs.macromol.8b00354
- Xiao, T., Li, S.-L., Zhang, Y., Lin, C., Hu, B., Guan, X., et al. (2012). Novel self-assembled dynamic [2]catenanes interlocked by the quadruple hydrogen bonding ureidopyrimidinone motif. *Chem. Sci.* 3, 1417–1421. doi: 10.1039/c2sc01004f
- Xiao, T., Zhou, L., Sun, X.-Q., Huang, F., Lin, C., and Wang, L. (2020). Supramolecular polymers fabricated by orthogonal self-assembly based on multiple hydrogen bonding and macrocyclic host-guest interactions. *Chin. Chem. Lett.* 31, 1–9. doi: 10.1016/j.cclet.2019.05.011
- Xu, K., Zhang, Z.-Y., Yu, C., Wang, B., Dong, M., Zeng, X., et al. (2020). A modular synthetic strategy for functional macrocycles. *Angew. Chem. Int. Ed.* 59, 7214–7218. doi: 10.1002/anie.202000909
- Xue, M., Yang, Y., Chi, X., Zhang, Z., and Huang, F. (2012). Pillararenes, a new class of macrocycles for supramolecular chemistry. *Acc. Chem. Res.* 45, 1294–1308. doi: 10.1021/ar2003418
- Yan, X., Xu, J.-F., Cook, T. R., Huang, F., Yang, Q.-Z., Tung, C.-H., et al. (2014). Photoinduced transformations of stiff-stilbene-based discrete metallacycles to metallosupramolecular polymers. *Proc. Natl. Acad. Sci. U.S.A.* 111, 8717–8722. doi: 10.1073/pnas.1408620111
- Yang, K., Chao, S., Zhang, F., Pei, Y., and Pei, Z. (2019). Recent advances in the development of rotaxanes and pseudorotaxanes based on pillar[n]arenes: from construction to application. *Chem. Commun.* 55, 13198–13210. doi: 10.1039/C9CC07373F
- Zeng, X., Deng, H., Jia, X., Cui, L., Li, J., Li, C., et al. (2018). Construction of [2]rotaxane-based supramolecular polymers driven by wheel-stopper  $\pi \dots \pi$  interactions. *Chem. Commun.* 54, 11634–11637. doi: 10.1039/C8CC07188H
- Zhu, J., Liu, X., Huang, J., and Xu, L. (2019). Our expedition in the construction of fluorescent supramolecular metallacycles. *Chin. Chem. Lett.* 30, 1767–1774. doi: 10.1016/j.cclet.2019.08.027

**Conflict of Interest:** The authors declare that the research was conducted in the absence of any commercial or financial relationships that could be construed as a potential conflict of interest.

Copyright © 2020 Su, Chen, Li, Li, Zhang and Li. This is an open-access article distributed under the terms of the Creative Commons Attribution License (CC BY). The use, distribution or reproduction in other forums is permitted, provided the original author(s) and the copyright owner(s) are credited and that the original publication in this journal is cited, in accordance with accepted academic practice. No use, distribution or reproduction is permitted which does not comply with these terms.





# Use of $\alpha$ -cyclodextrin to Promote Clean and Environmentally Friendly Disinfection of Phenolic Substrates via Chlorine Dioxide Treatment

Sauradip Chaudhuri<sup>1</sup>, Dana J. DiScenza<sup>2</sup>, Thomas B. Boving<sup>3</sup>, Alan Burke<sup>4</sup> and Mindy Levine<sup>5\*</sup>

<sup>1</sup> McGovern Medical School, University of Texas Health Science Center at Houston, Houston, TX, United States,

<sup>2</sup> Department of Chemistry, University of Virginia, Charlottesville, VA, United States, <sup>3</sup> Department of Geosciences/Department of Civil and Environmental Engineering, University of Rhode Island, Kingston, RI, United States, <sup>4</sup> Independent Researcher, North Kingstown, RI, United States, <sup>5</sup> Department of Chemical Sciences, Ariel University, Ariel, Israel

## OPEN ACCESS

### Edited by:

Yong Yao,  
Nantong University, China

### Reviewed by:

Yang Wang,  
Nantong University, China  
Chao-Guo Yan,  
Yangzhou University, China  
Ruibing Wang,  
University of Macau, China

### \*Correspondence:

Mindy Levine  
mindy.levine@gmail.com

### Specialty section:

This article was submitted to  
Supramolecular Chemistry,  
a section of the journal  
Frontiers in Chemistry

**Received:** 04 May 2020

**Accepted:** 22 June 2020

**Published:** 31 July 2020

### Citation:

Chaudhuri S, DiScenza DJ,  
Boving TB, Burke A and Levine M  
(2020) Use of  $\alpha$ -cyclodextrin to  
Promote Clean and Environmentally  
Friendly Disinfection of Phenolic  
Substrates via Chlorine Dioxide  
Treatment. *Front. Chem.* 8:641.  
doi: 10.3389/fchem.2020.00641

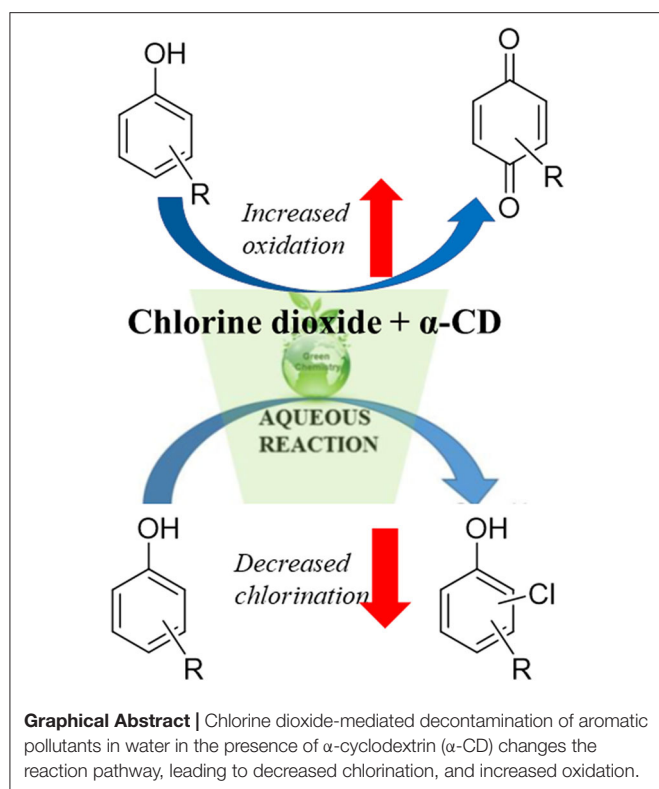
The use of chlorine dioxide to disinfect drinking water and ameliorate toxic components of wastewater has significant advantages in terms of providing safe water. Nonetheless, significant drawbacks toward such usage remain. These drawbacks include the fact that toxic byproducts of the disinfection agents are often formed, and the complete removal of such agents can be challenging. Reported herein is one approach to solving this problem: the use of  $\alpha$ -cyclodextrin to affect the product distribution in chlorine dioxide-mediated decomposition of organic pollutants. The presence of  $\alpha$ -cyclodextrin leads to markedly more oxidation and less aromatic chlorination, in a manner that is highly dependent on analyte structure and other reaction conditions. Mechanistic hypotheses are advanced to explain the cyclodextrin effect, and the potential for use of  $\alpha$ -cyclodextrin for practical wastewater treatment is also discussed.

**Keywords:** cyclodextrin, bisphenol (BPA), 2-phenylphenol, hydrophobic encapsulation, chlorination

## INTRODUCTION

The decontamination of the water supply from a variety of organic pollutants (Cravotto et al., 2005), including phthalates (Przybylinska and Wyszowski, 2016), biphenyls (Benoit et al., 2016), and bisphenol derivatives (Onundi et al., 2017) is an important challenge with a variety of industrial and public health applications (Foo and Hameed, 2010; Shah et al., 2016). Methods to achieve such decontamination to facilitate access to clean drinking water tend to rely on the application of large quantities of disinfectants, oxidants, or decomposition reagents (Kim et al., 1999), with newer methods including the use of photochemical (Laxma Reddy et al., 2017), electrochemical (Oturán et al., 2009), and sonochemical (Joseph et al., 2009) decontamination procedures. While these methods are effective in reducing the quantities of known organic pollutants (Besner et al., 2008), the decomposition products of both the pollutants and of chemicals used for disinfection have not been well-characterized (Wang et al., 2014), and methods to remove such decomposition products from the water stream are poorly developed. This is particularly concerning because many of these decomposition products are likely to have similar or even worse toxicities compared to their associated starting materials (Li and Mitch, 2018).

One popular disinfection agent is chlorine dioxide, which has been used for the decontamination of wastewater from pathogens (Banach et al., 2015), as part of the seawater desalination process (Kim et al., 2015), and for the removal of antibiotics and other pharmaceuticals from drinking



water (Dodd, 2012). Despite the widespread usage of chlorine dioxide, concerns remain about its toxicity (Ma et al., 2017), and about the toxicity of pollutant byproducts that result from chlorine dioxide treatment (Colman et al., 2011). Efforts to mitigate this toxicity have focused on alternative disinfection treatments (Meireles et al., 2016), on immobilization of chlorine dioxide to minimize the diffusion of toxic byproducts (He et al., 2014), and on the combined use of chlorine dioxide and other water treatments (Hsu and Huang, 2015). The use of supramolecular constructs and/or adducts of chlorine dioxide as strategies for mitigating chlorine dioxide-induced water treatment toxicity has not been reported to date, despite the fact that chlorine dioxide is known to form a variety of supramolecular adducts (Loginova et al., 2011; Palcsó et al., 2019), including with  $\alpha$ -cyclodextrin (Wambaugh et al., 2013). Moreover, supramolecular association with common organic pollutants is well-known, including cyclodextrin complexation with the classes of pollutants mentioned above [phthalates (Cromwell et al., 2019), biphenyls (Serio et al., 2013), and bisphenols (DiScenza et al., 2018)]. Finally, supramolecular complexation in general (Chang et al., 2017), and cyclodextrin complexation in particular (Aiassa et al., 2016), has been shown to result in significantly altered and often reduced toxicities, which provides another potential avenue by which toxicity of the water stream can be mitigated.

In general, cyclodextrin complexation has been shown to rely heavily on hydrophobic association of hydrophobic small molecules inside the hydrophobic interior cavity of the cyclodextrin hosts. Such host-guest complexes have a

strong dependence on the steric complementarity between the cavity size and the size of the guest, with single aromatic ring compounds reported to bind strongly in  $\alpha$ -cyclodextrin (Connors and Pendergast, 1984; Pendergast and Connors, 1985) and larger aromatic (and hydrophobic aliphatic compounds) reported to bind in  $\beta$ -cyclodextrin (Celebioglu et al., 2019; Yu et al., 2019). Of note, moving to the even larger  $\gamma$ -cyclodextrin oftentimes results in the formation of ternary complexes, where two small molecule guests bind simultaneously inside the larger  $\gamma$ -cyclodextrin core (Hamai, 2010; Saokham et al., 2018). For the most common analytes involved in aqueous contamination (*vide infra*), the single aromatic rings of these analytes indicate that they are likely to bind strongly in the  $\alpha$ -cyclodextrin cavity. Such strong and sterically matched binding, in turn, is expected to affect the reactivity of these substrates and the distribution of products obtained, an expectation that was effectively borne out by the results of our experiments (*vide infra*). The use of larger cyclodextrins, by contrast, would lead to the formation of less sterically matched complexes, which would in turn impart lower selectivities and lower overall cyclodextrin-induced effects.

Recent reports from our research groups have focused on the design, optimization, and sensing applications of cyclodextrin complexes (for the Levine group) (Serio et al., 2015; Chaudhuri et al., 2018; Haynes et al., 2019), and on the engineering, deployment, and evaluation of water purification filters (for the Boving group) (Schifman et al., 2016; Eberle et al., 2017; Blanford et al., 2018), which combined have provided us with unique insight into the potential of cyclodextrins to benefit the water purification process. Reported herein are the results of our investigations into the effect of  $\alpha$ -cyclodextrin complexation on chlorine dioxide-based water treatment, and how such complexation affects the quantity and distribution of degradation byproducts. Mechanistic insight into the specific role of  $\alpha$ -cyclodextrin is also discussed.

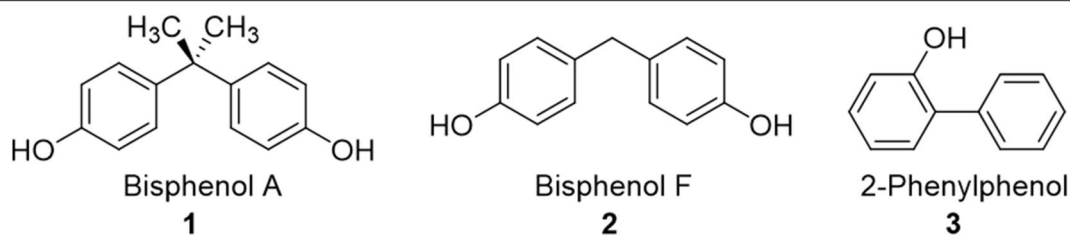
## EXPERIMENTAL SECTION

### Materials and Methods

$^1\text{H}$  NMR experiments were conducted using a 400 MHz Bruker Avance spectrometer with  $\text{D}_2\text{O}$  as a solvent. GC-MS analyses of reaction mixtures were carried out using a Shimadzu GCMS-QP2020 instrument. All chemicals were purchased from Sigma Aldrich chemical company or from Fisher Scientific and were used as received, without further purification.

### Method for the Preparation of Chlorine Dioxide Solution

An aqueous chlorine dioxide suspension was generated from the treatment of a solution of  $\text{NaClO}_2$  (ERCOPure<sup>TM</sup> 7.5) with activated HCl. A typical generation procedure involved the addition of 4 mL of 30–36% HCl to a mixture of 17.5 mL of ADOX<sup>TM</sup> 7.5 and 200 mL of deionized water. The reaction mixture was kept in a dark Amber bottle for  $\sim 24$  h at room temperature. Prior to usage, the reaction mixture was further diluted to render a final chlorine dioxide concentration of  $\sim 1,095$  ppm (confirmed via hand-held colorimetry using a Hach Digital Titrator).



**FIGURE 1** | Structures of common aqueous pollutants investigated herein as substrates for chlorine dioxide-mediated degradation.

## General Method for the Complexation of Chlorine Dioxide With $\alpha$ -cyclodextrin

The complexation of chlorine dioxide with  $\alpha$ -cyclodextrin was obtained by mixing a solution of 6.2 mL of 1,100 ppm of  $\text{ClO}_2$  (100  $\mu\text{mol}$ ) with solid  $\alpha$ -cyclodextrin (584 mg; 600  $\mu\text{mol}$ ) for 15–20 min.

## General Method for Determining the Reaction Progression

The reaction mixture containing the organic analyte (compounds **1–3**, **Figure 1**) was treated with  $\text{ClO}_2$  and allowed to react at the specified temperature for a certain amount of time, after which time the mixture was treated with concentrated sodium sulfite ( $\text{Na}_2\text{SO}_3$ ) solution to quench the excess chlorine dioxide. The resulting solution was extracted with ethyl acetate. An aliquot of the organic phase was injected into the GC-MS for analysis, which enabled us to identify unreacted starting material, as well as new peaks corresponding to the formation of a variety of oxidation and chlorination products.

## General Method for Measuring the Binding of Analytes in $\alpha$ -cyclodextrin

Binding of analytes with  $\alpha$ -cyclodextrin was investigated via  $^1\text{H}$  NMR titrations (Roselet and Kumari, 2017). A mixture of analytes (20  $\mu\text{mol}$ ) with  $\alpha$ -cyclodextrin (0.0–5.0 equivalents) in  $\text{D}_2\text{O}$  were investigated via  $^1\text{H}$  NMR spectroscopy, and the resulting shifts in the positions of the NMR signals were used to confirm supramolecular complexation.

## RESULTS AND DISCUSSION

### Analyte Selection

There are a broad variety of organic pollutants that contaminate water supplies, including phthalates, biphenyls, and bisphenol derivatives (*vide supra*). We have selected three common pollutants to focus on in this paper, all of which have been reported to interact with  $\alpha$ -cyclodextrin: bisphenol A (BPA) (analyte **1**) (Araki et al., 2001), bisphenol F (BPF) (analyte **2**) (Xiao et al., 2007), and 2-phenylphenol (analyte **3**) (Burkert et al., 1981), with the expectation that supramolecular interactions of the pollutants with  $\alpha$ -cyclodextrin is likely to affect their chlorine dioxide-mediated degradation. Moreover, the selection of three pollutants with similar structures is expected to provide important insight into the structural selectivity of  $\alpha$ -cyclodextrin

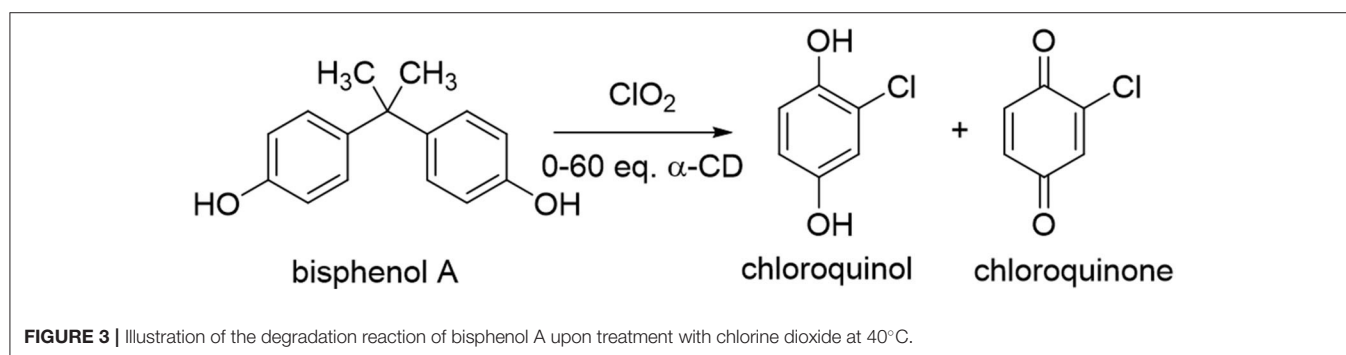
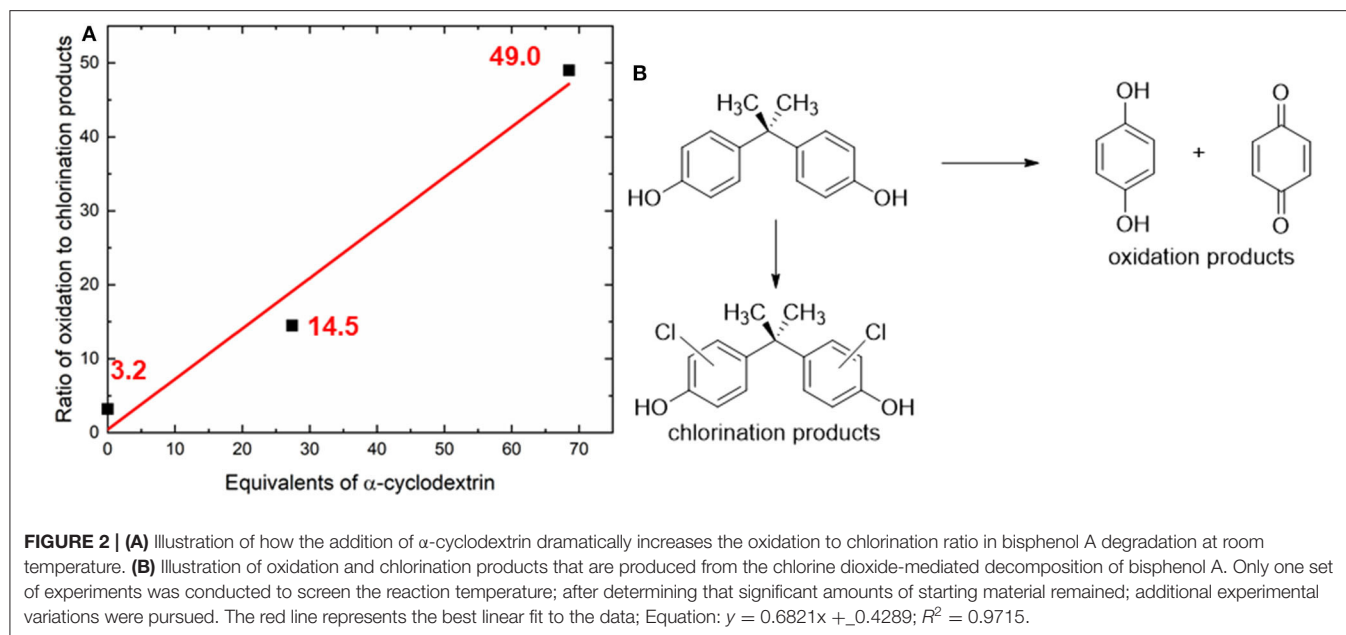
complexation, and how such selectivity affects the chlorine dioxide-mediated degradation processes. Finally, the inclusion of BPF in addition to BPA is important, as BPA derivatives such as BPF are increasingly used as commercially available substitutes for BPA (Bjornsdotter et al., 2017; Wu et al., 2018), with evidence indicating analogous or even worse toxicity compared to BPA (den Braver-Sewradj et al., 2020).

### Initial Screening

Initial screening of reaction conditions started with room temperature treatment of analyte **1** with chlorine dioxide and  $\alpha$ -cyclodextrin (0–60 equivalents relative to the substrate). BPA was found to undergo decomposition into single aromatic ring oxidized units (quinols and quinones), as well as undergo chlorination on residual starting material to form chlorinated BPA analogs. Under these conditions, increasing the equivalents of cyclodextrin led to a dramatic increase in the ratio of oxidation products to chlorination products, from a ratio of 3.2 without any cyclodextrin to a ratio of oxidation to chlorination of 49 measured at the highest concentration of  $\alpha$ -cyclodextrin (**Figure 2**).

However, even after 24 h, significant unreacted starting material remained (up to 72%). Raising the reaction temperature slightly, to 40°C, resulted in complete consumption of the starting material but dramatic changes in the reaction products, with nearly exclusive formation of chlorinated oxidation products chloroquinol and chloroquinone (**Figure 3**). This significant change in consumption of the starting material with only a mild increase in the temperature of the reaction is likely due to increased reaction kinetics at the elevated temperature. The stability of the cyclodextrin complexes is likely also affected by the increased reaction temperature, which in turn leads to changes in the distribution of products observed. Increasing the equivalents of  $\alpha$ -cyclodextrin in this system led to moderate increases in the ratio of chloroquinol to chloroquinone obtained, with overall limited changes in the overall oxidation products obtained (**Table 1**). This could likely be due to the stronger binding of quinols to  $\alpha$ -cyclodextrin, thereby inhibiting their subsequent oxidation into quinones.

In contrast to the results obtained for analyte **1**, treatment of bisphenol F (analyte **2**) with chlorine dioxide at 40°C led to 100% oxidation products, with both unsubstituted quinols and chloroquinols formed (**Figure 4**). The ratio of oxidation products (100% of the product mixture) to chlorination products (namely, the formation of chloroquinols) was calculated, and the results



**TABLE 1 |** Effects of  $\alpha$ -cyclodextrin addition on the distribution of decomposition products obtained from chlorine dioxide treatment of bisphenol A<sup>a</sup>.

Equivalents of $\alpha$ -cyclodextrin	Ratio of chloroquinol to chloroquinone	Overall oxidation product %
0	1.9	56.2%
27.4	3.5	53.6%
68.5	4.3	55.3%

<sup>a</sup>Reactions were run at 40°C for 24 h.

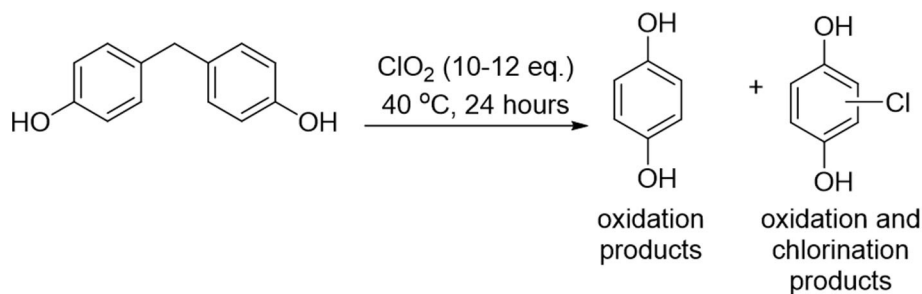
summarized in **Table 2**. Of note, substantial increases in the ratio of quinol to chloroquinol with increasing concentration of cyclodextrin indicates a decrease in the chlorination byproducts, which strongly suggests that cyclodextrin complexation plays a role in inhibiting that reaction pathway (*vide infra*).

In contrast to analytes 1 and 2, analyte 3 (2-phenylphenol) underwent complete decomposition with  $\text{ClO}_2$  treatment, yielding a much more complex product profile. Unlike analytes 1 and 2, which formed predominantly single aromatic ring oxidation products, the chlorine dioxide treatment of analyte

3 led to only minor amounts of such products, with the majority of oxidation products maintaining the core biphenyl structure. Such differences in product distribution between the analytes strongly suggests that the bridging methylene unit of the bisphenol structures of 1 and 2 (absent in analyte 3) provided a site for C-C bond cleavage that enabled single aromatic ring products to form. In addition to the biphenyl-containing oxidation products, a variety of chlorinated products were also formed, most of which resulted from chlorination of the initially formed oxidized compounds (**Figure 5**). The ratio of oxidation products to chlorination products formed from chlorine dioxide-mediated decomposition of analyte 3, with increasing equivalents of  $\alpha$ -cyclodextrin effectively protecting the aromatic ring from undesired chlorination reactions (as shown by increasing values of the oxidation to chlorination ratio observed, **Table 2**).

Overall, the results obtained for analyte 1 at room temperature, and analytes 2 and 3 at 40°C indicate that the presence of cyclodextrin markedly increases the percentage of non-chlorinated oxidation products formed, with the one anomalous result, obtained for the chlorine dioxide treatment of analyte 1 at 40°C, discussed later in the manuscript. Of note,





**FIGURE 4 |** Illustration of how the chlorine dioxide-mediated decomposition of bisphenol F leads to the formation of quinols and chloroquinols exclusively.

**TABLE 2 |** Ratio of oxidation to chlorination products formed by treating aromatic analytes **2** and **3** with chlorine dioxide with varying cyclodextrin equivalents<sup>a</sup>.

Analyte	0 eq. $\alpha$ -CD	24 eq. $\alpha$ -CD	60 eq. $\alpha$ -CD
<b>2</b>	1.2	1.5	1.5
<b>3</b>	3.2	4.5	5.1

<sup>a</sup>Reactions were run at  $40^\circ\text{C}$  for 24 h, and the ratio of oxidation to chlorination products was determined via GC-MS analysis.

both substrates with bridging methylene units (compounds **1** and **2**) decomposed primarily into single aromatic ring oxidized units [(chloro)quinols and (chloro)quinones]. Such results have substantial relevance from a practical as well as a fundamental scientific perspective. From a practical perspective, chlorinated byproducts formed from chlorine dioxide mediated decomposition generally have higher reported toxicities than the non-chlorinated, oxidation products formed (Li and Mitch, 2018). As a result, the ability to decrease the relative amount of chlorinated products through  $\alpha$ -cyclodextrin addition is particularly attractive, especially as  $\alpha$ -cyclodextrin itself has almost no reported toxicity (Cal and Centkowska, 2008), and in fact has been used for a variety of biomedical applications due to its generally recognized safety (Szente et al., 2018). From a fundamental perspective, the fact that  $\alpha$ -cyclodextrin complexation suppresses the chlorination processes is likely due to hydrophobic encapsulation of the phenyl rings in the cyclodextrin cavity, in a way that provides steric shielding and prevents aromatic chlorination from occurring (*vide infra*). Such supramolecular shielding provides insight into the mechanism of cyclodextrin complexation, how such complexation depends on the structure of the encapsulated guest, and how such complexes affect guest reactivity.

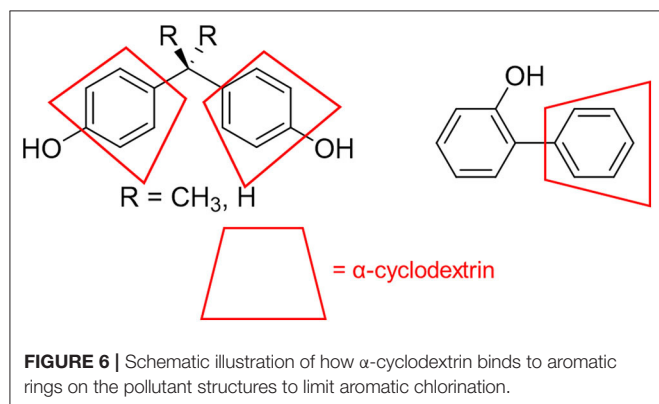
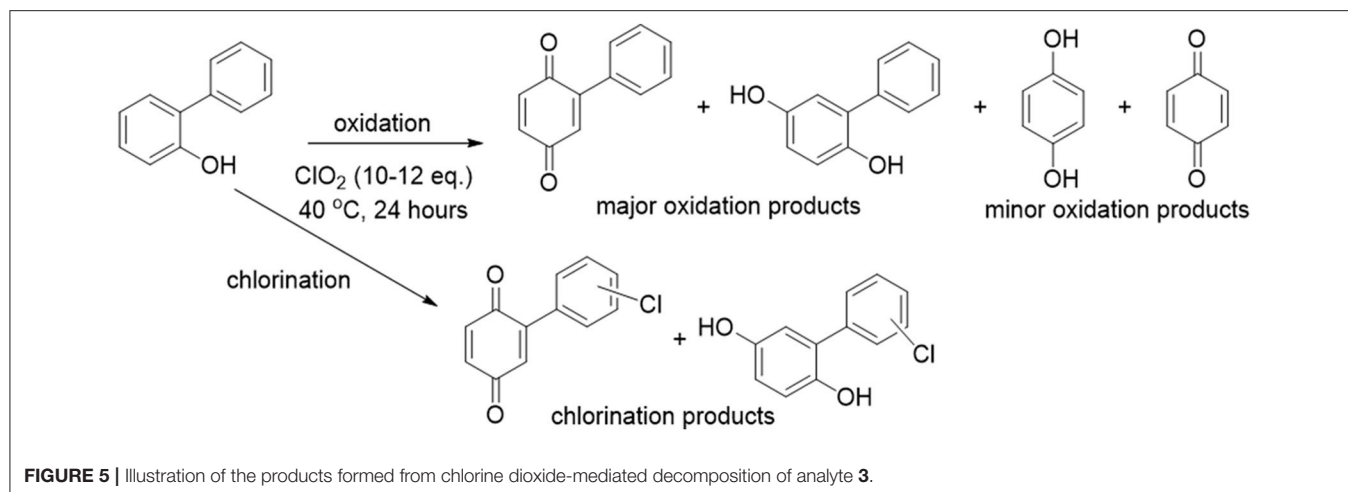
## Mechanistic Investigations

There are multiple fundamental mechanistic questions involved in this process, including how  $\alpha$ -cyclodextrin affects the product distribution of chlorine dioxide mediated degradation, as well as how variations in substrate structure affect product distribution and the underlying reaction mechanism. Most likely, the binding of phenyl groups in the cyclodextrin cavity (Figure 6) provides supramolecular steric shielding from

undesired aromatic chlorination. Moreover, the benzylic position on the substituent, which must be accessed to effect oxidation reactions, remains relatively unhindered. Electronic activation of that benzylic position through hydrogen bonding to the rims of cyclodextrins can also accelerate the desired oxidation reactions, and evidence for such activation is provided through  $^1\text{H}$  NMR analysis (*vide infra*).

Overall, the treatment of the analytes with chlorine dioxide led to highly analyte-specific results. Both analytes **1** and **2** yielded oxidation products with primarily single ring aromatic groups, whereas analyte **3** maintained its biphenyl structure, indicating that the bridging methylene group of analytes **1** and **2** plays a key role in facilitating oxidative bond cleavage. Differences in the product distribution of analytes **1** and **2** indicate a markedly more complex product mixture for analyte **1**'s treatment with chlorine dioxide, with major products of chloroquinol and chloroquinone and numerous minor products, generally with higher molecular weights (indicating radical-radical recombination). For analyte **1**, the fact that the ratio of chloroquinol to chloroquinone increased with increasing equivalents of  $\alpha$ -cyclodextrin indicates that the cyclodextrin effectively inhibits oxidation of chloroquinol. In contrast, increasing the equivalents of  $\alpha$ -cyclodextrin in the analyte **2** decomposition process led to an increased ratio of quinol to chloroquinol, which indicates that the chlorination reaction pathway was inhibited by  $\alpha$ -cyclodextrin.

The proposed mechanism is further supported by  $^1\text{H}$  NMR chemical shift studies of the analytes in presence of increasing equivalents of  $\alpha$ -cyclodextrin, and key results are summarized in Table 3 and Figure 7. In particular, all aromatic protons of the analytes demonstrated significant chemical shifts upon the addition of increasing concentrations of  $\alpha$ -cyclodextrin, supporting supramolecular encapsulation of the type shown in Figure 6. Moreover, for analytes **1** and **2**, significant changes in chemical shift were also observed for the methyl group protons at the bridging carbon (for analyte **1**) or for the protons directly on the methylene bridge (for analyte **2**), which indicates the existence of significant non-covalent interactions between this part of the molecule and the cyclodextrin host (Yang et al., 2008). Such interactions are likely intermolecular hydrogen bonding between the hydroxyls located at the cyclodextrin rim and the protons between the aromatic rings, which in turn activates the benzylic position for the desired oxidation reactions.



Of note, binding of aromatic compounds in cyclodextrin that leads to activation of benzylic positions through association with the cyclodextrin rim is a phenomenon that has been reported previously in the literature, both by our group (Chaudhuri et al., 2016) and by others (Andres and de Rossi, 2003; Lopez et al., 2007). In particular, a previous report by our group uses binding of aromatic rings in the cyclodextrin cavity to activate the benzylic position of benzylic alcohols and achieve effective and mild oxidation to the corresponding aldehydes (den Braver-Sewradj et al., 2020). Similarly, complexation in  $\alpha$ -cyclodextrin, reported herein, has the dual function of protecting the aromatic ring from undesired chlorination and of facilitating effective oxidation at the benzylic site.

## Practical Applications

Real-world municipal waste water effluent samples, prior to chlorination, were used to simulate this mediated oxidation in practice. Such samples were doped with 100 mg/L of BPA (analyte **1**), and then treated with chlorine dioxide in the presence or absence of  $\alpha$ -cyclodextrin. Results of these studies showed that  $\alpha$ -cyclodextrin promoted the decomposition of BPA to form hydroquinone and chlorohydroquinone, with

**TABLE 3** | Changes in the  $^1\text{H}$  NMR spectral signals of protons on bisphenol A as a function of added equivalents of  $\alpha$ -cyclodextrin ( $\alpha$ -CD)<sup>a</sup>.

Eq. of $\alpha$ -CD	Methyl protons ( $\Delta\text{ppm}$ )	Ortho protons ( $\Delta\text{ppm}$ ) <sup>b</sup>	Meta protons ( $\Delta\text{ppm}$ ) <sup>c</sup>
0.5	0.0291	0.0044	0.0609
1.0	0.0400	0.0071	0.0801
1.5	0.0443	0.0077	0.0870
2.0	0.0493	0.0089	0.0920
3.0	0.0522	0.0088	0.0953
5.0	0.0609	0.0135	0.1015

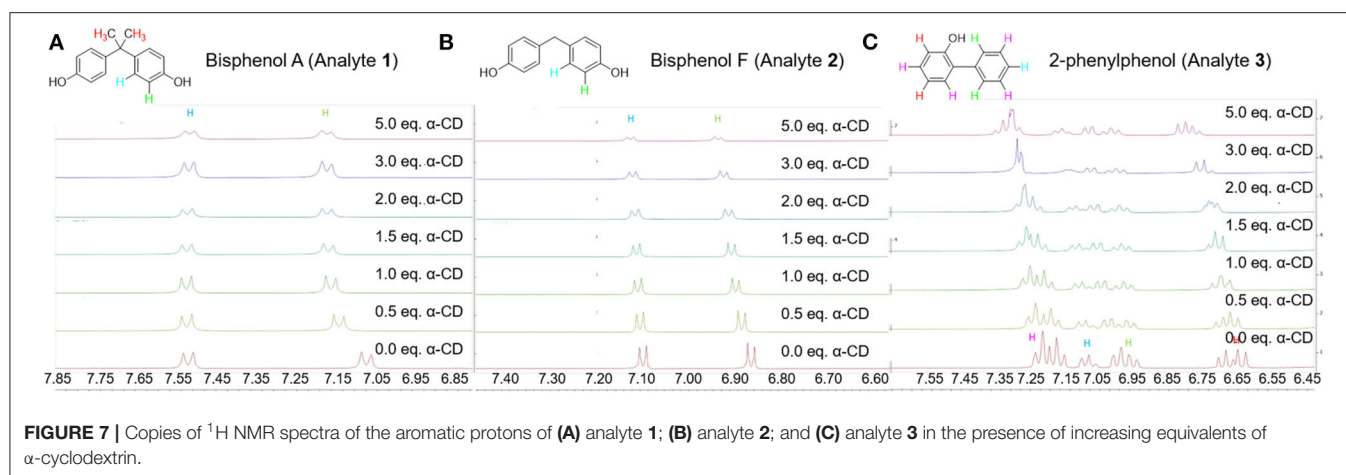
<sup>a</sup>  $\Delta\text{ppm}$  is defined as the difference in chemical shifts in the presence of cyclodextrin compared to the chemical shifts in the absence of cyclodextrin, according to the following equation.

$\Delta\text{ppm} = \delta_{\text{complex}} (\text{chemical shifts in presence of } \alpha\text{-CD}) - \delta_{\text{control}} (\text{chemical shifts without } \alpha\text{-CD})$ .

<sup>b</sup> Ortho protons are defined as the protons that are at the ortho positions of the aromatic ring relative to the non-aromatic bridge.

<sup>c</sup> Meta protons are defined as the protons that are at the meta positions of the aromatic ring relative to the non-aromatic bridge.

substantially more of these products formed in the presence of  $\alpha$ -cyclodextrin compared to the decomposition run in the absence of cyclodextrin (Table 4). Nonetheless, the ratio of hydroquinone to chlorohydroquinone remained roughly unchanged by the addition of  $\alpha$ -cyclodextrin, a result which is surprising based on the documented ability of  $\alpha$ -cyclodextrin to affect this product distribution (*vide supra*). Reasons for this anomalous behavior may relate to the presence of interfering species in the wastewater sample. In particular, higher ionic strength and/or other species complexing with cyclodextrin sites can limit the ability to target specific compounds for specific oxidation mechanisms. Such treatment might be better suited in the long-term for industrial wastewater streams where a more consistent water matrix and a higher concentration of the targeted pollutant is available for cyclodextrin-mediated oxidation. We expect that additional modifications to our cyclodextrin-based system will allow for improved performance in such samples, possibly through combining the  $\alpha$ -cyclodextrin with other additives that will address the more complex nature of real-world aqueous samples.



**TABLE 4** | Summary of the formation of hydroquinone and chlorohydroquinone from chlorine dioxide mediated decomposition of BPA in real-world wastewater samples, measured as normalized integrated peak emissions from GC-MS.

Decomposition product	Without $\alpha$ -CD	With $\alpha$ -CD
Hydroquinone <sup>a</sup>	0.17	0.31
Chlorohydroquinone <sup>a</sup>	0.51	1.00
Ratio of hydroquinone to chlorohydroquinone <sup>b</sup>	0.33	0.31

<sup>a</sup>Values reported herein represent the integrated area of the GC-MS peaks that correspond to each analyte, with the results normalized so that the highest value peak (chlorohydroquinone in the presence of  $\alpha$ -CD) is equal to 1.0.

<sup>b</sup>Ratio of hydroquinone to chlorohydroquinone is calculated as the quotient of the integrated area of the peak corresponding to hydroquinone divided by the integrated area of the peak corresponding to chlorohydroquinone.

## CONCLUSIONS

The ability to change the product distribution of chlorine dioxide mediated degradation of organic pollutants via supramolecular complexation of the pollutants has substantial practical benefit in improving wastewater treatment methodologies, and is of interest from a fundamental scientific perspective as well. Results reported herein highlight that the use of  $\alpha$ -cyclodextrin to bind small aromatic pollutants affects the accessibility of the structure to the chlorine dioxide reagent and the resulting distribution of oxidation to chlorination products in a way that is highly dependent on the structure of the reagent, the temperature of the treatment, and the molar equivalents of  $\alpha$ -cyclodextrin added, with most cases resulting in a marked decrease in the relative amounts of chlorinated byproducts obtained. Reasons for these effects rely on the supramolecular complexation of the pollutants, confirmed by  $^1\text{H}$  NMR analysis, which cause steric shielding of the phenyl groups of the pollutants to undesired chlorination. Overall, the addition of  $\alpha$ -cyclodextrin generally increases the ratio of water-soluble oxidation products and decreases the amount of toxic chlorination products, through the addition of a non-toxic, sugar-based cyclodextrin additive. The results reported herein provide significant groundwork for further

development of novel and highly effective water treatment procedures, and open the possibility of using cyclodextrin-mediated complexation in other water treatment and pollutant removal processes.

## DATA AVAILABILITY STATEMENT

All datasets generated for this study are included in the article/Supplementary Material.

## AUTHOR CONTRIBUTIONS

SC ran the initial experiments on purified laboratory systems, identified system components, did  $^1\text{H}$  NMR analysis, and drafted the initial manuscript. DD ran experiments on real-world wastewater samples, finalized experiments that were left from SC, and edited the manuscript. TB provided intellectual insight throughout the project and edited the manuscript. AB provided industrial perspective on the project, as well as real-world wastewater samples, and also edited the manuscript. ML provided intellectual insight on the project, worked with SC to draft the initial manuscript, and took responsibility for all edits and corrections to arrive at this final version. All authors contributed to the article and approved the submitted version.

## FUNDING

International Dioxide funded this work through a cooperative agreement with the University of Rhode Island. Fees to publish this work will be partially offset by an Open Access Fund at the University of Rhode Island and by discretionary funds at Ariel University.

## SUPPLEMENTARY MATERIAL

The Supplementary Material for this article can be found online at: <https://www.frontiersin.org/articles/10.3389/fchem.2020.00641/full#supplementary-material>

## REFERENCES

- Aiassa, V., Zoppi, A., Becerra, M. C., Albesa, I., and Longhi, M. R. (2016). Enhanced inhibition of bacterial biofilm formation and reduced leukocyte toxicity by chloramphenicol: $\beta$ -cyclodextrin:N-acetylcysteine complex. *Carbohydr. Polym.* 152, 672–678. doi: 10.1016/j.carbpol.2016.07.013
- Andres, G. O., and de Rossi, R. H. (2003). Mechanism of phthalate ester hydrolysis in water and in cyclodextrin mediated reactions. *ARKIVOC* 127–138. doi: 10.3998/ark.5550190.0004.a14
- Araki, M., Kawasaki, N., Nakamura, T., and Tanada, S. (2001). Removal of bisphenol A in soil by cyclodextrin derivatives. *Toxicol. Environ. Chem.* 79, 23–29. doi: 10.1080/02772240109358973
- Banach, J. L., Sampers, I., Van Haute, S., and van der Fels-Klerx, H. J. (2015). Effect of disinfectants on preventing the cross-contamination of pathogens in fresh produce washing water. *Int. J. Environ. Res. Public Health* 12, 8658–8677. doi: 10.3390/ijerph120808658
- Benoit, N., Dove, A., Burniston, D., and Boyd, D. (2016). Tracking PCB contamination in Ontario Great Lakes Tributaries: development of methodologies and lessons learned for watershed based investigations. *J. Environ. Protect.* 7, 390–409. doi: 10.4236/jep.2016.73035
- Besner, M.-C., Servais, P., and Prevost, M. (2008). Efficacy of disinfectant residual on microbial intrusion: a review of experiments. *J. Am. Water Works Assoc.* 100, 116–130. doi: 10.1002/j.1551-8833.2008.tb09752.x
- Bjornsdottir, M. K., de Boer, J., and Ballesteros-Gomez, A. (2017). Bisphenol A and replacements in thermal paper: a review. *Chemosphere* 182, 691–706. doi: 10.1016/j.chemosphere.2017.05.070
- Blanford, W. J., Pecoraro, M. P., Heinrichs, R., and Boving, T. B. (2018). Enhanced reductive de-chlorination of a solvent contaminated aquifer through addition and apparent fermentation of cyclodextrin. *J. Contaminant Hydrol.* 208, 68–78. doi: 10.1016/j.jconhyd.2017.10.006
- Burkert, W. G., Owensby, C. N., and Hinze, W. L. (1981). The use of an  $\alpha$ -cyclodextrin mobile phase in the thin-layer chromatographic separation of ortho, meta, and para substituted phenols. *J. Liq. Chromatogr.* 4, 1065–1085. doi: 10.1080/01483918108059604
- Cal, K., and Centkowska, K. (2008). Use of cyclodextrins in topical formulations: practical aspects. *Eur. J. Pharm. Biopharm.* 68, 467–478. doi: 10.1016/j.ejpb.2007.08.002
- Celebioglu, A., Topuz, F., Yildiz, Z. I., and Uyar, T. (2019). Efficient removal of polycyclic aromatic hydrocarbons and heavy metals from water by electrospun nanofibrous polycyclodextrin membranes. *ACS Omega* 4, 7850–7860. doi: 10.1021/acsomega.9b00279
- Chang, Y.-X., Zhang, X.-M., Duan, X.-C., Liu, F., and Du, L.-M. (2017). Supramolecular interaction of methotrexate with cucurbit[7]uril and analytical application. *Spectrochim. Acta A* 183, 131–137. doi: 10.1016/j.saa.2017.04.060
- Chaudhuri, S., Verderame, M., Mako, T. L., Bandara, Y. M. N. D. Y., Fernando, A. I., and Levine, M. (2018). Synthetic  $\beta$ -cyclodextrin dimers for squaraine binding: effect of host architecture on photophysical properties, aggregate formation and chemical reactivity. *Eur. J. Org. Chem.* 2018, 1964–1974. doi: 10.1002/ejoc.201800283
- Chaudhuri, S., Zaki, H., and Levine, M. (2016). Environmentally friendly procedure for the aqueous oxidation of benzyl alcohols to aldehydes with dibromodimethylhydantoin (DBDMH) and cyclodextrin: scope and mechanistic insights. *Synth. Commun.* 46, 636–644. doi: 10.1080/00397911.2016.1161801
- Colman, J., Rice, G. E., Wright, J. M., Hunter, E. S. III, Teuschler, L. K., Lipscomb, J. C., Hertzberg, R. C., et al. (2011). Identification of developmentally toxic drinking water disinfection byproducts and evaluation of data relevant to mode of action. *Toxicol. Appl. Pharmacol.* 254, 100–126. doi: 10.1016/j.taap.2011.02.002
- Connors, K. A., and Pendergast, D. D. (1984). Microscopic binding constants in cyclodextrin systems: complexation of  $\alpha$ -cyclodextrin with sym-1,4-disubstituted benzenes. *J. Am. Chem. Soc.* 106, 7607–7614. doi: 10.1021/ja00336a048
- Cravotto, G., Di Carlo, S., Tumiatto, V., Roggero, C., and Bremner, H. D. (2005). Degradation of persistent organic pollutants by Fenton's reagent facilitated by microwave or high-intensity ultrasound. *Environ. Technol.* 26, 721–724. doi: 10.1080/09593332608618513
- Cromwell, B., Dubnicka, M., Dubrawski, S., and Levine, M. (2019). Identification of 15 phthalate esters in commercial cheese powder via cyclodextrin-promoted fluorescence detection. *ACS Omega* 4, 17009–17015. doi: 10.1021/acsomega.9b02585
- den Braver-Sewradj, S. P., van Spronsen, R., and Hessel, E. V. S. (2020). Substitution of bisphenol A: a review of the carcinogenicity, reproductive toxicity, and endocrine disruption potential of alternative substances. *Crit. Rev. Toxicol.* 50, 128–147. doi: 10.1080/10408444.2019.1701986
- DiScenza, D. J., Lynch, J., Feder, E., and Levine, M. (2018). Detection of bisphenol A and derivatives in human urine via cyclodextrin-promoted fluorescence modulation. *Anal. Methods* 10, 3783–3790. doi: 10.1039/C8AY00733K
- Dodd, M. C. (2012). Potential impacts of disinfection processes on elimination and deactivation of antibiotic resistance genes during water and wastewater treatment. *J. Environ. Monitor.* 14, 1754–1771. doi: 10.1039/c2em00006g
- Eberle, D., Ball, R., and Boving, T. B. (2017). Impact of ISCO treatment on PFAA Co-contaminants at a former fire training area. *Environ. Sci. Technol.* 51, 5127–5136. doi: 10.1021/acs.est.6b06591
- Foo, K. Y., and Hameed, B. H. (2010). Decontamination of textile wastewater via TiO<sub>2</sub>/activated carbon composite materials. *Adv. Colloid Interface Sci.* 159, 130–143. doi: 10.1016/j.cis.2010.06.002
- Hamai, S. (2010). Complex formation of tetrakis(4-sulfonatophenyl)porphyrin with  $\gamma$ -cyclodextrin, phenylalanine, and tryptophan in aqueous solution. *J. Inclusion Phenom. Macrocyclic Chem.* 67, 471–481. doi: 10.1007/s10847-009-9730-7
- Haynes, A., Halpert, P., and Levine, M. (2019). Colorimetric detection of aliphatic alcohols in  $\beta$ -cyclodextrin solutions. *ACS Omega* 4, 18361–18369. doi: 10.1021/acsomega.9b02612
- He, S., Ruan, B., Zheng, Y., Zhou, X., and Xu, X. (2014). Immobilization of chlorine dioxide modified cells for uranium absorption. *J. Environ. Radioact.* 137, 46–51. doi: 10.1016/j.jenvrad.2014.06.016
- Hsu, C.-S., and Huang, D.-J. (2015). Disinfection of herbal spa pool using combined chlorine dioxide and sodium hypochlorite treatment. *Environ. Monitoring Assess.* 187, 1–11. doi: 10.1007/s10661-014-4242-3
- Joseph, C. G., Li, P. G., Bono, A., and Krishnaiah, D. (2009). Sonophotocatalysis in advanced oxidation process: a short review. *Ultrasonics Sonochem.* 16, 583–589. doi: 10.1016/j.ultsonch.2009.02.002
- Kim, D., Amy, G. L., and Karanfil, T. (2015). Disinfection by-product formation during seawater desalination: a review. *Water Res.* 81, 343–355. doi: 10.1016/j.watres.2015.05.040
- Kim, J. G., Yousef, A. E., and Dave, S. (1999). Application of ozone for enhancing the microbiological safety and quality of foods: a review. *J. Food Protect.* 62, 1071–1087. doi: 10.4315/0362-028X-62.9.1071
- Laxma Reddy, P. V., Kavitha, B., Kumar Reddy, P. A., and Kim, K.-H. (2017). TiO<sub>2</sub>-based photocatalytic disinfection of microbes in aqueous media: a review. *Environ. Res.* 154, 296–303. doi: 10.1016/j.envres.2017.01.018
- Li, X.-F., and Mitch, W. A. (2018). Drinking water disinfection byproducts (DBPs) and human health effects: multidisciplinary challenges and opportunities. *Environ. Sci. Technol.* 52, 1681–1689. doi: 10.1021/acs.est.7b05440
- Loginova, I. V., Rodygin, K. S., Rubtsova, S. A., Slepukhin, P. A., Kuchin, A. V., and Polukeev, V. A. (2011). Oxidation of polyfunctional sulfides with chlorine dioxide. *Russian J. Org. Chem.* 47, 124–130. doi: 10.1134/S1070428011010167
- Lopez, O. L., Marinescu, L., and Bols, M. (2007). New cup-shaped  $\alpha$ -cyclodextrin derivatives and a study of their catalytic properties in oxidation reactions. *Tetrahedron* 63, 8872–8880. doi: 10.1016/j.tet.2007.06.018
- Ma, J.-W., Huang, B.-S., Hsu, C.-W., Peng, C.-W., Cheng, M.-L., Kao, J.-Y., et al. (2017). Efficacy and safety evaluation of a chlorine dioxide solution. *Int. J. Environ. Res. Public Health* 14, 3291–3291/12. doi: 10.3390/ijerph14030329
- Meireles, A., Giauouris, E., and Simoes, M. (2016). Alternative disinfection methods to chlorine for use in the fresh-cut industry. *Food Res. Int.* 82, 71–85. doi: 10.1016/j.foodres.2016.01.021
- Onundi, Y., Drake, B. A., Malecky, R. T., DeNardo, M. A., Mills, M. R., Kundu, S., et al. (2017). A multidisciplinary investigation of the technical and environmental performances of TAML/peroxide elimination of bisphenol A compounds from water. *Green Chem.* 19, 4234–4262. doi: 10.1039/C7GC01415E
- Oturan, N., Sires, I., Oturan, M. A., and Brillas, E. (2009). Degradation of pesticides in aqueous medium by electro-fenton and related methods: a review. *J. Environ. Eng. Manage.* 19, 235–255.



- Palcso, B., Moldovan, Z., Suveg, K., Herczegh, A., and Zelko, R. (2019). Chlorine dioxide-loaded poly(acrylic acid) gels for prolonged antimicrobial effect. *Mater. Sci. Eng. C* 98, 782–788. doi: 10.1016/j.msec.2019.01.043
- Pendergast, D. D., and Connors, K. A. (1985). Complexes of disubstituted benzene positional isomers with  $\alpha$ -cyclodextrin. *Bioorg. Chem.* 13, 150–157. doi: 10.1016/0045-2068(85)90017-3
- Przybylinska, P. A., and Wyszowski, M. (2016). Environmental contamination with phthalates and its impact on living organisms. *Ecol. Chem. Eng. S* 23, 347–356. doi: 10.1515/eces-2016-0024
- Roselet, L., and Kumari, J. P. (2017). Inclusion studies on  $\alpha$ -cyclodextrin complexes of glipizide and gliclazide with effect of pH. *Asian J. Pharm. Clin. Res.* 10, 273–280. doi: 10.22159/ajpcr.2017.v10i1.15164
- Saokham, P., Do, T. T., Van den Mooter, G., and Loftsson, T. (2018). Inclusion complexes of p-hydroxybenzoic acid esters and  $\gamma$ -cyclodextrin. *J. Inclusion Phenom. Macrocyclic Chem.* 90, 111–122. doi: 10.1007/s10847-017-0776-7
- Schifman, L. A., Kasaraneni, V. K., Sullivan, R. K., Oyanedel-Craver, V., and Boving, T. B. (2016). Bacteria removal from stormwater runoff using tree filters: a comparison of a conventional and an innovative system. *Water* 8, 76/1–76/16. doi: 10.3390/w8030076
- Serio, N., Miller, K., and Levine, M. (2013). Efficient detection of polycyclic aromatic hydrocarbons and polychlorinated biphenyls via three-component energy transfer. *Chem. Commun.* 49, 4821–4823. doi: 10.1039/c3cc40534f
- Serio, N., Moyano, D. F., Rotello, V. M., and Levine, M. (2015). Array-based detection of persistent organic pollutants via cyclodextrin promoted energy transfer. *Chem. Commun.* 51, 11615–11618. doi: 10.1039/C5CC04153H
- Shah, A., Shahzad, S., Munir, A., Nadagouda, M. N., Khan, G. S., Shams, D. F., et al. (2016). Micelles as soil and water decontamination agents. *Chem. Rev.* 116, 6042–6074. doi: 10.1021/acs.chemrev.6b00132
- Szente, L., Singhal, A., Domokos, A., and Song, B. (2018). Cyclodextrins: assessing the impact of cavity size, occupancy, and substitutions on cytotoxicity and cholesterol homeostasis. *Molecules* 23, 1228/1–1228/15. doi: 10.3390/molecules23051228
- Wambaugh, J. F., Setzer, R. W., Reif, D. M., Gangwal, S., Mitchell-Blackwood, J., Arnot, J. A., et al. (2013). High-throughput models for exposure-based chemical prioritization in the ExpoCast project. *Environ. Sci. Technol.* 47, 8479–8488. doi: 10.1021/es400482g
- Wang, Y., Liu, H., Liu, G., and Xie, Y. (2014). Oxidation of diclofenac by aqueous chlorine dioxide: identification of major disinfection byproducts and toxicity evaluation. *Sci. Total Environ.* 473–474, 437–445. doi: 10.1016/j.scitotenv.2013.12.056
- Wu, L.-H., Zhang, X.-M., Wang, F., Gao, C.-J., Chen, D., Palumbo, J. R., et al. (2018). Occurrence of bisphenol S in the environment and implications for human exposure: a short review. *Sci. Total Environ.* 615, 87–98. doi: 10.1016/j.scitotenv.2017.09.194
- Xiao, J., Wang, G., Xue, X., Wu, F., Luan, H., and Deng, N. (2007). Enhanced photodegradation behavior of bisphenol F in the presence of  $\beta$ -cyclodextrin under UV light. *Environ. Eng. Sci.* 24, 812–820. doi: 10.1089/ees.2006.0107
- Yang, Z.-X., Chen, Y., and Liu, Y. (2008). Inclusion complexes of bisphenol A with cyclomaltoheptaose ( $\beta$ -cyclodextrin): solubilization and structure. *Carbohydr. Res.* 343, 2439–2442. doi: 10.1016/j.carres.2008.06.018
- Yu, Z., Grasso, M. F., Sorensen, H. H., and Zhang, P. (2019). Ratiometric SERS detection of polycyclic aromatic hydrocarbons assisted by  $\beta$ -cyclodextrin-modified gold nanoparticles. *Microchim. Acta* 186:391. doi: 10.1007/s00604-019-3511-9

**Conflict of Interest:** AB was employed by the company International Dioxide.

The remaining authors declare that the research was conducted in the absence of any commercial or financial relationships that could be construed as a potential conflict of interest. The authors declare that this study received funding from International Dioxide. The funder was not involved in the study design, collection, analysis, interpretation of data, the writing of this article, or the decision to submit it for publication.

Copyright © 2020 Chaudhuri, DiScenza, Boving, Burke and Levine. This is an open-access article distributed under the terms of the Creative Commons Attribution License (CC BY). The use, distribution or reproduction in other forums is permitted, provided the original author(s) and the copyright owner(s) are credited and that the original publication in this journal is cited, in accordance with accepted academic practice. No use, distribution or reproduction is permitted which does not comply with these terms.



# pH-Responsive Host-Guest Complexations Between a Water-Soluble Pillar[6]arene Dodecyl-Ammonium Chloride and Aromatic Sulfonic Acids

Qunpeng Duan<sup>1\*</sup>, Fei Wang<sup>1</sup>, Hongsong Zhang<sup>1</sup> and Kui Lu<sup>1,2\*</sup>

<sup>1</sup> Henan International Joint Laboratory of Rare Earth Composite Materials, School of Materials and Chemical Engineering, Henan University of Engineering, Zhengzhou, China, <sup>2</sup> School of Chemical Engineering and Food Science, Zhengzhou Institute of Technology, Zhengzhou, China

## OPEN ACCESS

### Edited by:

Tangxin Xiao,  
Changzhou University, China

### Reviewed by:

Shao-Lu Li,  
Tianjin Polytechnic University, China  
Chengyou Han,  
China University of Petroleum  
(Huadong), China

### \*Correspondence:

Qunpeng Duan  
qpduan@haue.edu.cn  
Kui Lu  
luckyluke@haue.edu.cn

### Specialty section:

This article was submitted to  
Supramolecular Chemistry,  
a section of the journal  
Frontiers in Chemistry

Received: 28 July 2020

Accepted: 13 August 2020

Published: 15 September 2020

### Citation:

Duan Q, Wang F, Zhang H and Lu K  
(2020) pH-Responsive Host-Guest  
Complexations Between a  
Water-Soluble Pillar[6]arene  
Dodecyl-Ammonium Chloride and  
Aromatic Sulfonic Acids.  
Front. Chem. 8:588201.  
doi: 10.3389/fchem.2020.588201

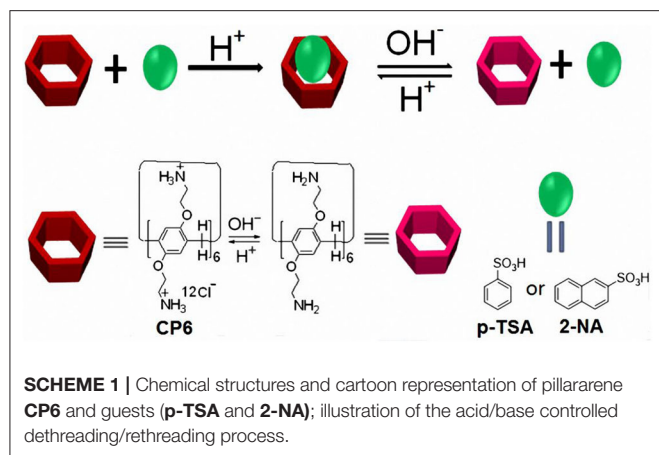
In the present work, new host-guest binding motifs based on a water-soluble pillar[6]arene dodecyl-ammonium chloride (CP6) with two aromatic sulfonic acids in aqueous media were fabricated. In accordance with the integrated results of <sup>1</sup>H NMR, 2D NOESY, and fluorescence titration experiments, it was demonstrated that the host-guest binding of CP6 with the two aromatic sulfonic acids in aqueous solution not only has high binding constants but also has pH-responsiveness.

**Keywords:** pillararenes, supramolecular chemistry, binding motif, pH-responsiveness, aromatic sulfonic acids

## INTRODUCTION

In the supramolecular chemistry field, stimuli-responsive molecular host-guest recognition motifs are attracting much attention because of their wide range of applications in the fabrication of various fascinating and important supramolecular systems, such as molecular devices and machines (Palmer and Rebek, 2004; Han and Chen, 2007; Zhang et al., 2014), responsive supramolecular polymers (Xu et al., 2013; Cantekin et al., 2015), and other smart supramolecular materials (Avestro et al., 2012; Guo and Liu, 2012; Li et al., 2012; Vukotic and Loeb, 2012). Up to now, pH, temperature, light, redox reagents, enzymes, and other external stimuli have been widely utilized for the fabrication of various responsive host-guest complexation systems (Guo and Liu, 2014; Han et al., 2014; Ma and Tian, 2014). Among these stimuli, pH response is very interesting for special applications in electronic devices, gene delivery, and drug delivery (Credit et al., 1997; Badjic et al., 2004; Yu et al., 2012; Duan et al., 2013; Zhang et al., 2013). Therefore, it is of particular importance to construct pH-responsive molecular host-guest complexation systems.

Pillararenes (Ogoshi et al., 2008, 2016; Cao et al., 2009, 2014; Xue et al., 2012; Yao et al., 2012; Si et al., 2014; Wang et al., 2019), as a new kind of supramolecular macrocyclic hosts, have gained growing attention due to their intrinsic unique rigid and symmetrical pillar-shaped architecture, tunable cavity size, easy modification, and superior host-guest properties. Pillararenes endowed with these outstanding features have been used to construct numerous supramolecular systems, such as supramolecular polymers (Zhang et al., 2011; Guan et al., 2012; Li, 2014), daisy chains (Zhang et al., 2012), transmembrane channels (Si et al., 2014), drug-release systems (Cao et al., 2014; Chang et al., 2014; Hu et al., 2016), and other advanced functional materials (Ni et al., 2016; Wang et al., 2018; Xiao et al., 2018; Zhou et al., 2020). Practically, a series of water-soluble pillararenes



have been synthesized and demonstrated to act as scaffolding hosts to various guests (Ogoshi et al., 2012; Hu et al., 2016; Yakimova et al., 2016). Among these water-soluble pillararenes, pH-responsive ones have been reported in the construction of plenty of supramolecular systems (Yu et al., 2012; Cao et al., 2014; Hu et al., 2016; Xiao et al., 2019). Recently, a pillar[6]arene dodecyl-ammonium chloride (CP6) with good water solubility was prepared by our group (Duan et al., 2019). The CP6 with 12 -NH<sub>3</sub><sup>+</sup> groups on both rims has response to acid/base reagent pairs (such as HCl and NaOH). Searching new guests for this positively charged pillar[6]arene to fabricate pH-responsive host-guest binding motifs is thus of great interest. In the present manuscript, two aromatic sulfonic acids, i.e., p-toluenesulfonic acid (p-TSA) and 2-naphthalenesulfonic acid (2-NA) were selected as guests, owing to their wide uses in rubbers, dyestuffs, insecticides, varnishes, and pharmaceuticals (Wu et al., 2011). The design and fabrication of pH-responsive host-guest recognition motifs are elaborated in Scheme 1. We show that CP6 can form highly stable host-guest complexes (p-TSA⊂CP6 and 2-NA⊂CP6) with p-TSA and 2-NA, respectively. Based on these two molecular recognition motifs, pH-responsive host-guest complexes were demonstrated.

## MATERIALS AND METHODS

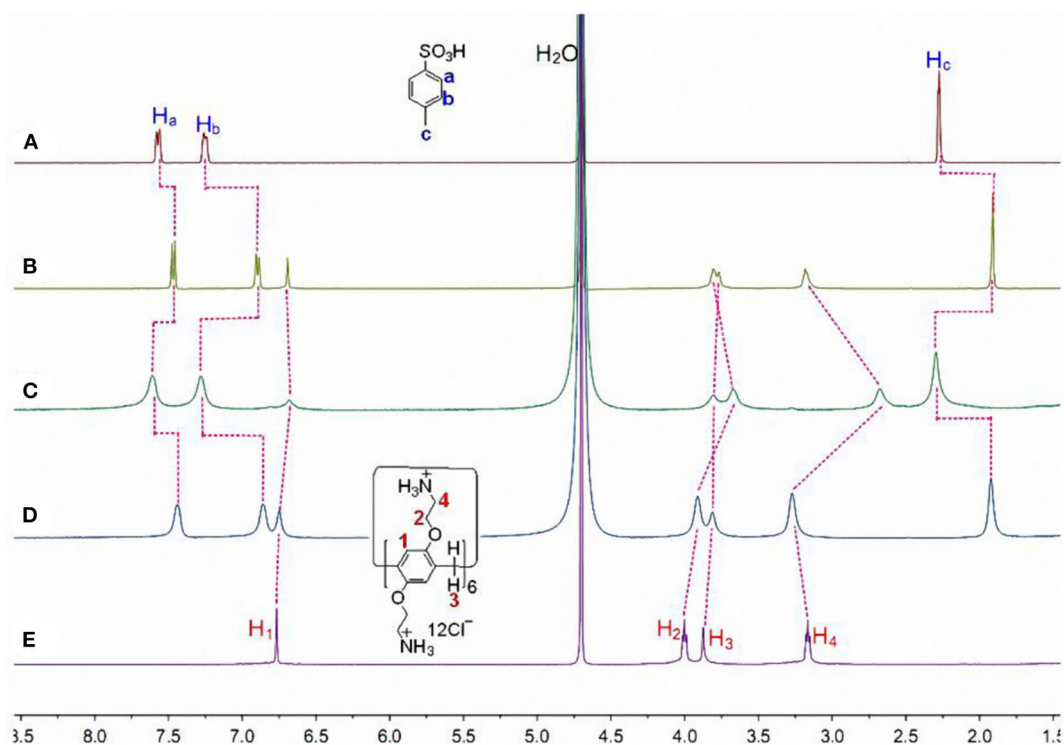
All reagents were commercially available and used as supplied without further purification. CP6 (Duan et al., 2019) was prepared according to the published procedures. NMR spectra were conducted on Bruker Avance III HD 400 spectrometer with the use of the deuterated solvent as the lock and the residual solvent as the internal reference. Fluorescence spectra were performed on an Agilent Cary Eclipse fluorescence spectrophotometer. 0.1 M phosphate buffer solution (PBS, pH = 6.0) was prepared by mixing 12 mL 1 M Na<sub>2</sub>HPO<sub>4</sub> and 88 mL 1 M NaH<sub>2</sub>PO<sub>4</sub> solution. The D<sub>2</sub>O solutions were adjusted to pD 6.0 by DCl or NaOD. The pH and pD values were verified on a Mettler Toledo pH meter calibrated with two standard buffer solutions. pH readings were converted to pD by adding 0.4 units (Glasoe and Long, 1960).

## RESULTS AND DISCUSSION

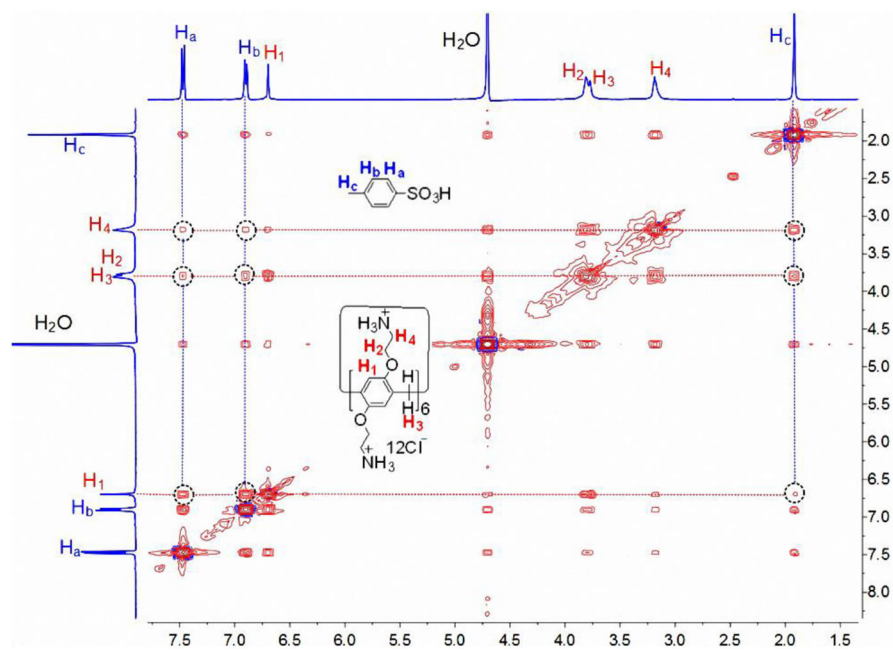
The host-guest complexation of CP6 with p-TSA in D<sub>2</sub>O was first investigated by <sup>1</sup>H NMR spectroscopy. As shown in Figure 1B, when adding about 0.1 equiv. of the host CP6, the signals of protons (a-c) on the guest p-TSA demonstrate significant upfield shifts against free guest p-TSA proton signals ( $\Delta\delta = -0.15$ ,  $-0.39$ , and  $-0.37$  ppm for proton a, b and c, respectively). Strong upfield chemical shifts ( $\Delta\delta$ ) of the aromatic and methyl protons indicate that the p-TSA guest was fully threaded into the host cavity, forming a stable threaded host-guest complex. And the presence of only one set of peaks for the solution of CP6 and p-TSA (Figure 1B) suggests that the host-guest complex formation is a fast exchange process on the NMR time scale. The host-guest binding of CP6 and p-TSA in water was then examined by 2D NOESY analysis. From the 2D NOESY spectrum (Figure 2), NOE correlation signals were observed between H<sub>a</sub>, H<sub>b</sub>, and H<sub>c</sub> on p-TSA and protons H<sub>1-4</sub> on CP6, respectively, supporting the assignment of a threaded structure p-TSA⊂CP6.

Subsequently, the complexation of CP6 by the larger 2-NA guest was also investigated. Similarly, <sup>1</sup>H NMR experiments were also performed to investigate the host-guest complexation of CP6 with 2-NA in D<sub>2</sub>O and MeOD. Figures 3A,B show the <sup>1</sup>H NMR spectra of 2-NA in D<sub>2</sub>O recorded in the absence and the presence of about 0.1 equiv. of the host CP6, respectively. In the presence of CP6 (Figure 3B), the signals of protons (a-g) on the guest 2-NA exhibit substantial upfield shifts compared to those of the free 2-NA ( $\Delta\delta = -0.24$  to  $-0.16$  ppm) (Figure 3A), suggesting the inclusion of the naphthalene moiety of 2-NA into the hydrophobic CP6 cavity. The assignment of these naphthyl proton signals of the inclusion complex can be verified by the analysis of the <sup>1</sup>H-<sup>1</sup>H COZY data (correlation spectroscopy; see Supplementary Figure 1). Furthermore, these shifts appeared due to fast proton exchange observed for complexation in the <sup>1</sup>H NMR timescale. The 2D NOESY data (Figure 4) show the NOE correlations between the aromatic protons (H<sub>a-g</sub>) of the entrapped 2-NA and the aromatic proton H<sub>1</sub> of CP6, which also revealed the interpenetrated geometry.

To quantitatively estimate the binding behaviors of p-TSA and 2-NA with host CP6, fluorescence titrations were conducted at 298 K in a PBS of pH 6.0. Job plots (Supplementary Figures 2,3) based on the fluorescence titrations data indicated that CP6 and the two guests form a 1:1 host-guest complex in aqueous solution, respectively. By using a non-linear curve-fitting method (Supplementary Figures 4,5), the association constants ( $K_a$ ) were calculated to be  $(2.23 \pm 0.15) \times 10^4 \text{ M}^{-1}$  and  $(1.97 \pm 0.28) \times 10^4 \text{ M}^{-1}$  for p-TSA and 2-NA, respectively. According to the pK<sub>a</sub> values of the two aromatic sulfonic acids (p-TSA:  $-2.1$ ; 2-NA:  $-1.8$ ), it can be concluded that the sulfonic groups of the two aromatic sulfonic acids should be in the deprotonated form at pH 6.0. Thus, we conclude that the interaction mechanism of CP6 with the two aromatic sulfonic acids is that the acidic aromatic sulfonic acids with one sulfonate anion could bind positively charged CP6 bearing 12 -NH<sub>3</sub><sup>+</sup> groups in aqueous solutions at pH 6.0, where the electrostatic interactions between sulfonate anion of the two



**FIGURE 1** | Partial <sup>1</sup>H NMR spectra (400 MHz, D<sub>2</sub>O, 298 K) of (A) 20.00 mM **p-TSA**, (B) 2.00 mM **CP6** and 20.00 mM **p-TSA**, (C) after addition of 1.0 μL of aqueous NaOD solution (30%) to b, (D) after addition of 2.0 μL of aqueous DCl solution (20%) to c, and (E) 2.00 mM **CP6** at pD 6.0.

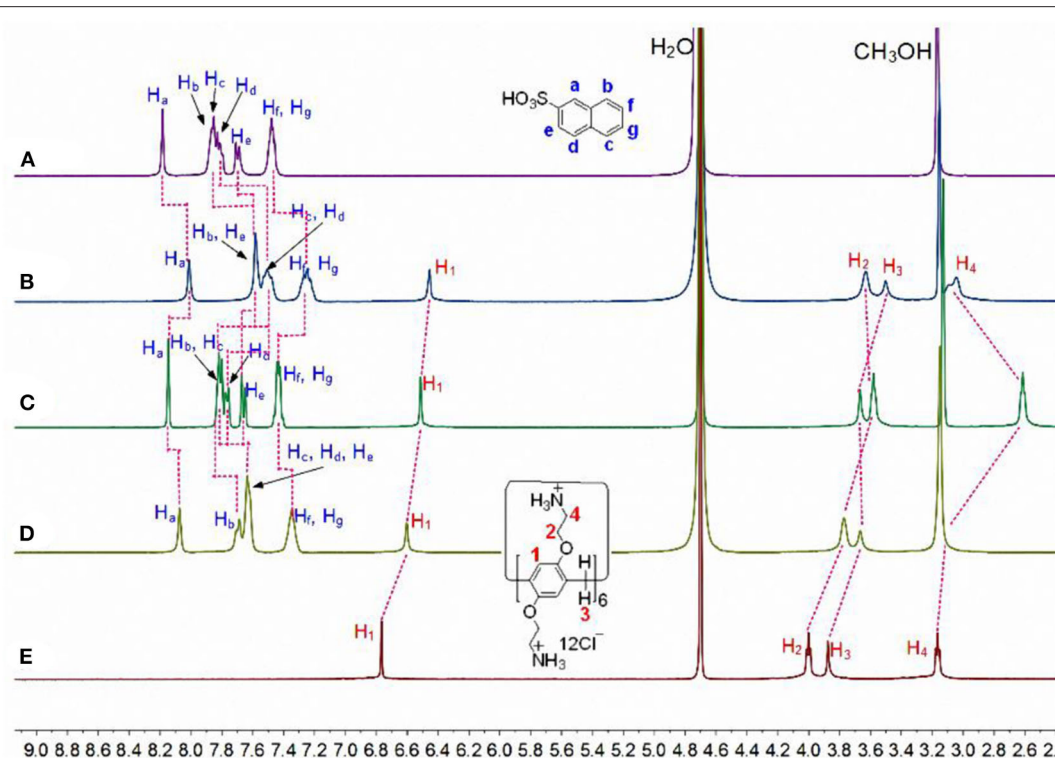


**FIGURE 2** | 2D NOESY NMR (400 MHz, D<sub>2</sub>O, 298 K, mixing time = 300 ms) spectrum of a solution of **CP6** (2.00 mM) and **p-TSA** (20.00 mM).

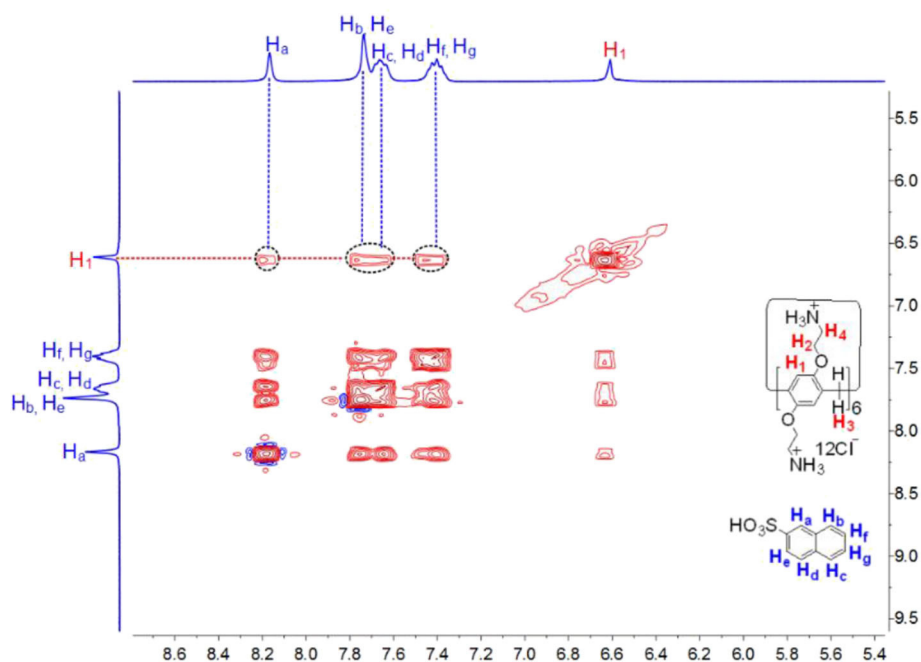
acidic aromatic sulfonic acids and the cationic portals of the host **CP6** play a dominant role in formation of the present host-guest complexation. By comparing **p-TSA** and **2-NA**, we can investigate the capability of these guests to form host-guest

complexes because of the changed size of the hydrophobic part. The  $K_a$  value for **p-TSA** is almost same as that for **2-NA**. Although **2-NA** has one more benzene ring than **p-TSA** and thus the larger  $\pi$ -conjugated system could afford a stronger





**FIGURE 3** | Partial  $^1\text{H}$  NMR spectra (400 MHz,  $\text{D}_2\text{O}/\text{CD}_3\text{OD} = 1/1$ , v/v, 298 K) of (A) 20.00 mM 2-NA, (B) 2.00 mM CP6 and 20.00 mM 2-NA, (C) after addition of 1.0  $\mu\text{L}$  of aqueous NaOD solution (30%) to b, (D) after addition of 2.0  $\mu\text{L}$  of aqueous DCl solution (20%) to c, and (E) 2.00 mM CP6 at pH 6.0.



**FIGURE 4** | 2D NOESY NMR (400 MHz,  $\text{D}_2\text{O}$ , 298 K, mixing time = 300 ms) spectrum of a solution of CP6 (2.00 mM) and 2-NA (20.00 mM).

$\pi$ - $\pi$  stacking interaction with the host cavity (Gómez et al., 2014), the electrostatic attractive forces are dominant in these two host-guest complexes.

Additionally, both the obtained p-TSA@CP6 and 2-NA@CP6 have pH-responsiveness, i.e., the dynamic behavior for the inclusion process of the two aromatic sulfonic acids and

CP6 can be reversed upon the addition of HCl and NaOH aqueous solutions. Proton NMR studies were conducted to affirm these two reverse processes (Figures 1, 3). As shown in Figures 1C, 3C, when adding NaOD to the mixed solution of p-TSA/CP6 and 2-NA/CP6, respectively, both signals of p-TSA and 2-NA returned to almost their uncomplexed positions, suggesting that both p-TSA and 2-NA dethreaded from the cavity of CP6. The reason is apparent: the addition of an aqueous NaOD solution yielded a basic solution and the  $\text{NH}_3^+$  groups on CP6 were deprotonated to produce the neutral amino groups, resulting in the disappearance of the electrostatic attractive forces between p-TSA or 2-NA and CP6. However, after adding DCl to these solutions,  $^1\text{H}$  NMR spectra similar to those of the original solutions of p-TSA/CP6 and 2-NA/CP6 were obtained (Figures 1D, 3D), resulting from the protonation of the amino groups and the regeneration of the complexes between p-TSA or 2-NA and CP6 in this solution. Thus, the host-guest complexes p-TSA/CP6 and 2-NA/CP6 can be reversed by the sequential addition of a base and an acid (NaOH and HCl, respectively) between its complexed and decomplexed states. In a word, the host-guest complexation between p-TSA or 2-NA and CP6 is pH-responsive and its reversible property can be used to serve as excellent motifs for a variety of controlled molecular release applications.

## CONCLUSIONS

In summary, novel pH-responsive host-guest recognition motifs based on a water-soluble pillar[6]arene dodecyl-ammonium chloride CP6 with p-TSA or 2-NA were successfully constructed. It was established that CP6 could form a stable 1:1 inclusion complex with the two aromatic sulfonic acids, p-TSA and 2-NA, respectively. Furthermore, both these host-guest complexes can be controlled reversibly through the sequential addition of a base and an acid (NaOH and HCl, respectively) between its complexed and decomplexed states. Consequently, the findings of this

work enrich the fields of controlled pillararene chemistry. Our further work will focus on expanding these new pH-responsive host-guest binding motifs to construct smart supramolecular materials in the treatment of sulfonated aromatic pollutants in aqueous media.

## DATA AVAILABILITY STATEMENT

All datasets generated for this study are included in the article/Supplementary Material.

## AUTHOR CONTRIBUTIONS

QD, FW, and KL designed the work. QD made contributions to the experiments and collective data. The paper was written by QD. All authors extensively discussed the results, reviewed the manuscript, and approved the final version of the manuscript to be submitted.

## FUNDING

This work was supported by the National Natural Science Foundation of China (no. 21402040), Henan Province Science and Technology Research Program (no. 192102210197), and Program for Innovative Research Team (in Science and Technology) in University of Henan Province (no. 20IRTSTHN008). Financial support from the Program of 543 team and Research and Cultivation Foundation of Henan University of Engineering (PYXM202009) is gratefully acknowledged.

## SUPPLEMENTARY MATERIAL

The Supplementary Material for this article can be found online at: <https://www.frontiersin.org/articles/10.3389/fchem.2020.588201/full#supplementary-material>

## REFERENCES

- Avestro, A.-J., Belowich, M. E., and Stoddart, J. F. (2012). Cooperative self-assembly: producing synthetic polymers with precise and concise primary structures. *Chem. Soc. Rev.* 41, 5881–5895. doi: 10.1039/C2CS35167F
- Badjic, J. D., Balzani, V., Credi, A., Silvi, S., and Stoddart, J. F. (2004). A molecular elevator. *Science* 303, 1845–1849. doi: 10.1126/science.1094791
- Cantekin, S., Markvoort, A. J., Elemans, J. A. A. W., Rowan, A. E., and Nolte, R. J. M. (2015). Allosterically controlled threading of polymers through macrocyclic dimers. *J. Am. Chem. Soc.* 137, 3915–3923. doi: 10.1021/jacs.5b00431
- Cao, D., Kou, Y., Liang, J., Chen, Z., Wang, L., and Meier, H. (2009). A facile and efficient preparation of pillararenes and a pillarquinone. *Angew. Chem. Int. Ed.* 48, 9721–9723. doi: 10.1002/anie.200904765
- Cao, Y., Hu, X.-Y., Li, Y., Zou, X., Xiong, X., Lin, C., et al. (2014). Multistimuli-responsive supramolecular vesicles based on water-soluble pillar[6]arene and SAINT complexation for controllable drug release. *J. Am. Chem. Soc.* 136, 10762–10769. doi: 10.1021/ja505344t
- Chang, Y., Yang, K., Wei, P., Huang, S., Pei, Y., Zhao, W., et al. (2014). Cationic vesicles based on amphiphilic pillar[5]arene capped with ferrocenium: a redox-responsive system for drug/siRNA co-delivery. *Angew. Chem. Int. Ed.* 53, 13126–13130. doi: 10.1002/anie.201407272
- Credit, A., Balzani, V., Langford, S. J., and Stoddart, J. F. (1997). Logic operations at the molecular level. An XOR gate based on a molecular machine. *J. Am. Chem. Soc.* 119, 2679–2681. doi: 10.1021/ja963572l
- Duan, Q., Cao, Y., Li, Y., Hu, X., Xiao, T., Lin, C., et al. (2013). pH-responsive supramolecular vesicles based on water-soluble pillar[6]arene and ferrocene derivative for drug delivery. *J. Am. Chem. Soc.* 135, 10542–10549. doi: 10.1021/ja405014r
- Duan, Q., Zhang, H., Mai, W., Wang, F., and Lu, K. (2019). Acid/base- and base/acid-switchable complexation between anionic-/cationic-pillar[6]arenes and a viologen ditosylate salt. *Org. Biomol. Chem.* 17, 4430–4434. doi: 10.1039/c9ob00398c
- Glasoe, P. K., and Long, F. A. (1960). Use of glass electrodes to measure acidities in deuterium oxide. *J. Phys. Chem.* 64, 188–190. doi: 10.1021/j100830a521
- Gómez, B., Francisco, V., Fernández-Nieto, F., García-Río, L., Paleo, M. R., and Sardina, F. J. (2014). Host-guest chemistry of a water-soluble Pillar[5]arene: evidence for an ionic-exchange recognition process and different

- complexation modes. *Chem. Eur. J.* 20, 12123–12132. doi: 10.1002/chem.201403194
- Guan, Y., Ni, M., Hu, X., Xiao, T., Xiong, S., Lin, C., et al. (2012). Pillar[5]arene-based polymeric architectures constructed by orthogonal supramolecular interactions. *Chem. Commun.* 48, 8529–8531. doi: 10.1039/c2cc33943a
- Guo, D.-S., and Liu, Y. (2012). Calixarene-based supramolecular polymerization in solution. *Chem. Soc. Rev.* 41, 5907–5921. doi: 10.1039/C2CS35075K
- Guo, D.-S., and Liu, Y. (2014). Supramolecular chemistry of p-sulfonatocalix[n]arenes and its biological applications. *Acc. Chem. Res.* 47, 1925–1934. doi: 10.1021/ar500009g
- Han, T., and Chen, C.-F. (2007). Formation of ternary complexes between a macrotricyclic host and hetero-guest pairs: an acid-base controlled selective complexation process. *Org. Lett.* 9, 4207–4210. doi: 10.1021/ol701770h
- Han, Y., Meng, Z., Ma, Y.-X., and Chen, C.-F. (2014). Iptycene-derived crown ether hosts for molecular recognition and self-assembly. *Acc. Chem. Res.* 47, 2026–2040. doi: 10.1021/ar5000677
- Hu, X.-Y., Liu, X., Zhang, W., Qin, S., Yao, C., Li, Y., et al. (2016). Controllable construction of biocompatible supramolecular micelles and vesicles by water-soluble phosphate pillar[5,6]arenes for selective anti-cancer drug delivery. *Chem. Mater.* 28, 3778–3788. doi: 10.1021/acs.chemmater.6b00691
- Li, C. (2014). Pillararene-based supramolecular polymers: from molecular recognition to polymeric aggregates. *Chem. Commun.* 50, 12420–12433. doi: 10.1039/c4cc03170a
- Li, S.-L., Xiao, T., Lin, C., and Wang, L. (2012). Advanced supramolecular polymers constructed by orthogonal self-assembly. *Chem. Soc. Rev.* 41, 5950–5968. doi: 10.1039/C2CS35099H
- Ma, X., and Tian, H. (2014). Stimuli-responsive supramolecular polymers in aqueous solution. *Acc. Chem. Res.* 47, 1971–1981. doi: 10.1021/ar500033n
- Ni, M., Zhang, N., Xia, W., Wu, X., Yao, C., Liu, X., et al. (2016). Dramatically promoted swelling of a hydrogel by pillar[6]arene-ferrocene complexation with multi-stimuli responsiveness. *J. Am. Chem. Soc.* 138, 6643–6649. doi: 10.1021/jacs.6b03296
- Ogoshi, T., Kanai, S., Fujinami, S., Yamagishi, T.-A., and Nakamoto, Y. (2008). para-Bridged symmetrical pillar[5]arenes: their Lewis acid catalyzed synthesis and host-guest property. *J. Am. Chem. Soc.* 130, 5022–5023. doi: 10.1021/ja711260m
- Ogoshi, T., Shiga, R., and Yamagishi, T.-A. (2012). Reversibly tunable lower critical solution temperature utilizing host-guest complexation of pillar[5]arene with triethylene oxide substituents. *J. Am. Chem. Soc.* 134, 4577–4580. doi: 10.1021/ja300989n
- Ogoshi, T., Yamagishi, T.-A., and Nakamoto, Y. (2016). Pillar-shaped macrocyclic hosts pillar[n]arenes: new key players for supramolecular chemistry. *Chem. Rev.* 116, 7937–8002. doi: 10.1021/acs.chemrev.5b00765
- Palmer, L. C., and Rebek, J. Jr. (2004). The ins and outs of molecular encapsulation. *Org. Biomol. Chem.* 2, 3051–3059. doi: 10.1039/B412510J
- Si, W., Li, Z.-T., and Hou, J.-L. (2014). Voltage-driven reversible insertion into and leaving from a lipid bilayer: tuning transmembrane transport of artificial channels. *Angew. Chem. Int. Ed.* 53, 4578–4581. doi: 10.1002/anie.201311249
- Vukotic, V. N., and Loeb, S. J. (2012). Coordination polymers containing rotaxane linkers. *Chem. Soc. Rev.* 41, 5896–5906. doi: 10.1039/C2CS35141B
- Wang, S., Xu, Z., Wang, T., Xiao, T., Hu, X.-Y., Shen, Y.-Z., et al. (2018). Warm/cool-tone switchable thermochromic material for smart windows by orthogonally integrating properties of pillar[6]arene and ferrocene. *Nat. Commun.* 9:1737. doi: 10.1038/s41467-018-03827-3
- Wang, X., Liu, Z.-J., Hill, E. H., Zheng, Y., Guo, G., Wang, Y., et al. (2019). Organic-inorganic hybrid pillararene-based nanomaterial for label-free sensing and catalysis. *Matter* 1, 848–861. doi: 10.1016/j.matt.2019.03.005
- Wu, T., Cai, X., Tan, S., Li, H., Liu, J., and Yang, W. (2011). Adsorption characteristics of acrylonitrile, p-toluenesulfonic acid, 1-naphthalenesulfonic acid and methyl blue on graphene in aqueous solutions. *Chem. Eng. J.* 173, 144–149. doi: 10.1016/j.cej.2011.07.050
- Xiao, T., Qi, L., Zhong, W., Lin, C., Wang, R., and Wang, L. (2019). Stimuli-responsive nanocarriers constructed from pillar[n]arene-based supramolecular amphiphiles. *Mater. Chem. Front.* 3, 1973–1993. doi: 10.1039/C9QM00428A
- Xiao, T., Xu, L., Zhong, W., Zhou, L., Sun, X.-Q., Hu, X.-Y., et al. (2018). Advanced functional materials constructed from pillar[n]arenes. *Isr. J. Chem.* 58, 1219–1229. doi: 10.1002/ijch.201800026
- Xu, J.-F., Chen, Y.-Z., Wu, D., Wu, L.-Z., Tung, C.-H., and Yang, Q.-Z. (2013). Photoresponsive hydrogen-bonded supramolecular polymers based on a stiff stilbene unit. *Angew. Chem. Int. Ed.* 52, 9738–9742. doi: 10.1002/anie.201303496
- Xue, M., Yang, Y., Chi, X., Zhang, Z., and Huang, F. (2012). Pillararenes, a new class of macrocycles for supramolecular chemistry. *Acc. Chem. Res.* 45, 1294–1308. doi: 10.1021/ar2003418
- Yakimova, L. S., Shurpik, D. N., Gilmanova, L. H., Makhmutova, A. R., Rakhimbekova, A., et al. (2016). Highly selective binding of methyl orange dye by cationic water-soluble pillar[5]arenes. *Org. Biomol. Chem.* 14, 4233–4238. doi: 10.1039/c6ob00539j
- Yao, Y., Xue, M., Chen, J., Zhang, M., and Huang, F. (2012). An amphiphilic pillar[5]arene: synthesis, controllable self-assembly in water, and application in calcein release and TNT adsorption. *J. Am. Chem. Soc.* 134, 15712–15715. doi: 10.1021/ja3076617
- Yu, G., Zhou, X., Zhang, Z., Han, C., Mao, Z., Gao, C., et al. (2012). Pillar[6]arene/paraquat molecular recognition in water: high binding strength, pH-responsiveness, and application in controllable self-assembly, controlled release, and treatment of paraquat poisoning. *J. Am. Chem. Soc.* 134, 19489–19497. doi: 10.1021/ja3099905
- Zhang, H., Zhou, B., Li, H., Qu, D. H., and Tian, H. (2013). A ferrocene-functionalized [2]rotaxane with two fluorophores as stoppers. *J. Org. Chem.* 78, 2091–2098. doi: 10.1021/jo302107a
- Zhang, M., Yan, X., Huang, F., Niu, Z., and Gibson, H. W. (2014). Stimuli-responsive host-guest systems based on the recognition of cryptands by organic guests. *Acc. Chem. Res.* 47, 1995–2005. doi: 10.1021/ar500046r
- Zhang, Z., Han, C., Yu, G., and Huang, F. (2012). A solvent-driven molecular spring. *Chem. Sci.* 3, 3026–3031. doi: 10.1039/C2SC20728A
- Zhang, Z., Luo, Y., Chen, J., Dong, S., Yu, Y., Ma, Z., et al. (2011). Formation of linear supramolecular polymers that is driven by C-H... $\pi$  interactions in solution and in the solid state. *Angew. Chem. Int. Ed.* 50, 1397–1401. doi: 10.1002/anie.201006693
- Zhou, Y., Jie, K., Zhao, R., Li, E., and Huang, F. (2020). Highly selective removal of trace isomers by nonporous adaptive pillararene crystals for chlorobutane purification. *J. Am. Chem. Soc.* 142, 6957–6961. doi: 10.1021/jacs.0c02684

**Conflict of Interest:** The authors declare that the research was conducted in the absence of any commercial or financial relationships that could be construed as a potential conflict of interest.

Copyright © 2020 Duan, Wang, Zhang and Lu. This is an open-access article distributed under the terms of the Creative Commons Attribution License (CC BY). The use, distribution or reproduction in other forums is permitted, provided the original author(s) and the copyright owner(s) are credited and that the original publication in this journal is cited, in accordance with accepted academic practice. No use, distribution or reproduction is permitted which does not comply with these terms.



# Stimuli-Responsive Biomass Cellulose Particles Being Able to Reversibly Self-Assemble at Fluid Interface

Yue Zhu<sup>1</sup>, Tingting Chen<sup>1\*</sup>, Zhenggang Cui<sup>2\*</sup>, Hong Dai<sup>1\*</sup> and Li Cai<sup>1</sup>

<sup>1</sup> School of Chemistry and Chemical Engineering, Nantong University, Nantong, China, <sup>2</sup> The Key Laboratory of Synthetic and Biological Colloids, Ministry of Education, School of Chemical and Material Engineering, Jiangnan University, Wuxi, China

## OPEN ACCESS

### Edited by:

Tangxin Xiao,  
Changzhou University, China

### Reviewed by:

Jinfeng Dong,  
Wuhan University, China  
Hengquan Yang,  
Shanxi University, China

### \*Correspondence:

Tingting Chen  
ttchen1980@126.com  
Zhenggang Cui  
cuizhenggang@hotmail.com  
Hong Dai  
dh123@ntu.edu.cn

### Specialty section:

This article was submitted to  
Supramolecular Chemistry,  
a section of the journal  
Frontiers in Chemistry

**Received:** 25 April 2020

**Accepted:** 09 July 2020

**Published:** 06 October 2020

### Citation:

Zhu Y, Chen T, Cui Z, Dai H and Cai L  
(2020) Stimuli-Responsive Biomass  
Cellulose Particles Being Able to  
Reversibly Self-Assemble at Fluid  
Interface. *Front. Chem.* 8:712.  
doi: 10.3389/fchem.2020.00712

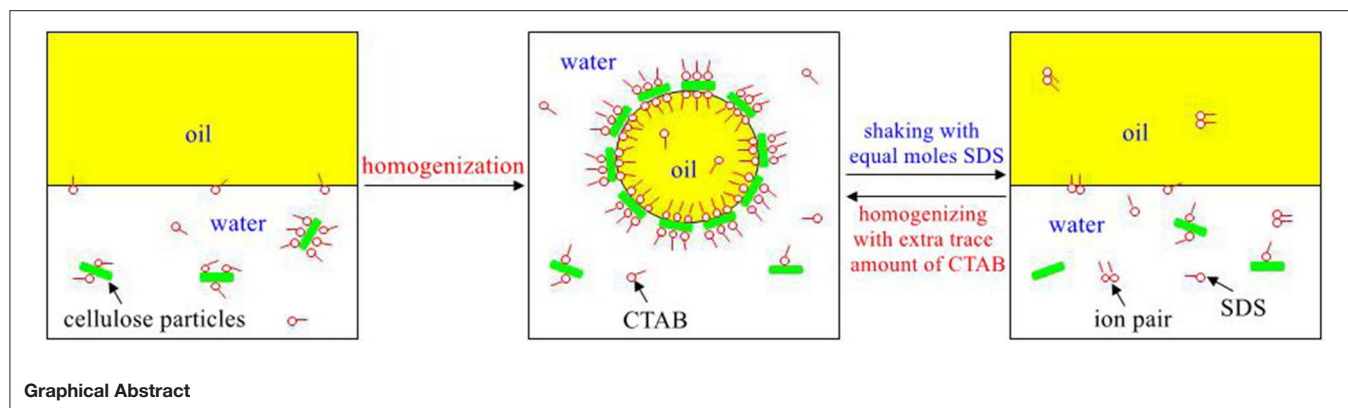
Stimuli-responsive surface-active microcrystalline cellulose (MCC) particles are obtained by interaction with conventional cationic surfactants such as cetyltrimethylammonium bromide (CTAB) in aqueous media, where MCC are *in situ* hydrophobized by adsorption of the cationic surfactant in water via electrostatic interaction and with the *in situ* hydrophobization removed by adding an equimolar amount of an anionic surfactant such as sodium dodecyl sulfate (SDS). The trigger is that the electrostatic interaction between the oppositely charged ionic surfactants is stronger than that between the cationic surfactant and the negative charges on particle surfaces, or the anionic surfactant prefers to form ion pairs with the cationic surfactants and thus making them desorbed from surface of MCC. Reversible O/W Pickering emulsions can then be obtained by using the MCC in combination with trace amount of a cationic surfactant and an anionic surfactant, and the anionic surfactant with a longer alkyl chain is more efficient for demulsification. With excellent biocompatibility, biodegradability, and renewability, as well as low toxicity, the biomass cellulose particles that can be made stimuli-responsive and able to reversibly self-assemble at fluid interface become ideal biocompatible particulate materials with extensive applications involving emulsions and foams.

**Keywords:** biomass cellulose particles, stimuli-responsive Pickering emulsions, *in situ* hydrophobization, reversibly self-assemble, amphiphiles

## INTRODUCTION

The emulsions stabilized by colloid particles are called Pickering emulsions. They are very stable because there is a dense particle film at the oil–water interface, providing a strong barrier to prevent coalescence of the droplets (Aveyard et al., 2003; Binks and Horozov, 2006). However, it is relatively difficult to demulsify when the emulsions are needed to be temporarily stable. Therefore, there has been much progress in preparing stimuli-responsive colloid particles, which can make the Pickering emulsions transit easily between stable and unstable. Various triggers have been developed such as pH (Binks et al., 2007; Fujii et al., 2011a,b; Liu et al., 2012, 2014; Morse et al., 2013; Tu and Lee, 2014), temperature (Binks et al., 2005; Saigal et al., 2010), CO<sub>2</sub>/N<sub>2</sub> (Lin and Theato, 2013; Yang et al., 2013; Zhang et al., 2013; Liang et al., 2014; Liu et al., 2014), redox (Quesada et al., 2013), light irradiation (Anwar et al., 2013; Tan et al., 2014), and magnetic field (Lam et al., 2011; Blanco et al., 2013), as well as dual stimuli such as pH–temperature (Ngai et al., 2005; Yang et al., 2013; Yamagami et al., 2014), light–temperature (Fameau et al., 2013), and magnetic





field intensity–temperature (Brugger and Richtering, 2007; Rahman et al., 2011). Nevertheless, the particles involved are mostly functional polymers, and their synthesis is relatively complicated. In recent years, commercially available inorganic nanoparticles with no surface activity in nature have been made surface-active by coating (Aveyard et al., 2003) or hydrophobized *in situ* (Cui et al., 2010, 2012). In addition, these inorganic particles such as silica nanoparticles can also be made stimuli-responsiveness through reversible hydrophobized *in situ* with the triggers including  $\text{CO}_2/\text{N}_2$ , pH, temperature, and ion pair formation (Jiang et al., 2013; Zhu et al., 2014, 2015a,b, 2017a; Liu et al., 2017).

However, the inorganic particles, lack of biocompatibility and biodegradability, are limited in the applications involving food, cosmetic, pharmaceuticals, and so on. Therefore, recently, there is a great interest in biomass particles of biological origin for stabilizing emulsions and foams involved in food and drug delivery (Lam et al., 2014). The biomass particles include cellulose, starch, chitosan, and chitin, as well as aromatic macromolecules and polypeptides.

Cellulose is the most abundant biological polymer in the world, which is a linear polysaccharide with the units of  $\beta$  (1,4) glucopyranose. Cellulose particles have excellent biodegradability, renewability, and biocompatibility, as well as low toxicity. All these characteristics make them quite perfect materials in daily products including foods, cosmetics, and pharmaceuticals (Lam et al., 2014). Many researchers have found that stable emulsions can be achieved by various sized cellulose including macroscopic fibers, microcrystalline cellulose (MCC), and nanofibrillated cellulose, in addition to cellulose nanocrystals (CNCs) as particulate emulsifiers in some certain conditions (Lam et al., 2014). It has also been found that there is significant difference in surface activity and film forming (Cherhal et al., 2016; Hu et al., 2016a; Varanasi et al., 2018; Alfassi et al., 2019; Costa et al., 2019) with cellulose of different origin, size, and surface property. The native cellulose is in general hydrophilic (not surface active), and the size and shape can be diverse (Lam et al., 2014); however, it has been reported that many hydrophobically modified cellulose particles have been made potentially applicable in foods, as well as drug delivery (Lam et al., 2014), thanks to great improvement of their surface activity by

hydrophobic modification (Hu et al., 2015, 2016b; Ching et al., 2016; Duffus et al., 2016; Ojala et al., 2016; Tang et al., 2017; Zhu et al., 2017b; Bai et al., 2018, 2019; Aaen et al., 2019).

With hydrophilic surfaces, cellulose particles typically stabilize water-continuous emulsions, and oil-continuous emulsions have been achieved by Andresen and Stenius (Andresen and Stenius, 2007) by using silylation to improve the hydrophobicity and surface wettability of cellulose. But the surface activity endowed in this way is not reversible. In recent years, stimuli-responsive cellulose particles by suitable surface modification have also been reported (Zoppe et al., 2012; Tang et al., 2014, 2016, 2017). For example, Zoppe et al. (2012) made thermo-responsive CNCs by grafting poly(*N*-isopropylacrylamine) (PNIPAM) onto their surfaces; Tang et al. (2014) reported pH–temperature–responsive CNCs grafted by poly(dimethylaminoethylmethacrylate), and then they further obtained another dual-responsive (pH and temperature) CNC nanoparticles based on grafting binary polymer brushes consisting of poly(oligoethylene glycol) methacrylate and poly(methacrylic acid) (Tang et al., 2016). Nevertheless, the synthesis of these particulate materials is complicated.

Herein we report that cellulose particles can be made surface-active by *in situ* hydrophobization in water via interaction with a cationic surfactant, and the surface activity of the particles can be switched off at room temperature to achieve reversible self-assembly at fluid interface. This is accomplished simply by adding an anionic surfactant of equimolar amount into the systems, forming ion pairs with the cationic surfactant and resulting in loss of surface activity of particles. The stimuli-responsiveness of the cellulose particles is characterized by stabilization and destabilization of emulsions, and both cationic and anionic surfactants with different chain length were examined for their efficiency in stabilization and demulsification.

## EXPERIMENTAL

### Materials

Microcrystalline cellulose (99%) with a primary particle diameter of 20  $\mu\text{m}$  was purchased from Sigma. Cetyltrimethylammonium bromide (CTAB, 99%), dodecyltrimethylammonium bromide

(DTAB, 98%), sodium dodecyl sulfate (SDS, 99%), sodium decyl sulfate (99%), and sodium octyl sulfate (99%) were all purchased from Sigma. Dodecane with a purity  $\geq 99\%$  was purchased from Aladdin and was columned two times through neutral alumina to remove possible polar impurities. Other chemicals were purchased from Sinopharm Chemical Reagent Co., which were all analytically pure. The ultrapure water used in all experiments with a resistance of  $18.1 \text{ M}\Omega \text{ cm}$  at  $25^\circ\text{C}$  was provided by Nantong University Analysis and Testing Center, China.

## Methods

### Preparation Aqueous Dispersion of MCC Particles

Powdered MCC particles were weighed into a glass vessel with height of 6.5 cm and diameter of 2.5 cm, followed by adding pure water or surfactant solution. Then the particles were dispersed using an ultrasound probe (FS-250N; Shanghai ShengXi Co.) working at 50 W for 1 min.

### Preparation and Characterization of Pickering Emulsions

The water phase (7 mL) containing MCC particles (dispersed in pure water or surfactant solution) was placed in a glass vessel, and then 1:1 by volume of dodecane (7 mL) was added. The two phases were emulsified using a A25 ultraturrax homogenizer (Shanghai OuHe Co.) operating at 7,000 revolutions/min (rpm) for 2 min.

The emulsion type was confirmed by drop test (Cui et al., 2010), and the photographs of the emulsions were taken 1 day and 7 days after preparation. To observe the microstructure of the emulsions, an emulsion drop was placed on a glass slide followed by diluted with water and then observed by a TL1530 microscope system (Shanghai DiLun Co.).

### Demulsification/Restabilization Cycling of Emulsions

Emulsions stabilized by 0.3 wt% MCC dispersed in 0.01 mM cationic surfactant were destroyed by adding 0.07 mL concentrated (1 mM) anionic surfactant solution followed by gentle agitation with a stick and then leaving standing for 30 min. And the emulsions were restabilized again by addition

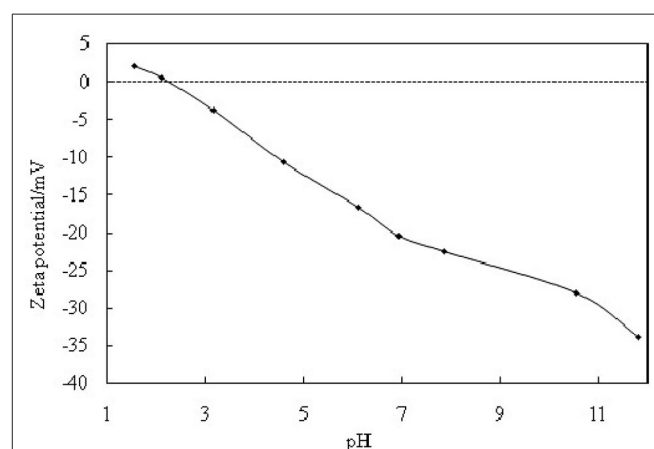
of 0.07 mL concentrated (1 mM) cationic surfactant solution followed by homogenization at 7,000 rpm for 2 min.

### Zeta Potential

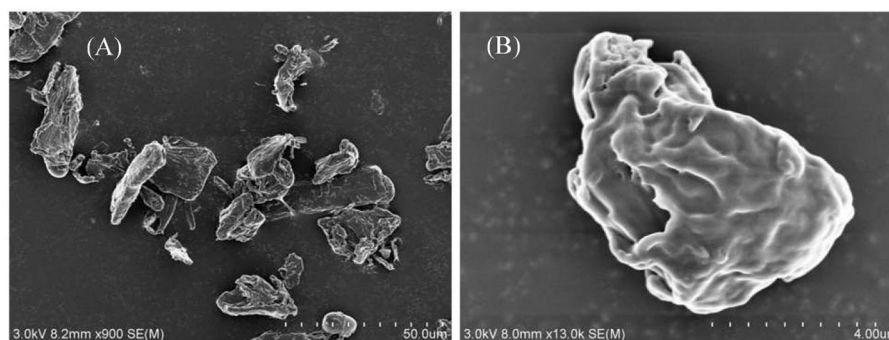
Microcrystalline cellulose 0.3 wt% was dispersed in surfactant solutions or pure water of different pH adjusted by adding aqueous HCl or NaOH at  $25^\circ\text{C}$ . The dispersion was left on stand for 24 h to reach equilibrium; the zeta potentials ( $\zeta$ ) of the particles were measured using a Zetasizer Nano (Malvern) instrument at room temperature.

### Interfacial Tension

The oil–water interfacial tension (IFT) was measured by drop shape method using Dropmeter A-100 drop shape analyzer (Ningbo Haishu Maishi Scientific Test Co., China), with the oil released from a U-shaped needle (outer diameter of  $0.86 \pm 0.005 \text{ mm}$ ) into water phase to form a reversed pendant drop at  $25^\circ\text{C}$ . Interfacial tension was calculated using the Young–Laplace method, and the result is an average of at least three measurements.



**FIGURE 2 |** Zeta potentials of cellulose particles in water (0.3%) of different pH at  $25^\circ\text{C}$ .



**FIGURE 1 |** SEM of cellulose particles as powders (A) and was ultrasonically dispersed in water (0.3%) (B).

## RESULTS AND DISCUSSION

### Dodecane-in-Water Pickering Emulsions Costabilized by Microcrystalline Cellulose and CTAB

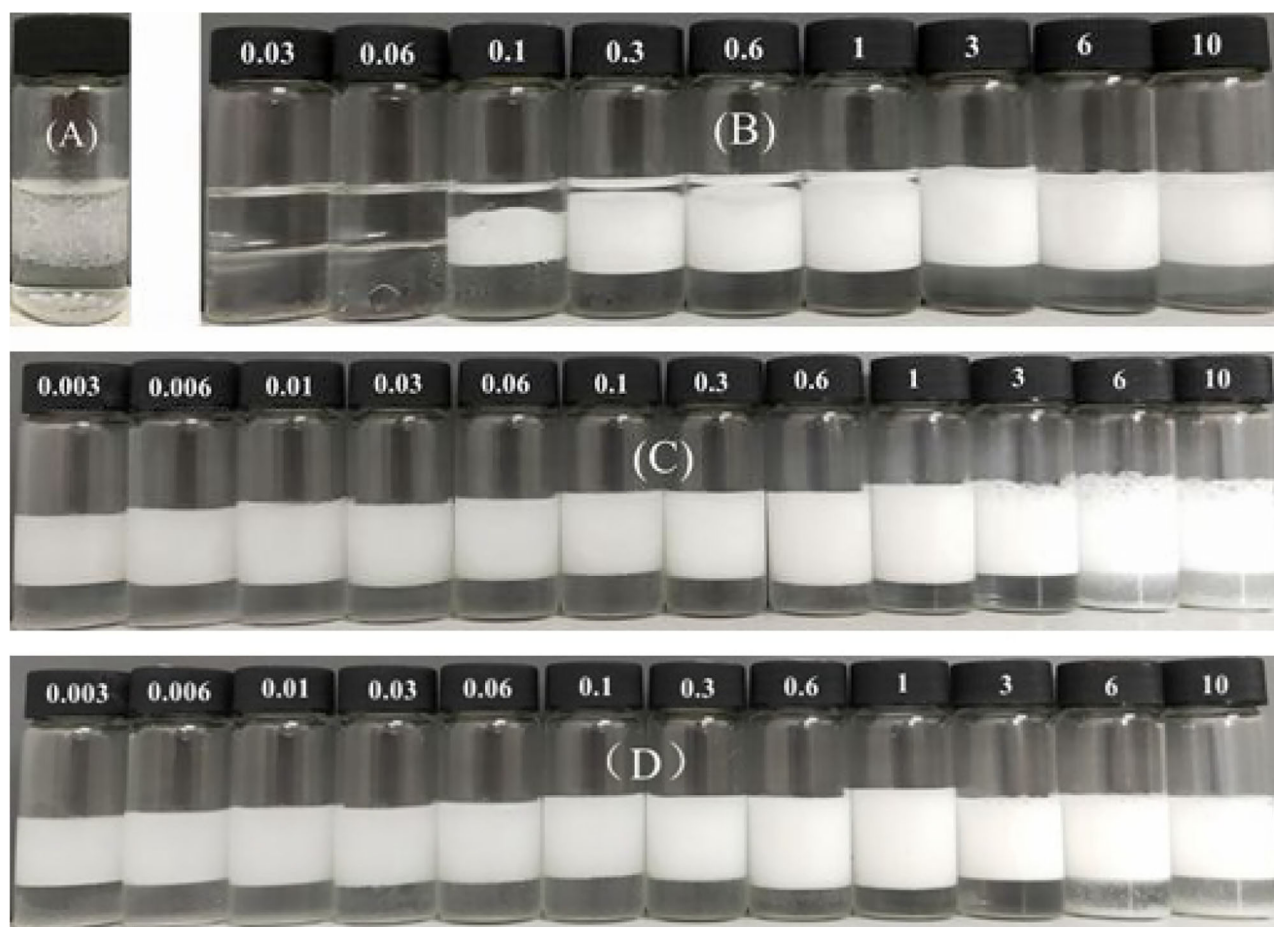
The hydrophilic bare MCC particles are rod-like with a primary diameter  $20\ \mu\text{m}$ , as shown by the scanning electron microscope (SEM) image in **Figure 1A**. When ultrasonically dispersed in water, small particles with diameter of approximately  $3\text{--}5\ \mu\text{m}$  can be obtained as shown in **Figure 1B**. They have an isoelectric point of 2.2 (**Figure 2**) and is negatively charged in neutral water. Microcrystalline cellulose particles alone at 0.3 wt.% cannot stabilize a dodecane-in-water emulsion, with big drops observed in the vessel, as shown in **Figure 3A**. Similarly, CTAB alone below its critical micelle concentration (cmc) of 0.9 mM (Zhu et al., 2015a) cannot stabilize a dodecane-in-water emulsion (**Figure 3B**). However, stable dodecane-in-water emulsions were obtained with 0.3 wt.% MCC particles plus CTAB, and almost no change appeared of the vessel after 24 h and 1 week as shown in **Figures 3C,D**. It was observed that the average droplet diameter decreases as CTAB concentration increases, as shown

in **Figure 4**. It is noticed that all droplets are much bigger than those stabilized by CTAB solely at 3 mM (**Figure 4D**), indicating that these droplets are stabilized mainly by particles coated with surfactant, or the emulsions formed are Pickering emulsions.

### Destabilization/Restabilization Transition of the Pickering Emulsions

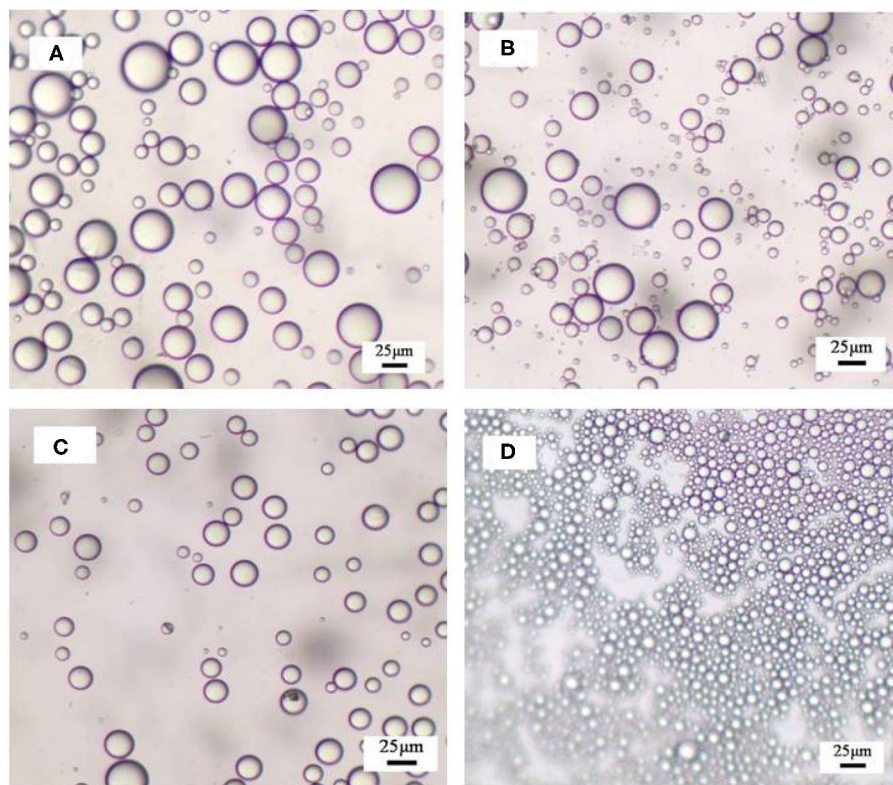
We have observed that if SDS, an anionic surfactant, was added (amount equal to that of CTAB) into an emulsion containing 0.3 wt.% MCC and CTAB of 0.01 mM, demulsification was observed with water phase and oil phase separated after gentle stirring. After an extra amount of CTAB (0.01 mM) was added into this system and the mixture was homogenized, stable Pickering emulsions can be formed again. This means that the Pickering emulsions stabilized by MCC and CTAB can be switched between stable and unstable, and MCC can be transferred between surface-active and surface-inactive.

For an emulsion comprising 0.3 wt.% MCC dispersed in 7 mL 0.01 mM CTAB solution and 7 mL dodecane (**Figure 5A**), once an equimolar amount of SDS (0.07 mL 1 mM SDS solution) was added (**Figure 5B**), almost complete demulsification was

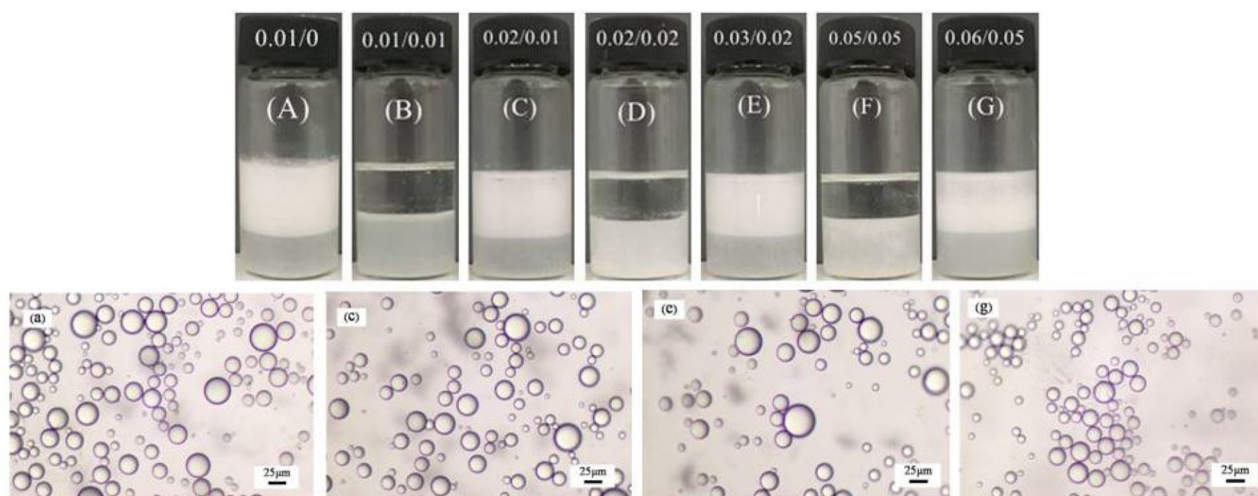


**FIGURE 3** | Dodecane-in-water emulsions stabilized by (A) 0.3 wt.% MCC particles solely, (B) CTAB alone at different concentration (mM), and 0.3 wt.% MCC particles plus CTAB at different concentration (mM), taken 24 h (A–C) and 7 days (D) after preparation.





**FIGURE 4** | Optical micrographs of obtained emulsions stabilized by (A–C) 0.3 wt.% MCC together with CTAB of various concentrations and by (D) CTAB solely recorded 24 h after preparation. The concentrations of CTAB are 0.01, 0.06, 0.3, and 3 mM (A–D).

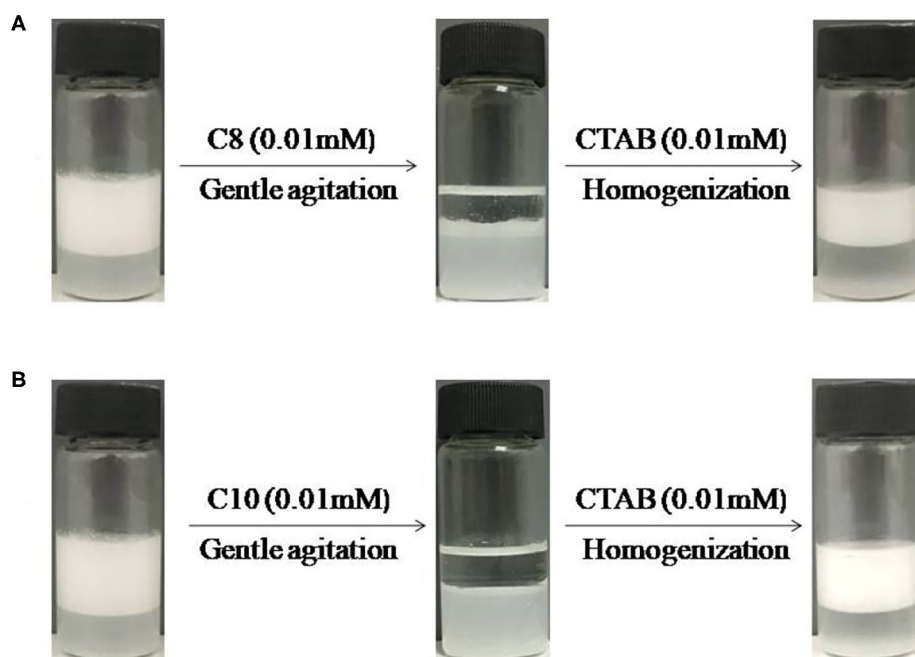


**FIGURE 5** | Photographs (A–G) of the dodecane-in-water Pickering emulsions stabilized by 0.3 wt.% MCC in combination with 0.01 mM CTAB undergoing unstable-stable cycles by adding 0.01 mM SDS and 0.01 mM CTAB alternately, and micrographs of the stable emulsions (A–G).

achieved after gentle agitation. Subsequently, when 0.01 mM free CTAB was added (adding extra 0.07 mL 1 mM CTAB solution), the stability of the emulsions was recovered by homogenization (Figure 5C). The emulsions are therefore stimuli-responsive by

alternate addition of an equimolar amount of SDS and extra CTAB, respectively, and the system can be recycled for at least five times as shown in Figure 5. Based on the micrographs shown in Figure 5, the average droplet sizes were statistically measured





**FIGURE 6 |** Switching dodecane-in-water emulsions containing 0.3 wt.% MCC with 0.01 mM CTAB between unstable by addition of (A) 0.01 M sodium octyl sulfate ( $C_8$ ) or (B) 0.01 M sodium decyl sulfate ( $C_{10}$ ) and restabilization by addition of extra 0.01 mM CTAB followed by homogenization.

to be 45, 45, 43, 41, and 40  $\mu\text{m}$ , respectively, for the five cycles, little change compared with the initial emulsion, suggesting that the droplet sizes depend only on the concentration of free CTAB in the aqueous phase.

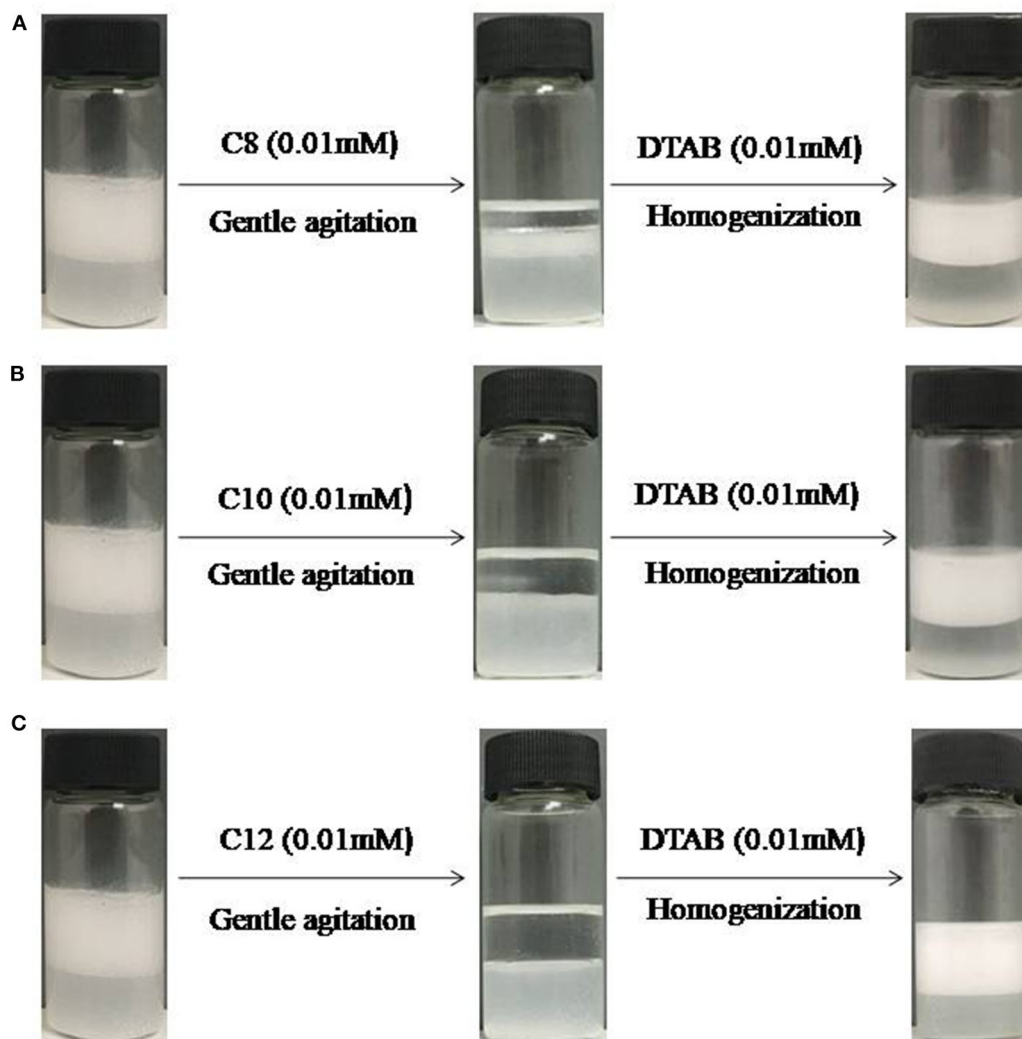
A question is whether other cationic surfactants and anionic surfactants are effective for *in situ* hydrophobization of the cellulose particles and demulsification. To find answers, DTAB as cationic surfactant and a series of sodium alkyl sulfates ( $C_8$ – $C_{12}$ ) as anionic surfactants were examined. **Figure 6** shows that in case of CTAB as cationic surfactant both  $C_8$  and  $C_{10}$  sodium alkyl sulfates are also effective at 0.01 mM for demulsification. And once CTAB was replaced by DTAB ( $C_{12}$ ) stimuli-responsive emulsions were obtained using  $C_8$  to  $C_{12}$  sodium alkyl sulfates as demulsifiers, as shown in **Figure 7**. However, the alkyl length did affect demulsification efficiency, as shown in **Figure 8**, where the oil phase is clearer after demulsification with increasing alkyl length of the anionic surfactants, and demulsification is not complete when using sodium octyl sulfate ( $C_8$ ), because the tendency of forming ionic pair increases with increasing total alkyl length. In fact, we have previously reported that for negatively charged silica nanoparticles the total alkyl length of cationic and anionic surfactants should be larger than  $C_{22}$  (Zhu et al., 2015a); this seems to be also true for the cellulose particles.

### Postulated Mechanism of MCC Reversibly Self-Assembling at Fluid Interface

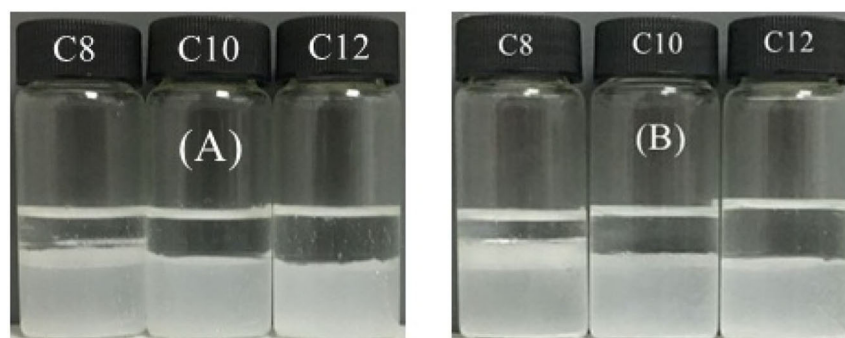
The stabilization and destabilization of emulsions indicate that MCC particles can reversibly self-assemble at fluid interface. The MCC particles are too hydrophilic, which has negatively charged when pH is beyond 2.2, as indicated in **Figure 2**. They are little

surface-active with a zeta potential of  $-22.5$  mV in the pure water (pH of dispersion 7.86). When MCC particles are dispersed in CTAB solution, the zeta potential is increased with increasing the concentration of CTAB, from negative to positive (**Figure 9**). It is proved that the cationic surfactant, CTAB, adsorbs to the negatively charged surfaces of MCC particles via electrostatic interaction and thus *in situ* hydrophobizes the surfaces. The particles then become surface-active to adsorb at the water-oil interface, stabilizing the Pickering emulsion, whereas, on the addition of SDS, an anionic surfactant, CTAB, prefers to form ion pairs with SDS (Kume et al., 2008; Tah et al., 2011), which makes CTAB desorb from MCC particles, resulting in demulsification as MCC particles return to the aqueous phase and become surface-inactive again. The mechanism is that there is much stronger electronic interaction between the anionic and cationic surfactants than that between particles and cationic surfactants with opposite charge. Here we provide the evidence of zeta potential, SEM, and the IFT to support the theory.

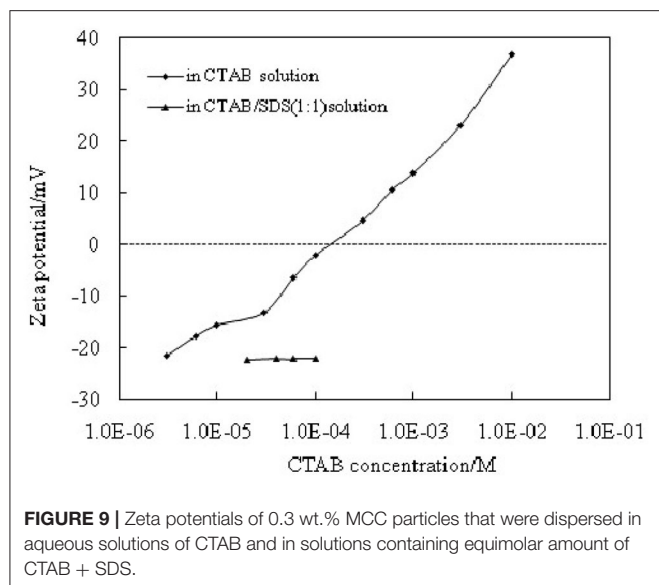
The change of zeta potential of 0.3 wt.% MCC during emulsification and demulsification cycling is shown in **Figure 10**. When 0.3 wt.% MCC is dispersed in the pure water, the zeta potential is  $-22.5$  mV (**Figure 10A**), and then it increases to  $-15.8$  mV (**Figure 10B**) in 0.01 mM CTAB solution. After addition of equimolar amount of SDS and an extra CTAB of 0.01 mM, respectively, the zeta potential decreases to  $-22.3$  mV (**Figure 10C**) and increases to  $-15.3$  mV (**Figure 10D**) in the first cycle and becomes  $-21.7$ – $-14.9$  mV (**Figures 10E,F**) in the second cycle, which indicates that the adsorption/desorption of the surfactant from the particle–water interface following adding CTAB and SDS is reversible. It is also indicated by



**FIGURE 7** | Switching between stable and unstable dodecane -in-water emulsions containing 0.3 wt% MCC with 0.01 mM DTAB followed by addition of **(A)** 0.01 M sodium octyl sulfate ( $C_8$ ) **(B)** 0.01 M sodium decyl sulfate ( $C_{10}$ ) **(C)** sodium dodecyl sulfate ( $C_{12}$ , SDS) and subsequently 0.01 mM DTAB.



**FIGURE 8** | Demulsification of Pickering emulsions stabilized by 0.3 wt.% MCC plus 0.01 mM CTAB **(A)** or by 0.3 wt.% MCC plus 0.01 mM DTAB **(B)** by adding an equimolar amount of sodium alkyl sulfate of different chain lengths (given) followed by gentle agitation, taken 2 h after addition.



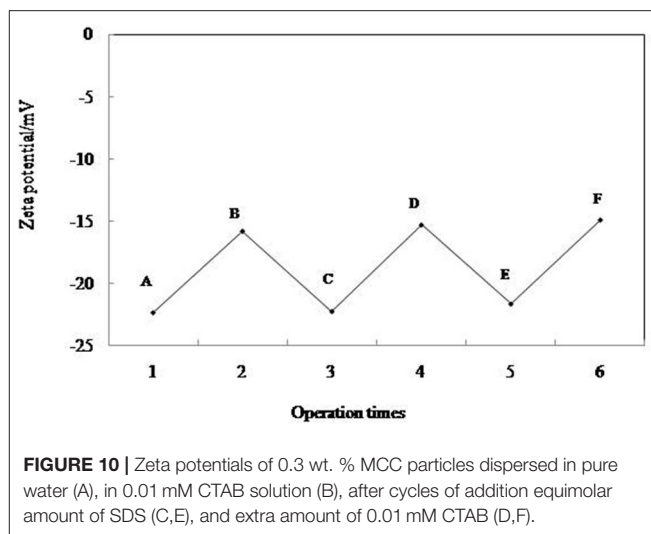
the photographs and micrographs shown in Figure 5. All these prove that cellulose particles can reversibly self-assemble at fluid interface.

Besides, the zeta potential of 0.3 wt.% MCC in the solution containing equimolar amount of SDS and CTAB at different concentration is almost not changed ( $-22.3 \pm 0.1$  mV) and is the same as in the pure water. It is believed that ion pairs consisting of anionic and cationic surfactants cannot adsorb to the particles, as shown in Figure 9. No stable emulsions were observed using this dispersion because particles are surface-inactive.

We have measured the dodecane/water IFT with either particles or surfactants or both in water, as shown in Table 1. The dodecane/pure water IFT is in good agreement with literature value (52.1 mN/m). Although the SEM of 0.3 wt.% MCC dispersed in 0.01 mM CTAB solution and in CTAB + SDS equimolar mixture at 0.01 mM shows no significant difference (Figure 11); the IFT (41.8 mN/m) between dodecane and dispersion of 0.3% particle in 0.01 mM CTAB solution is higher than that (35.8 mN/m) between dodecane and 0.01 mM CTAB solution, indicating adsorption of CTAB on particle surface, which reduced CTAB concentration in the dispersion. Actually flocculation was observed when 0.3 wt.% cellulose particles were dispersed in CTAB aqueous solution at CTAB concentration beyond 0.3 mM (not shown). When equal moles of SDS were added (0.3% cellulose particles dispersed in 0.01 mM CTAB + 0.01 mM SDS solution), the IFT (39.0 mN/m) is between the previous two systems. It is believed that the formation of ionic pairs reduces significantly the concentration of free CTAB and SDS, but the ionic pairs are also highly surface-active, which can strongly adsorb at oil–water interface to reduce the IFT.

## CONCLUSIONS

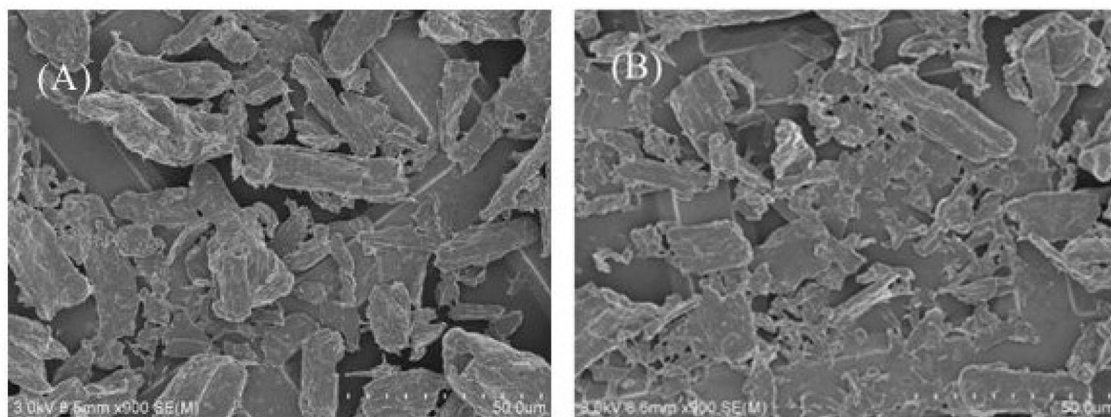
A simple protocol has been demonstrated to prepare the stimuli-responsive surface-active MCC particles, which are able



**TABLE 1 |** Interfacial tension between dodecane and aqueous phase with or without particles and surfactants at 25°C.

No.	Composition of aqueous phase	$\gamma$ /mN/m
1	Pure water	$52.1 \pm 0.1$
2	0.3% Cellulose	$48.7 \pm 0.1$
3	0.01 mM CTAB	$35.8 \pm 0.2$
4	0.3% Cellulose + 0.01 mM CTAB	$41.8 \pm 0.2$
5	0.3% Cellulose + 0.01 mM CTAB+0.01 mM SDS	$39.0 \pm 0.2$

to reversibly self-assemble at fluid interface via reversible *in situ* hydrophobization to stabilize stimuli-responsive Pickering emulsions. The stable Pickering emulsion is obtained by using negatively charged MCC particles *in situ* hydrophobized with a cationic surfactant in low concentration, whereas demulsification occurs by adding an anionic surfactant of equal moles. The restabilization of the Pickering emulsion is achieved again on addition of extra cationic surfactant which reestablishes the hydrophobization. The stimuli-responsiveness of the emulsions is due to the trigger that the electrostatic interaction between the oppositely charged ionic surfactants is stronger than that between the cationic surfactant and the particle surfaces. The added anionic surfactant prefers to form ion pairs, making cationic surfactant desorb from particle surfaces and particles surface-inactive returning to the water aqueous. This access avoids complicated synthesis of functional switchable particles as well as relative rigorous switching conditions. With excellent biocompatibility, biodegradability, and renewability, as well as low toxicity, the biomass cellulose particles, which are made stimuli-responsive and can then reversibly self-assembling at fluid interface, become ideal biocompatible particulate materials with more potential applications in many fields.



**FIGURE 11 |** SEM of 0.3 wt.% MCC dispersed in 0.01 mM CTAB solution **(A)** and in CTAB + SDS equimolar mixture at 0.01 mM **(B)**.

## DATA AVAILABILITY STATEMENT

The raw data supporting the conclusions of this article will be made available by the authors, without undue reservation.

## AUTHOR CONTRIBUTIONS

YZ wrote the manuscript. HD made the additional experiments according to the comments of reviewer. LC tested particles and Pickering emulsion. TC made the stimuli-responsiveness cellulose particles. ZC revised the article. All authors contributed to the article and approved the submitted version.

## REFERENCES

- Aaen, R., Brodin, F. W., Simon, S., Heggset, E. B., and Syverud, K. (2019). Oil-in-water emulsions stabilized by cellulosenanofibrils—the effects of ionic strength and pH. *Nanomaterials* 9, 259–272. doi: 10.3390/nano9020259
- Alfassi, G., Rein, D. M., and Cohen, Y. (2019). Cellulose emulsions and their hydrolysis. *J. Chem. Technol. Biotechnol.* 94, 178–184. doi: 10.1002/jctb.5760
- Andresen, M., and Stenius, P. (2007). Water-in-oil emulsions stabilized by hydrophobized microfibrillated cellulose. *J. Dispers. Sci. Technol.* 28, 837–844. doi: 10.1080/01932690701341827
- Anwar, N., Williams, T., Grimme, B., and Kuehne, A. J. C. (2013). Light-switchable and monodisperse conjugated polymer particles. *ACS Macro Lett.* 2, 766–769. doi: 10.1021/mz400362g
- Aveyard, R., Binks, B. P., and Clint, J. H. (2003). Emulsions stabilized solely by colloidal particles. *Adv. Colloid Interface Sci.* 10, 503–546. doi: 10.1016/S0001-8686(02)00069-6
- Bai, L., Huan, S.-Q., Xiang, W.-C., and Rojas, O. J. (2018). Pickering Emulsions by combining cellulose nanofibrils and nanocrystals: phase behavior and depletion stabilization. *Green Chem.* 20, 1571–1582. doi: 10.1039/C8GC00134K
- Bai, L., Lv, S.-S., Xiang, W.-C., Huan, S.-Q., McClements, D. J., and Rojas, O. J. (2019). Oil-in-water pickering emulsions via microfluidization with cellulose nanocrystals: 1. Formation and stability. *Food Hydrocoll.* 96, 699–708. doi: 10.1016/j.foodhyd.2019.04.038
- Binks, B. P., and Horozov, T. S. (Eds.). (2006). In *Colloidal Particles at Liquid Interfaces*. Cambridge: Cambridge University Press. doi: 10.1017/CBO9780511536670
- Binks, B. P., Murakami, R., Armes, S. P., and Fujii, S. (2005). Temperature-induced inversion of nanoparticle-stabilized emulsions. *Angew. Chem. Int. Ed.* 117, 4873–4876. doi: 10.1002/ange.200501073

## FUNDING

Financial support from the National Natural Science Foundation of China (NSFC 21802075) and funds received for open access publication fees.

## ACKNOWLEDGMENTS

Financial support from the National Natural Science Foundation of China (NSFC 21802075) is gratefully acknowledged.

- Binks, B. P., Murakami, R., Armes, S. P., Fujii, S., and Schmid, A. (2007). pH-responsive aqueous foams stabilized by ionizable latex particles. *Langmuir* 23, 8691–8694. doi: 10.1021/la700444a
- Blanco, E., Lam, S., Smoukov, S. K., Velikov, K. P., Khan, S. A., and Velez, O. D. (2013). Stability and viscoelasticity of magneto-pickering foams. *Langmuir* 29, 10019–10027. doi: 10.1021/la4014224
- Brugger, B., and Richtering, W. (2007). Magnetic, thermosensitive microgels as stimuli-responsive emulsifiers allowing for remote control of separability and stability of oil-in-water emulsions. *Adv. Mater.* 19, 2973–2978. doi: 10.1002/adma.200700487
- Cherhal, F., Cousin, F., and Capron, I. (2016). Structural description of the interface of pickering emulsions stabilized by cellulose nanocrystals. *Biomacromolecules* 17, 496–502. doi: 10.1021/acs.biomac.5b01413
- Ching, Y. C., Ali, M. D. E., Abdullah, L. C., Choo, K. W., Ching, K. Y., Julaihi, S. J., et al. (2016). Rheological properties of cellulose nanocrystal-embedded polymer composites: a review. *Cellulose* 23, 1011–1030. doi: 10.1007/s10570-016-0868-3
- Costa, C., Medronho, B., Filipe, A., Mira, I., Lindman, B., Edlund, H., et al. (2019). Emulsion formation and stabilization by biomolecules: the leading role of cellulose. *Polymers* 11, 1570–1587. doi: 10.3390/polym11101570
- Cui, Z.-G., Cui, C.-F., Zhu, Y., and Binks, B. P. (2012). Multiple phase inversion of emulsions stabilized by in situ surface activation of CaCO<sub>3</sub> nanoparticles via adsorption of fatty acids. *Langmuir* 28, 314–320. doi: 10.1021/la204021v
- Cui, Z.-G., Yang, L.-L., Cui, Y.-Z., and Binks, B. P. (2010). Effects of surfactant structure on the phase inversion of emulsions stabilized by mixtures of silica nanoparticles and cationic surfactant. *Langmuir* 26, 4717–4724. doi: 10.1021/la903589e
- Duffus, L. J., Norton, J. E., Smith, P., Norton, I. T., and Spyropoulos, F. (2016). A comparative study on the capacity of a range of food-grade particles to form



- stable O/W and W/O pickering emulsions. *J. Colloid Interf. Sci.* 473, 9–21. doi: 10.1016/j.jcis.2016.03.060
- Fameau, A. L., Lam, S., and Velez, O. D. (2013). Multi-stimuli responsive foams combining particles and self assembling fatty acids. *Chem. Sci.* 4, 3874–3881. doi: 10.1039/c3sc51774h
- Fujii, S., Mochizuki, M., Aono, K., Hamasaki, S., Murakami, R., and Nakamura, Y. (2011a). pH-responsive aqueous foams stabilized by hairy latex particles. *Langmuir* 27, 12902–12907. doi: 10.1021/la203062b
- Fujii, S., Suzuki, M., Armes, S. P., Dupin, D., Hamasaki, S., Aono, K., et al. (2011b). Liquid marbles prepared from pH-responsive sterically stabilized latex particles. *Langmuir* 27, 8067–8074. doi: 10.1021/la201317b
- Hu, Z., Marway, H. S., Kasem, H., Pelton, R., and Cranston, E. D. (2016a). Dried and redispersible cellulose nanocrystal pickering emulsions. *ACS Macro Lett.* 5, 185–189. doi: 10.1021/acsmacrolett.5b00919
- Hu, Z., Patten, T., Pelton, R., and Cranston, E. D. (2015). Synergistic stabilization of emulsions and emulsion gels with water-soluble polymers and cellulose nanocrystals. *ACS Sustain. Chem. Eng.* 3, 1023–1031. doi: 10.1021/acssuschemeng.5b00194
- Hu, Z., Xu, R., Cranston, E. D., and Pelton, R. (2016b). Stable aqueous foams from cellulose nanocrystals and methyl cellulose. *Biomacromolecules* 17, 4095–4099. doi: 10.1021/acs.biomac.6b01641
- Jiang, J.-Z., Zhu, Y., Cui, Z.-G., and Binks, B. P. (2013). Switchable pickering emulsions stabilized by silica nanoparticles hydrophobised *insitu* with a switchable surfactant. *Angew. Chem. Int. Ed.* 52, 12373–12376. doi: 10.1002/anie.201305947
- Kume, G., Gallotti, M., and Nunes, G. (2008). Review on anionic/cationic surfactant mixtures. *J. Surf. Det.* 11, 1–11. doi: 10.1007/s11743-007-1047-1
- Lam, S., Blanco, E., Smoukov, S. K., Velikov, K. P., and Velez, O. D. (2011). Magnetically responsive pickering foams. *J. Am. Chem. Soc.* 133, 13856–13859. doi: 10.1021/ja205065w
- Lam, S., Velikov, K. P., and Velez, O. D. (2014). Pickering stabilization of foams and emulsions with particles of biological origin. *Curr. Opin. Colloid Interface Sci.* 19, 490–500. doi: 10.1016/j.cocis.2014.07.003
- Liang, C., Liu, Q.-X., and Xu, Z.-H. (2014). Surfactant-free switchable emulsions using CO<sub>2</sub>-responsive particles. *ACS Appl. Mater. Interfaces* 6, 6898–6904. doi: 10.1021/am5007113
- Lin, S. J., and Theato, P. (2013). CO<sub>2</sub>-responsive polymers. *Macromol. Rapid Commun.* 34, 1118–1133. doi: 10.1002/marc.201300288
- Liu, H., Wang, C.-Y., Zou, S.-W., Wei, Z.-J., and Tong, Z. (2012). Simple, reversible emulsion system switched by pH on the basis of chitosan without any hydrophobic modification. *Langmuir* 28, 11017–11024. doi: 10.1021/la3021113
- Liu, K.-H., Jiang, J.-Z., Cui, Z.-G., and Binks, B. P. (2017). pH-responsive pickering emulsions stabilized by silica nanoparticles in combination with a conventional zwitterionic surfactant. *Langmuir* 33, 2296–2305. doi: 10.1021/acs.langmuir.6b04459
- Liu, P.-W., Lu, W.-Q., Wang, W.-J., Li, B.-G., and Zhu, S.-P. (2014). Highly CO<sub>2</sub>/N<sub>2</sub>-switchable zwitterionic surfactant for pickering emulsions at ambient temperature. *Langmuir* 30, 10248–10255. doi: 10.1021/la502749x
- Morse, A. J., Armes, S. P., Thompson, K. L., Dupin, D., Fielding, L. A., Mills, P., et al. (2013). Novel pickering emulsifiers based on pH responsive poly(2-(diethylamino)ethyl methacrylate) latexes. *Langmuir* 29, 5466–5475. doi: 10.1021/la400786a
- Ngai, T., Behrens, S. H., and Auweter, H. (2005). Novel emulsions stabilized by pH and temperature sensitive microgels. *Chem. Commun.* 3, 331–333. doi: 10.1039/b412330a
- Ojala, J., Sirviö, J. A., and Liimatainen, H. (2016). Nanoparticle emulsifiers based on bifunctionalized cellulose nanocrystals as marine diesel oil–water emulsion stabilizers. *Chem. Eng. J.* 312–320. doi: 10.1016/j.cej.2015.10.113
- Quesada, M., Muniesa, C., and Botella, P. (2013). Hybrid PLGAO-organosilica nanoparticles with redox-sensitive molecular gates. *Chem. Mater.* 25, 2597–2602. doi: 10.1021/cm400700g
- Rahman, M. M., Chehimi, M. M., Fessi, H., and Elaissari, A. (2011). Highly temperature responsive core-shell magnetic particles: synthesis, characterization and colloidal properties. *J. Colloid Interface Sci.* 360, 556–564. doi: 10.1016/j.jcis.2011.04.078
- Saigal, T., Dong, H.-C., Matyjaszewski, K., and Tilton, R. D. (2010). Pickering emulsions stabilized by nanoparticles with thermally responsive grafted polymer brushes. *Langmuir* 26, 15200–15209. doi: 10.1021/la1027898
- Tah, B., Pal, P., Mahato, M., and Talapatra, G. B. (2011). Aggregation behavior of SDS/CTAB catanionic surfactant mixture in aqueous solution and at the air/water interface. *J. Phys. Chem. B* 115, 8493–8499. doi: 10.1021/jp202578s
- Tan, T. T. Y., Ahsan, A., Reithofer, M. R., Tay, S. W., Tan, S. Y., Hor, T. S. A., et al. (2014). Photoresponsive liquid marbles and dry water. *Langmuir* 30, 3448–3454. doi: 10.1021/la500646r
- Tang, J.-T., Berry, R. M., and Tam, K. C. (2016). Stimuli-responsive cellulose nanocrystals for surfactant-free oil harvesting. *Biomacromolecules* 17, 1748–1756. doi: 10.1021/acs.biomac.6b00144
- Tang, J.-T., Lee, M. F. X., Zhang, W., Zhao, B.-X., Berry, R. M., and Tam, K. C. (2014). Dual responsive pickering emulsion stabilized by poly[2-(dimethylamino) ethyl methacrylate] grafted cellulose nanocrystals. *Biomacromolecules* 15, 3052–3060. doi: 10.1021/bm500663w
- Tang, J.-T., Sisler, J., Grishkewich, N., and Tam, K. C. (2017). Functionalization of cellulose nanocrystals for advanced applications. *J. Colloid Interf. Sci.* 494, 397–409. doi: 10.1016/j.jcis.2017.01.077
- Tu, F., and Lee, D. (2014). Shape-changing and amphiphilicity-reversing janus particles with pH-responsive surfactant properties. *J. Am. Chem. Soc.* 136, 9999–10006. doi: 10.1021/ja503189r
- Varanasi, S., Henzel, L., Mendoza, L., Prathapan, R., Batchelor, W., Tabor, R., et al. (2018). Pickering emulsions electrostatically stabilized by cellulose nanocrystals. *Front. Chem.* 6, 409–417. doi: 10.3389/fchem.2018.00409
- Yamagami, T., Kitayama, Y., and Okubo, M. (2014). Preparation of stimuli-responsive “mushroom-like” janus polymer particles as particulate surfactant by site-selective surface-initiated AGET ATRP in aqueous dispersed systems. *Langmuir* 30, 7823–7832. doi: 10.1021/la501266t
- Yang, H.-L., Liang, F.-X., Wang, X., Chen, Y., Zhang, C.-L., Wang, Q., et al. (2013). Responsive janus composite nanosheets. *Macromolecules* 46, 2754–2759. doi: 10.1021/ma400261y
- Zhang, Q., Yu, G.-Q., Wang, W.-J., Yuan, H.-M., Li, B.-G., and Zhu, S.-P. (2013). Switchable Block copolymer surfactants for preparation of reversibly coagulatable and redispersible poly(methyl methacrylate) latexes. *Macromolecules* 46, 1261–1267. doi: 10.1021/ma302505r
- Zhu, Y., Fu, T., Liu, K.-H., Lin, Q., Pei, X.-M., Jiang, J.-Z., et al. (2017a). Thermo-responsive pickering emulsions stabilized by silica nanoparticles in combination with alkyl polyoxyethylene ether nonionic surfactant. *Langmuir* 33, 5724–5733. doi: 10.1021/acs.langmuir.7b00273
- Zhu, Y., Jiang, J.-Z., Liu, K.-H., Cui, Z.-G., and Binks, B. P. (2015a). Switchable pickering emulsions stabilized by silica nanoparticles hydrophobised *insitu* with a conventional cationic surfactant. *Langmuir* 31, 3301–3307. doi: 10.1021/acs.langmuir.5b00295
- Zhu, Y., Jiang, J.-Z., Cui, Z.-G., and Binks, B. P. (2014). Responsive aqueous foams stabilized by silica nanoparticles hydrophobised *insitu* with a switchable surfactant. *Soft Matter* 10, 9739–9745. doi: 10.1039/C4SM01970A
- Zhu, Y., Luo, X.-G., Wu, X., Li, W., Li, B., Lu, A., et al. (2017b). Cellulose gel dispersions: fascinating green particles for the stabilization of oil/water pickering emulsion. *Cellulose* 24, 207–217. doi: 10.1007/s10570-016-1093-9
- Zhu, Y., Pei, X.-M., Jiang, J.-Z., Cui, Z.-G., and Binks, B. P. (2015b). Responsive aqueous foams stabilized by silica nanoparticles hydrophobised *insitu* with a conventional surfactant. *Langmuir* 31, 12937–12943. doi: 10.1021/acs.langmuir.5b03681
- Zoppe, J. O., Venditti, R. A., and Rojas, O. J. (2012). Pickering emulsions stabilized by cellulose nanocrystals grafted with thermo-responsive polymer brushes. *J. Colloid Interface Sci.* 369, 202–209. doi: 10.1016/j.jcis.2011.12.011

**Conflict of Interest:** The authors declare that the research was conducted in the absence of any commercial or financial relationships that could be construed as a potential conflict of interest.

Copyright © 2020 Zhu, Chen, Cui, Dai and Cai. This is an open-access article distributed under the terms of the Creative Commons Attribution License (CC BY). The use, distribution or reproduction in other forums is permitted, provided the original author(s) and the copyright owner(s) are credited and that the original publication in this journal is cited, in accordance with accepted academic practice. No use, distribution or reproduction is permitted which does not comply with these terms.



# Supramolecular Polymers With AIE Property Fabricated From a Cyanostilbene Motif-Derived Ditopic Benzo-21-Crown-7 and a Ditopic Dialkylammonium Salt

Haoran Wu and Tangxin Xiao\*

School of Petrochemical Engineering, Changzhou University, Changzhou, China

## OPEN ACCESS

### Edited by:

Suying Xu,  
Beijing University of Chemical  
Technology, China

### Reviewed by:

Xin Wu,  
The University of Sydney, Australia  
Qiuyu Gong,  
Independent Researcher,  
Singapore, Singapore

### \*Correspondence:

Tangxin Xiao  
xiaotangxin@cczu.edu.cn

### Specialty section:

This article was submitted to  
Supramolecular Chemistry,  
a section of the journal  
Frontiers in Chemistry

**Received:** 25 September 2020

**Accepted:** 16 October 2020

**Published:** 19 November 2020

### Citation:

Wu H and Xiao T (2020)  
Supramolecular Polymers With AIE  
Property Fabricated From a  
Cyanostilbene Motif-Derived Ditopic  
Benzo-21-Crown-7 and a Ditopic  
Dialkylammonium Salt.  
Front. Chem. 8:610093.  
doi: 10.3389/fchem.2020.610093

Fluorescent supramolecular polymers (FSP) have attracted considerable attention in recent years. Particularly, the incorporation of aggregation-induced emission (AIE) property to the FSP will bring this material into practical applications. Herein, we designed and synthesized a cyanostilbene motif derived ditopic benzo-21-crown-7 (B21C7) as a host molecule (**H**). The cyanostilbene motif endows **H** with AIE property while the B21C7 motif renders it with the capability to complex with electron deficient guest molecules. Upon the addition of a ditopic dialkylammonium salt molecule (**G**), a novel FSP with blue luminescent property can be constructed. This B21C7-based host-guest FSP with blue fluorescence may have potential application in supramolecular luminescent materials.

**Keywords:** supramolecular polymer, AIE, host-guest, fluorescent materials, B21C7

## INTRODUCTION

Supramolecular polymers, in which ordered and highly directional polymeric arrays of monomeric building blocks are brought together by reversible non-covalent bonds, are outstanding materials that generally exhibit stimuli-responsive and self-healing properties (Aida et al., 2012; Yang et al., 2015; Wehner and Würthner, 2020). The driving force of supramolecular polymers usually includes hydrogen bonds (Xiao et al., 2019b,e; Datta et al., 2020; Qi et al., 2020), metal-ligand bonds (Zheng et al., 2016; Shi et al., 2019), host-guest complexation (Guo et al., 2010; Harada et al., 2014; Wang et al., 2018; Xiao and Wang, 2018; Xiao et al., 2018, 2019d; Chen et al., 2019), donor-acceptor interaction (Han et al., 2018),  $\pi$ - $\pi$  stacking (Wagner et al., 2019; Xiao et al., 2019c), or a combination of them (Li et al., 2012; Wei et al., 2015; Xiao et al., 2020b). In recent years, supramolecular fluorescent materials have drawn much attention, such as fluorescent molecular switches (Cheng et al., 2017), fluorescent sensors (Kumawat et al., 2019), fluorescent metallacup (Wang et al., 2019), and artificial light-harvesting systems (Xiao et al., 2019g, 2020a). Particularly, the development of fluorescent supramolecular polymers (FSPs) has attracted more and more interest because of their potential application in the area of dynamic luminescent materials (Ji et al., 2013; Zhang et al., 2017, 2018; Li et al., 2019). Moreover, the emergence of aggregation-induced emission (Hong et al., 2011) (AIE) fluorophores laid the foundation for the application of FSP in practice.

Macrocycle-based host-guest interaction is an important driving force in supramolecular chemistry. For example, we have reviewed a series of supramolecular materials based on

pillararene (Xiao et al., 2019a,f,h). Benzo-21-crown-7 (B21C7) is one of the most important crown ethers (Zhang et al., 2007), and it shows interesting applications like adhesive materials (Dong et al., 2017; Zhang et al., 2019). B21C7 is the smallest crown ether that can complex with dialkylammonium salts, leading to a relatively strong host-guest interaction. Cyanostilbene is a well-known fluorophore and shows interesting AIE behavior, which is usually used for the construction of rotaxanes (Lee et al., 2013), nanoparticles with near-infrared emission (Shi et al., 2016), hydrogen-bonded supramolecular polymer (Lavrenova et al., 2017), and light-harvesting system (Kim et al., 2018; Sun et al., 2020). To the best of our knowledge, the integration of B21C7 unit and cyanostilbene unit to a host molecule to construct FSP has not yet been reported so far.

Previously, we have reported some orthogonal supramolecular polymers based on B21C7 (Xiao et al., 2013, 2020c). Herein, we designed and synthesized a new host molecule **H**, which bears both cyanostilbene motif and B21C7 units (Figure 1). The cyanostilbene motif endows **H** with the property of AIE, while B21C7 unit endows **H** with the capability to bind dialkylammonium salt. In the presence of guest molecule **G** (a ditopic dialkylammonium salt compound), a novel AA/BB-type FSP can be fabricated by crown ether-based host-guest complexation. Furthermore, the FSP could be assembled into macroscopic fibers with blue fluorescence from concentrated solution. This crown ether-based FSP with beautiful blue fluorescence both in solution and in the solid state may have potential application in supramolecular luminescent materials.

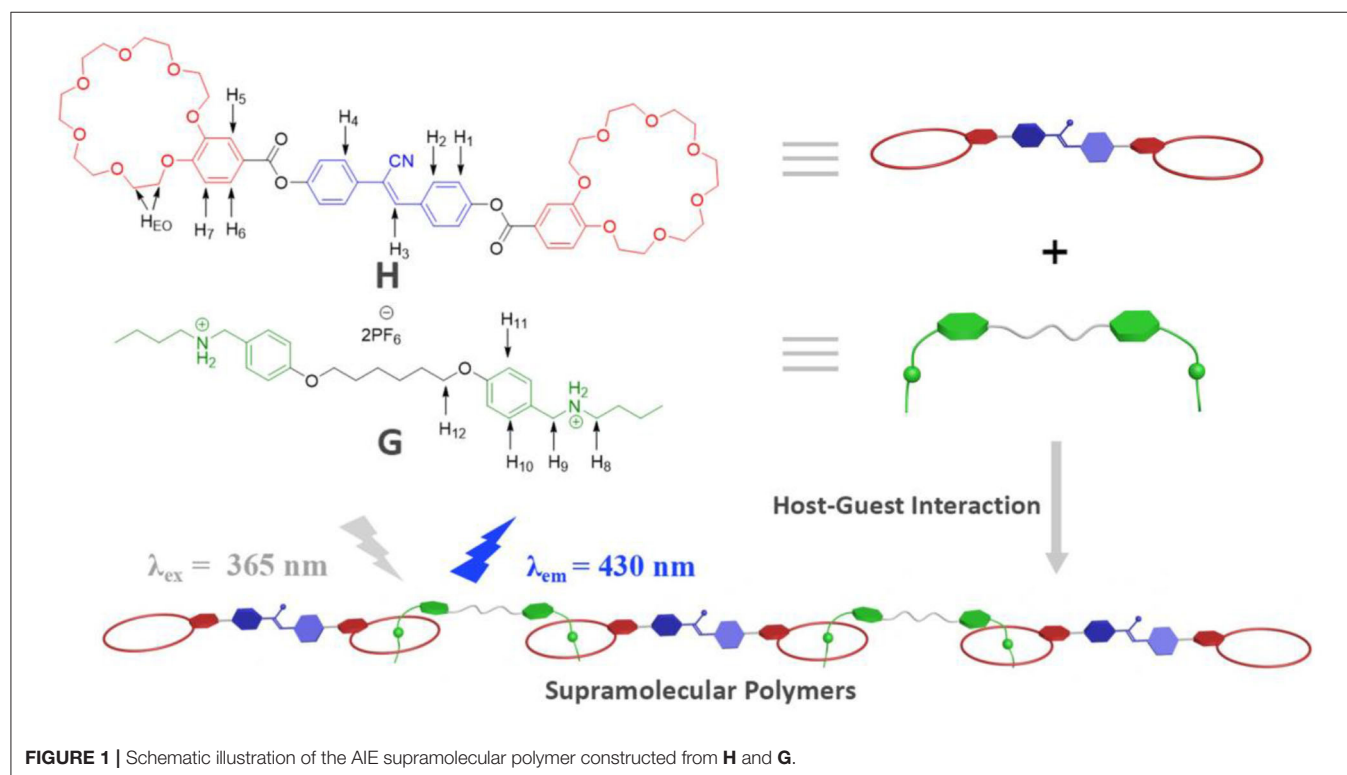
## RESULTS AND DISCUSSIONS

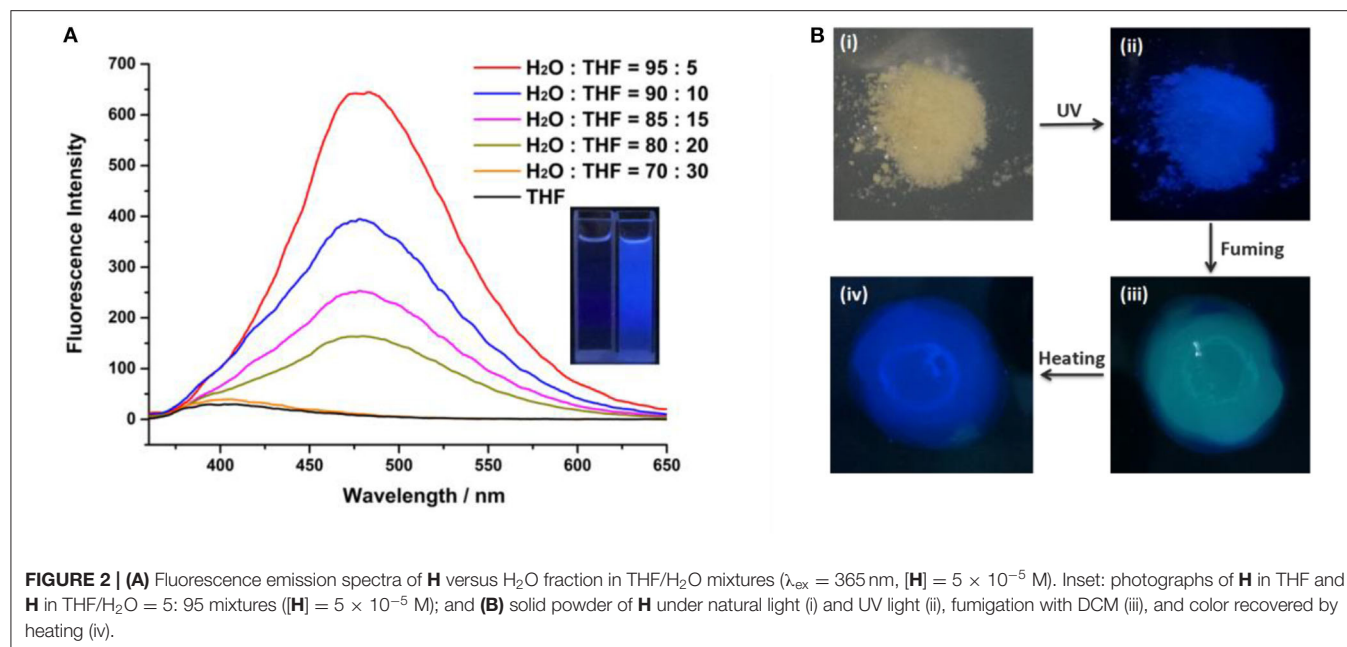
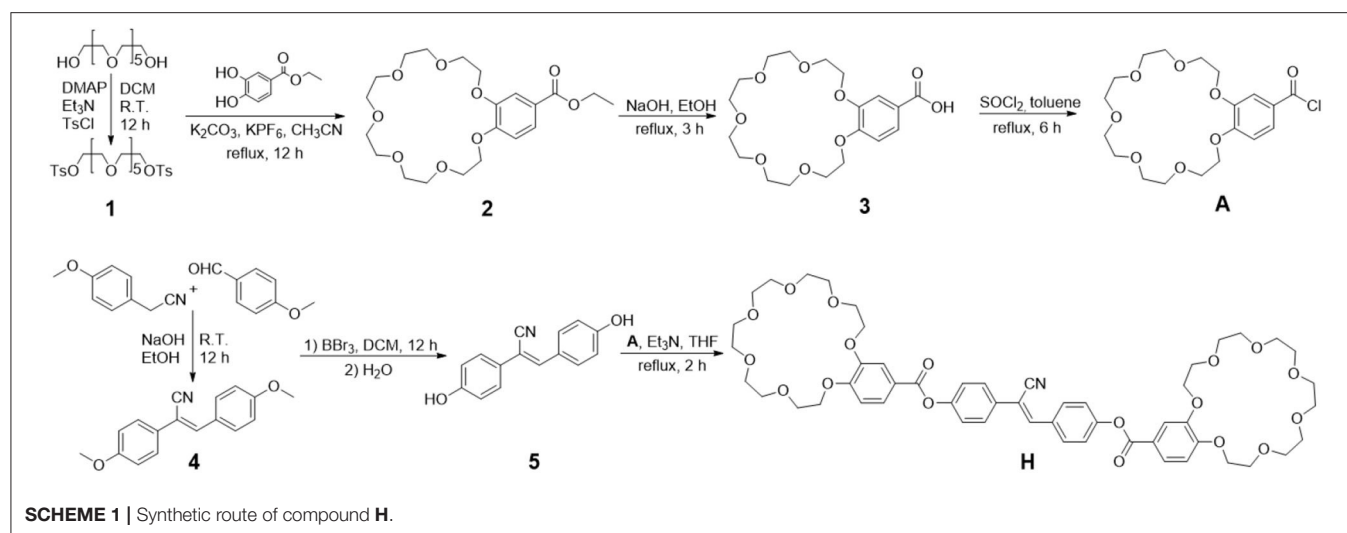
### Synthesis

The synthesis of organic molecules **H** and **G** are straightforward. Compound **H** was synthesized from B21C7-based derivative **A** (Lu et al., 2018) and cyanostilbene-derived compound **5** (Scheme 1). As shown in Scheme 1, starting from p-anisaldehyde and 4-methoxybenzyl cyanide, compound **4** was prepared in ethanol solution by condensation reaction. Demethylation of compound **4** with boron tribromide in dichloromethane (DCM) yields compound **5** (Gu et al., 2012). Compound **G** was synthesized according to literature report (Li et al., 2018). The compounds that have not been reported previously are carefully characterized by  $^1\text{H}$  NMR,  $^{13}\text{C}$  NMR, and HR-MS (Supplementary Figures 1–4).

### AIE and Vapochromic Behavior of **H**

In order to examine whether the cyanostilbene motif bridged B21C7 is AIE active, the fluorescence spectra of **H** in mixed  $\text{H}_2\text{O}$ /Tetrahydrofuran (THF) solutions were investigated. As shown in Figure 2, **H** shows an obvious AIE behavior. There is no fluorescence emission when **H** was in pure THF (a good solvent for **H**). When water (a poor solvent for **H**) content was increased gradually to 80%, a moderate emission was observed. The absorption spectrum of **H** is shown in Supplementary Figure 5. The emission wavelength was at 480 nm when excited at 365 nm. Upon increasing water content to 95%, the fluorescence intensity of **H** exhibits a dramatic enhancement with a bright blue color.





The dried powder of **H** was obtained as a light yellow solid, which exhibited intense blue luminescence under irradiation at 365 nm at room temperature (**Figure 2B**). Interestingly, exposing the sample to DCM vapor resulted in a distinct change of color from blue to green within only 30 s (**Figure 2B**). Notably, the blue color can be recovered by heating the sample to remove the DCM (**Figure 2B**).

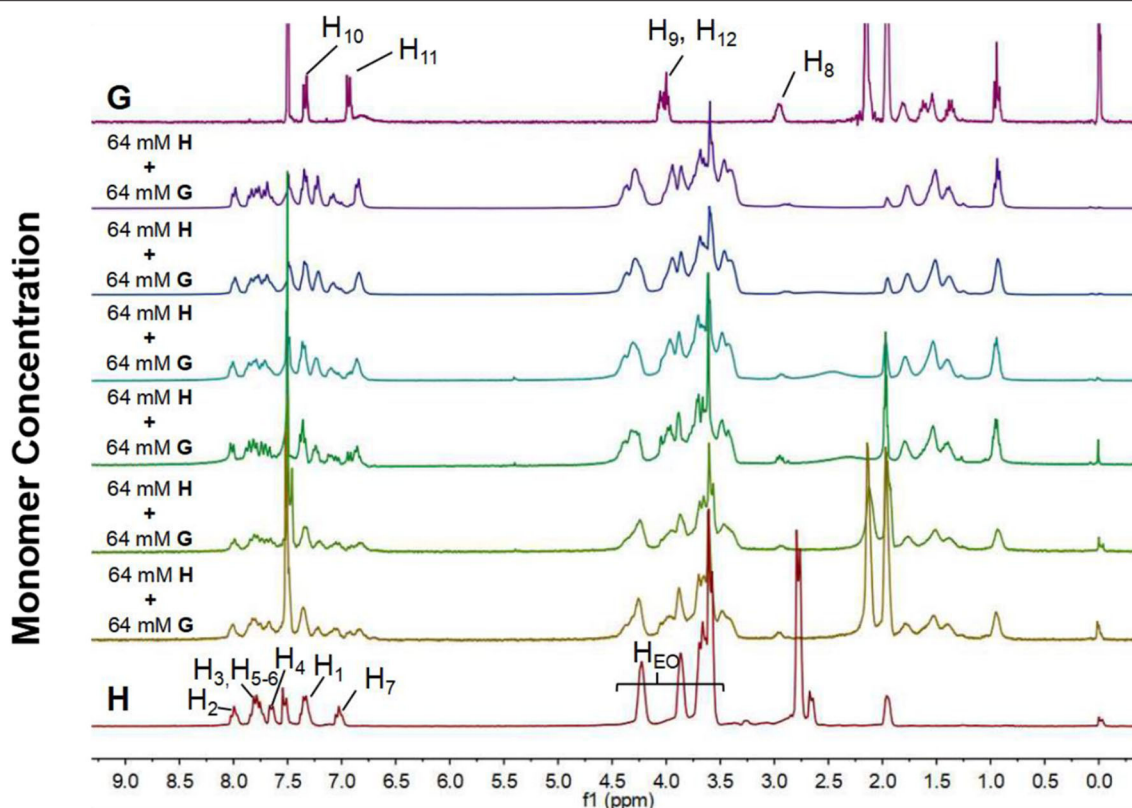
### Supramolecular Polymerization Studied by <sup>1</sup>H NMR and Viscometry

Supramolecular polymerization of **H** and **G** was first investigated by concentration-dependent <sup>1</sup>H NMR. It was measured in mixed CDCl<sub>3</sub>/CD<sub>3</sub>CN (1:1, v/v) at concentrations in the range of 2–64 mM (**Figure 3**). The concentration-dependent <sup>1</sup>H NMR spectra showed a complex picture owing to the slow-exchange

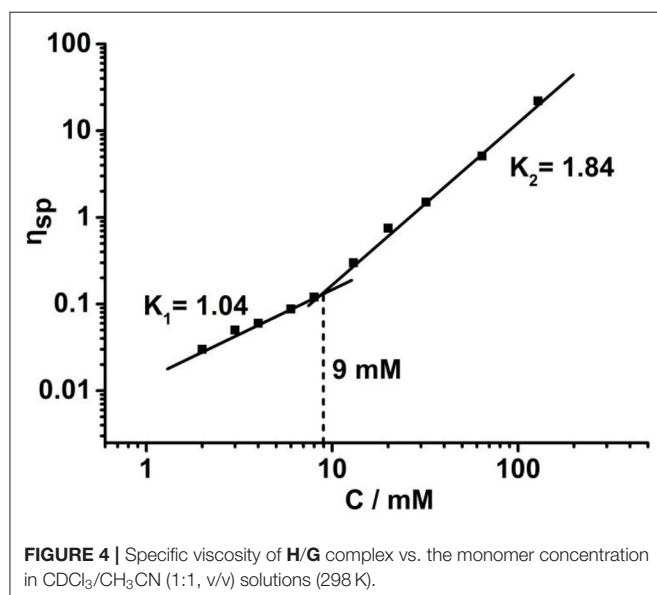
complexation of the B21C7 motif with the dialkylammonium salt on the NMR timescale. It should be noted that the peak splitting is relatively sharp at low concentrations (2–8 mM), suggesting that the cyclic oligomers are predominant species at this stage. As the concentration increases, these peaks became broad, indicating the formation of high-molecular-weight assemblies, such as supramolecular polymers. By contrast, the concentration-dependent <sup>1</sup>H NMR spectra of individual **H** shows no chemical shift change upon concentration increasing (**Supplementary Figure 6**).

To further study the supramolecular polymerization driven by crown ether-based host-guest interaction, viscosity measurements were performed by using a micro-Ubbelohde viscometer. A double logarithmic curve of specific viscosity toward monomer concentration is depicted in **Figure 4**. During





**FIGURE 3** |  $^1\text{H}$  NMR spectra (300 MHz,  $\text{CDCl}_3/\text{CD}_3\text{CN} = 1/1$ , v/v, 298 K) of individual **H** and **G**, and mixtures of them at different monomer concentrations ( $[\text{H}]/[\text{G}] = 1/1$ ).



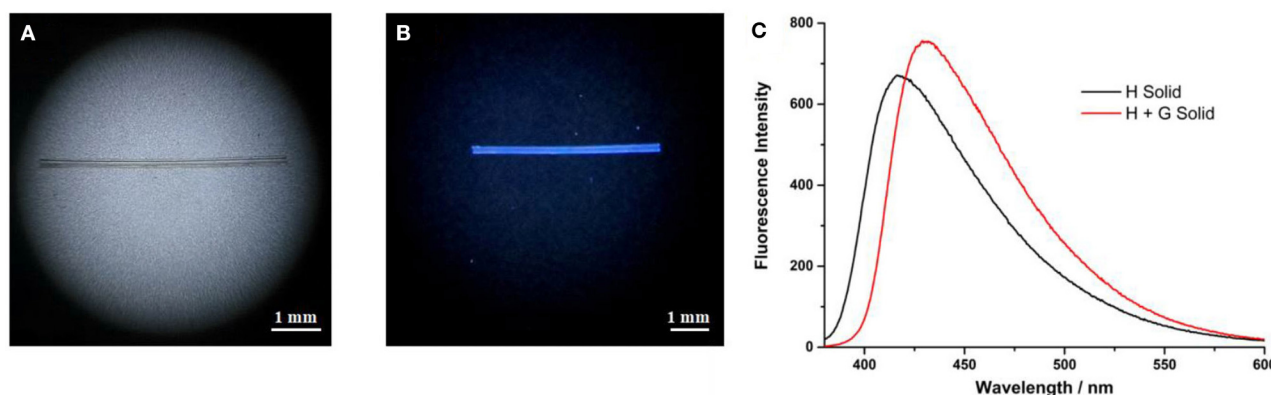
**FIGURE 4** | Specific viscosity of **H/G** complex vs. the monomer concentration in  $\text{CDCl}_3/\text{CH}_3\text{CN}$  (1:1, v/v) solutions (298 K).

the low concentration range, the slope value was tested to be 1.04, which is the characteristic of cyclic oligomers with constant size. When the concentration increased to 9 mM, a steeper curve with a slope 1.84 was obtained, suggesting

that the cyclic oligomers are gradually transformed into supramolecular polymers. This phenomenon was in line with concentration-dependent  $^1\text{H}$  NMR.

### Solid-State Fluorescence Spectroscopy

The formation of supramolecular polymers was further evidenced by its processibility. Fibers can be drawn from a concentrated solution of the host and guest with a molar ratio of  $\text{H/G} = 1/1$  (Figure 5A). Such fibers can be only made from entanglements of large aggregates. By contrast, no fiber can be pulled out from the concentrated solution of individual **H** or individual **G**. The fiber is colorless under visible light (Figure 5A) and generates blue fluorescence under UV light (Figure 5B). This fiber still has fluorescent luminescence after preparation for several days, indicating that the supramolecular polymer has potential applications in the area of supramolecular luminescent materials. The photophysical property of the supramolecular polymer was further investigated by solid-state fluorescence spectroscopy. As shown in Figure 5C, the emission wavelength of **H** shows a hypochromic shift from 480 nm in solution to 415 nm in the solid state. Compared with individual **H**, the supramolecular polymer in the solid state exhibited a stronger emission and bathochromic shift to 430 nm, indicating that the incorporation of the guest affected the packing of the fluorophores in the solid state, resulting in modified luminescent properties.



**FIGURE 5 |** (A) A rod-like fiber formed from **H** and **G** under visible light; (B) the rod-like fiber under UV (365 nm) lamp irradiation; and (C) fluorescence spectra of **H** and **H-G** in the solid state,  $\lambda_{\text{ex}} = 365$  nm.

## EXPERIMENTAL

### General

All chemicals, reagents, and solvents were purchased from commercial suppliers and used, unless otherwise stated, without further purification. If needed, solvents were dried by literature-known procedures. All yields were given as isolated yields. The  $^1\text{H}$  NMR and  $^{13}\text{C}$  NMR spectra were recorded with a Bruker AVANCE III (300 MHz) spectrometer and calibrated against the residual proton signal or natural abundance carbon resonance of the used deuterated solvent from tetramethylsilane as the internal standard. The chemical shifts  $\delta$  are indicated in ppm and the coupling constants  $J$  in Hz. The multiplicities are given as s (singlet), d (doublet), dd (doublet of doublets), t (triplet), and m (multiplet). High-resolution electrospray ionization mass spectra (HR-ESI-MS) were recorded on an Agilent Technologies 6540 UHD Accurate-Mass. Fluorescence measurements were performed on an Agilent Cary Eclipse spectrofluorometer. Viscosity measurements were carried out with Ubbelohde microviscometers (Shanghai Liangjing Glass Instrument Factory, 0.40 mm inner diameter) at 298 K in chloroform and acetonitrile.

### Synthesis of Compound H

To a solution of compound **5** (237 mg, 1.0 mmol) in THF (15 mL) was added compound **A** (1.26 g, 3.0 mmol) and 4-dimethylaminopyridine (18 mg, 0.15 mmol) at room temperature under  $\text{N}_2$  atmosphere. Then the  $\text{Et}_3\text{N}$  (303 mg, 3.0 mmol) was added with vigorous stirred over 15 min. The reaction mixture was heated at  $70^\circ\text{C}$  for 2 h and then poured into water (100 mL). The resulting mixture was extracted with DCM (50 mL  $\times$  3) and the combined extracts were washed with  $\text{H}_2\text{O}$  (100 mL  $\times$  3), brine (50 mL  $\times$  3), dried over anhydrous  $\text{Na}_2\text{SO}_4$  and concentrated under reduced pressure. The resulting residue was chromatographed over silica gel (DCM:MeOH = 60:1, v/v) to afford compound **H** as a light yellow solid (460 mg, 0.46 mmol), yield: 46%.  $^1\text{H}$  NMR (300 MHz,  $\text{CDCl}_3$ ):  $\delta$  (ppm) = 7.98 (d,  $J = 9.0$  Hz, 2H, ArH), 7.85 (dd,  $J = 8.4, 2.1$  Hz, 2H, ArH), 7.74 (d,  $J = 8.7$  Hz, 2H, ArH), 7.69 (d,  $J = 1.8$  Hz, 2H,

ArH), 7.54 (s, 1H, alkene-H), 7.32 (m, 4H, ArH), 6.96 (d,  $J = 8.7$  Hz, 2H, ArH), 4.33–4.19 (m, 8H,  $-\text{OCH}_2\text{CH}_2\text{O}-$ ), 4.03–3.93 (m, 8H,  $-\text{OCH}_2\text{CH}_2\text{O}-$ ), 3.82 (m, 8H,  $-\text{OCH}_2\text{CH}_2\text{O}-$ ), 3.76 (m, 8H,  $-\text{OCH}_2\text{CH}_2\text{O}-$ ), 3.69 (s, 16H,  $-\text{OCH}_2\text{CH}_2\text{O}-$ ).  $^{13}\text{C}$  NMR (75 MHz,  $\text{CDCl}_3$ ):  $\delta$  (ppm) = 164.6, 164.5, 153.7, 153.7, 152.6, 151.8, 148.5, 141.2, 132.0, 131.2, 130.6, 127.2, 124.9, 124.8, 122.6, 122.5, 121.7, 121.6, 117.9, 114.9, 112.3, 110.8, 71.4, 71.3, 71.2, 71.1, 71.0, 71.0, 70.6, 69.6, 69.5, 69.4, 69.2. HR-ESI-MS:  $m/z$  calcd for  $[\text{C}_{53}\text{H}_{64}\text{NO}_{18}]^+ = 1002.4118$ , found = 1002.4120.

## CONCLUSION

In summary, we have successfully synthesized a cyanostilbene motif bridged ditopic B21C7 compound, which exhibits good AIE property and vapoehromic behavior. Supramolecular polymers can be fabricated by such a host compound with a ditopic dialkylammonium salt guest. The host-guest supramolecular polymerization was fully characterized by concentration-dependent  $^1\text{H}$  NMR, viscosity measurements, and fiber formation test. Fluorescent properties of the supramolecular polymers in the solid state are also studied, which suggests that the supramolecular polymers can enhance the AIE of the individual host. The FSP described in this work may have potential applications in the field of dynamic luminescent materials.

## DATA AVAILABILITY STATEMENT

The original contributions generated for the study are included in the article/Supplementary Material, further inquiries can be directed to the corresponding author/s.

## AUTHOR CONTRIBUTIONS

TX conceived and designed the study and wrote and revised the manuscript. HW conducted the synthetic experiments. All authors analyzed and interpreted the data.

## ACKNOWLEDGMENTS

We gratefully thank the financial support from the National Natural Science Foundation of China (21702020).

## REFERENCES

- Aida, T., Meijer, E. W., and Stupp, S. I. (2012). Functional supramolecular polymers. *Science* 335, 813–817. doi: 10.1126/science.1205962
- Chen, Y., Sun, S., Lu, D., Shi, Y., and Yao, Y. (2019). Water-soluble supramolecular polymers constructed by macrocycle-based host-guest interactions. *Chin. Chem. Lett.* 30, 37–43. doi: 10.1016/j.ccl.2018.10.022
- Cheng, M., Zhang, J., Ren, X., Guo, S., Xiao, T., Hu, X. Y., et al. (2017). Acid/base-controllable fluorescent molecular switches based on cryptands and basic N-heteroaromatics. *Chem. Commun.* 53, 11838–11841. doi: 10.1039/C7CC07469G
- Datta, S., Kato, Y., Higashihara, S., Aratsu, K., Isobe, A., Saito, T., et al. (2020). Self-assembled poly-catenanes from supramolecular toroidal building blocks. *Nature* 583, 400–405. doi: 10.1038/s41586-020-2445-z
- Dong, S., Leng, J., Feng, Y., Liu, M., Stackhouse, C. J., Schonhals, A., et al. (2017). Structural water as an essential comonomer in supramolecular polymerization. *Sci. Adv.* 3:eaa0900. doi: 10.1126/sciadv.aao0900
- Gu, X., Yao, J., Zhang, G., Yan, Y., Zhang, C., Peng, Q., et al. (2012). Polymorphism-dependent emission for di(p-methoxyphenyl)dibenzofulvene and analogues: optical waveguide/amplified spontaneous emission behaviors. *Adv. Funct. Mater.* 22, 4862–4872. doi: 10.1002/adfm.201201482
- Guo, D.-S., Chen, S., Qian, H., Zhang, H.-Q., and Liu, Y. (2010). Electrochemical stimulus-responsive supramolecular polymer based on sulfonatocalixarene and viologen dimers. *Chem. Commun.* 46, 2620–2622. doi: 10.1039/b925157j
- Han, Y., Tian, Y., Li, Z., and Wang, F. (2018). Donor-acceptor-type supramolecular polymers on the basis of preorganized molecular tweezers/guest complexation. *Chem. Soc. Rev.* 47, 5165–5176. doi: 10.1039/C7CS00802C
- Harada, A., Takashima, Y., and Nakahata, M. (2014). Supramolecular polymeric materials via cyclodextrin-guest interactions. *Acc. Chem. Res.* 47, 2128–2140. doi: 10.1021/ar500109h
- Hong, Y., Lam, J. W. Y., and Tang, B. Z. (2011). Aggregation-induced emission. *Chem. Soc. Rev.* 40, 5361–5388. doi: 10.1039/c1cs15113d
- Ji, X., Yao, Y., Li, J., Yan, X., and Huang, F. (2013). A supramolecular cross-linked conjugated polymer network for multiple fluorescent sensing. *J. Am. Chem. Soc.* 135, 74–77. doi: 10.1021/ja3108559
- Kim, H.-J., Nandajan, P. C., Gierschner, J., and Park, S. Y. (2018). Light-harvesting fluorescent supramolecular block copolymers based on cyanostilbene derivatives and cucurbit[8]urils in aqueous solution. *Adv. Funct. Mater.* 28:1705141. doi: 10.1002/adfm.201705141
- Kumawat, L. K., Abogunrin, A. A., Kickham, M., Pardeshi, J., Fenelon, O., Schroeder, M., et al. (2019). Squaramide-naphthalimide conjugates as “turn-on” fluorescent sensors for bromide through an aggregation-disaggregation approach. *Front. Chem.* 7:354. doi: 10.3389/fchem.2019.00354
- Lavrenova, A., Balkenende, D. W. R., Sagara, Y., Schrettl, S., Simon, Y. C., and Weder, C. (2017). Mechano- and thermoresponsive photoluminescent supramolecular polymer. *J. Am. Chem. Soc.* 139, 4302–4305. doi: 10.1021/jacs.7b00342
- Lee, S., Chen, C.-H., and Flood, A. H. (2013). A pentagonal cyanostar macrocycle with cyanostilbene CH donors binds anions and forms dialkylphosphate [3]rotaxanes. *Nat. Chem.* 5, 704–710. doi: 10.1038/nchem.1668
- Li, B., He, T., Shen, X., Tang, D., and Yin, S. (2019). Fluorescent supramolecular polymers with aggregation induced emission properties. *Polym. Chem.* 10, 796–818. doi: 10.1039/C8PY01396A
- Li, S.-L., Xiao, T., Lin, C., and Wang, L. (2012). Advanced supramolecular polymers constructed by orthogonal self-assembly. *Chem. Soc. Rev.* 41, 5950–5968. doi: 10.1039/c2cs35099h
- Li, X., Wang, L., Deng, Y., Luo, Z., Zhang, Q., Dong, S., et al. (2018). Preparation of cross-linked supramolecular polymers based on benzo-21-crown-7/secondary ammonium salt host-guest interactions. *Chem. Commun.* 54, 12459–12462. doi: 10.1039/C8CC07657J
- Lu, C., Zhang, M., Tang, D., Yan, X., Zhang, Z., Zhou, Z., et al. (2018). Fluorescent metallacage-core supramolecular polymer gel formed by orthogonal metal coordination and host-guest interactions. *J. Am. Chem. Soc.* 140, 7674–7680. doi: 10.1021/jacs.8b03781
- Qi, L., Ding, Y., Xiao, T., Wu, H., Diao, K., Bao, C., et al. (2020). Supramolecular polymerization of dioxyphenylene bridged UPy derivatives and their host-guest behaviors with the bipyridinium-based cyclophane. *Chin. J. Org. Chem.* doi: 10.6023/cjoc202006070
- Shi, B., Jie, K., Zhou, Y., Zhou, J., Xia, D., and Huang, F. (2016). Nanoparticles with near-infrared emission enhanced by pillararene-based molecular recognition in water. *J. Am. Chem. Soc.* 138, 80–83. doi: 10.1021/jacs.5b11676
- Shi, B., Zhou, Z., Vanderlinden, R. T., Tang, J.-H., Yu, G., Acharyya, K., et al. (2019). Spontaneous supramolecular polymerization driven by discrete platinum metallacycle-based host-guest complexation. *J. Am. Chem. Soc.* 141, 11837–11841. doi: 10.1021/jacs.9b06181
- Sun, G., Qian, W., Jiao, J., Han, T., Shi, Y., Hu, X.-Y., et al. (2020). A highly efficient artificial light-harvesting system with two-step sequential energy transfer based on supramolecular self-assembly. *J. Mater. Chem. A* 8, 9590–9596. doi: 10.1039/D0TA03169K
- Wagner, W., Wehner, M., Stepanenko, V., and Würthner, F. (2019). Supramolecular block copolymers by seeded living polymerization of perylene bisimides. *J. Am. Chem. Soc.* 141, 12044–12054. doi: 10.1021/jacs.9b04935
- Wang, S., Xu, Z., Wang, T., Xiao, T., Hu, X.-Y., Shen, Y.-Z., et al. (2018). Warm/cool-tone switchable thermochromic material for smart windows by orthogonally integrating properties of pillar[6]arene and ferrocene. *Nat. Commun.* 9:1737. doi: 10.1038/s41467-018-03827-3
- Wang, Y., Cai, Y., Cao, L., Cen, M., Chen, Y., Zhang, R., et al. (2019). An amphiphilic metallacup with enhanced fluorescence emission in water: synthesis and controllable self-assembly into multi-dimensional microstructures. *Chem. Commun.* 55, 10132–10134. doi: 10.1039/C9CC04809J
- Wehner, M., and Würthner, F. (2020). Supramolecular polymerization through kinetic pathway control and living chain growth. *Nat. Rev. Chem.* 4, 38–53. doi: 10.1038/s41570-019-0153-8
- Wei, P., Yan, X., and Huang, F. (2015). Supramolecular polymers constructed by orthogonal self-assembly based on host-guest and metal-ligand interactions. *Chem. Soc. Rev.* 44, 815–832. doi: 10.1039/C4CS00327F
- Xiao, T., Feng, X., Wang, Q., Lin, C., Wang, L., and Pan, Y. (2013). Switchable supramolecular polymers from the orthogonal self-assembly of quadruple hydrogen bonding and benzo-21-crown-7-secondary ammonium salt recognition. *Chem. Commun.* 49, 8329–8331. doi: 10.1039/c3cc44525a
- Xiao, T., Qi, L., Zhong, W., Lin, C., Wang, R., and Wang, L. (2019a). Stimuli-responsive nanocarriers constructed from pillar[n]arene-based supramolecular polymers. *Mater. Chem. Front.* 3, 1973–1993. doi: 10.1039/C9QM00428A
- Xiao, T., and Wang, L. (2018). Recent advances of functional gels controlled by pillar[n]arene-based host-guest interactions. *Tetrahedron Lett.* 59, 1172–1182. doi: 10.1016/j.tetlet.2018.02.028
- Xiao, T., Wu, H., Sun, G., Diao, K., Wei, X., Li, Z.-Y., et al. (2020a). An efficient artificial light-harvesting system with tunable emission in water constructed from H-bonded AIE supramolecular polymer and Nile Red. *Chem. Commun.* 56, 12021–12024. doi: 10.1039/D0CC05077F
- Xiao, T., Xu, L., Götz, J., Cheng, M., Würthner, F., Gu, J., et al. (2019b). Supramolecular polymerization and cyclization of dioxynaphthalene motif bridged bifunctional UPys: minor variations in the molecular skeleton and drastic differences in self-assembly. *Mater. Chem. Front.* 3, 2738–2745. doi: 10.1039/C9QM00595A
- Xiao, T., Xu, L., Wang, J., Li, Z.-Y., Sun, X.-Q., and Wang, L. (2019c). Biomimetic folding of small organic molecules driven by multiple

## SUPPLEMENTARY MATERIAL

The Supplementary Material for this article can be found online at: <https://www.frontiersin.org/articles/10.3389/fchem.2020.610093/full#supplementary-material>

- non-covalent interactions. *Org. Chem. Front.* 6, 936–941. doi: 10.1039/C9QO00089E
- Xiao, T., Xu, L., Zhong, W., Zhou, L., Sun, X.-Q., Hu, X.-Y., et al. (2018). Advanced functional materials constructed from pillar[n]arenes. *Isr. J. Chem.* 58, 1183–1193. doi: 10.1002/ijch.201800026
- Xiao, T., Xu, L., Zhou, L., Sun, X.-Q., Lin, C., and Wang, L. (2019d). Dynamic hydrogels mediated by macrocyclic host–guest interactions. *J. Mater. Chem. B* 7, 1526–1540. doi: 10.1039/C8TB02339E
- Xiao, T., Zhong, W., Qi, L., Gu, J., Feng, X., Yin, Y., et al. (2019e). Ring-opening supramolecular polymerization controlled by orthogonal non-covalent interactions. *Polym. Chem.* 10, 3342–3350. doi: 10.1039/C9PY00312F
- Xiao, T., Zhong, W., Xu, L., Sun, X.-Q., Hu, X.-Y., and Wang, L. (2019f). Supramolecular vesicles based on pillar[n]arenes: design, construction, and applications. *Org. Biomol. Chem.* 17, 1336–1350. doi: 10.1039/C8OB03095B
- Xiao, T., Zhong, W., Zhou, L., Xu, L., Sun, X.-Q., Elmes, R. B. P., et al. (2019g). Artificial light-harvesting systems fabricated by supramolecular host–guest interactions. *Chin. Chem. Lett.* 30, 31–36. doi: 10.1016/j.cclet.2018.05.034
- Xiao, T., Zhou, L., Sun, X.-Q., Huang, F., Lin, C., and Wang, L. (2020b). Supramolecular polymers fabricated by orthogonal self-assembly based on multiple hydrogen bonding and macrocyclic host–guest interactions. *Chin. Chem. Lett.* 31, 1–9. doi: 10.1016/j.cclet.2019.05.011
- Xiao, T., Zhou, L., Wei, X., Li, Z., and Sun, X. (2020c). Supramolecular copolymers driven by quadruple hydrogen bonding and host–guest interactions. *Chin. J. Org. Chem.* 40, 944–949. doi: 10.6023/cjoc201911014
- Xiao, T., Zhou, L., Xu, L., Zhong, W., Zhao, W., Sun, X.-Q., et al. (2019h). Dynamic materials fabricated from water soluble pillar[n]arenes bearing triethylene oxide groups. *Chin. Chem. Lett.* 30, 271–276. doi: 10.1016/j.cclet.2018.05.039
- Yang, L., Tan, X., Wang, Z., and Zhang, X. (2015). Supramolecular polymers: historical development, preparation, characterization, and functions. *Chem. Rev.* 115, 7196–7239. doi: 10.1021/cr500633b
- Zhang, C., Li, S., Zhang, J., Zhu, K., Li, N., and Huang, F. (2007). Benzo-21-crown-7/secondary dialkylammonium salt [2]Pseudorotaxane- and [2]rotaxane-type threaded structures. *Org. Lett.* 9, 5553–5556. doi: 10.1021/ol702510c
- Zhang, C.-W., Ou, B., Jiang, S.-T., Yin, G.-Q., Chen, L.-J., Xu, L., et al. (2018). Cross-linked AIE supramolecular polymer gels with multiple stimuli-responsive behaviours constructed by hierarchical self-assembly. *Polym. Chem.* 9, 2021–2030. doi: 10.1039/C8PY00226F
- Zhang, M., Yin, S., Zhang, J., Zhou, Z., Saha, M. L., Lu, C., et al. (2017). Metallacycle-cored supramolecular assemblies with tunable fluorescence including white-light emission. *Proc. Natl. Acad. Sci. U.S.A.* 114, 3044–3049. doi: 10.1073/pnas.1702510114
- Zhang, Q., Li, T., Duan, A., Dong, S., Zhao, W., and Stang, P. J. (2019). Formation of a supramolecular polymeric adhesive via water-participant hydrogen bond formation. *J. Am. Chem. Soc.* 141, 8058–8063. doi: 10.1021/jacs.9b02677
- Zheng, W., Chen, L.-J., Yang, G., Sun, B., Wang, X., Jiang, B., et al. (2016). Construction of smart supramolecular polymeric hydrogels cross-linked by discrete organoplatinum(II) metallacycles via post-assembly polymerization. *J. Am. Chem. Soc.* 138, 4927–4937. doi: 10.1021/jacs.6b01089

**Conflict of Interest:** The authors declare that the research was conducted in the absence of any commercial or financial relationships that could be construed as a potential conflict of interest.

Copyright © 2020 Wu and Xiao. This is an open-access article distributed under the terms of the Creative Commons Attribution License (CC BY). The use, distribution or reproduction in other forums is permitted, provided the original author(s) and the copyright owner(s) are credited and that the original publication in this journal is cited, in accordance with accepted academic practice. No use, distribution or reproduction is permitted which does not comply with these terms.



# Advantages of publishing in Frontiers



## OPEN ACCESS

Articles are free to read  
for greatest visibility  
and readership



## FAST PUBLICATION

Around 90 days  
from submission  
to decision



## HIGH QUALITY PEER-REVIEW

Rigorous, collaborative,  
and constructive  
peer-review



## TRANSPARENT PEER-REVIEW

Editors and reviewers  
acknowledged by name  
on published articles

## Frontiers

Avenue du Tribunal-Fédéral 34  
1005 Lausanne | Switzerland

Visit us: [www.frontiersin.org](http://www.frontiersin.org)

Contact us: [frontiersin.org/about/contact](http://frontiersin.org/about/contact)



## REPRODUCIBILITY OF RESEARCH

Support open data  
and methods to enhance  
research reproducibility



## DIGITAL PUBLISHING

Articles designed  
for optimal readership  
across devices



## FOLLOW US

@frontiersin



## IMPACT METRICS

Advanced article metrics  
track visibility across  
digital media



## EXTENSIVE PROMOTION

Marketing  
and promotion  
of impactful research



## LOOP RESEARCH NETWORK

Our network  
increases your  
article's readership